



UNIVERSITY *of the*
WESTERN CAPE

PETROPHYSICAL EVALUATION OF THE ALBIAN AGE GAS BEARING SANDSTONE
RESERVOIRS OF THE O-M FIELD, ORANGE BASIN, SOUTH AFRICA

By

OPUWARI, MIMONITU

A thesis Submitted in Partial fulfilment of the requirement for the degree of Philosophae Doctor
(PhD) in the Faculty of Science, Earth Sciences Department
University of the Western Cape, Bellville, South Africa

Supervisor: Professor Paul Carey
Co-supervisor: Escordia De Poquioma

May, 2010.

ABSTRACT

Petrophysical Evaluation of the Albian Age Gas Bearing Sandstone Reservoirs of the O-M field,
Orange Basin, South Africa

Opuwari, Mimonitu

Petrophysical evaluation of the Albian age gas bearing sandstone reservoirs of the O-M field, Offshore South Africa has been performed. The main goal of the thesis is to evaluate the reservoir potentials of the field through the integration and comparison of results from core analysis, production data and petrography studies for the evaluation and correction of key petrophysical parameters from wireline logs which could be used to generate an effective reservoir model. A total of ten wells were evaluated and twenty eight sandstone reservoirs were encountered of which twenty four are gas bearing and four are wet within the Albian age depth interval of 2800m to 3500m. Six lithofacies (A1, A2, A3, A4, A5 and A6) were grouped according to textural and structural features and grain size from the key wells (OP1, OP2 and OP3). Facies A6 was identified as non reservoir rock in terms of reservoir rock quality and facies A1 and A2 were regarded as the best reservoir rock quality. This study identifies the different rock types that comprise reservoir and non reservoirs. Porosity and permeability are the key parameters for identifying the rock types and reservoir characterization. Pore throat radius was estimated from conventional core porosity and permeability with application of the Winland's method for assessment of reservoir rock quality on the bases of pore throat radius. Results from the Winland's method present five Petrofacies (Mega porous, Macro porous, Meso porous, Micro porous and Nanno porous). The best Petrofacies was mega porous rock type which corresponds to lithofacies A1 and A2. The nano porous rock type corresponds to lithofacies A6 and was subsequently classified as non reservoir rock. The volume of clay model from log was taken from the gamma-ray model corrected by Steiber equations which was based on the level of agreement between log data and the x-ray diffraction (XRD) clay data. The average volume of clay determined ranged from 1 – 28 %. The field average grain density of 2.67 g/cc was

determined from core data which is representative of the well formation, hence 2.67 g/cc was used to estimate porosity from the density log. Reservoir rock properties are generally good with reservoir average porosities between 10 – 22 %, an average permeability of approximately 60mD. The laterolog resistivity values have been invasion corrected to yield estimates of the true formation resistivity. In general, resistivities of above 4.0 Ohm-m are productive reservoirs, an average water resistivity of 0.1 Ohm-m was estimated. Log calculated water saturation models were calibrated with capillary pressure and conventional core determined water saturations, and the Simandoux shaly sand model best agree with capillary and conventional core water saturations and was used to determine field water saturations. The reservoir average water saturations range between 23 – 69 %. The study also revealed quartz as being the dominant mineral in addition to abundant chlorite as the major clay mineral. The fine textured and dispersed pore lining chlorite mineral affects the reservoir quality and may be the possible cause of the low resistivity recorded in the area. The reservoirs evaluated in the field are characterized as normally pressured with an average reservoir pressure of 4800 psi and temperature of 220 °F. An interpreted field aquifer gradient of 0.44 psi/ft (1.01 g/cc) and gas gradient of 0.09 psi/ft (0.2 g/cc) were obtained from repeat formation test measurements. A total of eight gas water contacts were identified in six wells. For an interval to be regarded as having net pay potential, cut-off values were used to distinguish between pay and non-pay intervals. For an interval to be regarded as pay, it must have a porosity value of at least 10 %, volume of clay of less than 40 %, and water saturation of not more than 65 %. A total of twenty four reservoir intervals meet the cut-off criteria and was regarded as net pay intervals. The gross thickness of the reservoirs range from 2.4m to 31.7m and net pay interval from 1.03m to 25.15m respectively. In summary, this study contributes to scale transition issues in a complex gas bearing sandstone reservoirs and serves as a basis for analysis of petrophysical properties in a multi-scale system.

DECLARATION

I declare that *Petrophysical Evaluation of the Albian Age Gas Bearing Sandstone Reservoirs of the O-M field, Orange Basin, South Africa* is my own work, that it has not been submitted before for any degree or examination in any other university, and that all the sources I have used or quoted have been indicated and acknowledged as complete references.

Opuwari, Mimonitu

May 2010

Signed:

ACKNOWLEDGEMENTS

I would like to give the Almighty God all the glory, honour and adoration for seeing me through this great journey of overwhelming challenges. With His presence, it has really been an interesting and fulfilling venture. A number of persons have contributed throughout the period of this project and deserve credit for the completion of this project.

To my supervisors, Professor Paul Carey and Escordia de Poquioma (Mrs), I say a big thank you for your untiring efforts and interest in this work. You introduced me to the world of Petrophysics and ensured that I receive water, care and nourishment from time to time. Your confidence in me was indeed a great inspiration. From time to time, you were ever willing to attend to my “don’t knows”. The fruit of your support is evident, and I am indeed very grateful.

This research project was financially supported by the Petroleum oil and gas company of South Africa (PETROSA) and I am deeply grateful for such an opportunity. The contributions of Petroleum Agency of South Africa (PASA) and Forest Oil Exploration International for providing data used in this thesis are highly acknowledged. I am also grateful to Schlumberger Company and Senergy for providing the Interactive Petrophysics Software package used in the modeling.

Mr Jeff Aldrich is gratefully acknowledged for his general support, motivation and the trust he demonstrated especially at the early phase of this research work. Mr Andrew and Jody Frewin’s contributions to the success of this work are appreciated. Thanks a lot.

The dean of Science, Professor Donker is deeply appreciated for his support at critical stages of this work.

To the Department of Earth Sciences, University of the Western Cape, Bellville, South Africa, the Head of the department, Prof. Charles Okujeni and all the members of staff, I say a big thank you for the good and cordial working relationship I enjoyed during my studies. Fellow students in the department, especially Solomon Adekola, Segun Adeyemi, Corlyne Barlie, Fadipe,

Wisemen, Yafeh, Funke Ojo, are appreciated for the professional and non- professional conversations during this period. The secretary, Ms Washiela Davids is thanked for her support.

This study would not have been completely satisfying without the working relationship I had with my colleagues and good brothers, including James Ayuk, Dr Richard Akinyeye, Anthony Duah, Ebenezer Kingsley, Jerry Egwu, Joe Daniel, Greene Avor, Seth Udeme, Dr Patrick Ogidi, Sunmi Iyela, Femi Adigun , and Victor Amadi. Your contributions are highly appreciated.

I wish to thank Rev Segun Adeleke, Professor and Mrs Meshack Ogunniye, Professor and Dr Charles Ile, Professor George Amabeoku, Rev George Ogenetega, Pastor Akinyeye, Lanre Fatoba, and members of Boston Cell group of Bellville Baptist Church for their prayers and support. I am indeed very proud of you.

Mr Abdullah Jamoodian, Mandla N,Rasheed ,and Sbusiso all of PetroSA are appreciated for their support. Also to be remembered is Mr Juan Carlos Porrás of International rock Analysts for the short course he presented on rock typing. Thank you.

I am particularly grateful to my parents, Mr and Mrs Ahams Opuwari for my education and upbringing and my in-laws for their prayers and support. It is delightful to see you all alive as I progress in life. All my other family members are equally gratefully acknowledged. Thanks for the love and care.

Finally, my dear wife, Chinyerum and son David are thanked for showing an enormous patience and understanding during this period of study. I could not have carried out this research without her caring support. I really appreciate and love you dearly.

DEDICATION

This project is dedicated to

The

ALMIGHTY GOD

for

His

Enabling Grace that was

Sufficient for me.

TABLE OF CONTENTS

	Page No
<i>Abstract</i>	<i>i</i>
<i>Declaration</i>	<i>iii</i>
<i>Acknowledgements</i>	<i>iv</i>
<i>Dedication</i>	<i>v</i>
<i>Table of contents</i>	<i>vii</i>
<i>List of Figures</i>	<i>xvi</i>
<i>List of Tables</i>	<i>xxiii</i>
<i>List of Appendices</i>	<i>xxvi</i>

SECTION ONE: BASIC CONCEPTS

<i>Chapter One: Introduction</i>	1
1.1 Background Information	1
1.2 Approach and outline of thesis	2
1.3 Geological Overview	5
1.4 Location of Study Area/ Well Location	7
1.5 Aims and Objectives	9
1.6 Research Methodology	9
<i>Chapter Two: Wireline Logging</i>	13
2.1 Introduction	13
2.2 The Nuclear Logs	14
2.2.1 Conventional Natural Gamma Ray (GR)	14
2.2.2 Spectral Gamma Ray (SGR)	16
2.2.3 Density logs	16
2.2.3.1 Formation Bulk Density Log (RHOB)	19

2.2.3.2	Photo-electric Effect Density Log (PEF)	20
2.2.4	Neutron Logs	21
2.2.4.1	Compensated Neutron Log (CNL)	23
2.2.4.2	Sidewall Neutron Porosity Log (SNP)	23
2.3	Acoustic Log	23
2.4	Electrical logs	26
2.4.1	Spontaneous Potential (SP)	26
2.4.2	Resistivity Logs	28
2.4.2.1	Induction Logs	28
2.4.2.2	Laterolog	29
2.4.2.3	Microresistivity Logs	30
2.5	Auxiliary Logs	31
2.5.1	Caliper Log	31
2.5.2	Temperature Log	31
2.5.3	Dipmeter Log	32
2.6	Overview of new generation logging tools	33
<i>Chapter Three: Description of Petrophysical Properties</i>		34
3.1	Introduction	34
3.2	Porosity	34
3.2.1	Porosity Alteration	37
3.3	Permeability	38
3.4	Fluid Saturation	40
3.4.1	Electrical Formation water	41
3.4.2	Water Saturation	43
3.4.3	Influence of Clay on Rock Resistivity	44
3.5	Capillary Pressure	44
3.5.1	Capillary Pressure Curves	45
3.5.2	Capillary Pressure and Seal	47
3.5.3	Saturation-Height Equations	49
3.5.3.1	Leverett's J Function Approach	49

3.5.3.2	Johnson Capillary method	50
3.5.3.2	Skelt-Harrison Capillary Pressure and log Based Method	50

SECTION TWO: PETROPHYSICAL EVALUATION

Chapter Four: Wireline Log Editing and Normalization **51**

4.1	Introduction	51
4.2	Log data Collection and Creation of Database	53
4.2.1	Wireline logged Intervals for Wells	53
4.3	Log Editing	55
4.3.1	Depth Shifting	55
4.3.2	Borehole environmental correction	56
4.3.3	Mud filtrate Invasion Correction	60
4.3.4	Smoothing, De-Spiking and Noise Removal	62
4.4	Curve Splicing/Merging	63
4.5	Curve Normalization	64

Chapter Five: Core Analysis and Interpretation **68**

5.1	Introduction	68
5.2	Conventional Core Analysis	69
5.2.1	Interval Cored	69
5.2.1.1	Well OP1	69
5.2.1.2	Well OP2	71
5.2.1.3	Well OP3	73
5.3	Core-Log Depth Match	75
5.4	Lithofacies Description	76
5.4.1	Well OP1 Lithofacies	78
5.4.2	Well OP2 Lithofacies	79
5.4.3	Well OP3 Lithofacies	80
5.5	Analysis and Interpretation of Results	82

5.5.1	Grain Density	82
5.5.2	Well OP1 Grain Density	83
5.5.3	Well OP2 Grain Density	84
5.5.4	Well OP3 Grain Density	84
5.5.5	Comparison of Grain Density Distributions for Wells	85
5.6	Interpretation of Core Porosity	86
5.6.1	Well OP1 Porosity	87
5.6.2	Well OP2 Porosity	89
5.6.3	Well OP3 Porosity	91
5.6.4	Porosity distribution for Wells	94
5.7	Interpretation of Permeability	96
5.7.1	Well OP1 Permeability	97
5.7.2	Well OP2 Permeability	99
5.7.3	Well OP3 Permeability	101
5.7.4	Permeability Distribution for Wells	104
5.8	Interpretation of Fluid Saturation	105
5.8.1	Well OP1 Fluid Saturation	106
5.8.2	Well OP3 Fluid Saturation	107
5.9	Comparison of Porosity- Permeability and Facies Distribution	109
5.9.1	Porosity-Permeability and facies Distribution for Well OP1	109
5.9.2	Porosity-Permeability and Facies Distribution for Well OP2	110
5.9.3	Porosity-Permeability and facies Distribution for Well OP3	112
5.9.4	Comparison of Porosity, Permeability and Facies for All Wells	113
5.10	Special Core Analysis (SCAL)	114
5.10.1	Porosity, Permeability and Grain density Measurements	115
5.10.1.1	Well OP1 Porosity, Permeability and Grain density Measurements	115
5.10.1.2	Well OP3 Porosity, Permeability and Grain density Measurements	116
5.10.2	Formation Resistivity Factor (FRF) Measurements	117
5.10.2.1	Formation Resistivity Factor (FRF) measurement Results for Well OP1	118
5.10.2.2	Formation Resistivity Factor (FRF) measurement Results for Well OP3	118
5.10.2.3	Formation Resistivity Index (RI) Measurements	119

5.10.3.1	Formation Resistivity Index Results for Well OP1	120
5.10.3.2	Formation Resistivity Index Results for Well OP3	120
5.10.4	Interpretation of Results	121
5.10.4.1	Porosity Overburden Correction	121
5.10.5	Derivation of Cementation exponent From Formation Resistivity Factor	125
5.10.5.1	Well OP1 cementation Exponent (m) at Room Condition	126
5.10.5.2	Well OP3 cementation Exponent (m)	127
5.10.5.3	Effect of overburden Pressure on Cementation	128
5.10.5.4	Comparison of cementation exponent with Porosity	130
5.10.5.5	Comparison of Cementation exponent with permeability	133
5.10.6	Determination of Saturation Exponent (n)	134
5.10.6.1	Well OP1 Formation Resistivity Index (RI) versus Saturation at Room Condition	135
5.10.6.2	Well OP3 Saturation Exponent (n) Determination at Room Condition	136
5.10.6.3	Comparison of Saturation Exponent (n)	137
5.10.7	Petrography Studies	138
5.10.7.1	Thin Section Analysis	138
5.10.7.1.1	Well OP3	139
5.10.7.2	X-Ray Diffraction (XRD)	140
5.10.7.2.1	Well OP2 XRD	140
5.10.7.2.2	Well OP3 XRD	142
5.10.7.3	Scanning Electron Microscopy (SEM)	145
5.10.7.3.1	Well OP3	146
5.10.7.4	Relationship between Chlorite and Facies	147
5.10.8	Cation Exchange Capacity (CEC)	150
5.10.8.1	Presentation of CEC Analysis Results	151
5.10.8.2	Q _v , the Shale Indicator determination	151
5.10.8.3	Clay Bound Water (CBW), Porosity and Q _v	153
5.10.9	Capillary Pressure Measurements	158
5.10.9.1	Well OP1 Air-Brine capillary pressure measurement Results	159
5.10.9.2	Well OP3 Air-Brine capillary pressure measurement Results	159

5.10.9.3	Well OP2 Mercury-Injection capillary pressure measurement Results	160
5.10.10	Interpretation of Capillary Pressure Results	160
5.10.10.1	Well OP1 Water Saturation determination from Capillary pressure curves	161
5.10.10.2	Well OP3 Water Saturation determination from Capillary pressure curves	163
5.10.10.3	Well OP2 Water Saturation determination from Capillary pressure curves	164
5.11	Saturation –Height Determination from Leverett’s J-Function Method	166

Chapter Six: Petrophysical Model of Volume of Shale, Porosity and Water Saturation from Core and Log

6.1	Introduction	171
6.2	Volume of Shale	171
6.2.1	Gamma-Ray Method	173
6.2.2	Spontaneous Potential (SP) Method	174
6.2.3	Neutron Log Method	174
6.2.4	Resistivity Method	175
6.2.5	Correction of Shale Volume	175
6.2.6	Double Clay Indicators	177
6.2.7	Parameters used for determination of Volume of Clay	178
6.2.8	Calibration of Volume of Clay (Vcl) Models	179
6.2.9	Use of Spectral Gamma-Ray log as an Estimator of Clay type	183
6.3	Porosity Model	186
6.3.1	Porosity Determination from Density Log	186
6.3.2	Porosity from Neutron Log	187
6.3.3	Porosity from Sonic (acoustic) Log (Φ_S)	188
6.3.4	Effective Porosity Determination (Φ_e)	189
6.3.5	Comparison of Log and Core Porosity	190
6.4	Water Saturation Models	195
6.4.1	Parameters	197
6.4.1.1	Formation Temperature Determination	197
6.4.1.2	Determination of formation Water Resistivity (Rw)	199
6.4.1.2.1	SP Method for Formation Resistivity water Estimation	200

6.4.1.2.2	Pickett Plot method For Formation water Resistivity Estimation	202
6.4.1.3	Cation Exchange Capacity per Pore Volume (Q_v) and Equivalent Conductance of Clay Cations (B)	203
6.4.2	Water Saturation (S_w) Models	203
6.4.2.1	Archie's Model	204
6.4.2.2	The Shaly-Sand Model	205
6.4.2.2.1	The Simandoux Model	205
6.4.2.2.2	Indonesian Model	206
6.4.2.2.3	Waxman-Smits Model	207
6.4.2.2.4	Dual-Water Model	208
6.4.2.2.5	Juhasz Model	211
6.4.3	Comparison of Core and Log Water saturations	211
6.5	Bulk Volume of Water (BVW)	215
<i>Chapter Seven: Permeability, Rock Typing and Flow Units</i>		217
7.1	Introduction	217
7.2	Permeability	218
7.2.1	Permeability from Core Analysis (Permeability–Porosity Function)	218
7.3	Permeabilities Estimate from Log	223
7.4	Permeability from the Repeat Formation Test (RFT)	229
7.4.1	Relative Permeability	229
7.5	Determination of Rock types (Petrofacies)	233
7.5.1	Well OP1 Petrofacies determination	235
7.5.2	Well OP2 Petrofacies determination	236
7.5.3	Well OP3 Petrofacies determination	238
7.6	Comparison of Petrofacies and Lithofacies	240
7.7	K/PHI Relationship	244
7.8	Hydraulic Flow Zone Indicator (FZI)	246
<i>Chapter Eight: Determination of Fluid Contact</i>		258
8.1	Introduction	258
8.2	Wireline Pressure data analysis and Interpretation	258

8.2.1	Well OP1	260
8.2.2	Well OP2	261
8.2.3	Well OP3	262
8.2.4	Well OP4	262
8.2.5	Well OP6	263
8.2.6	Well MA1	264
8.2.7	Well MA2	265
8.2.8	Well MA3	266
8.3	Comparison of Log, DST and RFT data fluid contact	269
 <i>Chapter Nine: Application of Results, Determination of Cut-Off and Net Pay</i>		278
9.1	Introduction	278
9.2	Determination of Petrophysical Properties in Non-Cored Wells	279
9.3	Cut-off Determination	287
9.3.1	Porosity Cut-Off Determination	288
9.3.2	Volume of Shale Cut-Off Determination	290
9.3.3	Water Saturation Cut-Off Determination	292
9.4	Determination of Net Pay	293
 <i>Chapter Ten: Conclusions and Recommendations</i>		304
<i>References</i>		310
<i>Appendices</i>		324

LIST OF FIGURES

		Page No
1.1	Outline of Research	3
1.2	Chronostratigraphic and sequence stratigraphic diagram of the Orange Basin	6
1.3	Well location map	8
1.4	Section one of the flow chat of research methodology	11
1.5	Section two of Research methodology flow chart	12
2.1	Diagram of GR log	15
2.2	Compton Scattering of Gamma Rays	17
2.3	Density and litho density (photoelectric) logging in relation of gamma ray energy	18
2.4	Neutron speed versus source (MeV)	22
2.5	The positions of transmitters and Receivers in Sonic tool	24
2.6	Graphics of Self Potential Curve showing Static Self Potential (SSP) and Shale line	27
2.7	Example of presentation of dip log	32
3.1	Example of pore space and mineral grain space	35
3.2	Example of Effective and total Porosity	36
3.3	Packings of spheres of primary or intergranular porosity	37
3.4	Directions of measurement of permeability	39
3.5	Rock Permeability Ranges	40
3.6	Contact angles for water-wet and oil-wet surfaces	45
3.7	Pressure vs Depth plot	48
4.1	Flow chart of Log editing	52
4.2	Example of gamma-ray log Run at the same depth with other logs	59
4.3	Example of density log affected by borehole	61
4.4	Graphics of uncorrected and environmentally corrected logs	63
4.5	Thin bed Recognition on Resistivity logs	65
4.6	Example of spike and de-spiking of sonic log	66
4.7a	Example of Log at different runs (unspliced curves)	67

4.7b	Examples of graphics of spliced curves	68
4.8a	GR log values for all Well before Normalization	69
4.8b	Possible Reference Wells (OP4 and OP5) used for Normalization	70
4.8c	Normalized curves	71
5.1	Example of Log and Core data comparison before depth shifting	79
5.2	Well OP1 showing core facies in track 3	82
5.3	Well OP2 graphics showing Core facies in track 3	83
5.4a	Well OP3 core 1 Facies shown in track 3	84
5.4b	Well OP3 core 2 Facies shown in track 3	85
5.5	Histogram of Well OP1 Core Grain densities	87
5.6	Grain Density Histogram of Well OP2	88
5.7	Well OP3 core grain density cumulative frequency plot	89
5.8	Grain density histogram plot for all Well	90
5.9a	Well OP1 Core Porosity versus depth Plot	92
5.9b	Histogram Of porosity distribution of Well OP1	93
5.10a	Well OP2 Porosity versus depth plot	94
5.10b	Well OP2 core porosity histogram and plot against depth	95
5.11a	Well OP3 porosity versus depth plot	96
5.11b	Histogram of Well OP3 core porosity distribution	97
5.12a	Histogram of Porosity distribution for Wells	98
5.12b	Histogram of Core Porosity Shaly/Silt interval for all Well	99
5.12c	Histogram of Core Porosity Massive Sands for Wells	100
5.13a	Well OP1 Permeability versus depth Plot	102
5.13b	Well OP1 Permeability Histogram Plot	103
5.14a	Well OP2 Depth versus permeability plot	104
5.14b	Well OP2 permeability histogram plot	105
5.15a	Well OP3 depth-permeability plot	106
5.15b	Well OP3 core1 and 2 Permeability Histogram Plot	107
5.16	Permeability histogram for Wells	108
5.17	Well OP1 Fluid Saturation versus depth plot	110
5.18a	Well OP3 core 1 Fluid saturation versus depth plot	111

5.18b	Well OP3 core 2 fluid saturation versus depth plot	112
5.19	Porosity-Permeability and Gamma ray log and Facies Plot for Well OP1	113
5.20	Porosity-Permeability and Facies and GR plot for Well OP2	114
5.21	Porosity-Permeability and Facies GR plot for Well OP3	115
5.22	Porosity-permeability and Facies distribution for Wells	117
5.23a	Well OP3 Porosity at Overburden Pressure vs Porosity at room condition	126
5.23b	Formation resistivity factor (FRF) vs Porosity Plot for Well OP1	129
5.24	Plot of Well OP3 FRF Vs Fractional Porosity	131
5.25	Formation Resistivity factor vs Porosity at Overburden pressure	132
5.26	Well OP1 and OP3 cementation versus porosity plot at room conditions	134
5.27	Cementation versus porosity at Overburden condition of Well OP3	135
5.28	Well OP1 and OP3 cementation exponent vs permeability at room condition	136
5.29	Well OP1 resistivity Index versus water saturation plot	138
5.30	Well OP3 Resistivity Index versus saturation Plot	139
5.31	Resistivity Index versus Saturation plots for Well OP1 and OP3	140
5.32	Well OP3 thin section at depth 3236m and 3283m showing fine grain, sub angular to angular, and sparsely distributed organic matter and pore filling Chlorite	142
5.33	Whole Rock mineralogy of Well OP2	145
5.34	Whole rock mineralogy of core 1 and 2 of Well OP3	147
5.35	Different ways of Shale distribution in a formation	148
5.36	Example of Well OP3 SEM analysis result	149
5.37	Distribution of chlorite for Well OP2	150
5.38a	Well OP3 core 1 Chlorite distribution	151
5.38b	Well OP3 core 1 Chlorite distribution	152
5.39	Plot of Q_v versus saturation of bound water for all Wells	158
5.40a	Plot of Q_v versus Total and effective porosities for all Wells	159
5.40b	Multi-Well Porosity versus Saturation of bound water plot	160
5.41	Schematic relationship between Capillary pressure curve and	

	oil accumulation	164
5.42	Capillary Pressure Curve for Well OP1	165
5.43	Capillary Pressure Curve for Well OP3	166
5.44	Capillary Pressure Curve for Well OP2	167
5.45	Capillary Pressure Curves with Permeability and Porosity	168
5.46	Leverett's Saturation determination J-Function	171
5.47	J-function curves for Well OP1 and OP3	172
5.48	Saturation-height function for Wells OP1 and OP3	172
6.1a	Schematic diagram of variation of sediments with clay mineral content increasing from left to right	175
6.1b	Volume of shale correction chart	179
6.2	Example of Neutron-Density cross plot as clay indicator	180
6.3	Log determined volume of clay overlain with XRD volume of clay for Well OP2	183
6.4	Log determined volume of clay overlain with XRD volume of clay for Well OP3	184
6.5	Well OP1 Spectral Gamma ray log	187
6.6	Well OP1 potassium/thorium cross plot for identification of clay type	188
6.7	Well OP1 Comparison of log and core porosity	194
6.8	Well OP2 comparison of log and core porosity	195
6.9	Well OP3 comparison of log and core porosity	196
6.10	Multi-Well overburden porosity versus log porosity	197
6.11	Example of Resistivity of water from SP method	204
6.12	Pickett Plot for determination of resistivity of water (R_w) for Well OP1, OP2, and OP3 respectively	205
6.13a	Estimate of Resistivity of shale (R_{sh}) from Wells	209
6.14	Comparison of core and log determined bound water saturation for Well OP1	212
6.15	Comparison of core and log estimated bound water saturation and XRD mineralogy data for Well OP2	213
6.16	Comparison of Core and log water saturation models for Well OP1	215

6.17	Comparison of Core and log water saturation models for Well OP3	217
6.18	Bulk Volume of water and Effective Porosity Plot for Well OP3	219
7.1	Porosity –Permeability Cross Plots for determination of function	222
7.2	Well OP1 Plot of Predicted Permeability Overlaying original core permeability in track 4	223
7.3	Well OP2 Plot of Predicted Permeability Overlaying original core permeability in track 4	224
7.4	Well OP3 Plot of Predicted Permeability Overlaying original core permeability in track 4	225
7.5	Example of irreducible water saturation estimate point from capillary pressure measurement	227
7.6	Log estimated permeability and overlaid core permeability for Well OP1	229
7.7	Log estimated permeability and overlaid core permeability for Well OP2	230
7.8	Log estimated permeability and overlaid core permeability for Well OP3	231
7.9	Relative Permeability curves for Well OP2 and OP3 within the reservoir intervals	233
7.10	Comparison of permeabilities derived from log, RFT and Krh equations for Well OP2	234
7.11	Comparison of Permeabilities derived from core, log and cross plot	235
7.12	Correlation of Winland and Pittman’s plots for Well OP1	239
7.13	Correlation of Winland and Pittman’s plots for Well OP2	241
7.14	Correlation of Winland and Pittman’s plots for Well OP3	243
7.15a	Comparison of lithofacies and Petrofacies for Well OP1	244
7.15b	Comparison of Lithofacies and Petrofacies for Well OP2	245
7.15c	Comparison of lithofacies and Petrofacies for Well OP3	246
7.15d	Comparison of lithofacies and Petrofacies for entire Well	247
7.15e	Permeability/Porosity Ratio (K/PHI) for Wells	248
7.16a	Well OP1 Flow Zone Indicator, Rock Types and Facies plot	253
7.16b	Well OP1 NPI Vs RQI Plot	254
7.17a	Well OP2 Flow Zone Indicator, Rock Types and Facies plot	255
7.17b	Plot of NPI Versus RQI for Well OP2	256

7.18a	Well OP3 Flow Zone Indicator, Rock Types and Facies plot	258
7.18b	Plot of NPI Versus RQI for Well OP3	259
7.18c	Plot of NPI Versus RQI for all Wells	260
8.1	Well OP1 Pressure versus depth Plot for identification of Gas/Water Contact (GWC) and Fluid densities	263
8.2	Well OP2 Pressure versus Depth Plot	264
8.3	Well OP3 Pressure Versus Depth Plot showing possible GWC at measured depth 3361.3m	265
8.4	Well OP4 Pressure versus Depth Plot	266
8.5	Well OP6 Pressure versus Depth Plot	267
8.6	Well MA1 Pressure versus Depth Plot	268
8.7	Well MA2 Pressure versus Depth Plot	269
8.8	Well MA3 Pressure versus Depth Plot	270
8.9	Overlaid gas and water gradients in the field	271
8.10	Well OP1 comparison of log and Pressure data Gas Water Contact	273
8.11	Well OP3 Comparison of Log and Pressure data Gas water Contact	274
8.12	Well OP4 Comparison of Log and Pressure data Gas Water Contact	276
8.13	Well OP6 Comparison of Log and Pressure data Gas Water Contact	277
8.14	Well MA 2 Comparison of Log and Pressure data Gas Water Contact	278
8.15	Well MA3 Comparison of Log and Pressure data Gas water contact	279
9.1	Well MA1 results estimated petrophysical properties	283
9.2	Well MA2 results of estimated of Petrophysical Properties	284
9.3	Well MA3 Results of Estimated Petrophysical Properties	285
9.4	Well MA4 Results of Estimated Petrophysical Properties	286
9.5	Well OP4 Results of Estimated Petrophysical Properties	287
9.6	Well OP5 Results of Estimated Petrophysical Properties	288
9.7	Well OP6 Results of Estimated Petrophysical Properties	289
9.8a	Multi-Well Porosity-Permeability Plot for Cut-Off determination	291
9.8b	Multi-Well Permeability and Porosity Histogram distributions	292
9.8c	Application of Permeability and Porosity Cut-Off to Petrofacies	293
9.9a	Volume of shale versus porosity and gamma-ray log plot	294

9.9b	Multi-Well Vclay frequency distribution and cut-off point	295
9.10	Multi-Well Porosity vs Water Saturation and Frequency Distribution	296
9.11	Well OP1 showing Calculated Reservoir Parameters and Pay Flags	298
9.12	Well OP2 showing Calculated Reservoir Parameters and Pay Flag	299
9.13	Well OP3 graphics of Calculated Reservoir Parameters and Flags	300
9.14	Well OP4 showing calculated reservoir parameters and Flags	301
9.15	Well OP5 showing Calculated Reservoir Parameters and Flags	302
9.16	Well OP6 showing calculated Reservoir Parameters and Flags	303
9.17	Well MA2 Showing Calculated Reservoir Parameters and Flags	304
9.18	Well MA3 Showing Calculated Reservoir Parameters and Flags	305
9.19	Well MA4 Graphics of Calculated Reservoir Parameters and Flags	306

LIST OF TABLES

		Page No
1.1	Summary of data used for study	10
2.1	Depth of investigation of density tool and typical readings	19
2.2	Photo-electric absorption factor for common minerals	21
2.3	Typical Sonic matrix travel times of some rocks	26
2.4	Curve names and mnemonics of laterolog	29
2.5	Common curve names of microresistivity logs	30
3.1	Cementation of various rock types	42
3.2	Interfacial Tension and Contact Angle Values	47
4.1	Suite of Logs Run in wells at various Intervals	54
4.2	Summary of environmental corrections applied to logs	57
4.3	Guide for borehole condition	58
5.1	Well OP1 Routine Core Analysis	70
5.2	Well OP2 Routine core analysis results	72
5.3	Well OP3 core1 analysis results and lithology description	73
5.4	Well OP3 core 2 Routine core analysis results and lithology description	74
5.5	Cored Intervals and Core-log Shift Summary for Wells	76
5.6	Lithofacies descriptions and classification of Reservoir Facies	78
5.7	Matrix density of common lithology	82
5.8	Permeability classification scale	98
5.9	Porosity, Permeability and Grain Density test results of Well OP1 at room condition	115
5.10	Porosity, Permeability and Grain Density test results of Well OP3 at room condition	106
5.11	Result of Well OP1 FRF measurement at room condition	118
5.12	Result of Well OP3 FRF measurement at room and overburden conditions	118
5.13	Resistivity Index results for Well OP1	119
5.14	Resistivity Index results for Well OP3	120
5.15	Well OP3 core 2 data used for porosity overburden correction	121

5.16	Wells OP1, OP2 and OP3 calculated Overburden Corrected Porosities	123
5.17a	Classification of Cementation exponent	124
5.17b	Cementation exponent (m) from Formation resistivity factor measurement	125
5.18	Cementation exponent for Well at Room Condition	126
5.19	Well OP3 cementation exponent at overburden pressure (4,830 psi)	128
5.20	Well OP3 comparison of cementation exponents	129
5.21	Well OP1 result of resistivity index measurements and n values	134
5.22	Well OP3 Result of Saturation exponent (n) derived from RI vs Saturation	136
5.23	Whole rock Mineralogy of Well OP2	140
5.24	Whole Rock Mineralogy of Well OP3	142
5.25	Result of Cation Exchange Capacity (CEC) for Wells	150
5.26	Calculated values of cation exchange capacity per pore volume for Wells	151
5.27	Calculated effective porosity and clay bound water for Wells	153
5.28	Well OP1 Capillary Pressure test data	158
5.29	Well OP3 Capillary Pressure test data	159
6.1	Summary of Parameters used for Volume of Clay calculations	181
6.2	Summary of Parameters used for log Effective porosity calculation	192
6.3	Calculated Formation temperature (T2) and Resistivity of mud filtrate	201
7.1	Established Porosity-Permeability Functions for Wells	222
7.2	Classification of Rock Types 7.3	237
7.3	Rock types classification based on winland and Pittman calculations	238
7.4	Rock types classification based on winland and Pittman calculations for Well OP2	240
7.5	Reservoir rock classifications of Well OP3	242
7.6	Well OP1 Calculated values for RQI, NPI and FZI	251
7.7	Well OP2 Calculated values for RQI, NPI and FZI	254
7.8	Well OP3 Calculated values for RQI, NPI and FZI	257
8.1	Ranges of density and pressure gradients for hydrocarbon	262
8.2	Summary of pressure gradients and densities for Wells	270
8.3	Summary of Gas Water Contact	280
9.1	Well OP1 Summary of calculated Reservoir Pay Parameters	297

9.2	Well OP2 Summary of Calculated Reservoir Pay Parameters	299
9.3	Well OP3 Summary of calculated Reservoir Pay Parameters	300
9.4	Well OP4 Summary of calculated Reservoir Pay Parameters	301
9.5	Well OP5 Summary of calculated Reservoir Pay Parameters	302
9.6	Well OP6 Summary of calculated Reservoir Pay Parameters	303
9.7	Well MA2 Summary of calculated Reservoir Pay Parameters	304
9.8	Well MA3 Summary of calculated Reservoir Pay Parameters	305
9.9	Well MA4 Summary of calculated Reservoir Pay Parameters	306

LIST OF APPENDICES

		Page No
Appendix A	Logging tool code and tool description	327
Appendix B	Core photos	328
Appendix C	Well resistivity index vs saturation plot	330
Appendix D	Well OP2 capillary pressure data	337
Appendix E	Well J-Function and height parameters	338
Appendix F	Neutron versus Density and GR log plots	340
Appendix G	Log versus Core overburden Porosity for Wells	341
Appendix H	Pickett plot for Wells	342
Appendix I	Results of RFT measurements for Wells	343

CHAPTER ONE

INTRODUCTION

1.1 BACKGROUND INFORMATION

Petrophysics is regarded as the process of characterising the physical and chemical properties of the rock-pore-fluid system through the integration of the geological environment, well logs, rock and fluid sample analyses and their production histories. A reservoir is a subsurface layer or a sequence of layers of porous rock that contain hydrocarbon. Depending on their geological origin, these layers are usually sandstone rock or carbonate rock. The hydrocarbon resides in the open spaces in the rock matrix called pores. The parameters that determine the behaviour of pore system are known as the petrophysical properties.

In reservoir evaluation and development, the assessment of petrophysical properties such as porosity, permeability, and water saturation, percentage of shale volume, mineralogy, and type of pore fluid are deduced from well logs, core analysis, and well tests. The successful evaluations of these properties are necessary for determining the hydrocarbon potential of a reservoir system performance and also help us predict the behaviour of complex reservoir situations. The integration of comprehensive mineralogical studies with the evaluation of petrophysical properties provides a valuable basis for reservoir systems studies. Thus, it aids in understanding the influence of minerals in rock properties when correlated with wire line geophysical logs. The operators in the Petroleum Industry need quick and reliable methods by which the fundamental properties of the rocks and the fluid contents can be determined in the subsurface. This is easily achieved by the use of wire line geophysical logs.

Geophysical logs are not direct measures of the petrophysical properties of the formation. The logs measure different formation parameters that are then translated to properties of geological significance during log interpretations. The parameters measured by the logs may be inherent to the formation itself such as the formation resistance to an electric current. Logs also measure mechanical parameters in the

borehole such as the hole diameter and the down hole temperature. The petrophysical properties determined from cores and logs are not always comparable, hence considerable care must be observed when comparing data from core and log analysis. Core analysis is one of the reservoir assessment tools that directly measure many important formation properties. The analysis determines porosity, permeability, grain-size distribution, grain density, mineral composition, sensitivity of fluids, and effect of overburden stress (Bateman, 1985).

The Albian reservoir intervals in the Orange Basin consists of an overall association of coursing-upward, laminated and bioturbated mudstone to massive and planar cross-bedded sandstones with evidence of reducing conditions. The reservoirs are heterogeneous consisting of massive sands and are encountered at depths below 2700m with varying thicknesses.

The Albian age gas bearing reservoir sandstones evaluated in this study range between 2800m to 3500m depending on the position of the well. The study area is zoned into two. The MA wells in the Northern part of the field and the OP wells in the central and southern part of the study area. Ten wells are the focus of the study, of which three (OP1, OP2 and OP3) were regarded as the key wells because core analysis was performed in some of the reservoir sections of these wells.

1.2 APPROACH AND OUTLINE OF THE THESIS

This thesis started with the review of previous studies and literature search in comparable oil and gas fields. This is to get familiarize with the basin architecture, tectonic and structural features, sediment source and transport history, flow units and inter play of accumulation. Emphasis has been placed on classic reservoirs because the techniques that were developed in this study focus on sandstone and shale lithology.

The petrophysical evaluation approach adopted in this study is a probabilistic log analysis technique which takes all continuous log data and uses the response to create an answer. The answer which yields the least difference between the raw and re-computed logs from that answer is chosen. Core and production data are used to calibrate the answer derived from the log by adjusting in order to obtain better performance.

The thesis is grouped into two sections which are depicted in Figure 1.1 below.

<h1 style="text-align: center;">THESIS STRUCTURE</h1>	
Section one (Basic concepts)	Section two (Petrophysical evaluation)
<ul style="list-style-type: none"> • Chapter one (Introduction) • Chapter two (Wireline logs) • Chapter three (Petrophysical properties) 	<ul style="list-style-type: none"> • Chapter four (Log editing and normalization) • Chapter five (Core analysis and interpretation) • Chapter six (Calibration of volume of shale, porosity and water saturation) • Chapter seven (Permeability, petrofacies and flow zone indicators) • Chapter eight (Fluid contact determination) • Chapter nine (Application of results, cut-off and net pay determination) • Chapter ten (conclusions and recommendations).

Figure 1.1: Outline of Research.

In petroleum evaluation, the importance of mineralogical studies has been demonstrated in the northern North Sea where porosity evaluation from logs was complicated by radioactive and heavy minerals and the evaluation had to resort to an integrated approach with core and log analysis (Nyberg et al, 1978). The integrated analysis and interpretation of core and log information together with fluid and pressure analysis, by geologists, petrophysicists and reservoir engineers has resulted in a valuable base for field development studies, particularly in circumstances where major investment decisions are taken with the benefit of few appraisal wells (Hurst & Archer, 1986).

Petrophysical properties are derived from individual characteristics of the mineral constituents forming the rock (Serra, 1986), but the mineral themselves are seldom considered in the evaluation of rock properties. Laboratory studies of sandstones showed the various petrophysical properties, such as density, radioactivity, resistivity, porosity, magnetic susceptibility, might vary considerable depending on clay and heavy minerals, carbonaceous matter and on rock fabrics (Emerson, 2000).

The geochemistry of sandstone diagenesis is routinely applied to problems of reservoir simulation and enhances recovery (Hearn et al., 1984). Clay minerals affect all log measurements and logs have potential for determining clay mineralogy. However, the sensitivity of logs to mineralogy requires that log responses be calibrated for mineralogy effects (Patchett & Coalson, 1982; Suau & Spurlin, 1982).

Mineralogy input into geophysical analysis has also provided porosity evaluation results that are more comparable with direct measurements carried out on core samples (Guest, 1990).

Saturation profiles can also be used to understand the distribution of water saturation within a field or prospect Hartmann & Coalson (1990) showed how cores and logs from four field wells of the Sorrento field, southeast Colorado was determined through saturation profiles. Bastia (2004) in his study of the depositional model and reservoir architecture of tertiary deep water sedimentation, Krishna Godavari offshore Basin, India, reveal that the reservoir of the gas field tertiary sands originally deposited in the deep water channel-levee system with relatively clean channel and laminated levee facies as shown in his study.

Core analysis has evolved from qualitative geology descriptions to the use of sophisticated analysis tool, such as the scanning electron microscopy (SEM), energy dispersive x-ray spectrometry, x-ray diffraction, infrared spectroscopy, and imaging analysis techniques Juhasz (1990)

Mineralogical techniques have shown that small variations in the clay mineral content and rock texture can have an influence on the permeability and on different geophysical log responses Hurst & Archer (1986). It has thus been suggested that log derived mineralogical evaluation might be used in conjunction with mineralogical analysis of core samples in order to validate the quantification from logs, and provide additional information on mineral texture and distributions.

1.3 GEOLOGICAL OVERVIEW

The Orange Basin extends along the coast of Western Africa for 1500 km from the Aguilhas Arch in the south to the Walvis Ridge in the north. The Basin is one of the most lightly explored passive margin systems in the world with the South African portion of the basin encompasses 130,000 km² with water depths ranging to greater than 3000m. More than 75% of the prospective area is in water depths shallower than 500m and half of the prospective region lies in water depths shallower than 250m. To date only 47 wells have been drilled in the basin. This exploration effort has led to the discovery of one gas field in Namibian waters (Kudu) and one gas field in South African waters.

Deposition in the area took place in an overall shallow marine shelf-type environment. Sand deposition mostly resulted from wave reworked dominated delta front and shelf marine and storm bars. The sandstones are appears greenish which is indicative of the presence of glauconite marine conditions. The greenish sandstones are massive and exhibit a wave influenced type of lamination. The sandstones are generally well sorted ranging in grain size from very fine to medium. The lower and upper contacts of the sandstones are characterized by an abrupt lower contact, gradual, bioturbated upper contact Petroleum Agency Brochure (2000).

Earliest sedimentation is dated as pre-Hauterivian and likely began in the Kimmeridgian or Tithonian (~152-154 Ma), although fossil control in the older rocks is absent due to the lack of marine facies in Wells drilled to date (Figure 1.2).

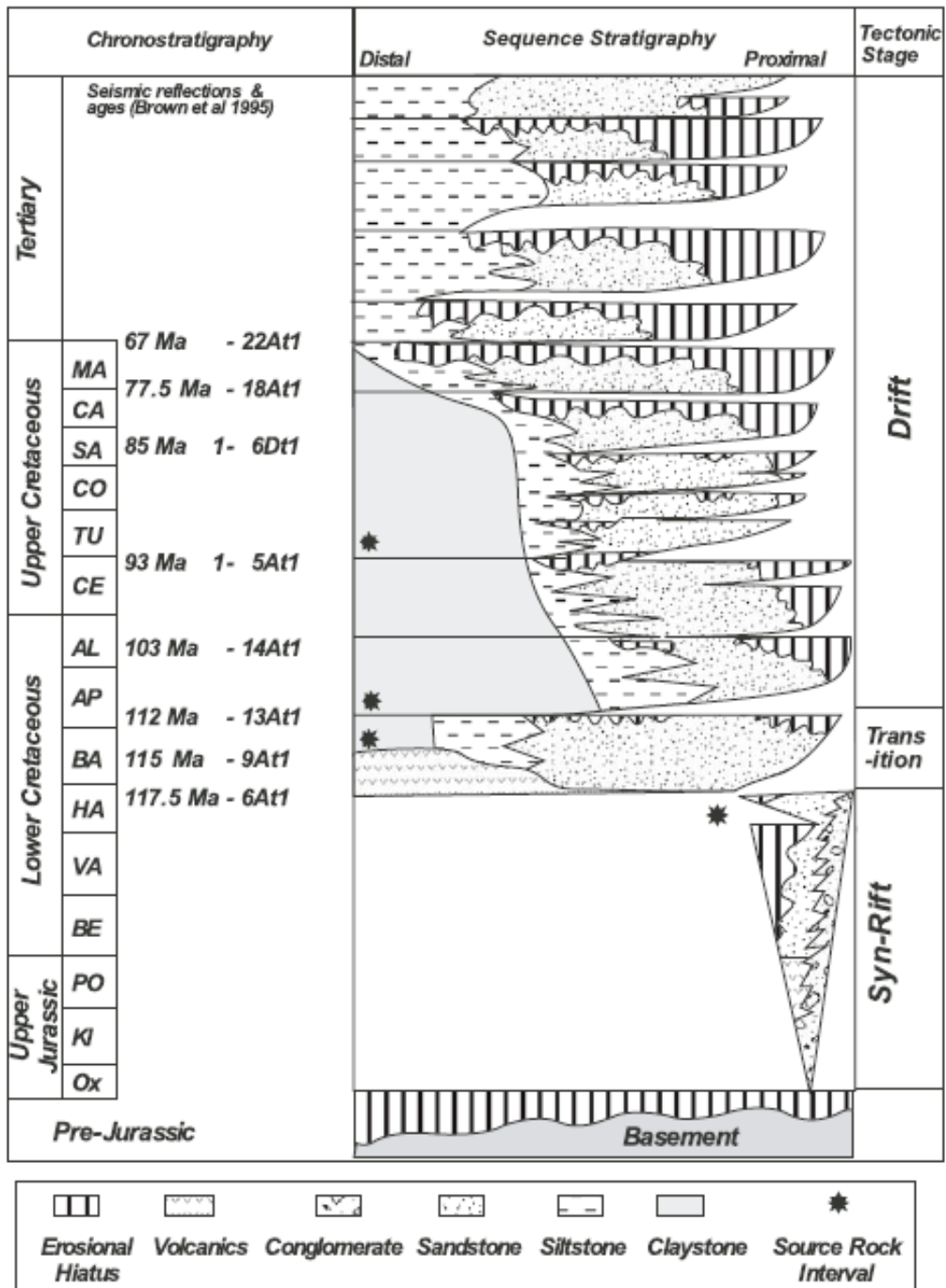


Figure 1.2: Chronostratigraphic and sequence stratigraphic diagram of the Orange Basin (Brown et al., 1995).

Two source rocks are present, the lacustrine shales restricted to the Pre-Hauterivian section in rift phase half-graben sub basins and, terrigenous derived Type II kerogen in Upper Cretaceous shales of the drift section. Both source rock sequences are currently generative. The channels are part of a meandering system. Reservoir rocks

in the rift section are fluvial and deltaic sandstones and conglomerates derived from the Palaeozoic Karoo section and underlying basement. Drift sequence reservoir facies on most of the broad shelf are primarily fluvial sandstones and floodplain deposits (Jungslager, 1999).

Numerous play types are present in the area. The rift plays are presented by possible lacustrine sandstones trapping oil from organic rich claystones .The other major play is represented by synrift sediments and drift plays which include the early cretaceous Aeolian sandstone play, the Albian incised valley play, structural plays in younger shelf sediments and deeper water plays comprising roll-over anticlines in growth fault zones (Vander Spuy, 2002).

Detailed mapping of the numerous reservoir channels at Ibhubesi field, Orange Basin South Africa necessitated the building of a stratigraphic framework within the Albian section. This framework was derived from a sequence stratigraphic study of the Orange Basin by Brown et al which the area was referred as series of incised valley fill sequences (Brown et al., 1995).

1.4 LOCATION OF STUDY/ WELL LOCATIONS

The study area is located within Orange Basin, Offshore South Africa (Figure 1.3) below. Ten (10) exploration wells located within the O-M field is the focus of the work. The field (O-M) and well names used in this study are imaginary names of gas field and wells located in the Orange Basin South Africa. The wells are as follows:

- OP1
- OP2
- OP3
- OP4
- OP5
- OP6
- MA1
- MA2
- MA3
- MA4

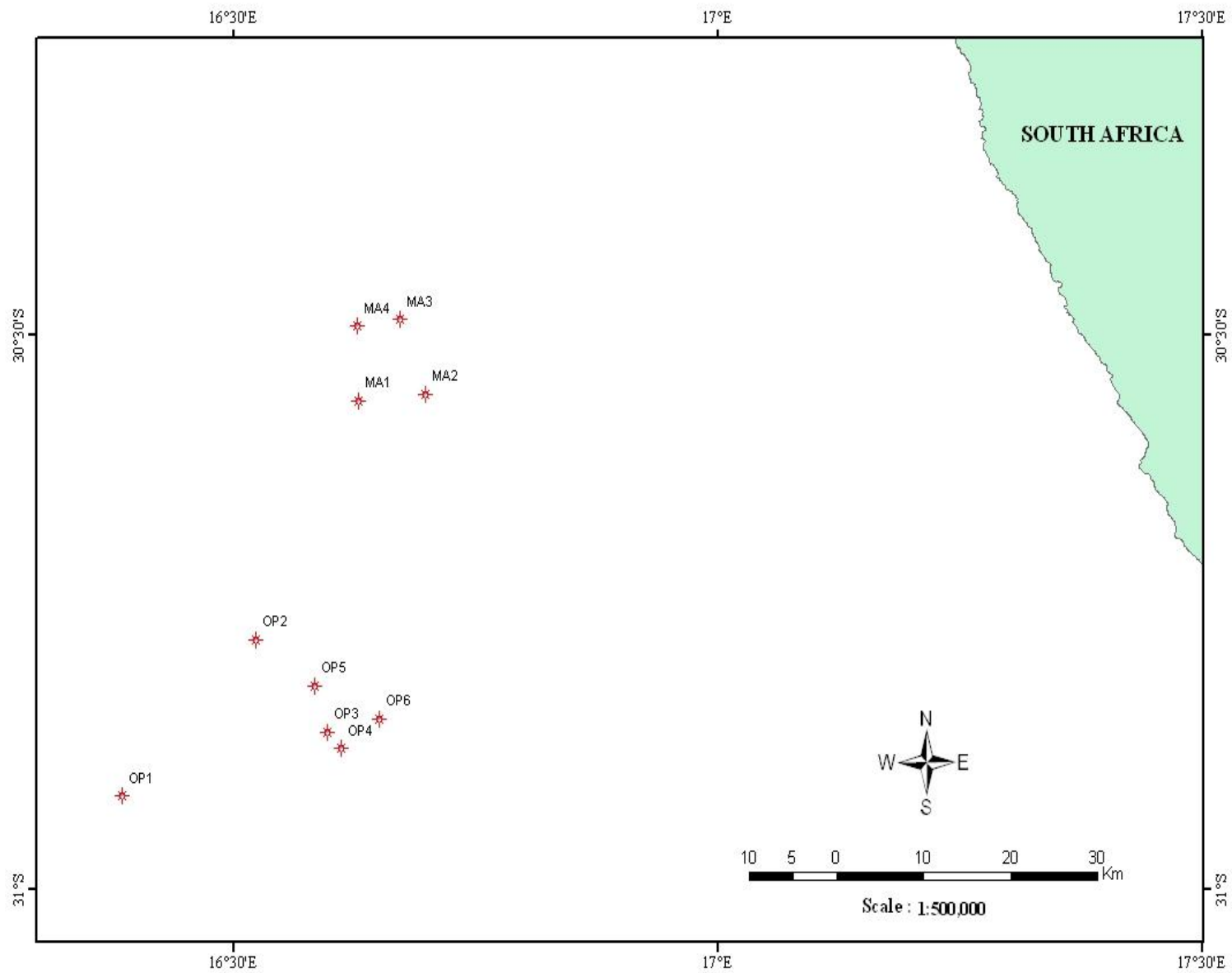


Figure 1.3: Well Location map

1.5 AIMS AND OBJECTIVES

The research is aimed at evaluating the reservoir potentials of O-M field, Offshore South Africa with limitation to the available data. This could be achieved through the integration and critically comparing results from core analysis, petrography studies for evaluating and correcting key petrophysical parameters obtained from wireline logs and generates an effective static reservoir model.

The specific objectives include the following:

- Editing and normalization of raw wireline log data.
- Classification of lithofacies, petrofacies and flow zone indicators
- Calibration of logs/ core data to obtain parameters for petrophysical log interpretations.
- Integrated studies of Sedimentology and petrophysics to determine the percentages of clay, type and distributions within the reservoir sections and its effect on water saturation.
- Determination of Porosities from logs
- Determination of true formation resistivity water and accurate estimate of bound and free water saturations.
- Determination of water/oil/gas contacts from water saturation calculations and Repeat Formation Tests (RFT)

1.6 RESEARCH METHODOLOGY

This process started with review of previous studies and utilizes the probabilistic Petrophysics log analysis approach for multi-mineral evaluation for a static reservoir model. This method takes all continuous log data and response equations to the proposed formation components and computes an answer. Core and production data are used to adjust this answer to produce a conceptual static petrophysical model.

Demonstrations will be carried out on integration of different subsurface data at relevant and appropriate scales in order to construct reliable static reservoir models.

The Table below present summary of data used for this study:

Table 1.1: Summary of data used for study

<i>Well Name</i>	<i>Conventional Logs</i>	<i>Conventional Core</i>	<i>Special Core Analysis</i>	<i>Petrography</i>	<i>RFT</i>	<i>DST</i>	<i>Completion Report</i>
<i>MA1</i>	X				X		X
<i>MA2</i>	X				X		X
<i>MA3</i>	X				X		X
<i>MA4</i>	X						X
<i>OP1</i>	X	X	X		X		X
<i>OP2</i>	X	X	X	X	X		
<i>OP3</i>	X	X	X	X	X	X	X
<i>OP4</i>	X				X		
<i>OP5</i>	X						
<i>OP6</i>	X				X		

A conventional suite of open-hole wireline logs were run by Schlumberger in all the wells. The main measurements acquired in all the wells at different Runs include:

- Gamma-Ray, Caliper, Spontaneous Potential
- Porosity Logs – Density, Neutron and sonic
- Resistivity Logs- Deep Induction, Spherically focused Laterolog, Micro-Spherically focused logs.

The collected data was first edited /reviewed and then loaded into the database for petrophysical modeling at different stages.

The flow charts (Figures 1.4, 1.5) below represent summary of workflow which starts from data collection and terminates at submission of report.

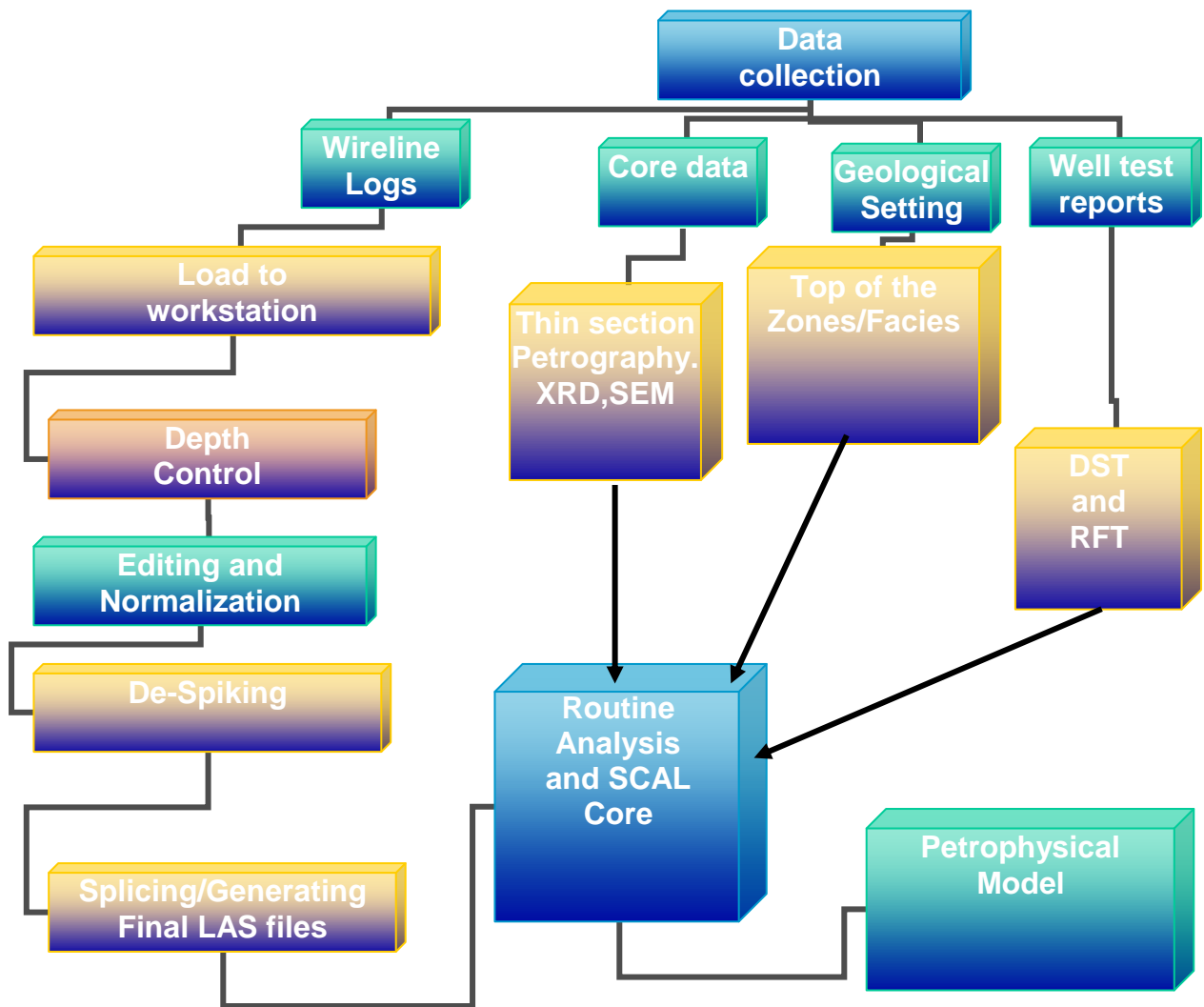


Figure 1.4: Section one of the flow chat of research methodology.

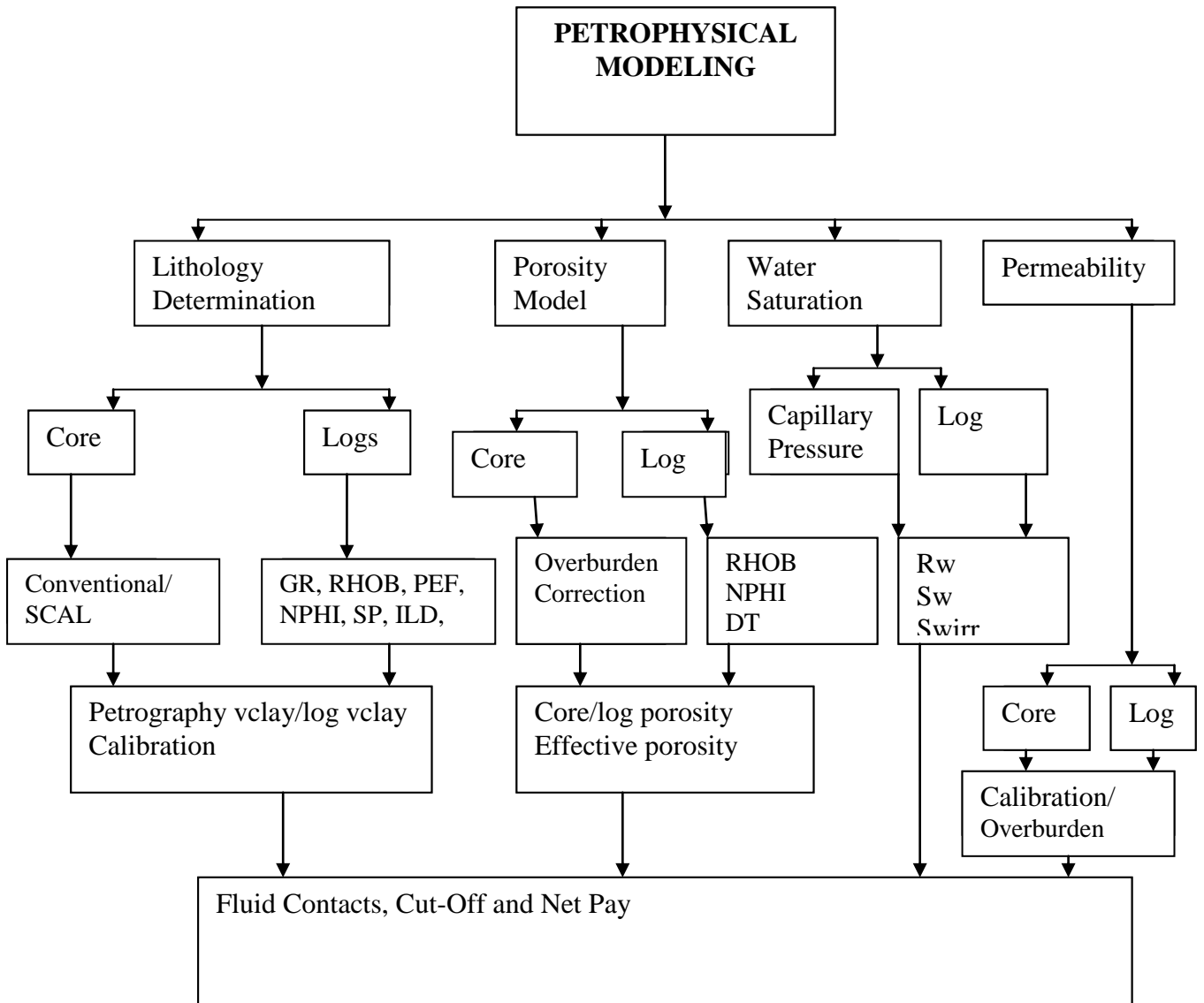


Figure 1.5: Section two of Research methodology flow chart.

CHAPTER TWO

WIRELINING LOGGING

2.1 INTRODUCTION

Wireline logging is a process that depends on lowering the logging cable into a drill well by loggers for the measurements of physical, chemical, electrical, or other properties of rock/fluid mixtures penetrated by drilling a well into the Earth's mantle. Well logging is usually carried out with instruments that are either suspended from a steel cable (wireline) or embedded in the drill string (logging while drilling, LWD). The wireline log is a graph and the data are continuous measurements of a log parameter against depth. When a log is made, it is said to be RUN. A log run is made at the end of a drilling phase and before casing is put in the hole and each of the run is numbered being counted from the first time that the particular log is recorded.

When logs are used for purposes other than evaluation of oil and gas, they are often called geophysical logs instead of well logs. The science is called borehole geophysics instead of petrophysics. The theory of well logging remains the same just the nomenclature and sometimes the emphasis (Rider, 1996).

The geophysical well logging was first developed for the petroleum Industry by Marcel and Conrad Schlumberger in 1927. The Schlumberger brothers developed a resistivity tool to detect differences in the porosity of the sandstones of the oilfield at Merkwiller- Pechelbronn in eastern France (Schlumberger, 1989).

The wireline logging can be grouped into two. They are the open-hole and cased- hole logging. The open-hole logging is based on measurements of the formations electrical, acoustic, and nuclear properties. Cased-hole logging includes measurements of nuclear, acoustic and magnetic properties. The open-hole logging will be the focus of this research. Some well logs are made of data collected at the surface; examples are the core log, mud sample logs, drilling time logs, etc.

Wireline logging is the established way of gathering about hydrocarbon bearing reservoirs over the length of the well and the objective is to obtain information on hydrocarbon. Physical properties such as resistivity, density, natural gamma radiation, and magnetic resonance are recorded as a function of depth. These physical properties are converted into petrophysical properties of the rock.

The wireline logging tools can be grouped into active and passive tools. The active tools measure the response of formation to some form of excitations. Examples include density, neutron, resistivity, and the nuclear magnetic resonance (NMR) tools. The passive tools measure natural occurring phenomenon such as the gamma radiation that is emitted by elements in the rock or electric potential caused by difference in salinity of the mud in the well and the formation water. Examples include gamma ray (GR) and Spontaneous Potential (SP) logs.

2.2 THE NUCLEAR LOGS

The Nuclear logs record radioactivity that may be either naturally emitted or induced by particle bombardment. Radioactive materials emit alpha, beta and gamma radiation. Only the gamma radiation has sufficient penetrating power to be used in well logging. Neutrons are used to excite atoms by bombardment in the well logging. They have high penetrating power and are only significantly absorbed by hydrogen atoms. The hydrogen atoms in the formation fluids are very effective in slowing neutrons and thus tend to be an important property in well logging.

The basic nuclear logs that will be discussed briefly are the following:

- Conventional Natural Gamma-Ray (GR)
- Spectral Gamma-Ray (SGR)
- Formation Density (RHOB)
- Photoelectric Effect (PEF)
- Compensated Neutron (CNL)
- Sidewall Neutron Porosity (SNP)

2.2.1 Conventional Natural Gamma-Ray Log (GR)

The natural radiation is due to the disintegration of nuclei in the subsurface. Potassium, Thorium and Uranium are the major decay series that contribute to natural radiation. These elements Potassium, Thorium and Uranium tend to be concentrated in shales, and are present in feldspars and micas that occur in many sandstone reservoirs.

The gamma-ray log is a log of this naturally occurring radiation. The units are American Petroleum Institute (API). Clean sands has fairly low levels of <45 API and shales has high gamma reading > 75 API. The measurements are used to calculate the

amount of shale as a function of depth and the vertical resolution of the tool is approximately 0.6m with a depth of investigation of 0.15 – 0.3m depending on the density of the rock. The gamma ray log is used for basic lithology analysis, quantitative estimation of clay content, correlation of formations, and the depth matching of multiple tool runs.

The simple gamma ray log is usually recorded in track one and scales chosen locally, but 0 – 100 and 0 – 150 API are common. A deflection of GR log to the right indicates shales, where the maximum and constant recorded radioactivity to the right shows shale line. A deflection to the left indicates sandstone, where the maximum and constant recorded radioactivity to the left shows sandstone line as indicated in Figure 2.1 below.

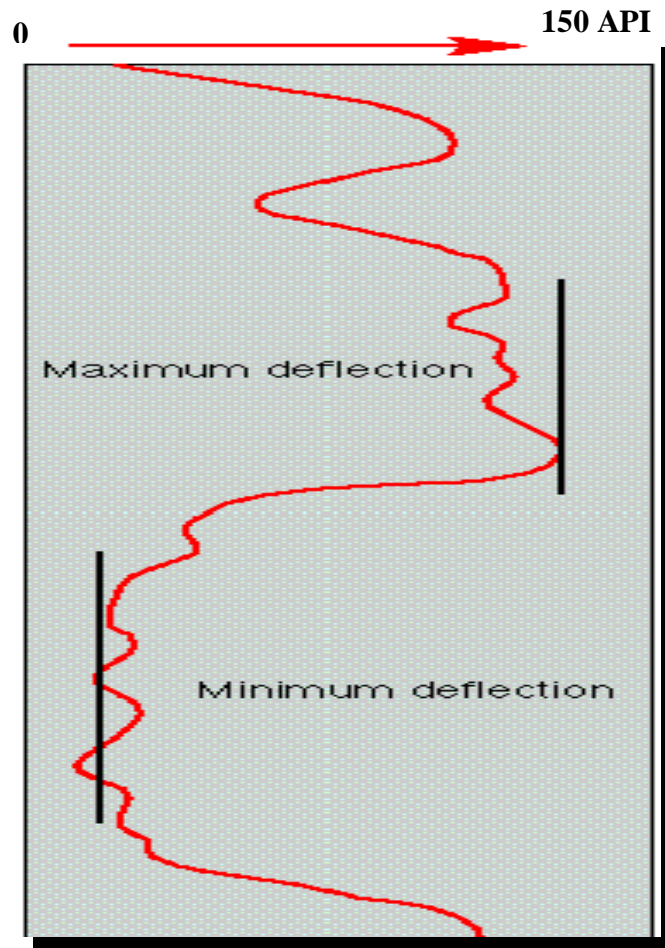


Figure 2.1: Diagram of GR log (Modified after Russel, 1944).

In the conventional gamma sonde, a scintillation counter detects total disintegration from sources in the radial region close to the hole. The scintillation detector uses a sodium iodide crystal coupled to a photomultiplier tube to detect tiny flashes of light associated with penetrations of the crystal by gamma rays.

2.2.2 Spectral Gamma Ray (SGR)

The spectral gamma ray log record individual responses for potassium, thorium and Uranium bearing minerals. The detectors record radiation in several energy windows as Gamma-Ray – Potassium, Gamma-Ray- Thorium, and Gamma-Ray-Uranium. In the three window tool, estimates of the concentrations of the three radioactive elements can be made as follows:

- Potassium: Gamma Ray Energy 1.46MeV (K40)
- Thorium Series: Gamma Ray Energy 2.62 MeV (Tl205)
- Uranium-Radium Series: Gamma Ray Energy 1.76 MeV (Bi214)

Spectral gamma sondes also provide a total GR counts from a fourth window that is equivalent to a conventional gamma log. The main applications of spectral gamma logs are:

- Clay Content Evaluation – Spectral logs will distinguish between clays and other radioactive minerals such as phosphate.
- Clay type identification – Ratios such as Th: K are used to distinguish particular clay minerals.
- Source Rock Potential – There is an empirical relationship between U: K ratios and organic carbon in shales.

2.2.3 Density Logs

Density logging employs incident gamma radiation which results in two important interactions with the electron cloud and its parent atoms which are the Compton scattering and photo-electric absorption. The density logging techniques are the Bulk electron density and the photo-electric density.

Compton scattering allows the measurement of bulk density based on electron concentration moderating the gamma flux. The Photo-electric response occurs at

lower energies where gamma rays are absorbed by atoms which then eject secondary gamma rays. The low energy portion of the spectrum is dominated by the PE effect. The source emits high energy gamma rays that pass through the formation until they are scattered (Compton scattering) and then eventually captured (Absorbed) having lost most of their energy. Two sodium iodide detectors are placed within the cloud capturing a portion of the scattered rays and counting them (Figure 2.2).

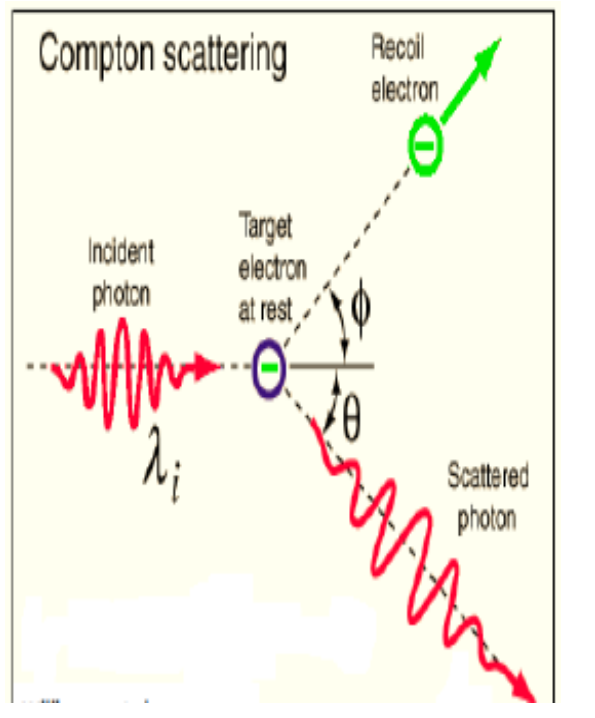


Figure 2.2: Compton scattering of gamma rays.

The count rate at each detector is proportional to the electron density of the rock and is proportional to the bulk density. The radioactive source most often used in density logging is the isotope Cs137. This is because it has energy of 662 KeV in the centre of the range of energies where the probability of Compton scattering is highest (Figure 2.3 below).

A density log is a measure of the number of low energy gamma rays surrounding the sonde which is due to elastic scattering and is proportional to the electron density of the rock. We actually measure electron density but what is needed is the bulk density of the rock, therefore the ratio of atomic number and weight are important.

The density tools use a gamma ray source and three gamma ray detectors. The number of gamma rays returning to the detector depends on the number of electrons present

and the electron density. The electron density (ρ_e) can be related to the bulk density (ρ_b) of the minerals by an equation below

$$\rho_e = \rho (2Z/A) \dots \dots \dots (2.1)$$

Where Z is the number of electrons per atom and A is the atomic weight.

The assumption made in the interpretation is that $Z/A = 0.5$ which is very close for most elements commonly encountered, except hydrogen which has little effect on the measurement. Therefore, $\rho_e = \rho$. The tool measured density has been experimentally related to the electron density as:

$$\rho_b = 1.0704\rho_e - 0.1883 \dots \dots \dots (2.2)$$

The tool has a shallow depth of investigation and the fluid is assumed to be mud filtrate with a density of 1.0 g/cm^3 for fresh water and 1.1 g/cm^3 for salt water.

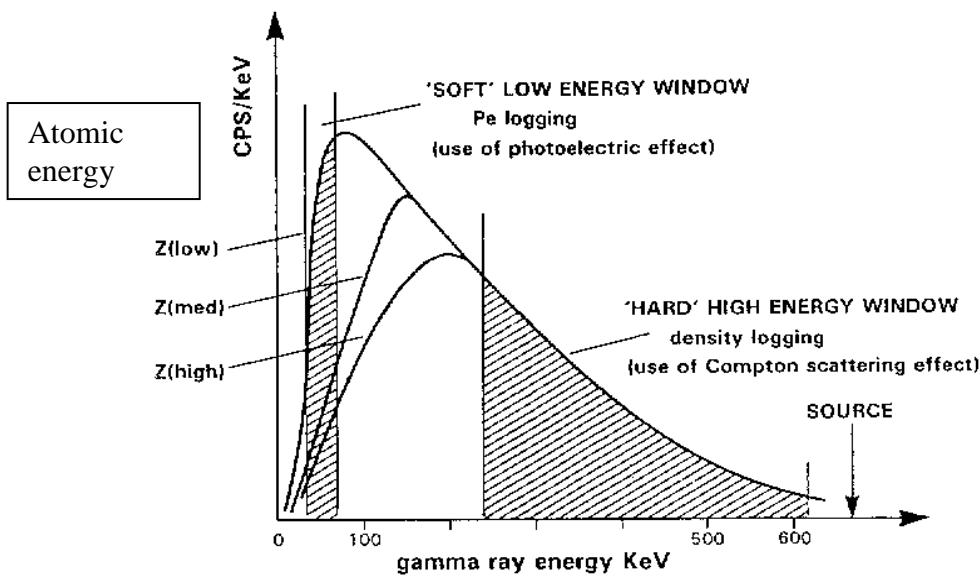


Figure 2.3: Density and litho density (photoelectric) logging in relation of gamma ray energy. (Modified after Ellis & Singer 1987).

2.2.3.1 Formation Bulk Density Log (RHOB)

The density log is a continuous record of formation bulk density. This is the over all density of a rock including solid matrix and the fluid enclosed in the pores. The unit of bulk density measurement is gram per centimetre cubed (g/cm³).

The density log is normally plotted on a linear scale of bulk density and run in tracks two and three most often with a scale between 2.0 and 3.0 g/cm³ (Rider, 1996). Table 2.1 present density parameters.

Table 2.1: Depth of investigation of density tool and typical readings

Density Parameters

Standard	18 inches
Depth of investigation	6 inches Vertical resolution 6' to 9 inches
Limestone (0%)	2.71
Sandstone (0%)	2.65
Dolomite (0%)	2.87 Reading in Zéro porosity
Anhydrite	2.98
Salt	2.03
Shale	2.2-2.7
Coal	1.5+ Typical Readings

The density tool is extremely useful as it has high accuracy and exhibits small borehole effects. The major uses are in the determination of porosity as given below :

- Determination of porosity-

$$\phi = \frac{\rho_{ma} - \rho_b}{\rho_{ma} - \rho_f} \dots\dots\dots(2.3)$$

Where:

Φ = Porosity

ρ_{ma} =matrix density

ρ_b =density from log

ρ_f =Fluid density of the mud filtrate

The other uses of the density log are:

- Lithology identification in combination with Neutron tool
- Gas indication in combination with Neutron tool
- Formation acoustic impedance in combination with Sonic tool
- Shaliness of formation in combination with Neutron log

2.2.3.2 Photo-electric Effect density Log (PEF)

The photo-electric effect log is influenced more by atomic number than by electron density. The photo-electric effect only occurs at low energy; generally below 100KeV (Figure 2.3).It measures the absorption of low energy gamma rays by the formation and is calibrated into units of barns per electron.

The logged value is a function of the aggregate atomic number of all the elements in the formation and so is a sensitive indicator of mineralogy. The log is less sensitive to porosity and caving effects since hydrogen has a very low atomic number. The Photoelectric response depends on the atomic number of the elements in the formation and varies according to the chemical composition. The photoelectric effect log provides a direct indication of lithology. The Table below present the photoelectric absorption factors (Pe) for common sedimentary minerals.

Table 2.2: Photo-electric absorption factor for common minerals

Mineral	Pe
Quartz	1.81
Kaolinite	1.83
Montmorillonite	2.04
Dolomite	3.14
Illite	3.45
Halite	4.65
Anhydrite	5.05
Calcite	5.08
Chlorite	6.30

2.2.4 Neutron Logs

The Neutron log was introduced commercially by Well Surveys Incorporated two years after the gamma ray log. Gus Archie working for Shell used the neutron porosity log in his equation of 1942.

In Neutron logging, fast neutrons are emitted by a chemical source (Americium-Beryllium) in the sonde and travel through the formation where they are slowed mainly by collision with hydrogen atom. Slow neutrons are captured by the atoms with the emission of a gamma ray at various energies and velocities as indicated in Figure 2.4 below:

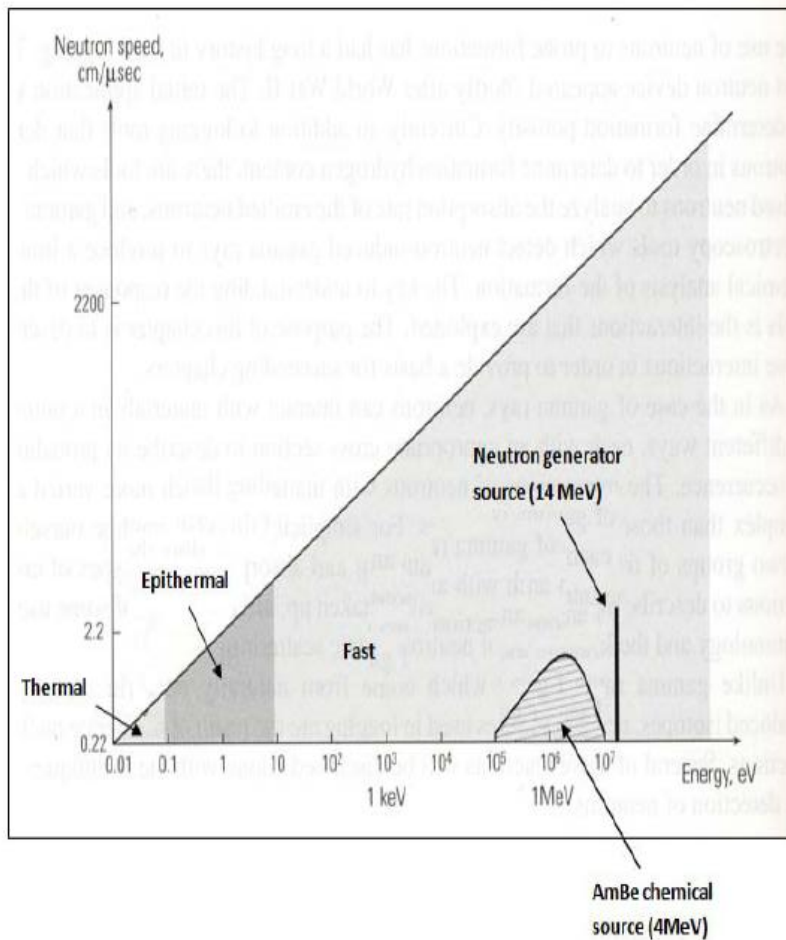


Figure 2.4: Neutron speed versus source (MeV; Ellis & Singer, 1987).

Various logs detect the following:

- Capture gamma Rays
- Slow (thermal) Neutrons
- Partly slowed (epithermal) neutrons

There are two interactions that generally affect counts at the neutron sonde's detector. The presence of hydrogen in the formation which is thermalisation and the presence of chlorine or iron which is early absorption. The log reacts to the presence of hydrogen, and so water in the formation. This in turn indicates the formation porosity, both primary and secondary and the system can be calibrated to estimate the percentage of pore space in the clean sandstone, limestone or dolomite.

2.2.4.1 Compensated Neutron Log (CNL)

The compensated Neutron log (CNL) tool has two detector spacings and is sensitive to slow neutrons. The tool detects thermal neutrons. The logs can be run in open and cased holes.

2.2.4.2 Sidewall Neutron Porosity Log (SNP)

The sidewall neutron porosity tools is a single detector pad tool that detect partly slowed epithermal neutrons. All neutron tools can be run in cased holes to determine formation porosity. Corrections must be made for the presence of casing and cement (Krygowski, 2003).

Principal uses of the Neutron logs are listed below:

- Porosity display directly on the log
- Lithology determination in combination with Density and Sonic logs
- Gas indication in combination with Density log
- Clay content estimation with gamma Ray log
- Correlation in open or cased holes

2.3 ACOUSTIC (SONIC) LOG

The traditional sonic logging involves just the compressional wave measurement done in the sonde in real time and converted to velocity for lithology, seismic and geotechnical applications. The sonic log provides a formation's acoustic interval travel time, designated Δt . The travel time or slowness of a sonic primary (P) or compressional wave through rocks varies due to rock type, compaction. The P-wave is a refracted wave that passes through the rock mass. It is a fast wave and the first arrival at our receivers so it is easy to discriminate.

The sonic tools create an acoustic signal and measure how long it takes to pass through a rock by simply measuring this time we can get an indication of the formation properties. The amplitude of the signal will also give information about the formation. The tool uses a pair of transmitters and four receivers to compensate for

caves and sonde tilt. The normal spacing between the transmitters and receivers is about 3 to 5 inches. The diagram (Figure 2.5) below presents the configuration.

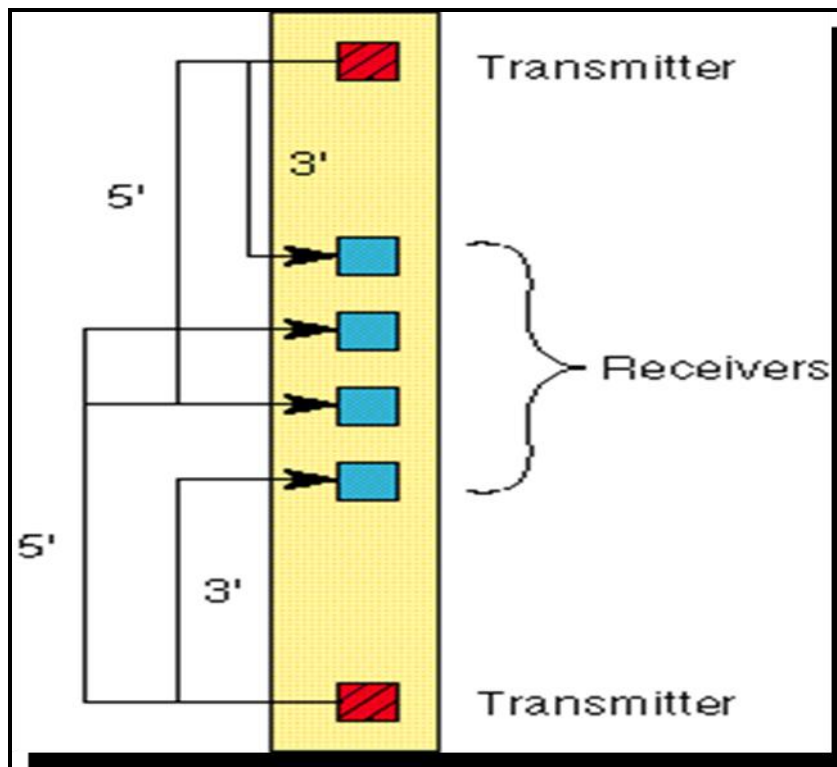


Figure 2.5: The positions of transmitters and receivers in sonic tool.

The figure above presents a simple tool that uses a pair of transmitters and four receivers to compensate for caves and sonde tilt. The normal spacing is between 3 to 5 inches. The configuration produces a compressional slowness by measuring the first arrival transit times. The sonde is centralised and run at about 6 metres per minutes in water while transmitting at 10 times per seconds at 20 kHz. Each arrival at a receiver generates a voltage whose first arrival within a prescribed time gate is discriminated. Noise and cycle skips result in spikes on the log but a de-spiker in the sonde removes most of these spikes.

The sonic log in sedimentary rocks is considered a porosity log and can generate a sonic based sandstone or limestone porosity log to compare with those created from neutron and density logs. No calibration is necessary because it relies on a fixed, perfectly spaced geometry. The sonic log will display raw transmit times in micro-

seconds per foot. The most common interval transit times fall between 40 and 140 ms.

The sonic log is presented in tracks 2 and 3. The major uses are listed below:

- Correlation.
- Porosity.
- Lithology.
- Seismic tie in time-to-depth conversion.

The porosity from the sonic slowness is different from the density and Neutron tools. It reacts to primary porosity only and as such does not see fractures or vugs. The basic equation for sonic porosity is the Wyllie Time Average given below:

$$\phi = \frac{\Delta t_{\log} - \Delta t_{ma}}{\Delta t_f - \Delta t_{ma}} \dots\dots\dots(2.4)$$

Where:

Φ = Sonic Porosity

Δt_{\log} = Formation of interest sonic log reading

Δt_{\max} = Matrix travel time

Δt_f = Mud Fluid travel time

There is another way of transforming slowness to porosity called “Raymer Gardner Hunt”. This formula tries to take into account some irregularities observed in the field.

The simplified Version of Ramer –Gardner Hunt is given in equation 5 below:

$$\phi = C \frac{\Delta t_{\log} - \Delta t_{ma}}{\Delta t_{\log}} \dots\dots\dots(5)$$

Where C is a compaction constant usually taken as 0.67.

Table 2.3 presents the sonic porosity readings of some common sedimentary rocks.

Table 2.3: Typical sonic matrix travel times of some rocks

Mineral	Matrix Travel time (Δt_{max})ms
Sandstone	51 - 55
Limestone	47.6 -53
Dolomite	38.5 -45
Anhydrite	50
Salt	67 - 90
Shale	62.5 - 167

(Rider, 1996).

2.4 ELECTRICAL LOGS

The electrical logs measure electrical properties of the formation in different frequency ranges. This includes the Spontaneous Potential (SP) and the Resistivity Logs.

2.4.1 Spontaneous Potential (SP)

The self Potential originated from the electric currents flowing in the mud of a borehole caused by electromotive forces in formations. The Self Potential (SP) log is a measurement of a very small electrical voltages resulting from electrical currents in the borehole caused by the differences between in the salinities of the formation water and the drilling mud filtrate. The voltage changes are measured by a downhole electrode relative to the ground surface. They are naturally occurring potentials within the earth.

The SP currents are measured in millivolts (mV) and the scale positive or negative millivolts. The potential read for shales normally varies very little with depth. The SP is measured relative to this base line zero called the shale base line.

Negative deflections to the left of the shale base line occurs opposite sands and reach a maximum in clean porous sands called the static self potential(SSP) as shown in Figure 2.6 .

The SP is positive if the mud filtrate is saltier than the formation water and negative if the formation water is more saline than the mud filtrate.

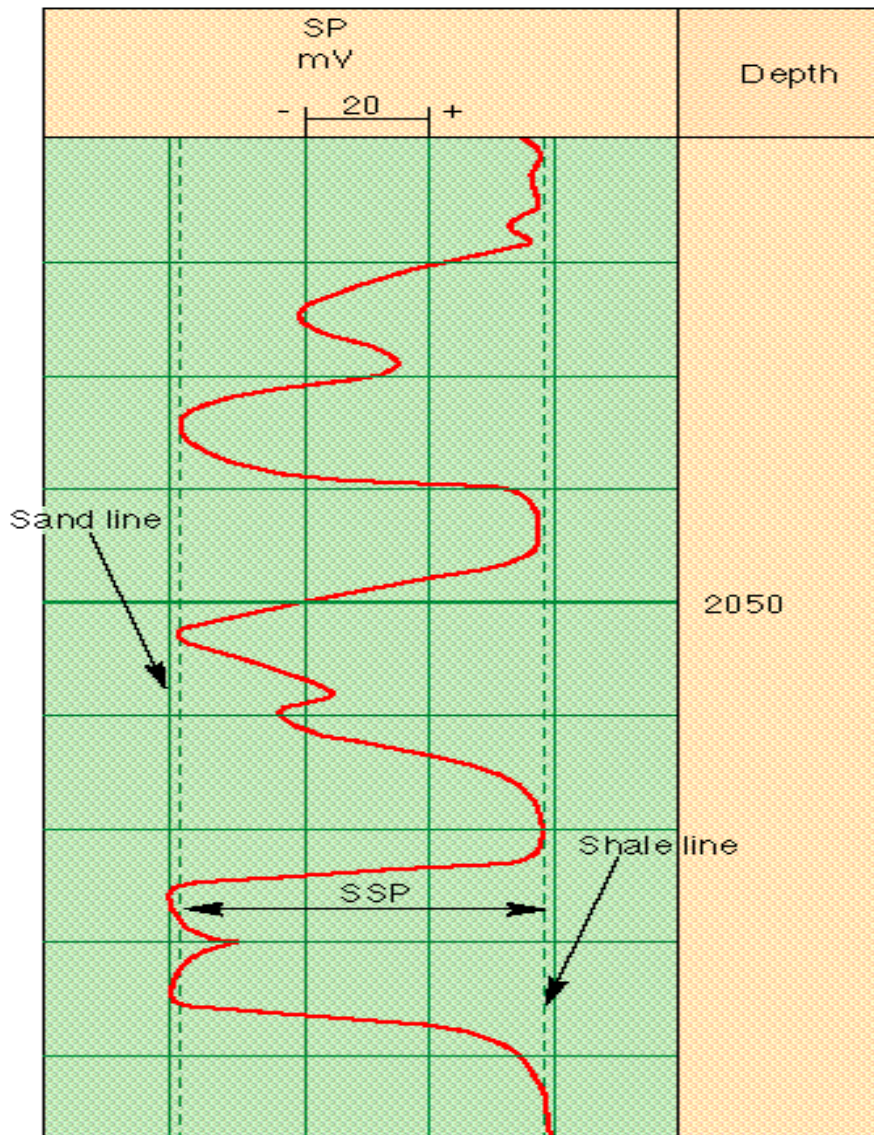


Figure 2.6: Graphics of self potential curve showing static self potential (ssp) and shale line.

The SP log is used to determine the resistivity of water by applying the following equation:

- Determination of resistivity of water (R_w)

$$SSP = -k \log \frac{R_{mfe}}{R_{we}} \dots (2.6)$$

Where:

K = Constant that depend on formation temperature

R_{mf} = Resistivity of mud filtrate at reservoir temperature

R_{we} = Equivalent resistivity of water

SSP= Static SP value.

The other uses of the SP log are the following:

- Differentiate potentially porous and permeable reservoir rocks impermeable clays
- Define Bed Boundaries.
- Give an indication of shaliness

2.4.2 Resistivity Logs

The Resistivity log is a measurement of the formation resistivity with direct current using the principles of Ohm's law. The resistivity of a substance is a measure of its ability to impede the flow of electric current. The basic measuring system has two current electrodes and two voltage electrodes. Resistivity is the key to hydrocarbon saturation determination and the measuring unit is ohm-meters and they are plotted on a logarithm scales in track 2 or 3.

The Resistivity logs can be grouped into three measurements; Induction logs, Laterologs, and Microresistivity measurements.

2.4.2.1 Induction Logs

The Induction logs measure the resistivity of the undisturbed part of the formation laterally distant from the borehole. An induction tool uses a high frequency electromagnetic transmitter to induce a current in a ground loop of formation. This in turn induces an electric field whose magnitude is proportional to the formation conductivity. Induction logs measure conductivity rather than resistivity.

The Induction tool is designed for an 8.5 inches hole and can be run successfully in much larger hole sizes in which logging is usually performed with a 1.5 inch stand off from the borehole wall. The tools work best in low resistivity formations and in Wells drilled with high resistivity muds. Tool resolution is in the order of 6 feet. Depth of investigation is 4 – 6 feet for the Medium Induction log (ILm) and about 10 feet for the Deep Induction log (ILd).

- The Typical applications of the Induction Logs are:

- Measure the true(undisturbed) formation resistivity (Rt)
- Ideal in Fresh or Oil -based environments
- Ideal for Low resistivity measurements
- Fluid saturation determination

2.4.2.2 Laterologs

The laterolog tools use focusing or bucking currents into a planar disc shape and monitor the potential drop between an electrode on the tool and a distant electrode. The potential drop changes as the current and the formation resistivity changes and therefore the resistivity can be determined. Table 2.4 below present laterolog curves display generic names commonly used.

Table 2.4: Curve names and mnemonics of laterolog

<i>Curve Name</i>	<i>Mnemonics</i>
Deep Laterolog Resistivity	DLL,LLD,RLLD
Shallow laterolog resistivity	SLL,LLS,RLLS

(Krygowski, 2003)

The resolution of the tool is about 3-5 feet and depth of investigation of about 3 feet for the LLs and 9-12 feet for the LLd.

Laterolog applications include the following:

- Measures True(Undisturbed) formation resistivity Rt
- Useful in medium to high resistivity environments
- Overpressure detection
- Fluid saturation determination
- Diameter of invasion determination

Limitations of the Laterologs are:

- Affected by the Groningen effects in some environments
- Cannot be used in oil-based muds
- Cannot be used in air-filled holes

2.4.2.3 Microresistivity Log

The microresistivity logs are pad mounted tools with shallow depth of investigation and of higher resolution. Tools are focused to pass through the mud cake. The tool uses a set of five electrodes which focus the signal into the invaded zone just before the mud cake.

The shallow reading versions of this resistivity tool are always pad-mounted. First was the Micro-log which is still in use, second was the Micro-Laterolog (MLL), replaced by Proximity (PI) tool and thirdly the Micro-Spherically Focused Log (MSFL) which has another version as Micro-Cylindrical Focused Log (MCFL). The tools are variously affected by factors like mud cake thickness of the invaded zone.

Table 2.5 below shows common names used for the microresistivity logs.

Table 2.5: Common curve names of microresistivity logs

<i>Curve Name</i>	<i>Mnemonics</i>
Micro normal resistivity	MNOR
Micro inverse resistivity	MINV
Micro Spherically Focused resistivity	MSFL
Micro Laterolog	MLL

(Krygowski, 2003).

Microresistivity log applications are:

- Determination of flushed zone formation resistivity R_{xo}
- Flushed zone water saturation (S_{xo}) through Archie's Equation
- Invasion corrections deep resistivity tools
- Thin bed definition

Limitations of the tools are:

- Rugose hole
- Oil-Based mud
- Heavy or thick mud cake

2.5 AUXILIARY LOGS

These are logs that are required to assist in the quantitative interpretation of many other logs that are sensitive to borehole diameter, wall roughness, hole deviation, and fluid temperature. This includes; the calliper, temperature, and dipmeter logs.

2.5.1 Caliper Log

The calliper logs are the first runs in borehole to measure the diameter of the hole or casing for corrections to other logs and measurements. The measurement of the borehole diameter is done using two or four flexible arms, symmetrically placed on each side of a logging tool.

The calliper shows where deviations occur from the nominal drill bit diameter. The simple calliper log records the mechanical response of formations to drilling. Holes with larger diameter than the bit size is caved or washed out. The curve is traditionally a dashed line and usually plotted in track one with a scale of 6 to 16 inches. The log also provides information on fracture identification, lithologic changes, well construction and serve as input for environmental corrections for other measurements. It can be run in any borehole conditions.

2.5.2 Temperature Log

The temperature tools measures the temperature of borehole fluids. Temperature logging is used to detect changes in thermal conductivity of the rocks along the borehole or to detect water flow through cracks or fractures.

The temperature log is normally plotted so that changes in the temperature gradient (change in temperature to depth) might be related to lithological boundaries or aquifers. Ideally the logging sonde is run twice; once immediately after drill rods are withdrawn and after 24 hours in order to describe the temperature gradient.

The unit of measurement is normally in Degree Fahrenheit (^oF). The logs are to be run in fluid-filled boreholes and are also used for temperature corrections to other logs and measurements.

2.5.3 Dipmeter Log

The dipmeter was the first structural logging tool (originally an SP dipmeter). The log provides a continuous record of formation dip and direction of dip or azimuth. The dipmeter measurements of borehole tilt and azimuth are based on magnetic and gyroscopic sensors in the sonde. All recorded data are corrected to true dip and strike and log is usually presented in a tadpole or arrow plot form with respect to true north as presented in Figure 2.7.

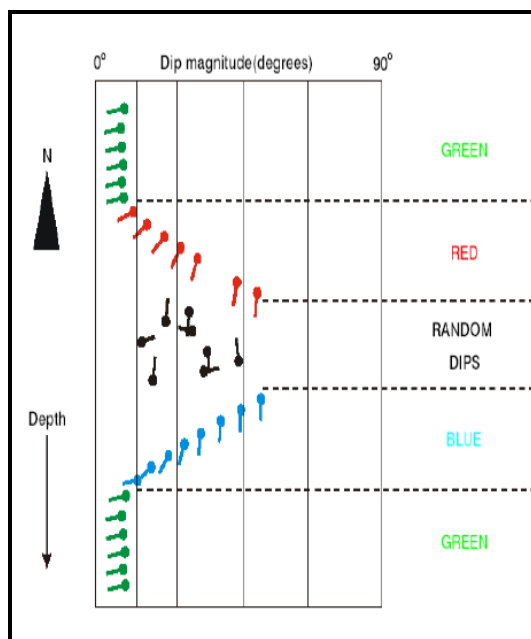


Figure 2.7: Example of presentation of dip log

The log describes a correlation solution as tadpole with a prescribed frequency. Tool rotation, magnetic field and gamma ray logs are included for quality control of the log. Quality is dependent on low rotation frequency and calibration of the tool.

The dip angle is the angle formed between a normal to a bedding plane and vertical. A horizontal bed has a dip angle of 0° and a vertical bed has a dip of 90° .

The dip azimuth is the angle formed between the geographic north and the direction of greatest slope on the bedding plane. Dip azimuth is conventionally measured clockwise from north so that a plane dipping to east has a dip azimuth of 90° .

A group of dips of more or less constant low dip magnitude and more or less constant azimuth is coloured green (Figure 2.7). Group of dips of more or less constant azimuth

showing an increase in dip magnitude with depth is coloured red, and that showing decrease in dip magnitude with depth is coloured blue (Bateman, 1985). Depositional features like sand bars and channels might be identified from the dipmeter plot.

2.6 OVERVIEW OF NEW GENERATION LOGGING TOOLS

The new generation of logging tools technology are developed to capture complete map of the borehole wall in terms of diameter, deviation, light and colour. They have higher resolutions. They can be divided into two categories:

Qualitative and quantitative devices.

The Qualitative devices include the following:

❖ Dipmeter:

- Stratigraphical high Resolution Dipmeter tool (SHDT)
- Oil Base Dipmeter tool (OBDT)

❖ Image Logs:

- Formation Micro-scanner (FMS) tool
- Full-bore Formation Micro-image (FMI) tool
- Borehole imaging in oil-base mud (OBMI)
- Borehole televiewer (BHTV)
- Azimuth Resistivity Imager (ARI)
- Array Induction Tool (AIT)

❖ Quantitative Devices:

- Nuclear Magnetic Resonance (NMR)
- Combinable Magnetic Resonance (CMR)
- Pulsed Neutron Capture Log (PNC)

CHAPTER THREE

DESCRIPTION OF PETROPHYSICAL PROPERTIES

3.1 INTRODUCTION

Petrophysics is regarded as the study of rock and fluid systems. Petrophysical measurements are made on cores in the laboratories and boreholes to determine the major reservoir properties which include porosity, permeability, fluid saturations and capillary pressure. The petrophysical parameters obtained from cores are used to calibrate borehole measurements and for volume calculations. The petrophysical parameters will be reviewed.

3.2 POROSITY

The porosity of a rock is the fraction of the total rock volume that can be filled with gas, oil, water or a mixture of these fluids. The porosity developed in sedimentary rocks is a function of the grain size distribution, grain shape, orientation and sorting. When all the grains are of the same size, sorting is regarded as good and if grains of diverse sizes are mixed together, sorting is regarded as poor.

The ratio of a volume of void spaces within a rock to the total bulk volume of that rock is expressed as a percentage denoted as Φ . This is expressed mathematically as

$$\Phi = \frac{\text{Pore Volume}}{\text{Pore volume} + \text{Grain Volume}} * 100$$

An example of pore space and grain space is given the Figure 3.1.

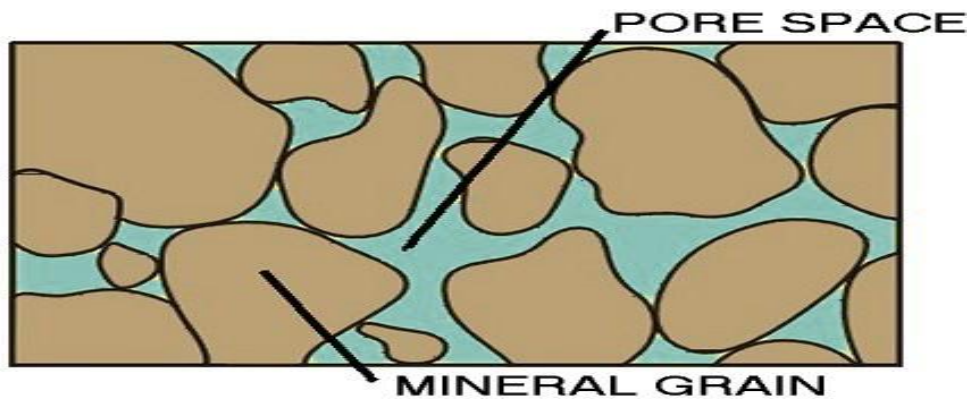


Figure 3.1: Example of pore space and mineral grain space.

There are many descriptions of porosity but the two common are the total and effective porosities. The total porosity Φ_T is defined as the ratio of total pore volume within a rock to the total bulk volume including voids. The effective porosity Φ_e is defined as the ratio of the interconnected pore space to the total bulk volume. The Figure 3.2 below presents an example of effective, non-effective or isolated, and total porosity of a rock.

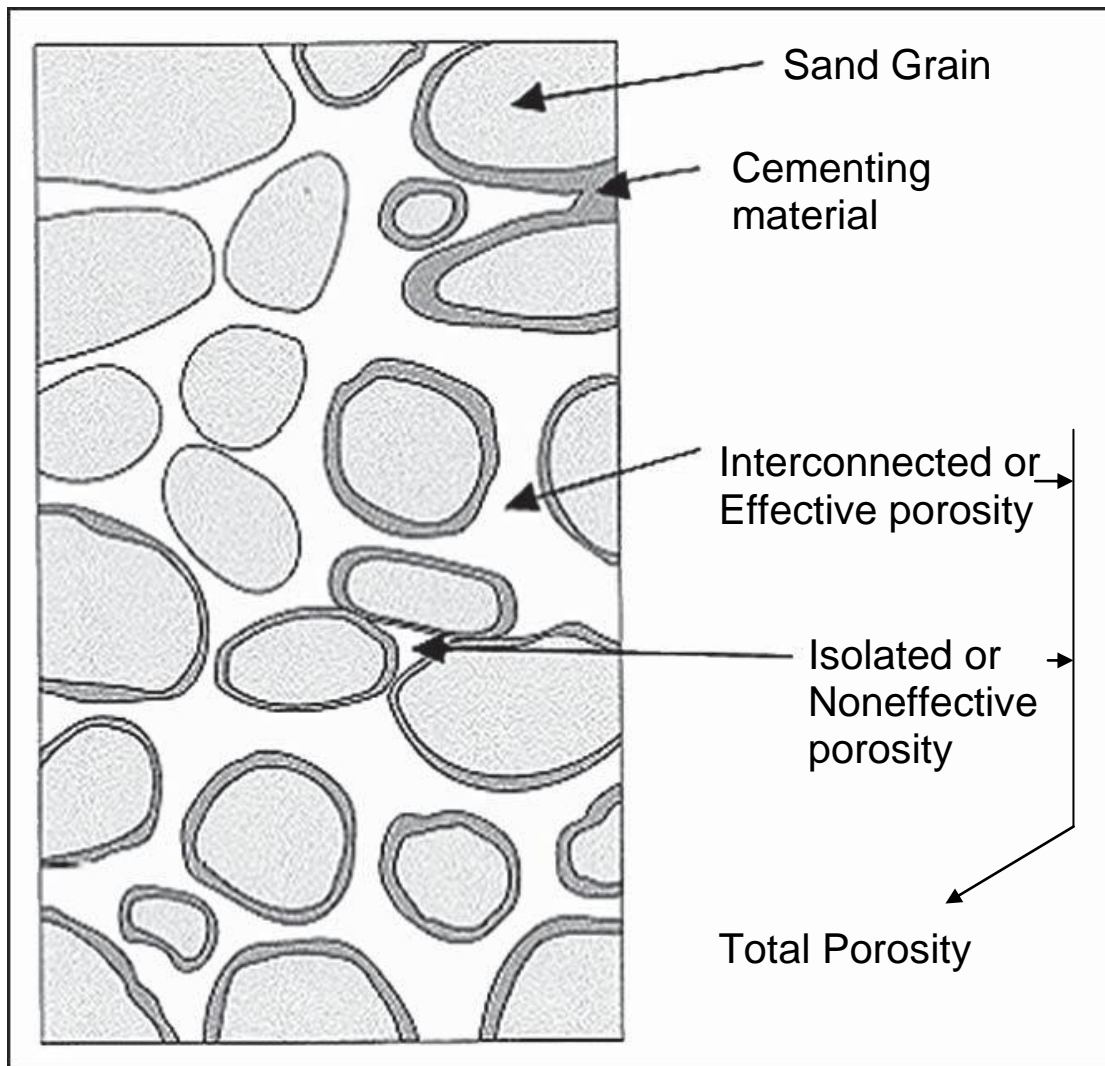


Figure 3.2: Example of effective and total porosity.

The amount of porosity is mainly caused by the arrangement (cubic or rhombohedral), size and sorting of rock. The cubic arrangement of grains has a maximum porosity of about 48% and rhombohedral packing of maximum porosity of about 26% (Figure 3.3).

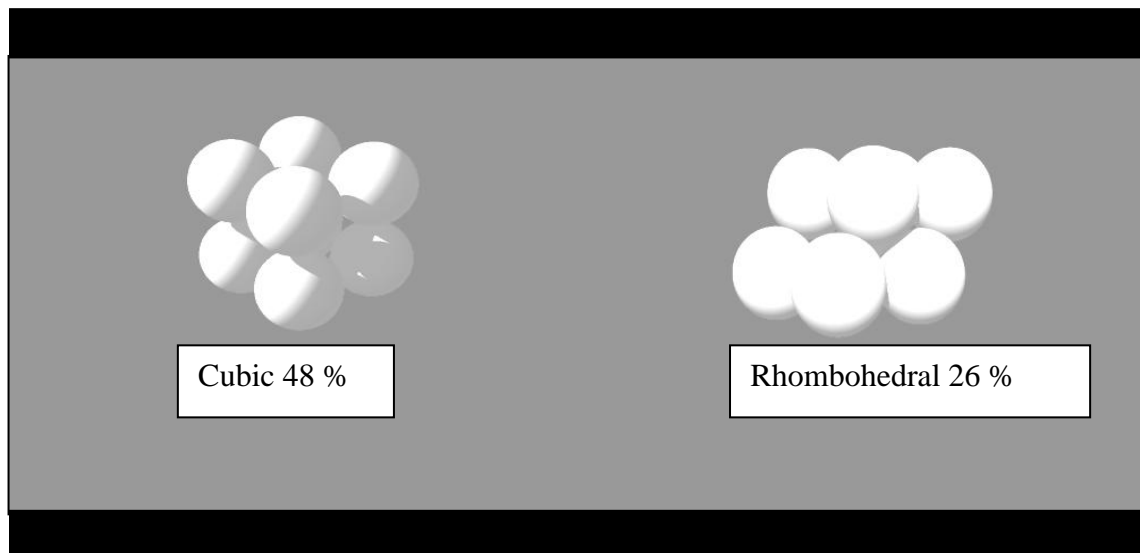


Figure 3.3: Packings of spheres of primary or intergranular porosity (Fraser & Graton, 1935).

In sedimentological terms, a wide grain size distribution is called poorly sorted; a narrow distribution is considered well sorted. Well sorted systems approach the ideal rhombohedral packing which gives porosity higher than poorly sorted grains. Porosity can be measured indirectly by the wireline logs and directly by core analysis methods.

3.2.1 Porosity Alteration

When sediment has been deposited it has an initial porosity known as the primary porosity. Over geological times the primary porosity is altered by the following factors:

- ❖ Diagenesis – The physio-chemical precipitation of minerals from the pore fluids. Cementation is the most important diagenetic effect because it binds the grains together and thereby reduces the porosity.
- ❖ Compaction – Compaction is caused by the load of the overlying sediments. Compaction leads to a more compact arrangement of the grains. It is a mechanical phenomenon and dependent on the rock types, the pore fluid type and weight of the overburden.

- ❖ Leaching – Leaching occurs when minerals dissolve in the pore fluids. This type of porosity is referred to as secondary porosity because it is produced after deposition of the sediments.
- ❖ Bioturbation – The mixing of deposited sediments caused by bioactivity of small organisms such as worm that move through the sediments and leave a trace of fine particles behind.
- ❖ Clay coating – This involves crystals that grow on the surface of the grains over geological times and can even completely fill pores (Schutjens, 1991).

3.3 PERMEABILITY

The permeability is the measure of the ease at which fluid flows through connecting pore spaces of reservoir rock. The fluid flow is proportional to the gradient of pressure. Permeability is controlled by size of pore openings, degree and size of pore connectivity, type of cementing material between rock grains.

The concept of permeability originates from the laboratory flow tests carried out by Henri Darcy in 1856. The following equation is an expression of Darcy's equation to determine permeability.

$$K = Q \mu / A (\Delta P/L) \dots\dots\dots (3.1)$$

Where:

- K = Permeability (darcy)
- Q = Flow per unit time (cm/s)
- μ = Viscosity of flowing medium (cp)
- A = Cross section of rock (cm²)
- L = Length of rock (cm)
- ΔP = Change in pressure (psi)

The unit of measurement of permeability is in Darcies, more commonly in millidarcies (md). A reservoir productive capacity is largely determined by its permeability. Permeability is measured horizontally and vertically (Figure 3.4). The

horizontally measured permeability is accepted as the rock permeability because it is measured parallel to the bedding which is the major contributor to fluid flow into a typical reservoir. Vertical permeability (K_v) is usually less than horizontal permeability (K_h) because of layering effects of sedimentation (Hughes, 2002).

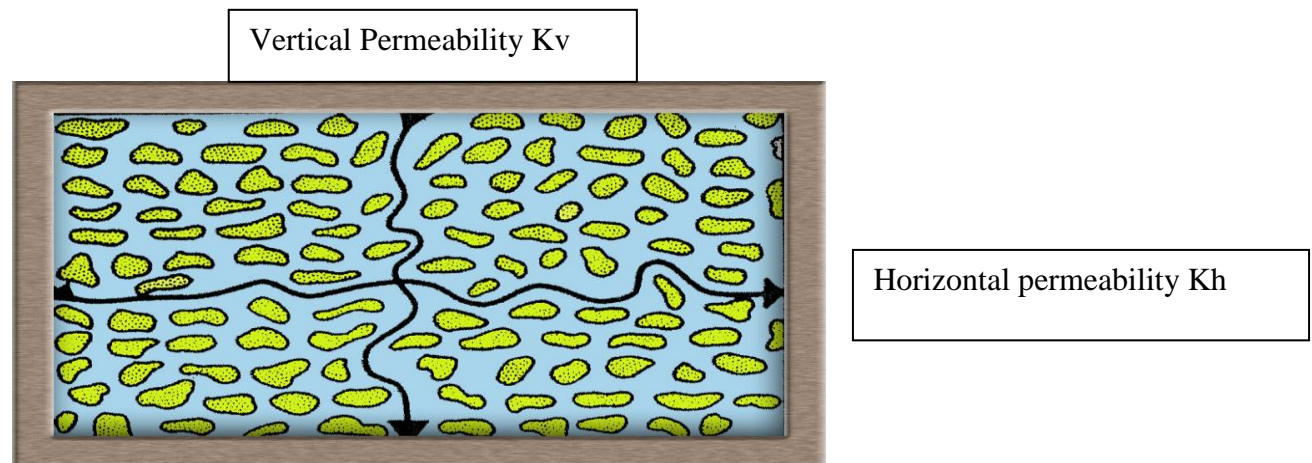


Figure 3.4: Directions of measurement of permeability.

Three types of permeability are employed in Petroleum applications; absolute, effective and relative. Permeability is absolute when the reservoir rock is completely saturated with the flowing fluid. Permeability is effective to a particular fluid when that fluid occupies less than 100 % of the pore space. An example is a gas or oil permeability in a rock which contains connate water. Relative permeability is the ratio of the effective to absolute permeability.

The permeability which could describe fluid flow in reservoirs is effective or relative permeability. The values of permeability can be determined from Core analysis, well tests, and drill stem test analysis. Permeability measured from core data is the most accurate and values can be classified fair is permeability is between 1 to 10md; Good from 10 to 100md; very good from 100 to 1000md. The Figure below present rock permeability ranges (Garven, 1986).

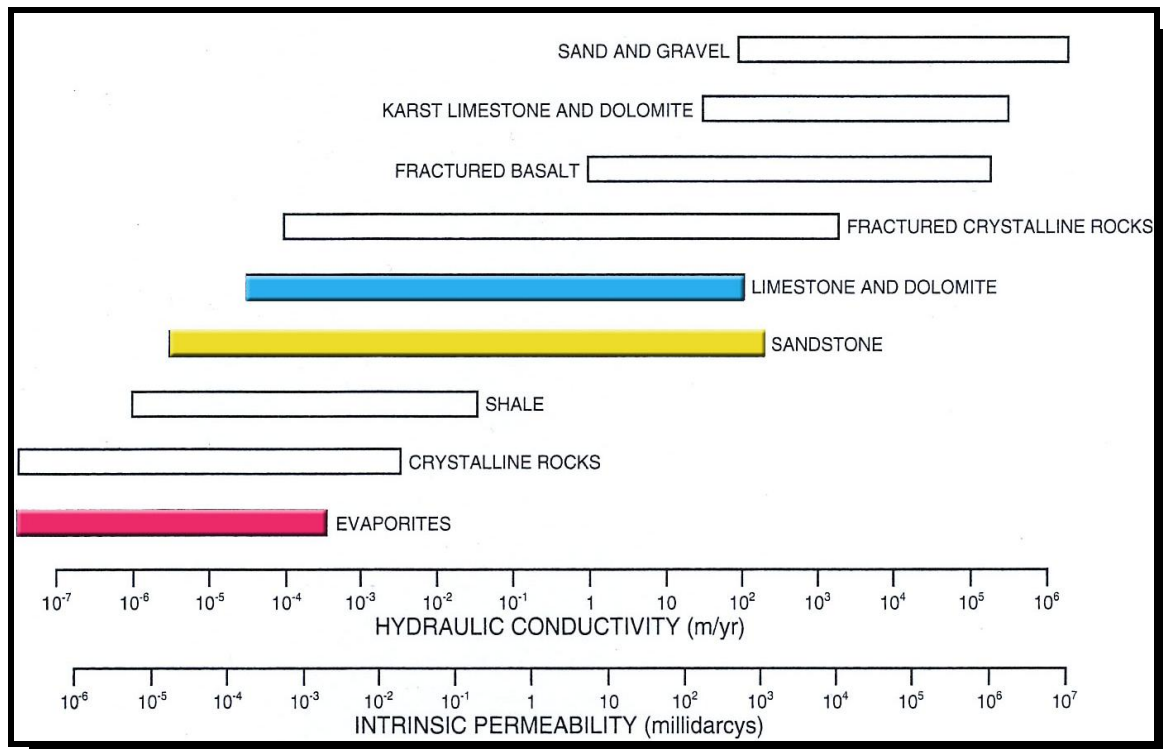


Figure 3.5: Rock permeability ranges (Garvin, 1986).

3.4 FLUID SATURATION

The fluid saturation is the fraction or percentage occupied by a certain fluid. This could be expressed mathematically as the volume of fluid divided by the volume of pores in which the fluid resides. That is,

$$\text{Fluid saturation } (S_f) = \frac{\text{Formation fluid occupying pores}}{\text{Total pore space in Rock}}$$

The total saturation of fluid in rock is 100%. Reservoir rocks often contains two (oil and water, gas and water) and three (gas, oil and water) fluids. Water in a formation usually contains dissolved salts that facilitate ionic conductivity but the hydrocarbon in the formation is non conductive fluids. A relationship between electric conductivity and saturation can be established. Investigation of the electrical properties of wet and oil bearing rocks was pioneered by Archie in 1942.

3.4.1 Electrical Formation Water

The method Archie used to arrive at the conclusion of his investigation on resistivity and saturation was simple. He took a number of cores of different porosity and saturated each one with a variety of brines. He measured the resistivity of the water R_w and the resistivity of the 100% water saturated rock R_o . When the results were plotted, he found a series of straight lines of slope F referred to as the electrical formation factor (Bateman, 1985).

The rock formation factor is the resistivity of a rock sample completely saturated with water to the resistivity of the water. Mathematically; it can be expressed as follows:

$$F = \frac{R_o}{R_w} \dots\dots\dots (3.2)$$

Where:

R_o = Resistivity of 100 % saturated rock (Ohm-m)

R_w = Resistivity of water (Ohm-m)

Archie found out that measured value of F could be related to the porosity of the rock by an equation of the form

$$F = \frac{1}{\Phi^m}$$

Where:

Φ = Porosity

m =cementation exponent

Another empirical equation relating F and Φ was also suggested by the results of experiment measurements conducted by Winsauer et al (Bassouni, 1994). The equation is of the form

$$F = \frac{a}{\Phi^m} \dots\dots\dots (3.3)$$

Where:

a=tortuosity factor

m=cementation exponent

Some commonly used formation factor to porosity relations are as follows:

$$F = 0.81 / \Phi^2 \text{ in most sandstones (consolidated)}$$

$$F = 0.62 / \Phi^{2.15} \text{ unconsolidated sandstones (Humble formula)}$$

$$F = 1.45 / \Phi^{1.54} \text{ (Phillips Equation)}$$

$$F = 1.13 / \Phi^{1.73} \text{ (Chevron Formula)}$$

$$F = 1.97 / \Phi^{1.29} \text{ (Porter and Carothers)}$$

$$F = 1 / \Phi^2 \text{ (Carbonates)}$$

The reasons for the observed variations in the cementation factor (m) in the above relations has been attributed to number of factors which includes; degree of cementation, shape, sorting and packing of the particular system, compaction due to overburden pressure, type of pore system etc (Helander, 1984).

Fresh water yields low formation factor and cementation values. Cementation factors for various rock types are presented in Table 3.1 below.

Table 3.1: Cementation of various rock types

Lithology	Cementation Factor (m)
<i>Sandstones</i>	
Loose un -cemented sands	1.3
Slightly cemented sands	1.3 – 1.7
Moderately cemented sands	1.7 - 1.9
Well cemented sands	1.9 – 2.2
<i>Limestones</i>	
Moderately porous limestones	2
Some oolitic limestones	2.8

(Piron, 1958)

3.4.2 Water Saturation (Sw)

Archie experiment showed that water saturation could be related to its resistivity. He defined the resistivity index I_R as the ratio of the resistivity of a partially water saturated rock R_t to the resistivity of the fully brine saturated rock R_o .

$$I_R = \frac{R_t}{R_o} \dots\dots\dots (3.4a)$$

If the rock sample was originally fully saturated with water, then R_t will equal R_o and I_R will equal one. The presence of hydrocarbon is indicated by the value of the resistivity index. Saturation can be expressed as a ratio of the resistivities:

$$S_w^n = \frac{R_o}{R_t} \dots\dots\dots (3.4b)$$

Where n is the saturation exponent an empirical constant and taken as two in most case. Substituting for R_o in equation 3.4a and F in equation 3.4b above, the expression the water saturation becomes

$$S_w^n = \frac{a}{\phi^m} \frac{R_w}{R_t}$$

The Archie's equation links the porosity and resistivity with the amount of water present S_w in the formation. Increasing porosity will reduce the water saturation for the same R_t . Once the water saturation is known; the hydrocarbon saturation can be calculated.

$$S_{HC} = 1 - S_w$$

Where:

S_{HC} = Hydrocarbon saturation.

S_w = Water Saturation.

The Archie's model considers the electrolytes in the pores as the only conductive path, hence the relationship is valid for only clean sand formations. Shaly sand formations exhibit more complex behaviour because clay minerals present in the formation contribute an additional parallel conductive path in addition to the formation salinity.

3.4.3 Influence of Clay on rock resistivity

The presence of clay in a rock will influence the resistivity of the rock depending on the type and distribution of the clay. The presence of cation exchangeable clays often cause apparent low resistivity index values to be observed which also causes a decrease in water saturation calculations. The conductivity of the clay is related to the cation exchange capacity (CEC). The higher the CEC, the lower the formation factor at any salinity.

Active sites exist on clay surfaces where cations may be exchanged with drilling mud fluid. This ion exchange may alter formation porosity, reduce permeability, formation resistivity and also result in erroneous high calculation of water saturations from downhole logs. Waxman-Smit-Thomas and other researchers proposed equations that allow calculations of a formation factor independent of the clay conductivity effects (Core laboratories, 1982).

3.5 CAPILLARY PRESSURE

Capillary pressure reflects the interaction of rock and fluids and is controlled by the pore geometry, interfacial tension and wettability. Hydrocarbon reservoirs can be regarded as a capillary system where in the absence of other forces, the distribution of the fluids is determined by the interaction of gravity, interfacial tension and wettability.

The wettability is defined as the contact angle between droplets of liquid on a horizontal surface. It is a measure of which fluid adheres to the rock. The wettability describes the affinity between a liquid and a solid. The fluid/fluid interaction dominated by intermolecular van der Waal forces is regarded as the interfacial tension. The gravity plays a role in both wettability and interfacial tension situations.

In order to understand the distribution of fluids in a reservoir and the position of oil/gas and oil/water, knowledge of wettability and interfacial tension is essential.

In situations when the adhesive affinity between water and the rock matrix is larger than the force between oil and rock, the reservoir is considered water wet. In oil wet rocks, the affinity between oil and the rock matrix is larger than the affinity between water and rock. Most sandstone reservoirs are assumed to be water wet. The pores are assumed to be initially filled with water that was forced out by the oil because it floats on water.

The capillary pressure concept is an important parameter in volumetric studies where it is used to calculate saturation- height relationships from core and log informations. It is also used to infer the free water level (FWL) from oil transition zone saturation-height relation when pressure gradient data for both oil and water legs may not be available. The saturation-height function is able to predict the saturation anywhere in the reservoir for a given height above the free water level and for a given reservoir permeability or porosity or to estimate permeability once water saturation is known (Harrison & Jing, 2001).

3.5.1 Capillary Pressure curves

The wettability of a rock for a fluid can be expressed by the contact angle σ . When contact angles are smaller than 90° between the water surface and the solid, the solid is considered water wet. For contact angles more than 90° between the same substance and the rock are considered oil wet (Figure 3.6).

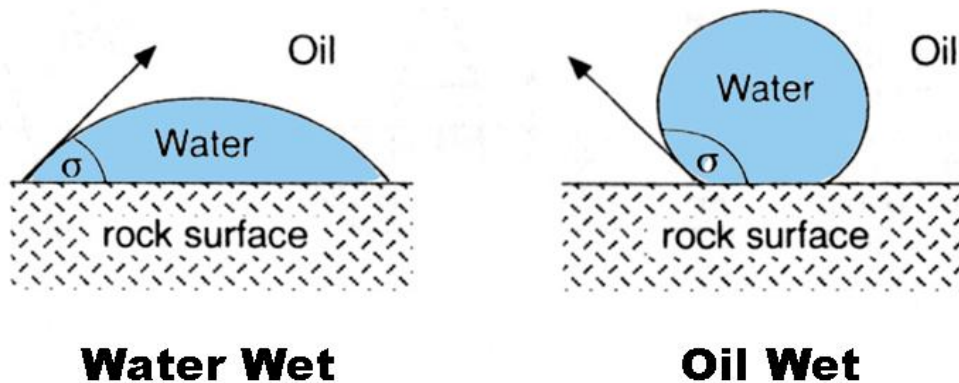


Figure 3.6: Contact angles for water-wet and oil-wet surfaces.

In capillary pressure measurements, a non wetting fluid invades the pore system that was originally occupied by a wetting fluid whereby the latter is displaced by the former. The capillary pressure of a non wetting fluid invading into the pores is described by Laplace's equation (Dullien, 1979) as follows:

$$P_c = \frac{2\gamma}{R_{\text{pore}}} = \frac{2\gamma \cos\sigma}{R_{\text{pore}}} \dots\dots\dots (3.5)$$

Where:

P_c = Capillary pressure

γ = interfacial tension

R = Average radius of pores

σ = contact angle

The Laplace equation (3.5) describes the relationship between the radius of the pore and the pressure that is required for the fluid to enter the pore. The laboratory values of capillary pressure can be converted to equivalent reservoir condition values as follows:

$$P_{c(\text{res})} = P_{c(\text{lab})} \frac{(\gamma \cos\sigma)_{\text{res}}}{(\gamma \cos\sigma)_{\text{lab}}} \dots\dots\dots (3.6)$$

Typical values for interfacial tension and contact angles taken from core laboratory manual are given in Table 3.2. The laboratory to reservoir condition conversion considers the difference in capillary pressure due to interfacial tension and contact angle. The interfacial angle can be measured at laboratory and reservoir conditions but the contact angle is difficult to measure especially for systems that are not strongly wet.

Table 3.2: Interfacial tension and contact angle values

<i>Wetting Phase</i>	<i>Non-Wetting Phase</i>	<i>Conditions: Temperature(T) Pressure(P)</i>	<i>Contact Angle(σ)</i>	<i>Interfacial Tension (dynes/cm)</i>
Brine	Oil	Reservoir,T,P	30	30
Brine	Oil	Laboratory,T,P	30	48
Brine	Gas	Laboratory,T,P	0	72
Brine	Gas	Reservoir,T,P	0	50
Oil	Gas	Reservoir,T,P	0	4
Gas	Mercury	Laboratory,T,P	140	480

(Core Laboratories, 1982)

Reservoir water saturation decreases with increasing height above the free water level where capillary pressure is zero. A minimum water saturation (S_{wirr}) is reached at a great height above the free water level and this water saturation is immobile. The transition zone is defined as the zone which can produce both hydrocarbon and water. Changes in the capillary pressure radius are controlled by the pore geometry which is a function of rock properties such as permeability and porosity. The pore size distribution also has a great influence on the magnitude of the irreducible water saturation (S_{wirr}) and height of the transition zone. The hydrocarbon water contact will vary with depth as a function of the reservoir quality. The higher the permeability, the smaller the separation between oil water contact and free water level (Harrison & Jing, 2001).

3.5.2 Capillary pressure and seal

The seal is a rock which prevents natural buoyancy related upward migration of hydrocarbon. Hunt (1990) extended the definition to any rock which is capable of preventing all pore fluid movement over a substantial period. A seal is controlled by the largest flaw in the sealing rock generally near the crest. The weakness of the seal can be due to diagenesis and tectonic force. For a hydrocarbon to be trap, the upward buoyancy must be smaller than the downward capillary pressure.

Figure 3.7 below pressure versus depth and capillary pressure plot for typical reservoir showing the petroleum and water gradients, position of free water level, thickness of hydrocarbon interval and the position of seal.

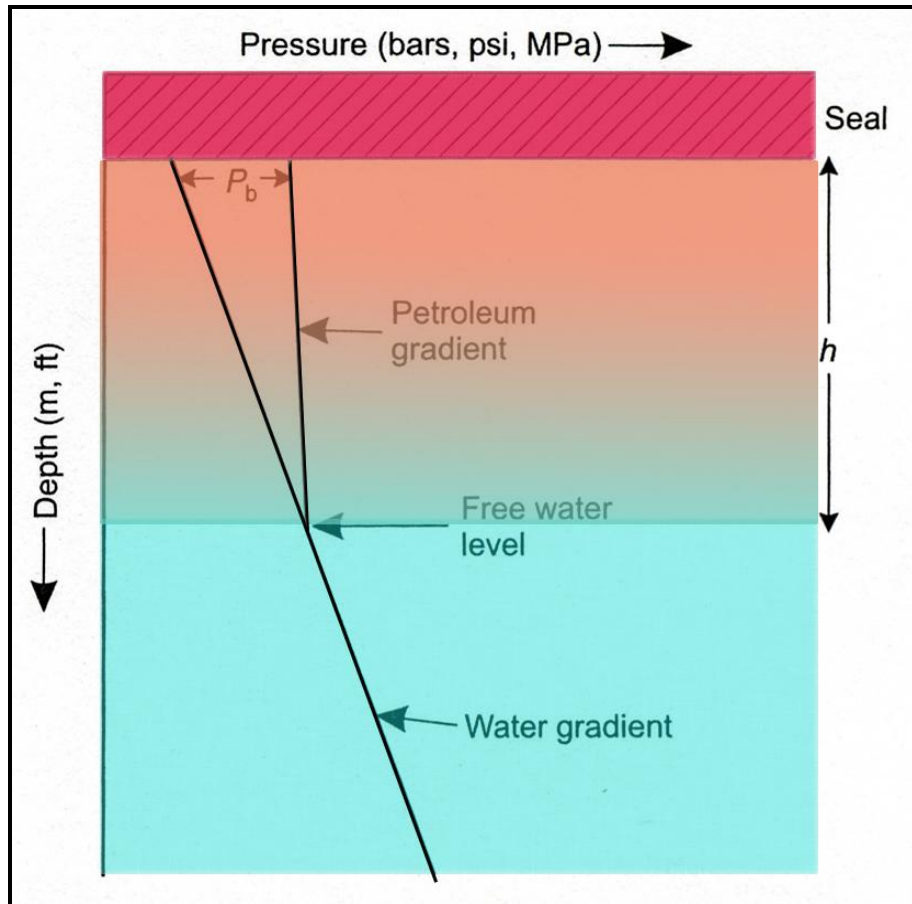


Figure 3.7: Pressure versus depth plot.

The pressure gradients for oil and water phases are determined by the fluid densities. The water saturation distribution above or below the free water level are controlled by the balance of capillary and buoyancy forces. The relationship can be expressed as follows:

$$P_c = h (\text{water gradient} - \text{oil gradient}) \dots \dots \dots (3.7)$$

3.5.3 Saturation-Height Equations

The correlation of capillary pressure curves according to rock type for a formations and generating field saturation – height function that relates capillary pressure curves to porosity, permeability or rock types have various equations. The methods include the Leverett’s J-function approach, Cuddy et al (1993), Johnson (1987), Skelt-Harrison (1996), and others.

3.5.3.1 Leverett’s J Function Approach

In 1941, Leverett investigated the effect of fluids interfacial tension and a rock property on capillary pressure. Leverett was the first to introduce a dimensionless capillary pressure correlation function. Based on experiments, he proposed the following dimensionless group as a function of wetting fluid saturation (S_w) for capillary pressure (P_c) modelling as

$$J(S_w) = \frac{P_c \sqrt{K/\Phi}}{\sigma \cos \theta} \dots \dots \dots (3.8)$$

Where:

P_c = Capillary pressure (psi)

K = Permeability (mD)

Φ = Porosity

The $\cos \theta$ term was added to adjust for wettability. The $(\sqrt{K/\Phi})$ is proportional to size of typical pore throat radius and J-function is dimensionless for a particular rock type. Special core analysis measurements of capillary pressure on core samples provide the most reliable means to establish J –function for rock types with similar geometries. Capillary pressure measurements are performed on each core plugs and then converted to reservoir conditions and finally converted to J values for each samples and plotted against saturation. This function which is sometimes termed universal J-function did not produce a single correlation for different types of formations (Leverett, 1941).

The J-function is useful for averaging capillary pressure data from a given rock type of a reservoir and sometimes can be extended to different reservoirs having the same lithologies though usually not accurate correlating different lithologies.

3.5.3.2 Johnson Capillary method

Johnson (1987) proposed another way of correlating capillary pressure data water saturation to permeability. Using special core analysis data, Johnson observed that the plots of water saturation versus permeability for each capillary pressure de-saturation step were approximate straight and parallel lines when drawn on log/log axes. His permeability averaging method gives an empirical function that relates capillary pressure to water saturation and permeability as follows:

$$\text{Log}(S_w) = B \cdot P_c^{-c} - A \cdot \log(K) \dots\dots\dots(3.9)$$

Where:

A, B, and C = Constant

S_w = Water saturation (percent)

K = Permeability (mD)

P_c = Capillary Pressure (psi)

The constants A, B and C are derived from special core analysis measurements capillary pressure data using series of cross plots. Johnson states that his method is not universal but it has proved effective in some North Sea reservoirs (Johnson, 1987).

3.5.3.3 Skelt-Harrison Capillary Pressure and log Based Method

Skelt recommends the fitting of a curve to a set of height and saturation data. It was initially to the capillary pressure data from special core analysis measurements and then refines this to fit the log derived water saturation data. Each data point was assigned a different weight during the regression (Skelt & Harrison, 1995).

The strength of the Skelt's function is that rather than linearise the function using logarithms, it makes use of its non-linearity to provide a fitted curve shape that actually looks like a capillary pressure curve. The equation is of the form:

$$S_w = 1 - A \exp. [-(B / h + D)^c] \dots\dots\dots(3.10)$$

Where:

A, B, C and D = Coefficients found by regression to core and log data. h=Height above free water level

CHAPTER FOUR

WIRELINE LOG EDITING AND NORMALIZATION

4.1 INTRODUCTION

The aim of wireline logging is to measure and record a given formation's properties in its undisturbed state and convert it to petrophysical parameter. The objective is rarely achieved because the drilled hole where the logging operation is performed is not perfect and the logging environment also is often affected by drilling mud type, mud salinity, that need to be removed in order to get the actual response of the logs.

When raw log data are collected for formation evaluations it is essential to check the quality of the data and perform editing if necessary before performing quantitative interpretation. Log editing is basically a form of log interpretation aimed at removing or correcting problems that affect logs and provides the best possible presentation of the in-situ properties measured and recorded by logs. Some of the problems encountered by logs that need to be edited before using it for quantitative interpretations are the following:

- ❖ Depth Shifting/Matching
- ❖ Borehole environmental corrections
- ❖ Smoothing/De-spiking/Noise Removal
- ❖ Merging/splicing of curves

After performing the editing process, the next stage is curves normalization. Normalization is a mathematical process that adjusts for differences among data from varying sources in order to create a common basis for comparison.

The flow chart starting from data collection through the editing processes to quantitative analysis is given in Figure 4.1 below. However, this chapter starts with the process of wireline log data collection and end on log normalization of the ten wells within the study area.

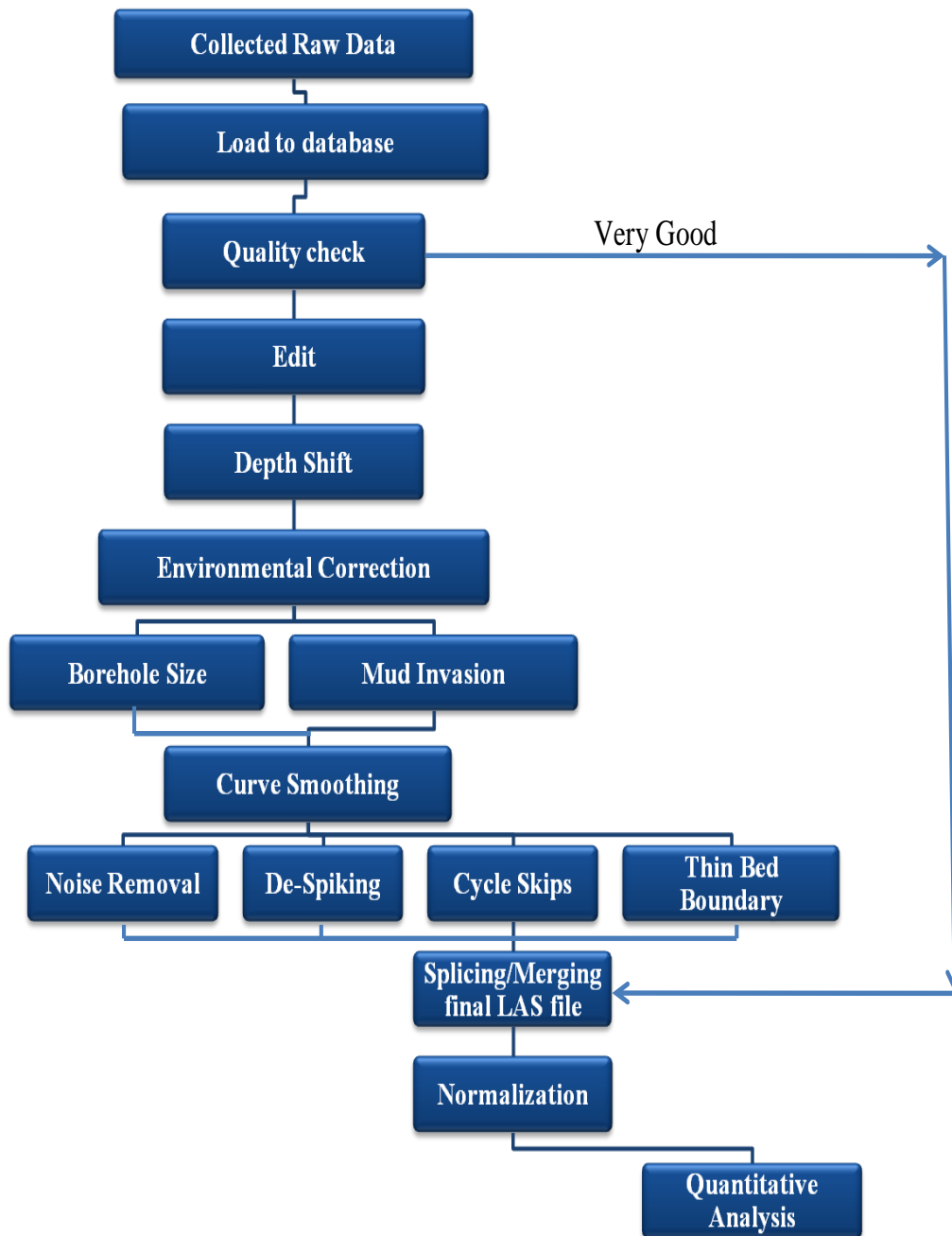


Figure 4.1: Flow chart of Log editing.

4.2 LOG DATA COLLECTION AND CREATION OF DATABASE

A conventional suite of open –hole wireline log data were run by Schlumberger in all the vertical exploration wells drilled between 1987 and 2003 and logged by Schlumberger wireline Company. Water based mud (WBM) were used to drill wells MA1 ,MA2, MA3, MA4, OP1, and OP3, while oil based mud (OBM) were used to drill wells (OP2, OP4, OP5 and OP6).

All the wells were logged with basic log data suites and the data were provided by Petroleum agency of South Africa (PASA) and PetroSA in Log ASCII format (LAS), comprising measurements of:

- Gamma- Ray, Caliper, Spontaneous Potential
- Porosity – Density, Neutron, and Sonic
- Resistivity Logs
 - Water Based Mud wells – Dual laterolog, MSFL.
 - Oil Based mud wells – Dual Induction

Digital data were provided in LAS format files at different Runs across the wells. The logs were loaded into Interactive Petrophysics software created database. The log header information and well completion report provides information on the interval of wireline log for wells as given in the next subsection below. The logging suite tool code name and description are shown in appendix A.

4.2.1 Wireline logged Intervals for Wells

The objectives of the well drilling project were to drill, log and test the primary target intervals in order to prove a commercially viable gas reserve. Schlumberger Company provided the wireline data with overall log quality very good. A suite of wireline logs were available and successful Runs were conducted with well problems limited to minor tight hole conditions at various intervals but were remedied by washing and reaming during wiper trips. The static bottom hole temperature was estimated using the Dowdle and Cobb method.

The Table 4.1 presents the suite of wireline logs available and successful Runs conducted at different intervals as indicated in the Table 4.1 below.

Table 4.1: Suite of Logs Run in wells at various intervals

<i>Well</i>	<i>Run Number</i>	<i>Hole size (in)</i>	<i>Interval (m)</i>	<i>Logging Suite</i>
MA1	1	12 1/4	1118 - 240.6	HALS/ DSI/ TLD/ MCFL/ PEX.
	2	8 1/2	3309.4 - 1107	HALS/DSI/TLD/MCFL/PEX
MA2	1	12 1/4	1114 - 280.4	HALS/DSI/TLD/MCFL
	2	8 1/2	3171 - 1117	HALS/DSI/TLD/MCFL
MA3	1	12 1/4	1118 - 240.6	HALS/ DSI/ TLD/ MCFL/ PEX.
	2	8 1/2	3309.4- 1107	HALS/DSI/TLD/MCFL/PEX
MA4	1	12 1/4	1134.9 - 256	HALS/ DSI/ TLD/ MCFL/ PEX.
	2	8 1/2	3487.74 - 1090	HALS/DSI/TLD/MCFL/PEX
OP1	1	12 1/4	1781 - 3010	ISF-MSFL-BHC-SP-GR, LDT-CNL-GR,SHDT-GR
	2	8 1/2	3020 - 3520	MSFL-ILD-BHC-GR-SP,LDT-CNL,SHDT,VSP
	3	8 1/2	3552 - 3071	ISF-MSFL-ILD-BHC-GR
OP2	1	8 1/2	1256.7 - 3520	DIL/LDT/CNL/Sonic/GR
OP3	1	12 1/4	1386 - 3115	ISF-MSFL-SP-BHC-GR,LDT-CNL,SHDT
	2	8 1/2	3107 - 3681	ISF-MSFL-SP-BHC-GR;LDT-CNL;SHDT
OP4	1	8 1/2	1575 - 3430	AIT/LDT/CNL/DSI/GR
OP5	1	8 1/2	772.5 - 3463	SP-AIT-NGT-DSI-PEX
OP6	1	8 1/2	1750 - 3412	AIT/LDT/CNL/DSI/GR

4.3 LOG EDITING

4.3.1 Depth Shifting

When combining measurements made during separate log runs through the same borehole, discrepancies often arise and it is important that the measurements be correctly correlated in depth with one another before performing quantitative interpretation. Logs from different wireline tool strings may have slight mismatches that may exist because of ship heave during recording, cable stretch, tidal changes in sea level etc (Hagelberg et al., 1992). A curve is chosen e.g. natural gamma-ray log or resistivity as a reference curve that provide means of depth shifting for correlation with other curves and appropriate adjustments or shifts are applied.

For this study, the Interactive Petrophysics (IP) triple combination (triple combo) module was applied for depth checking and was confirmed that no depth matching was required except for wells that have core data that need to be depth matched with the log data. Figure 4.2 below present example of curve run in all track with the gamma ray log to check corresponding depth.

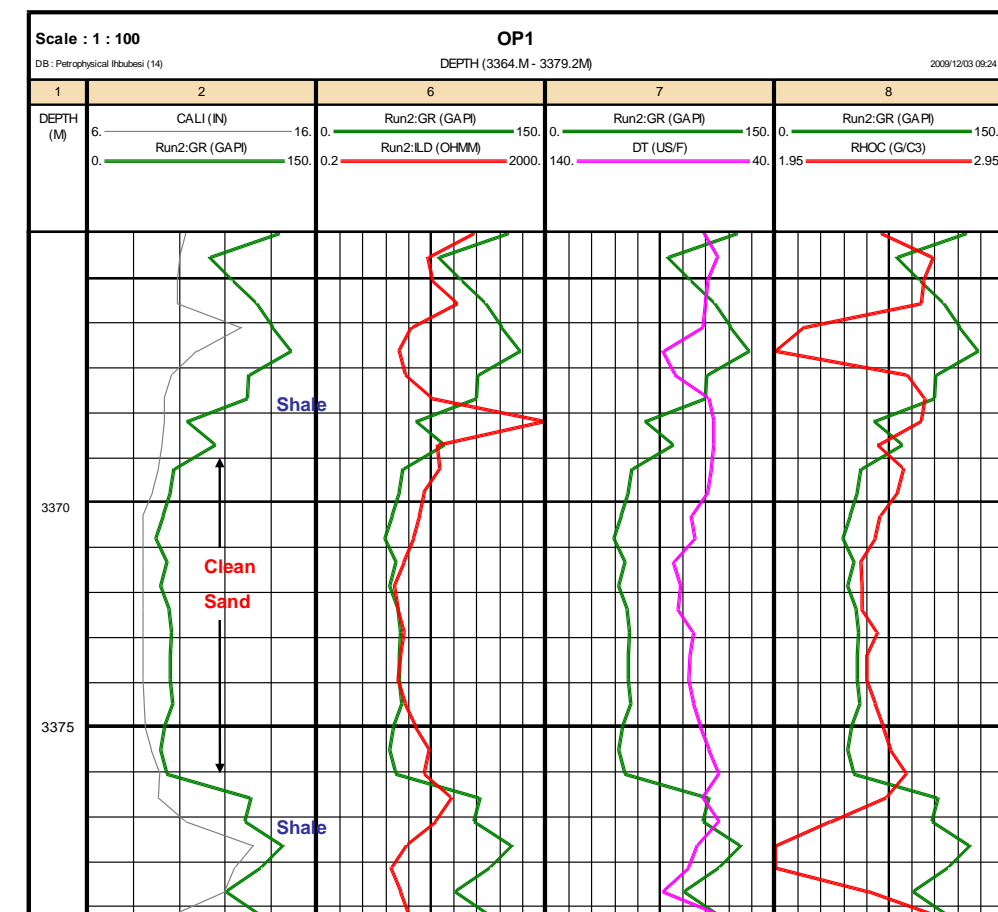


Figure 4.2: Example of gamma-ray log Run at the same depth with other logs.

The Figure above shows gamma –ray log (green colour) in track 2 and resistivity (red) in track 6, sonic log (Foschini) in track 7, and density log (red) in track 8 both recorded at the same depth and Run, while the gamma-ray log is used to check if they all record the same formation at a given depth. The gamma-ray or resistivity log could be used as the reference shift curve.

No depth shift was required except for well that have core data that was depth shifted with logs.

4.3.2 Borehole environmental correction

Logs are affected by borehole size and the environment, thus environmental corrections by computer programs are applied. Borehole environmental influence is caused by stress, mud weight, temperature, etc. All pad type devices such as the density, sidewall neutron log, microlog, and dipmeter will not perform effectively in large holes where the hole diameter is beyond the reach of the pad. The tools will read the mud values or jump from high to low values due to the intermittent contact with the borehole wall (Crain, 2001). Rough or rugose holes and shale intervals due to washout will also leave excessive mud between the pad and the borehole wall and can be observed from the Caliper and density correction DRHO logs as it will be very high in such intervals.

Borehole environmental corrections have been applied to the following logs using mud/borehole properties identified from log headers as presented in Table 4.2 below.

Table 4.2: Summary of environmental corrections applied to logs

LOG	CORRECTION APPLIED
Gamma-Ray (GR)	Hole size, mud weight and tool position.
Density (RHOB)	Hole size, mud weight
Neutron (NPHI)	Mudcake, mudweight, borehole salinity, pressure and stand-off
Deep and Shallow Laterolog (LLD & LLS)	Hole size and mud resistivity
Microspherical (MSFL)	Mudcake resistivity
Spontaneous potential (SP)	Baseline correction

An example of a density log in rough and enlarged borehole diameter is shown in Figure 4.3 below:

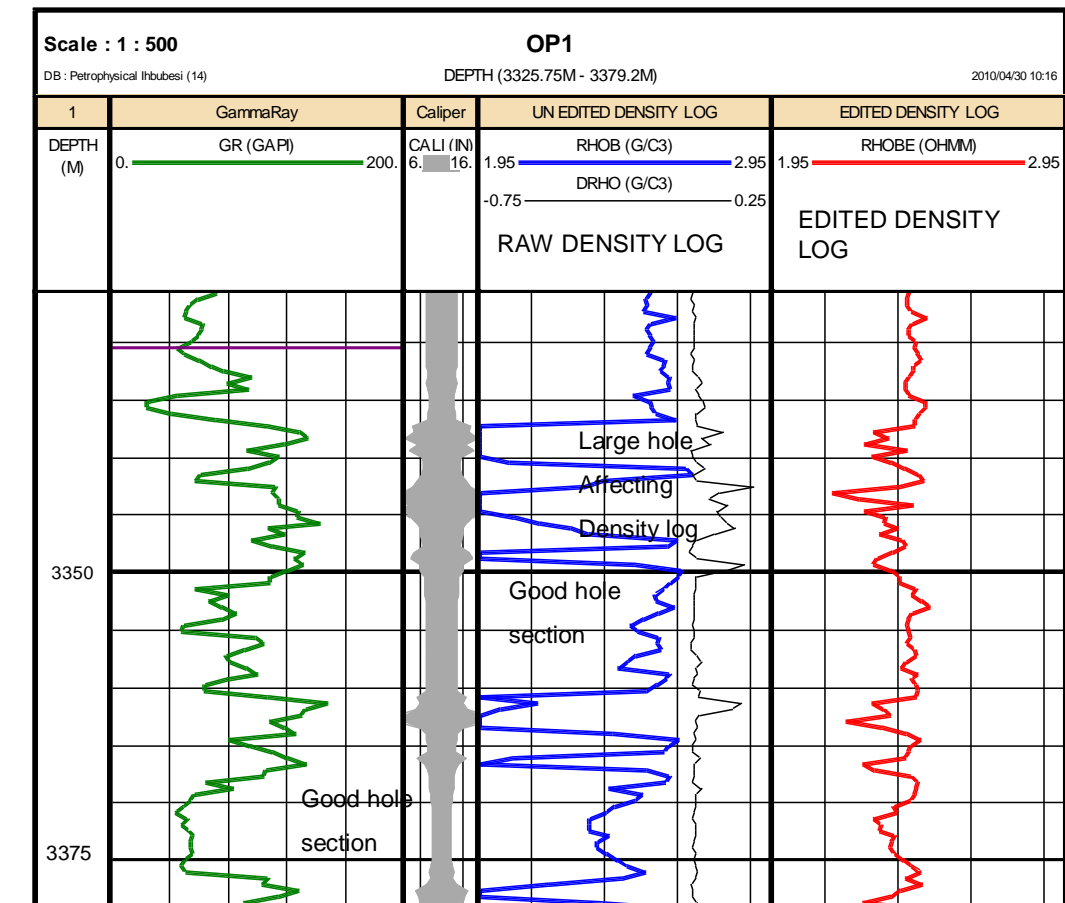


Figure 4.3: Example of density log affected by borehole.

The Table 4.3 below presents guide as to know when to apply corrections due to borehole condition (Yan et al., 2008).

Table 4.3: Guide for borehole condition

Caliper and Bit size(BS) logs	Condition
Caliper – BS = 0 %	Excellent condition, no need for correction
Caliper – BS < 10 %	Logs are good quality, refer to DRHO log
Caliper – BS =10 – 30%	Logs probably need to be corrected
Caliper –BS >30 – 50%	Logs incorrect, need to correct
Caliper – BS > 50 %	Very bad borehole conditions. incorrect logs

(Yan et al., 2008)

The use of service company chart books provide options for environmental corrections and the input parameters includes raw log data, tool type, caliper log, drilling bit size (BS), and mud information.

The mud properties used were taken from log data files and Well completion reports. Hole size was taken from recorded bit size and Caliper log.

Figure 4.4 below presents an example of an uncorrected log and environmentally corrected logs. Green colour curves with C appended to the suffixes are corrected curves, while Red coloured curves are the uncorrected curves. After performing the corrections, the curves tend to increase in values except the resistivity logs as presented in the Figure.

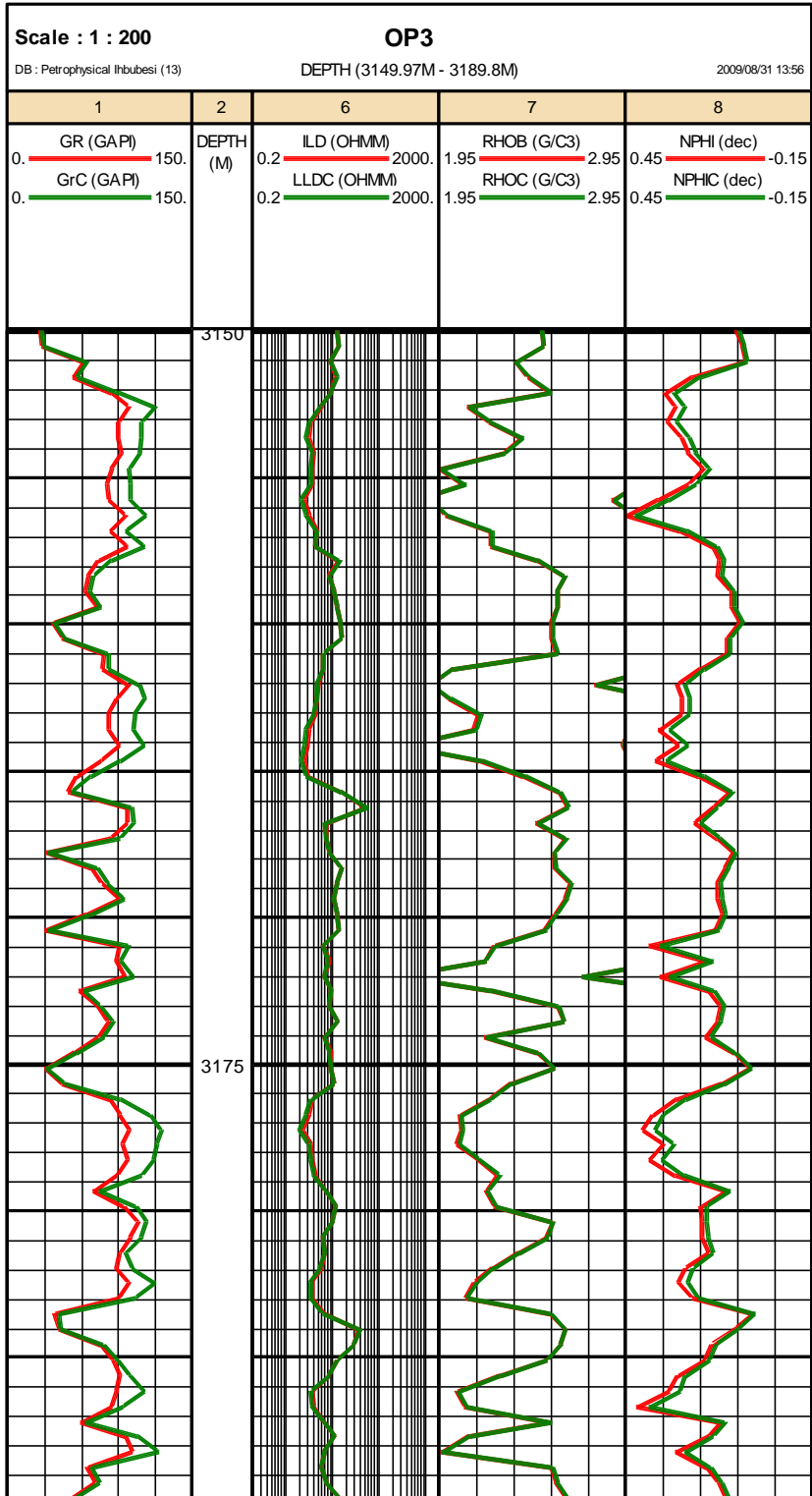


Figure 4.4: Graphics of uncorrected and environmentally corrected logs

4.3.3 Mud filtrate Invasion Correction

The sonic, shallow resistivity and density logs have shallow depths of investigations and their measured values comes from the near the wellbore so are all affected by invasion. The mud filtrate invasion into the borehole can be up to 0.5m to 0.8m when using water based mud in the drilling process. Studies by Chi et al (2004) showed that the maximum invaded distance is about 2m therefore if the invasion depth is beyond the depth of the investigation of the logging tool; it will result in tool showing values from the invaded zone.

The conductive mud used in drilling also causes the induction log to read too low values due to invasion and invasion correction charts could be used in such cases. The correction for a fresh mud in a hydrocarbon zone will reduce resistivity values instead of increasing it. The resistivity logs can be used to identify invasion zones.

Presented in Figure 4.5 is an example of the use of the resistivity log for recognition of thin bed.

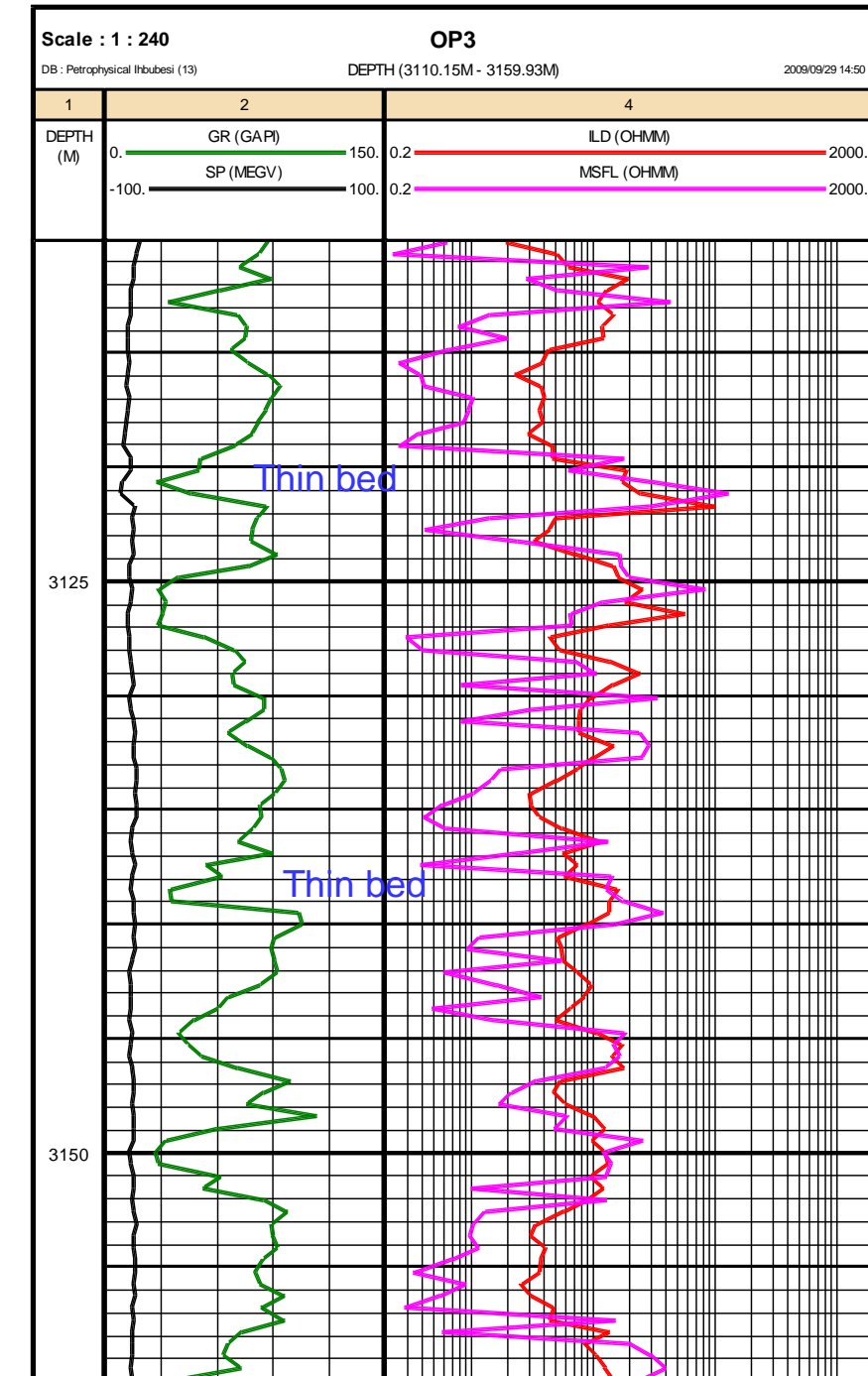


Figure 4.5: Thin bed recognition on resistivity logs

4.3.4 Smoothing, De-Spiking and Noise Removal

The process of de-spiking is an editing that involves removing of unwanted signals in form of cycle skip, noise and spike that is associated with sonic logs. Care must be taken in editing noise because some of the noise may be as a result of thinly bedded porous layers. Track 6 in Figure 4.6 below present a sonic log data with spike. On Track 9 is the edited sonic log without spike. When spikes are removed, the quality of the sonic log data is improved (track 9).

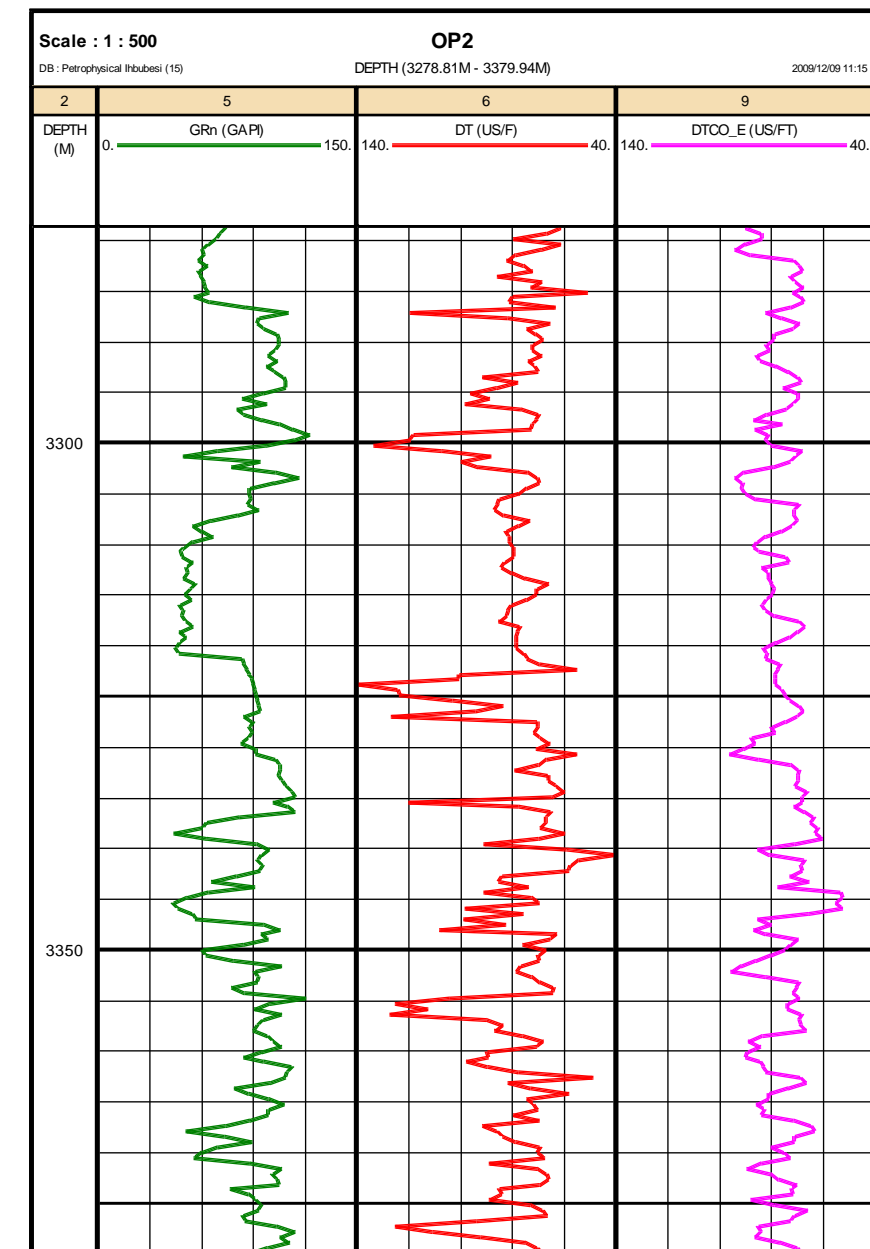


Figure 4.6: Example of spike and de-spiking of sonic log

4.4 CURVE SPLICING/MERGING

Log splicing or merging is a process of bringing together all the RUNS logged in a well to form a continuous LAS file. The logs runs at different depths were spliced or merged into a continuous log. Figures 4.7a and b are examples of un-spliced and spliced logs.

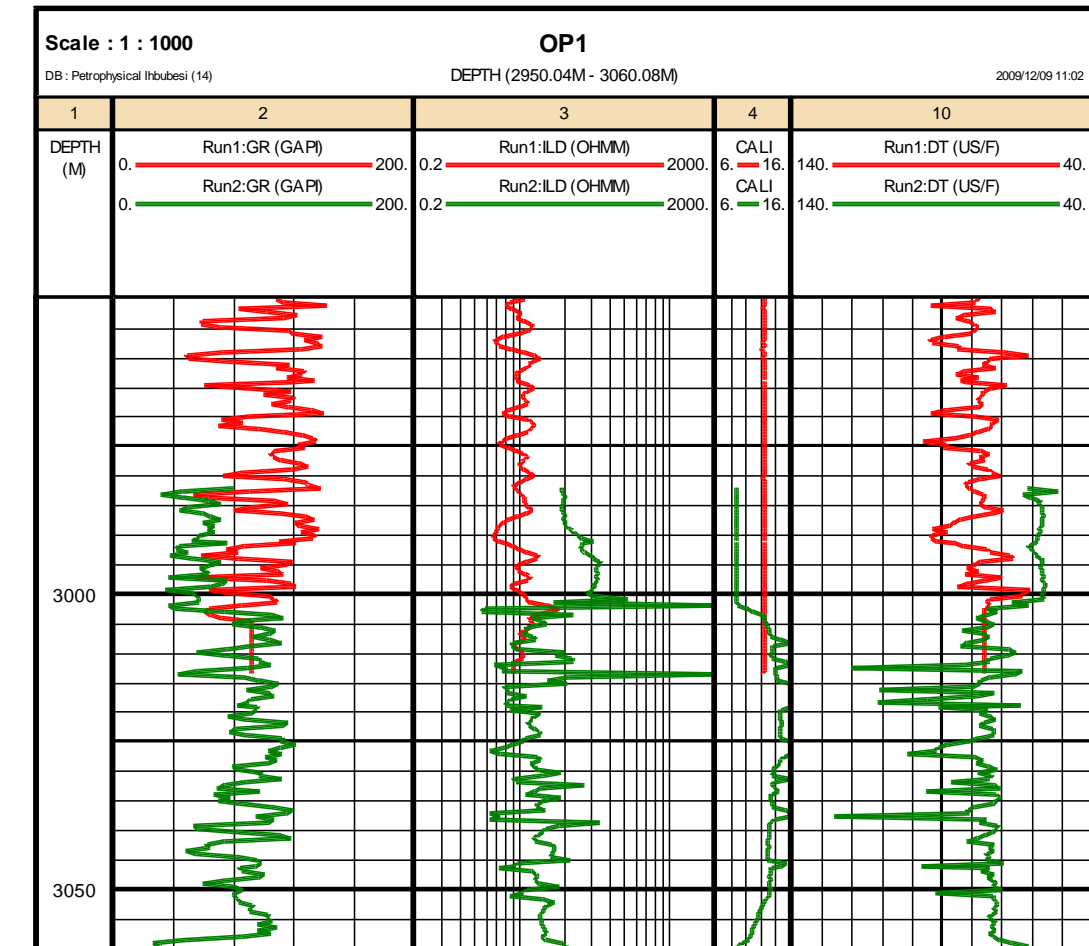


Figure 4.7a: Example of Log at different runs (unspliced curves)

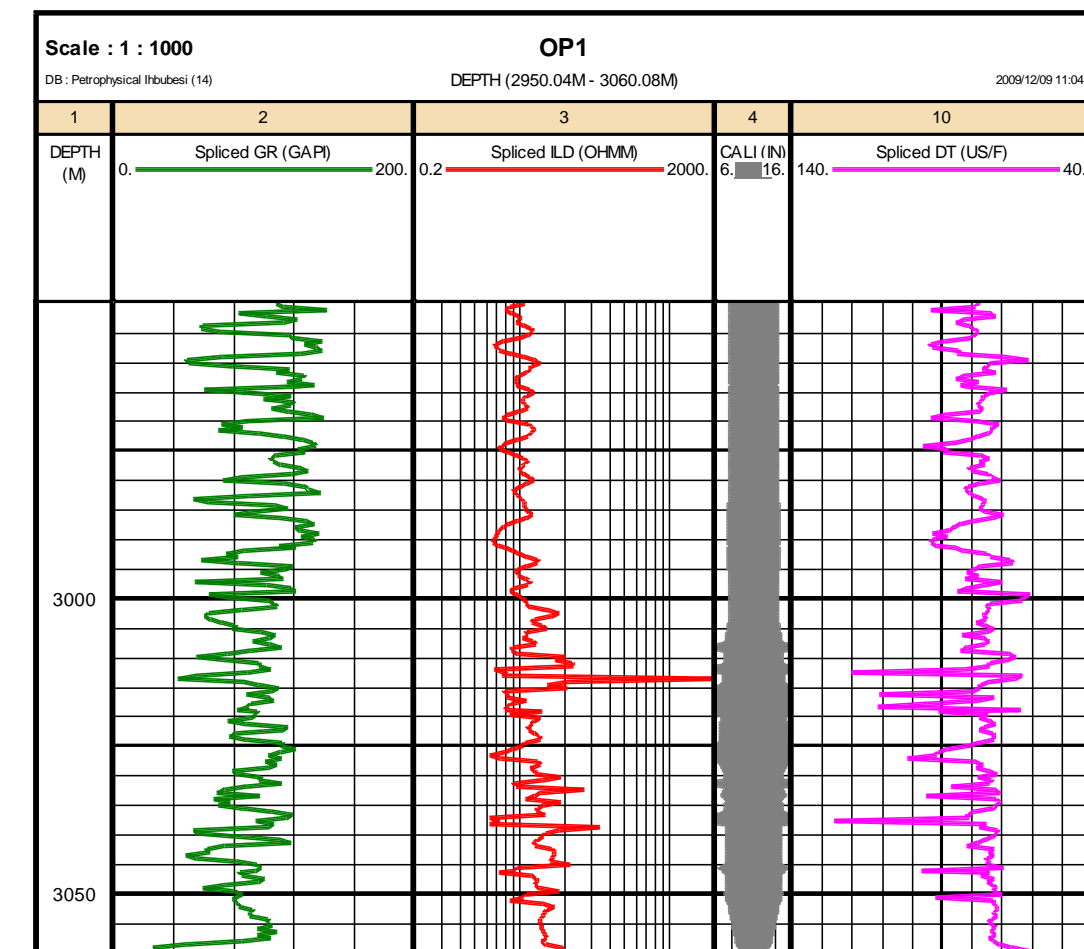


Figure 4.7b: Examples of graphics of spliced curves

4.5 CURVE NORMALIZATION

The objective of curve normalization is to adjust certain curves in each well so that they register similar values in the similar rock type. Normalization is a mathematical process that adjusts for differences among data from varying sources in order to create a common basis for comparison (Shier, 2004).

Three types of curve normalization operation are enabled in the Interactive Petrophysics package that is used to perform the curve normalization. One of the types is the one point linear shift which adds or subtracts a fixed value to or from the selected curve for normalization. The other type is the one point scale factor that multiply the user selected curve by a fixed value. Also is the two point type that combines the first two types, allowing a scaling plus a linear shift operation.

Well log normalization especially the gamma-log is useful for multi-well characterisation of facie types, assessing the lateral continuity of reservoir sands, geological analysis and mapping and determining net pay (Scott et al., 2004).

The first step in the log normalization was the histogram plot of GR values of all the wells over the intervals and compared as shown in Figure 4.8a below.

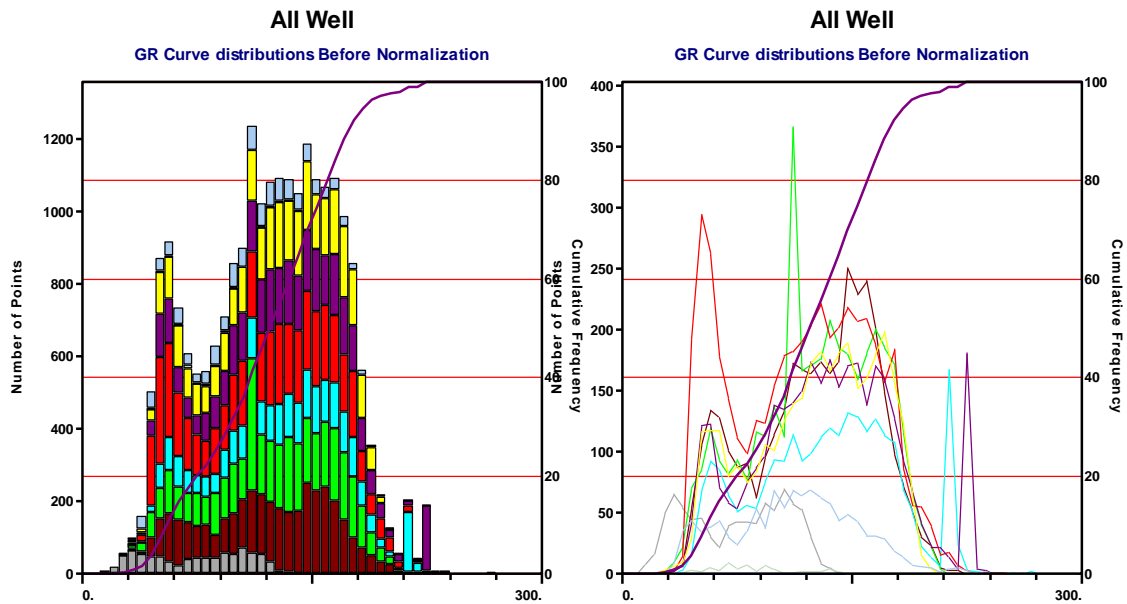


Figure 4.8a: GR log values for all Well before Normalization.

The second step in the normalization process is to choose a standard or reference well whose histogram is very similar and its geographical location is central to other wells. In this case, well OP4 and OP5 were chosen as the reference wells and histogram distributions are given in Figure 4.8b .

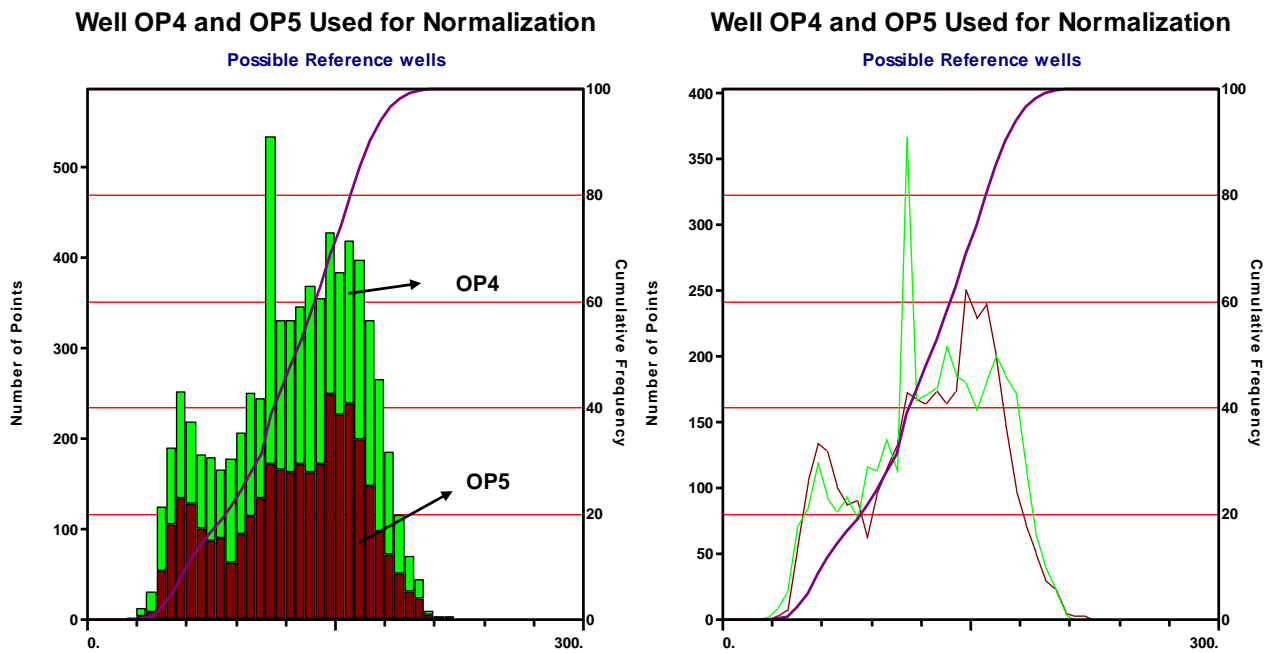


Figure 4.8b: Possible Reference wells (OP4 and OP5) used for Normalization

The next step in the process is to carry out the normalization process. Because all the wells were logged by the same Company (Schlumberger), the range of the gamma-ray log responses were similar and the normalization required was a simple shift. The two point type of normalization was adopted in this study which is of the form given below:

$$GR_n = \text{Input GR curve} * X + C$$

Where:

GR_n = Normalized curve

X = Factor to be multiplied with input curve

C = Value to be added to curve.

The normalized curves have n appended to the curve mnemonic and are presented in Figure 4.8c below.

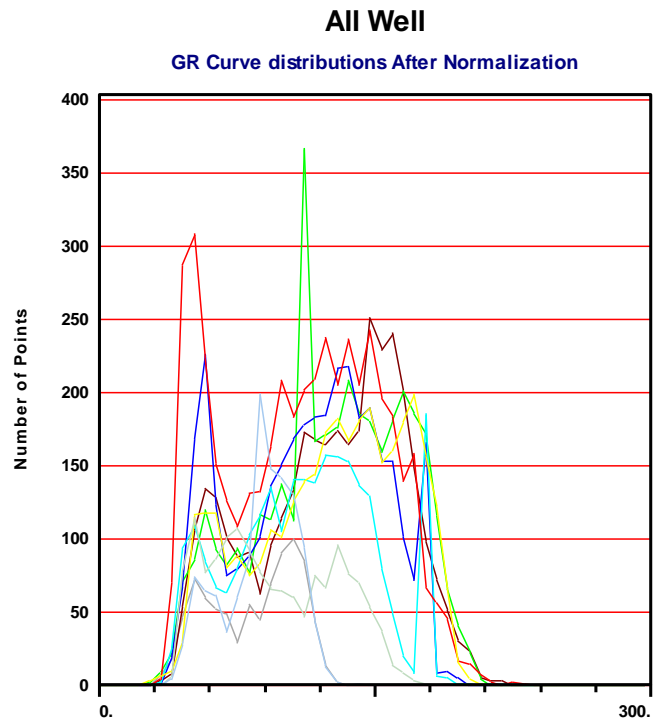
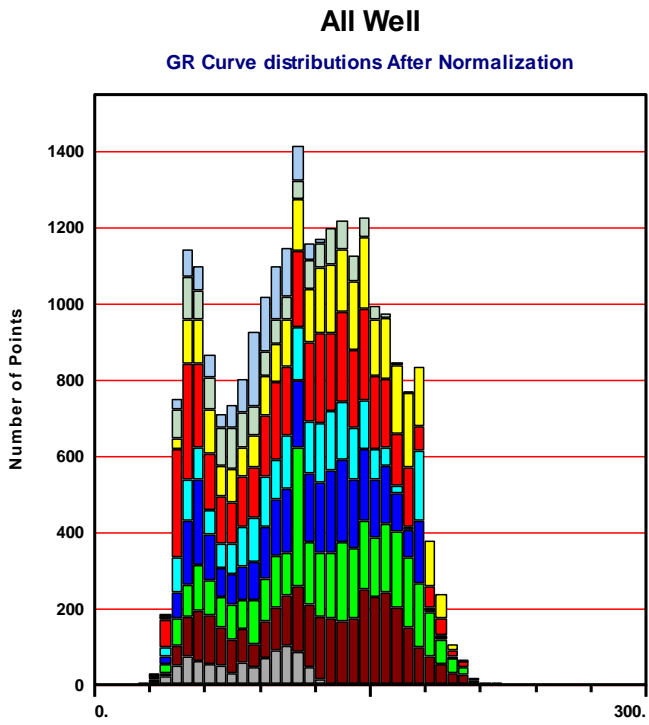


Figure 4.8c: Normalized curves

CHAPTER FIVE

CORE ANALYSIS AND INTERPRETATION

5.1 INTRODUCTION

The core analysis is done to establish ground truth for other formation evaluation measurements and is essential for calibration of well logs. Core Analysis is a tool in reservoir assessment that directly measures many important formation properties. The objective of performing this analysis is to bring a sample of the formation and its pore fluids to the surface in an unaltered state to preserve the sample and then transport it to the laboratory for analysis. The analysis may aim to determine porosity, permeability, fluid saturation, grain size distribution, mineral composition, grain density; etc. Samples for this analysis may come from conventional core, sidewall cores or plugs, and cuttings (Bateman, 1985).

The core analysis is usually carried out on core plugs, samples that are taken from the bulk core. In the core laboratory, core plugs are drilled from whole core that typically have a length of about 5cm and diameter of 2.5cm. The petrophysical properties are then measured on these core plugs. Laboratory core analysis can provide very accurate measurements and are regarded as the ground truth. Porosity determinations in the laboratory are accurate within $\pm 0.5\%$ of the porosity value and $\pm 5\%$ for permeability when the limits and procedures are properly observed. Samples of core taken with either water or oil base mud and are preserved and subsequently tested without cleaning and drying are referred to as fresh cores. Sample of cores cleaned and dried prior to testing are referred to as restored core. An advantage is that air permeability and porosity are available to assist in sample selection (Core Laboratories, 1973).

The special core analysis (SCAL) are measurements that are made on core plugs that complement the routine core analysis measurements which provides information on the electrical properties, relative permeability, capillary pressure, cation exchange capacity (CEC) and wettability. The results of electrical properties of rock measured from SCAL analysis include the resistivity formation factor, cementation exponent, resistivity index, and also the determination of saturation exponent.

The results of the relative permeability measurements helps to make quantitative estimates of formation damage, quantifies effective permeabilities of water, oil and gas, and calculate cumulative permeabilities to each different fluid.

The petrography studies which is the scientific description and study of rocks used different mineralogical analysis techniques which include X-ray diffraction (XRD), thin sections of the rock which gives visual study of textural properties of rock, and the scanning electron microscopy (SEM) which allows visual examination of pore throats and walls. These analyses were performed in some of the wells studied; results and interpretations will be presented.

5.2 CONVENTIONAL CORE ANALYSIS

The conventional or plug type core analysis is the logging, sampling, and analysis of cores where by a portion of each interval to be analysed is selected to represent the interval of interest. This analysis is performed on homogeneous formations such as sandstones, carbonates and shaly-sand formations at three to four inches of each foot of core.

This analysis was performed in three wells OP1, OP2 and OP3 of the study area by Core laboratory in order to determine the petrophysical properties of reservoir formations.

5.2.1 Interval Cored

5.2.1.1 Well OP1

A conventional core was cut in well OP1 on the basis of good drilling break and associated gas shows at a reservoir within the Albian age from 3370 to 3383m predominantly consisting of sandstones with about 20% claystones and silty-claystones. A total of 12.95m of core was cut and 12.43m was recovered giving a recovery percentage of approximately 96 %. The routine core analysis measurements were provided in excel spreadsheet format and the measurements were available for horizontal plugs which includes; grain density, gas expansion (helium) porosity; air and liquid permeabilities, fluid saturations, and calcimetry (calcite and dolomite). Core photos were available and are presented in appendix B.

Table 5.1 below presents the results obtained from the conventional core measurements of well OP1.

Table 5.1: Well OP1 routine core analysis Results

Depth (m)	Porosity (%)	K (mD)	Kair (mD)	Sg (%)	So (%)	Sw (%)	Calcite (%)	Dolomite (%)	Grain Density (g/cc)	Lithology Description
3370.05	18.9	96	108	49	0	51	0.5	5	2.64	Massive sandstone interval sandstone, poor ,white to grey, fine to very fine predominantly fine, sorted to rounded consolidated,lithoclasts ,calcite.
3370.35	19.6	60	69						2.68	
3370.6	20.2	55	64						2.68	
3370.85	14.6	10	13						2.69	
3371.07	16.9	34	40	52	0	48	0.5	0.5	2.65	
3371.4	16.4	11	14						2.71	
3371.65	16.7	15	19						2.71	
3371.9	16.5	21	26						2.69	Sandstone, very fine to fine, poorly to Well sorted, non calcite, argillaceous mixtures, brown Lithoclasts.
3372.03	12.7	4.5	6	56	0	44	0.5	0	2.65	
3372.28	12	0.91	1.3						2.69	
3372.53	9.5	0.2	0.32						2.68	
3372.82	8.5	0.09	0.149						2.68	
3373.75	5	0.01	0.018						2.69	
3373.88	3.2	0.01	0.01	22	27	51	1	0	2.64	Claystone interval with siltstone & sandstone interbeds. laminated coal, black ,and fractured Brittle.
3375.6	3	0.01	0.017						2.69	
3375.98	2	0.01	0.016						2.71	
3376.62	7.7	0.02	0.03	45	0	55	0.5	0	2.66	
3376.86	8.6	0.09	0.151						2.65	A massive sandstone interval with claystones and siltstone interbeds, and claystones Laminations.
3377.12	10.1	0.21	0.33						2.69	
3377.36	9.6	0.09	0.151						2.69	
3377.54	7	0.05	0.079	45	0	55	0.5	0	2.65	
3377.78	7.9	0.07	0.104						2.68	
3378.23	9.2	0.01	0.028						2.68	
3378.48	8.6	0.01	0.025						2.67	Sandstones, with ,calcite, lithic
3378.58	7.6	0.01	0.025	15	11	74	0.5	0	2.64	
3379.24	6.8	0.01	0.018						2.67	
3379.64	1.2	0.01	0.013						2.64	A massive claystones interval. Dark grey and carbonated.
3379.82	4.9	0.01	0.01	19	0	81	1	1	2.64	
3380.15	3.3	0.01	0.015						2.67	

5.2.1.2 Well OP2

A conventional core of about 25 meters was cut at reservoir interval 3446 to 3471m. At the depth of 3446 to 3465.17m was described as sandstones, very fine to medium grained with rare shale deposited in fining-upward depositional units separated sharp contact. Below 3465.17m was described as sandstones, siltstone, and shale deposited in coarsing-upward depositional units separated by sharp to gradational contacts.

A total of 25m core was cut and about 24.5m was recovered which shows a recovery of about 98 percent. The core photos of are presented in appendix A.

The routine core analysis measurements were taken on thirty five (35) plug samples to determine grain density, porosity and permeability by Core laboratories. The results of this analysis and lithology description are shown in Table 5.2.

Table 5.2: Well OP2 routine core analysis results

Depth (m)	Porosity (%)	Klin (mD)	Kair (mD)	Grain density (g/cc)	Lithology Description
3446.20	23.06	380	392	2.682	Sandstone, fine to medium, well sorted.
3447.08	24.24	225	227	2.681	Sandstone, very fine to fine, well sorted grains.
3447.11	24.17	163	166	2.668	
3447.83	18.65	13.600	14.2	2.578	Sandstone, dark grey, laminated moderately sorted.
3448.69	22.01	27.4	30.3	2.684	Sandstone, fine grain and moderate to well sorted.
3449.52	20.27	11.4	13.3	2.696	
3450.58	22.32	162	165	2.685	
3451.70	23.54	365	366	2.669	Fine to medium grain sandstone, moderate to well sorted, and possible horizontal burrow at 3451.35m.
3452.14	23.83	605	606	2.679	
3452.59	24.01	432	435	2.684	
3453.68	23.03	293	296	2.679	Fine grain sandstones, well sorted
3454.72	24.25	890	909	2.677	
3455.08	22.96	1074	1095	2.673	
3455.55	18.83	25.6	28.1	2.700	
3455.86	10.42	1.67	2.07	2.665	Sandstone, fine to medium grains, silty to shaly lamination, poorly sorted.
3456.15	4.59	.011	.019	2.744	
3456.65	3.37	.013	.021	2.705	Sandstone, fine to very fine grain, rich in calcite and moderately sorted.
3457.18	3.27	.003	.006	2.767	
3457.74	21.39	223	225	2.690	Sandstone is fine to medium grain, moderately well sorted
3458.69	21.36	268	270	2.683	
3459.59	20.11	208	213	2.681	
3460.00	21.93	396	399	2.674	
3460.10	22.05	659	675	2.686	
3461.48	23.07	460	473	2.689	
3462.54	18.91	31.0	33.1	2.727	Sandstone is fine, moderately sorted.
3463.48	19.55	108	110	2.695	
3464.59	8.19	.055	.100	2.694	Fine grain scattered clasts, poorly sorted.
3464.81	4.92	.025	.037	2.677	Sandstone, fine grain, moderately sorted.
3465.40	2.95	.003	.005	2.752	Limestone is very light gray.
3466.47	6.23	.007	.015	2.714	Siltstone is light to medium gray,
3466.75	4.43	.055	.092	2.720	Shale is dark gray, laminated with minor burrows.
3467.50	4.12	.034	.054	2.750	Siltstone is light to medium gray, heterolithic shaly lamina with ripples.
3467.60	3.89	.012	.018	2.732	
3468.17	5.96	.011	.020	2.686	
3468.89	7.23	.012	.028	2.695	

5.2.1.3 Well OP3

Two conventional cores were cut in sandstones associated with hydrocarbon shows. Core one ranges from 3236 to 3244.93m consisting of 3m of massive sandstones underlain by about 6m of predominantly claystones with thin interbedded sandstones. Core two ranges from 3283.2 to 3296.3m consist predominantly of sandstones which become more argillaceous below 3288m (PASA report, 1989).

The percentages of core recovery were 75 % in core 1 and 78 % was recovered in core 2. Core photos of this well are presented in appendix B. Presented below in Tables 5.3 and 5.4 are the results of the routine core analysis and lithology descriptions obtained from core plugs.

Table 5.3: Well OP3 core1 analysis results and lithology description

Depth (m)	Porosity (%)	Klin (mD)	Kair (mD)	Sg (%)	So (%)	Sw (%)	Grain Density (g/cc)	Lithology Description
3236.1	24.2	121	135	-	-	-	2.7	Massive sandstone interval, very fine to fine, Well sorted, consolidated sandstones occasional calcite presence
3236.4	22.6	140	156	-	-	-	2.68	
3236.5	21.3	75	86	41	0	59	2.69	
3236.8	21.4	67	77	-	-	-	2.71	
3237.1	18.1	28	34	-	-	-	2.71	
3237.3	18.1	36	43	-	-	-	2.69	Siltstone
3237.5	15	17	21	-	-	-	2.68	Sandstone, low angle cross stratification, poorly sorted, parallel lamination.
3237.8	12.9	6.6	8.6	-	-	-	2.85	
3238	9.1	0.42	0.63	59	0	41	2.64	
3238.3	8.9	0.13	0.22	-	-	-	2.66	
3238.5	6.3	0.04	0.074	-	-	-	2.66	
3238.5	8.8	0.14	0.23	-	-	-	2.66	
3239.1	4.3	0.04	0.06	-	-	-	2.68	Silty claystone, non parallel wavy lamination, mm scale bed.
3243.6	0.6	0.02	0.04	15	0	85	2.67	

Table 5.4: Well OP3 core 2 Routine core analysis results and lithology description.

Depth (m)	Porosity (%)	Klin (mD)	Kair (mD)	Sg (%)	So (%)	Sw (%)	Grain Density (g/cc)	Lithology Description	
3283.2	19.2	3.7	4.9	30	0	70	2.68	Silty sandstone, poorly sorted, pararell lamination	
3283.6	17.8	12	15	-	-	-	2.68		
3283.85	17.8	25	30	-	-	-	2.68	Sandstone, poorly sorted with rip up clasts, very fine to fine.	
3284.1	20.4	35	41	-	-	-	2.68		
3284.35	21.3	34	40			-	2.68		
3284.45	22	53	62	36	0	64	2.68		
3285.05	22.2	43	50				2.69		
3285.3	22.8	40	47				2.67		
3285.34	20.6	12	15	41	0	59	2.67		
3285.83	17.3	3.6	4.8				2.69		
3286.08	14.3	38	45				2.67		
3286.3	20.4	45	53				2.68		
3286.55	22.3	41	48				2.69		
3286.6	22.2	69	79	39	0	61	2.68		
3287.25	23.3	1.9	2.7				2.69		
3287.3	15.8	67	77				2.67		Clay mudstone, burrowed horizontally.
3287.9	3.7	0.12	0.194	45	0	55	2.66		
3290.06	2.3	0.01	0.013	16		84	2.69	Claystones and siltstone, Vertical burrows, siderite concretion.	
3291.76	2.7	0.01	0.016	35		65	2.65		
3292.79	2.6	0.01	0.023	35		65	2.66		

5.3 CORE-LOG DEPTH MATCH

The petrophysical properties measured on core are used to verify log interpretation models. Using the core data to verify the log interpretation models also allow the log and core data to be compared and the uncertainties in the log-derived properties to be quantified (Adams, 2005).

The routine core analysis results have been depth match to the log data by overlaying core measured data and wireline log data. Visual examinations of the routine core were carried out and the routine core data was depth shifted or matched to the wireline logs to enable direct comparison. This core to log data depth match is necessary especially in offshore wells because the driller's depth do not always match with the logger's depth.

Presented in Figure 5.1 below is an example of core-log overlay before depth shift was applied of well OP2.

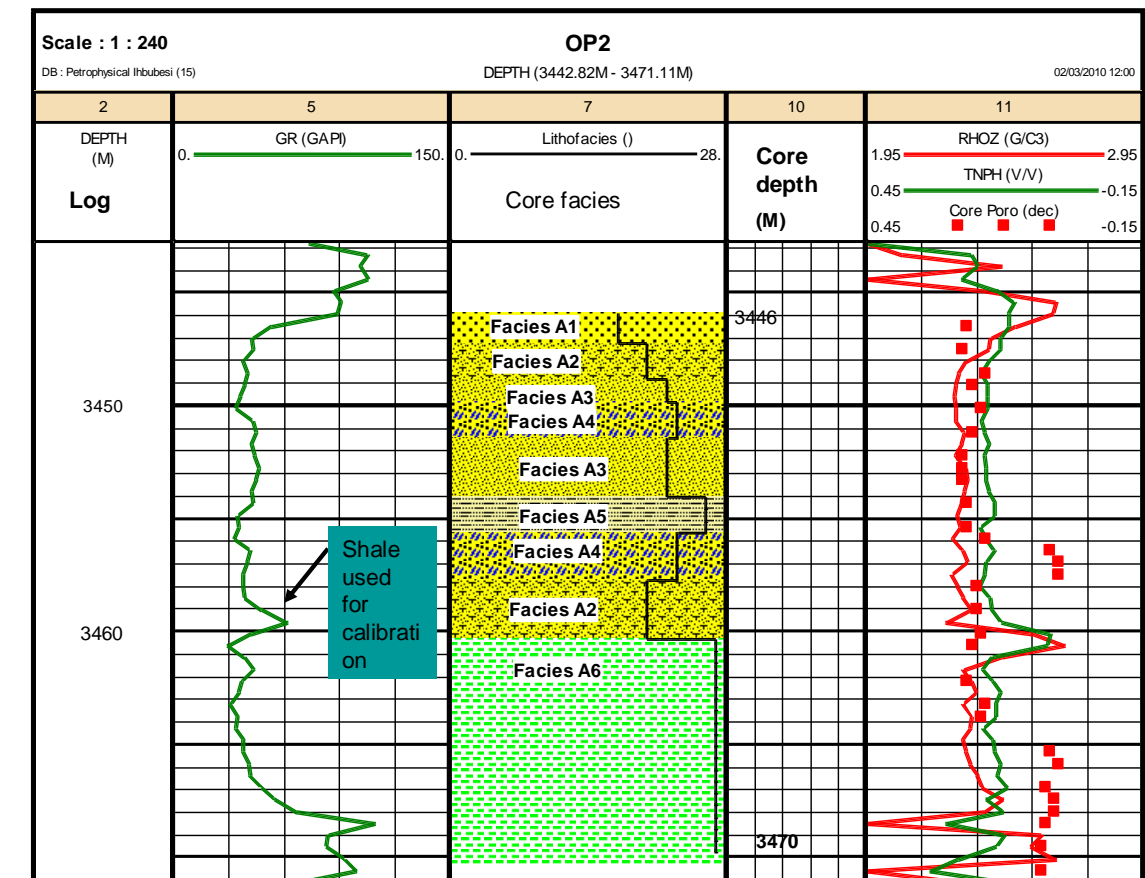


Figure 5.1: Example of Log and Core data comparison before depth shifting.

Before carrying out the depth shift of log and core data, both are overlaid and a visible shale or clay point is used as a reference point for appropriate shifting. In this particular well, core depth plus 3.43m equals the log depth.

The amount of variable shifts required in each routine core to match with the log data is presented in Table 5.5 below.

Table 5.5: Cored Intervals and Core-log Shift Summary for wells.

		Core Drillers Depths						Core-log match. Log Equiv. Depth		Log Equiv. depth	
		Top	Base	Cut	Recovered	Recovery	Core-Log Shift (m)	Cored interval		Recovered interval	
Well	Core	m	m	m	m	%		Top (m)	Base (m)	Top (m)	Base (m)
OP1	1	3370.05	3383	12.95	12.43	96	+2.8	3372.85	3385.8	3367.25	3383.9
OP2	1	3446	3471	25	24.5	98	+3.43	3449.43	3474.43	3449.43	3473.9
OP3	1	3236.1	3244.93	8.93	6.69	75	+0.21	3236.31	3245.14	3236.1	3234
OP3	2	3283.2	3296.3	13.1	10.1	78	-1	3282.2	3296.3	3282.2	3293
TOTAL				59.98	53.72						

5.4 Lithofacies Description

The term facies according to Roger and Noel (1992) is a body of rock characterized by a particular combination of lithology, physical and biological structures that shows an aspect different from the bodies of rock above, below and laterally adjacent.

An existing core sedimentological description of the routine core analysis was used in this study. The study and description of reservoir core is fundamental in the development of petrophysical model. This description helps to find a relation between log data and routine and special core analysis.

The approach adopted by Nieto and Rojas (1998) for grouping of lithofacies was used in this work. The lithofacies of the rock units were grouped according to textural and structural features and grain sizes.

The Table 5.6 below presents the lithofacies classifications of rock units grouped into six different facies.

Table 5.6: Lithofacies descriptions and classification of reservoir facies

Facies	Description	Reservoir Quality	Facies photos
A1	Sandstone, fine to medium grains, well sorted.	Good	
A2	Very fine to medium grained, moderate to well sorting, fining upward depositional unit.	Very Good	
A3	Fine grain sandstone, yellowish gray to light brownish gray, horizontally bedded to low angle cross bedded. Locally rippled. Moderately sorted with calcite.	Moderate	
A4	Argillaceous sandstone is light gray to dark gray, bioturbated and burrowed.	Fair	
A5	Siltstone is light to medium gray, heterolithic shaly laminae, ripples	Poor	
A6	Claystone, laminated with minor burrows shale, occasional siltstone presence, poorly sorted.	Non Reservoir	

5.4.1 Well OP1 Lithofacies

Four lithofacies were identified in well OP1. They are facies A3, A4, A5 and A6 as shown in track 3 (Figure 5.2) below. In terms of reservoir quality, lithotype A3 represents the best petrophysical reservoir quality with good permeability and porosity values, facies A4 is intermediate quality and Facies A5 and A6 are considered to have poor reservoir rock quality for this well.

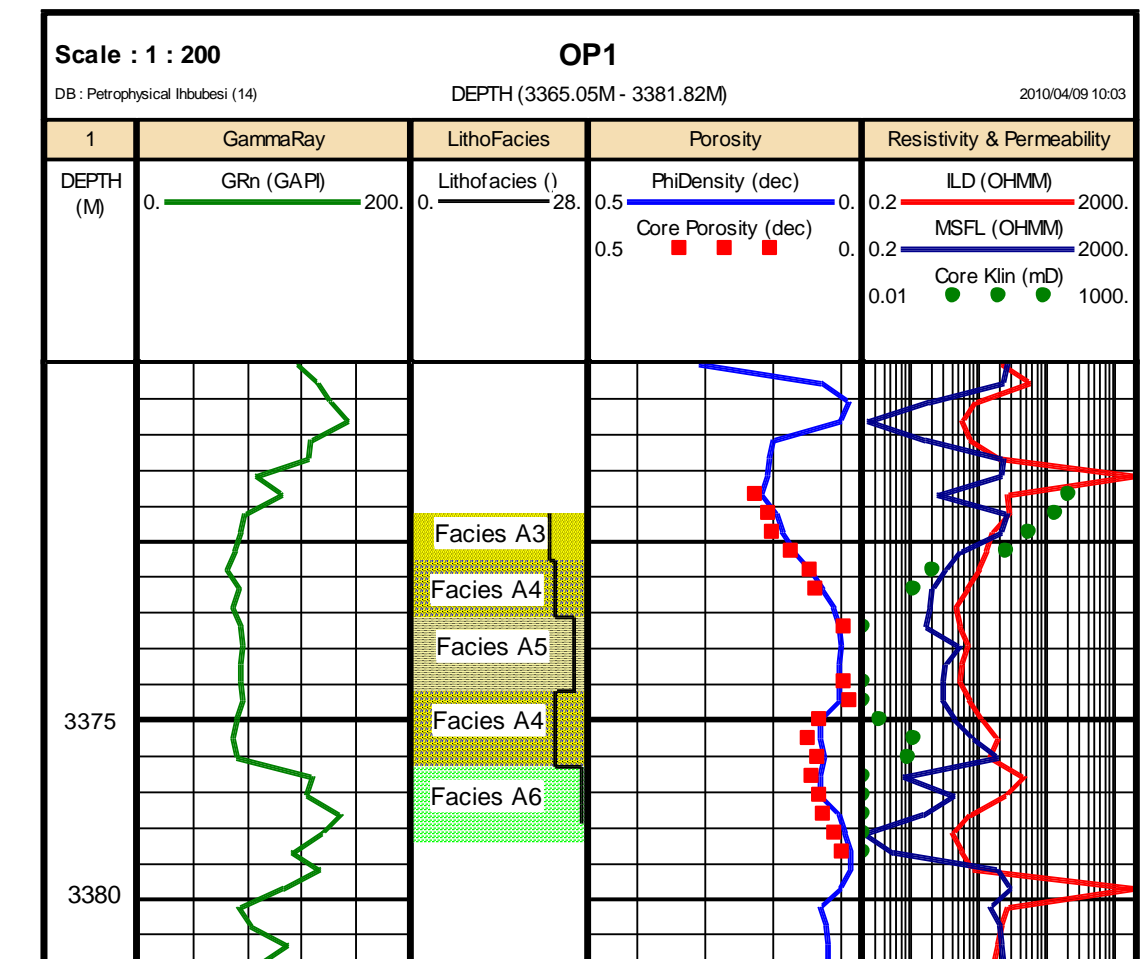


Figure 5.2: Well OP1 showing core facies in track 3.

5.4.2 Well OP2 Lithofacies

In well OP2, six lithofacies were identified, they are A1, A2, A3, A4, A5, and A6 as shown in track 6 (Figure 5.3) below. The best reservoir rock quality are facies A1 and A2, while A3 and A4 can be considered good quality, A5 is classified as poor reservoir rock quality and A6 is not considered as a reservoir rock.

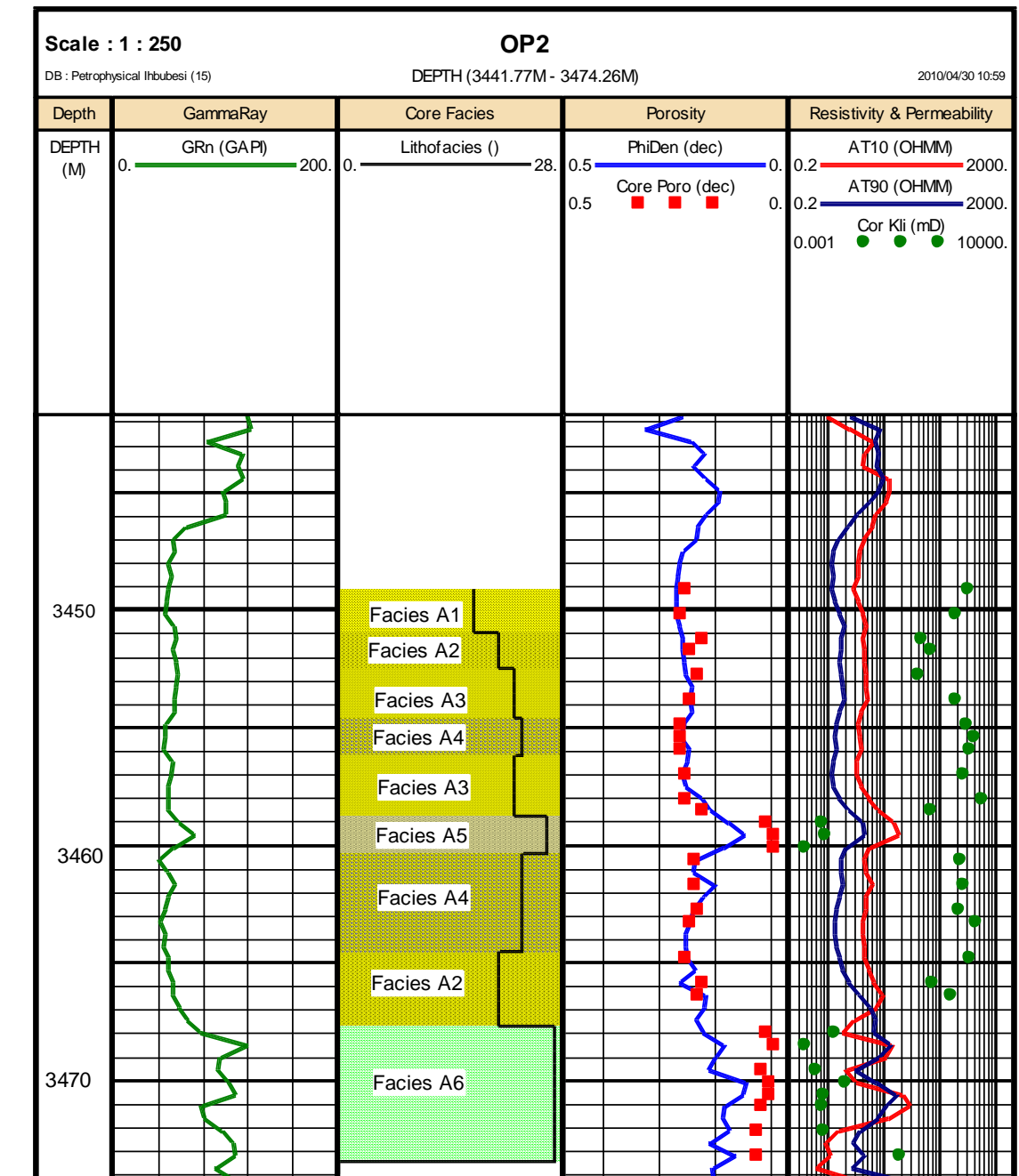


Figure 5.3: Well OP2 graphics showing core facies in track 3.

5.4.3 Well OP3 Lithofacies

In well OP3, four facies (A3, A4, A5 and A6) were identified in core 1 as shown in track 3 (Figure 5.4a) below. The best facies for this well is facies A3 because it has good porosity and permeability values.

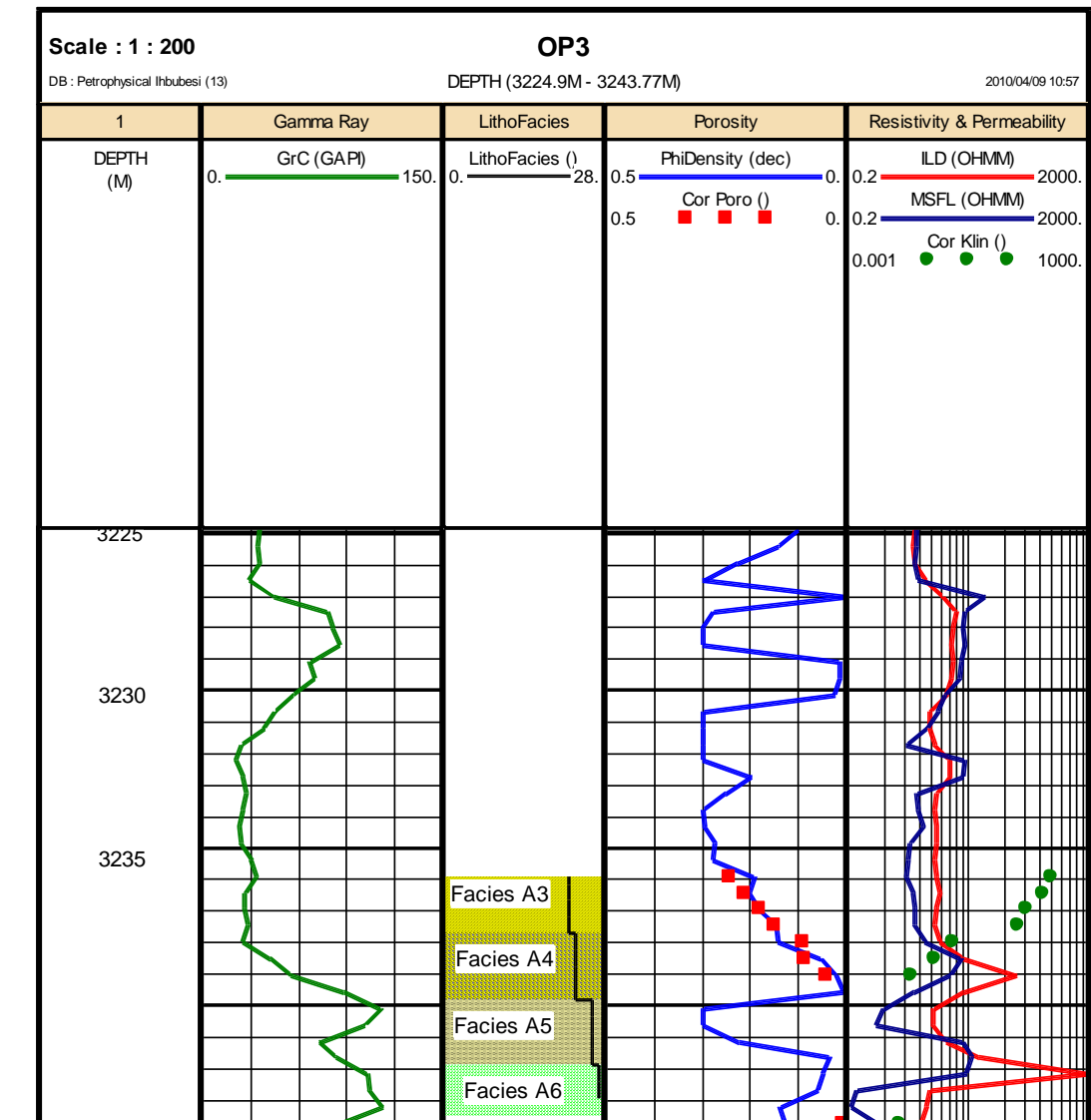


Figure 5.4a: Well OP3 core 1 facies shown in track 3.

Three facies were identified in core 2 of well OP3 as indicated in track 3 (Figure 5.4b) below. Two reservoir facies A3 and A4 were identified and non reservoir facie A6 in the cored interval.

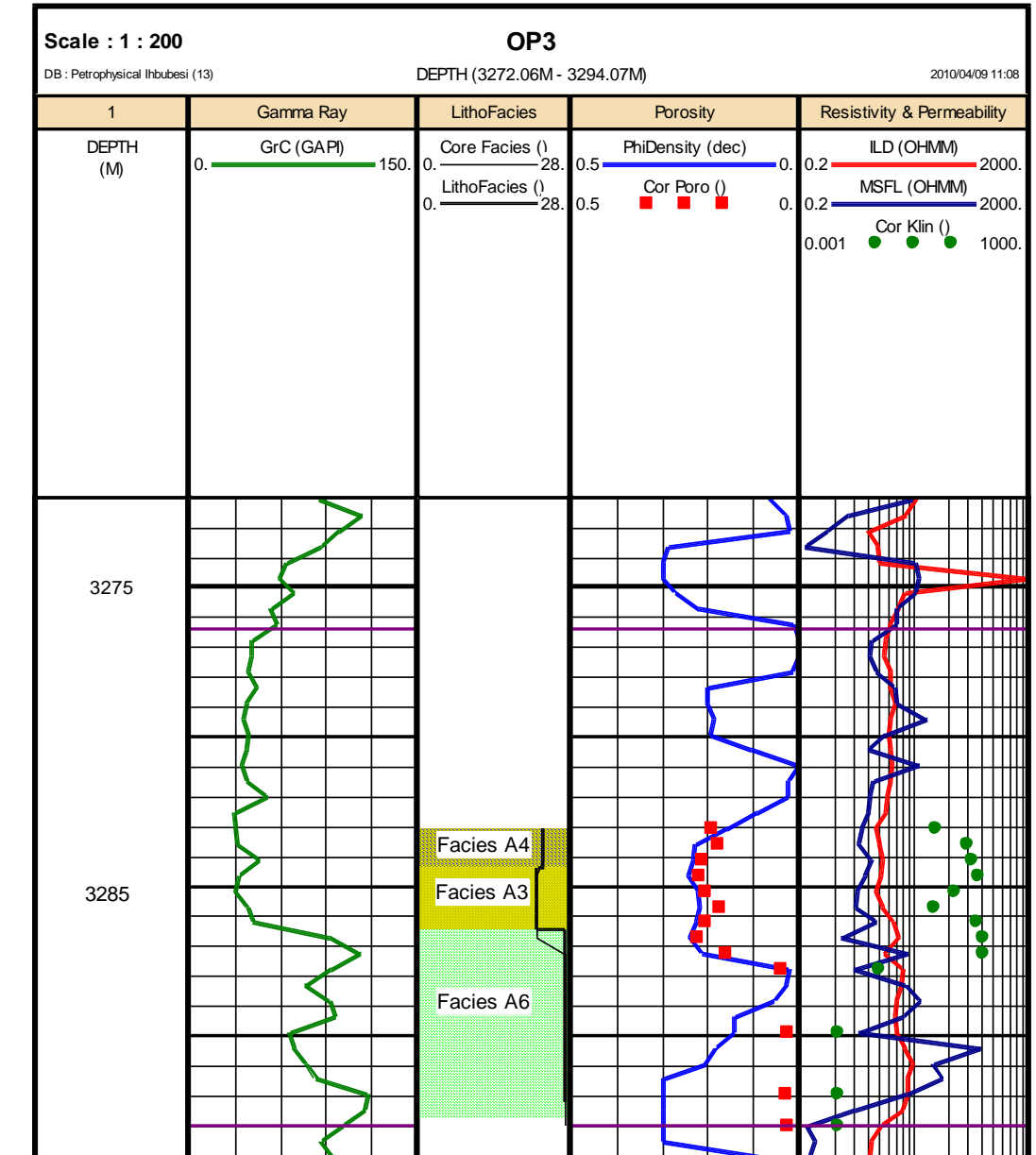


Figure 5.4b: Well OP3 core 2 facies shown in track 3.

5.5 Analysis and Interpretation of Results

5.5.1 Grain Density

The grain density pertains to the density of the solid material of the sample, excluding the pore spaces. The grain density values were calculated from the dry weight and grain volume of the core plugs determined from porosimeter analysis. This was calculated as the ratio of the dry weight to grain volume.

The grain or matrix density is the density of the solid components of a rock excluding the density of the fluids contained in the pores. The value of the grain density depends on the density and proportion of the individual mineral components.

The matrix densities of some common lithology are given in Table 5.7 below:

Table 5.7: Matrix density of common lithology

Lithology	Matrix value (g/cm³)
Clay Minerals	Varies between 2.02 – 2.81
Chlorite	2.81
Illite	2.61
Kaolinite	2.55
Smectite	2.02
Coal	1.19
Halite	2.04
Sandstones(quartz)	2.65
Limestones	2.71
Dolomites	2.85
Orthoclase	2.57
Plagioclase	2.59
Anhydrite	2.98
Siderite	3.88
Pyrite	4.99

(Schlumberger, 2003)

5.5.2 Well OP1 Grain Density

The grain density of well OP1 range from 2.64 to 2.71 g/cc with a mean value of 2.67 g/cc as shown in Figure 5.5 below.

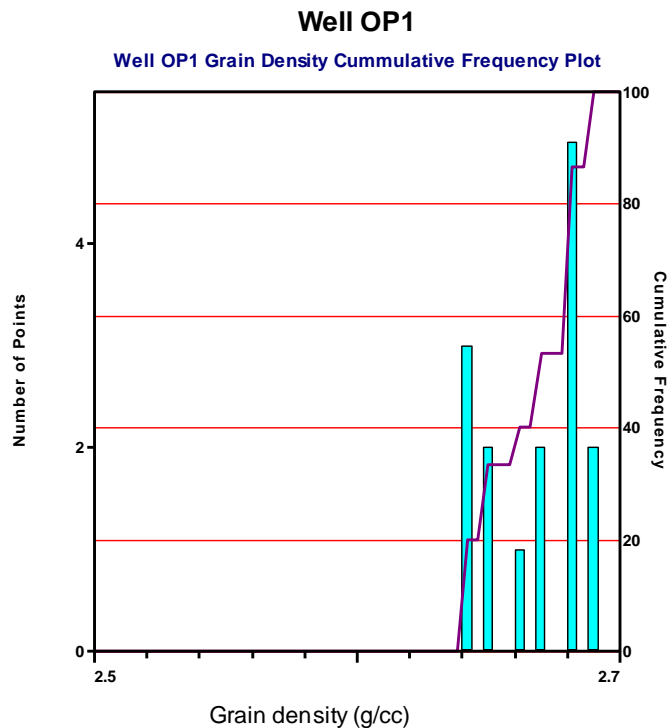


Figure 5.5: Histogram of well OP1 core grain densities.

In a clean quartz sand reservoir, a grain density of 2.65 g/cc is expected. Core results do not indicate persistent carbonate cements because the presence of calcite and dolomite is very insignificant in core analysis results of Table 5.1. The grain density value of 2.71g/cc at measured depths of 3371.4, 3371.65, and 3375.98 m suggest the presence of very thin interval of calcite which was also seen on the core.

A standard deviation value of 0.0242 g/cc was recorded in the histogram plot which implies a mean distribution of 2.649 g/cc to 2.694 g/cc. However, for an accurate determination of the mean value of grain density for sandstones, the grain density values of calcite were excluded.

5.5.3 Well OP2 Grain Density

The grain density of well OP2 determined from the routine core analysis measurements ranges from 2.58 g/cc to 2.77 g/cc with a mean value of 2.69 g/cc (Figure 5.6).

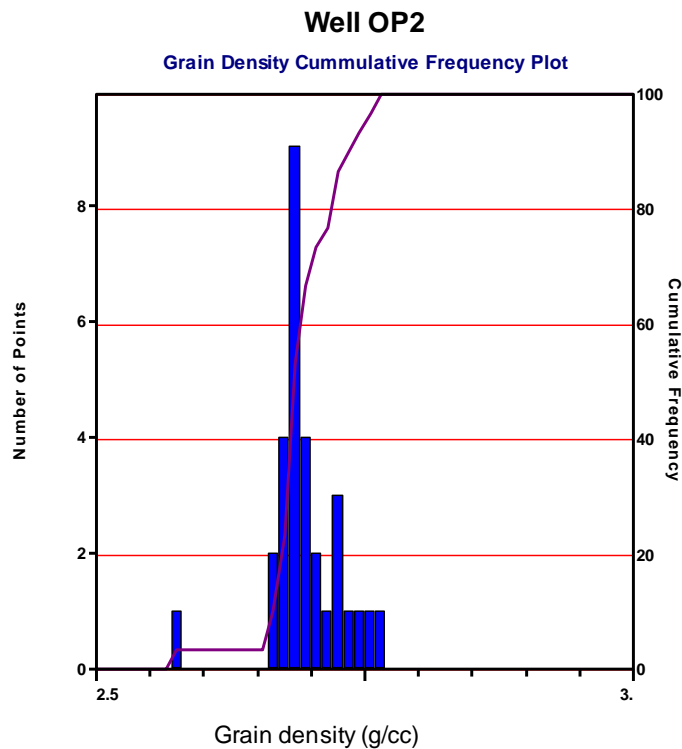


Figure 5.6: Grain density histogram of well OP2

A grain density value of about 2.57 g/cc observed in the histogram could be due to the presence of laminated shaly sandstone. The values of 2.71g/cc to 2.75 g/cc indicate the presence of calcite in four of the samples analysed. The standard deviation which is a number that shows approximately how far the values in the data set deviate from the mean value also present a value of 0.033 g/cc, which implies that the values vary from 2.661 g/cc to 2.7272 g/cc.

5.5.4 Well OP3 Grain Density

In well OP3, two non-continuous core samples were taken for analysis and the grain densities of core 1 ranges from 2.64 to 2.71g/cc with a mean value of 2.69 g/cc while core 2 grain densities ranges from 2.65 g/cc to 2.69 g/cc with mean value of 2.68 g/cc Figure 5.7.

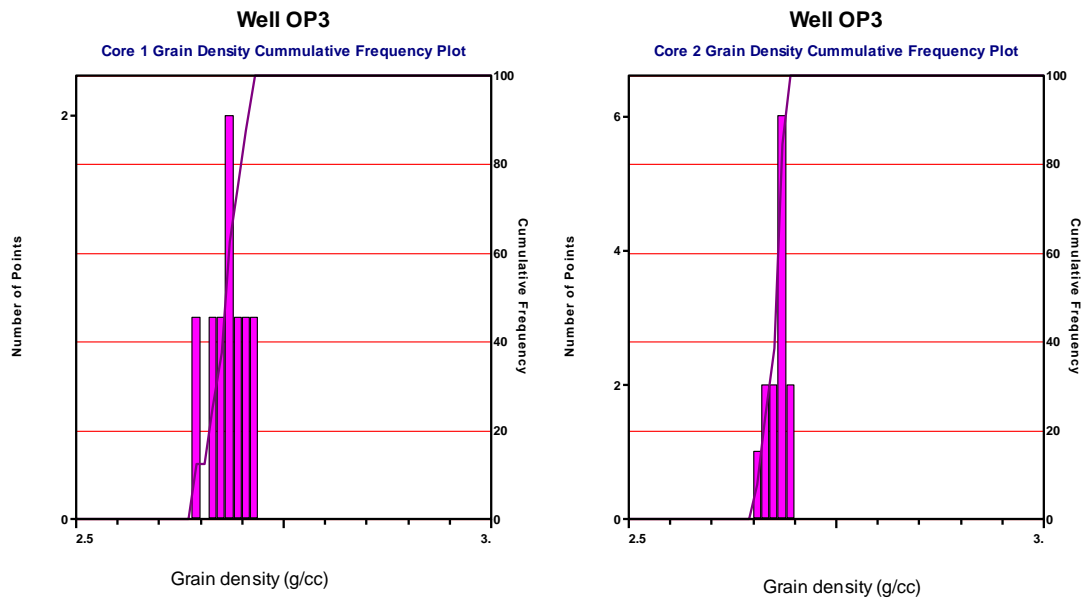


Figure 5.7: Well OP3 core grain density cumulative frequency plot.

The grain density values recorded in core 1 display higher standard deviation value of 0.05 g/cc from the mean which gives a range of 2.64 g/cc to 2.74 g/cc. The high standard deviation value recorded in core 1 may be due to the presence of calcite in two of the samples analysed. The low standard deviation value of about 0.01198 g/cc recorded in core 2 implies a mean range of 2.68 g/cc to 2.71g/cc.

5.5.5 Comparison of Grain Density Distributions for Wells

The grain density value for all the wells with core analysis results showed a range of 2.58 g/cc to 2.76 g/cc with mean value of 2.68 g/cc and standard deviation value of 0.028 g/cc (Figure 5.8) which means variation 2.65 g/cc to 2.71g/cc . The presence of calcite was observed in all the cored wells with relatively small proportion .Well OP2 showed the highest mean grain density with mean value of 2.69 g/cc as against values of about 2.67 g/cc recorded in well OP1 and OP3 respectively. The mean grain density of 2.67 g/cc was obtained from the analysis, excluding that of calcite which will be adopted as the matrix grain density for log analysis.

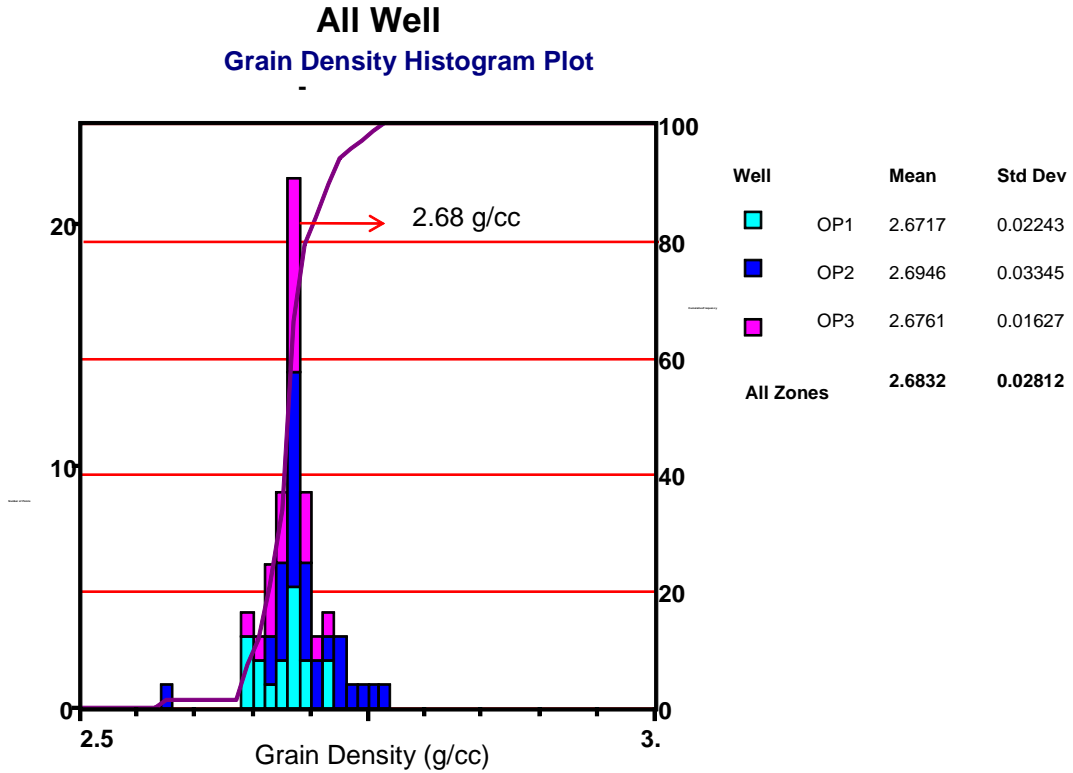


Figure 5.8: Grain density histogram plot for well OP1, OP2 and OP3

5.6 Interpretation of Core Porosity

The porosity of a reservoir rock was defined in chapter three as the percentage of the volume of the rock that is not occupied by the solid framework of the reservoir. This determines the amount of water or other fluids that a rock can contain. Fraser and Gratton (1935) determined the porosity of various packing arrangements of uniform spheres and concluded that the cubic packed system has a porosity of 47.6 % and the rhombohedra or closed packed system has a porosity of 25.9 %.

After cleaning of the core plugs and removal of fluids, porosity is determined from the grain volume and the bulk volume of the sample. Depending on the technique used, different types of porosity are estimated. With a gas expansion method, the connected porosity is measured, while the destruction of the sample to estimate grain volume, a measure of total porosity is obtained.

Determination of the core plug porosities for the wells was done using helium gas based on Boyle's law for gas expansion ($P_1 V_1 = P_2 V_2$). Porosity measurement by gas expansion indicates only pores that are interconnected (effective porosity) thereby

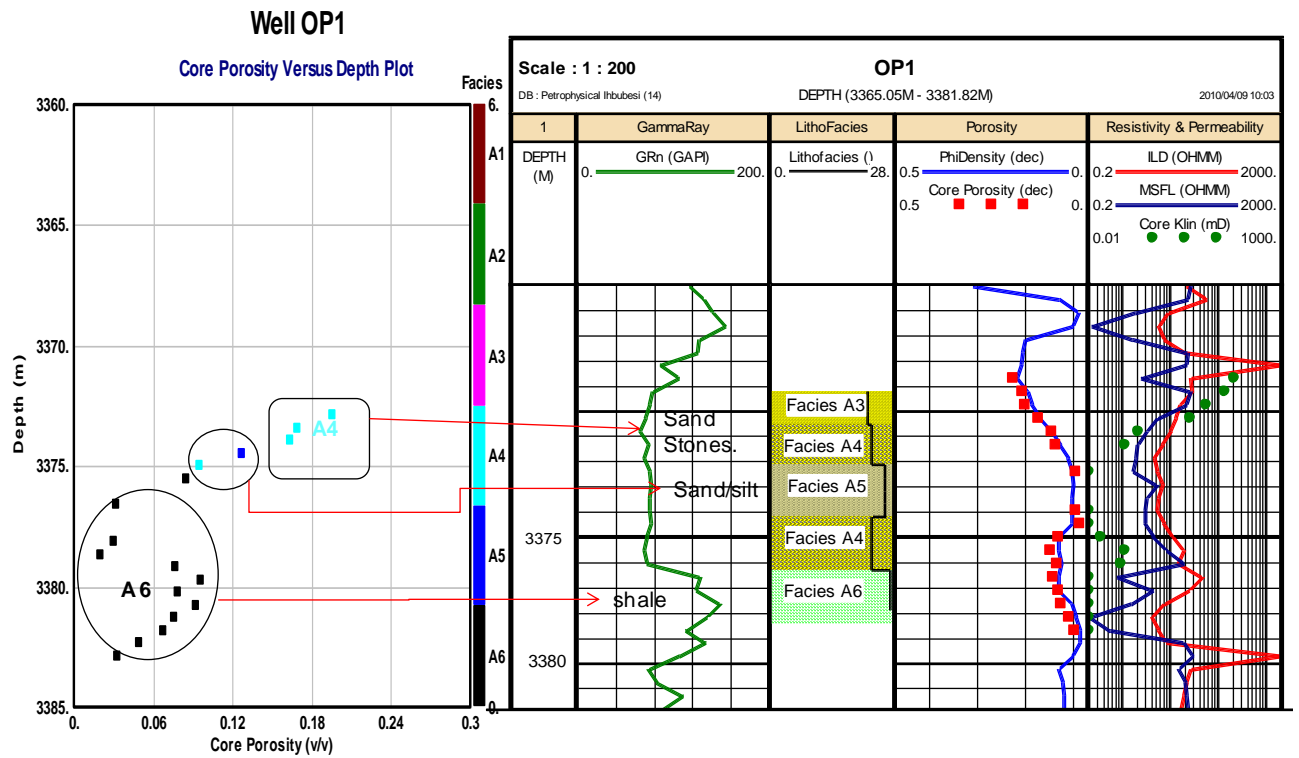
providing a very good estimate of effective porosity for the purpose of reservoir evaluation.

The porosities of petroleum reservoirs range from about 5 % to 45 % and factors determining the magnitude of porosity in sediments are grain sorting, degree of cementation or consolidation, amount of compaction and methods of grain packing (Djebbar, 1999). If all the grains are of the same size, sorting is said to be good and porosity may be high. If grains are of many sizes and are mixed together, sorting is regarded as poor and porosity in that condition will be reduced. Poorly sorted sediments usually have lower porosity because the fine grained fragments tend to fill in the open space.

Cementation that takes place during diagenesis also tends to fill in the pore space, so highly cemented sedimentary rocks have lower porosity than poorly cemented sedimentary rocks. Although, round grains and a high content of grain cement gives a high porosity, and angular grains and low cement content gives lower porosity.

5.6.1 Well OP1 Porosity

The core porosity values of well OP1 ranges from 1.2 % to 20.2 % at the cored interval. The low porosity values were observed in intervals that are associated with claystones and siltstone interbedded lamina. The relatively high porosity interval was observed in massive sandstones intervals that are very fine to fine grains and are well sorted as observed in depth of 3368.5 to 3369.2 m (Figure 5.9a). In this well, the decrease in porosity is observed in the rocks associated with clay. The core porosity histogram of well OP1 is given in Figure 5.9b below.



Facies A4 is a reservoir sand and A 6 is non-reservoir facies

Figure 5.9a: Well OP1 Core Porosity versus depth Plot.

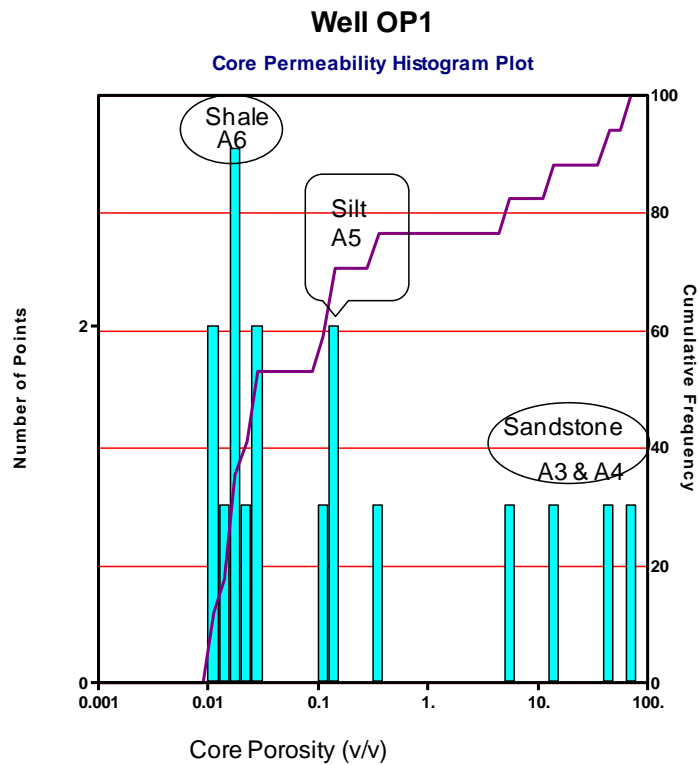


Figure 5.9b: Histogram of porosity distribution for well OP1

The porosity histogram plot of this well showed an average porosity value of 9.9 % (Figure 5.9b) above. A standard deviation value of 5.3 % was recorded which ranged from 4.7 % to 15.2 %.

The high cumulative frequency values observed within the shaly/sand interval showed that the interval of core measured porosity is predominantly of shaly/sand formation.

5.6.2 Well OP2 Porosity

The porosity value of this well range from 3.27 % to 24.25 % with mean value of 15 % within the cored interval .Two different zones were observed, one with decreasing porosity values at depth 3450 m to 3469 m and the other with slightly increasing values at depth 3460 to 3472 m (Figure 5.10a) below.

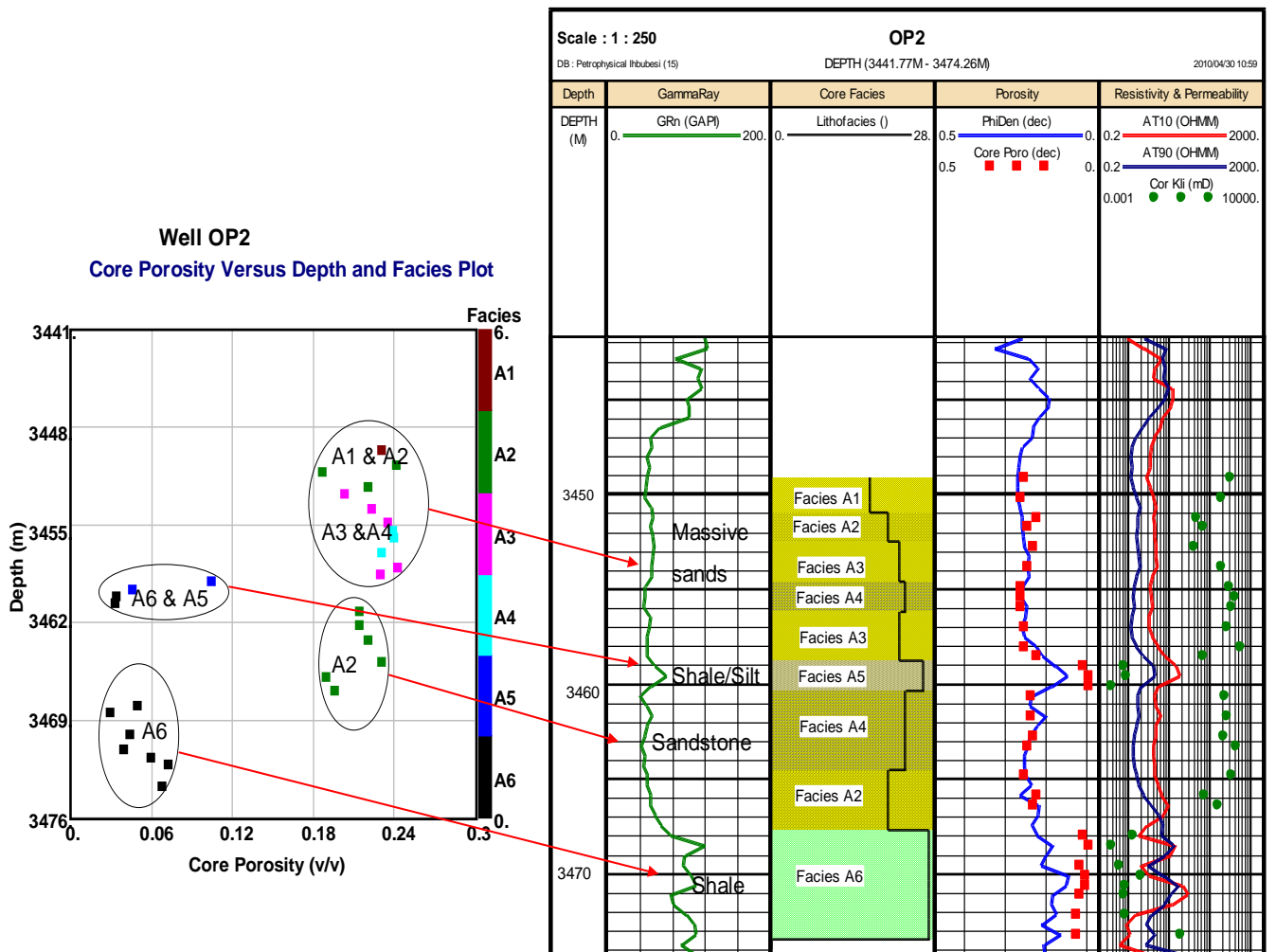


Figure 5.10a: Well OP2 porosity versus depth plot.

The high porosity intervals are medium fine and well sorted sandstones, while the low porosity values are associated with laminated shaly intervals.

On the porosity histogram, a bimodal frequency were observed showing the shaly/silt mode and the clean sandstone mode, with mean value of about 15 % recorded within the cored interval with standard deviation value of about 8.4% which implies a variation of 6.8 % to 23.7 % (Figure 5.10b).

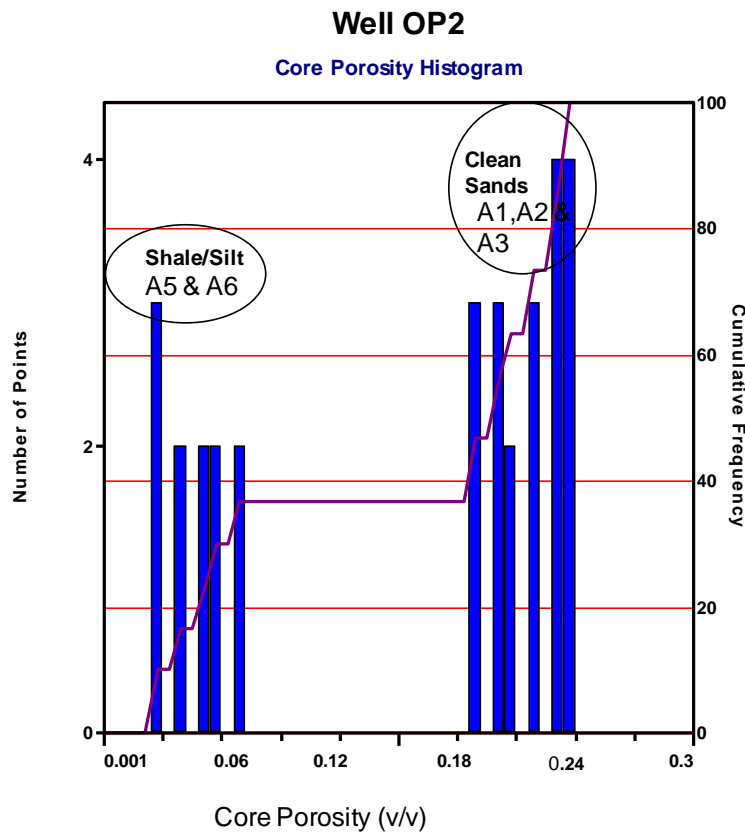


Figure 5.10b: Well OP2 core porosity histogram and plot against depth.

The differences in variations of porosity in the zones may be attributed to the type of facies present in each zone. The interval of porosity values less than 6 % is comprised mostly of facies A5 and A6 which is shaly/silt and shale intervals. The interval with porosity values of more than 18 % is comprised of the clean sandstones of facies A1, A2 and A3 respectively.

5.6.3 Well OP3 Porosity

The porosity value of well OP3 ranged from 0.6 % to 24.2 % in core 1 and 2.3 % to 23.3 % in core 2 within the cored intervals. The silty claystones interval in core 1 contribute to the low porosity values observed while the massive sandstone units that are very fine to fine, well sorted with occasional calcite intervals are with high porosity values (Figure 5.11a).

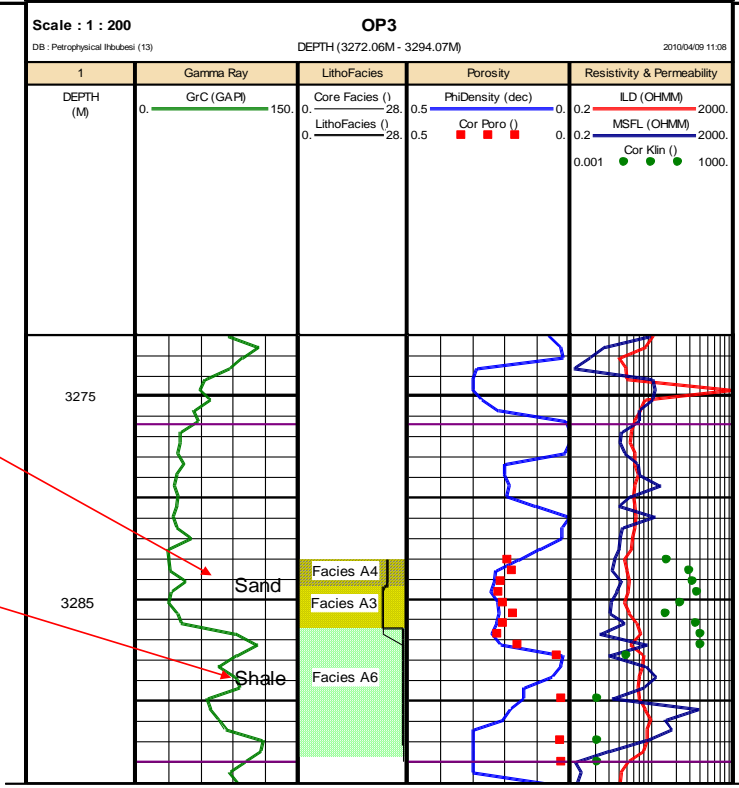
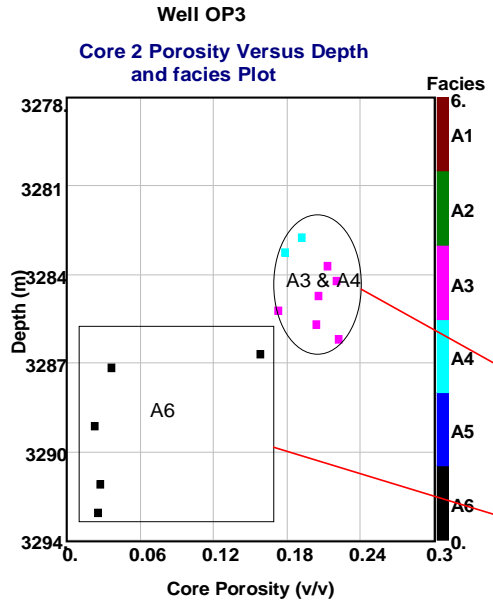
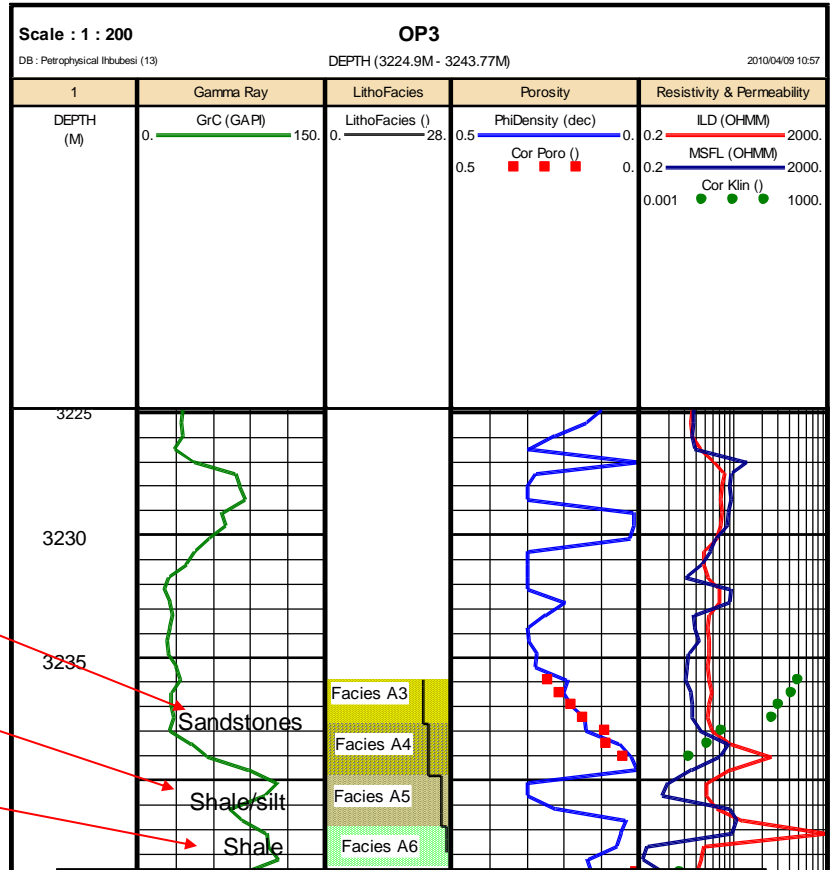
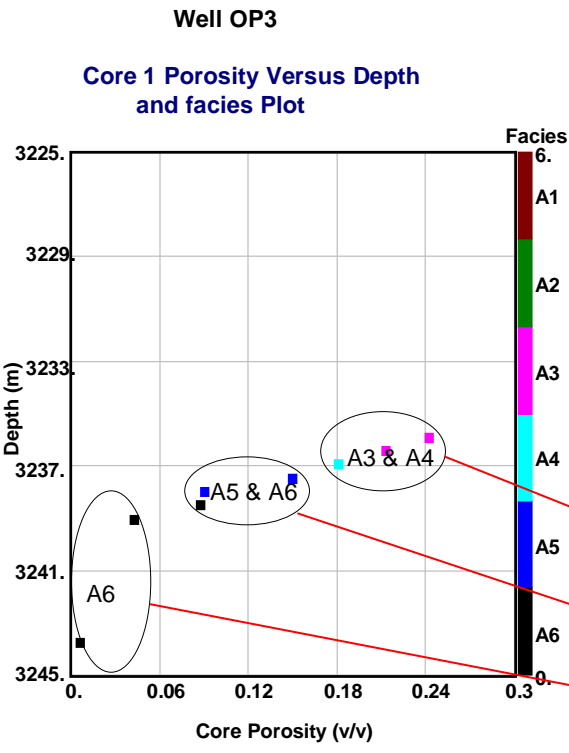


Figure 5.11a: Well OP3 porosity versus depth plot

The core porosity histogram for well OP3 is presented in Figure 5.11b below.

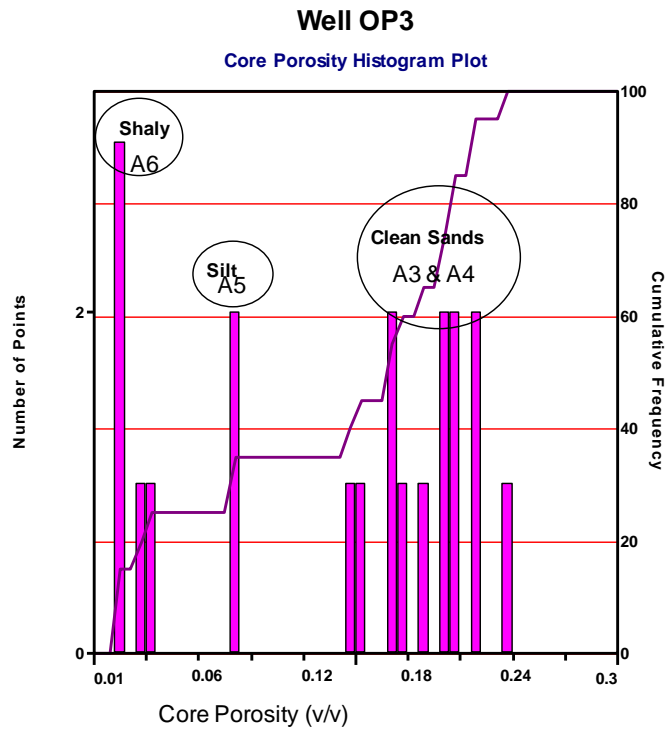


Figure 5.11b: Histogram of well OP3 core porosity distribution.

The histogram showed three different porosity zones. One zone was showed porosity values of less than 3 % which is comprised of facies A6. Another zone showed porosity values between 6 to 10 % and is predominantly of facies A5. A zone of porosity values of more than 12 % was also observed from the histogram plot which is comprised of clean sandstones and facies A3 and A4.

The differences in porosity may be due to the nature of sediments that are associated in area as shown in the core data. The low porosity intervals are observed in claystones and silty vertical burrow intervals while the high porosity values are in the very fine to fine grains sandstones.

5.6.4 Porosity distribution for wells

The histogram of porosity distribution for all wells is presented in Figure 5.12a below.

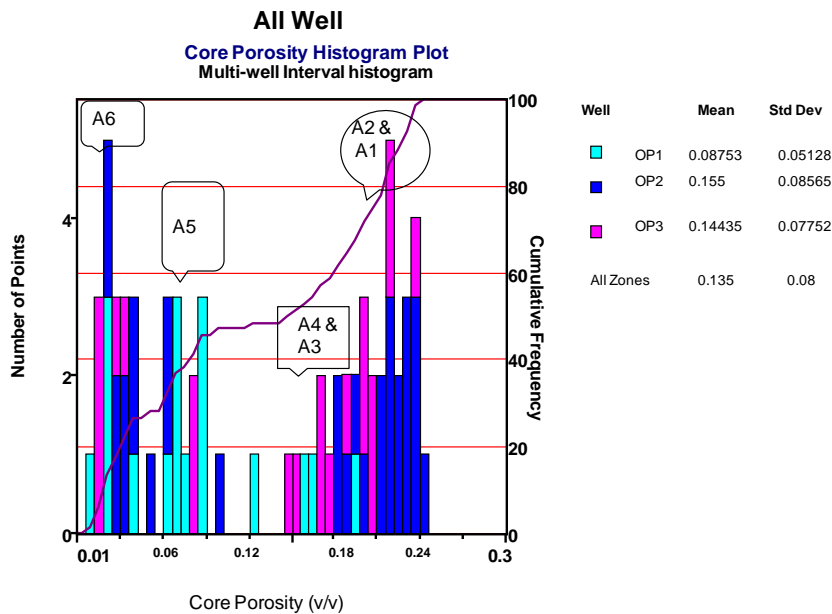


Figure 5.12a: Histogram of Porosity distribution for wells.

Two distinct areas were observed on the histogram, an area of low porosity values and an area of high porosity values. The zone of porosity values of less than 10 % is comprised of facies A6 and A5. The area of porosity values between 12 to 18 % is comprised of facies A4 and A3, while facies A2 and A1 dominates the intervals with porosity values greater than 18 %.

An average porosity value of 13.5 % was recorded on the histogram plot with a corresponding standard deviation value of 7%.

The low porosity values recorded are due to the presence of clay/silt in such intervals while the high porosity values are associated with clean sandstone intervals.

The histogram plot of the low porosity interval is presented in Figure 5.12b below.

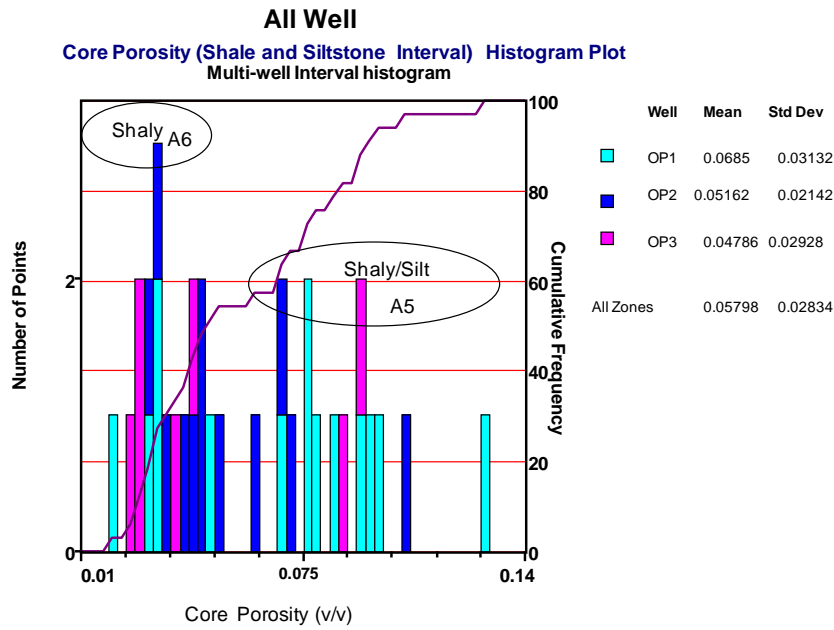


Figure 5.12b: Histogram of Core Porosity Shaly/Silt interval for all well.

The low porosity values were dominant in well OP1 within the shale and siltstone intervals of the histogram and generally features in entire well. The plot clearly showed the distinctions between the shaly and silty intervals with an intermediary porosity value of approximately 6 % .

The high porosity value as plotted in the histogram (Figure 5.12c) below shows area of massive sandstone intervals with well sorted grains that are well sorted with medium to fine grains in the well.

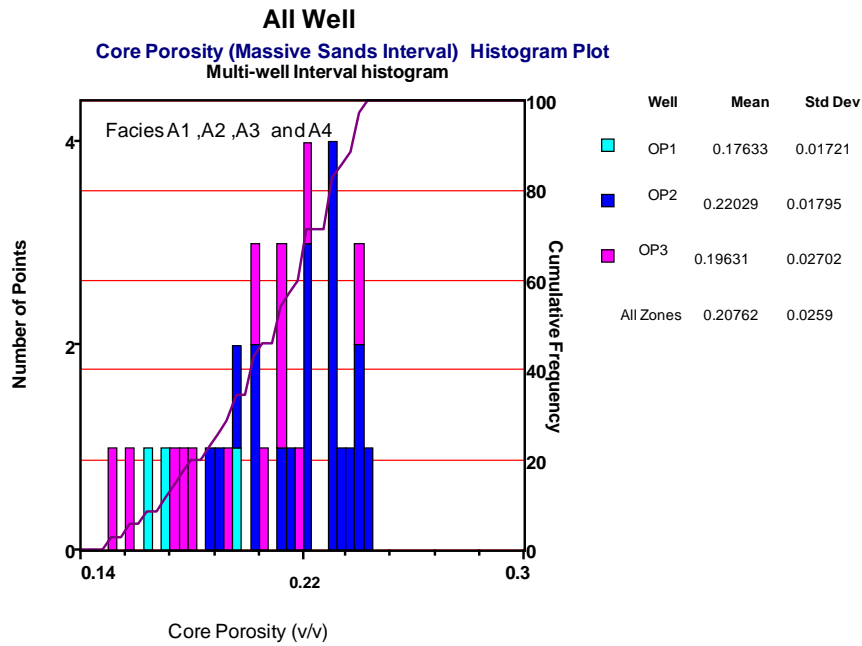


Figure 5.12c: Histogram of core porosity massive sands for Wells.

The histogram plot present well OP2 as the dominant well in the most porous intervals of the plot and well OP3 with the least porosity values recorded in the interval.

5.7 Interpretation of Permeability

The permeability of a rock which is the ability of the rock to allow fluids to flow through its connected pores is controlled by rock grain size, grain shape, degree of cementation or consolidation, grain packing, and clay. Permeability of reservoir rocks may vary from less than 1 mD to over 1000 mD.

To determine the permeability of the core plugs, the plugs were placed in a compliant sleeve within a cylinder. A pressure on the sleeve ensures that the injected gas or liquid flows parallel to the core plug axis. Fluid, usually gas is injected with an inflow pressure and flows almost linearly through the plug to atmospheric pressure. The permeability is then determined from Darcy's law. Due to difference in flow physics between gas and liquid especially in low permeable media, a correction is done on the gas or air permeability which is known as Klinkenberg Correction. The permeability values are reported as permeabilities to air and liquid (corrected for the Klinkenberg

effect). Gas permeability corrected for the Klinkenberg effect is considered equivalent to the permeability if a liquid medium is present in the pores.

The quality of a reservoir as determined by permeability in mD may be scaled as shown in the Table 5.8 below:

Table 5.8: Permeability classification scale

Permeability Values (mD)	Classification
Less than 1	Poor
Between 1 and 10	Fair
Between 10 and 50	Moderate
Between 50 and 250	Good
Above 250	Very Good

(Modified after Djebbar, 1999)

5.7.1 Well OP1 Permeability

The permeability of well OP1 was measured horizontally and vertically. The horizontally measured permeability is accepted as the rock permeability because it is measured parallel to the bedding which is the major contributor to fluid flow into a typical reservoir.

The permeability values of this well were reported as permeability to air and liquid (corrected for the Klinkenberg effect). Gas permeability corrected for the Klinkenberg effect is considered equivalent to the permeability if a liquid medium is otherwise present in the pores. The air permeability values ranges from 0.01 mD to 108 mD and the liquid permeability values from 0.01 mD to 96 mD. Air permeabilities measure higher than the liquid permeabilities.

For consistencies, the liquid permeability values are used in this study. Plot of permeability in log scale against depth in linear scale is given in Figure 5.13a below.

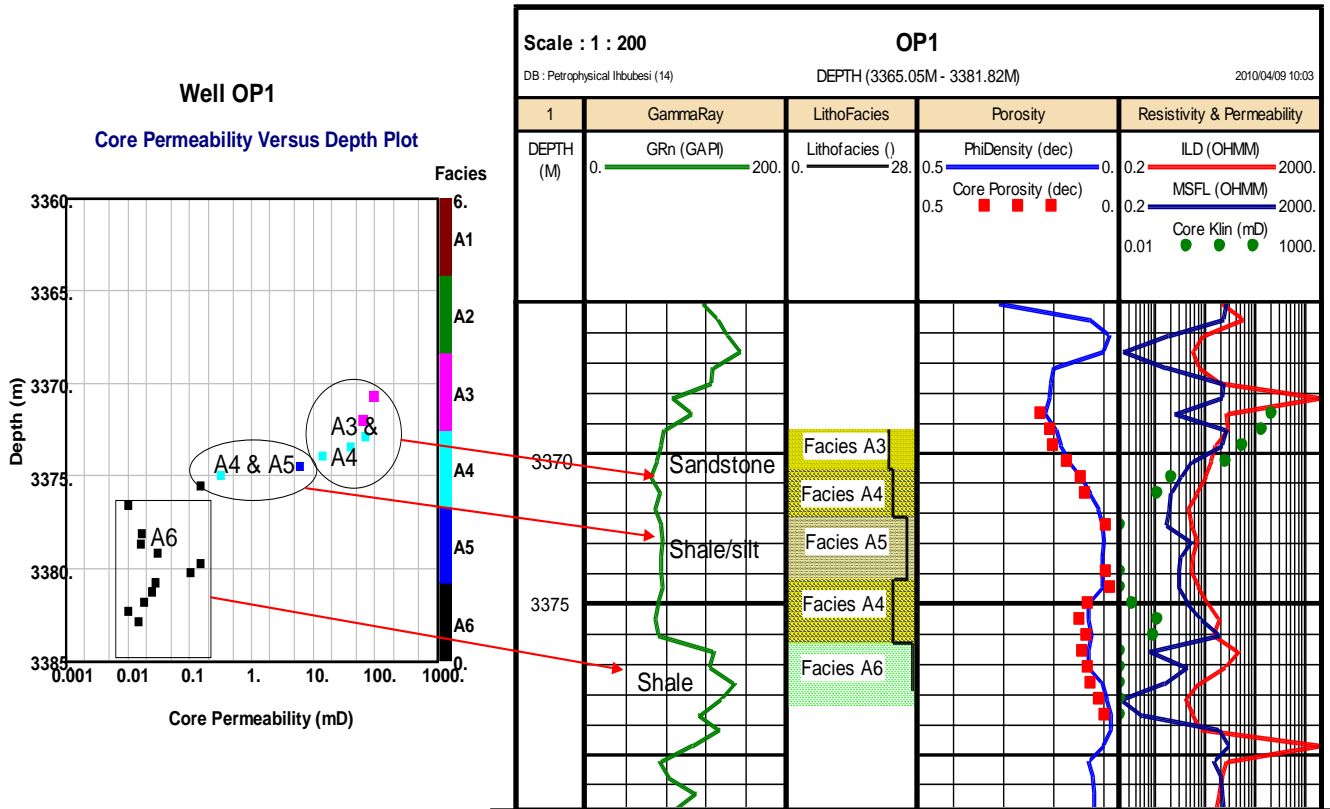


Figure 5.13a: Well OP1 permeability versus depth Plot.

The poor permeability values (<1 mD) shown in the depth interval of 3381 m to 3383.15 m in the plot is because of the claystones lamination interval which act as a barrier to the permeability and comprised of facies type A6. Moderate to good permeability values were indicated in depth interval of 3370.0 m to 3372 m. This may be attributed to the very fine to fine grain sandstone interval that is well sorted, though with the presence of calcite cement. This sandstone interval is made up of facies A3 and A4.

The histogram plot of the core permeability of the well is presented in Figure 5.13b below.

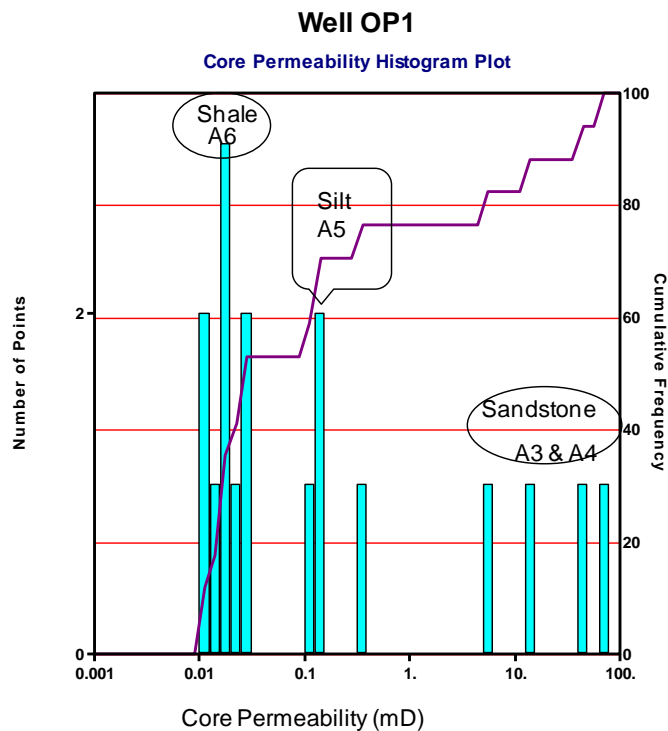


Figure 5.13b: Well OP1 Permeability Histogram Plot

The histogram plot showed three distinct zones. A shale zone or area was observed with permeability values of less than 0.1mD and comprised of facies A6 which is regarded as a non-reservoir facies. Another zone observed was of siltstone that is composed of permeability values in the range of 0.08 mD to 0.5 mD which is comprised of facies A5. Sandstones with permeability values exceeding 8mD were also observed and correspond to facies A3 and A4.

5.7.2 Well OP2 Permeability

The permeability values of this well were reported as Klinkenberg corrected (Klin) in mD and permeability to air (Kair) in mD. The values of the Klinkenberg corrected permeability ranges from 0.003 mD to 1074 mD and permeability to air ranges from 0.006 mD to 1095 mD. It was observed that the permeability to air is higher than Klinkenberg corrected permeability because it has been converted to equivalent liquid values. The plot of Klinkenberg corrected permeability in log scale to depth in linear scale is depicted in Figure 5.14a below.

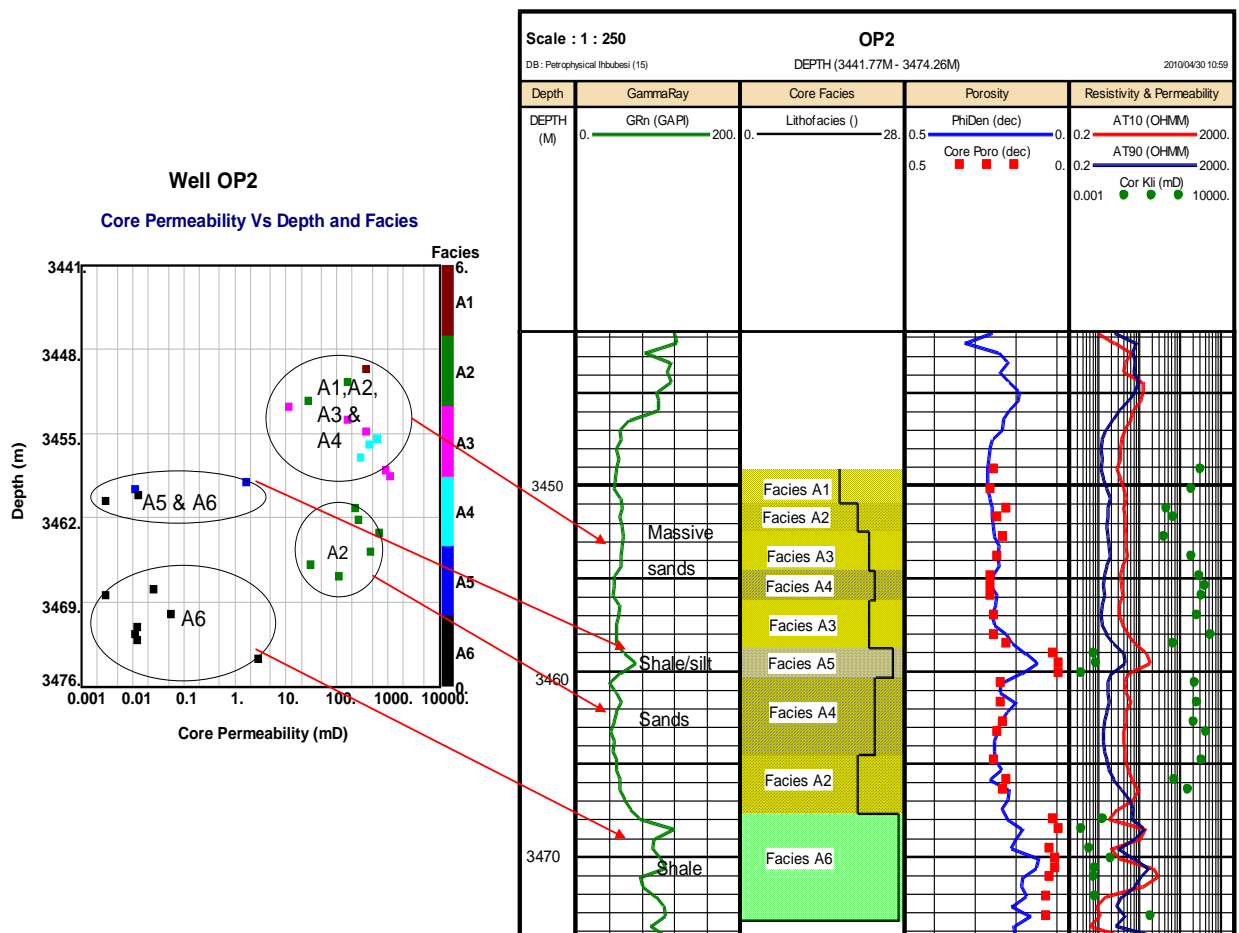


Figure 5.14a: Well OP2 Depth versus permeability plot.

The massive clean sandstone interval present good to very good permeability values and is associated with core facies types A1 and A2. The sand with sparingly distributed siltstone interval showed fair to good permeability values which are attributed to the presence of silt in the interval and corresponds to facies A3 and A4. The silt interval lies between the sand and shaly interval and corresponds to facies A5. A poor permeability interval was also observed in the plot and corresponds to the non-reservoir facies A6. The permeability histogram (Figure 5.14b) is presented below.

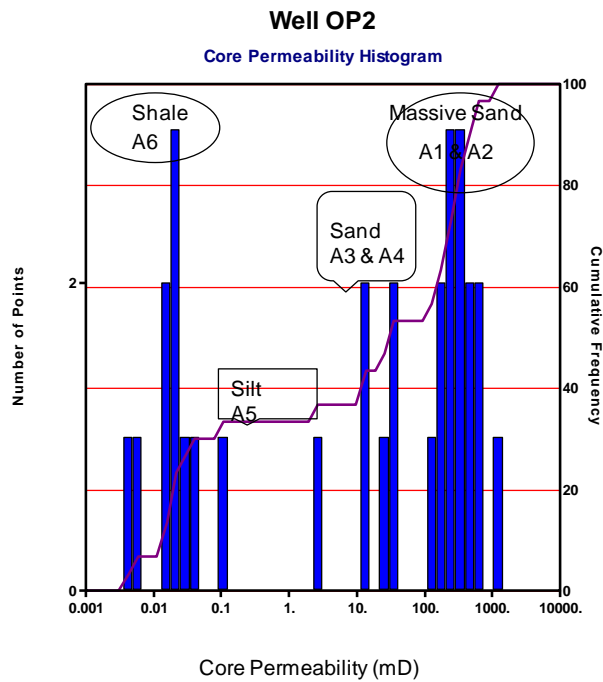


Figure 5.14b: Well OP2 permeability histogram plot.

Four intervals were delineated in terms of permeability and facies on the histogram plot as shown in Figure 5.14b above. The shale interval has permeability values of less than 0.1mD which represents facies A6. Next to this interval is the siltstone which has permeability values between 0.1mD to less than 10 mD. The sandstone intervals represented by facies A3 and A4 showed permeability values of 10 mD to less than 100 mD .The massive clean sandstone intervals showed permeability values higher than 100 mD and is dominated by facies A1 and A2. This is the best reservoir sandstones observed in terms of permeability interpretations and the worst permeability values were observed in facies A6 which is non-reservoir sand.

5.7.3 Well OP3 Permeability

The liquid permeability values of core 1 ranges from 0.02 mD to 140 mD and permeability values to air ranges from 0.04 mD to 156 mD. In core 2 of the same well, the liquid permeability value ranges from 0.01 mD to 69 mD and permeability to air from 0.013 mD to 79 mD. The reduced permeability values recorded in both cores may be attributed to the type of facies that is present in such interval.

The plot of permeability in log scale -depth in linear scale is shown in Figure 5.15a below.

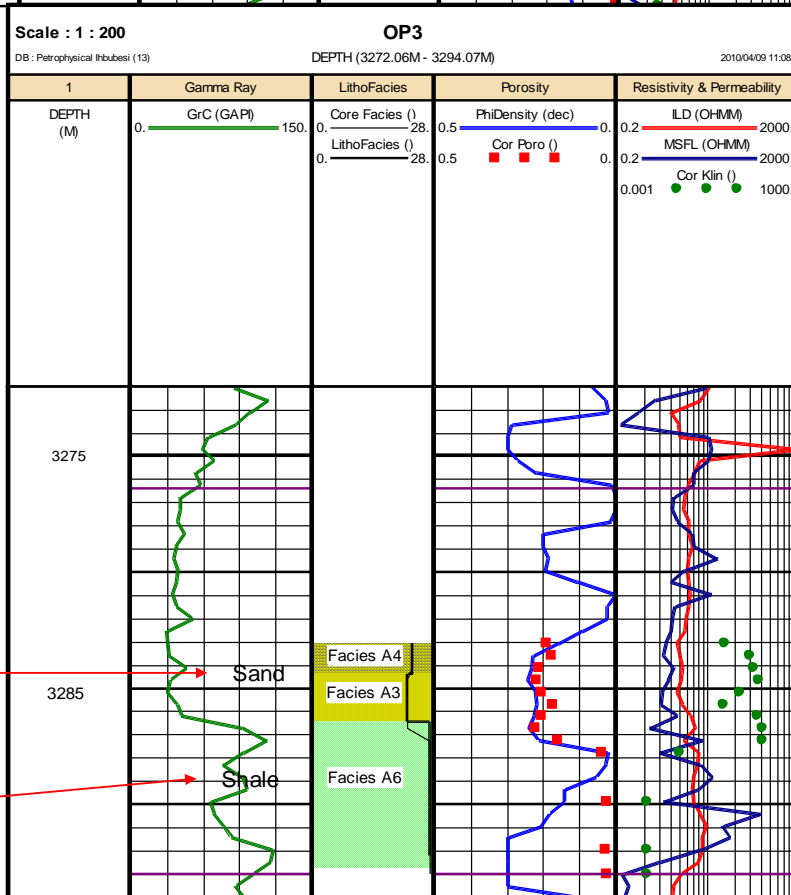
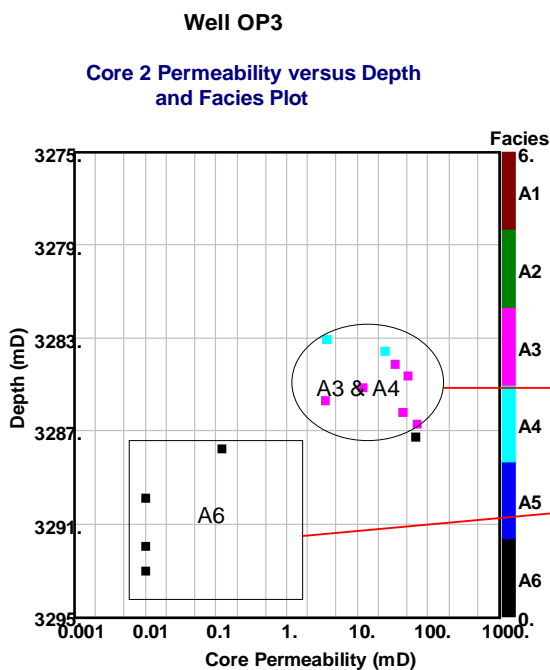
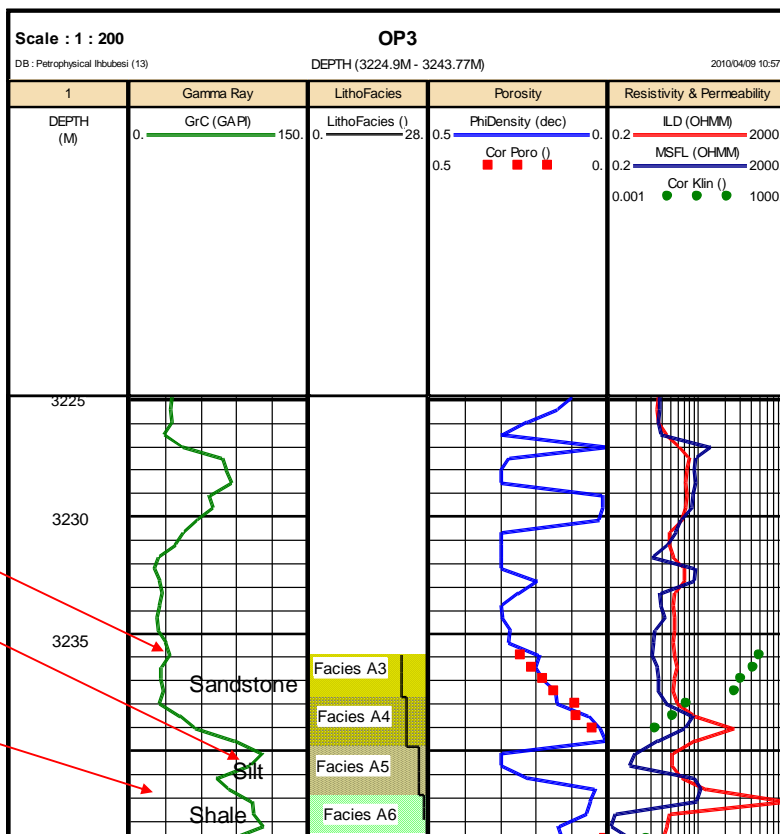
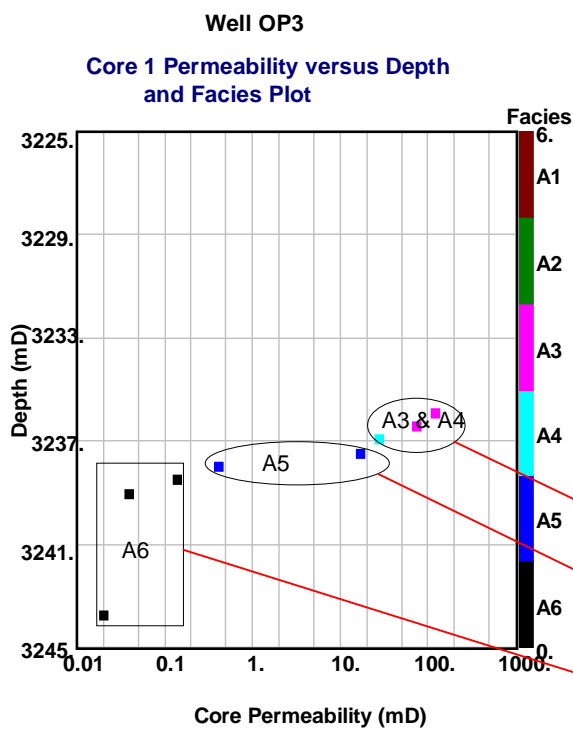


Figure 5.15a: Well OP3 depth-permeability plot.

Core 1 permeability values which are indicated between 3230 m to 3244 m on the plot shows a relatively fair to good permeability values within the massive sandstone interval and poor values at shaly sand interval.

A similar pattern of fair to good permeability was also observed in the sand interval of core 2 between 3283 m to 3300 m. A constant permeability value of 0.01 mD was observed at interval of 3290 m to 3292.79 m which is associated with claystones and siltstone that are vertically burrows. The moderate to good permeability values noticed in both cores may be attributed to the massive sandstones that are well sorted. Facies type A3 and A4 for this well are the dominant facies in the sand interval while facie A5 dominate the shaly-sand interval of poor permeability values as shown in the plots Figure 5.15a above.

The histogram plot is presented in Figure 5.15b below.

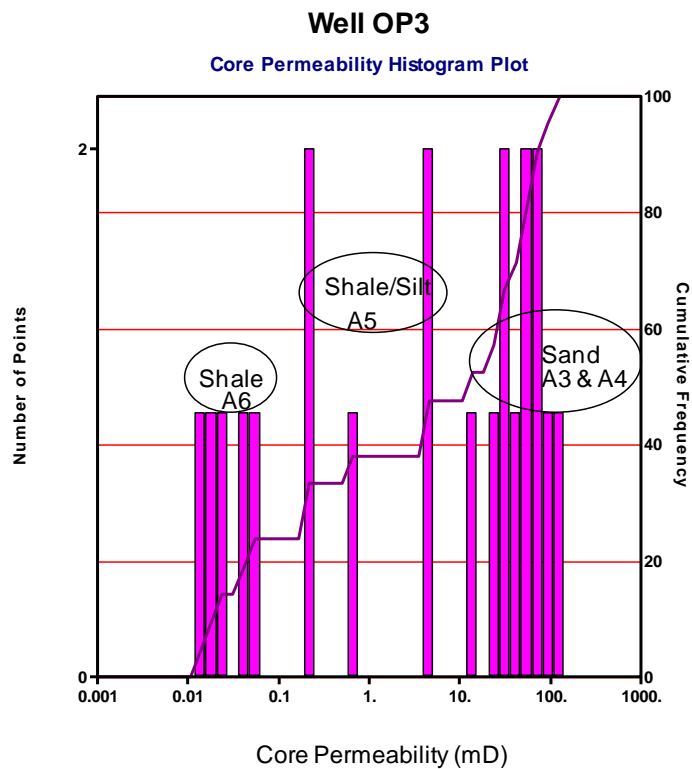


Figure 5.15b: Well OP3 core1 and 2 permeability histogram plot.

The shale intervals have permeability values of less than 1 mD and represented by facies A6. The shale/silt interval showed values of permeability in range of 0.1mD to less than 10 mD. The massive sand intervals correspond to facies A3 and A4 with permeability values in range of 10 mD to 100 mD.

5.7.4 Permeability Distribution for wells

A histogram plot for the entire wells is presented in Figure 5.16 below.

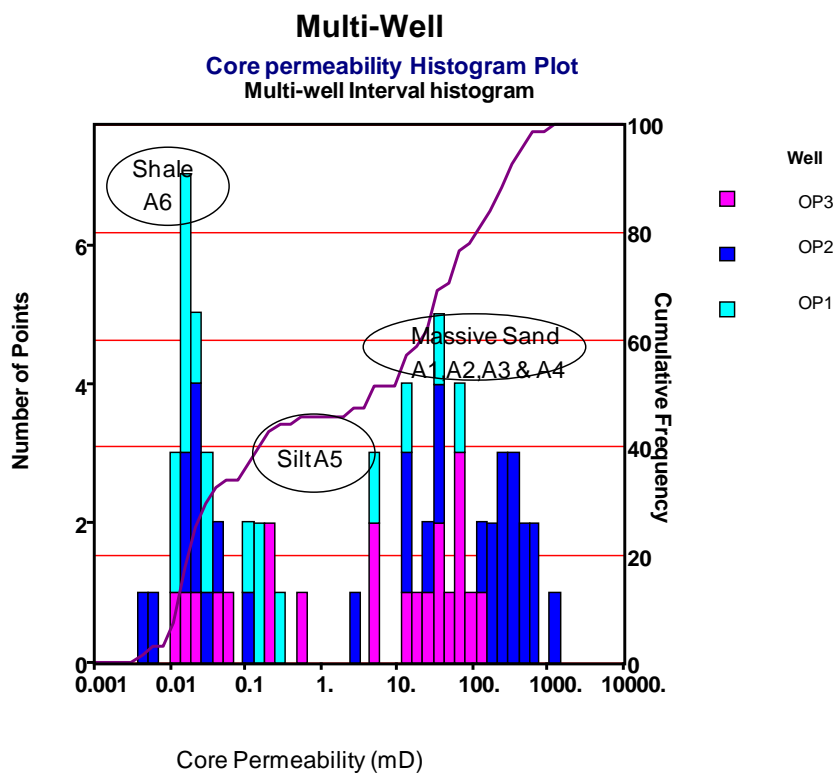


Figure 5.16: Permeability histogram for Wells.

From the histogram plot, three different areas in terms of permeability distribution were delineated. An area of poor permeability values less than 0.1mD was classified as the non reservoir rock (shale) and corresponds to facies A6. Poor to fair reservoir quality rocks was observed with permeability values in the range of 0.1mD to less than 10 mD and correspond to facies A5. Another area of moderate to very good

permeability values greater than mD was also delineated in the permeability plot and represents the massive sandstone interval that corresponds to facies A1, A2, A3 and A4 respectively.

This massive sandstone interval was regarded as the best reservoir rock in terms of permeability distribution.

Well OP2 dominate the good permeability area while well OP1 dominates the poor permeability area. The modal class was noticed at permeability value of 0.01 mD centred on well OP1 and OP2.

The distribution of permeability for all the well investigated showed that good reservoir rocks and best facies are located at the top of the reservoirs and the poor permeability were observed to be predominant in the lower part of the reservoirs and consists of facies A5 and A6.

5.8 Interpretation of Fluid Saturation

The saturation of a formation is regarded as the fraction of its pore volume occupied by the fluid. The symbol used for saturation is S and various subscripts are used to represent saturation of different fluids. In this study the symbol used to represent water saturation is S_w . Oil saturation is S_o , Gas saturation is S_g , and hydrocarbon saturation is S_h .

The summation of all saturations in a given rock must equal 100 %, and water saturation of a formation can vary from 100% to much smaller percentage but will never be zero because there is always a small amount of capillary water or irreducible water that cannot be displaced. Also for an oil or gas bearing reservoir rock, all the hydrocarbon saturation cannot be removed or displaced, some of the oil or gases remain trapped in the pore volume and this hydrocarbon saturation is regarded as residual oil saturation.

The fluid saturation was determined by using the plug-end trims of the core plug The method used involves using both heat and organic solvent to extract the pore fluids and is called Dean-Stark extraction.

5.8.1 Well OP1 Fluid Saturation

Three types of fluid saturation values (saturation of gas, S_g , Saturation of oil S_o , and saturation of water S_w) were reported in well OP1. The average saturation of water (S_w) measured was 57 %; gas saturation (S_g) of 38 % and oil saturation of approximately 5 % was measured as presented in Figure 5.17 below.

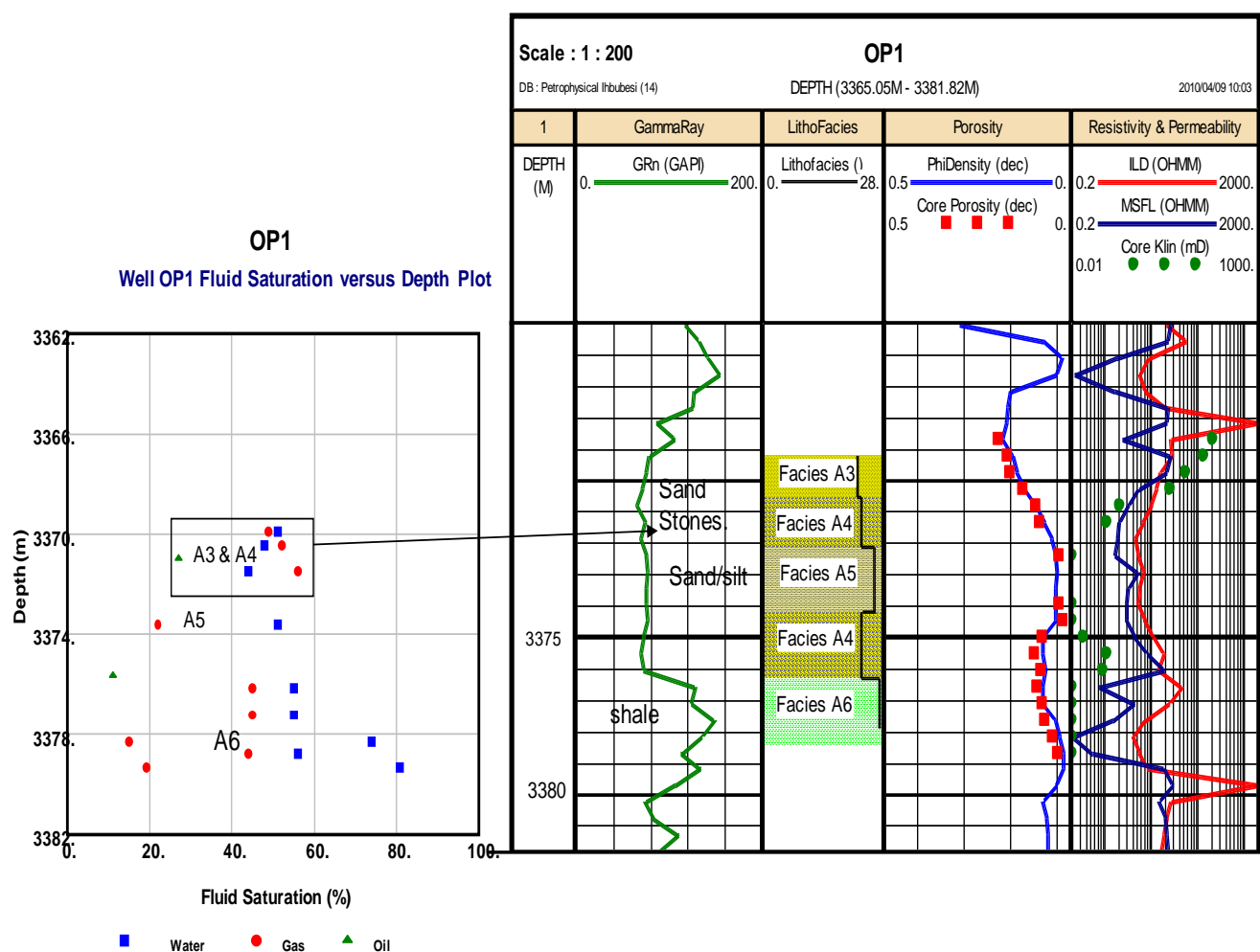


Figure 5.17: Well OP1 fluid saturation versus depth plot.

The plot of fluid saturation versus depth present an interval of increasing hydrocarbon saturation at depth 3370 m to 3373 m which corresponds to facies A3 and A4. The presence of decreasing water in this interval may represent irreducible water

saturation. Below this interval at facies A4, the water and hydrocarbon saturation was constant to a depth of about 3378m which suspected to be the transition zone. The water saturation tends to increase with a decrease in gas saturation at depth 3376m which correspond to facies A6.

5.8.2 Well OP3 Fluid Saturation

In core 1 of well OP3, the fluid saturations reported were water saturation (S_w) with an average value of 62 % and gas saturation of an average value of 38 %. No oil saturation was observed in this interval. At depth of 3236.5m to 3238m (Figure 5.18a) below, a decrease in water saturation was noticed from 60 % to about 40 %, while the gas saturation at this interval increases from 40 % to 60 % and correspond to facies A3 and A4. Sample for fluid saturation determination was not performed on facies A5. At measured depth of 3242 m (facies A6), gas and water saturation were observed at 18 % and 84 % respectively.

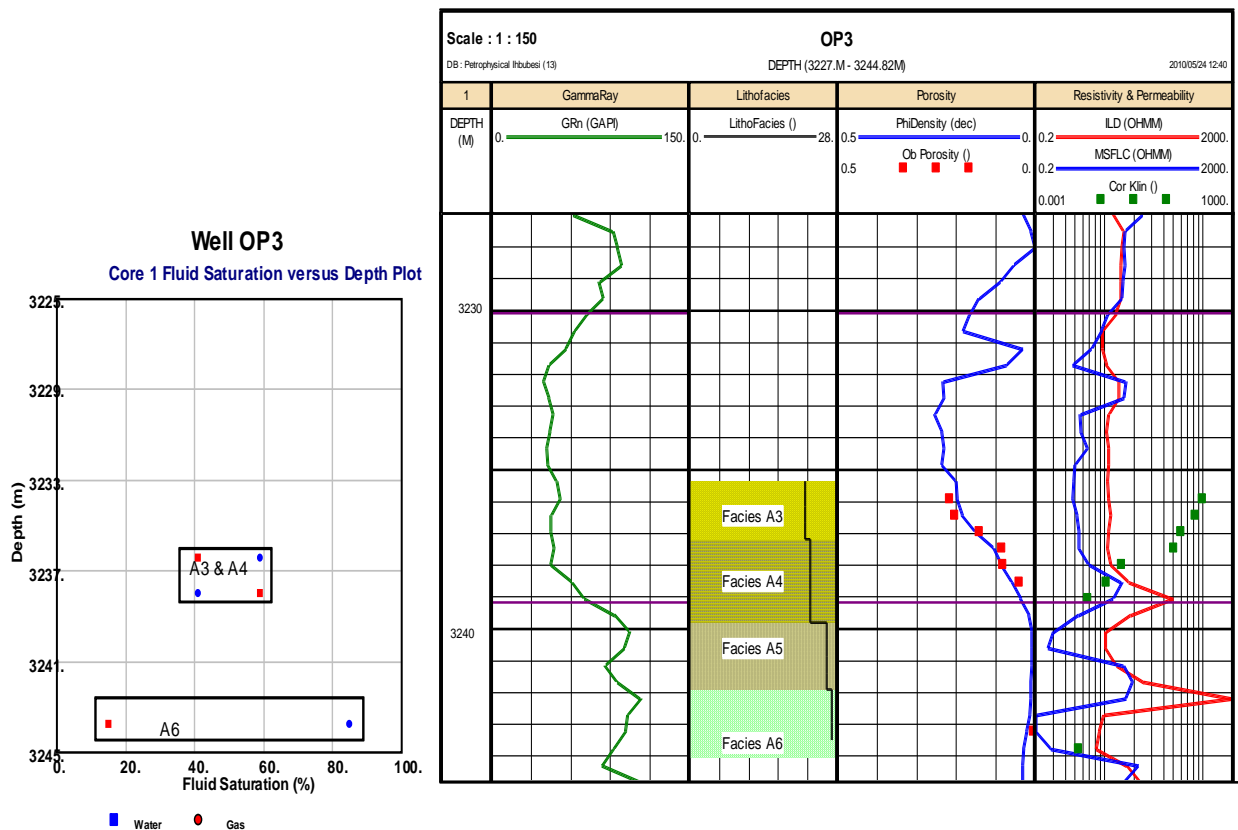


Figure 5.18a: Well OP3 core 1 fluid saturation versus depth plot.

In core 2 of well OP3 (Figure 5.18 b) below, the average water saturation determined was 65 % and gas saturation of 35 %, no oil saturation was measured. An increase of gas saturation from about 30% to 48% was noticed at depth 3283.2m to 3287.9m (facies A3 and A4) and a corresponding decrease in water saturation from 70 % to about 54% was also observed. At facies A6 relatively constant saturation of water and gas saturations were observed which is suspected to be the transition interval.

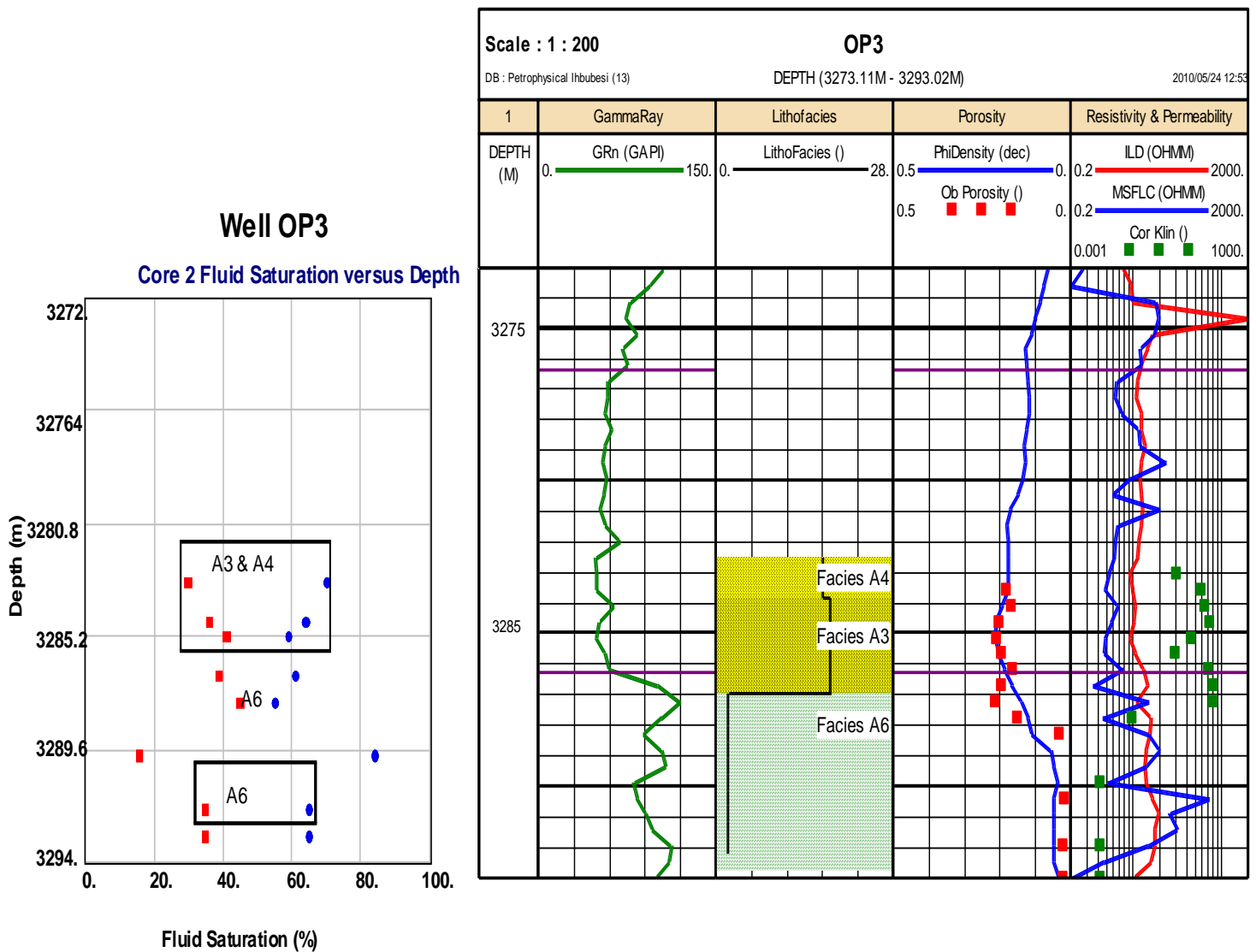


Figure 5.18b: Well OP3 core 2 fluid saturation versus depth plot

5.9 Comparison of Porosity- Permeability and Facies Distribution

The porosity-permeability cross plots are used to distinguish between rock types and also show the trend between porosity and permeability. Porosity-permeability and facies relationships vary from exploration well to well. The Klinkenberg Permeability measured in mD is plotted on a logarithmic scale (y-axis) versus the porosity measured as fraction is plotted on a linear scale (x-axis), and facies were assigned linear values based on description were plotted on the (z-axis). The purpose of the z-plot is to show the distribution of four variables (porosity, permeability, facies and GR) instead of two (porosity and permeability).

Composition and abundance of principal framework grains have a great impact on diagenetic processes controlling porosity reduction, preservation and enhancement with burial. Heterogeneity and facies variations such as the vertical and lateral changes from cross-bedded to ripple-laminated sandstone, affect reservoir performance.

5.9.1 Porosity-Permeability and facies Distribution for well OP1

The core permeability was plotted in log scale on the y-axis against the core porosity in linear scale on the x-axis, and facies and gamma ray on the z-axis as shown in Figure 5.19 below.

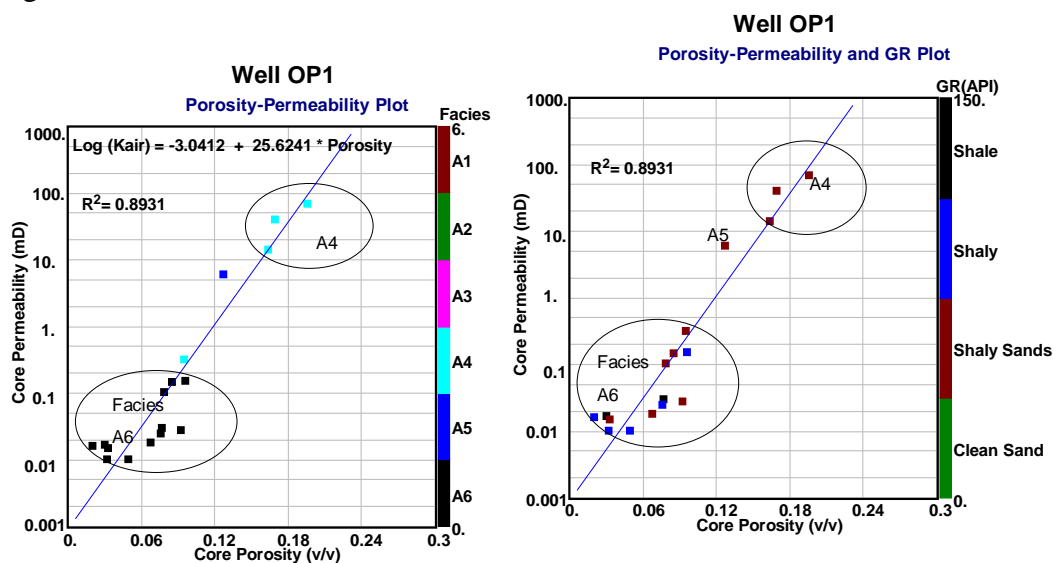


Figure 5.19: Porosity-Permeability and gamma ray log and facies plot for well OP1

The gamma ray log plot on the z-axis with values of 0 to 37 API represents clean sandstone, 37.5 to 75 API as shaly sandstones, and 76 to 150 API as shale.

Three facies were observed, facies A4, A5 and A6 on the cross-plot of this well. Facies A6 falls within gamma ray values of 75 to 150 API, with permeability values of less than 1 mD and porosity values of less than 10%. This facies is recognized as predominantly clay/siltstone and was classified as non reservoir rock. Facies A5 with gamma ray value between 40 and 75 API was regarded as shaly sand formation which posses a permeability value of slightly less than 10 mD and porosity value of about 13 %. Facies A4 is also regarded as a shaly sand formation based on the gamma ray values that it represents. The permeability values are poor to good and porosity values are above 10%.

Porosity permeability relationship of the interval is good with correlation coefficient of $R^2 = 0.8931$. The following relationship was established from the regression analysis plot:

$$\text{Log (K)} = -3.1626 + 24.8170 * \text{Core Porosity} \dots\dots\dots (5.1)$$
$$R^2 = 0.8931$$

Where:

K= Permeability (mD)

R = Correlation coefficient

5.9.2 Porosity-Permeability and Facies Distribution for well OP2

The cross plot of porosity-permeability and facies GR of well OP2 is presented in Figure 5.20 below.

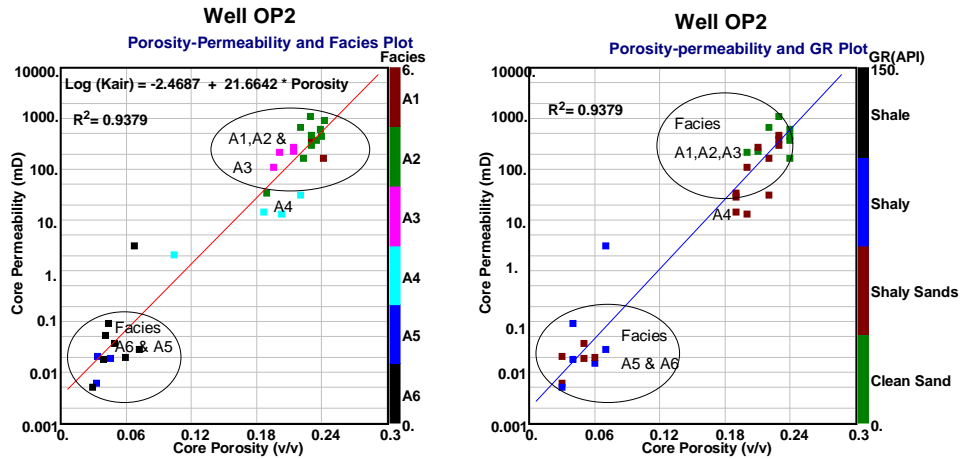


Figure 5.20: Porosity-Permeability and facies and GR plot for well OP2

The plot shows three different data clustering points of different rock types and facies. Facies A6 is of low porosity and permeability and is made up of GR values greater than 76 API and could be interpreted as silt/shale to shaly formation. The other data clustering point is composed of facies A5 and A4 having predominantly GR values between 37.5 to 75 API values which represents shaly-silt formation with high porosity and moderate permeability values.

Facies A1, A2 and A3 are made up of data clustering of high porosity and very good permeability values and a GR values below 75 API which is predominantly of clean sand formation and slight intercalation of shaly sand formation.

An empirical relationship between measured porosity and permeability was derived using the following linear regression analysis:

$$K = 10^{(21.6648 * \text{Porosity} - 2.687)} \dots\dots\dots (5.2)$$

$$R^2 = 0.9379$$

Where:

K = Permeability (mD)

R = Correlation Coefficient

5.9.3 Porosity-Permeability and facies Distribution for well OP3

The permeability, porosity and facies of core 1 and 2 of well OP3 are plotted in Figure 5.21 below.

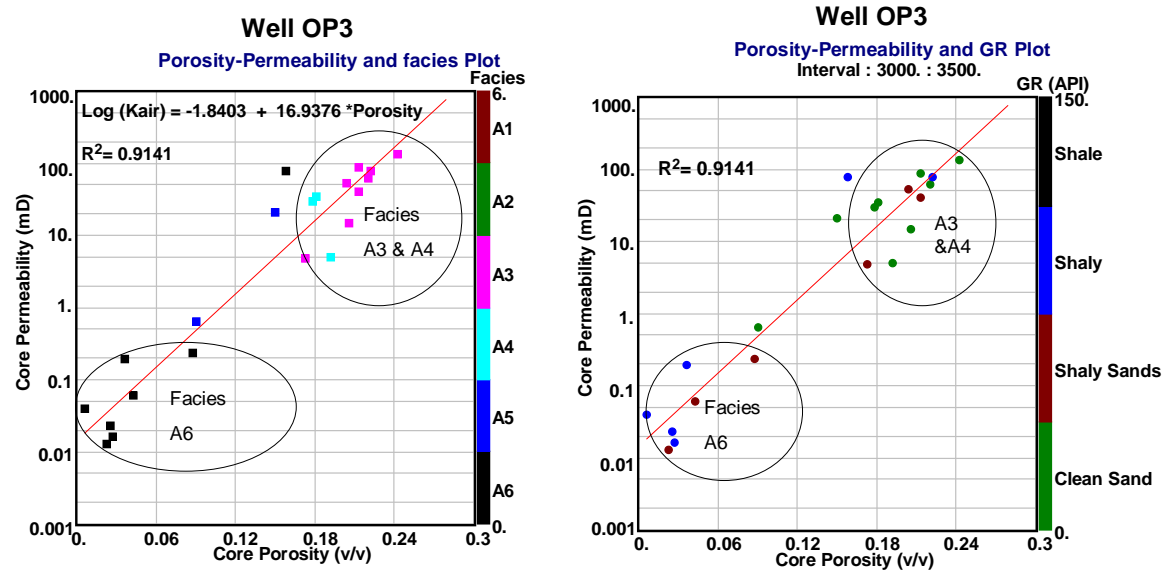


Figure 5.21: Porosity-Permeability and facies GR plot for Well OP3

In the cross plot of well OP3, three facies were represented. Low porosity and permeability values were associated with facies A6 which is represented by GR values showing shaly/silt to shale formation. Facies A5 has low to moderate porosity and permeability values and predominantly of GR between clean and shaly/silt which could be associated with clean sandstone or limestone formation. Facies A4 has moderate porosity and good permeability values and represented by a clean sandstone formation. Facies A3 showed high porosity and good permeability values and represented by typically of clean sandstone formation and the presence of high GR value observed in this facies could be sandstone that is rich in potassium. This may be identified as sand on spectral gamma-ray and on Density/Neutron cross plot. The best reservoir type in this well is facies A3.

An empirical relationship between the porosity and permeability was achieved using the following linear regression analysis equation below:

$$K = 10^{(16.9376 * \text{Porosity} - 1.8403)} \dots \dots \dots (5.3)$$

Where K= Permeability (mD)

5.9.4 Comparison of Porosity, Permeability and Facies for all wells

In order to determine a relationship between porosity-permeability and identify facies that will contribute to flow of hydrocarbon of the study area, the porosity-permeability and facies were plotted (Figure 5.22) below. The relationship established from the cross plot will also serves as the field permeability predictor in un-cored intervals and for Wells without core.

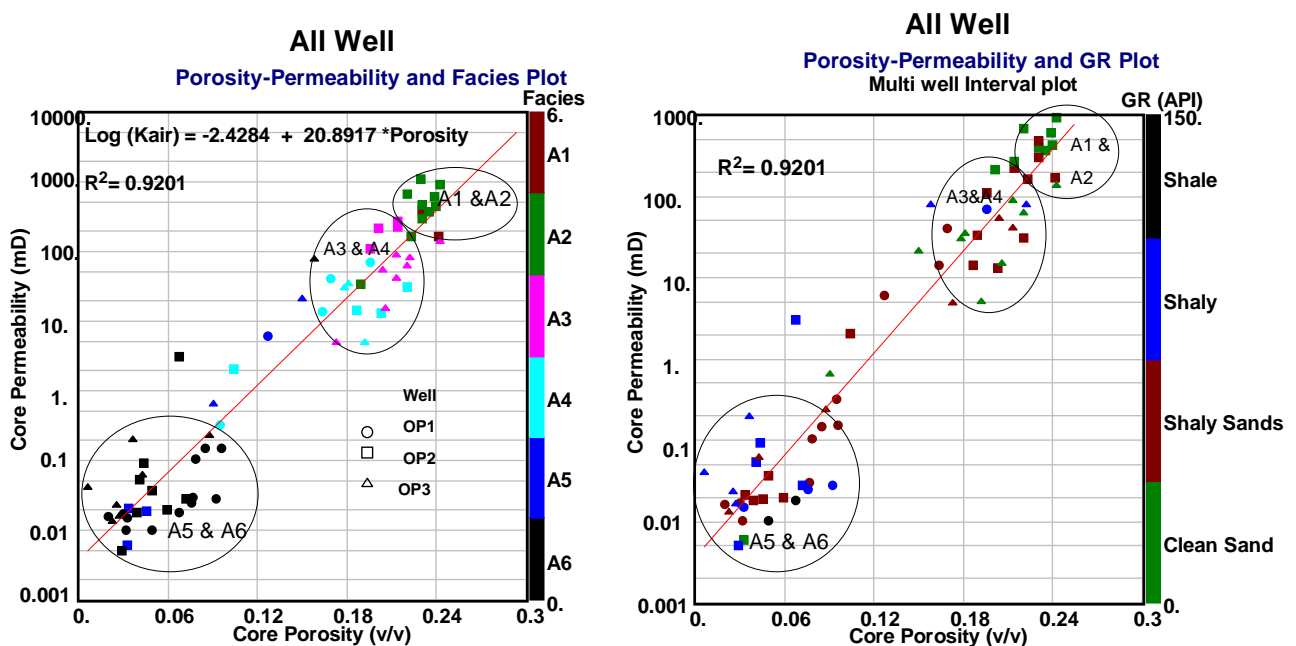


Figure 5.22: Porosity-permeability and facies distribution for wells

The facies A6 in the cross plot are predominant in the low porosity (porosity less than 10 %) and poor permeability (less than 1 mD) plot area coloured black which represent shale formation. Facies A5 in the cross plot showed area of poor to fair permeability and low to high porosity values. This facies fall between the low porosity-permeability and high porosity-permeability interval and represent sandstones and shaly- sands as compared with the GR plot. Sediments in this interval may be intercalation of clean sandstone, siltstone and claystones.

Facies A4 and A3 are closely related having permeability values of moderate to good and porosity values above 12 %. The high values recorded in this area may be due to sandstone represented by GR clean sands which are moderately sorted grains and the

low values may be due to the shaly sands as predominantly represented by GR shaly formation.

Facies A2 and A1 were observed to have the best reservoir rock quality with porosity of higher than 18 % and good to very good permeability values and predominantly represented by GR of clean sandstone and few shaly-sands. The sediments in this facies are well sorted grains.

It is evident that a linear porosity-permeability relationship exists and a permeability predictor could easily be constructed by means of a simple linear regression. An empirical relationship was derived from the cross plot as given below:

$$K = 10^{(20.8917 * \text{Porosity} - 2.4284)} \dots\dots\dots (5.4)$$

$$R^2 = 0.9201$$

Where K = Permeability (mD)
 Porosity = Porosity (v/v)
 R= Correlation Coefficient

The equation 5.4 above shows a correlation coefficient of 0.92 which is very good from statistical point of view and thus can be used provisionally to estimate permeability provided the porosity is known either from log for other wells that do not have core data . An accurate method will be used later in the study to determine the values of permeabilities. From this analysis, it was observed that for one particular value of porosity and permeability, it can be represented by different facies.

The low values of porosity and permeability values recorded may be due to the poorly sorted sediments, the finer grained material tends to block the pore throats giving decrease in permeability. Porosity is independent of grain size but decreases with decreasing sorting while permeability depends on both grain size and sorting.

5.10 SPECIAL CORE ANALYSIS (SCAL)

The special core analysis are measurements made on core plugs that complements conventional analysis measurements which are concern with measurements of reservoir properties that allows calculation of static fluid distribution and dynamic flow performance of a reservoir.

In this section, discussions will be focused on results of special core analysis measurement (SCAL) analyses on core plug samples from well OP1, OP2 and OP3 that were undertaken by Core Laboratories on behalf of South African Oil Exploration (Pty) limited (PASA report, 1993) to determine the following:

- ❖ Additional Routine analysis of Permeability to air, Klinkenberg corrected permeability to air, and helium injection porosity and grain density at room conditions.
- ❖ Formation Resistivity Factor (FRF) at room conditions and as a function of overburden pressure.
- ❖ Formation Resistivity Index (RI) at room conditions
- ❖ Capillary pressure measurements – Air-Brine porous plate cell and mercury injection methods.

The special core analysis overburden measurements are laboratory measurements of petrophysical properties aimed at determining the exact values under stress, pressure and temperature conditions. The laboratory overburden pressure tests stimulate the net overburden pressure which is the difference between the overburden pressure caused by the weight of sediments and the reservoir pressure.

SCAL measurements are performed on a relatively small number of representative samples and analysis can be performed at reservoir conditions using fluid samples.

5.10.1 Porosity, Permeability and Grain density Measurements

The permeability to air and porosity data obtained for each core sample after the cleaning and drying processes help in sample selections for other SCAL tests because it defines a minimum values for samples to meet before been utilized for other analyses. Results of two wells OP1 and OP3 are presented below.

5.10.1.1 Well OP1 Porosity, Permeability and Grain density Measurements

In well OP1, six (6) samples were selected for SCAL analyses but following air permeability and helium porosity measurements, two samples at depth 3372.93 and 3373.8 were found to be below test limits therefore was not suitable for further testing.

Table 5.9 present results from porosity, permeability, and grain density measurements.

Table 5.9: Porosity, Permeability and Grain Density test results of well OP1 at room condition.

Depth (m)	Porosity (%)	Klin (mD)	Kair (mD)	Grain Density (g/cc)	Remarks
3370.4	17.7	34	38	2.67	SuiTable for analysis
3371	18.6	35	38	2.67	SuiTable for analysis
3371.6	16.7	15	17	2.69	SuiTable for analysis
3372.3	11.7	0.76	1.1	2.67	SuiTable for analysis
3372.93	8.1	0.07	0.16	2.66	Not SuiTable
3373.8	5.2	0.006	0.015	2.68	Not SuiTable

The values of the routine core analysis measurements compared with the previous routine core analysis results showed a very good relationship as values are all most the same.

The overburden porosity and permeability measurements are measurements made in the laboratory at equivalent or net confining reservoir temperature and pressure.

5.10.1.2 Well OP3 Porosity, Permeability and Grain density Measurements

In well OP3, thirteen samples at measured depth ranges of 3283.2m to 3288.25m were selected for SCAL analysis. Based on air permeability and helium porosity measurements, three samples were found to be un-suitable for all requested analyses as the permeability to air data obtained was below 1 mD. Results are presented in Table 5.10 below.

Table 5.10: Porosity, permeability and grain density test results of well OP3 at room condition.

Depth (m)	Porosity (%)	Klin (mD)	Kair (mD)	Grain Density (g/cc)	Remarks
3283.2	20.2	4.5	6	2.71	Suitable for analysis
3283.4	18.7	3.3	4.4	2.71	Suitable for analysis
3283.5	17.7	2.5	3.5	2.7	Suitable for analysis
3284.74	23.5	70	80	2.7	Suitable for analysis
3284.77	23.4	49	57	2.7	Suitable for analysis
3284.85	23.6	60	69	2.7	Suitable for analysis
3286.95	24.2	51	59	2.72	Suitable for analysis
3286.99	24.3	93	105	2.7	Suitable for analysis
3287	24.3	69	79	2.69	Suitable for analysis
3287.1	24.4	79	90	2.69	Suitable for analysis
3288.09	9.5	0.06	0.14	2.68	Not Suitable
3288.15	6.8	0.03	0.06	2.67	Not Suitable
3288.25	6.1	0.02	0.04	2.68	Not Suitable

5.10.2 Formation Resistivity Factor (FRF) Measurements

The formation resistivity factor (FRF) is defined as the ratio of resistivity of the 100 percent water saturated rock sample to the water resistivity. It is a function of porosity and pore geometry of rock.

The core plugs used in this measurement were first cleaned dry plugs and later evacuated and pressure saturated with simulated formation brine. Electrical resistance of the brine saturated core plugs were measured at room conditions on consecutive days until results stabilized indicating ionic equilibrium within the core plugs.

The formation brine used in this study consists of sodium chloride (NaCl) and calcium chloride (CaCl₂). The calcium chloride was used to minimise any possible reactive clay problems. The formation resistivity values were determined at ambient condition for 100 percent brine saturated samples and also simulated to net overburden pressure which will be presented later.

The cementation exponent (m) which is a very useful parameter for the determination of water saturation is calculated from the slope of plotting measured values of FRF against porosity setting the intercept “a” to unity.

5.10.2.1 Formation Resistivity Factor (FRF) measurement Results for well OP1

The FRF measurement for well OP1 was performed at temperature of 77 °F which is equivalent to 25°C and the brine resistivity of 0.32 Ohm-m was used at room condition. The brine used consisted of approximately 18,500 ppm of dissolved solids consisting of 80 % sodium chloride (NaCl) and 20 % calcium chloride (CaCl₂).

The result of formation resistivity factor (FRF) performed on four samples of well OP1 is presented in Table 5.11 below.

Table 5.11: Result of well OP1 FRF measurement at room condition

Depth (m)	Porosity (%) Room Condition	FRF Room Condition
3370.40	17.7	25.47
3371.00	18.6	24.63
3371.60	16.7	30.38
3372.30	11.7	54.49

The room condition as used means measurements made at surface atmospheric condition at 25 °C or 77 °F

5.10.2.2 Formation Resistivity Factor (FRF) measurement Results for well OP3

The formation resistivity measurement for well OP3 was performed at room condition at a temperature of 77 °F and overburden condition. The resistivity of brine used was 0.13 Ohm-m. The water composition was confirmed with the Schlumberger log interpretation chart Gen-9.

The total dissolved solids were 51.282 mg/l and constituents were sodium chloride (NaCl) having 41.026 mg/l and calcium chloride 10.256 mg/l. Shown in Table 5.12 is results obtained from FRF measurements.

Table 5.12: Result of well OP3 FRF measurement at room and overburden conditions

Room Condition			Overburden Pressure 4,830psig	
Depth (m)	Porosity (%)	FRF	Porosity (%)	FRF
3283.20	20.2	24.7	19.2	33.0
3283.40	18.7	29.1	17.7	42.2
3283.50	17.7	33.7	16.7	49.4
3284.74	23.5	16.2	22.4	20.8
3284.77	23.4	16.7	22.0	21.1
3284.85	23.6	16.1	22.4	21.1
3286.95	24.2	15.3	23.2	18.5
3286.99	24.3	14.1	23.0	17.3
3287.00	24.3	14.7	23.0	20.2
3287.10	24.4	14.6	23.3	17.6

The overburden pressure of about 4,830 psi and temperature of 217.4 °F which is equivalent to 103°C in Table 5.12 above is the pressure or stress imposed on the core samples by the weight of overlying materials which was taken as pressure at reservoir condition and measurements were taken at that pressure. A reduction of porosity values and an increase of formation resistivity factor were observed at measurements at overburden pressure.

5.10.2.3 Formation Resistivity Index (RI) Measurements

The Resistivity Index (RI) is defined as the ratio of the resistivity of a formation bearing hydrocarbons to the resistivity it would have if 100 % saturated with formation water (SPWLA, 1984). It is a function of water saturation and pore geometry.

This test is normally performed in conjunction with air-brine capillary pressure after formation resistivity factor measurements were made on rock samples. A minimum of three saturation measurements were obtained on each core and individual sample resistivity index values are plotted against water saturation to determine a saturation

exponent (n) which is a slope of a line relating saturation and resistivity index (Core laboratory, 1982).

These measurements were performed in the Albian age reservoir sections of two wells (OP1 and OP3) in the study area. The results from resistivity index measurements are presented.

5.10.3.1 Formation Resistivity Index Results for well OP1

In well OP1, formation resistivity index measurements were conducted on four samples at room condition as presented in Table 5.13. About six different resistivity index measurements were performed on each sample at different brine saturations.

Table 5.13: Resistivity Index results for well OP1

Depth (m)	Brine Saturation (%)							Resistivity Index (RI)						
	91	71	57	52	50	46	43	1.1	1.6	2.2	2.4	2.9	3.1	3.4
3370.4	91	71	57	52	50	46	43	1.1	1.6	2.2	2.4	2.9	3.1	3.4
3371	64	51	48	45	42	40		1.9	2.8	3	3.5	3.7	4	
3371.6	75	56	51	48	45	42		1.5	2.4	2.8	3.3	3.5	3.7	
3372.3	71	64	57	52				1.6	1.9	2.1	2.3			

5.10.3.2 Formation Resistivity Index Results for Well OP3

In well OP3, formation resistivity index measurements were performed on ten samples at different brine saturation percent pore spaces as shown in Table 5.14.

Table 5.14: Resistivity Index results for well OP3

Depth (m)	Brine Saturation (%)							Resistivity Index (RI)			
	100	71.4	63.2	53.3	50	1	1.98	2.41	2.91	3.27	
3283.2	100	71.4	63.2	53.3	50	1	1.98	2.41	2.91	3.27	
3283.4	100	71.2	62.7	55.7	52.1	1	2.1	2.34	2.57	3.3	
3283.5	100	72.8	63.5	55.9	51.6	1	2.23	2.53	3.06	3.44	
3284.74	100	54.9	48.1	40.3	37.9	1	2.11	2.71	4.3	6	
3284.77	100	57.6	50.5	41.2	38	1	1.85	2.92	3.79	5.5	
3284.85	100	55.2	49.7	40.9	37.4	1	2.07	3.18	5.27	6.13	
3286.95	100	56	49	41.8	36.3	1	2.12	3.01	4.07	6.3	
3286.99	100	52.4	45.5	37.3	33	1	2.57	3.85	4.91	8.43	
3287	100	50.7	44.4	35.9	32.5	1	2.64	3.78	4.97	8.3	
3287.1	100	50.4	44.2	35.7	32.4	1	1.59	3.21	5.05	8.18	

5.10.4 Interpretation of Results

5.10.4.1 Porosity Overburden Correction

When the core is brought to the surface, all confining forces are removed and the rock tends to expand in all directions. This expansion causes a modification of the pore geometry which may impact on the rock permeability and porosity depending on pressure differential, the consolidation state of the rock and clay content. Discrepancy between laboratory and in situ measurements is due the increase in volume that occurs when the core is brought to a lower pressure and temperature at the surface because of the removal of overlying sediment column (Moran, 1995).

Overburden correction is regarded as the correction from laboratory condition measurements to net effective overburden stress at in situ reservoir conditions. This correction is carried out because routine core analysis measurements may incorporate systematic errors because these values are measured at low pressure which may lead to an over estimation.

An overburden correction should always be applied to the routine core data. When overburden measurements are available, a correction function for the routine data can be constructed otherwise empirical relationships can be applied (Luca & Jean-Claude, 2001).

In this study, the overburden corrections were applied to routine core porosity values due to the availability of porosity measurement data at overburden pressure. An empirical relationship between porosity at overburden and ambient conditions is established for porosity overburden corrections. No special core analysis measurements of permeability values at overburden equivalent or net confining pressures were recorded; therefore no permeability overburden corrections will be applied to the routine core analysis permeabilities.

The special core analysis data of well OP3 at room and overburden pressure conditions provide data for this correction. The overburden corrected porosity values will be used to calibrate wireline log porosity measurements. Table 5.15 present data for overburden correction.

Table 5.15: Well OP3 core 2 data used for porosity overburden correction.

Depth (m)	Porosity (%)	Porosity (%)
	Room condition	overburden pressure
3283.20	20.2	19.2
3283.40	18.7	17.7
3283.50	17.7	16.7
3284.74	23.5	22.4
3284.77	23.4	22.0
3284.85	23.6	22.4
3286.95	24.2	23.2
3286.99	24.3	23.0
3287.00	24.3	23.0
3287.10	24.4	23.3

The porosity at overburden pressure (4,830 psi) was plotted against porosity values at room condition on a linear scale as shown in Figure 5.23a below.

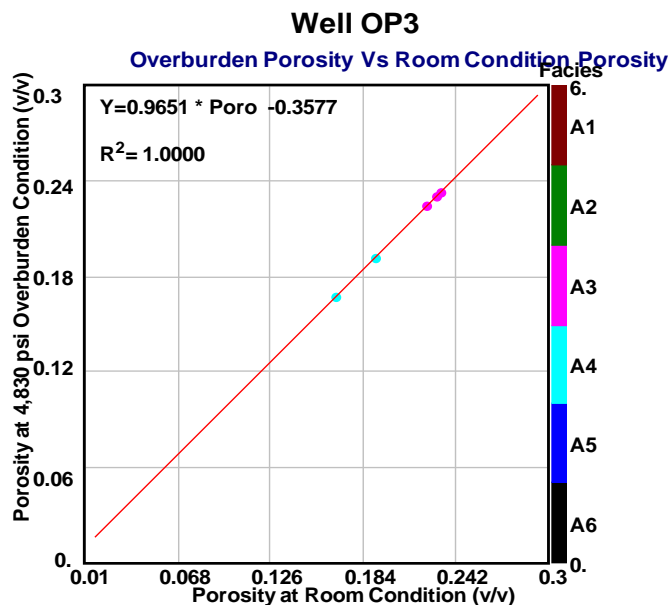


Figure 5.23a: Well OP3 porosity at overburden pressure versus porosity at room condition

To obtain an empirical linear relationship for the application of porosity overburden corrections, the regression equation from the plot of porosity at overburden pressure against porosity at room condition is used as given in the equation below:

$$\Phi_{\text{correct}} = 0.9651 (\Phi_{\text{routine}}) - 0.3577 \dots\dots\dots (5.5)$$

Where:

Φ_{correct} = Overburden corrected porosity

Φ_{routine} = Routine core porosity

Another useful parameter is the Pore Volume Reduction Factor (PRF) which is defined as the ratio of the overburden corrected porosity to routine core porosity. An average porosity reduction factor of 0.95 was obtained. Adopting a mean PRF would result in an over correction in higher porosity sections and under correction in the lowest porosity sections, hence equation 4.6 above is used to correct the routine core porosity measured at room conditions to in situ reservoir conditions.

The routine core porosity corrected values to the equivalent in situ reservoir conditions are given in Table 5.16 below.

Table 5.16: Wells OP1, OP2 and OP3 calculated overburden corrected porosities

Well OP1			Well OP2			Well OP3		
Depth (m)	Routine Porosity (%)	Corrected Porosity (%)	Depth (m)	Routine Porosity (%)	Corrected Porosity (%)	Depth (m)	Routine Porosity (%)	Corrected Porosity (%)
3370.05	18.9	17.9	3446.20	23.06	21.9	3236.1	24.2	23.0
3370.6	20.2	19.1	3447.08	24.24	23.3	3236.35	22.6	21.5
3371.07	16.9	15.9	3447.11	24.17	23.0	3236.51	21.3	20.2
3371.4	16.4	15.5	3447.83	18.65	17.6	3236.81	21.4	20.3
3371.9	16.5	15.6	3448.69	22.01	20.9	3237.05	18.1	17.1
3372.03	12.7	11.9	3449.52	20.27	19.2	3237.26	18.1	17.1
3372.53	9.5	8.8	3450.58	22.32	21.2	3237.51	15.0	14.1
3378.98	6.9	6.3	3451.70	23.54	22.4	3237.77	12.9	12.1
3373.75	5.0	4.5	3452.14	23.83	22.6	3237.95	9.1	8.4
3375.6	3.0	2.5	3452.59	24.01	22.8	3238.3	8.9	8.2
3375.98	2.0	1.6	3453.68	23.03	21.9	3238.5	6.3	5.7
3376.62	7.7	7.1	3454.72	24.25	23.0	3238.52	8.8	8.1
3376.86	8.6	8.0	3455.08	22.96	21.8	3239.05	4.3	3.8
3377.12	10.1	9.4	3455.55	18.83	17.8	3243.6	0.6	0.2
3377.36	9.6	8.9	3455.86	10.42	9.7	3283.2	19.2	18.2
3377.54	7.0	6.4	3456.15	4.59	4.1	3283.6	17.8	16.8
3377.78	7.9	7.3	3456.65	3.37	2.9	3283.85	17.8	16.8
3378.23	9.2	8.5	3457.18	3.27	2.8	3284.1	20.4	19.3
3378.48	8.6	7.9	3457.74	21.39	20.3	3284.35	21.3	20.2
3378.58	7.6	7.0	3458.69	21.36	20.3	3284.45	22	20.9
3379.24	6.8	6.2	3459.59	20.11	19.0	3285.05	22.2	21.1
3379.64	1.2	0.8	3460.00	21.93	20.8	3285.3	22.8	21.6
3379.82	4.9	4.4	3460.10	22.05	20.9	3285.34	20.6	19.5
3380.15	3.3	2.8	3461.48	23.07	21.9	3285.83	17.3	16.3
			3462.54	18.91	17.9	3286.08	14.3	13.4
			3463.48	19.55	18.5	3286.3	20.4	19.3
			3464.59	8.19	7.5	3286.55	22.3	21.2
			3464.81	4.92	4.4	3286.6	22.2	21.1
			3465.40	2.95	2.5	3286.7	22.2	21.1
			3466.47	6.23	5.7	3287.25	23.3	22.1
			3466.75	4.43	3.9	3287.3	15.8	14.9
			3467.50	4.12	3.6	3287.9	3.7	3.2
			3467.60	3.89	3.4	3290.06	2.3	1.9
			3468.17	5.96	5.4	3291.76	2.7	2.2
						3292.79	2.6	2.2

5.10.5 Derivation of Cementation exponent From Formation Resistivity Factor

The cementation of a rock is defined as the process of deposition of dissolved mineral components in the interstices of sediments. The process involves coming together of sediment to form a new rock during diagenesis or lithification (Boggs, 2006).

The cementation exponent which is represented by “ m ” is a function of the shape and distribution of pores and it is determined from the slope of the plot of the formation resistivity factor versus the porosity. The degree of cementation of sand particles depends on the nature and distribution of the cementing materials; less cemented sandstones normally have higher porosity values and lower formation resistivity factor values.

The value of the cementation exponent reflects the tortuosity of the interconnected pore space and ranges between 1 and 2.3 (Luca, 2001). The more complex the current path is, the higher the cementation exponent which implies higher value of “ m ”. The cementation exponent plays a critical role in the determination of water saturation calculations.

The typical values used in classification of cementation for rocks are given in the Table below:

Table 5.17a: Classification of cementation exponent

Classification	Cementation ($-m$) values
Highly Cemented	2.0 -2.2
Moderately Cemented	1.8 -1.9
Slightly cemented	1.6 -1.7
Very Slightly Cemented	1.4 -1.5
Not Cemented	1.30

(Pirson, 1958)

5.10.5.1 Well OP1 Cementation Exponent (m) at Room Condition

The cementation exponent m was derived from the slope of the cross plot of formation resistivity factor versus porosity by setting the tortuosity “ a ” the intercept to unity as shown in Figure 5.23b below for well OP1.

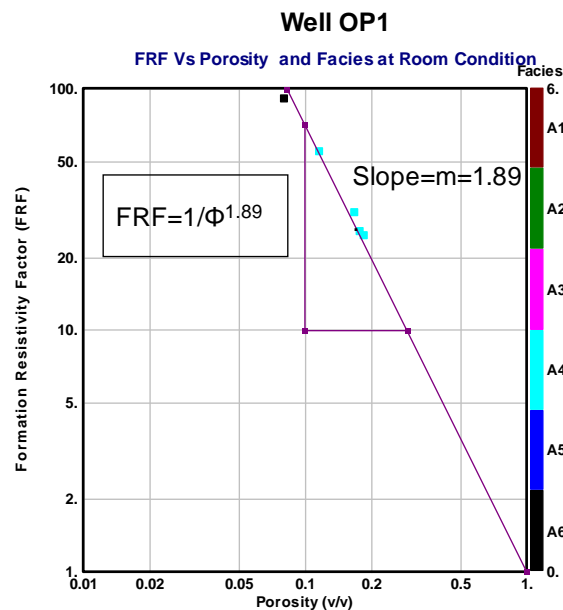


Figure 5.23b: Formation resistivity factor (FRF) vs porosity plot for Well OP1

The slope gives the cementation exponent (m) from the equation, $FRF = 1 / \Phi^m$.

The values of cementation exponent (m) are given in Table 5.17b below. The values range from 1.80 to 1.9 with a mean value of 1.89.

Table 5.17b: Cementation exponent (m) from Formation resistivity factor measurement

Depth (m)	Porosity (%)	FRF	Cementation exponent (-m)
3370.40	17.7	25.47	1.88
3371.00	18.6	24.63	1.90
3371.60	16.7	30.38	1.90
3372.30	11.7	54.49	1.87

Well OP1 was classified as moderately cemented based on the average cementation exponent value of 1.89 obtained.

5.10.5.2 Well OP3 cementation Exponent (m)

The cementation exponent (m) values of well OP3 at room condition varies from 1.89 to 2.04 (Table 5.18) below.

Table 5.18: Cementation exponent for Well at room condition

Room Condition

Depth (m)	Porosity (%)	FRF	Cementation exponent (-m)
3283.20	20.2	24.7	2.01
3283.40	18.7	29.1	2.0
3283.50	17.7	33.7	2.04
3284.74	23.5	16.2	1.92
3284.77	23.4	16.7	1.94
3284.85	23.6	16.1	1.92
3286.95	24.2	15.3	1.90
3286.99	24.3	14.1	1.89
3287.00	24.3	14.7	1.92
3287.10	24.4	14.6	1.90

The formation resistivity factor (FRF) was plotted against the fractional porosity to obtain an average value of 1.95 (slope) as the cementation exponent of the Well (Figure 5.24).

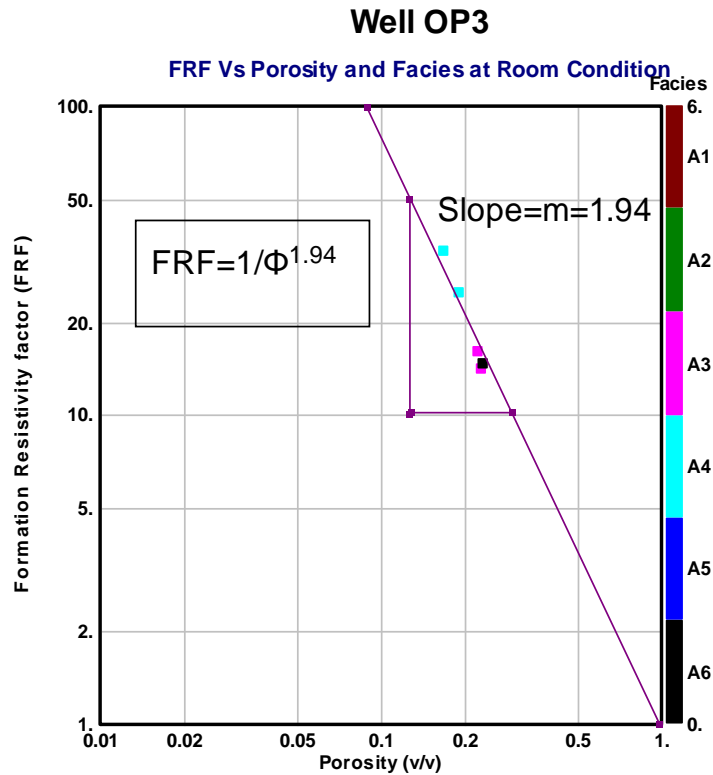


Figure 5.24: Plot of Well OP3 formation resistivity factor versus fractional porosity

In this particular well, the cementation exponent was determined from two types of facies (A4 and A5) within the interval measured at room conditions. Facies A4 showed higher formation resistivity factor values than facies A3. In terms of porosity, facies A3 appeared to be more porous than facies A4 which indicate that facies A4 is more cemented than facies A3. The cementation exponent determined in well OP3 was classified as moderately cemented having an average cementation value of 1.95.

5.10.5.3 Effect of Overburden Pressure on Cementation

The formation resistivity factor and porosity of well OP3 were measured at overburden pressure of 4,830 psi, and cementation exponent values derived from the cross plot of FRF vs. porosity varies from 1.94 to 2.17 with mean of 2.05 as shown in Figure 5.25 below.

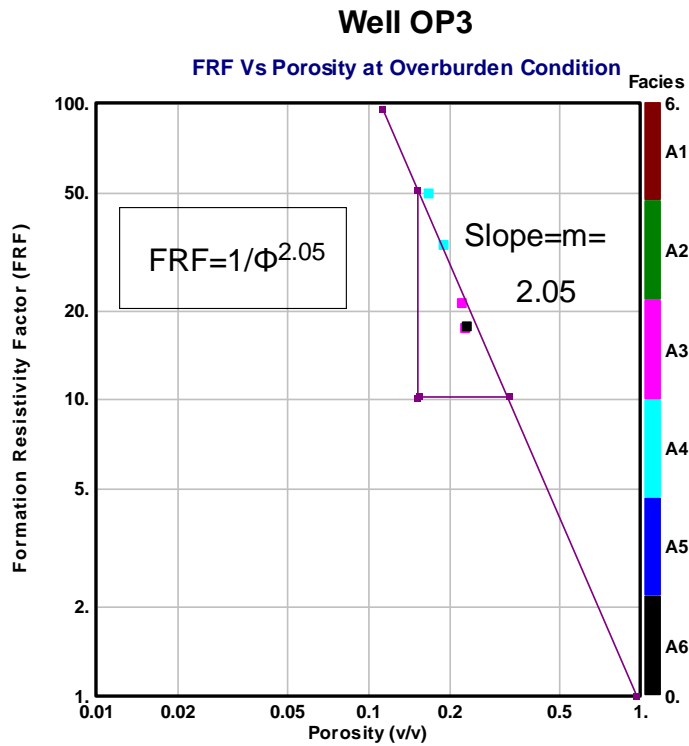


Figure 5.25: Formation resistivity factor versus porosity at overburden pressure

The cementation exponent values determined at overburden condition for well OP3 varies from 1.94 to 2.17 as shown in Table 5.19 below.

Table 5.19: Well OP3 cementation exponent at overburden pressure (4,830 psi)

Depth (m)	Porosity (%)	FRF	Cementation Exponent (-m)
3283.20	19.2	33.0	2.11
3283.40	17.7	42.2	2.17
3283.50	16.7	49.4	2.17
3284.74	22.4	20.8	2.03
3284.77	22.0	21.1	2.03
3284.85	22.4	21.1	2.03
3286.95	23.2	18.5	2.02
3286.99	23.0	17.3	1.94
3287.00	23.0	20.2	2.05
3287.10	23.3	17.6	1.98

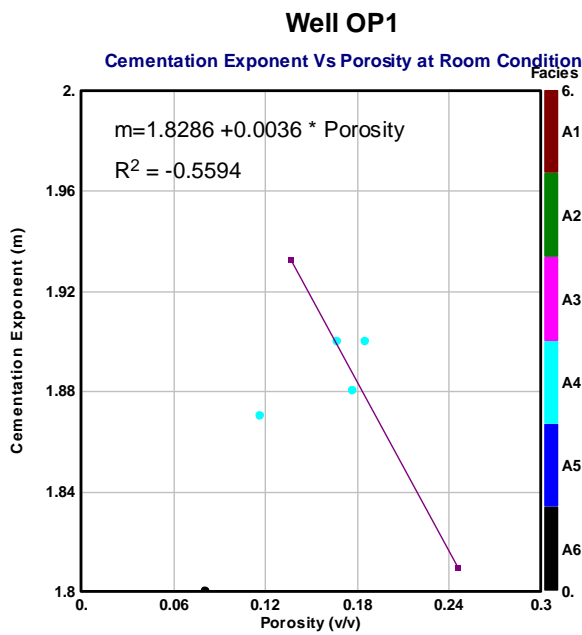
The cementation exponents (m) determined at room condition and at overburden condition are presented in Table 5.20 below. Overburden pressure has an effect on cementation (m) as m increases at overburden condition as compared to room condition.

Table 5.20: Well OP3 comparison of cementation exponents

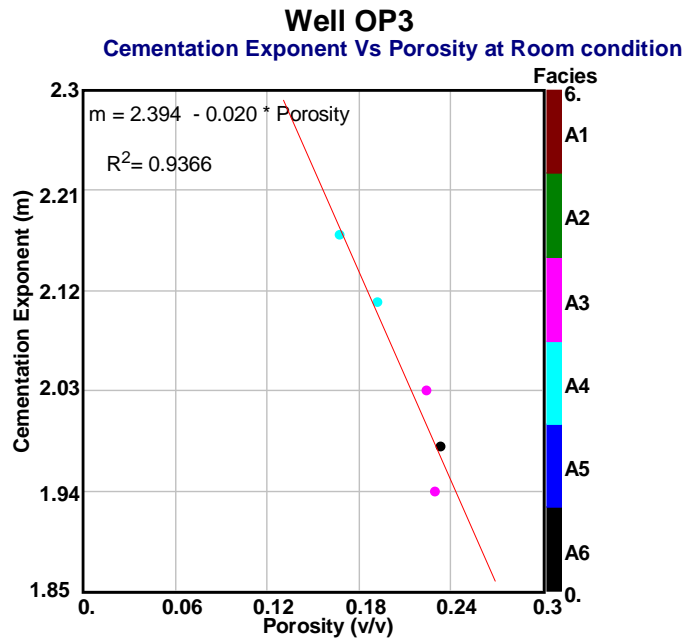
Depth (m)	Cementation (-m)	Cémentation (-m)
	Room Condition	Overburden 4,830psi
3283.20	2.01	2.11
3283.40	2.0	2.17
3283.50	2.04	2.17
3284.74	1.92	2.03
3284.77	1.94	2.03
3284.85	1.92	2.03
3286.95	1.90	2.02
3286.99	1.89	1.94
3287.00	1.92	2.05
3287.10	1.90	1.98

5.10.5.4 Comparison of Cementation Exponent with Porosity

The cementation exponent values for well OP1 and OP3 at room conditions were plotted on linear scale of y-axis against the porosity on the linear scale in order to determine an empirical linear relationship between the two variables as shown in Figure 5.26 below.



Just one type of rock (Facies A4).



Two types of rock (Facies A3 & A4)

Figure 5.26: Well OP1 and OP3 cementation versus porosity plot at room conditions.

From the plot, it was observed that the data was made up of facies A4 and as the cementation exponent increases, the porosity of the formation also increases and linear regression equation was derived from the cross plot as given below:

$$m = 0.0036 * \text{Porosity} + 1.8286 \dots\dots\dots (5.6)$$

$$R^2 = 0.5594$$

Where m= Cementation exponent

The trend of the plot for well OP3 is different from what was obtained in well OP1. Well OP3 data were composed of core facies A3, A4 and A5. As cementation values decrease, the porosity values also decrease and a linear empirical regression equation was obtained from the cross plot as expressed in equation 4.8 below:

$$m = 2.394 - 0.020 * \text{Porosity} \dots\dots\dots (5.7)$$

$$R^2 = 0.9366$$

The differences in the trend line of cementation versus porosity plots for well OP1 and OP3 at room condition may be due to diagenetic effect and the shape of the grains of the core samples. A linear scale plot was also made for cementation exponent

versus porosity for well OP3 at overburden condition as presented in Figure 5.27 below. Both wells are moderately cemented.

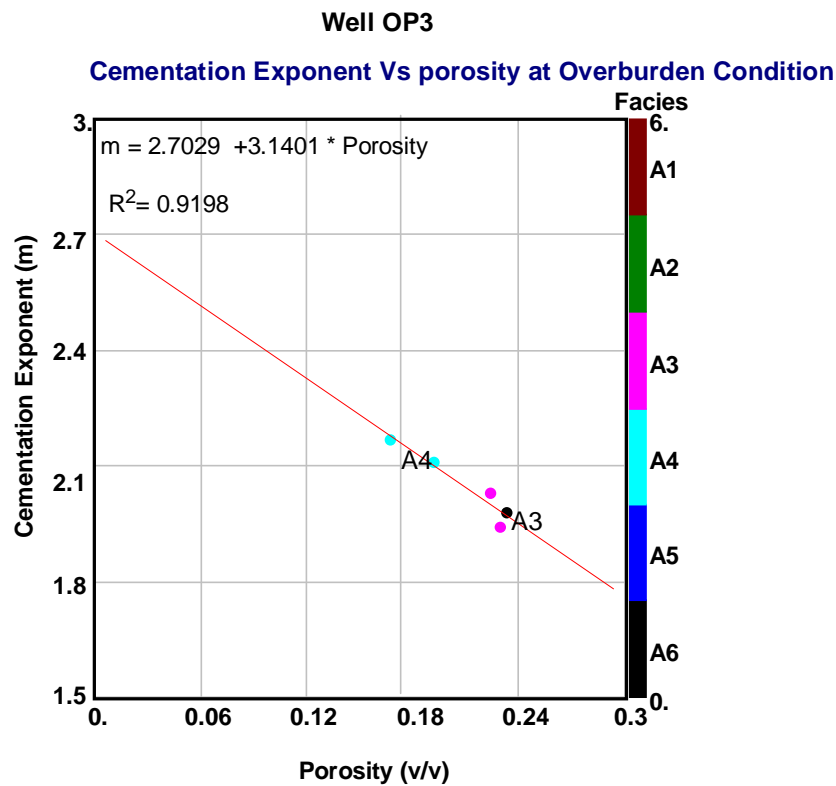


Figure 5.27: Cementation versus porosity at Overburden condition of Well OP3

The plot shows constant cementation values between the depth intervals of 3283.4m to 3283.5m and 3284.74m to 3284.85m with slight changes in porosity values at these depths. The constant values may be due to the closeness of the core samples and shape and nature of sediments which are almost the same.

An empirical linear regression analysis relationship between the cementation exponent and porosity at overburden condition for the well is given below:

$$m = 2.6555 - 0.0283 * \text{Porosity} \dots\dots\dots (5.8)$$

$$R^2 = 0.8542$$

Where m=cementation exponent and porosity is in percent.

Comparison of the plots showed that well OP3 at room condition and overburden conditions portrayed the same trend line as opposed to that of well OP1. The best

correlation coefficient was obtained from well OP3 cementation versus porosity plot at room condition with value of about 0.94. Based on the number of data used for the correlation and the higher correlation coefficient obtained from well OP3 at room condition, therefore equation 5.8 above will be used for the evaluation.

5.10.5.5 Comparison of Cementation Exponent with Permeability

The cementation exponent plot on a linear scale against the permeability values on a log scales for well OP1 and OP3 at room condition is presented in Figure 5.28 below.

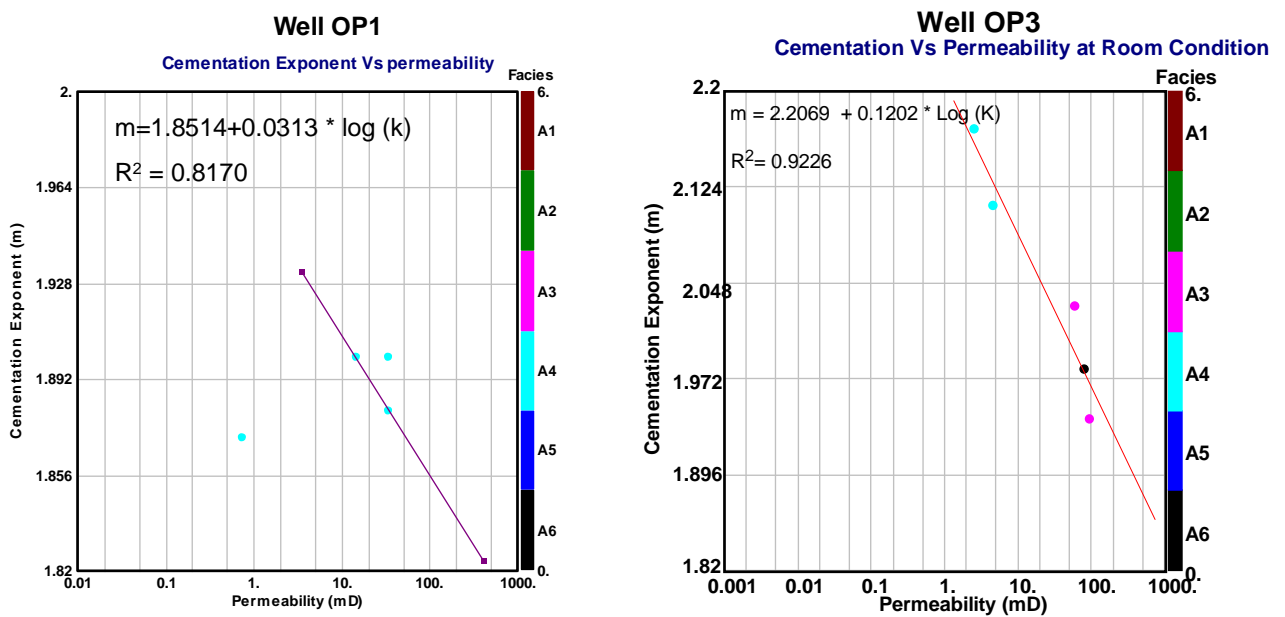


Figure 5.28: Well OP1 and OP3 cementation exponent Vs permeability at room temperature

The plot of Well OP1 was on core facies A4 and it showed that as cementation increases, the permeability values tend to decrease and linear relationship between the cementation exponents was obtained from the regression analysis as shown in the equation below:

$$m = 0.0058 * (\log K) + 1.8782 \dots\dots\dots (5.9)$$

$$R^2 = 0.4827$$

Where m= cementation exponent and K is the permeability in mD.

A poor regression analysis value of 48% was obtained which implies that a poor relationship exists between the plotted data and equation 5.9 could be used with caution.

In well OP3, the permeability values decreases as the cementation increases as shown in Figure 5.28 above and cementation also decreases as the depth increases. A good relationship exists between the cementation exponent values and permeability as shown in the regression coefficient value of about 94 % confidence.

The empirical relationship is given by the regression analysis below:

$$m = 2.0597 - 0.035 * (\log K) \dots\dots\dots (5.10)$$

Where m is cementation exponent and K is permeability in mD.

Equation 5.10 above demonstrates a better relationship between cementation exponent and permeability and hence could be used to estimate values of cementation exponent provided permeability values are known.

It could be concluded that in well OP1, the slight increment in cementation observed may be due to the closeness of the data and the core Facies A4, while in well OP3 cementation reduce porosity and permeability and the core facies were facies A3, A4 and A5.

5.10.6 Determination of Saturation Exponent (n)

The saturation exponent “n” is determined from the slope of a plot of resistivity index on a lo-log scale versus the water saturation. The saturation exponent depends on rock type and the way in which the pores are connected. The value of n is affected by wettability, overburden pressure, type and amount of clay, and nature and distribution of reservoir fluids (Djebbar, 1999).

5.10.6.1 Well OP1 Formation Resistivity Index (RI) versus Saturation at Room Condition

The saturation exponent (n) of well OP1 was determined from the slope of resistivity index versus water saturation as shown in Figure 5.29 below showing facies A4 as the dominant facies in the interval plotted.

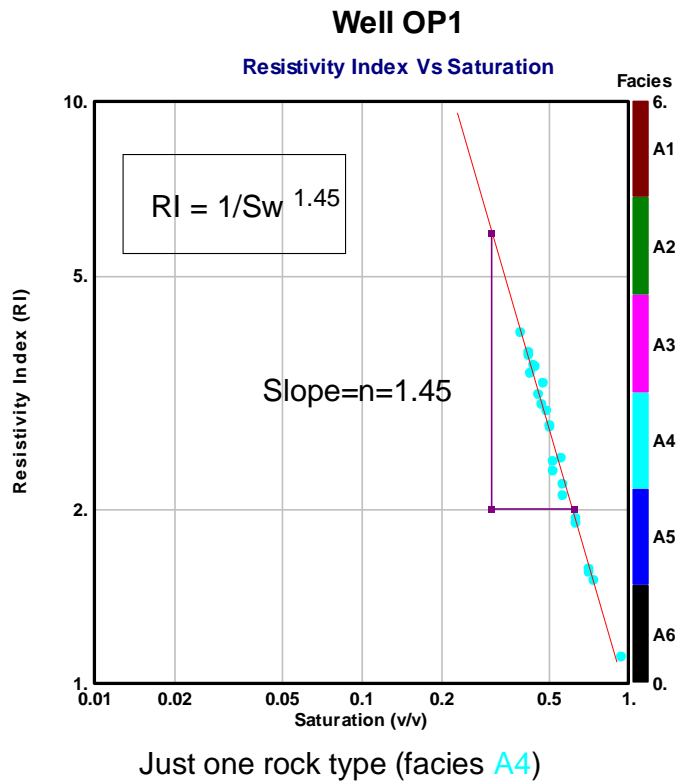


Figure 5.29: Well OP1 resistivity index versus water saturation plot.

The values of n vary from 1.43 to 1.53 with mean value of 1.45 as presented in Table 5.21.

Table 5.21: Well OP1 result of resistivity index measurements and n values

Depth (m)	Brine Saturation (%)							Resistivity index (RI)							(-n)
	91	71	57	52	50	46	43	1.1	1.6	2.2	2.4	2.9	3.1	3.4	
3370.4	91	71	57	52	50	46	43	1.1	1.6	2.2	2.4	2.9	3.1	3.4	1.43
3371	64	51	48	45	42	40	-	1.9	2.8	3.0	3.5	3.7	4.0	-	1.51
3371.6	75	56	51	48	45	42	-	1.5	2.4	2.8	3.3	3.5	3.7	-	1.53
3372.3	71	64	57	52				1.6	1.9	2.1	2.3				1.34

A plot of resistivity index versus saturation for well OP1 is given in Figure 5.29 above and individual depth plots are in appendix C.

5.10.6.2 Well OP3 Saturation Exponent (n) Determination at Room Condition

The saturation exponent (n) was determined from the slope of plotting resistivity index versus water saturation gives an average value of 1.94 as shown in Figure 5.30. Facies A3 and A4 were observed at the interval plotted.

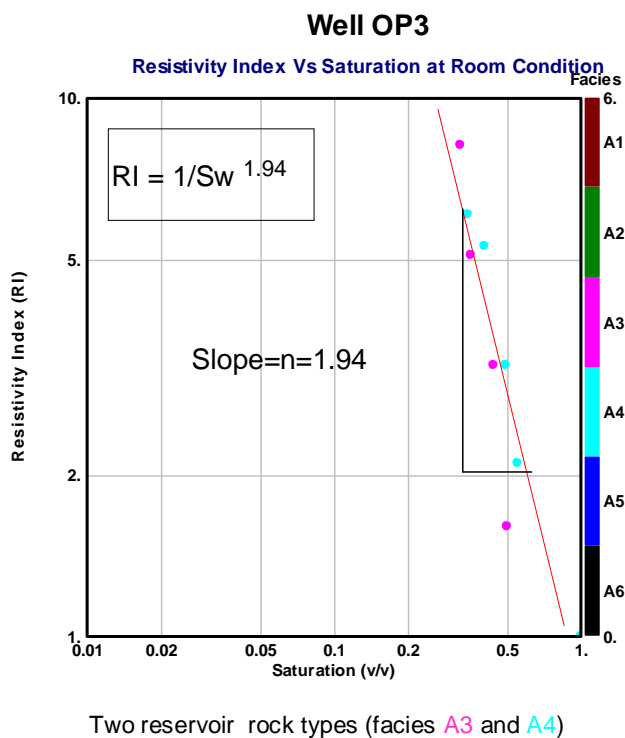


Figure 5.30: Well OP3 resistivity index versus saturation plot

The depth plots of “n” for this well are presented in appendix C. The n values vary from 1.89 to 2.02 with an average value of 1.94 as indicated in Table 5.22 below.

Table 5.22: Well OP3 result of saturation exponent (n) derived from resistivity index versus saturation.

Depth (m)	Brine Saturation %					Resistivity Index (RI)					(-n)
	100	71	63	53	50	1	2	2.41	2.91	3.27	
3283.2	100	71	63	53	50	1	2	2.41	2.91	3.27	1.89
3283.4	100	71	63	56	52	1	2.1	2.34	2.57	3.30	2.02
3283.5	100	73	64	56	52	1	2.2	2.53	3.06	3.44	1.96
3284.74	100	55	48	40	38	1	2.1	2.71	4.3	6.00	1.91
3284.77	100	58	51	41	38	1	1.9	2.92	3.79	5.50	1.90
3284.85	100	55	50	41	37	1	2.1	3.18	5.27	6.13	1.89
3286.95	100	56	49	42	36	1	2.1	3.01	4.07	6.30	1.91
3286.99	100	52	46	37	33	1	2.6	3.85	4.91	8.43	2.02
3287	100	51	44	36	33	1	2.6	3.78	4.97	8.30	1.95
3287.1	100	50	44	36	32	1	1.6	3.21	5.05	8.18	1.94

5.10.6.3 Comparison of Saturation Exponent (n)

The resistivity Index which is a function of water saturation and pore geometry was plotted for wells OP1 and OP3 to compare and confirm which of the wells will have a higher saturation exponent value (Figure 5.31).

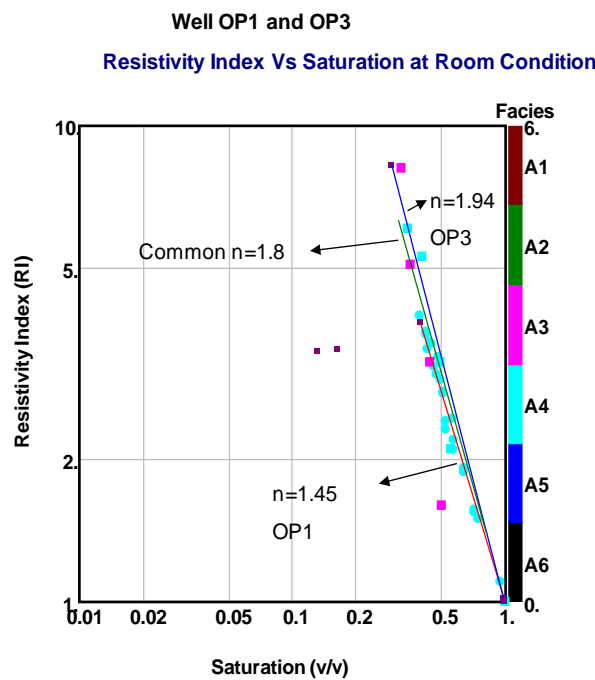


Figure 5.31: Resistivity index versus saturation plots for well OP1 and OP3

Well OP3 present a cleaner sandstone trend with higher saturation exponent value of 1.94 than OP1 which display a lower saturation exponent mean value of 1.45 as shown in Figure 5.31. The differences in the saturation exponent trend may be due to the distribution of fluids within the pore systems and types of facies present. A common value of saturation index of 1.8 was obtained for both well.

In rocks containing clay minerals such as chlorite, the saturation exponent becomes increasingly lower as the water saturation is reduced. In most shaly-sand saturation equations such as the Waxman-Smith and Dual-water models, the value of the saturation exponent is determined in high water salinity or with the clay effects removed and the variations of resistivity index with the saturation is then predicted from equations.

5.10.7 Petrography Studies

The petrography study is defined as the scientific description and study of rocks. Varieties of techniques and instrumentation have been devised to assist the geologist. This study includes thin sections, X-Ray Diffraction (XRD), and Scanning Electron Microscopy (SEM) (Core laboratories, 1982). OMNI laboratories performed the petrography studies in well OP2 and OP3 within the Albian age formation of the study area.

The petrography studies is included in this research because it will aid in the mineral identification and also help in understanding the textural nature of mineral and better understanding of the pore space as it will be used to validate other results.

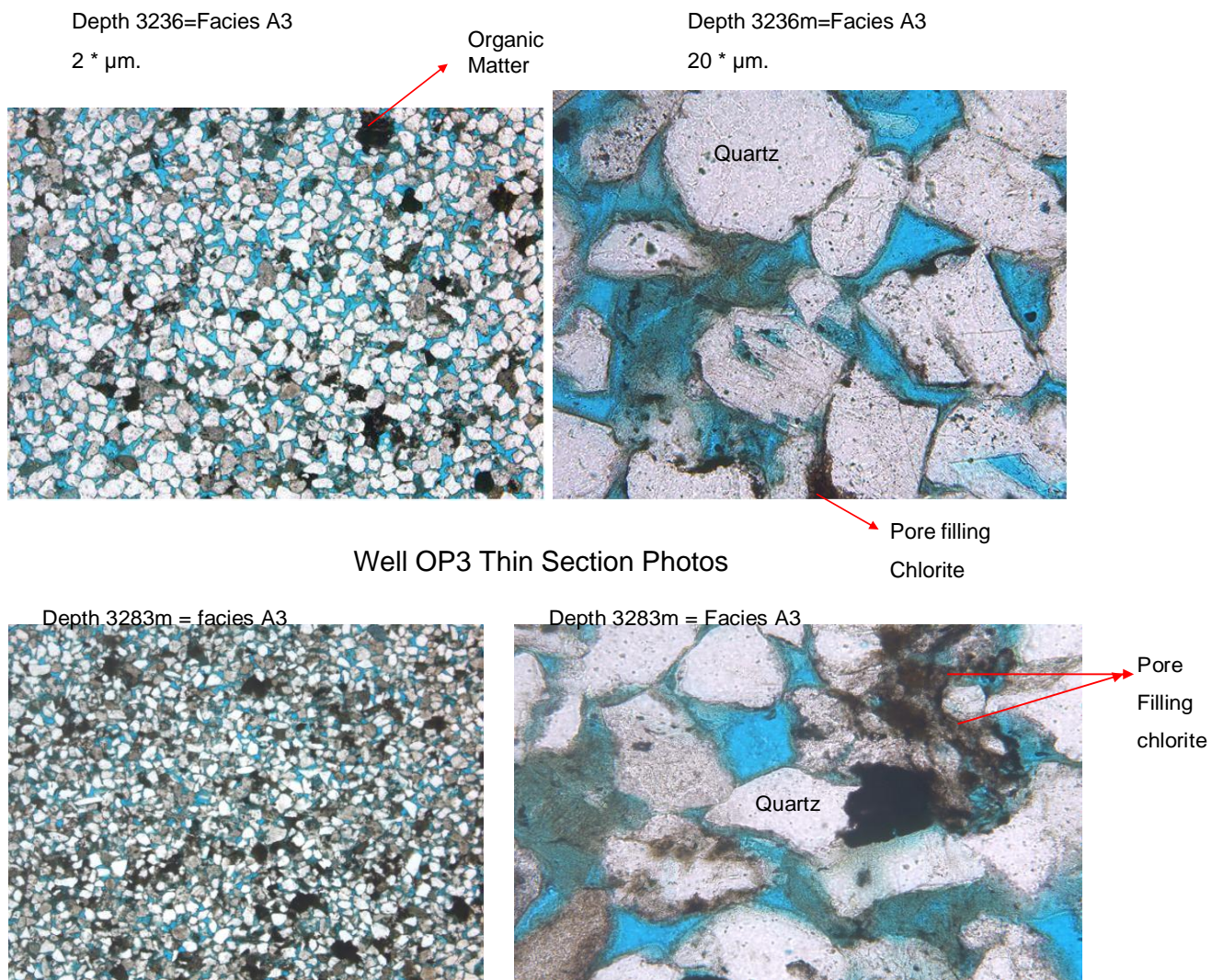
5.10.7.1 Thin Section Analysis

Selected reservoir sandstone samples from well OP2 and OP3 were investigated in thin sections in order to obtain information on the occurrence and distribution of different mineral components. The information obtained from the thin section investigations will be used to supplement the quantitative mineralogy data determined by X-Ray Diffraction and Scanning electron microscopy. The petrophysical properties of the reservoir sequence studied are influenced not by the proportion of the mineral constituents alone but also by the way the minerals occur in the rocks.

The sandstone samples in thin sections typically consist of quartz as the dominant framework grains, with minor feldspar and opaque grains. Lithic fragments include shale, siltstone and quartz. Traces of glauconite, siderite may also be noted in some of the samples.

5.10.7.1.1 Well OP3

Thin sections of well OP3 are shown in Figure 5.32 below.



Well OP3 Thin Section Photos at depth 3283m.

Figure 5.32: Well OP3 thin section at depth 3236m and 3283m showing fine grain, sub angular to angular, and sparsely distributed organic matter and pore filling Chlorite.

They are mostly fine grain, sub-angular to angular and organic matters are sparingly distributed. The porosities are generally good and grain is dissolved and secondary porosity observed within the samples (depth 3236m). Fe coatings and little quartz overgrowth were also observed. The thin sections at depth 3283m look much finer grains and the organic materials are more as compared to depth 3236m. Pore filling chlorite clay minerals was also observed. The thin section analysis was performed on facies A3 in both core of well OP3.

5.10.7.2 X-Ray Diffraction (XRD)

The X-Ray diffraction tests are made on crushed core samples and complement thin section analysis by providing quantitative mineral identification as Well amount of clay minerals present in each sample.

Clay minerals comprise of small percentages of the reservoir rock total composition and it is necessary to separate clay size particles from larger sand grain particles and make a separate analysis of clay sizes alone. The X-Ray diffraction analysis is more suitable because it gives more detailed information on different types of clay based on their unique x-ray diffraction pattern that is comparable to finger print. Samples of five to ten gram sizes are usually preferred for this analysis. The X- ray diffraction does not allow identification of non-crystalline (amorphous) materials such as organic material and volcanic glass.

This analysis was carried out within the Albian age formation of the study area of well OP2 and OP3 by OMNI laboratories.

5.10.7.2.1 Well OP2 XRD

The whole rock mineralogy results of well OP2 from forest report 2001 is presented in Table 5.23 below. A total of thirty five samples were taken for analysis and result shows dominance of quartz having percentage by weight of 67 %, clay minerals with 14 %, and minor occurrences of carbonates and heavy minerals as shown.

Table 5.23: Whole rock mineralogy of Well OP2

Depth(m)	Whole Rock Mineralogy (Weight %)									Relative Clay Abundance (Normalized to 100%)		
	Quartz	Ksp	Plag	Cal	Dol/Fe-Dol	Sid	Pyr	Anh	Clay	I/S*	Ill	Chl
3446.00A	75	4	14	0	1	Tr	0	0	6	0	28	72
3446.00B	54	3	12	0	0	1	11	0	19	0	30	70
3447.08	73	2	15	Tr	Tr	0	0	0	10	0	24	76
3447.83	62	3	16	0	1	0	1	0	17	0	21	79
3448.69	70	2	17	0	0	Tr	0	0	11	0	25	75
3449.52	70	2	16	0	0	1	Tr	0	11	0	26	74
3450.58	73	2	14	0	Tr	0	0	0	11	0	24	76
3451.70	75	2	13	0	0	Tr	0	0	10	0	21	79
3452.14	77	2	11	0	1	Tr	Tr	0	9	0	24	76
3452.59	74	2	12	0	1	0	0	0	11	0	18	82
3453.68	76	2	11	0	0	Tr	Tr	0	11	0	26	74
3454.72	78	2	10	0	1	1	Tr	0	8	0	23	77
3455.08	78	2	9	0	2	0	0	0	9	0	24	76
3455.55	69	3	14	0	0	0	Tr	0	14	0	17	83
3455.86	84	2	8	Tr	0	0	Tr	0	6	0	26	74
3456.15	55	3	10	0	0	Tr	0	0	32	0	32	68
3456.65	52	1	9	30	0	Tr	0	0	8	0	31	69
3457.18	37	1	5	31	0	18	0	0	8	0	26	74
3457.74	74	3	12	0	0	0	0	0	11	0	23	77
3458.69	73	2	12	0	1	0	0	0	12	0	20	80
3459.59	75	3	11	0	Tr	1	0	0	10	0	24	76
3460.10	74	3	10	0	2	1	0	1	9	0	24	76
3461.48	75	1	11	0	2	0	0	0	11	0	23	77
3462.54	71	1	14	0	0	1	Tr	0	13	0	22	78
3463.48	73	2	11	0	0	0	0	0	14	0	19	81
3464.59	72	2	11	0	0	0	0	0	15	0	14	86
3464.81	76	1	6	10	0	0	0	0	7	0	23	77
3466.20	72	4	11	1	3	Tr	0	0	9	0	32	68
3466.47	70	2	12	1	0	0	0	0	15	0	18	82
3466.75	49	3	22	0	0	0	1	0	25	0	21	79
3467.50	49	4	10	0	0	0	3	0	34	22	23	55
3468.17	57	2	14	15	0	0	0	0	12	17	25	58
3468.89	65	2	17	3	0	0	1	0	12	13	20	67
3469.39	46	3	19	0	0	0	0	0	32	11	20	69
3470.35	37	3	7	0	0	2	3	0	48	22	34	44
Average:	67	2	12	13	2	3	3	1	14	2	24	74

The X-ray diffraction analysis of the samples indicates the presence of clay mineral as the dominant clay type in the well. The presence of chlorite and Illite in the samples will contribute to grain coating. Kaolinite is absent (Figure 5.33) below.

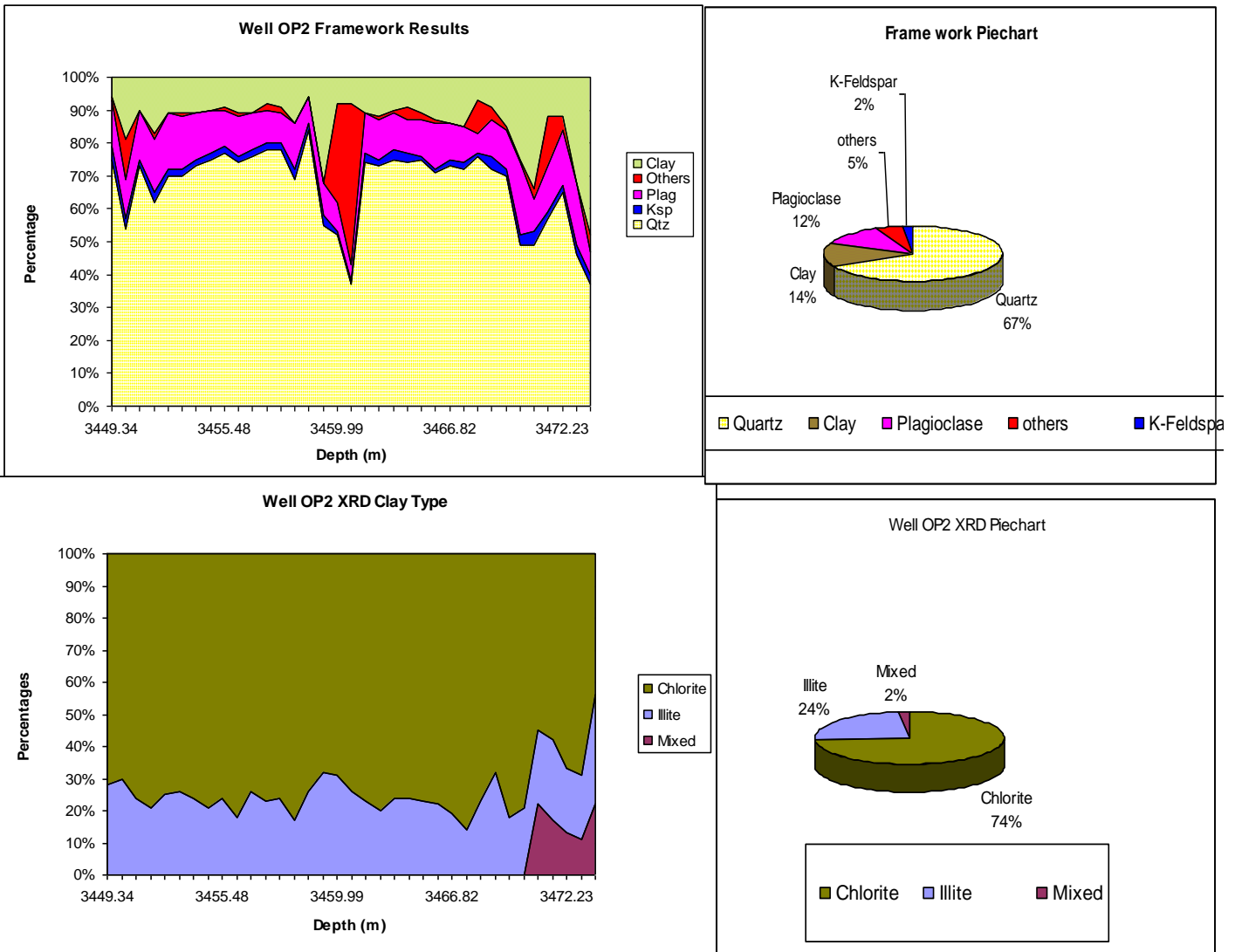


Figure 5.33: Whole rock mineralogy of Well OP2

5.10.7.2.2 Well OP3 XRD

The mineralogy results of fourteen samples within the Albian age from core1 and two of well OP3 are presented in Table 5.24 below. The results shows the dominance of quartz percentage by weight of 57 to 58 % in both cores, clay minerals with about 25 and 20 % in both cores, carbonates in small proportions in both cores.

Table 5.24: Whole rock mineralogy of Well OP3 (PASA Report, 2000)

Depth	Whole Rock Mineralogy (Weight %)								Relative Clay Abundance (Normalized to 100%)		
	Quartz	K-Feldspar	Plagioclase	Calcite	Dolomite	Siderite	Pyrite	Total Clay	Smectite & Smectite*	Illite & Mica Mica	Chlorite
3236.0	75	0	13	0	0	3	0	9	0	13	87
3236.34	79	0	13	0	0	2	0	6	0	14	86
3237.06	71	0	16	1	0	4	0	8	7	14	79
3237.12	61	0	11	1	1	2	6	18	11	16	73
3238.12	78	0	12	1	1	0	0	8	10	16	74
3238.51	82	0	11	1	0	0	0	6	12	19	69
3239.36	35	0	12	0	0	0	1	52	41	44	15
3240.25	47	0	6	0	0	0	6	41	40	45	15
3241.5	49	0	19	0	0	0	0	32	33	36	31
3242.67	34	0	6	0	0	0	6	54	42	47	11
3243.71	60	4	17	1	0	0	1	17	23	26	51
3244.42	43	2	15	0	0	0	2	38	35	38	27
3245.33	41	0	11	0	0	0	0	48	35	42	23
3245.43	46	3	26	0	0	3	0	22	19	22	59
Average	57.2	0.6	13.4	0.4	0.1	1	1.6	25.6	22	28	50
Core2											
3283.0	61	0	24	0	0	2	1	12	12	13	75
3283.51	28	4	22	0	0	0	0	46	27	36	37
3285.0	71	0	17	0	0	3	Tr	9	13	14	73
3285.90a	72	0	17	0	0	0	0	11	9	13	78
3286.47	74	0	14	0	0	2	0	10	10	14	76
3287.33	64	0	16	11	0	1	0	8	9	14	77
3288.1	76	0	16	0	0	0	0	8	8	15	77
3288.3	34	0	9	0	0	0	4	53	37	48	15
3289.37	41	3	11	0	0	0	6	39	45	44	11
3290.6	49	0	17	0	0	0	0	34	32	41	27
3291.75	76	2	13	2	0	0	0	7	14	21	65
3293.12a	69	3	9	11	0	0	0	8	14	18	68
3293.12b	50	3	22	1	0	1	1	22	25	29	46
3296.18	52	6	20	1	0	0	1	20	28	32	40
Average	58.4	1.5	16.1	1.9	0	0.6	0.9	20.5	20.2	25.1	54.7

The results of the X-ray diffraction studies include detailed evaluations of the clay minerals and the quantification of the whole rock matrix components. The mineral phases identified by x-ray diffraction include quartz, K-feldspar, plagioclase, calcite, dolomite, siderite, pyrite and clay minerals. The clay mineral types in the samples studied include smectite, Illite and mica, and chlorite. Dolomite, calcite, siderite, pyrite, and K-feldspar were identified in few samples.

The sandstones of the formation in both cored intervals contain quartz particles as the dominant framework grains consisting of more than 57 % with clay which account for over 20 % proportion and plagioclase with 13 % and minor proportion of pyrite, siderite and calcite (Figure 5.34).

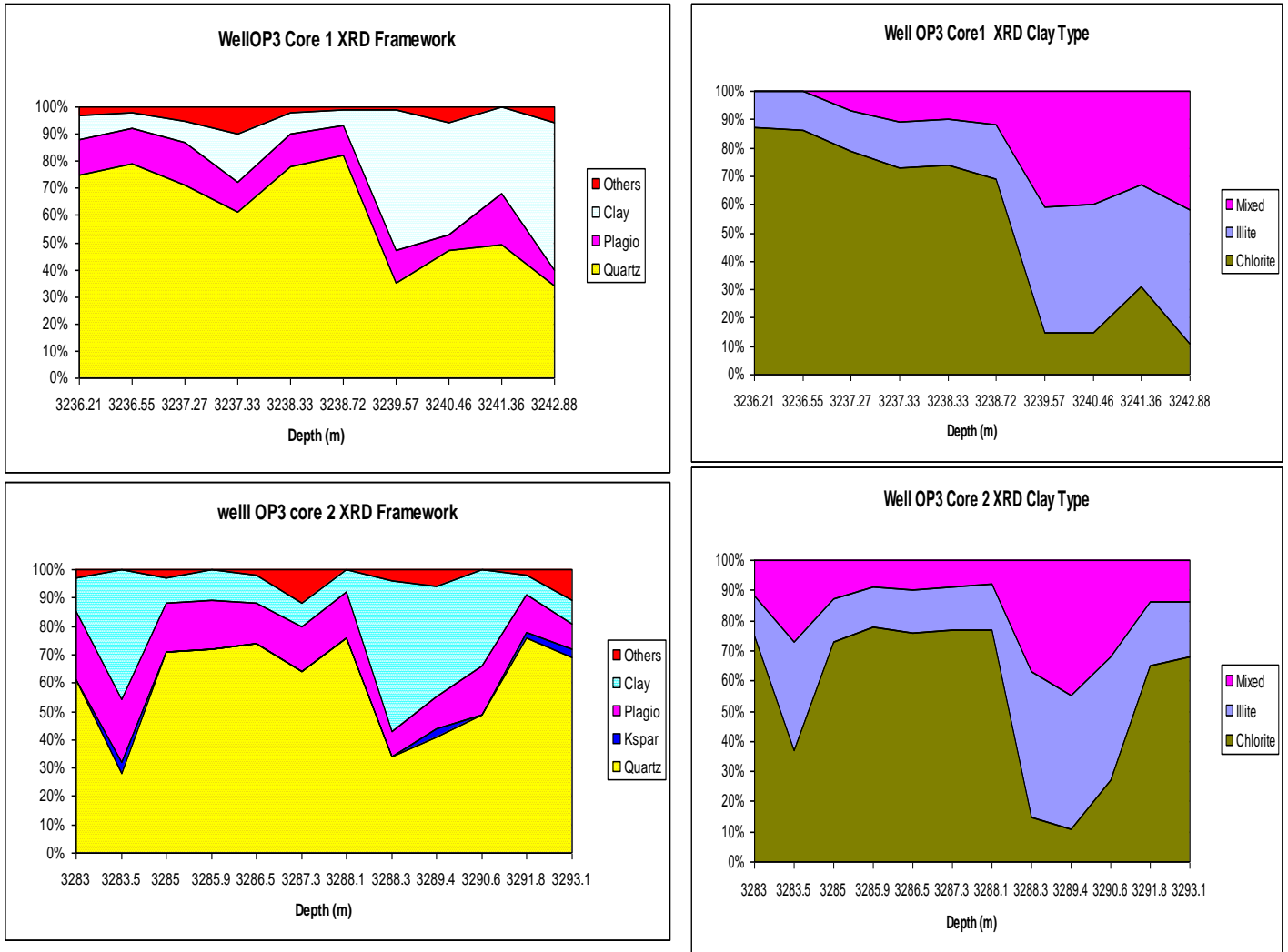


Figure 5.34: Whole rock mineralogy of core 1 and 2 of well OP3

Whole rock X-Ray Diffraction indicates that Chlorite is the main clay mineral type in both cored intervals. The proportion of Illitic clay (illite, mixed layer illite-smectite and mica) was also found with good proportion.

5.10.7.3 Scanning Electron Microscopy (SEM)

The shale materials in sandstone reservoirs can be distributed in the formation in three ways which are laminated, structural and dispersed. Shale can exist in the form of a lamina between layers of clean sand, and could also exist as structural grains or nodules within the formation matrix. The shaly material could also exist as dispersed throughout the sand, partially filling the inter-granular interstices or can be coating the grains (Schlumberger, 1987). Figure 5.35 below presents the three forms of existence of shale in sandstone reservoirs.

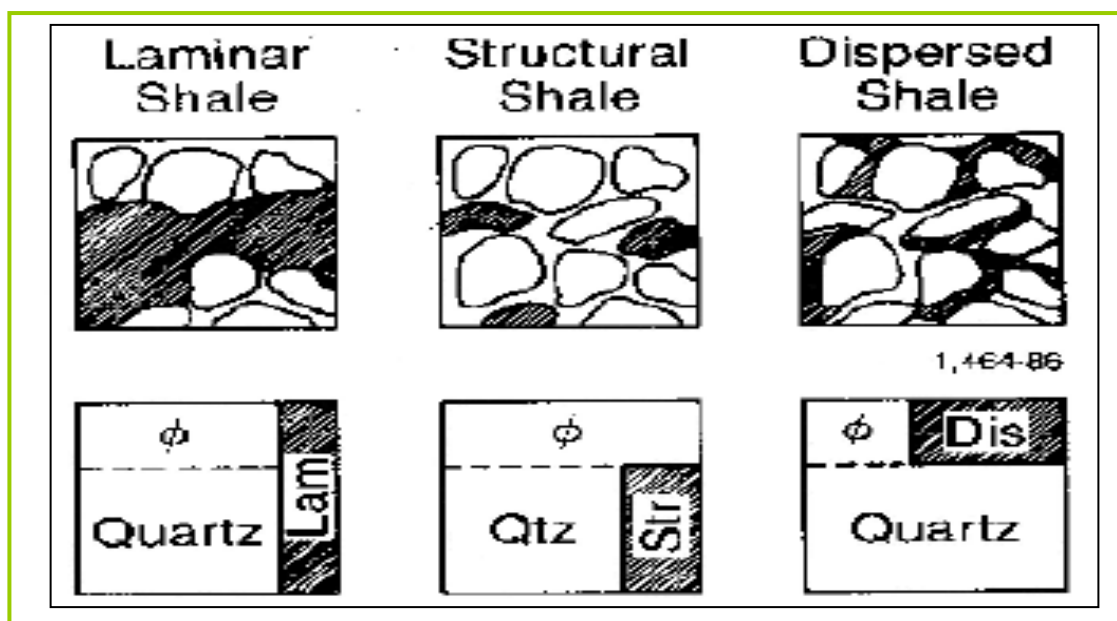


Figure 5.35: Different ways of shale distribution in a formation (Serra, 1984).

The most commonly found clay minerals in sedimentary rocks are the chlorite, Kaolinite, illite and smectite. The Scanning electron microscopy (SEM) shows images of these minerals because each has its own unique feature.

The two principle methods used to obtain images applied to reservoir rock samples are the transmission electron microscopy (TEM) and Scanning electron microscopy (SEM). In transmission electron microscopy, a high energy beam penetrates an ultra-thin sample and the image is formed from the projection of the transmitted electrons. Scanning electron microscopy uses a beam of medium energy electrons to scan the

surface of a sample. In this study, the SEM is used to have a visual examination of clay minerals that coat and fill the pore channels.

The limited resolution of optical microscopy does not allow detailed inspection of reservoir rock and particularly clay structures. Clay structures with dimensions below 0.5 micron cannot be resolved because the physical resolution of optical microscopy is limited to the wavelength of visible light of approximately 0.5 microns. The resolution that is required for inspection of clay structures can be provided by scanning electron microscopy which is able to reveal details to several nano-meters (Fens, 2000). The SEM analysis was carried out in well OP2 and OP3 by OMNI laboratories (forest report, 2005).

5.10.7.3.1 Well OP3

In well OP3, scanning electron microscopy (SEM) analyse was carried out in four samples with the Albian age as presented in the photos below. Pore filling chlorites was noticed on SEM as shown in the Figure 5.36 below.

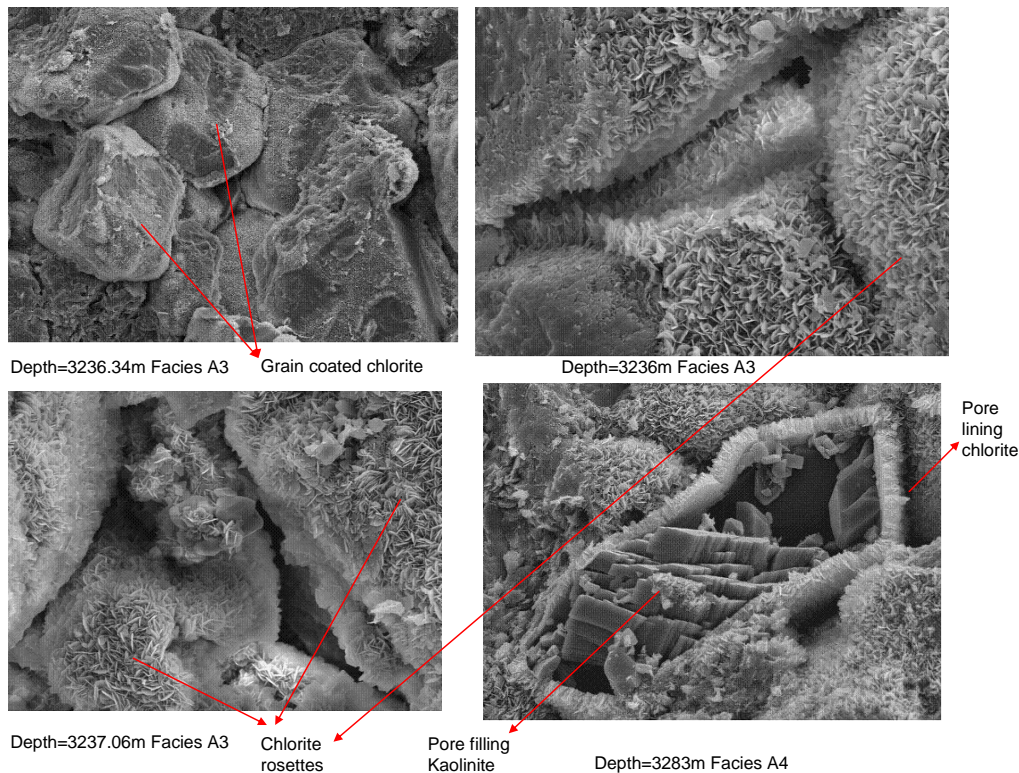


Figure 5.36: Example of Well OP3 SEM analysis result

5.10.7.4 Relationship between Chlorite and Facies

The petrographic analysis analyses revealed mineralogy with quartz being the dominant mineral in addition to abundant chlorite as the major clay mineral. The fine textured dispersed pore lining and pore filling chlorite mineral is detrimental to permeability and hence affect the reservoir quality and may be the possible causes of the low resistivity, hence the special focus on the effect of chlorite on the facies and its distribution.

The distribution of chlorite for well OP2 is presented in Figure 5.37 below.

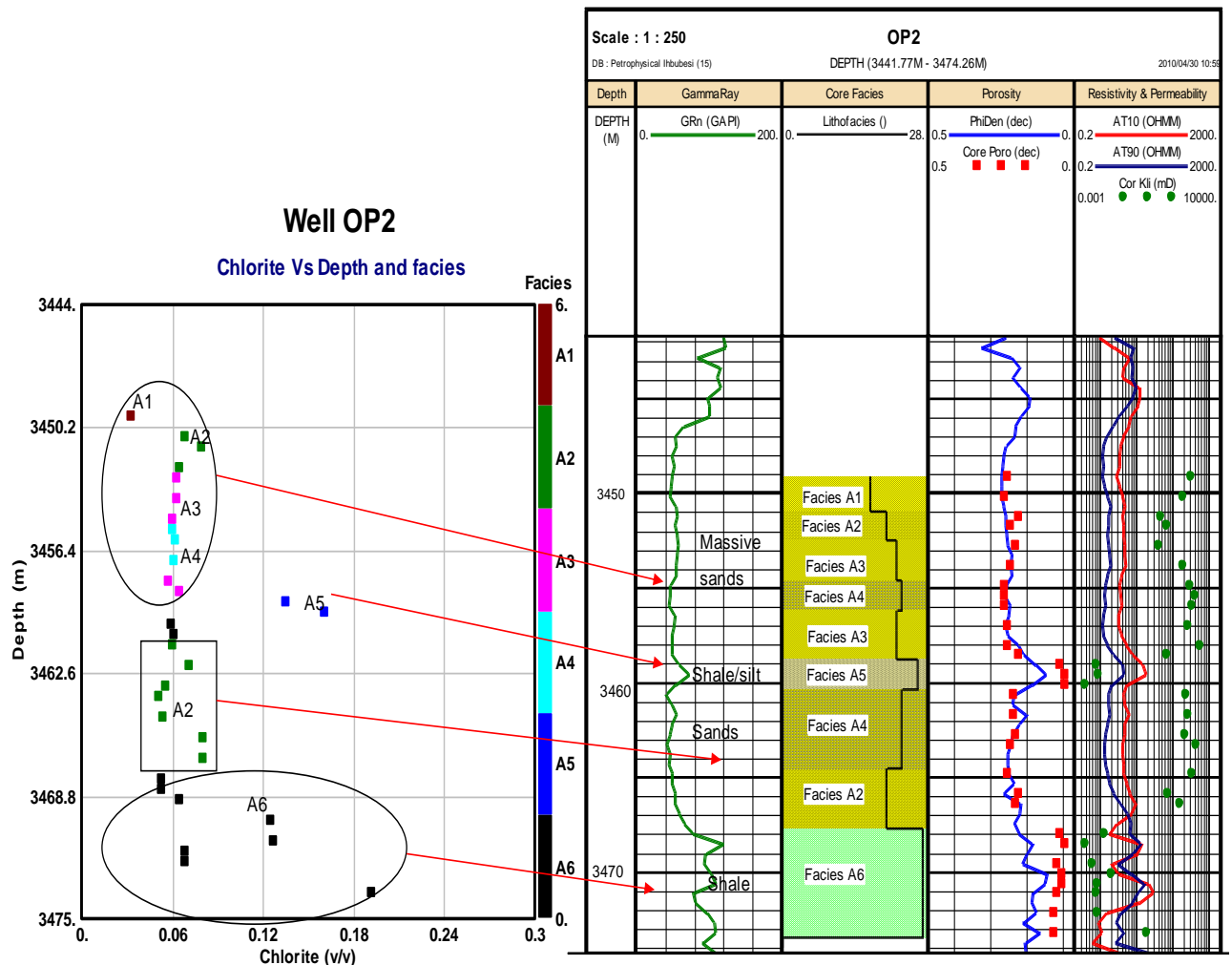


Figure 5.37: Distribution of chlorite for Well OP2

The plot shows that facies A1 has the lowest volume of chlorite of less than 3% and highest amount of chlorite was observed in facies A6 with chlorite volume that range from 5 % to 20 %. At the shale/silt interval (facies A5 and A6) relatively high chlorite content was also observed. It can be concluded that in well OP2, textural parameters and grain composition has a relationship with chlorite mineral in the pore-space of sandstone reservoirs.

The chlorite distribution with facies for well OP3 core 1 is presented in Figure 5.38 a below.

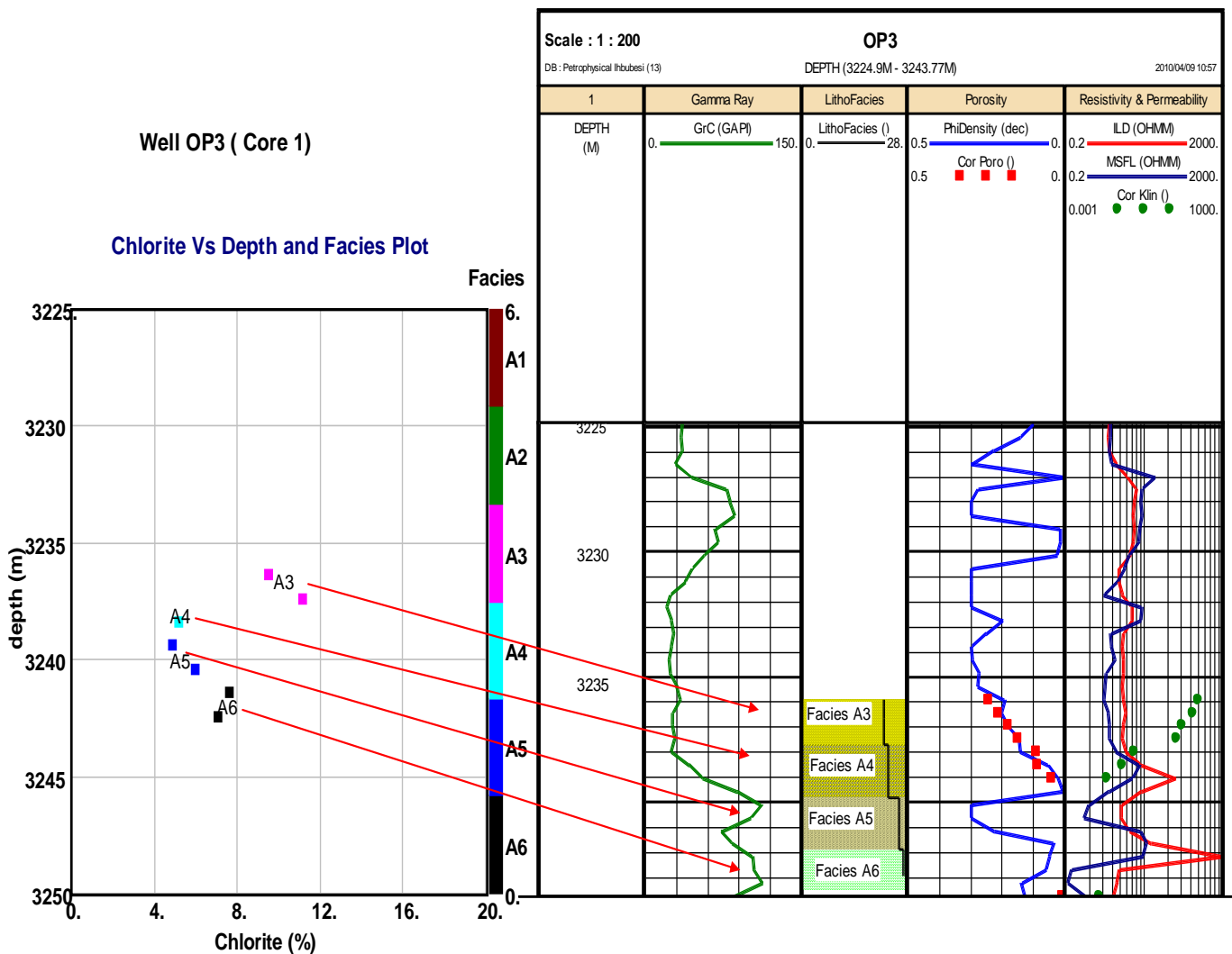


Figure 5.38a: Well OP3 core 1 chlorite distribution

In core 1 of well OP3, the highest amount of chlorite was observed in facies A3 in the range of 9 % to 11 %. The least amount of chlorite was recorded in facies A4. However, within the reservoir area (3235m to 3240m) the amount of chlorite tends to

decrease and a gradual increment was observed at below the reservoir interval (facies A5).

The plot of chlorite and facies for core 2 of well OP3 is shown below.

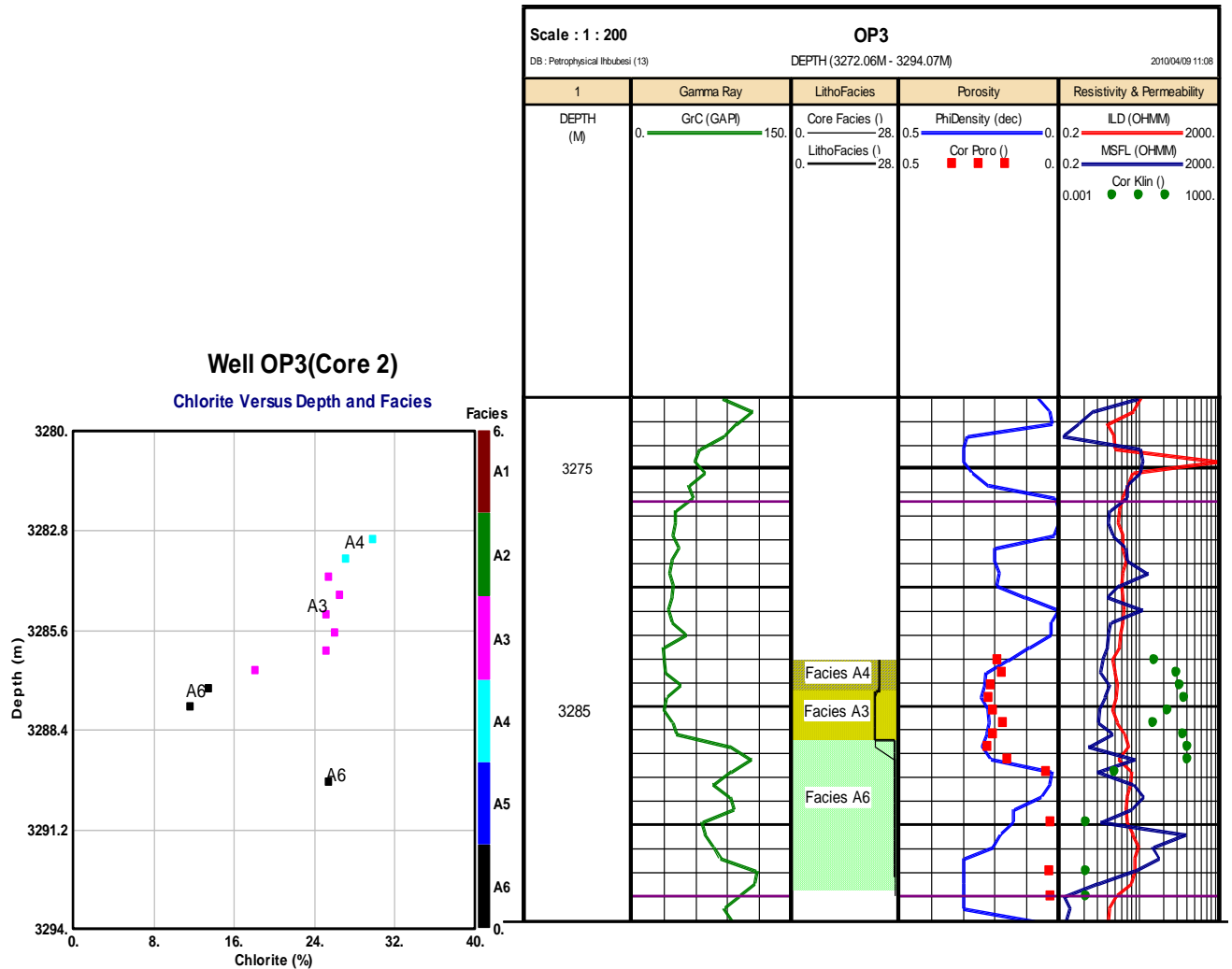


Figure 5.38b: Well OP3 core 1 chlorite distribution

In core 2 of well OP3, the highest amount of chlorite was observed in facies A4 within the reservoir section and a gradual decrease in chlorite from facies A4 to A3. At the base of the reservoir interval (measured depth 3287m) which is represented by facies A6, an increase in chlorite was also noticed.

In conclusion, the reservoir quality changes with proportion of chlorite and grain size, sorting and composition do influence the amount of chlorite in facies.

5.10.8 Cation Exchange Capacity (CEC)

The cation exchange capacity (CEC) is an important property of clay in shaly sand evaluation because it is the source of the excess conductivity in addition to the formation salinity. The cation exchange capacity (CEC) actually measures the concentration of sodium cations by chemical means and is termed cation exchange capacity and it is a reflection of the specific surface area of clay regardless of type. The results from this measurement can be related to the clay bound water and also help to identify producible shaly sands.

Crystalline surfaces of clay have what is known as exchange sites where ions can temporarily reside because of the charge imbalance on the external surface of clay's molecular building blocks (Bate, 1985). These exchange sites offer an electrical path through the clay by means of surface conductance. When in contact with saline solution, the cations on the surface layers of clay may be easily exchanged by other cations and are called exchangeable cations. The number of these cations can be measured and is called cation exchange capacity. The higher the amount of these cations in the formation, the higher the cation exchange capacity in the formation which implies higher surface conductance of clays. This shows that CEC can be used as an effective shaliness indicator.

The cation exchange capacity models result from a phenomena called the double layer. Winsaur and Mc Cardell (1953) are the first that introduced the double layer model. They stated that the excess conductivity, the double layer conductivity of shaly reservoir rocks was attributed to absorption on the clay surface and a resultant concentration of ions adjacent to this surface (Worthington, 1985). The most commonly used CEC models are the Waxman-Smith and Dual-Water shaly sand models.

Cation exchange capacity is expressed in milli-equivalents per gram of dry clay. For practical purpose Q_v , the cation exchange capacity per unit pore volume is used. For petrophysical evaluations, the cation exchange capacity is commonly determined by using the titration method using barium chlorite at or ammonium acetate. A piece of core plug end was crushed and weighed and a solution was used to exchange the cations. The solution was titrated while the conductivity also was monitored and CEC measured. For this study, the core plug samples were crushed and weighed and then sent to the Agricultural Research Council (ARC) Pretoria South Africa were the

ammonium acetate method was used to extract the cations using inductively coupled plasma spectroscopy.

The laboratory measurements of CEC was conducted on twenty five core plug ends samples of different facies of wells OP1, OP2 and OP3 at Agricultural Research Council and the results indicated existence of some degree of shaliness. This shaliness is represented by the value of Q_v as presented below.

5.10.8.1 Presentation of CEC Analysis Results

The laboratory measurement of cation exchange capacity was conducted on twenty five core samples of well OP1, OP2 and OP3 as presented in the Table 5.25 below.

Table 5.25: Result of cation exchange capacity (CEC) for Wells

Well OP1			Well OP2			Well OP3		
Depth (m)	CEC (meq/100g)	Type	Depth (m)	CEC (meq/100g)	Type	Depth (m)	CEC (meq/100g)	Type
3370.240	4.700	A3	3450.500	2.270	A1	3230.35	1.870	
3371.280	4.480	A3	3452.500	1.700	A1	3236.270	1.690	A3
3372.700	2.040	A4	3454.000	2.160	A2	3236.960	1.920	A3
3375.020	11.080	A5	3455.500	1.500	A2	3239.180	1.800	A4
3376.230	6.790	A4	3457.050	2.420	A3	3244.750	17.530	A6
			3460.240	3.970	A4	3283.600	1.450	A4
			3463.050	2.580	A3	3283.900	4.930	A4
			3465.800	5.020	A4	3284.300	1.520	A3
			3466.450	2.270	A4	3285.970	8.010	A3
			3469.200	5.640	A4	3289.590	2.690	A6

5.10.8.2 Q_v , the Shale Indicator Determination

The cation exchange capacity per volume (Q_v) which is regarded as shale indicator was determined from the laboratory measured cation exchange capacity (CEC) data. The equation for the calculation of Q_v is given below:

$$Q_v = \frac{CEC (1 - \Phi) \rho_{ma}}{\Phi * 100} \dots \dots \dots (5.11)$$

Where:

Q_v = Cation exchange capacity per pore volume

CEC = cation exchange capacity

ρ_{ma} = Grain density (g/cc)

Φ = Porosity (fraction)

Applying equation 5.11, the following values for Q_v were obtained:

Table 5.26: Calculated values of cation exchange capacity per pore volume for Wells

Well OP1			Well OP2			Well OP3		
Depth (m)	CEC (meq/100g)	Qv (meq/l)	Depth (m)	CEC (meq/100g)	Qv (meq/l)	Depth (m)	CEC (meq/100g)	Qv (meq/l)
3370.240	4.700	0.532428	3450.500	2.270	0.212762	3230.35	1.870	Nil
3371.280	4.480	0.618885	3452.500	1.700	0.144273	3236.270	1.690	0.15511508
3372.700	2.040	0.588528	3454.000	2.160	0.193799	3236.960	1.920	0.19110819
3375.020	11.080	9.637015	3455.500	1.500	0.174926	3239.180	1.800	1.07362047
3376.230	6.790	2.165022	3457.050	2.420	1.964299	3244.750	17.530	7.332799
			3460.240	3.970	0.355514	3283.600	1.450	0.17945461
			3463.050	2.580	0.285748	3283.900	4.930	0.61014566
			3465.800	5.020	4.463617	3284.300	1.520	0.15051283
			3466.450	2.270	0.930693	3285.970	8.010	1.02235843
			3469.200	5.640	1.96272	3289.590	2.690	3.07376943

5.10.8.3 Clay Bound Water (CBW), Porosity and Qv

The clay bound water is the volume of water retained by or associated with clay surfaces and clay interlayer due to electrochemical bonding. The bound water includes fresh water absorbed to clay surfaces and the hydration water of clay exchange cations but does not include water retained by capillary or formation water. The volume of the clay bound water is proportional to the surface area and is significant with clay minerals having moderate to high surface area such as chlorite, illite and mixed-layer illite/smectite and varies according to salinity of the formation (John and Marin (2006)).

According to John Dewan (1983), a relationship between the fraction of pore water (Swb) that is bound to the clay and Qv is given below:

$$S_{wb} = W * Q_v \dots\dots\dots (5.12)$$

Where:

S_{wb} = Fraction of pore water

W = Amount of bound water approximated as 0.3 cc/ meq.

Q_v = Cation exchange capacity per pore volume (meq/l)

In order to determine the effective porosity measured on core samples, the clay bound water is subtracted from the total porosity as shown below:

$$\Phi_e = \Phi_t - CBW \dots\dots\dots (5.13)$$

Where

Φ_e = Effective Porosity (v/v)

Φ_t = Total Porosity (v/v)

CBW = Clay bound water (v/v)

Equation 4.14 can then be written as follows:

$$\Phi_e = \Phi_t (1 - S_{wb}) \dots\dots\dots (5.14)$$

Equation 5.14 was applied to determine the effective porosity by removing the clay effect on the porosity. Table 5.27 below present results of the effective porosity and clay bound water calculated.

Table 5.27: Calculated effective porosity and clay bound water for Wells

Well OP1							
Depth (m)	CEC(meq/100g)	Qv (meq/l)	Swb (v/v)	Φ_t (v/v)	Φ_e (v/v)	CBW (v/v)	Remark
3370.240	4.700	0.5324279	0.159	0.189	0.158	0.031	Not Used
3371.280	4.480	0.6188847	0.186	0.164	0.133	0.031	
3372.700	2.040	0.588528	0.177	0.085	0.069	0.016	
3375.020	11.080	9.6370147	2.89	0.03	-0.056		
3376.230	6.790	2.1650224	0.65	0.077	0.027	0.05	
Well OP2							
Depth (m)	CEC(meq/100g)	Qv (meq/l)	Swb (v/v)	Φ_t (v/v)	Φ_e (v/v)	CBW (v/v)	Remark
3450.500	2.270	0.2127621	0.063	0.223	0.208	0.015	Not Used
3452.500	1.700	0.1442733	0.04	0.24	0.229	0.011	
3454.000	2.160	0.193799	0.058	0.23	0.216	0.014	
3455.500	1.500	0.1749255	0.052	0.188	0.178	0.01	
3457.050	2.420	1.9642993	0.58	0.033	0.0135	0.0195	
3460.240	3.970	0.3555144	0.11	0.231	0.206	0.025	
3463.050	2.580	0.2857482	0.85	0.196	0.179	0.017	
3465.800	5.020	4.4636167	1.33	0.03	-0.01	0.04	
3466.450	2.270	0.9306927	0.27	0.062	0.044	0.018	
3469.200	5.640	1.96272	0.588	0.072	0.029	0.043	
Well OP3							
Depth (m)	CEC(meq/100g)		Swb (v/v)	Φ_t (v/v)	Φ_e (v/v)	CBW (v/v)	Remark
3230.35	1.870						Not Used
3236.270	1.690	0.1551151	0.046	0.226	0.215	0.011	
3236.960	1.920	0.1911082	0.057	0.214	0.2	0.014	
3239.180	1.800	1.0736205	0.322	0.043	0.029	0.014	
3244.750	17.530	7.332799	2.199	0.06	-0.07		
3283.600	1.450	0.1794546	0.053	0.178	0.1684	0.0096	
3283.900	4.930	0.6101457	0.183	0.178	0.1454	0.0326	
3284.300	1.520	0.1505128	0.045	0.213	0.2033	0.0097	
3285.970	8.010	1.0223584	0.3	0.173	0.119	0.054	
3289.590	2.690	3.0737694	0.92	0.023	0.0017	0.0213	

Three of the core sample plugs one each from each well was not used for other analysis because they gave erroneous values. The Qv was plotted against the fractional values of pore water saturation (Swb) on a linear scale for all the wells in Figure 5.39 below.

All Well

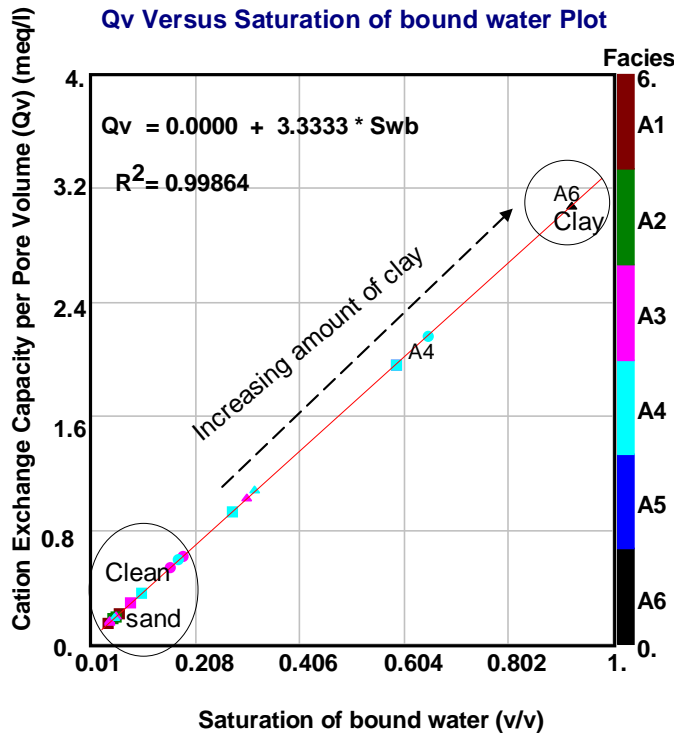


Figure 5.39: Plot of Qv versus saturation of bound water for all Well.

It was observed from the plot that core facies A1 and A2 have very low amount of cation exchange capacity per pore volume (Qv) and saturation of bound water (Swb). Highest amount of both Qv (2.69 meq/l) and saturation of bound water (92 %) was observed in facies A6. It could be interpreted that Facies A6 would retain the highest amount of bound water in its surfaces, followed by Facies A4, A3 and A2 and A1. Generally, as the amount of cation capacity per pore volume increases, the amount of clay increases and the saturation of bound water also increases.

A linear empirical relationship was established from the cross plot as follows

$$Q_v = 3.3333 * (S_{wb}) \dots\dots\dots (5.15)$$

$$R^2 = 0.99864$$

The cation exchange capacity per pore volume (Qv) was also plotted against porosity on a linear scale to establish an empirical relationship between them as shown in Figure 5.40a below.

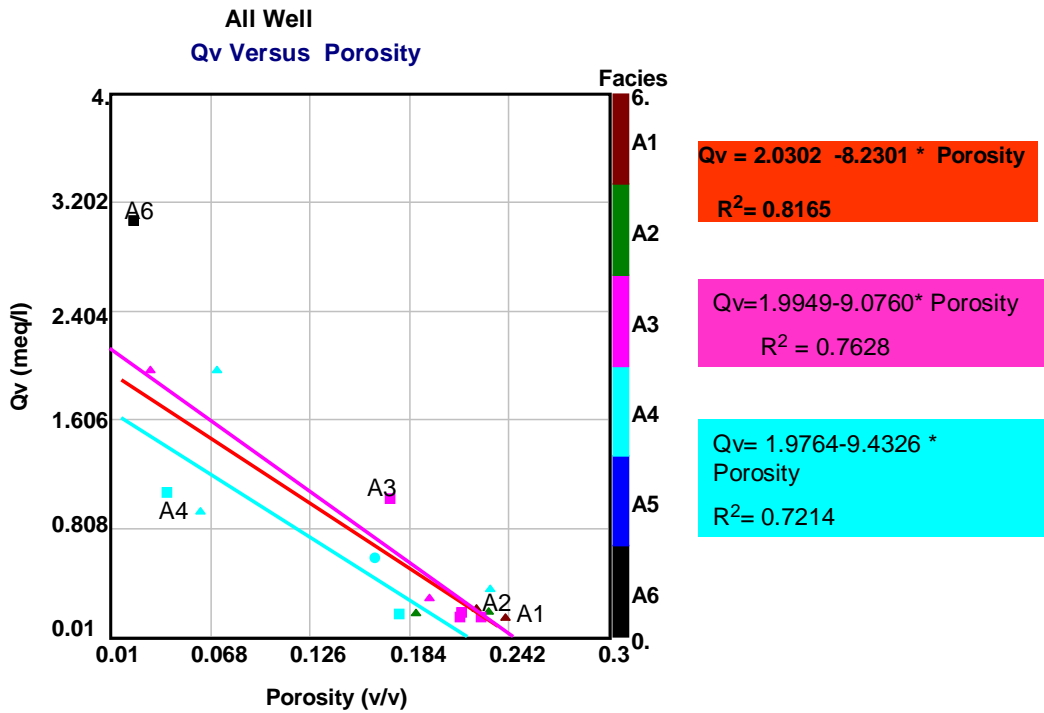


Figure 5.40a: Plot of Qv versus Total and effective porosities for all Well

The plot of Qv versus porosities in Figure 5.40 above presents an inverse relationship between the cation exchange capacity per pore volume and porosities. Facies A1, A2, and A3 showed porosity values greater than 12 % at very low Qv values less than 0.1 meq/l. While facies A4 generally presents Qv values of above 0.8 meq/l and porosities below 10 % except in two core samples and highest value of Qv was obtained in facies A6 at very low porosity value (less than 1 %).

The empirical relationship between the Qv and the porosities for different facies was obtained as given in the following equations below.

$$Q_v \text{ (meq/l)} = 2.0302 - 8.2301 * \text{Porosity} \dots\dots\dots (5.16a)$$

$$R^2 = 0.8165 \text{ (for all well)}$$

$$Q_v \text{ (meq/l)} = 1.9949 - 9.0760 * \text{Porosity (v/v)} \dots\dots\dots (5.16b)$$

$$R^2 = 0.7628 \text{ (facies A3)}$$

$$Q_v \text{ (meq/l)} = 1.9764 - 9.4326 * \text{Porosity} \dots\dots\dots(5.16c)$$

$$R^2 = 0.7214 \text{ (facies A4)}$$

An empirical relationship between saturation of bound water and porosity was also determined through the linear cross plot of porosity versus saturation of bound water. The idea is to be able to predict saturation of bound water from log porosity in Wells without Qv data. The saturation of bound water is required in calculation of water saturation using the cation exchange capacity shaly sand model.

The plot is presented in Figure 5.40b below.

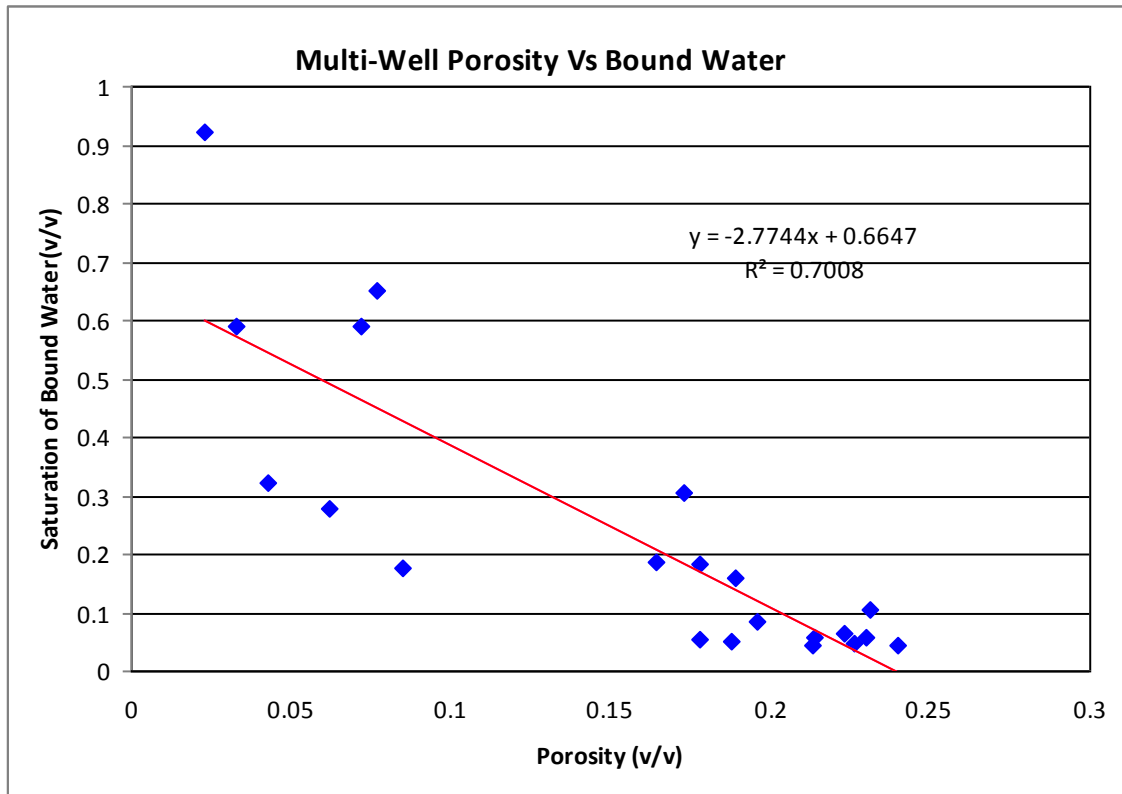


Figure 5.40b: Multi-Well porosity versus saturation of bound water plot.

An empirical relationship was established from the cross plot with good regression coefficient as given in the equation below.

$$S_{wb} = 0.6647 - 2.7744 * \text{Porosity} \dots\dots\dots(5.16d)$$

$$R^2 = 0.7008$$

It could be concluded from the cation exchange capacity analysis that shaly sands with cation exchange capacity per pore volume (Qv) value higher than 1 have higher quantity of clay bound water as indicated in the saturation of bound water (Swb) values. As the Qv increases there is a corresponding increase in saturation of bound

water (Figure 5.39 and Table 5.30) meaning that more water will be bound at the surfaces of the shaly sand formation.

It was also observed that cation exchange capacity has a good relationship with porosity. At low Q_v values, porosities tend to increase as shown in the cross plots of Figure 5.40. Facies A6 has the highest bound water retention capacity and facies A1 and A 2 the least bound water retention capacity.

5.10.9 Capillary Pressure Measurements

Capillary Pressure is defined as the difference in pressure between the non-wetting and wetting phases of fluid. The difference in pressure causes the interface between the two phases to be curved. The curvature of the interface between the two fluids and the shape of the pore space or the grain determine the saturation of the two phases. The relationship between the saturation and the capillary pressure is expressed in terms of a capillary pressure curve. The capillary pressure curves may be determined under drainage or imbibition conditions. Under drainage condition, a non-wetting phase is displacing a wetting phase; an example is mercury displacing air. Under imbibition condition, a wetting phase is displacing a non wetting phase; example is displacement of oil by water in water wet rock.

The special core analysis capillary pressure measurements are measurements made on core plugs at increasing pressures. The laboratory capillary pressure curves are used to define water saturations, pore throat size and distribution, depth of reservoir fluid contacts, and computation of height above free water level, transition zone height and relative permeability.

The capillary measurements are of three types. They are the restored porous plates, centrifuge capillary pressure, and the mercury injection measurements. The results from the capillary pressure measurements gives location and amount of irreducible and mobile water saturations, identifies hydraulic units in pressure communication, highlights rock type differences, height and location of reservoir transition zones, and pore entry pressure.

The restored state cell (Air-Brine porous plate cell) method involves cleaning and drying of samples and pressure saturated with simulated formation brine. The fully saturated samples are placed in a porous plate cell and de-saturated using humidified nitrogen as the displacing phase at increasing incremental pressures up to 180 psig.

After a minimum of four days at each pressure, equilibrium saturations are determined gravimetrically. These measurements were performed in two wells (OP1 and OP3).

The mercury injection capillary pressure measurements method was made on three core plugs of well OP2. Before carrying out the measurements, the core plug samples were cleaned using a simple distillation to extract hydrocarbon and other pore-fillings. Compound and samples were dried to remove residual moisture. Injected mercury was monitored at 52 pressure points from 1.01 to 54,900 psia.

The results from this analysis include drainage curves for each sample based on wetting phase saturation, pore aperture diameter distribution, and mercury derived porosity and permeability.

5.10.9.1 Well OP1 Air-Brine Capillary Pressure Measurement Results

The restored state cell capillary pressure method was performed on four core plug samples at increasing pressures from 2 to 180 psig (Table 5.28).

Table 5.28: Well OP1 capillary pressure test data

Depth (m)	Brine saturation (%)							Capillary Pressure (psi)						
	91	71	57	52	50	46	43	2	4	8	15	35	80	180
3370.4	91	71	57	52	50	46	43	2	4	8	15	35	80	180
3371	64	51	48	45	42	40		4	8	15	35	80	180	
3371.6	75	56	51	48	45	42		4	8	15	35	80	180	
3372.3	71	64	57	52				15	35	80	180			

5.10.9.2 Well OP3 Air-Brine Capillary Pressure Measurement Results

The air-brine restored state cell capillary pressure measurement method was performed on ten core plug samples of well OP3 as presented in Table 5.29 below.

Table 5.29: Well OP3 capillary pressure test data

Depth (m)	Brine Saturation (%)								Capillary Pressure (psi)							
3283.2	100	100	98.4	82.7	71.4	63.2	53.3	50	1	2	4	8	15	35	100	180
3283.4	100	100	97.9	83.9	71.2	62.7	55.7	52.1	1	2	4	8	15	35	100	180
3283.5	100	100	97.8	87.6	72.8	63.5	55.9	51.6	1	2	4	8	15	35	100	180
3284.74	100	94.8	67.6	59.8	54.9	48.1	40.3	37.9	1	2	4	8	15	35	100	180
3284.77	100	95.7	72.6	62.9	57.6	50.5	41.2	38	1	2	4	8	15	35	100	180
3284.85	100	96.1	68.4	60.4	55.2	49.7	40.9	37.4	1	2	4	8	15	35	100	180
3286.95	97.9	85.8	68	61.2	56	49	41.8	36.3	1	2	4	8	15	35	100	180
3286.99	98.2	80.7	62.9	57.2	52.4	45.5	37.3	33	1	2	4	8	15	35	100	180
3287	97.6	78.7	60.9	55.4	50.7	44.4	35.9	32.5	1	2	4	8	15	35	100	180
3287.1	97.1	78.8	60.7	55	50.4	44.2	35.7	32.4	1	2	4	8	15	35	100	180

5.10.9.3 Well OP2 Mercury-Injection Capillary Pressure Measurement Results

The mercury injection capillary pressure test method was performed on three core plug samples of well OP2. Injected mercury was monitored at 52 pressure points from 1.01 to 54,900 psia (appendix D).

5.10.10 Interpretation of Capillary Pressure Results

The capillary pressure curve is based on the observation that the entry pressure and the plateau of a capillary pressure curve are very closely related to the permeability. The permeability is also related to the pore size distribution because at the entry pressure and the start of the plateau in a capillary pressure curve, the invading non-wetting fluid is entering into the sample and the flow is in the Darcy regime (Mishra & Sharma, 1988; Dias & Payatakes, 1996). A theoretical example of capillary pressure curve is given in Figure 5.41 below.

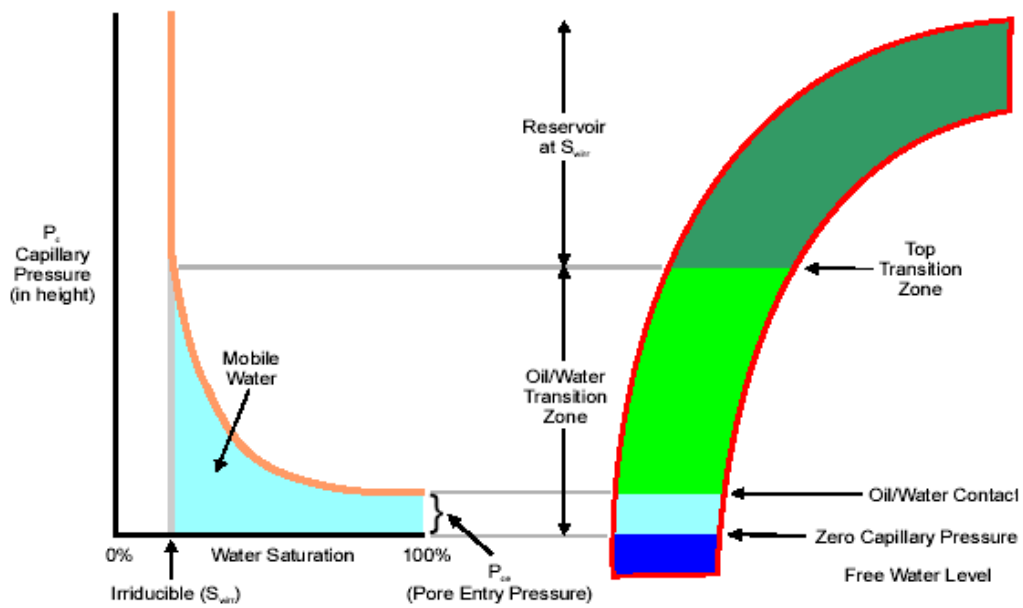


Figure 5.41: Schematic relationship between capillary pressure curve and oil accumulation (Holmes, 2002).

The standard techniques to obtain the capillary pressure curves are the porous plate method, centrifuge and the air-mercury injection methods. Application of the capillary pressure curve is the estimation of the irreducible water saturation (S_{wirr}) which is used to determine the maximum volume of hydrocarbons in the reservoir and the mobile water saturation (S_w). The hydrocarbon-water contact is the maximum depth with either water free production or economic production. The free water level is regarded as the intersection of hydrocarbon pressure gradient line and water pressure gradient line where hydrocarbon and water pressure are equal.

The restored state cell (Air-Brine porous plate cell) method was conducted on fourteen samples in well OP1 and OP3, while the mercury injection capillary pressure method was applied on three samples of well OP2.

5.10.10.1 Well OP1 Water Saturation Determination from Capillary Pressure Curves

The porous plate method of capillary pressure measurement was undertaken on four samples of well OP1 (Table 5.28) above. To construct the curve, the capillary

pressure data measurement at laboratory condition was plotted on the y-axis against the brine saturation on linear scales as shown (Figure 5.42).

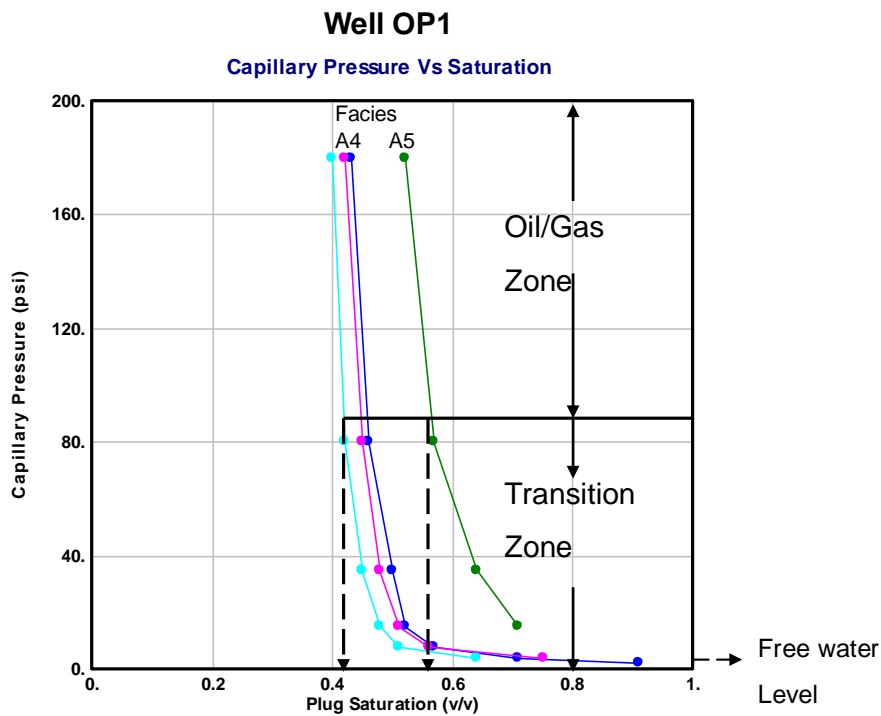


Figure 5.42: Capillary pressure curve for well OP1

The capillary pressure curve of the well indicate the minimum irreducible water saturation (S_{wirr}) of about 42 % at measured depth 3271m of facies A4 , while the highest irreducible water saturation of about 56 % was observed of facies A5 at measured depth of 3372.3m . The differences in the irreducible water saturation may be attributed to clay type and mode of distribution and pore geometry, permeability and the type of facies.

The point at which the capillary pressure is zero is equivalent to the free water level. The transition zone (point were hydrocarbon and water could be produce) would have been sharp if all the pores are of the same size. At depth 3372.3m (facies type A5), different pore size is clearly shown (Figure 5.42) and this may be fine grain that has the ability to retain high amount of irreducible water.

5.10.10.2 Well OP3 Water Saturation Determination from Capillary Pressure Curves

The porous plate method of capillary pressure measurement was undertaken on ten samples of well OP3 (Table 5.29) above. To construct the curve, the capillary pressure data was plotted on the y-axis against the brine saturation as shown (Figure 5.43).

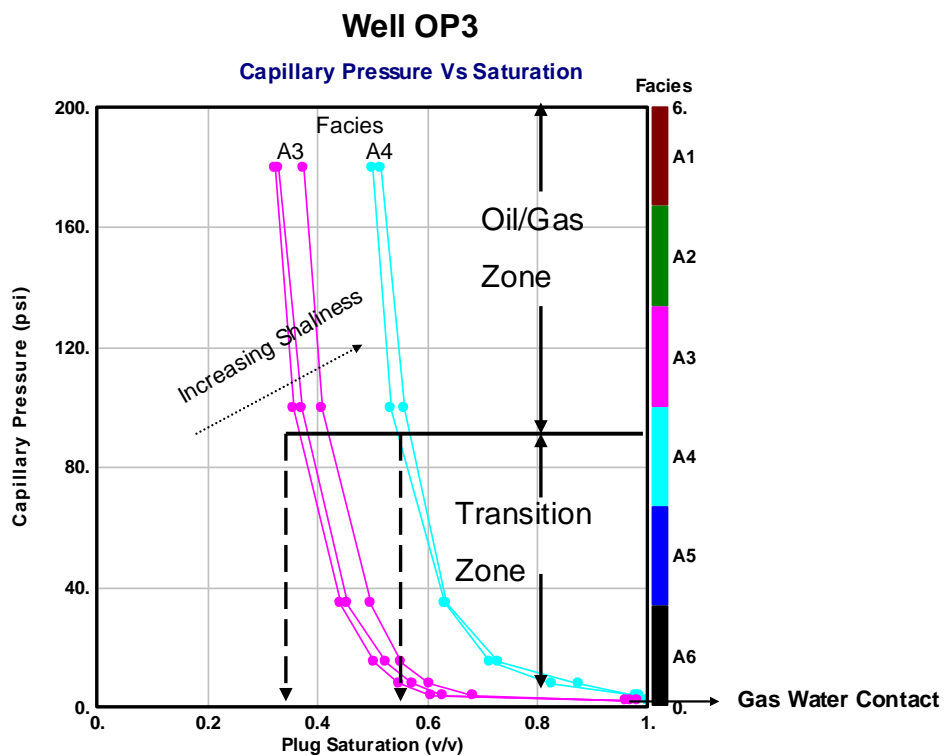


Figure 5.43: Capillary pressure curve for Well OP3

The minimum value of irreducible water saturation (S_{wirr}) of well OP3 was estimated to be 38 % (Figure 5.43) on facies A3 at a measured depth of 3287.1m and maximum irreducible water saturation of 56 % was estimated on facies A4 at a measured depth of 3283.5m. It was observed that the cleaner the sand, the lower the irreducible water saturation.

5.10.10.3 Well OP2 Water Saturation Determination from Capillary Pressure Curves

The mercury injection capillary pressure method was performed on three core samples of well OP2. Injected mercury was monitored at 52 pressure points from 1.01 to 54,900 psia (appendix D). Figure 5.44 below present the linear scale plot of injected mercury pressure against saturation.

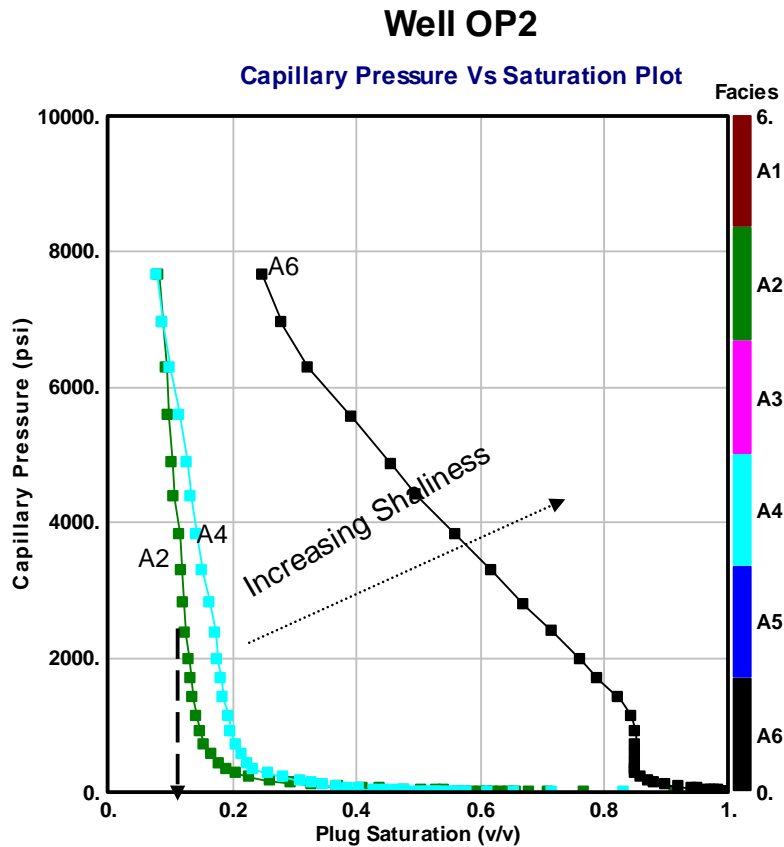


Figure 5.44: Capillary Pressure Curve for Well OP2

The minimum point of irreducible water saturation was estimated at about 11 % at a measured depth of 3447.08m which represents core facies A2, while the highest irreducible water saturation was observed at depth 3467.5m which represents core facies A6 with an estimated value of about 84 %. This shows that non reservoir rock samples like facies A6 gives very high values of irreducible water saturation values and therefore may not be useful for further analysis.

The point at which the capillary pressure is zero equals to the free water level. The possible gas water contact (GWC) for this well was located at the free water level.

Above the gas water contact, it is expected that oil will displace water first in the large pores, then in the medium pores, and finally in a smaller pores as elevation increases. The medium grains will be associated with depth 3447.08m and fine grains at depth 3467.5m.

Comparison of the mercury injection with the porous plate capillary pressure measurement showed that the mercury injection measurements do not provide a corresponding measurement for oil and water system but shows how various rock types can expel a non-wetting phase when pressure is reduced. The porous-plate capillary pressure method gives accurate results irrespective of the types of facies or rock measured. Mercury injection also provides the same good results as well but a scaling factor equal to the interfacial tensions ratio and a contact angle equal to zero is often used (Omeregje, 1986).

The mercury injection method is a repetitive and fast method but the representative of the capillary pressures are doubtful for high clay content porous media (Gauchet, 1993).

A plot of capillary pressure curves with porosity and permeability clearly showed that as the sandstone becomes cleaner and as permeability increases, the irreducible water saturation becomes smaller (Figure 5.45) below. Porosity does not have much effect on capillary pressure curves as shown in the Figure 5.45 below.

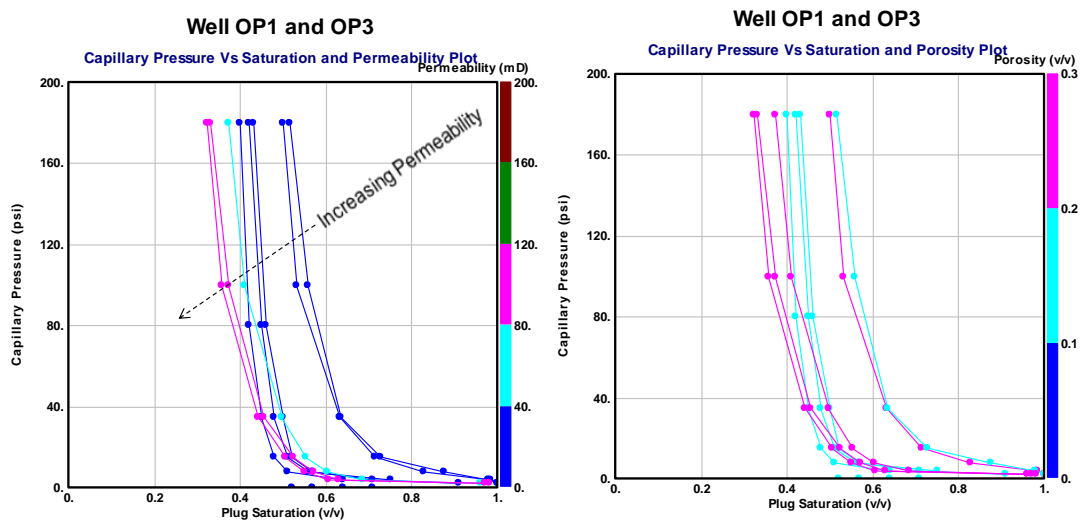


Figure 5.45: Capillary pressure curves with permeability and porosity

In conclusion, it has been demonstrated that coarse-grained sandstones and other rocks with large pores will have relatively low irreducible water saturation and good

to excellent permeability values. Facies A2 present value of irreducible water saturation of less than 12%; facies A3 in the range of 38 to 44 %; facies A4 between 52 to 56 %; facies A5 about 58 %, and facies A6 of 84 %. Fine-grained sandstones and rocks with small pores tend to have relatively high irreducible water saturation. Permeability also depends on pore dimensions and sandstones with large connected pores have high permeability values while fine-grained sandstones have low permeability values. Porosity however does not necessarily depend on pore dimension or configuration.

5.11 Saturation –Height Determination from Leverett’s J-Function Method

The capillary pressure derived saturation height function can be used to calculate the free water level for geological modelling and reservoir simulation to normalize capillary pressure curves. There are many forms of the saturation-height functions as mentioned in chapter three of this work, but discussions will be focused on the Leverett’s J-Function method.

In 1940, Leverett introduced a dimensionless J-function or equation to convert all capillary data with similar pore geometry to a universal curve. Leverett was the first to introduce a dimensionless capillary function correlating capillary pressure curves with petrophysical properties of the reservoir rock (Leverett, 1941). Based on experiments, he proposed the following dimensionless group as a function of wetting fluid saturation (S_w) for capillary pressure (P_c) modelling as

$$J(S_w) = 0.2166 * \frac{P_c \sqrt{K/\Phi}}{\sigma \cos \theta} \dots\dots\dots (5.17)$$

Where:

$J(S_w)$ = Leverett’s water Saturation J function

P_c = Capillary pressure at laboratory condition (psi)

K = Core plug permeability (mD)

Φ = Core Plug porosity (fractional)

σ = Interfacial tension, (dynes/cm)

θ = Contact angle in a gas/water or oil/water system, (degrees).

The J-function considers the changes of permeability, porosity and wettability of the reservoir as long as the pore geometry remains constant. Different rock types show different J-function correlations and all the capillary pressure data from a specific formation can be reduced to a single J-function versus saturation curve.

To convert capillary pressure from laboratory to reservoir conditions the following was used:

$$P_c \text{ res} = \frac{P_c \text{ lab} * (\sigma * \cos \theta) \text{ res}}{(\sigma * \cos \theta) \text{ lab}} \dots\dots\dots(5.18)$$

$$J (\text{Sw}) \text{ res} = \frac{P_c \text{ res}}{(\sigma * \cos \theta) \text{ lab}} \sqrt{K/\Phi} \dots\dots\dots(5.19)$$

Where:

$P_c \text{ res}$ = Capillary pressure at reservoir condition (psi)

$P_c \text{ lab}$ = Capillary pressure at laboratory condition (psi)

$(\sigma * \cos \theta) \text{ res}$ = Interfacial tension and contact angle at reservoir condition=50

$(\sigma * \cos \theta) \text{ lab}$ = Interfacial tension and contact angle at laboratory condition = 72

$J (\text{Sw}) \text{ res}$ = Saturation function at reservoir condition

To convert the capillary pressure pressures to height, the following relation was used:

$$P_c \text{ res} = \frac{(\text{den} (w) \text{ res} - \text{den}(g \text{ res}) * H_t}{0.3048} \dots\dots\dots(5.20)$$

Where:

$\text{den} (w \text{ res})$ = Density of water at reservoir condition= 0.44 psi/ft=1.42 psi/m =1.02 g/cc.

$\text{den} (g \text{ res})$ = Density of gas at reservoir condition = 0.088 psi/ft=0.28 psi/m=0.2 g/cc.

H_t = Height in m.

The fluid densities of the respective wells at reservoir conditions were determined from the wireline repeat formation test (RFT) as indicated in appendix K.

J-function can also be calibrated to wetting phase saturation in the form given below.

$$J(S_w) = a * S_w^b \dots \dots \dots (5.21)$$

Where “a” and “b” are constant derived from an equation for all the capillary pressure curves regression analysis of J (S_w) versus saturation plot Figure (5.46) below.

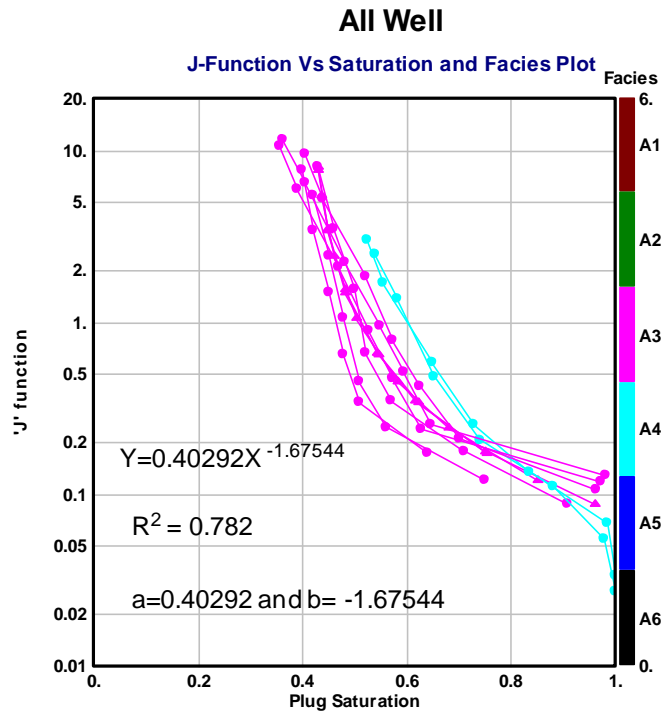


Figure 5.46: Leverett’s saturation determination J-function

The application of the normalized capillary pressure curve using the universal J-function gives a better picture of the capillary pressure curves as they appear to be closer to each other as presented in Figure 5.47 below.

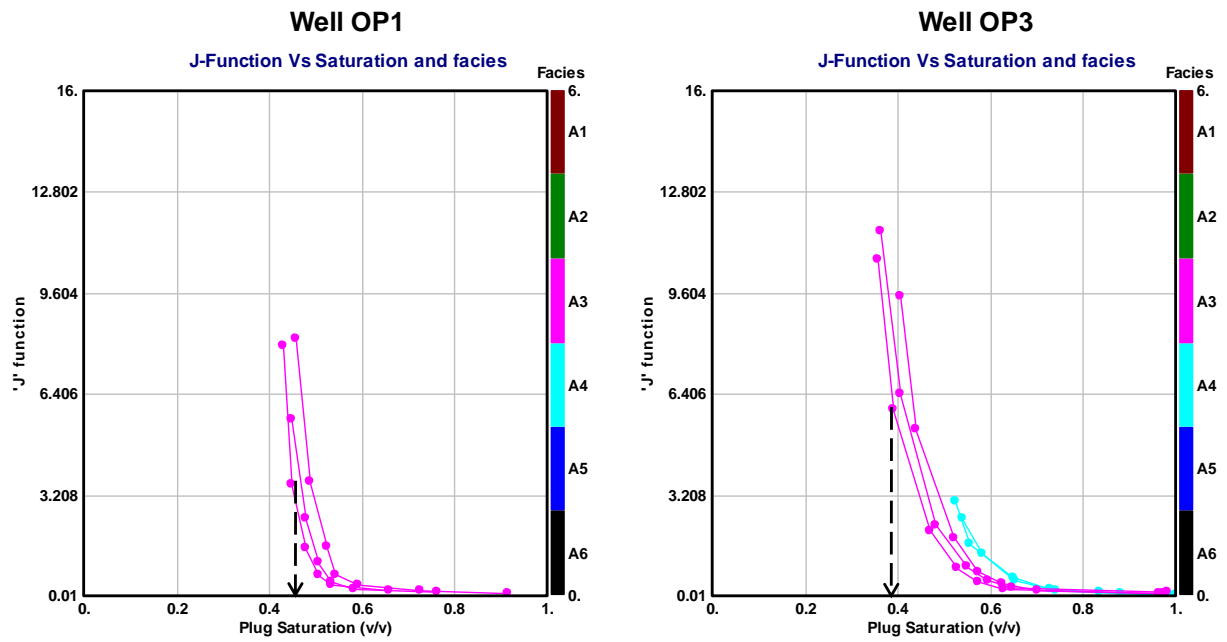


Figure 5.47: J-function curves for well OP1 and OP3

The saturation-height function have been established from the capillary pressure data using the J-function technique for estimated water saturation from height, porosity, and permeability as presented in Figure 5.48 .

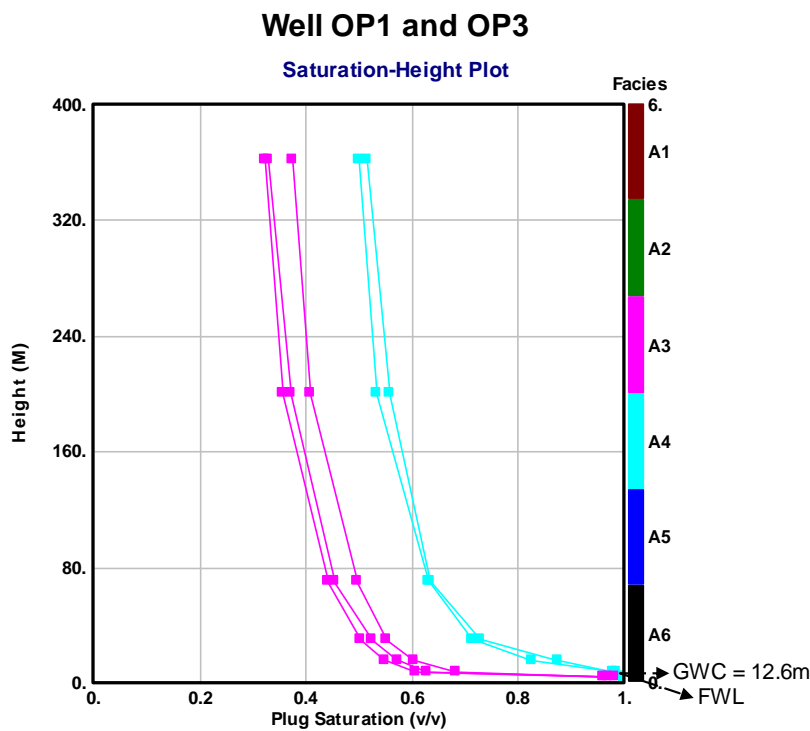


Figure 5.48: Saturation-height function for wells OP1 and OP3

The free water level is the point where the brine is completely saturated and the capillary pressure at that particular point is at zero psi. A possible gas water contact (GWC) of about 12.6 m was estimated in the saturation-height plot of Figure 5.48 above. Facies A3 presents smaller separation between the gas water contact point as compared to facies A4 and the reason for this may be attributed to the higher permeability values in the facies.

CHAPTER SIX

PETROPHYSICAL MODEL OF VOLUME OF SHALE, POROSITY AND WATER SATURATION FROM CORE AND LOG

6.1 INTRODUCTION

The static reservoir modelling involves the integration of core data, log and engineering data which are used in order to understand the behaviour of the reservoir at in situ condition. The goal of this chapter is to incorporate core description and analysis data of the key wells (OP1, OP2 and OP3) into log analysis models of volume of shale, porosity and water saturation for uncored intervals and field study.

6.2 VOLUME OF SHALE MODEL

The volume of shale (Vsh) quantity is defined as the volume of wetted shale per unit volume of reservoir rock. Wetted shale is the space occupied by water confined to the shale known as bound water. A shale can be described by listing some of its attributes as presented by Holt & Olav-Magnar (2008). Shale can be regarded clay minerals that constitute the load bearing framework and shale's have nannometer pore sizes and nanno-darcy permeability; surface area is large, and water is absorbed on surfaces or bound inside clay platelets (Keith, 2008). The difference in rock properties can be used to distinguish sands from shale as presented by Heslop in Figure 6.1a below.

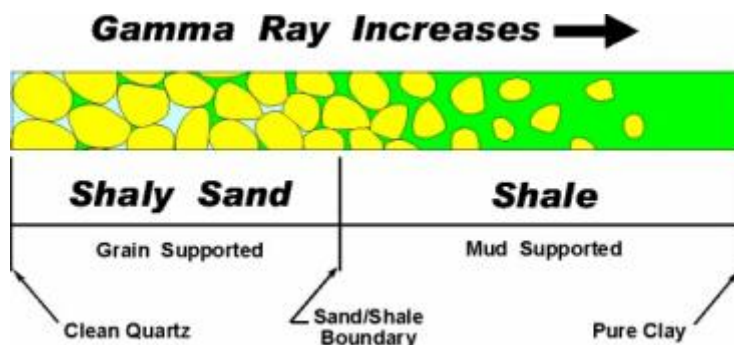


Figure 6.1a: Schematic diagram of variation of sediments with clay mineral content increasing from left to right (modified after Heslop, 1972).

Figure (6.1a) above shows what happens as clay content is increased from clean sandstones on the left to clay rich shale on the right. In the sands on the left, stresses are supported by rigid sand grains and grain contacts. Small amounts of clay are accommodated in the intergranular spaces and do not support external stress. With increasing clay, eventually the sand and silt grains cannot form a continuous network with stresses supported by grain-grain contacts and the grains then float in a clay mineral matrix that is load bearing. Heslop used the gamma ray (GR) log response as a means of clay content.

Shaly sands are sands with a shale component. These shales are very significant component of shaly sand reservoirs. Increased volumes of shale decrease the effective reservoir capacity and conductive shales reduce the formation resistivity and if not corrected for, give wrong volume of hydrocarbon calculations (Kenneth & Alan Heslop, 2003). The volume of shale need to be calculated in petrophysical evaluation in order to correct porosity and water saturation results for the biased effects of shale. The volume of shale is considered as an indicator for reservoir quality. In addition to the shale volume, it is important to determine the types of shale for choosing the appropriate shale model which can be utilized for selecting suitable models.

The shale content is determined using different shale indicators. The following methods were used to define the shale volume in this study:

- Gamma-Ray (GR) log
- Spontaneous Potential (SP) log
- Neutron log
- Resistivity logs
- Double clay indicators:
 - Neuron/Density
 - Sonic / Density
 - Neutron/Sonic

The estimated volume of shale determined from log will be compared with clay volume determined from petrography analysis (X-Ray Diffraction) data acquired from core samples in wells.

6.2.1 Gamma-Ray Method

The gamma ray log is the most common shale volume indicator. The log responds to the changes in natural radiation emitted by formation. In shaly sands the level of gamma radiation emitted is a function of clay volume. The gamma ray log does not measure the volume of silts or other inclusions within the shales. The maximum gamma ray response is taken as the shale point and minimum response as the clean sand point.

The Gamma-Ray clay indicator can be calculated using the following methods (Dresser Atlas, 1979).

Linear Method:

$$\text{Volume of Shale (Vsh)} = \frac{\text{GR value (log)} - \text{GR (min)}}{\text{GR (max)} - \text{GR (min)}} \dots\dots\dots (6.1)$$

Where

GR value (log) = GR log value reading of formation to be evaluated

GR (min) = Clean formation

GR (max) = GR value of maximum shale reading in the formation

Non linear Gamma- Ray Method:

Z = Calculated volume of shale = Vsh

Let Z = Vsh as discussed in linear method above

If Z is less than 0.55

$$\text{Vsh} = 0.0006078 * (100 * Z)^{1.58527}$$

If $0.73 < Z > 0.55$

$$\text{Vsh} = 2.1212 * Z - 0.81667$$

If $1.0 < Z > 0.73$

$$Z = \text{Vsh}$$

6.2.2 Spontaneous Potential (SP) Method

The volume of shale (Vsh) could be determined from the spontaneous potential (SP) log using the following relationship.

$$V_{sh} = \frac{SP_{clean} - SP_{log}}{SP_{clean} - SP_{shale}} \dots\dots\dots (6.2)$$

Where:

Vsh = Volume of shale or clay

SPlog = SP in the zone of interest (read from log)

SPclean = Maximum SP deflection from a nearby clean wet zone in the same Well.

SPshale = SP value in a shale (assumed to be zero)

6.2.3 Neutron Log Method

The neutron log measures the hydrogen content of formation. It records a nearly constant response through sand formations and increases in shales.

This method can be used for determining the shale volume in case of high clay content and low effective porosity from the relationship below:

$$V_{sh} = \left(\frac{\Phi_{neu} * \Phi_{neu} - \Phi_{neu\ clean}}{\Phi_{neu\ clay} \Phi_{neu\ clay} - \Phi_{neu\ clean}} \right)^{0.5} \dots\dots\dots (6.3)$$

Or

$$V_{sh} \leq \frac{\Phi_{nlog}}{\Phi_{nsh}}$$

Where:

Φnlog = the neutron log reading of study zone

Φnsh = neutron log reading in front of a shaly zone

6.2.4 Resistivity Method

This method can be used to calculate the shale volume in case of high clay content and low true resistivity (Rt) values from the relationships below:

$$V_{sh} \leq \frac{R_{sh}}{R_t}$$

If this ratio is less than 0.5 then:

$$Z = \frac{R_{clay}}{R_t} * \frac{(R_{clean} - R_t)}{(R_{clean} - R_{clay})} \dots\dots\dots (6.4)$$

If Rt is greater than 2 Rclay then

$$V_{sh} = 0.5 * (2 * Z)^{0.67 * (Z+1)}$$

Otherwise Vsh= Z

Where

Rclay = resistivity log reading of a shaly zone

Rsh = Resistivity of the adjacent shale unit

Rclean = Resistivity of a clean formation

6.2.5 Correction of Shale Volume

The values of Z or Vsh calculated above have to be corrected to obtain the optimum shale values suitable in log interpretation. The formulae are as follows:

Clavier (Clavier et al, 1971):

$$V_{sh} = 1.7 (3.38 * (Z + 0.7)^2)^{0.5}$$

Larionov (Tertiary rocks)

$$V_{sh} = 0.33 (2^{2*Z} - 1)$$

Steiber(Steiber,1973):

$$V_{sh} = \frac{0.5 * Z}{1.5 - Z}$$

However, the different zones were classified into clean, shaly and shale zones according to the following:

If $V_{sh} < 10\%$ = Clean zone

If V_{sh} is between 10 to 35 % = Shaly zone

If $V_{sh} > 35\%$ = Shale zone

The graphics for the correction of the shale volume derived from the above mentioned methods from gamma-ray is presented in Figure 6.1b below.

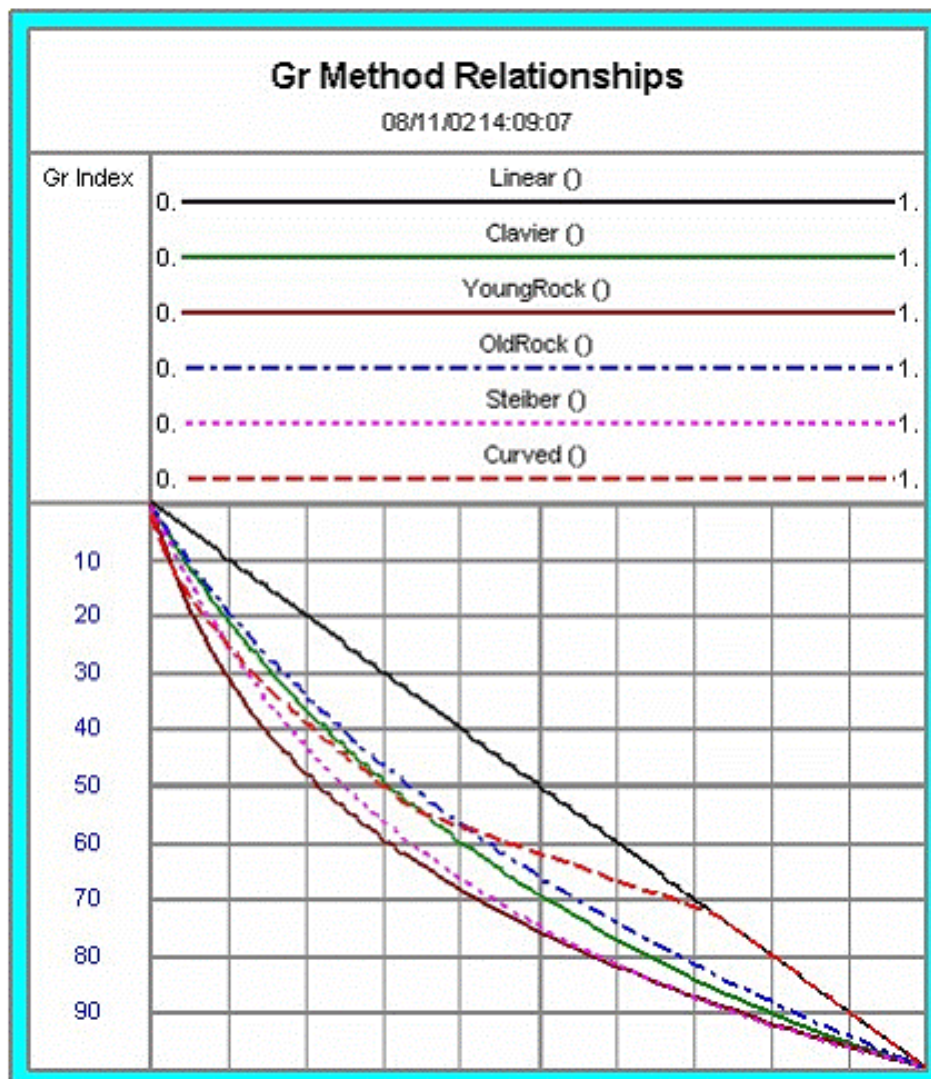


Figure 6.1b: Volume of shale correction chart (Schlumberger,1995)

The approach used in deciding which of the resulted shale volume model to be used was based on overlaying the resulted shale volumes with that derived from

petrography studies. The best match with the petrography volume of shale was chosen.

6.2.6 Double Clay Indicators

The double clay indicators utilize the principle of defining a clean line and a clay point. The clay volume is calculated as the distance the input data falls between the clay point and the clean line. An example of double clay indicator is shown in Figure 6.2 below.

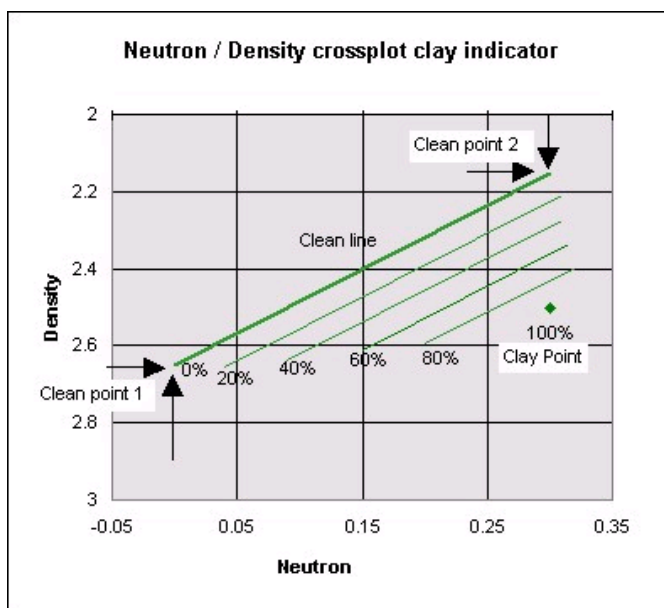


Figure 6.2: Example of neutron-density cross plot as clay indicator

The double clay indicators equations are given below:

The Neutron-Density double clay indicator relationship:

$$V_{sh} = \frac{(D_{enc2} - D_{enc1}) * (Neu - Neu_{cl1}) - (D_{en} - D_{enc1}) * (Neu_{cl2} - Neu_{cl1})}{(D_{enc2} - D_{enc1}) * (Neu_{clay} - Neu_{cl1}) - (D_{enclay} - D_{enc1}) * (Neu_{cl2} - Neu_{cl1})}$$

Where

D_{enc1} , Neu_{cl1} , D_{enc2} and Neu_{cl2} are the density and neutron values for the two ends of the clean line.

Neutron-Sonic clay indicator relationship:

$$V_{sh} = \frac{(\text{Neucl2} - \text{Neucl1}) * (\text{son} - \text{soncl1}) - (\text{Neu} - \text{Neucl1}) * (\text{soncl2} - \text{soncl1})}{(\text{Neucl2} - \text{Neucl1}) * (\text{sonclay} - \text{soncl1}) - (\text{Neuclay} - \text{Neucl1}) * (\text{soncl2} - \text{soncl1})}$$

Where

Neucl1 and soncl1 and neucl2 and Neucl2 and soncl2 are the neutron and sonic values for the two ends of the clean line.

The sonic-Density double clay indicator for Vsh is given as:

$$V_{sh} = \frac{(\text{Denc12} - \text{Denc11}) * (\text{son} - \text{soncl1}) - (\text{Den} - \text{Denc11}) * (\text{soncl2} - \text{soncl1})}{(\text{Denc12} - \text{Denc11}) * (\text{sonclay} - \text{soncl1}) - (\text{Denclay} - \text{Denc11}) * (\text{soncl2} - \text{soncl1})}$$

Where:

Denc11 and soncl1 and Denc12 and soncl2 are the density and sonic values for the two ends of the clean line.

6.2.7 Parameters used for Determination of Volume of Clay

The following parameters were used for performing the volume of shale analysis from logs as presented in Table 6.1 below.

Table 6.1: Summary of parameters used for volume of clay calculations

Well	GRmin (API)	GR max(API)	NPHI clean(v/v)	NPHI clay(v/v)	RHOB (g/cc)	DT clean	DT clay
OP2	18	120	0.06	0.30	2.63	55	102
OP3	15	117	-.006	0.32	2.68	54	100

The cross plots for the determination of clay and matrix values are shown in appendix F. The commonly applied GR model is for a simple linear relationship between GR and clay volume. There is a possibility for over-estimation of clay volumes in the presence of non clay radioactive minerals in matrix. Non-linear models which lower the level variations in GR were also applied. The GR matrix response is selected from the frequency distribution of the normalized gamma-ray data on the cumulative distribution curve.

The density of clay was estimated from the Density-Gamma-Ray cross plot and wet clay properties were established from the Neutron-Density cross-plot as presented in the appendix I. The DT matrix (clean) and clay were selected from the frequency distribution of the sonic log data on the cumulative distribution and cross-plots with gamma-ray log.

6.2.8 Calibration of Volume of Clay (Vcl) Models

This part of the study deals with the integration of the quantitative mineralogy results obtained from X-Ray analysis (XRD) with wireline logs. The mineralogy results were presented in chapter four (5) were correlated with the wireline logs for wells OP2 and OP3. Evaluations of logs produce proportions by volume so the XRD results have been converted to proportion by volume based on the relationship below:

$$\text{Weight Volume \% of rock} = \frac{(\text{Dry weight \%}) * (1 - \text{Porosity}) * (\text{Rock Grain Density})}{\text{Mineral Grain Density}}$$

Where:

Dry weight % = Dry weight percentage of rock in percent

Porosity = Porosity from routine core analysis in fractions

Rock Grain density = Routine core grain density in g/cc

Mineral Grain density = Fixed mineral for a particular mineral and taken from standard log chart reference Tables or book.

The volume of clay models derived from logs have been assessed against the independent X-ray diffraction (XRD) data acquired in well OP2 and OP3. The XRD data have been converted to proportion by volume since evaluations from logs generate proportions by volume.

Presented in Figures 6.3 and 6.4 below are the models of clay volumes from based on logs been overlaid XRD clay volume on each other.

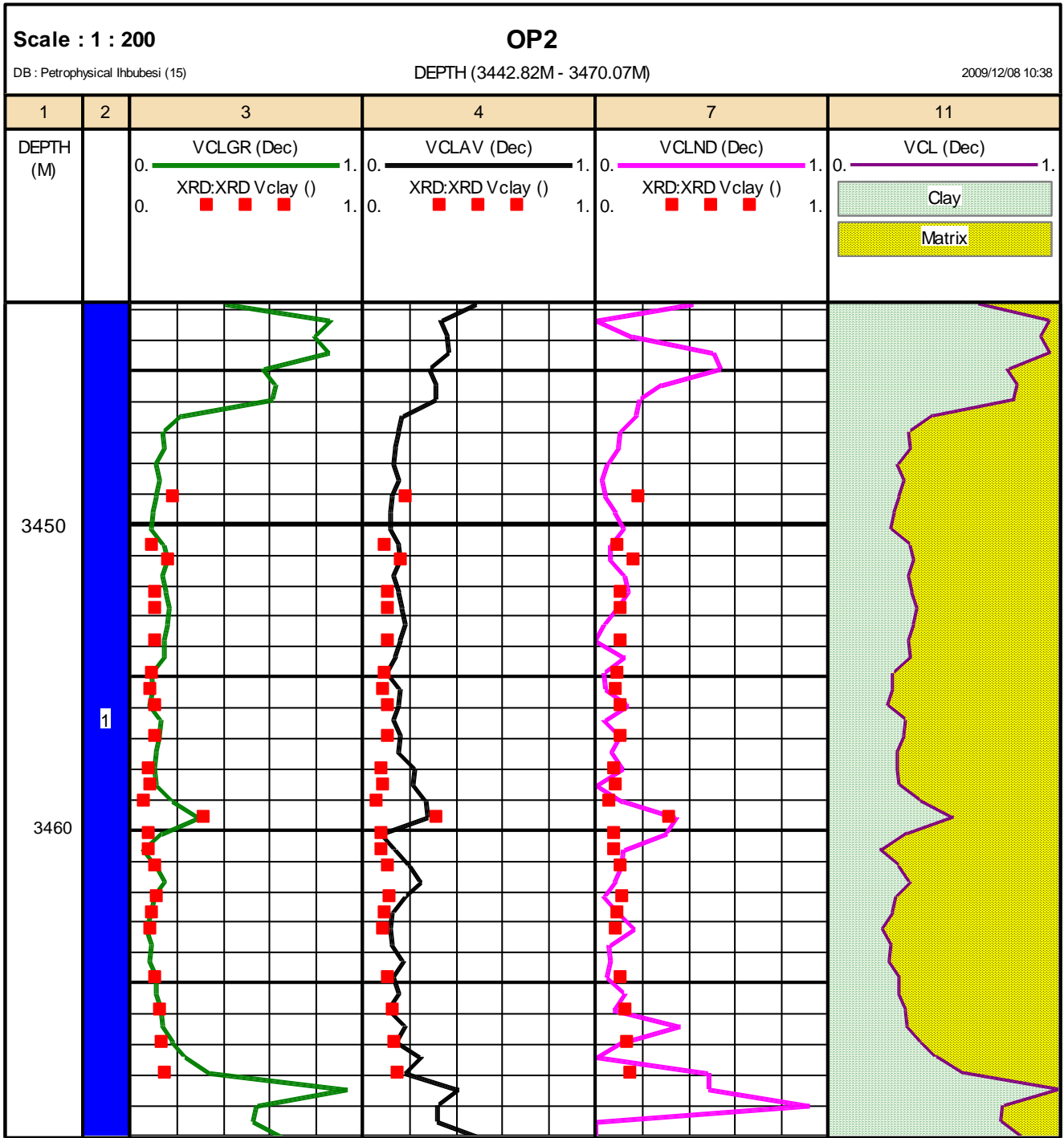


Figure 6.3: Log determined volume of clay overlain with XRD volume of clay for well OP2.

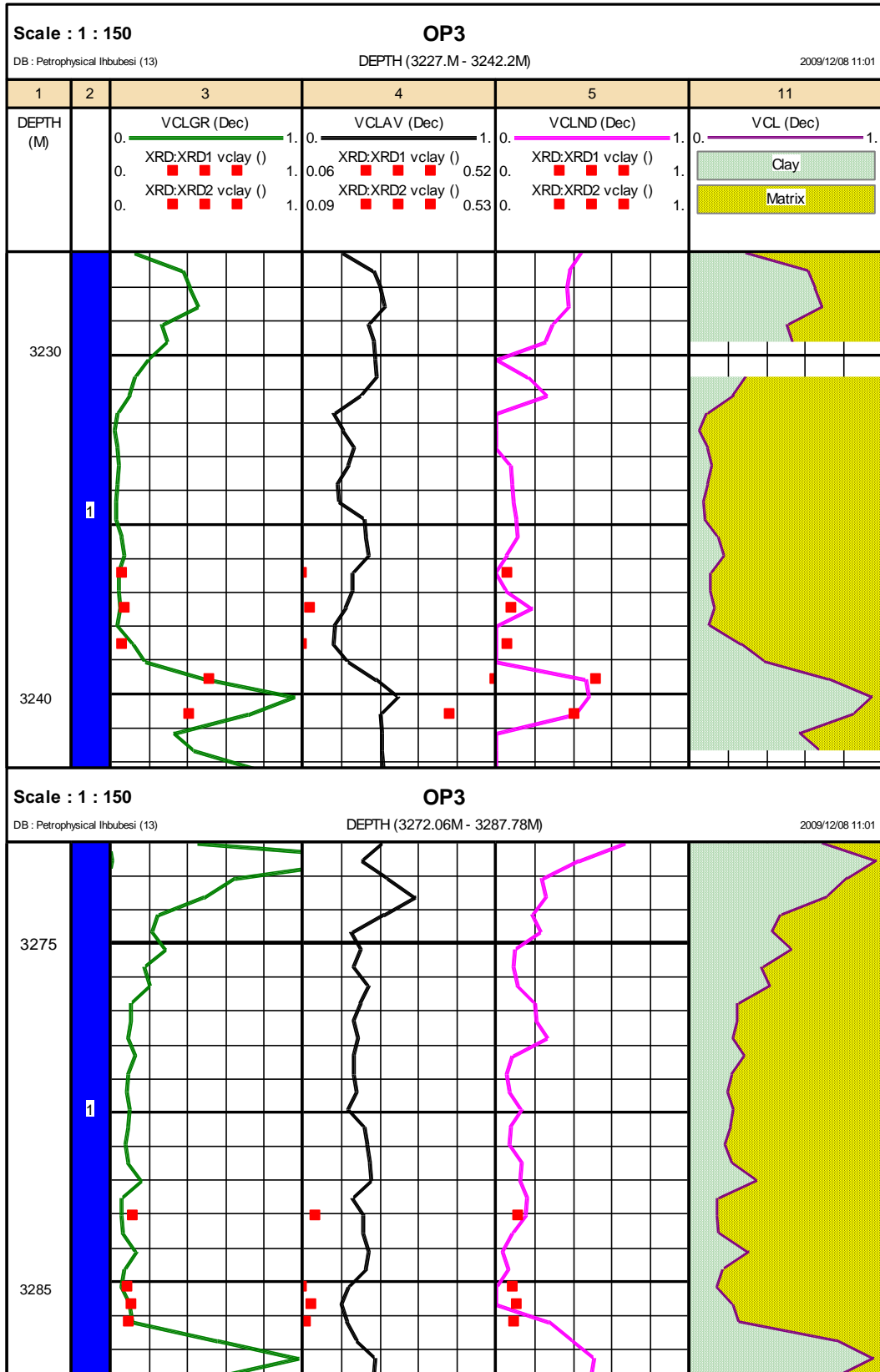


Figure 6.4: Log determined volume of clay overlain with XRD volume of clay for Well OP3

In both plots of Figures 6.2 and 6.3 above, the volume of clay derived from the XRD is plotted on the red dot line against the well derived volume of clay models from logs. The green coloured curves are the volume of clay from gamma-ray non-linear model (Steiber VCLGR); the pink coloured are the volume of clay from the double clay Neutron-Density (VCLND) model; and black colour represents the average volume of clay (VCLAV) from all the log models.

The linear Gamma-ray model over-estimated the initial volume of clay calculated, therefore the Larinov, Clavier and Steiber non-linear model was adopted and the Steiber model was observed to be more compatible with the XRD volume of clay model in both Wells.

Another log volume of clay model that generates clay volume that was compatible with the XRD model was the Neutron-Density model. The model has its limitations in that it may under-estimate clay volumes in the presence of light hydrocarbons such as gas and may also over-estimate clay volumes where carbonate cements or heavy minerals are present. The XRD data indicate no significant carbonate and heavy minerals such as pyrite and siderite so the Neutron-Density model volume of clay was Not over-estimated. Well OP2 Neutron-Density volume of clay model is more compatible with the XRD volume of clay than in well OP2.

There exist significant scale similarities between the XRD volume of clay and the log derived volume of clay in the gamma-ray and N-D double clay models in both wells in the level of clay. The volume of clay from the resistivity log and the averaged volume of clay from logs indicate significantly higher clay volumes than the XRD and hence will not be used for the final volume of clay model.

The final volume of clay model from logs is taken from the gamma-ray model corrected by Steiber equation. This is based on the observed higher levels of agreement between the log and XRD volume of clay data as shown in the plots of both wells.

6.2.9 Use of Spectral Gamma-Ray log as an Estimator of Clay type

The spectral gamma-ray log measures the natural gamma-ray radiation from formation split into contributions from the radio-isotopic sources of potassium, uranium and thorium. The spectral gamma-ray log is displayed as three curves of thorium (ppm), uranium (ppm) and potassium (%). Track 1 in the log presentation is normally is the spectral gamma ray (SGR) which is the record of the total gamma-ray count from all sources, as Well as the computed gamma-ray (CGR) log which is the sum of potassium and thorium responses.

The calculated gamma ray log (CGR) is an important log because it is used to estimate clay content that is free of uranium. Common application of the spectral gamma ray log are in determination of clay mineral volume and types, and the recognition of fractures that had uranium salt precipitated in them by ground water system (Fertl et al, 1980).

Thorium and Uranium are usually presented in track 2 (ppm) and the percentage of potassium (%) in the formation is presented in track 3. The spectral gamma ray log was only run in well OP1. Presented in Figure 6.5 below is well OP1 spectral gamma ray log.

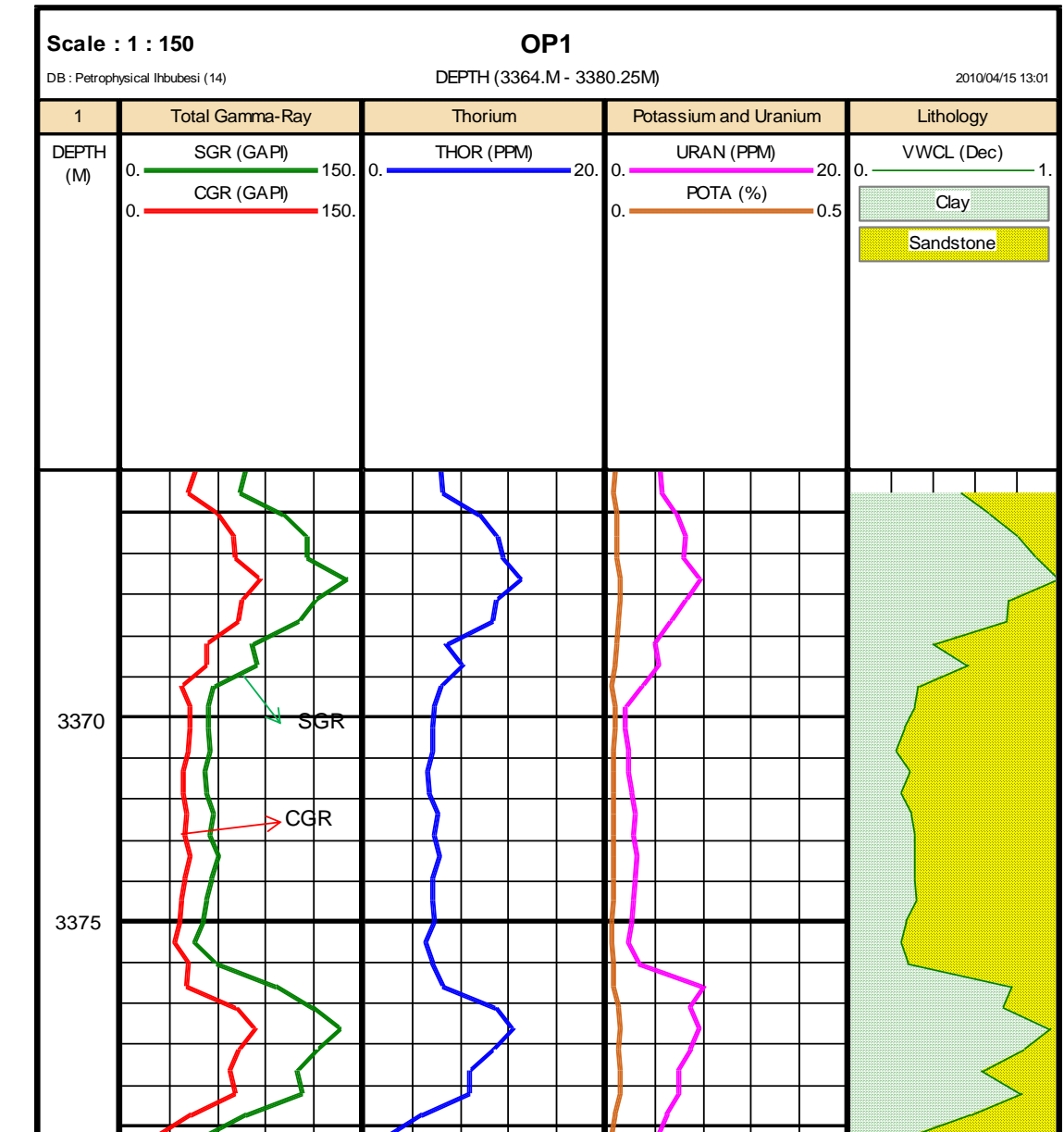
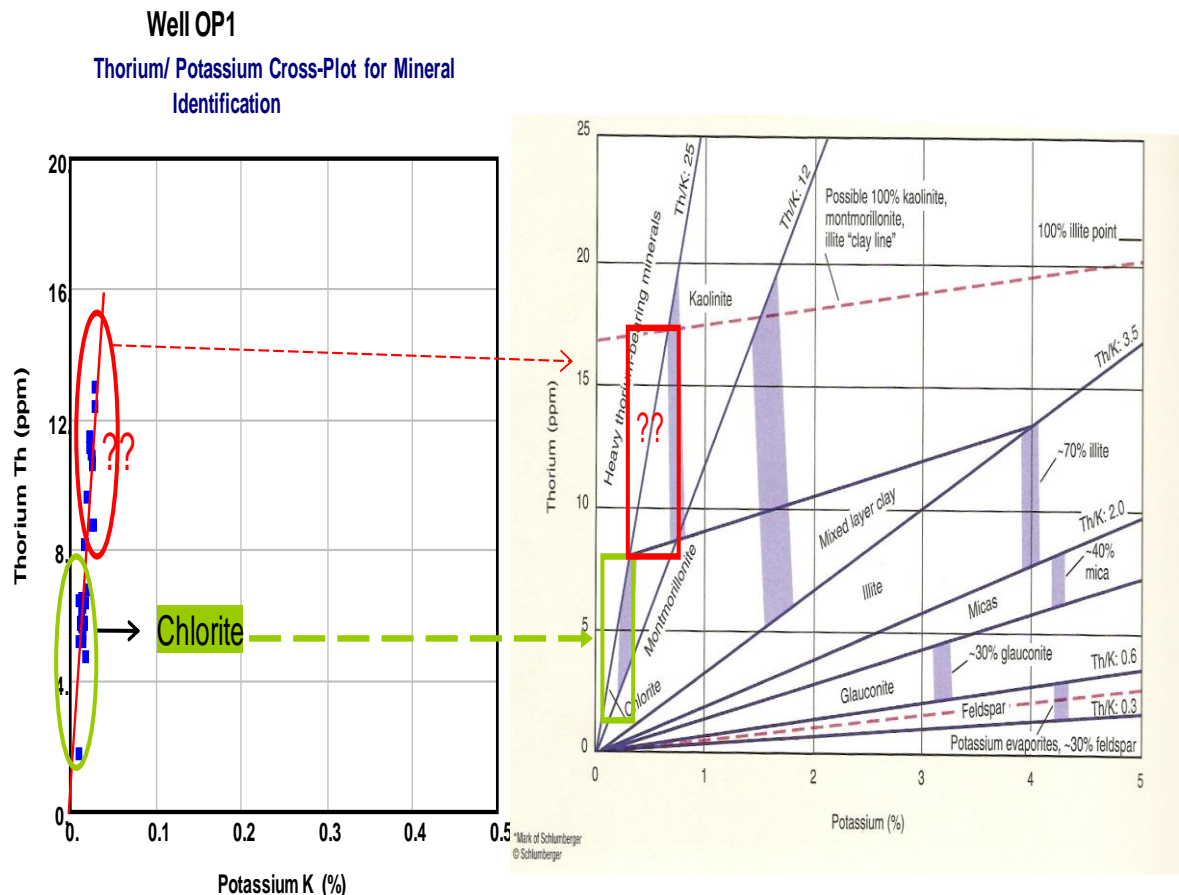


Figure 6.5: Well OP1 spectral gamma ray log

Figure 6.5 above showed an average concentration of thorium within the reservoir interval of well OP1 of approximately 7 ppm, uranium 2 ppm, and potassium 0.03 %. The low percentage of potassium within the reservoir area is as expected because the whole rock analysis results of adjacent wells showed insignificant percentage of potassium feldspars. This shows that sandstones in the reservoir intervals do not contain feldspars, micas, glauconite, and heavy minerals (Tables 5.23 and 5.24). Clay bearing sandstones and types of clay minerals may be identified by the potassium-thorium cross plot. Illite clay mineral has higher potassium than mixed-

layered, while Kaolinite and chlorite clay minerals have little or none. Presented in Figure 6.6 below is the potassium/thorium cross plot for well OP1.



Schlumberger Chart CP-19 (Schlumberger, 1995)

Figure 6.6: Well OP1 potassium/thorium cross plot for identification of clay type

The red line on the cross plot that originate from the origin of the plot have gradients matched with the values of the ratio Th/K ratio that correspond to chlorite mineral point on the Schlumberger chart CP-19. The ratio is a measure of potassium richness as related to thorium. The cluster of points (light green circle) to the left showing values of potassium of less than 0.1 percent indicates the presence of chlorite in the Schlumberger thorium/potassium chart for mineral identification. This is the reservoir interval. Above this interval (circled red with question mark) may be Kaolinite mineral that has transformed to chlorite at deeper depth (reservoir interval) or the presence of heavy mineral.

A sandstone reservoir with varying amounts of shaliness with Illite as the principal clay mineral usually plots in the illite segment of the chart to the right with Th/k

between 2.0 and 2.5. Less shaly parts of the reservoir plot closer to the origin and more shaly parts plot closer to the 70 % illite area of the chart (Schlumberger, 1995).

6.3 POROSITY MODEL

The porosity of a rock is the volume of the non-solid portion of the rock that is filled with fluids divided by the total volume of the rock. Porosity is considered to be a primary porosity if it is developed during the original sedimentation process by which the rock is created. Secondary porosity is created by processes which synthesize vugs in rocks by ground water (Crain, 1986). In general, porosities tend to be lower in deeper and older rocks due to cementation and overburden pressure stress on the rock. The porosity from logs can be estimated from a single porosity log (density, neutron, sonic) or a combination of porosity logs. The porosity derived directly from logs without correction for clay content is regarded as total porosity. Effective porosity is the resultant porosity determined after removal of the effect of clay. However, in an interval of no shale, the total porosity equals the effective porosity.

Estimation of porosities from wireline logs requires information on lithology, core data which includes grain matrix and pore fluid. The porosity from log can be determined in both clean and shaly zones as presented below.

6.3.1 Porosity Determination from Density Log

The porosity derived from the density log (Φ_D) is defined by the following relationships (Wyllie, 1963).

$$\text{Porosity } (\Phi_D) = \frac{(\rho_{ma} - \rho_b)}{(\rho_{ma} - \rho_f)} \dots\dots\dots (6.5)$$

Where:

ρ_{ma} = matrix (or grain) density= 2.67g/cc from core.

ρ_b = Bulk density as measured by the tool

ρ_f = Fluid density (derived from pressure test). Field water density of 1.02 g/cc and gas density of 0.2 g/cc.

For:

$$\left. \begin{array}{l} \text{Fresh water mud, } \rho_f = 1.0 \text{ g/cm}^3 \\ \text{Salt water mud, } \rho_f = 1.1 \text{ g/cm}^3 \\ \text{Gas mud, } \rho_f = 0.7 \text{ g/cm}^3 \end{array} \right\}$$

According to Dresser Atlas 1979, density porosity in a shaly formation is calculated using the following equation:

$$\Phi_{D \text{ corr}} = \frac{(\rho_{ma} - \rho_b)}{(\rho_{ma} - \rho_f)} - V_{sh} \frac{(\rho_{ma} - \rho_{sh})}{(\rho_{ma} - \rho_f)} \dots\dots\dots (6.6)$$

Where:

- $\Phi_{D \text{ corr}}$ = Corrected density for shale effect
- V_{sh} = Volume of shale
- ρ_{sh} = Density value of adjacent shale formation

6.3.2 Porosity from Neutron Log

Neutron log porosity is calculated by the acquisition software and is displayed directly on the log (Krygowski, 2003). The logs must be interpreted from a specific chart because they are not calibrated in physical units. A convenient standard for the neutron log is the neutron porosity index given in limestone.

In a shaly formation, the neutron log will appear to be more porous. The effect of shale on the neutron log can be corrected by the following equation:

$$\Phi_{N \text{ corr}} = \Phi_{N \text{ log}} - V_{sh} \times \Phi_{N \text{ sh}} \dots\dots\dots (6.7)$$

Where

- $\Phi_{N \text{ corr}}$ = Corrected neutron porosity
- $\Phi_{N \text{ log}}$ = Neutron log reading of the interval
- V_{sh} = Volume of shale
- $\Phi_{N \text{ sh}}$ = neutron log of the adjacent shale formation

6.3.3 Porosity from Sonic (acoustic) Log (Φ_S)

The acoustic travel time is a function of the formation lithology and porosity. The following equations are used to calculate the sonic porosity in consolidated and compacted formations (Wyllie et al, 1958).

Wyllie Time – Average Equation:

$$\Phi_S = \left(\frac{DT - DT_{Ma}}{DT_{Fl} - DT_{Ma}} \right) * \frac{1}{B_{cp}} \dots\dots\dots(6.8)$$

Where:

Φ_S = Sonic (acoustic) porosity

DT = Sonic travel time from the log

DT_{Ma} = Matrix travel time

B_{cp} = compaction correction = $\frac{DT_{Shale}}{100} > 1.0$

Raymer-Hunt Gardner (1980) equation:

$$\Phi_S = \frac{5}{8} * \left(\frac{DT - DT_{Ma}}{DT} \right) \dots\dots\dots (6.9)$$

Hilchie, 1978 suggested the following empirical correction for the hydrocarbon effects on sonic derived porosity in a gas formation:

$$\Phi_{corr} = \Phi_{sonic} * 0.7 \dots\dots\dots (6.10)$$

However, a combination of any of the two porosity logs can be used to determine porosity in clean and shaly sand environments.

6.3.4 Effective Porosity Determination (Φ_e)

Effective porosity(Φ_e) excludes all the bound water associated with clays but involves all the connected pores in the pore system that can contribute to flow has been determined from the density log as follows:

$$\text{Eval Phie} = \left(\frac{\rho_{ma} - \rho_{log}}{\rho_{ma} - \rho_{fl}} \right) - V_{clay} * \left(\frac{\rho_{ma} - \rho_{clay}}{\rho_{ma} - \rho_{fl}} \right) \dots\dots\dots (6.11)$$

Where

Eval Phie = Effective density from density log (v/v)

ρ_{ma} = Matrix density (g/cc) = 2.67g/cc from core grain density.

ρ_{log} = Log bulk formation density (g/cc)

The summary of the parameters used for the effective porosity from the density log for all the wells are given in Table 6.2 below.

Table 6.2: Summary of parameters used for log effective porosity calculation

	PARAMETERS				
Well	ρ_{ma} (g/cc)	Clay (g/cc)	ρ_{H_2O} (g/cc)	Hyd (g/cc)	Vcl (v/v)
OP1	2.67	2.67	1.02	0.23	VCLGR
OP2	2.67	2.63	1.02	Nil	VCLGR
OP3	2.67	2.69	0.98	0.22	VCLGR

The matrix density (ρ_{ma}) was derived from the mean value of the histogram of core grain densities of the field as was presented in chapter five. The fluid densities were estimated from the Repeat formation test (RFT) analysis which represents the in-situ densities of the fluid (appendix F). The VCGL is volume of clay from gamma-ray log (non-linear) Steiber model.

Gas indication can be determined in the formation by comparison of the corrected porosity values of neutron and density.

If Φ_{Ncorr} is less than $\Phi_{D corr}$ then gas is suspected in the formation. The effective porosity in a shaly sand formation can also be determined from the combination of the neutron and density porosity logs (John 1983) as follows:

$$(\Phi_e) = \sqrt{(\Phi_{D corr}^2 + \Phi_{Ncorr}^2)} / 2 \dots\dots\dots (6.12)$$

6.3.5 Comparison of Log and Core Porosity

The porosities computed from the logs have been calibrated with the overburden corrected core porosities (ob core). The results when overlaid with the corrected core data shows that the data sets are generally consistent with one another though there are cases of discrepancies which may be as a result of the different scales of measurements and as a result of lithology factor as the routine core measured porosities are generally lower than the log derived porosities in all wells. The evaluated effective porosity is also shown in each of the plot tracks as shown in Figure 6.7 below for well OP1.

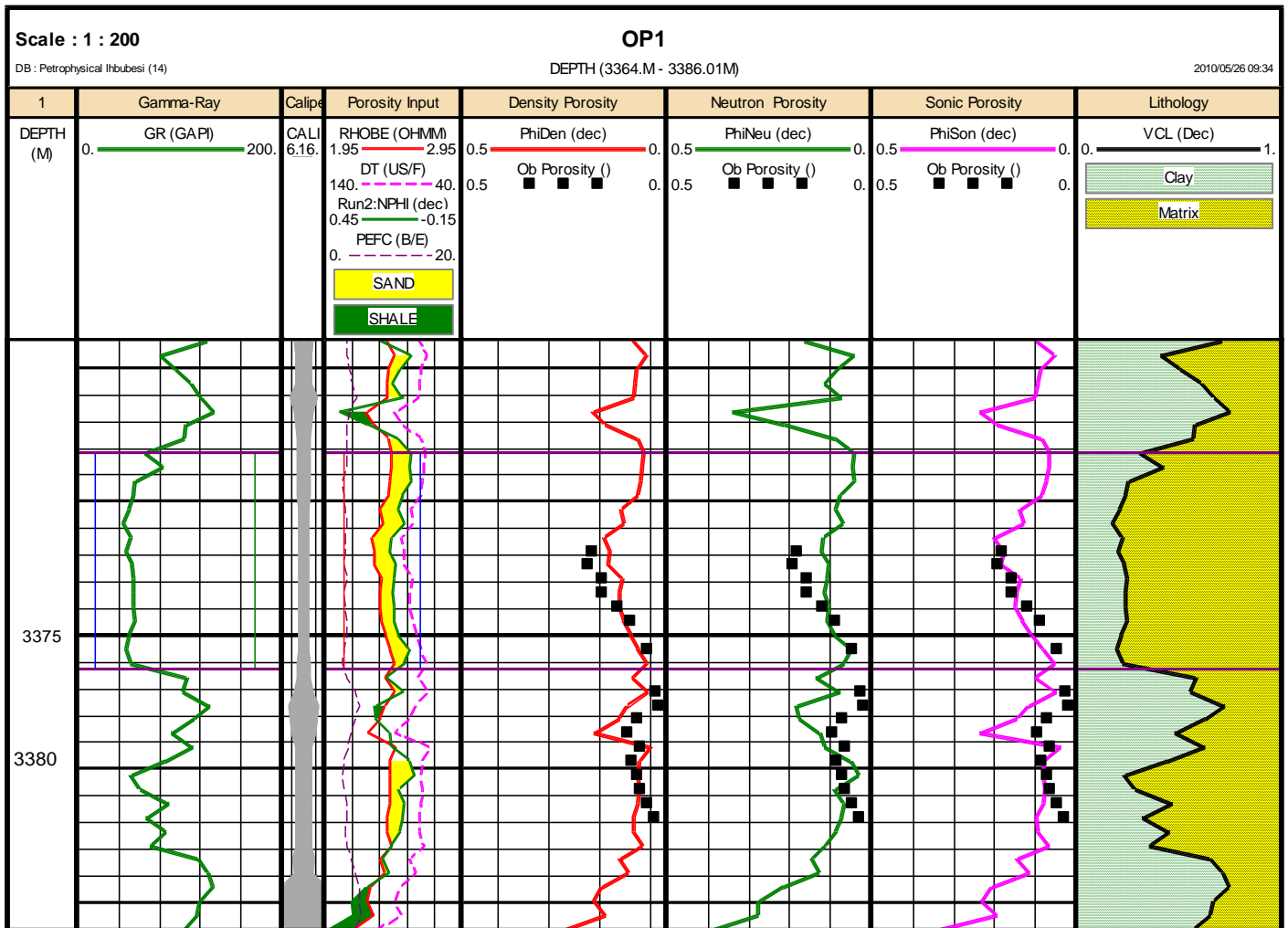


Figure 6.7: Well OP1 comparison of log and core porosity

Track 5 in Figure 6.7 above present the log derived porosity from the density (Phi-den) red colour , track 6 is neutron porosity (PhiNeu- green colour), and track 7 is the sonic porosity (PhiSon- Pink colour). The porosity logs in their respective tracks were plotted against the routine core derived porosity (ob-porosity) black dots for comparison.

The sonic derived porosity and density porosity best compared with the routine core porosity. The plot for well OP2 is presented in Figure 6.8 below.

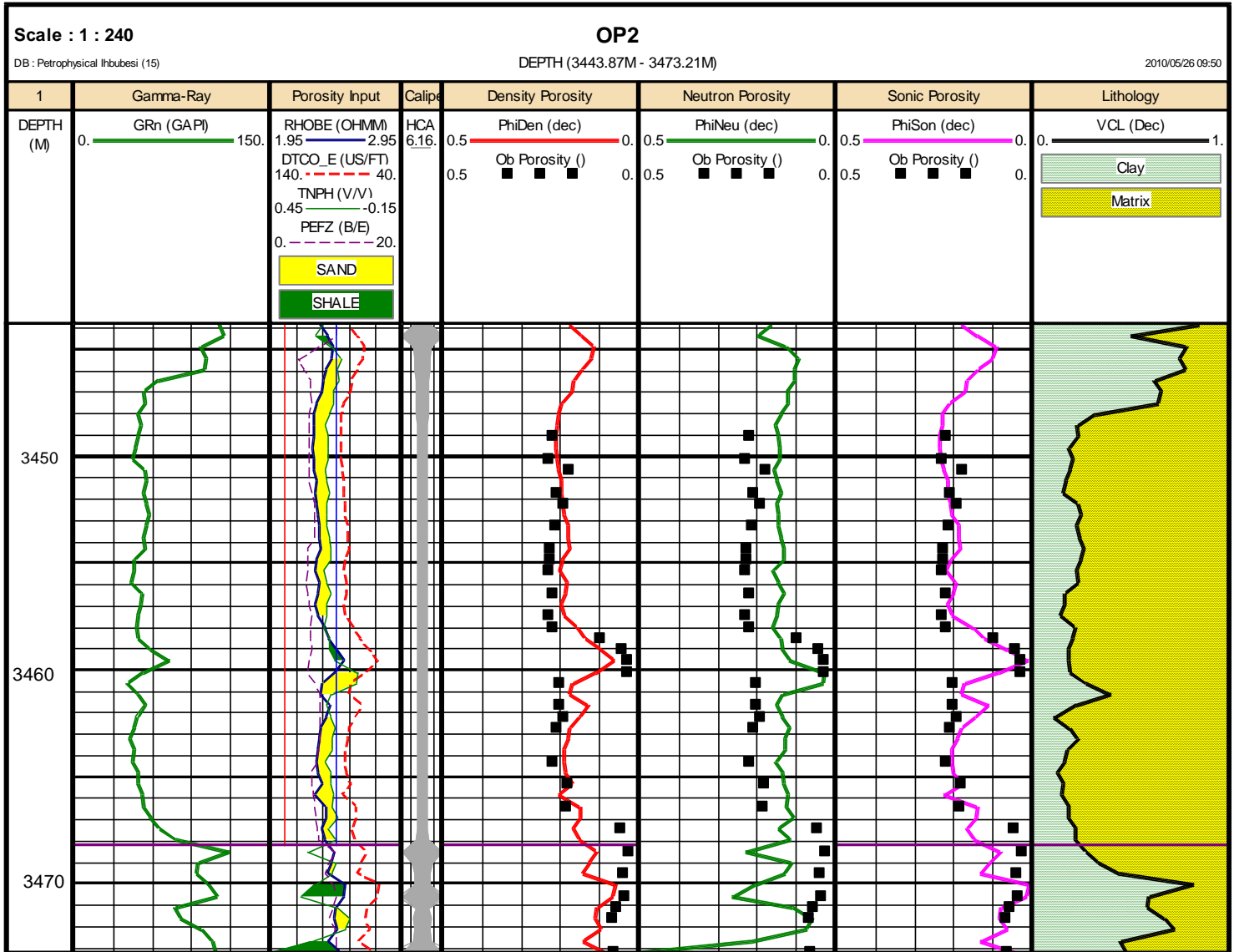


Figure 6.8: Well OP2 comparison of log and core porosity.

Plotted in track 5 of Figure 6.8 above is the density porosity log (Phiden-red colour), track 6 is the neutron porosity log (Phineu-green colour) and track 7 is the sonic porosity (Phison-pink colour). The log derived porosity curves were overlain with the routine core porosity for comparison purposes. The porosity derived from the sonic log best match with the routine core porosity as shown.

The presence of clay and enlarge borehole presents a difficulty because of variability with respect to concentrations of elements with large thermal neutron absorption cross section which has a strong effect on the thermal neutron log as shown in the lower part of the neutron porosity log. The capiler log was introduce in track 4 to check hole

enlargement. Figure 6.9 below presents the log and core porosity data comparison for well OP3.

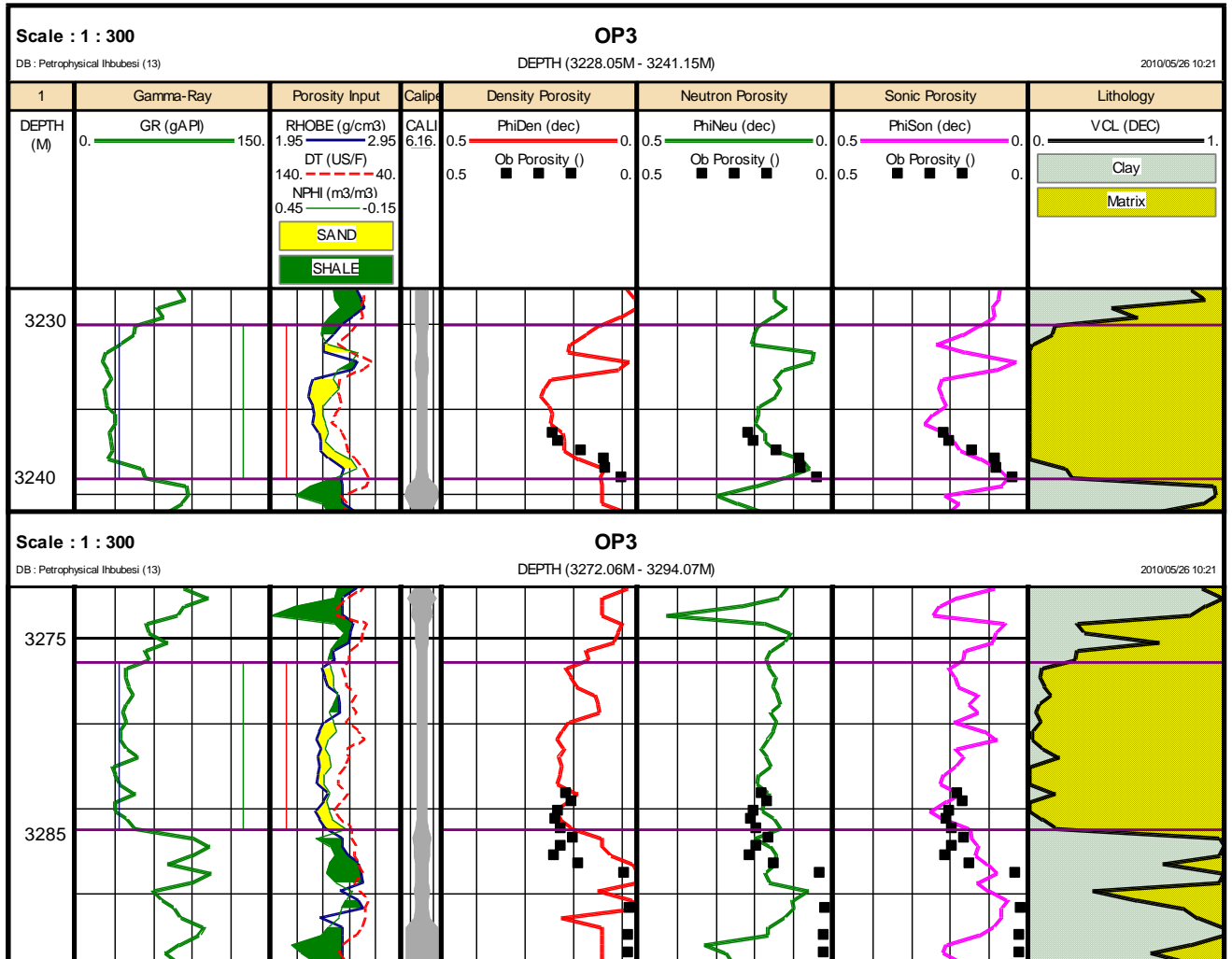


Figure 6.9: Well OP3 comparison of log and core porosity

Two non-continuous core samples were measured in this Well and the porosity results were compared with the log derived porosity as presented in Figure 6.8 above. Track 5 is the density porosity (Phidensity –red colour), track 6 is the neutron porosity (Phineu-green colour) and track 7 is the sonic porosity (Phison- Pink colour), all plotted against the core porosity (ob porosity –black dots) for comparison.

The best match of log derived porosity to routine core porosity were the density porosity and sonic in core 1. The caliper log was also introduced in track 4 to check hole enlargement. The effect of clay material on the thermal neutron porosity log was

also observed in the lower section of core 2 of the neutron porosity log as a result of the discrepancy between both data at clay section.

Generally, the intervals where the log and core porosity shows a departure from each other is associated with clay materials which may expand slightly because of rebound effects leading to an increase in volume which causes a decrease in bulk density and at intervals where there is an increase in hole diameter. The cross plots of log and core data porosities are shown in appendix G. It could be deduced from the above that the differences in porosity measurements between core and log may be due to the effect of authigenic clays which reduce effective porosity at reservoir conditions but caused an over-estimation of porosity in the air-dried cores measured in the laboratory.

In conclusion, the density and neutron logs have to be corrected for the effect of shale and the sonic log derived porosity generally showed the best match with the core derived porosity and hence will be used for the porosity model. An empirical relationship between the overburden corrected porosity from core and log derived porosity from the sonic porosity log was established by plotting the overburden corrected porosity determined in all the Well versus the sonic porosity on a linear scale. The plot is presented in Figure 6.10 below.

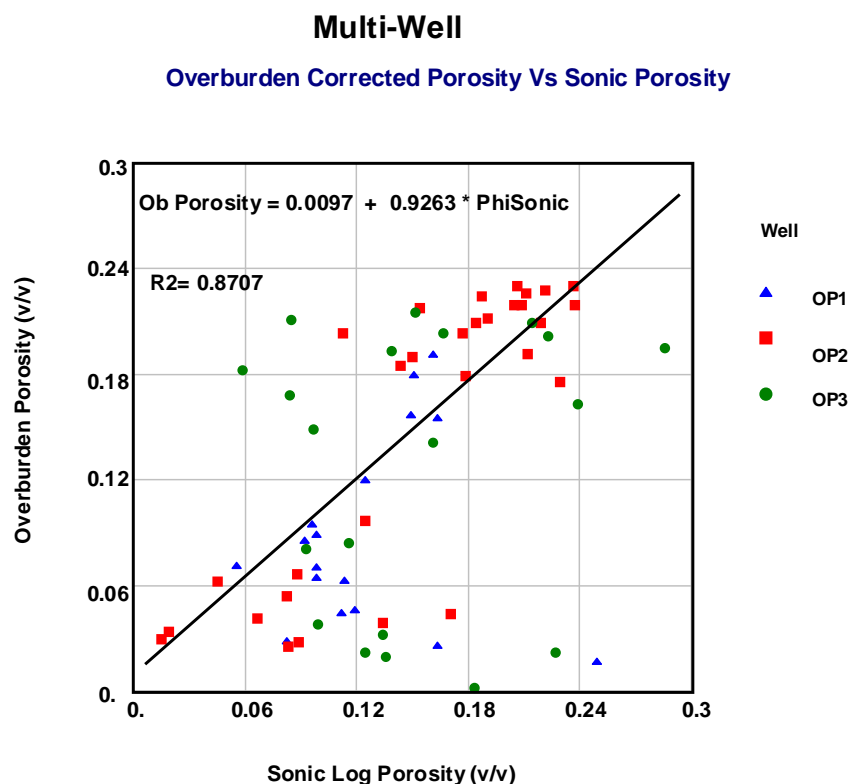


Figure 6.10: Multi-Well overburden porosity versus log porosity

A common equation for predicting the overburden porosity in un-cored intervals and Wells without core was established through the cross plot. A correlation coefficient of 0.87 was realized which shows that an excellent relationship exist between the two plotted data from the statistical point of view.

The common equation is given in equation 6.13 below:

$$\text{Overburden Porosity} = 0.0097 + 0.9263 * \text{Phisonic} \dots\dots\dots (6.13)$$

$$R^2 = 0.8707$$

Where:

Overburden porosity = Predicted overburden porosity (v/v)

Phisonic = Sonic Porosity (v/v)

6.4 WATER SATURATION MODEL

The saturation of fluid of a reservoir rock is referred to as the percentage of the pore space filled with a particular fluid, and the sum of all the fluids in the pore spaces equals one hundred percent. The saturation of water is always part of the fluids that occupy the pore spaces of reservoir rock.

The water in a reservoir rock at the time of discovery is referred to as connate water which is derived from the marine environment in which the sediments were first deposited. The term interstitial water is often used synonymous with connate water but it could represent water which resulted from compaction of the rock, the expulsion of water, and from lateral migration (Levorsen, 1967). Both connate and interstitial water are used to refer to the water present in all oil or gas reservoirs and is considered residual or irreducible and immobile.

According to Engineering data book of 1977, the water saturation in any given rock sample depends upon the size of the pores, the distribution of pore sizes in the rock, and the height of the sample above the water bearing zone. Connate water usually is in the range of 10 % to 40 % in most rocks which means that it only occupies about 10 to 40 percent of the pore volume of the rock and other fluids (hydrocarbon) occupy the rest. In general, coarse grained sandstones, vuggy limestones and other rocks with large pores will have low connate water saturations and fine grained sandstones and rocks with small pores tend to have relatively high water saturation.

The knowledge of the quantity and distribution of different types of water contained in the interconnected pore spaces of a reservoir is essential for formation evaluation. Three main water types has been identified as bound, capillary and free waters .The bound water includes water that is strongly held to the clay mineral surfaces and the water of hydration associated with the mineral charge balancing cations. The Capillary water is the immobile water held by capillary forces in regions of micro-porosity. Free water is water that resides within the macro-porosity region of the interconnected pore space of a reservoir and is able to flow under an applied pressure gradient (Newman, 1987).

The water saturation of reservoir rocks can be determined from the following:

- ❖ Wireline Logs
- ❖ Core data
- ❖ Capillary Pressure Measurements
- ❖ Drill Stem Test (DST)

However, in this part of the analysis and interpretation, emphasis will be on log derived water saturation models and compared with water saturation models derived earlier in chapter five from conventional and special core data results and from production test data.

Determination of water saturation from logs can be grouped into two, namely the Clean Sand (Shale free) and Shaly-Sand models. The Clean Sand or shale free group is determined from the Archie's relationship while the Shaly-Sand models can further be sub-divided into two main equation groups according to Petrolog (2006) as follows:

Group 1: The volume of Shale or Resistivity model:

- ✚ Simandoux
- ✚ Modified Simandoux
- ✚ Poupon Leveaux
- ✚ Fertl and Hammack
- ✚ Indonesia

This particular group uses the effective porosity as the input porosity in the water saturation equation.

Group 2: Cation Exchange or Conductivity model

- ✚ Waxman-Smiths
- ✚ Modified Waxman-Smiths
- ✚ Dual –Water
- ✚ Juhasz

The group 2 as listed above uses the total porosity values in the water saturation equation. Before discussing in details the water saturation models, some of the basic input parameters to these models such as the formation temperature and resistivity of water at formation temperature will be estimated and verified in as many ways as possible. Other basic parameters like cementation and saturation exponents (m and n) earlier determined from special core analysis will be used for the evaluations of water saturations.

6.4.1 Parameters

6.4.1.1 Formation Temperature Determination

The following equation was used for formation temperature determination.

$$T_2 = \frac{D(BHT - T_1)}{TD} + T_1 \dots\dots\dots(6.13)$$

Where

- T₂ = Formation Température
- D = Log depth
- BHT = Bottom hole temperature
- T₁ = Surface temperature
- TD = Total depth

The resistivity of mud filtrate (Rmf) at formation temperature can also be determined using the following equation:

$$Rmf_2 = Rmf_1 \frac{(T_1 + 6.77)}{(T_2 + 6.77)} \dots\dots\dots (6.14)$$

Where

- Rmf₂ = Resistivity of mud filtrate at formation temperature (ohm-m in °F)
- Rmf₁ = Known resistivity of mud filtrate at surface temperature (in °F)

Table 6.3 below present the parameters used for the calculation of Resistivity of mud filtrate (Rmf) at formation temperature and reservoir formation temperature values of all the Wells. The parameters used were taken from the well completion report and log header information of wells. The depths indicated in the Table 6.3 below are measured depths (MD) in meters.

Table 6.3: Calculated formation temperature (T_2) and resistivity of mud filtrate

<i>Well</i>	<i>Zone</i>	<i>Top (m)</i>	<i>Bottom (m)</i>	<i>T₁ (°F)</i>	<i>Rmf₁ (Ωm)</i>	<i>T₂ (°F)</i>	<i>Rmf₂ (Ωm)</i>	<i>TD (m)</i>	<i>BHT (°F)</i>
MA1	1	3212.5	3237.9	78.8	0.141	205	0.057	3320	208
MA2	1	2939.9	2950	71.6	0.153	179	0.065	3171	187
	2	2956.6	2966.2	71.6	0.153	179	0.065	3171	187
	3	2968.0	2980.1	71.6	0.153	180	0.065	3171	187
OP1	1	3181.0	3196.3	64.0	0.16	204	0.054	3749	229
	2	3303.0	3330.9	64.0	0.16	210	0.052	3749	229
	3	3368.0	3376.3	64.0	0.16	212	0.052	3749	229
	4	3390.1	3416	64.0	0.16	214	0.051	3749	229
OP3	1	3230.1	3239.2	71.6	0.23	206	0.085	3681	225
	2	3276.4	3286.3	71.6	0.23	208	0.085	3681	225
	3	3310.1	3317.1	71.6	0.23	209	0.083	3681	225
	4	3354.1	3370.1	71.6	0.23	211	0.083	3681	225
OP4	1	3107.5	3122.5	69.0	0.133	OBM	OBM	3440	229
	2	3236.8	3257.6	69.0	0.133	OBM	OBM	3440	229
OP5	1	3207.3	3213.1	72.0	0.276	OBM	OBM	3468	216
	2	3321.1	3330	72.0	0.276	OBM	OBM	3468	216
OP2	1	3184.4	3203.1	68.0	0.574	OBM	OBM	3511	169
	2	3306.0	3320.7	68.0	0.574	OBM	OBM	3511	169
	3	3445.9	3468.2	68.0	0.574	OBM	OBM	3511	169
MA3	1	3062.8	3070.4	73.4	0.136	179	0.059	3287	190
	2	3085.8	3091.9	73.4	0.136	183	0.058	3287	190
M A4	1	3150.6	3161.0	70.7	0.185	207	0.067	3470	220
	2	3293.0	3301.0	70.7	0.185	213	0.065	3470	220
	3	3332.1	3359.8	70.7	0.185	215	0.065	3470	220
OP 6	1	3196.0	3227.7	68.0	0.104	OBM	OBM	3367	226
	2	3306.6	3309.0	68.0	0.104	OBM	OBM	3367	226
	3	3314.0	3318.0	68.0	0.104	OBM	OBM	3367	226
	4	3330.0	3339.6	68.0	0.104	OBM	OBM	3367	226

In the Table 6.3 above, OBM represents wells drilled with oil based mud. The resistivity of the mud filtrate at formation (R_{mf2}) and the formation temperature (T_2) could not be estimated because oil based mud will influence the results. The other wells were drilled with water based mud and thus were easy to determine the resistivity of mud filtrate and temperature at reservoir conditions.

6.4.1.2 Determination of Formation Water Resistivity (R_w)

Formation water resistivity represents the resistivity value of the water which is uncontaminated by drilling mud that saturates the porous formation. The formation water resistivity can be determined from the calculation of Spontaneous Potential (SP) log (Asquith & Gibson, 1983), water catalogue, chemical analysis, water sample measurements, calculation from nearby water bearing formation, from R_{wa} technique, and from various cross plots (Mostafa & Walid, 2002).

The relationship for formation water resistivity obtained from water bearing formation is given below:

$$R_w = \left(\frac{R_{mf} * R_t}{R_{xo}} \right) \dots\dots\dots (6.15)$$

Where:

R_w = Water resistivity in uninvaded zone = 0.1 Ohm-m.

R_{mf} = Resistivity of mud filtrate

R_t = True resistivity from deep resistivity log reading

R_{xo} = Water resistivity from the flushed zone (shallow resistivity reading)

The formation water resistivity estimated from the SP log method and the Pickett cross plots are discussed below. The values obtained from these methods will be verified by comparison with one another and the use of standard log chart book.

6.4.1.2.1 SP Method for Formation Resistivity Water Estimation

The water formation resistivity value can be estimated from the static spontaneous potential of the SP log in water bearing clean sand. The baseline shift is first applied to the SP curve with a shale baseline set to 0.0mV. A formation temperature curve is entered if available otherwise it is created using the temperature gradient module of the IP software package.

The result (resistivity of water from SP curve R_{wSP}) curve is then calculated and corrected to the output temperature entered. Also created is the equivalent salinity of the R_{wSP} results to salinity in units of Kppm Nacl equivalent. The equation used for SP water resistivity calculations are given below:

$$ESSP = - Kc \log[R_{mfq} / R_w] \dots\dots\dots (6.16)$$

Where

ESSP = Static SP. in mV.

Kc = Temperature of formation

R_{mfq} = Equivalent Resistivity of mud filtrate

R_w = Resistivity of formation water.

K_c = temperature dependent factor = $65 + 0.24 * ^\circ C = 61.3 + 0.133F$

This method may not be successfully being applied to Wells drilled with an oil based mud because sufficient SP will not be generated. Also in shaly formations and hydrocarbon bearing intervals, SP measurements will be reduced and therefore for the determination of formation water resistivity, SP is determined in a clean water bearing sands (Bateman, 1985).

This method was not applied to the oil based mud (OBM) wells. The SP and temperature logs were not run in some of the wells in the study area; therefore it could not be used for comparison purposes. Porosity and deep resistivity logs were run in all wells; therefore the Pickett plot method for water resistivity determination was used for the determination of resistivity of water and compared with other methods and standard log chart book.

The resistivity of mud filtrate at surface condition and temperature are entered and then the SP curve will be created. An example of RwSP curve is presented in Figure 6.11 below.

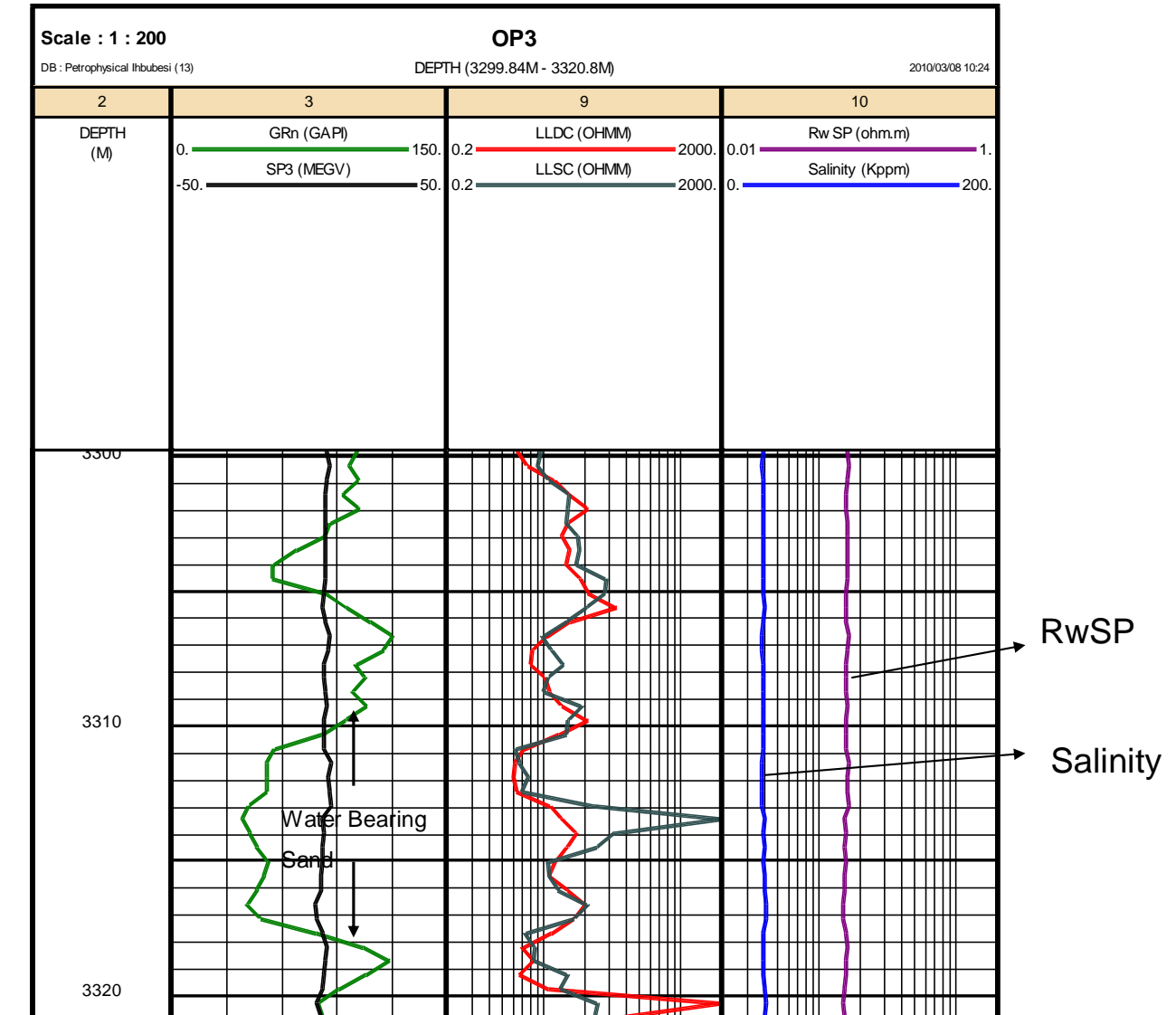


Figure 6.11: Example of resistivity of water from SP method

The water resistivity from SP (RwSP) and the salinity curves of the water bearing interval of well OP3 is shown in track 10 of Figure 6.11 above. Average values of salinity of 28 kppm and water resistivity of about 0.08 ohm-m were estimated in this water bearing sand interval at reservoir temperature of 212 °F. The Schlumberger Log

interpretation Chart Gen-9 was used to confirm the salinity and water resistivity values calculated.

6.4.1.2.2 Pickett Plot method For Formation Water Resistivity Estimation

The concept of the Pickett plot is based on double logarithm plot of a resistivity measurement on the x-axis versus porosity measurement on the y-axis. After the points are plotted, the one hundred percent water saturation is fixed by drawing it through the lowest resistivity points corresponding to different porosities. Points of constant water saturation will be plotted on straight line and the water resistivity (R_w) can be determined from point on the straight line (Bate, 1985).

The Pickett plot for water resistivity determination for well OP1, OP2, OP3, and OP4 taken at water bearing intervals is presented in Figure 6.12 below.

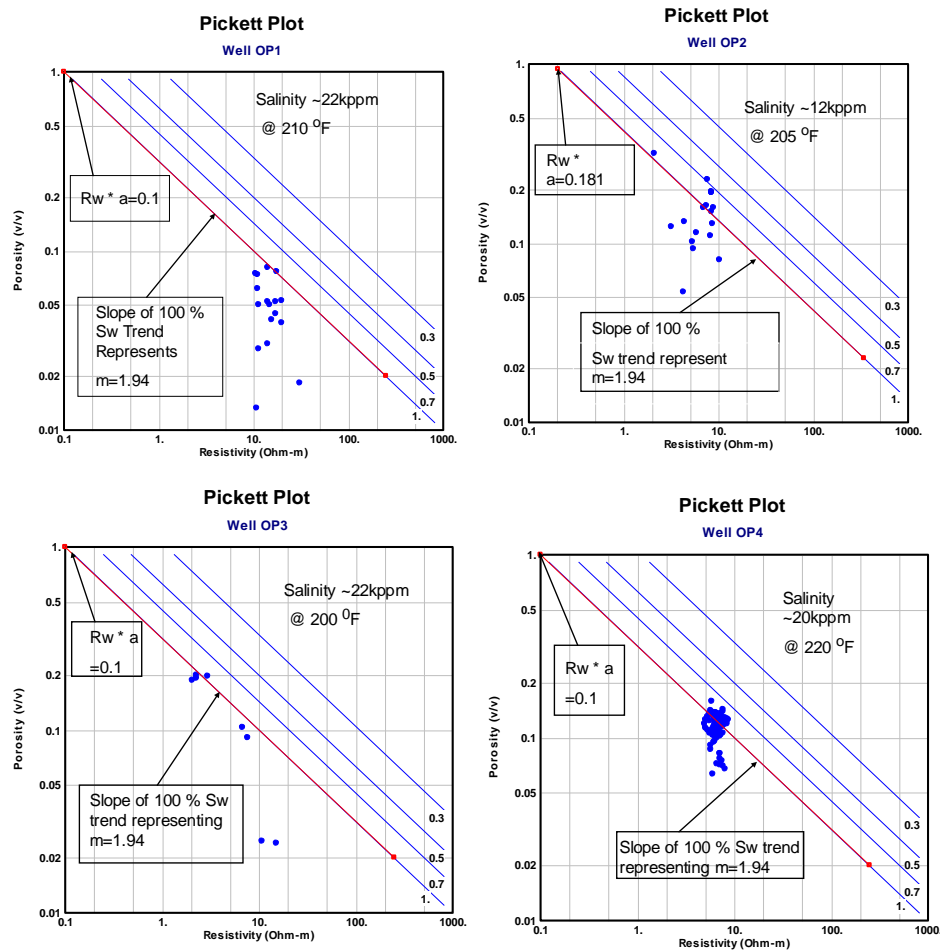


Figure 6.12: Pickett Plot for determination of resistivity of water (R_w) for well OP1, OP2, OP3, and OP4 respectively.

The Pickett plot above present the resistivity of water of 0.1 ohm-m for wells (OP1, OP3, and OP4) using cementation exponent of 1.94 derived from the special core analysis results and saturation exponents of 1.8 respectively at formation temperatures determined from repeat formation test measurements. The Pickett plots for other wells are presented in appendix I.

The resistivity of formation water to be used in subsequent water saturation modeling will be 0.1 ohm-m for wells.

6.4.1.3 Cation Exchange Capacity per Pore Volume (Q_v) and Equivalent Conductance of Clay Cations (B)

The cation exchange capacity per pore volume (Q_v) and equivalent conductance of clay cations are essential parameters in water saturation cation exchange capacity models. The cation exchange capacity per pore volume was determined from core plugs of wells OP1, OP2 and OP3 as earlier discussed in chapter five. The determined Q_v values are entered as input curves while the equivalent conductance of clay cations (B) was calculated from the following relationship.

$$B = \frac{-1.28 + 0.225 * T - 0.0004057 * T^2}{1 + R_w^{1.23} (0.045 * T - 0.27)} \dots\dots\dots (6.17)$$

Where:

B = Equivalent conductance of clay cations

T = Formation temperature

R_w = Resistivity of water =0.1 Ohm-m

The equivalent conductance of clay cations parameter will be used in the volume of shale cation Exchange Capacity (CEC) water saturation model (example is the Waxman-Smits, Dual-Water ,and Juhasz).

6.4.2 Water Saturation (S_w) Models

The estimates of water saturation are needed when evaluating the potential of a reservoir. Water saturations of the invaded and un-invaded zones (S_{xo} and S_w) of a

formation can be calculated for clean sands and Shaly-sand models by using one of the Sw equations below.

6.4.2.1 Archie's Model

The first and still the most popular clean sands model for electrical measurements and saturation were provided by Archie (1942). He characterised the conductivity of a porous media having a non-conductive matrix as a function of the porosity and of the conductivity of the saturating fluid.

Archie's equation is in the form given below:

$$S_w^n = R_w / (\Phi^m * R_t) \dots\dots\dots (6.18)$$

where:

S_w = Water Saturation of the un-invaded zone

n = Saturation Exponent which varies from 1.7 to 4 but normally equals 2 for Archie's-type rocks. In this study, $n = 1.8$ determined from special core analysis will be used.

R_w = Formation Water Resistivity at formation temperature = 0.1 Ohm-m

Φ = Porosity

m = Cementation Exponent which varies from 1.4 to 3.0 but normally equals 2.0 for Archie's -type of rock. The value of m used in this study is 1.94 determined from special core analysis as discussed in chapter 5.

R_t = True Resistivity of the formation corrected for invasion, borehole, thin bed and other effects.

The Archie's equation works very well in a high salinity condition provided there exist a current path through the formation. In an extremely low salinity clean sands condition, the equation may give an error which is due to surface conductance effects. The shaly-sand models are models that include in the water saturation equations, terms that consider the conduction path of the clay mineral double layer which are interlayer and clay surface water. The Shaly-Sand models are presented below:

6.4.2.2 The Shaly-Sand Models (Volume of Shale and CEC)

In evaluating the Shaly-Sand reservoirs, the Archie's equation may give a misleading result because it assumes that the formation water is the only electrically conductive material in the formation. Shale conduct electricity and Shaly-sand conductivity varies with clay type, shale origin and fluid composition. The Shaly-sand models consider the conductivity from shale and the formation water, hence two conductivity pathways are considered.

The Shaly-sand models are grouped into the volume of shale and the cation exchange capacity models. The volume of shale model is comprised of Simandoux, Fertl and Hammock, Indonesia, etc. The cation exchange capacity models comprised of the Waxman-Smit, Dual-Water, Juhasz, etc.

6.4.2.2.1 The Simandoux Model (Volume of Shale)

Simandoux (1963) proposed a model based on the experimental work on homogeneous mixtures of sand and shale and come up with the following relationship:

$$S_w = aR_w / 2\Phi^m \left[V_{sh}/R_{sh} + \sqrt{(V_{sh}/R_{sh})^2 + 4/F * R_w * R_t} \dots \right] \dots \dots \dots (6.19)$$

Where:

S_w = Water Saturation

a = Equation Coefficient

R_w = Resistivity of water

R_{sh} = Resistivity of shale =5 Ohm-m

V_{sh} = Volume of shale

F = Formation Resistivity factor

R_t = True formation resistivity from corrected deep resistivity log.

Φ = Effective Porosity, fraction

m = Cementation exponent =1.94 from special core analysis.

The estimated resistivity of shale of 5 Ohm-m was used for the evaluation. This value was determined from the resistivity correlation of wells as shown in Figure 6.13a below)

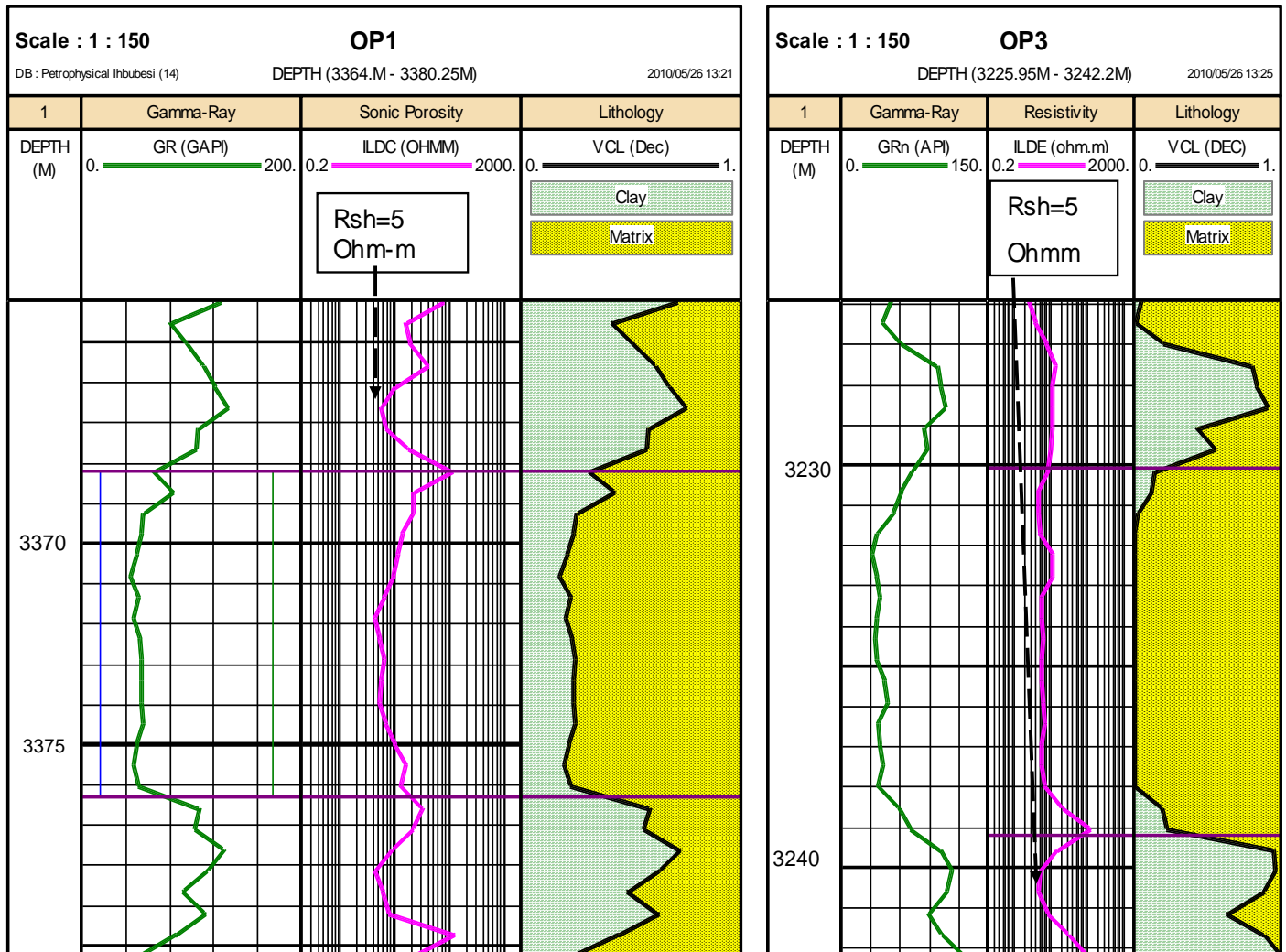


Figure 6.13a: Estimate of resistivity of shale (Rsh) from Wells.

6.4.2.2.2 Indonesian Model

In 1971, Poupon and Leveaux proposed an empirical model called Indonesia formula (Poupon and Leveaux1971).The equation was based on characteristic of fresh waters and high degrees of shaliness that were present in many oil reservoirs in Indonesia.

The empirical relationship can be written as follows:

$$1/\sqrt{R_t} = \left[\sqrt{\frac{\Phi_e^m}{a \cdot R_w}} + \frac{V_{cl}^{(1-V_{cl}/2)}}{\sqrt{R_{cl}}} \right] * S_w^{n/2} \dots\dots\dots(6.20)$$

where:

R_t = Resistivity curve from deep log reading

R_{cl} = Resistivity of wet clay

Φ_e = Effective porosity calculated from equation 5.12 above.

S_w = Water saturation, fraction

V_{cl} = Volume of shale, fraction

R_w = Formation water resistivity = 0.1 Ohm-m.

m = Cementation exponent = 1.94 from special core analysis

a = Tortuosity factor

n = Saturation exponent = 1.8 from special core analysis

6.4.2.2.3 Waxman-Smith Model

Waxman and Smith (1968) based on an extensive laboratory work and theoretical studies proposed a saturation-resistivity relationship for shaly formation based on the assumption that cation conduction and the conduction of normal formation sodium chloride act independently in the pore space resulting to a parallel conduction path.

The model is expressed as follows:

$$1/R_t = \left[\frac{\Phi^m * S_w^n}{a * R_w} \right] * \left[1 + B * Q_v \frac{R_w}{S_w} \right] \dots\dots\dots(6.21)$$

Where:

R_t = Resistivity from deep log reading

Φ = Total porosity

S_w = Water saturation

R_w = Formation water resistivity

n = Saturation exponent

B = Equivalent conductance of clay cations

Q_v = cation exchange capacity per pore volume (from equation 5.11)

m^* = Cementation factor obtained from special core analysis measurement determined from equation 5.6.

6.4.2.2.4 Dual-Water Model

The Dual-Water model is a modification of the Waxman-Smiths equation by considering counterion conductivity to be restricted to the bound water where counterion resides and the free water which is found at a distance away from the clay surface. The model shows that the apparent water conductivity will depend on the relative volume of clay bound water and free water. Clavier et al. (1984) first proposed this model called the dual water.

The Dual-Water equation is given below:

$$1/R_t = \left(\frac{\Phi^{m^*} * S_w^n}{a} \right) * \left(\frac{1}{R_w} + \frac{S_{wb}}{S_w} \left(\frac{1}{R_{wb}} - \frac{1}{R_w} \right) \right) \dots\dots\dots(6.22)$$

Where:

R_t = Resistivity from deep log reading

Φ = Total porosity

S_w = Water saturation

S_{wb} = Bound water saturation.

R_w = Formation water resistivity

R_{wb} = Bound water resistivity

n = Saturation exponent

m^* = Cementation factor obtained from special core analysis measurement.

Bound water is the water that is held close to the surface of the rock matrix. Bound water is mainly associated with the surfaces of clay minerals because of their small size. The saturation of bound water (S_{wb}) determination is essential for an accurate estimation of total water present in a reservoir. The presence of clay minerals and mode of distribution in sandstone reservoirs often develop an overgrowth on the sand grains that tends to provide additional pore spaces known as micro-pores that contain

only water. This results in high surface areas on which large quantity of water are absorbed.

Chlorite and mixed-layer Illite commonly form grain coating cements concentration within particular intervals. Grain coating cementation is often associated with primary deposition or immediate post depositional processes (Hurst and Archer, 1986).

Presented in Figures 7.6 to 7.8 below are capillary pressure estimated irreducible water saturation (Sw_J, CEC saturation of bound water (CEC Sw_b), log determined bound water saturations (Sw_b) and XRD clay type mineralogy.

Presented in Figures 6.14 to 6.15 below are the comparison of log determined bound water saturation with core for wells.

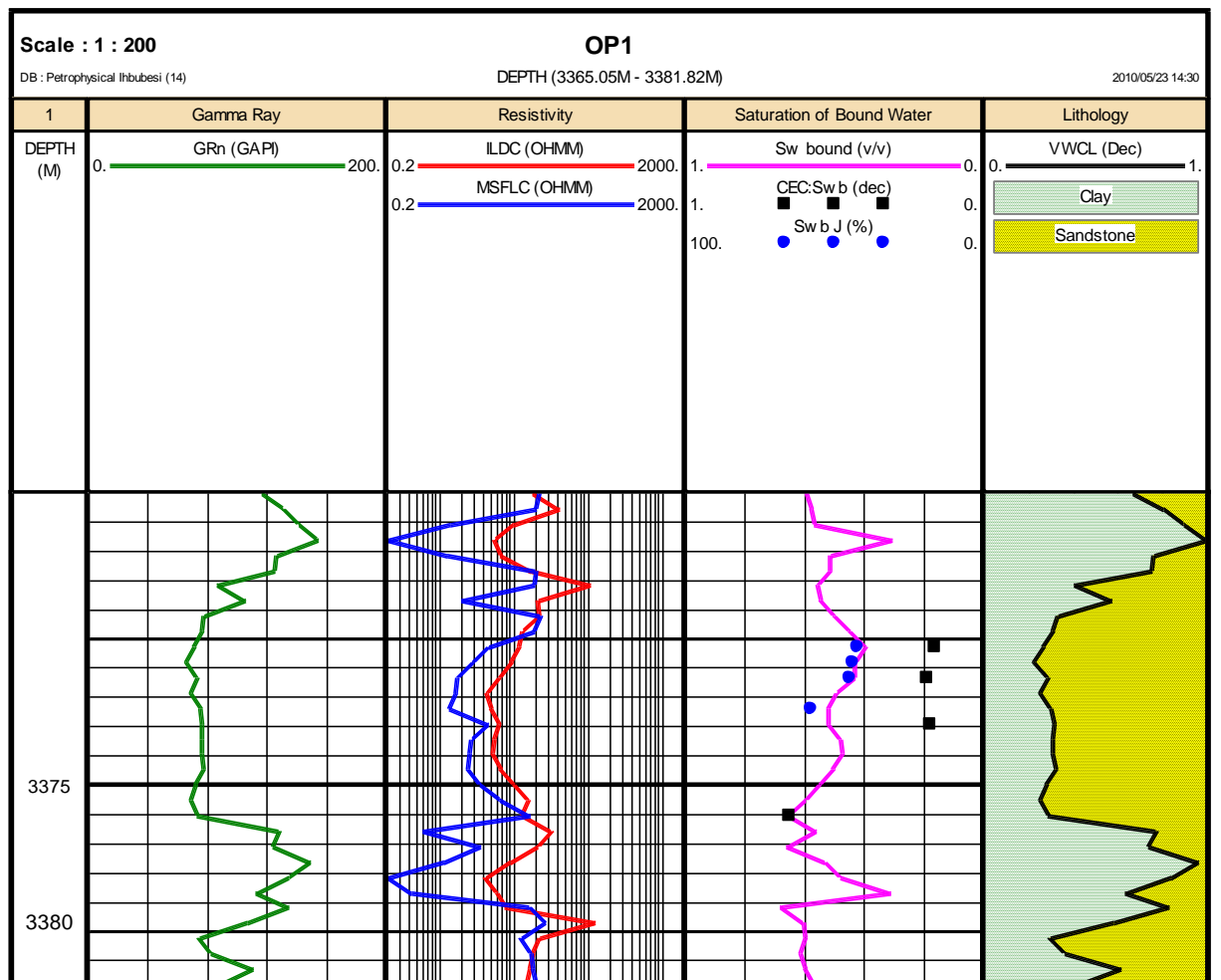


Figure 6.14: Comparison of core and log determined bound water saturation for Well OP1

In well OP1 (Figure 6.14 above), 100 % bound water saturation was recorded at the clay intervals top and below the reservoir zone. The core and log data overlaid do not match and there was no XRD clay type result for this well. The minimum saturation of bound water of about 62 % was recorded at measured depth 3272m.

In well OP2 (Figure 6.15), there exists a good agreement between the log and CEC derived saturation of bound water. Within the reservoir interval, very low (less than 10 %) saturation of bound water was recorded and the dominant clay mineral present is chlorite (track 5). The low resistivity values observed in track 3 may be due to the presence of chlorite and illite.

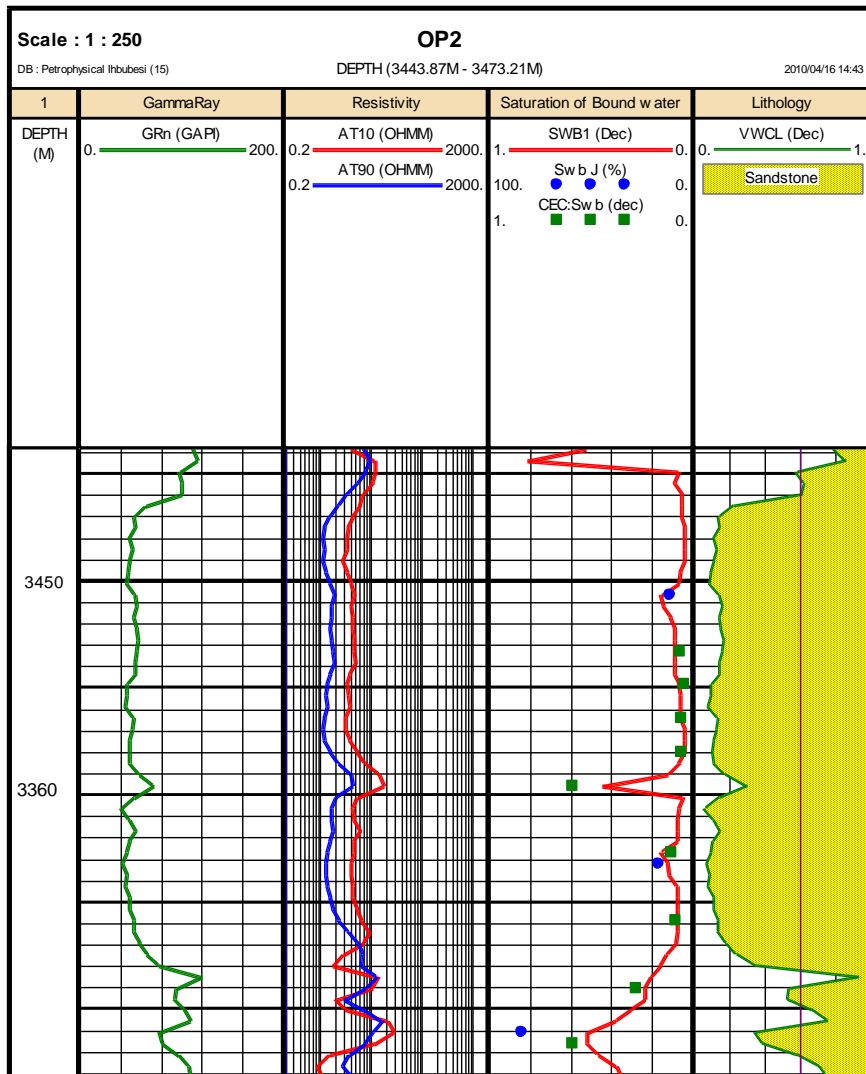


Figure 6.15: Comparison of core and log estimated bound water saturation and XRD mineralogy data for Well OP2

6.4.2.2.5 Juhasz Model

Juhasz (1981) developed a relationship for determination of water saturation based on the concept of Waxman and Smith (1968).

$$1/R_t = \left(\frac{\Phi^m * S_w^n}{a * R_w} \right) * \left(1 + B_n * Q_{vn} \frac{R_w}{S_w} \right) \dots\dots\dots(6.23)$$

Given that $Q_{vn} = \frac{V_{cl} * \Phi_{clay}}{\Phi}$

Where:

R_t = Resistivity from deep log reading

Φ = Total porosity

Φ_{clay} = Total porosity of adjacent clay

S_w = Water saturation

R_w = Formation water resistivity

n = Saturation exponent

B_n = Normalized equivalent conductance of clay cations

Q_{vn} = Normalized cation exchange capacity per pore volume

m = Cementation factor

V_{cl} = Volume of clay, fraction.

6.4.3 Comparison of Conventional Core, Capillary Pressure and Log Water Saturation

Water saturations were estimated from Dean-Stark conventional core based measurements in well OP1 and OP3, and capillary pressure measurements in both wells (chapter 5) which provide a reference against which log derived saturations can be compared. Presented in Figures 6.16 to 6.17 below are the comparisons of conventional core and capillary pressure water saturation measurements with log calculated water saturation models.

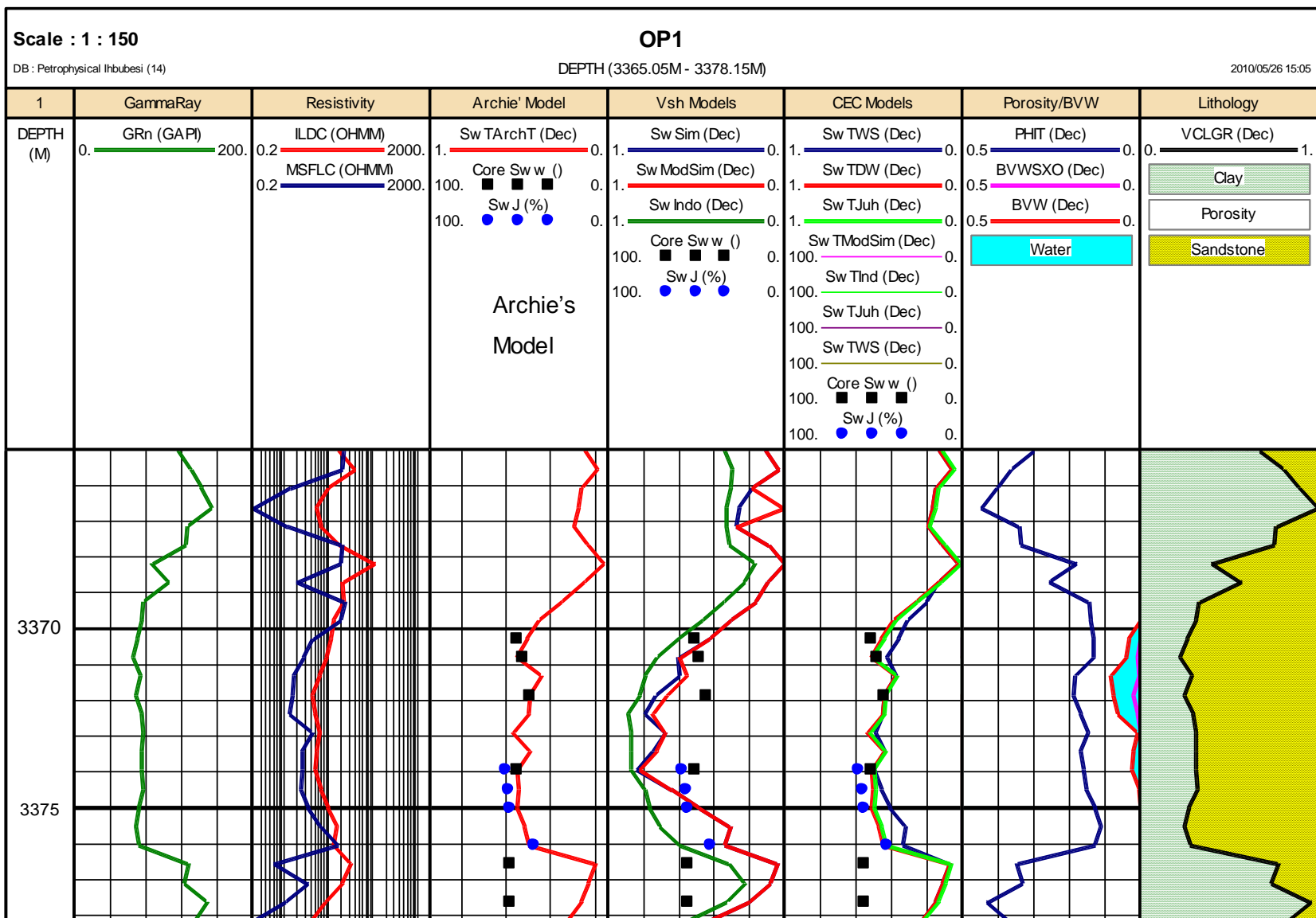


Figure 6.16: Comparison of core and log water saturation models for Well OP1

The water saturation model derived from the Archie's model is plotted in track 4 (red colour), shaly sand volume of shale models (Simandoux (Sws- navy blue colour, modified Simandoux (Swmodsim-red, and Indonesia (Sw Ind-green) in track 5; and the CEC models (Waxman-Smit (Sw WS(navy blue, Dual water (Sw DW-red), and Juhasz (Sw Juh –lime colour) in track 6 respectively.

In well OP1 (Figure 6.16) above, the average water saturation estimated from the Archie's model was about 48%, Simandoux 67 %; Indonesia 84 %; Waxman-Smith 44 %,Dual –Water and Juhasz about 50 % respectively within the reservoir section. The Waxman-Smith model in track 6 (navy blue colour) best matches with the water saturation from routine core analysis and J-function saturation data.

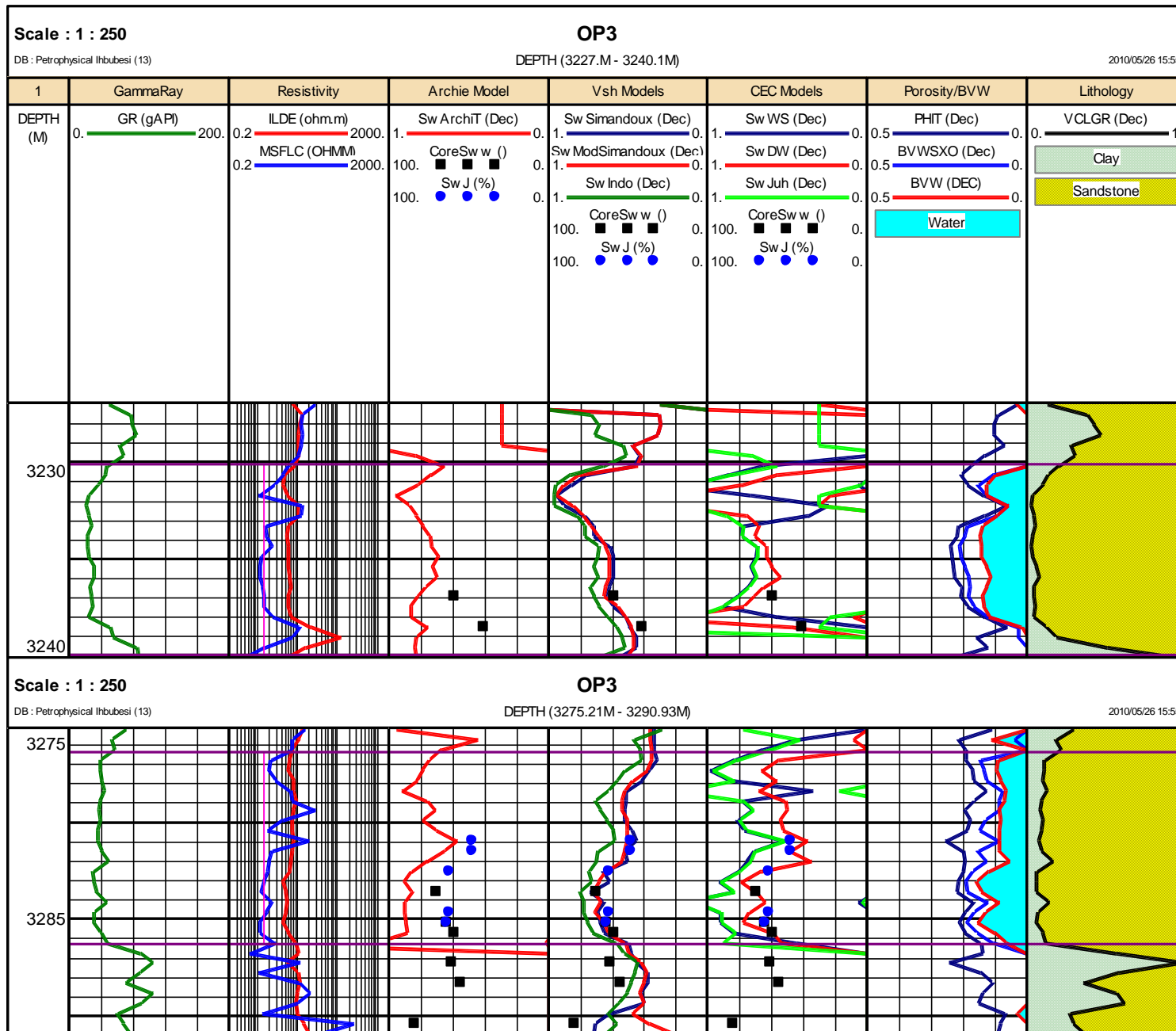


Figure 6.17: Comparison of core and log water saturation models for Well OP3

For well OP3 (Figure 6.17) above, the estimated water saturation from Archie's model was 44 % and 49 % ,Simandoux and Indonesia 40 % and 51 %, Waxman-Smith, Dual-water and Juhasz 62 % and 48 % in both cored intervals respectively. A good agreement between the capillary pressure water saturation and log determined water saturation was observed in core 2 interval. The Simandoux and Indonesia saturation models best match with the capillary pressure water saturation data.

Generally, the core based water based saturations are higher than those derived from log. The higher water saturations in the core based saturations may be due to the water based mud used to drill these wells which provide an alternate source for water found in the core. Consistent mismatch in water saturation levels between log and core was observed in all Well. It was apparent that from the logs and core data interpreted that the reservoir formations contained shaly sands. The log interpretation compared water saturation predictions from the clean sand (Archie) and Shaly Sand (Volume of shale (Vsh) and Cation Exchange Capacity (CEC)) models. The Dual -Water and the Simandoux models were the closest match with the core data.

6.5 BULK VOLUME OF WATER (BVW)

The bulk volume of water is defined as the product of water saturation and porosity. The bulk volume of water can also be used as a hydrocarbon indicator (Walid, 2005). This method simply plots a bulk volume of water (BVW) and effective porosity versus reservoir depth interval. At points when the bulk volume of water is nearly or equal to the effective porosity indicates that the zone or interval is wet or completely saturated with water.

A separation between the bulk volume of water and effective porosity indicates the presence of hydrocarbon. Presented in Figure 6.19 below is an example of the use of bulk volume of water as hydrocarbon indicator for well OP3.

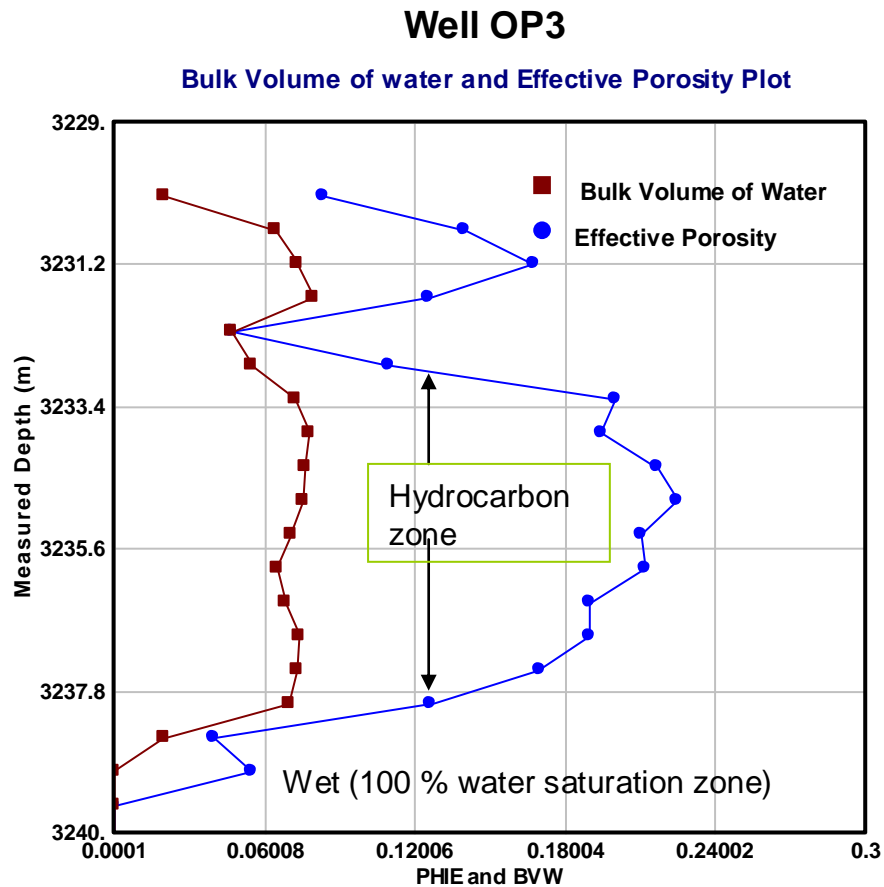


Figure 6.18: Bulk volume of water and effective porosity plot for well OP3

In conclusion, the Simandoux volume of shale water saturation model will be adopted for water saturation calculations because there was an agreement with the conventional core data and the water saturation derived from the capillary pressure measurements. The input parameters into the Simandoux model can be controlled much easier than the Dual-Water model.

CHAPTER SEVEN

PERMEABILITY, ROCK TYPING AND FLOW UNITS

7.1 INTRODUCTION

Permeability is the property of a rock that characterises the flow of fluids through its interconnected pores. It is a measure of the fluid conductivity of a rock. The permeability of a flow unit in a reservoir is not an absolute value but it is a relative value that varies with water saturation. Understanding how permeability is measured is important to determine reservoir rock quality or compare the quality of one flow unit to another. Permeability is not actually measured but is calculated and could be determined horizontally or vertically.

The horizontal permeability is measured parallel to the bedding plane and is generally greater than vertical because of vertical changes in sorting and because grains tends to align and overlap parallel to the depositional surface. The vertical permeability is measured across the bedding plane. Most permeability calculations are made from horizontal measurements (Halliburton, 2001).

Reservoir contains water, oil and gas in varying amounts. Each of the fluid present in the reservoir interferes with and impedes the flow of other fluid. The permeability of a reservoir calculated with only one fluid present in the pores of a formation is regarded as absolute (K_a). Effective permeability (K_e) is the ability of a rock to conduct one fluid in the presence of another, provided that both fluids are immiscible. Relative permeability (K_r) can be expressed as the ratio of a fluid's effective permeability to the formation's absolute permeability. It can be expressed as a number between zero and one or as a percent.

The calibration of test data made at in situ reservoir conditions with laboratory measurements is very important in reservoir description. In situ permeability is a measure of effective permeability of a given fluid in the presence of other fluids. Permeability measured under laboratory conditions is the absolute permeability to a single fluid (Hurst & Archer, 1986).

A petrophysical flow unit is defined as an interval of sediment with similar petrophysical properties such as porosity, permeability, water saturation, pore throat radius and flow capacity that are different from the intervals immediately above and below it (Porras & Campos, 2001).Petrophysical flow units are grouped to define

containers and rock types having similar flow capacity are grouped and used to determine reservoir flow units.

Ebanks (1987) defined the fundamental concept of hydraulic flow units as a map- able portion of the reservoir within which geological and petrophysical properties controlling the flow of fluids, are consistent and predictably different from the properties of other reservoir rock portion. Methods for flow unit zonation include application of Lorenz plots and the use of flow zone indicator (Saibal et al., 2008).

Both methods require the knowledge of porosity and permeability distributions. Different techniques and methods have been used to define flow units. Comparative studies of different methods of flow unit determination have been reported by Porras et al. (1999), Amaefule et al. (1993) and Stolz & Graves (2003).

Rock typing is the process of classifying reservoir rocks into distinct units, each of which was deposited under similar geological conditions and has undergone similar diagenetic alterations (Gunter et al., 1997). When properly applied, rock typing can lead to an accurate estimation of formation permeability in uncored intervals of uncured well (Genliang et al., 2007).

The flow rate depends on the permeability, formation pressure, and viscosity of the fluid and saturation of the fluids present.

7.2 PERMEABILITY

The permeability values in this study are derived from three potential sources. They are core measured permeabilities, permeability estimated from the regression analysis of the core porosity versus permeability plot; log predicted permeabilities and permeability determined from the repeat formation test measurements.

7.2.1 Permeability from Core Analysis (Permeability–Porosity Function)

This particular aspect of the study was aimed at establishing a correlation between core permeability and porosity and other wireline log porosity responses. The objective was to identify or predict permeability in uncured intervals and also to estimate permeability in wells without core data. The Figure 7.1 below present the graphics of core analysis porosity-permeability plots for well OP1, OP2, OP3, and combination of all the wells.

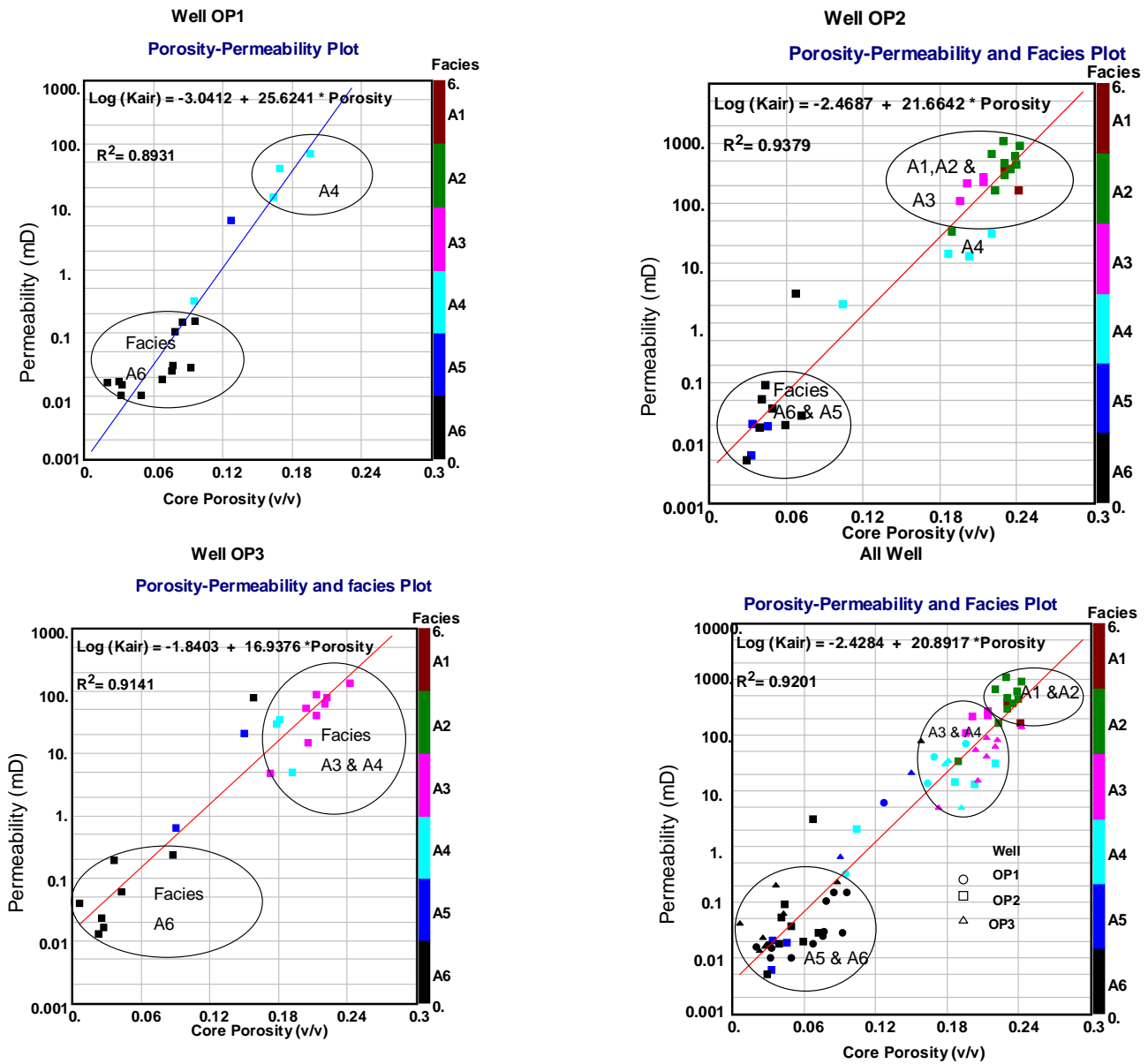


Figure 7.1: Porosity –Permeability cross plots for determination of function

The following based permeability-porosity functions were established from the cross plots as discussed in chapter four of this study as shown in Table 7.1 below

Table 7.1: Established porosity-permeability functions for wells

Well	Porosity-Permeability functions	Correlation Coefficient (R^2)
OP1	$\text{Log}(K) = -3.1626 + 24.817 * \text{Porosity}$	0.8931
OP2	$\text{Log}(K) = -2.687 + 21.6648 * \text{Porosity}$	0.9379
OP3	$\text{Log}(K) = -1.8403 + 16.9376 * \text{Porosity}$	0.9141
All Well	$\text{Log}(K) = -2.4284 + 20.8917 * \text{Porosity}$	0.9201

The functions established in Table 7.1 above have been validated by comparing predicted permeabilities from the functions against the original core measured permeabilities. The comparison of the functions are illustrated in Figures 7.2 to 7.4 below where the predicted permeabilities (red colour curve in track 4) are directly overlain with the core permeabilities (green colour dots in track 4) in wells OP1, OP2 and OP3 respectively.

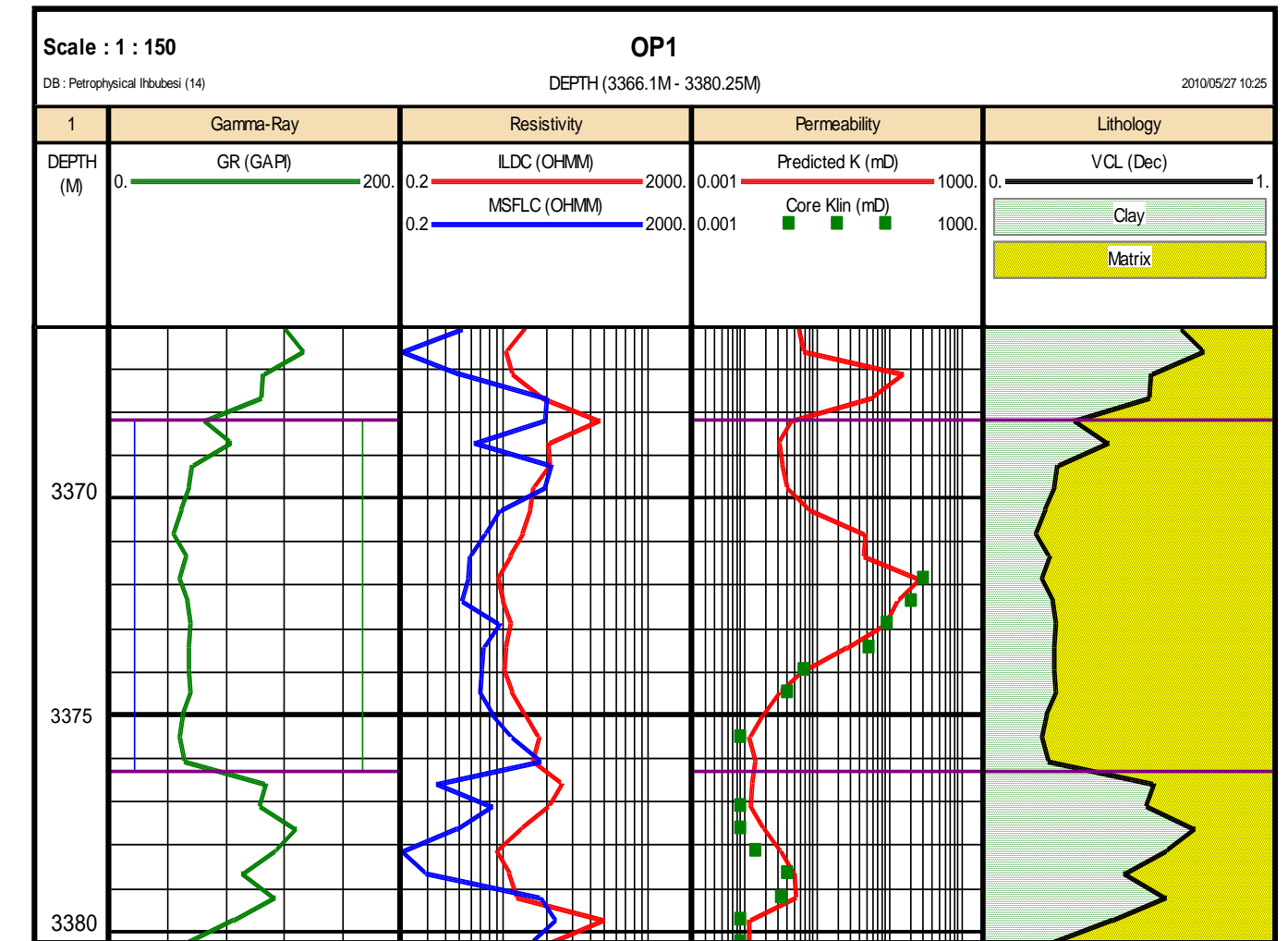


Figure 7.2: Well OP1 plot of predicted permeability overlaying original core permeability in track 4

In well OP1 (Figure 7.2), the predicted permeability (track4 red) values from log derived porosity matched very well with the core measured permeability (track 4 green dots). A good relationship was observed between both curves though they both portray the same trend pattern. The plot for well OP2 is presented in Figure 7.3 below.

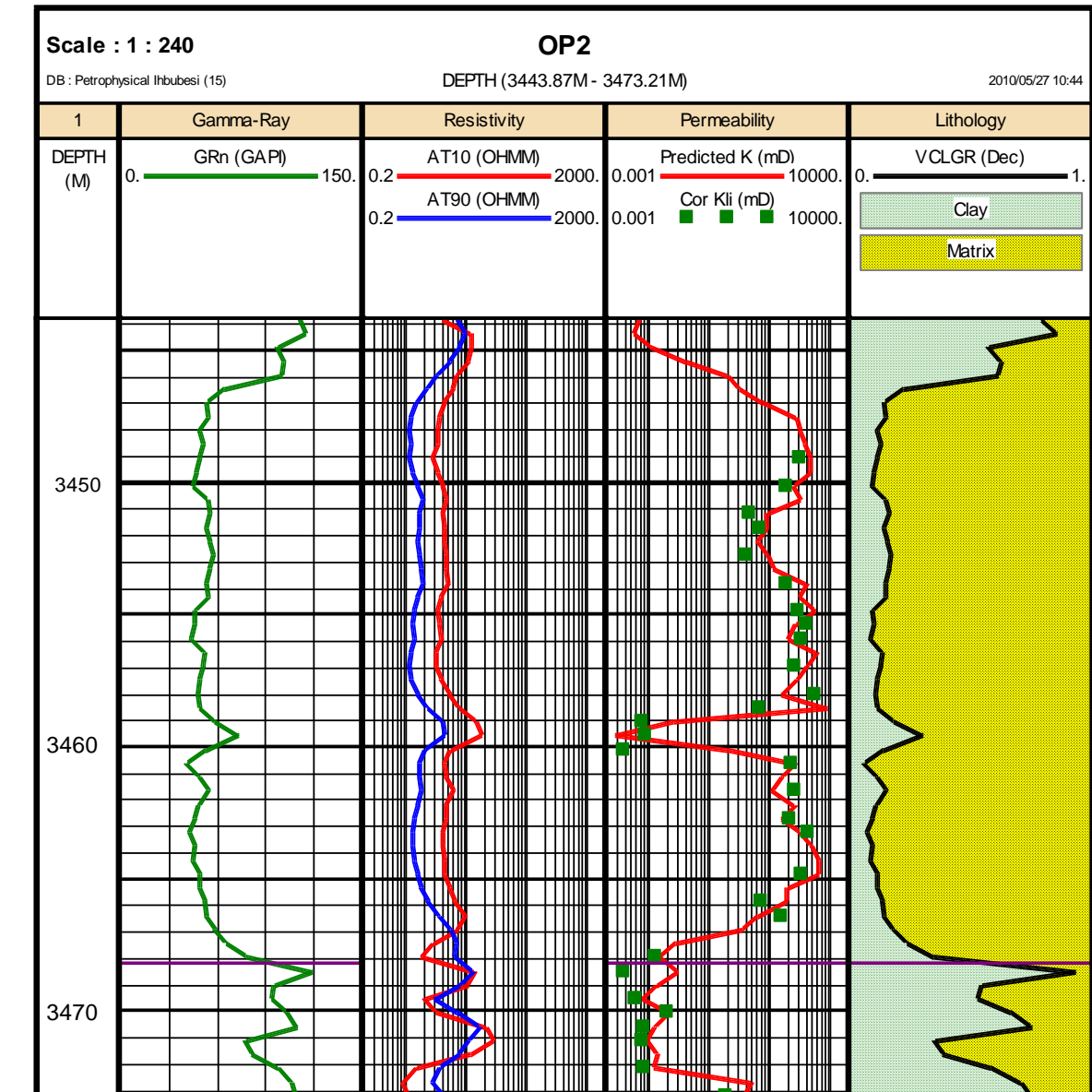


Figure 7.3: Well OP2 plot of predicted permeability overlaying original core permeability in track 4

In well OP2 (Figure 7.3), the predicted permeability curve (track 4 red) showed a good and close agreement with the core measured permeabilities (track 4 green dots). Though a few scatter points were observed, this may be due to the inherent scale differences between the two measurements.

Presented in Figure 7.4 below is the core and log permeability overlay for well OP3.

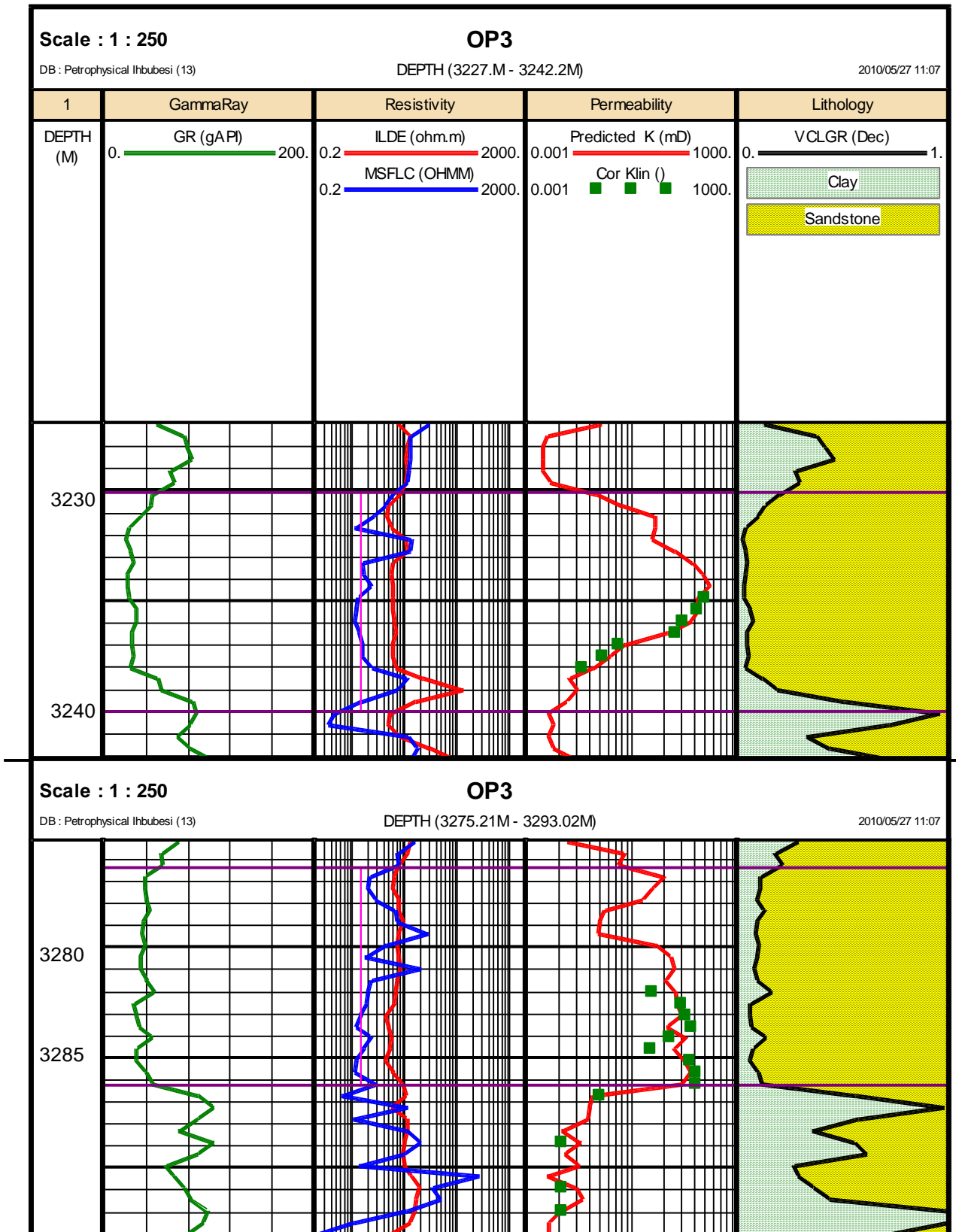


Figure 7.4: Well OP3 plot of predicted permeability overlaying original core permeability in track 4

For well OP3 (Figure 7.4), the predicted permeability matched the core permeability on a one to one trend in core 1(measured depth interval between 3230m to 3240m).In

core 2 (measured depth interval 3275 to 3290 meters), discrepancies were observed between both curves. Generally, a good agreement exist between core measured permeability and predicted permeability. In conclusion, for non-cored Wells, the absolute permeability could be predicted from the core porosity-permeability derived function because the predictor showed good match with the Klinkenberg corrected core permeability in all the wells compared.

7.3 PERMEABILITIES ESTIMATE FROM LOG

There exist several equations proposed for the estimate of permeability from measurements of porosity and irreducible water saturation. A general empirical relationship for the estimation of permeability from porosity and irreducible water saturation was first proposed by Wyllie and Rose (1950).

The Wyllie and Rose relationship is of the form given below:

$$\sqrt{K} = C \Phi^3 / S_{iw} \dots\dots\dots (7.1)$$

Where:

K = Permeability (mD)

C = Factor that depends on the density of the hydrocarbon.

Φ = Porosity

S_{iw} = Irreducible water Saturation.

The irreducible water saturation was estimated from the capillary pressure measurements. An example for the determination of the irreducible water saturation is presented in the Figure 7.5 below.

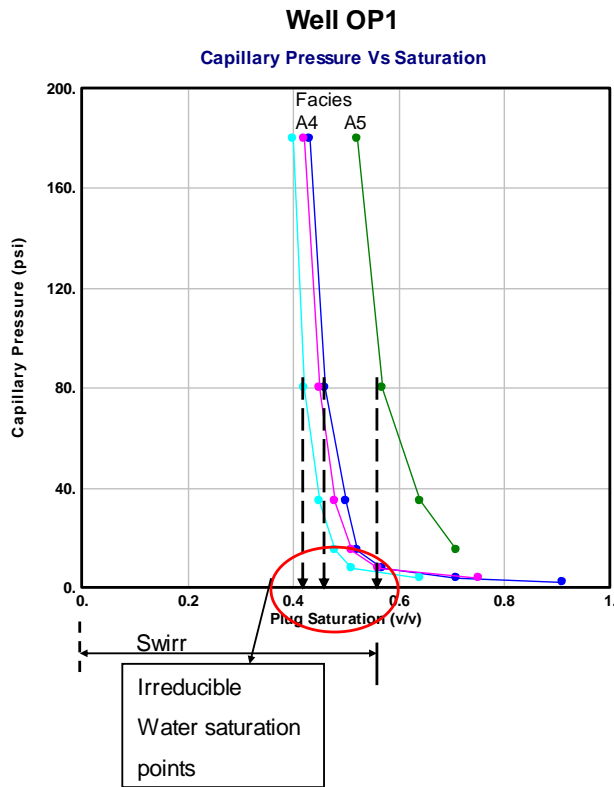


Figure 7.5: Example of irreducible water saturation estimate point from capillary pressure measurement

The irreducible water saturation was estimated at points where the black arrows intersecting the plug saturation line on the x-axis as measured from the left (zero plug saturation points).

In this study, methods proposed by Timur (1968), Morris and Biggs (1967), and Schlumberger (1972) to estimate permeability from measurements of porosity and irreducible water saturation was used. The general equation used with the aid of the Interactive Petrophysics Software package is of the form given below:

$$K = a * (\Phi^b / S_{iw}^c) \dots\dots\dots(7.2)$$

Where:

K = Permeability

Φ = Porosity

S_{iw} = Irreducible water saturation

The constants a, b and c for Timur, Morris and Biggs, and Schlumberger equations are given below:

Timur equation= $a = 8581$; $b = 4.4$ and $c = 2$

Morris Biggs gas = $a = 62500$; $b = 6$ and $c = 2$

Schlumberger = $a = 10000$; $b = 4.5$ and $c = 2$

Comparison of log permeability values are presented in Figures 7.4 to 7.6. The Morris and Biggs equation is plotted in track 3 (red colour curve), Schlumberger in track 4 (blue colour curve), and the Timur equation in track 5 (Pink colour curve). The curves were overlaid with the core measured permeability data (green colour dots) in tracks 3 to 5 for comparison.

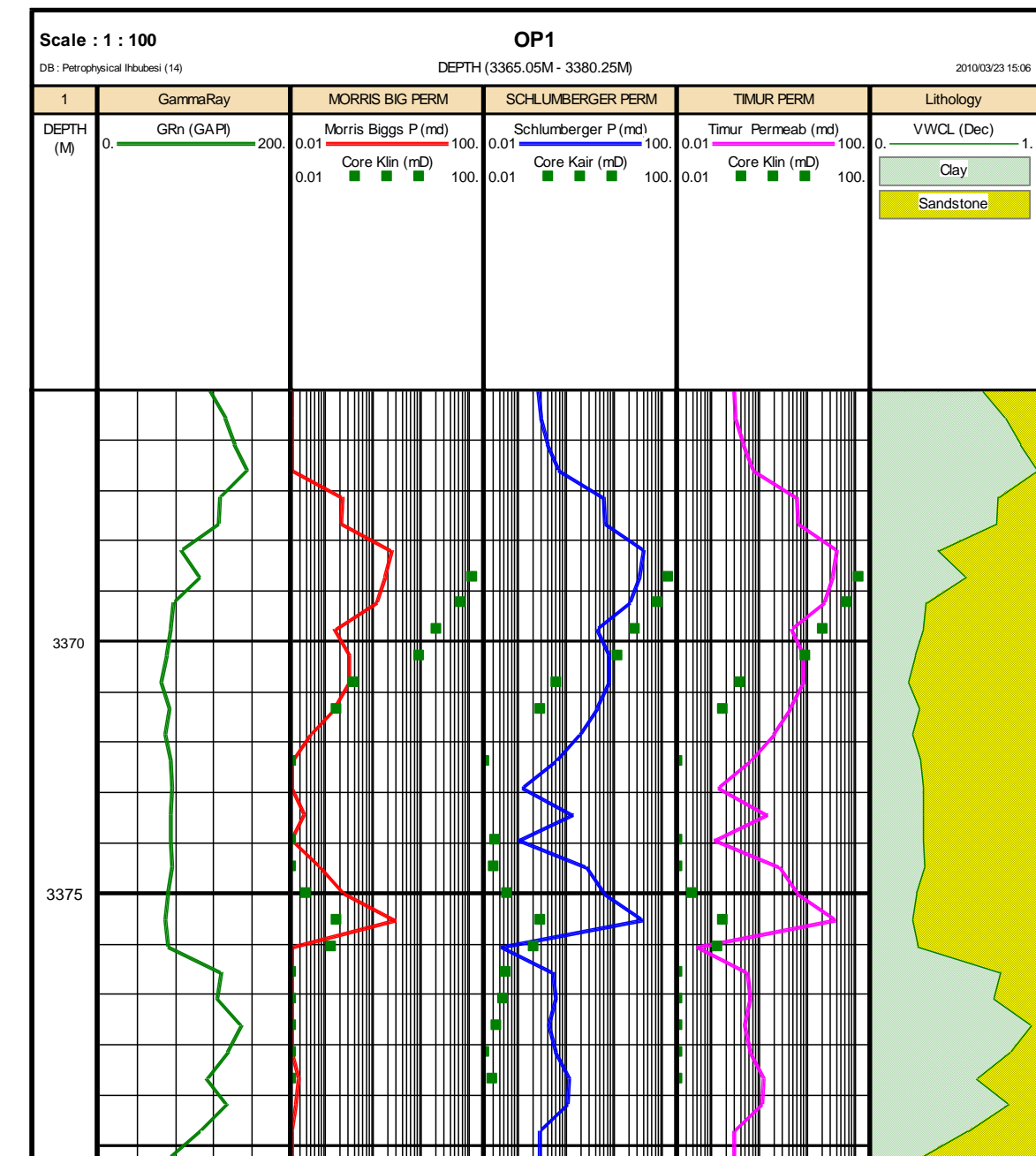


Figure 7.6: Log estimated permeability and overlaid core permeability for well OP1

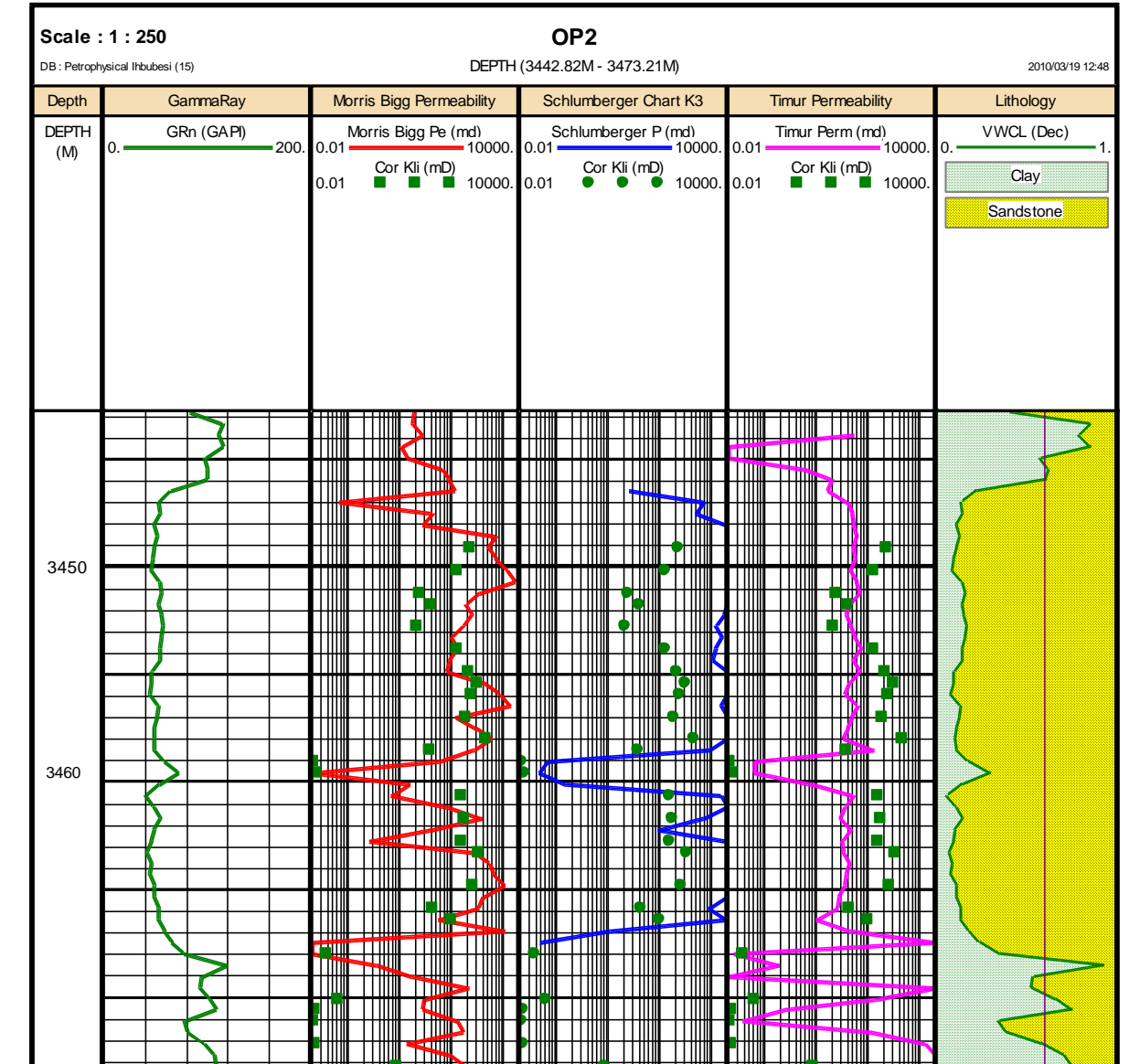


Figure 7.7: Log estimated permeability and overlaid core permeability for well OP2

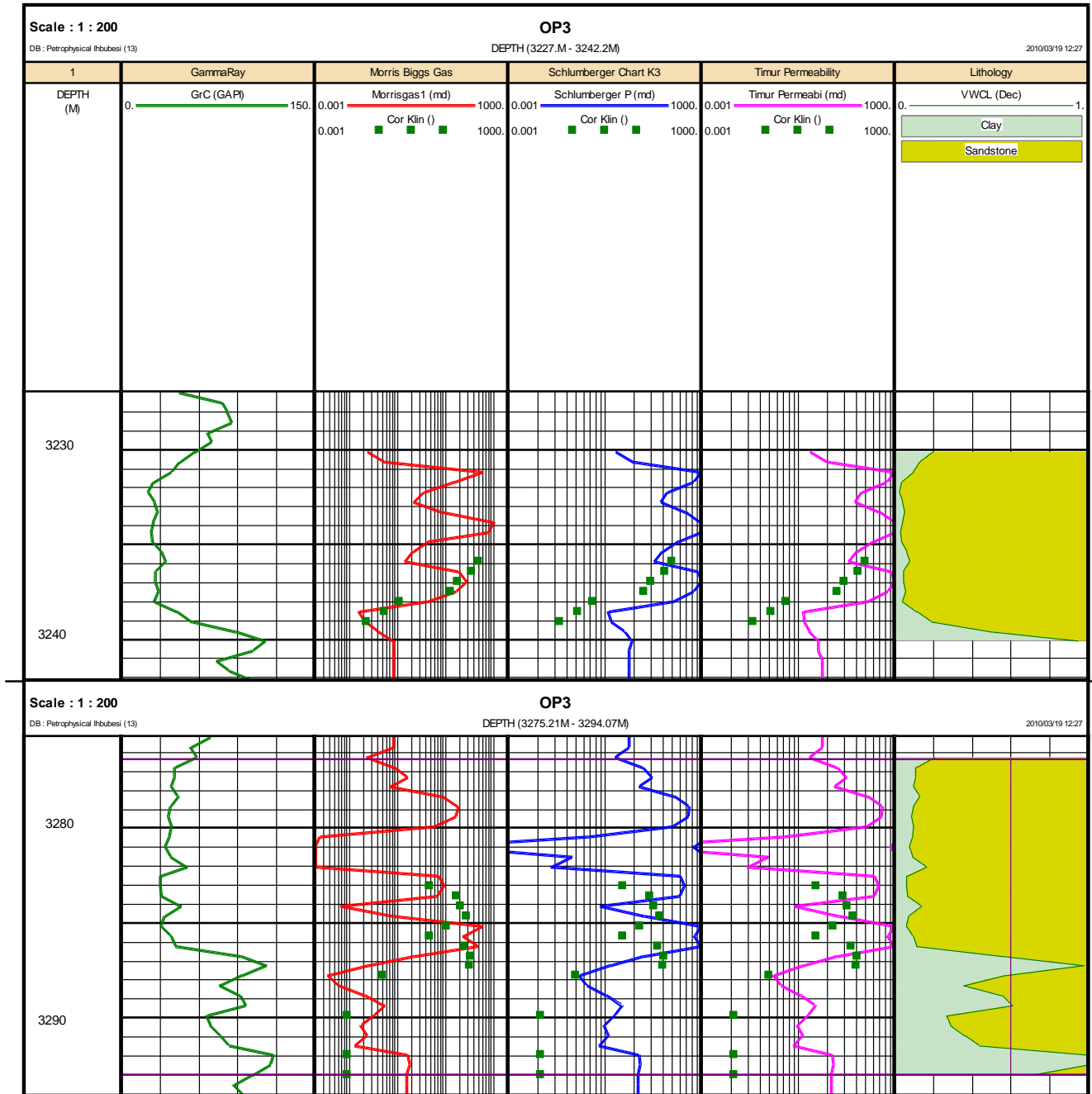


Figure 7.8: Log estimated permeability and overlaid core permeability for well OP3

The Morris and Biggs equation best match with the core measured permeability followed by the Timur equation in all well. The reason of for this investigation was to estimate in situ permeability using capillary pressure irreducible water saturation and log porosity with the models proposed by Timur, Morris Biggs for gas, and Schlumberger to determine which model best agree with the core permeability

7.4 PERMEABILITY FROM THE REPEAT FORMATION TEST (RFT)

In addition to the previous methods of determining permeability, permeability can also be determined from the repeat formation test measurement by analysing the pressure changes. The two flowing periods and the subsequent pressure build-up provide information for calculating permeability. The pressure draw down during fluid flow depends on the effective permeability of the formation to the flowing fluid which in practice is the mud filtrate from the invaded zone. Analysis of the pressure build up curve plots provides estimate of effective permeability some distance from the borehole which corresponds to the effective permeability of the uninvaded formation to the mobile phase of the formation fluid.

The Repeat formation test measurement gives an effective permeability while the results of core analysis permeability values are usually expressed in absolute permeability. The permeabilities derived from the RFT measurements are often smaller than core permeabilities (Pelliaier- Combescure et al., 1979).

The results of the RFT measurements are presented in appendix J for wells with mobility values. The effective permeability from RFT was derived from the relationship below.

Effective Permeability (mD) = Mobility (mD/cp) * Viscosity (cp).

7.4.1 Relative permeability

The relative permeability is regarded as the ratio of effective permeability to absolute permeability and it is usually determined from special core analysis measurements. However, this measurement was not performed in wells of the study area; therefore other methods were used to determine the relative permeability.

To relate absolute permeability to effective permeability, the use of the relative permeability concepts developed by Coates and Denoo (1981) was applied as follows:

$$K_{rw} = \left\{ \frac{(S_w - S_{wi})}{(1 - S_{wi})} \right\}^3 \dots\dots\dots (7.3)$$

$$K_{rh} = (1 - S_w)^{2.1} / (1 - S_{wi})^2 \dots\dots\dots (7.4)$$

Where:

K_{rw} = Water Relative permeability

S_w = Water saturation

S_{wi} = Irreducible water saturation

K_{rh} = Hydrocarbon relative permeability.

The results of the application of equations 7.3 and 7.4 above to wells OP2 and OP3 are presented in Figure 7.9 below.

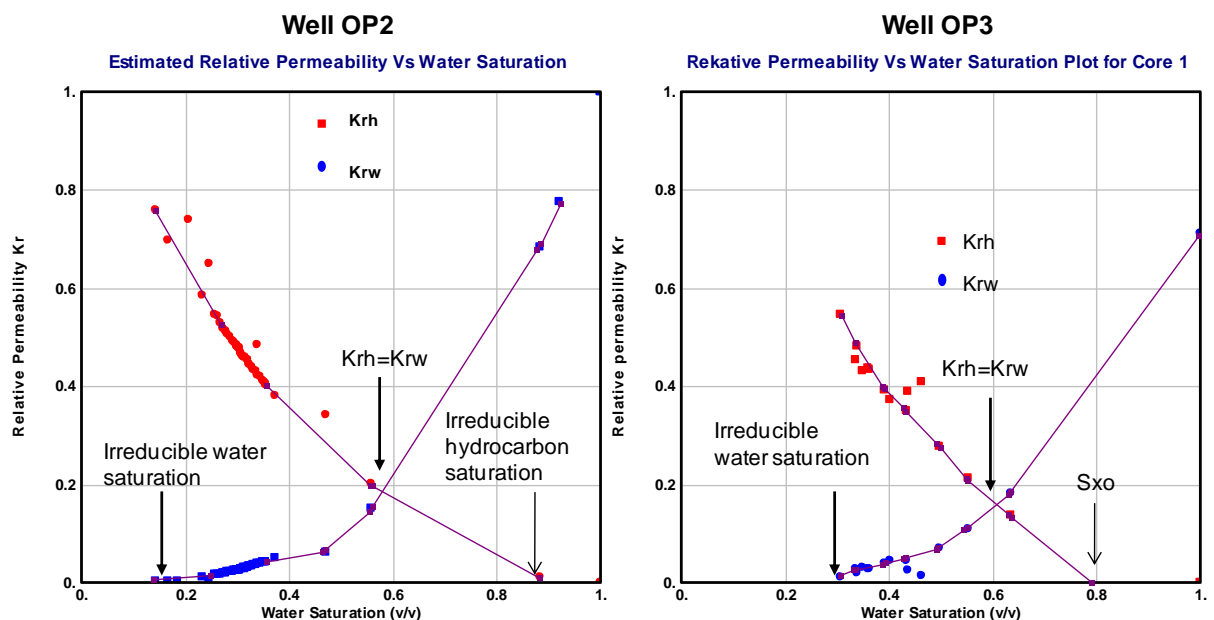


Figure 7.9: Relative permeability curves for well OP2 and OP3 within the reservoir intervals

According to Timmerman (1982), clays usually have poor relative permeability characteristics and higher or in-situ irreducible water saturation. Considering the relative permeability curves of Figure 7.9 above of well OP2 and OP3, it was observed that the irreducible water saturation of well OP2 is approximately 17 % and Well OP3 is approximately 30 %. From this result, it can be inferred that well OP2 has better rock quality as compared to well OP3 in terms of irreducible water saturation.

At the intersection of K_{rh} and K_{rw} curves, hydrocarbon and water flow at ease.

The comparison of permeabilities derived from core, log, RFT, and relative permeability equation for well OP2 is presented in Figure 7.10 below.

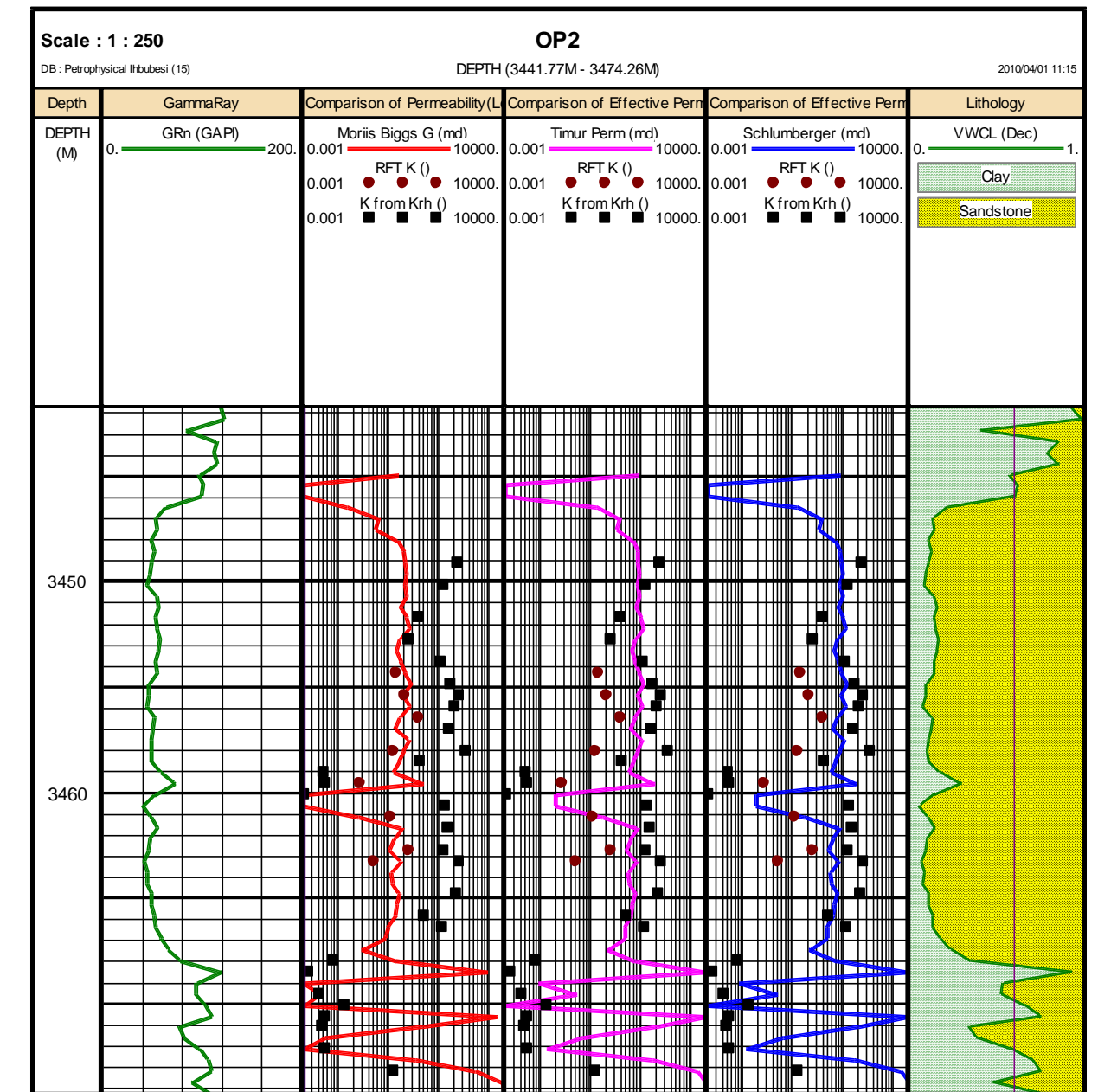


Figure 7.10: Comparison of permeabilities derived from log, RFT and Krh equations for well OP2

Tracks 3, 4 and 5 of Figure 7.10 above are the log estimated permeability curves overlain with RFT determined effective permeability (brown dots), and effective permeability estimated from the product of Krh with core permeability (K from K_{rh} , black dots).

The Morris Biggs log estimated permeability (track 3) best agree with the effective permeability derived from the RFT measurement.

In conclusion, it has been demonstrated that permeability derived from the repeat formation test (RFT) measurements are effective permeabilities and showed good agreement with log derived permeability using the Morris Biggs gas model. The predicted permeability from convention core porosity-permeability data best agree with the Klinkenberg corrected permeability as presented in track 4 of Figure 7.11 below.

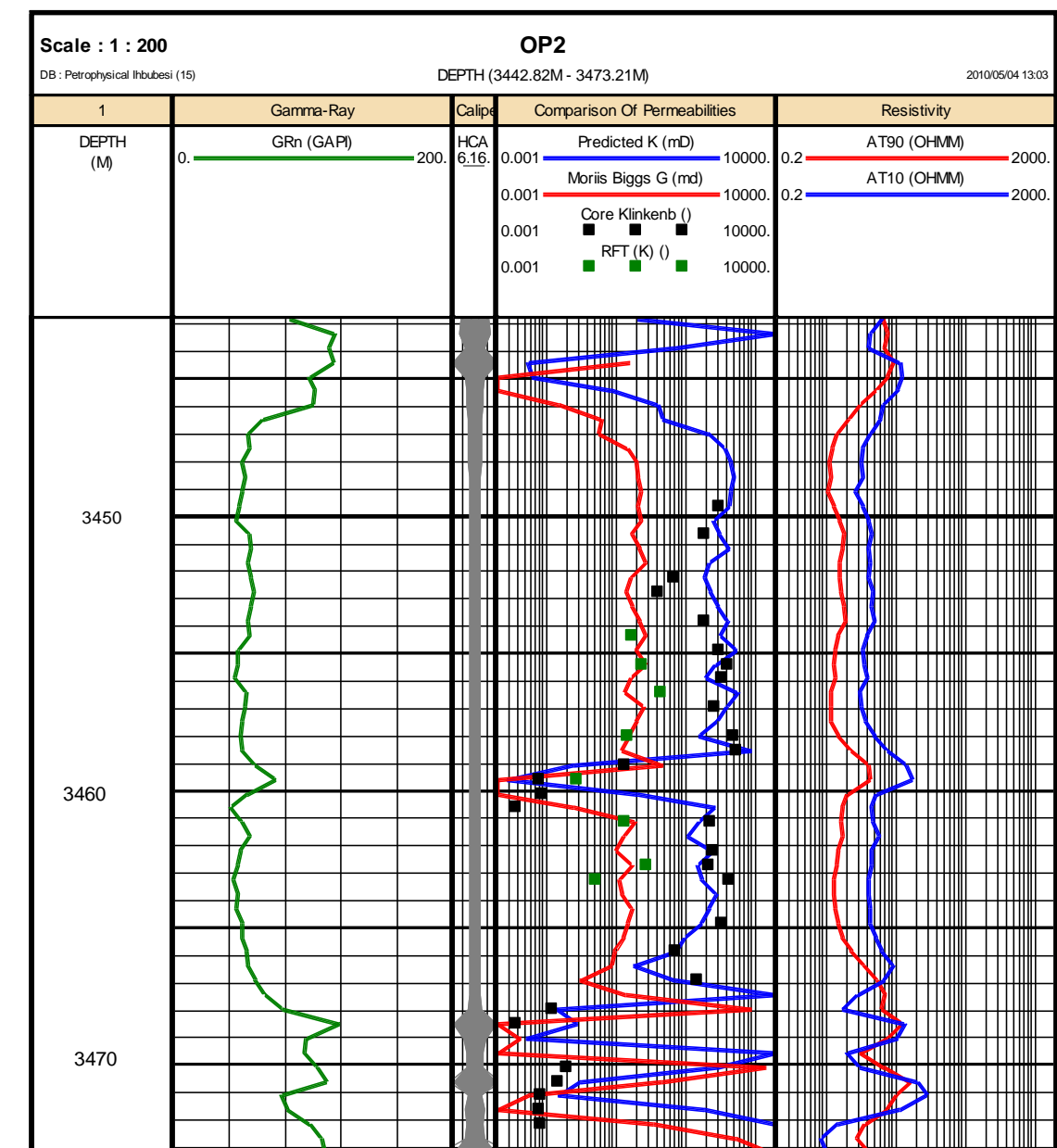


Figure 7.11: Comparison of permeabilities derived from core, log and cross plot

7.5 DETERMINATION OF ROCK TYPES (PETROFACIES)

The petrofacies concept is used for the study of rock units according to their petrologic characteristics as opposed to their form, boundaries or in relation to other rock units. The quality of reservoirs is controlled by depositional structures, textures and composition, diagenetic processes and pore types distribution. The term petrofacies is defined in the sedimentary literature by different meanings (De Ros & Goldberg, 2007). Petrofacies analysis in this part of the study is applied based on flow units that relates pore types, porosity and permeability as an assessment of reservoir continuity and quality.

Petrofacies are defined as intervals of rocks with a similar average in pore throat radius having similar fluid flow characteristics. The characterization of the rock type is based on the flow capacity and storage of the rock carried out from capillary results, porosity and permeability values (Boada et al., 2001).

Pore throat size may be estimated from routine core analysis porosity and permeability data at ambient conditions. Rock type characterization can be based on integration of routine core analysis data, capillary pressure data, thin section, scanning electron microscopy, and X-Ray diffraction analysis in core samples to determine dominant pore throat radius of the interconnected pore system. Two methods commonly used to assess reservoir quality on the basis of pore throat are the Winland method and Pittman's methods are used in this study.

Winland (1972) of Amoco tested 322 different water wet rocks using mercury injection capillary pressure curves to develop an empirical relationship between porosity, permeability and pore throat radius on reservoir rocks from Spindle field, Colorado. Winland's experiments showed that the effective pore system that dominates flow through a rock corresponds to a mercury saturation at 35 %. That pore system has pore throat radii equal to or smaller than the pore throats entered when a rock is saturated 35% with a non-wetting phase. After 35 % of the pore system fills with a non-wetting fluid, the remaining pore system does not contribute to flow; instead it contributes to storage (Winland, 1972).

The r_{35} pore throat radii is a function of entry size and pore throat sorting, and is a good measure of the largest connected pore throats in a rock with intergranular porosity (Hartmann & Coalson, 1990). The Winland equation was used and published by Kolodzie in 1980 and the equation is given as below:

$$\text{Log}(r_{35} \%) = 0.732 + 0.588 \log(K_{\text{air}}) - 0.864 \log(\Phi) \dots \dots \dots (7.5)$$

Where:

r_{35} = Pore aperture radius in microns corresponding to 35th percentile

K_{air} = Uncorrected air permeability in mD

Φ = Porosity (%)

Pittman (1992) based on Winland's work, developed $r_{45} \%$ equation for pore throats corresponding to mercury saturations of 45 % which allow calculation of pore throat sizes. Pittman's $r_{45} \%$ equation is given below:

$$\text{Log}(r_{45} \%) = 0.609 + 0.6089 \log(K_{\text{air}}) - 0.974 \log(\Phi) \dots \dots \dots (7.6)$$

Where:

r_{45} = Pore aperture radius in microns corresponding to 45th percentile

K_{air} = Uncorrected air permeability

Φ = Porosity (%)

Rock type classification will be based on permeability and porosity relationship from conventional core analysis and capillary pressure that will allow the identification of rock types and division into five petrophysical categories in the ranges in Table 7.2 below:

Table 7.2: Classification of rock types

Petrofacies	Pore Throat radius(Micron)	Rock Type
1	More than 10	Mega porous
2	2.0 -10.0	Macro porous
3	0.5-2.0	Mesoporous
4	0.1-0.5	Micro porous
5	Less than 0.1	Nanoporous

Rock types can be semi-quantitatively related to several reservoir response characteristics useful in formation evaluation.

7.5.1 Well OP1 Petrofacies determination

To determine the dominant pore throat radius that best reproduce capillary pressure data, permeability and porosity of the well, the Winland and Pittman's equations (7.5 and 7.6) are used and the results are shown in Table 7.3 below.

Table 7.3: Rock types classification based on winland and Pittman calculations

Depth (m)	Porosity (%)	Kair (mD)	Winland (r35) (Microns)	Pittman (r45) (Microns)	Rock Type (Petrofacies)
3370.05	18.9	108	6.6	4.10	2=Macro
3370.6	20.2	64	4.6	2.69	2=Macro
3371.07	16.9	40	4.1	2.45	2=Macro
3371.4	16.4	14	2.2	1.32	3=Meso
3371.9	16.5	26	3.3	1.95	2=Macro
3372.03	12.7	6.0	1.7	1.02	3=Meso
3372.53	9.5	0.32	0.4	0.23	4=Micro
3372.98	6.9	0.16	0.3	0.20	4=Micro
3373.75	5.0	0.018	0.03	0.07	5=Nanno
3375.6	3.0	0.017	0.2	0.12	4=Micro
3375.98	2.0	0.016	0.26	0.17	4=Micro
3376.62	7.7	0.03	0.1	0.06	5=Nanno
3376.86	8.6	0.151	0.26	0.16	4=Micro
3377.12	10.1	0.33	0.38	0.22	3=Meso
3377.36	9.6	0.151	0.25	0.14	4=Micro
3377.54	7.0	0.079	0.22	0.13	4=Micro
3377.78	7.9	0.104	0.24	0.14	4=Micro
3378.23	9.2	0.028	0.09	0.05	5=Nano
3378.48	8.6	0.025	0.09	0.05	5=Nano
3378.58	7.6	0.025	0.1	0.06	5=Nano
3379.24	6.8	0.018	0.09	0.05	5=Nano
3379.64	1.2	0.013	0.36	0.24	4=Micro
3379.82	4.9	0.01	1.4	0.05	3=Meso
3380.15	3.3	0.015	1.96	0.09	3=Meso

Table 7.3 above shows the calculated pore throat radii from Winland and Pittman equations of the reservoir rock porosity, permeability and pore throat radii ranges by rock type. Four possible petrophysical rock types were identified based on pore throat radii and results will be validated with thin section analysis and Scanning electron microscopy results. Petrofacies 2 represent the best reservoir rock type in this Well characterised by a porosity range between 16 % and 20 % and an average permeability of 59mD. The rock types in this depth interval (3370.40 to 3371.6m) represents rocks having similar flow capacity and higher storage capacity than other rocks. Petrofacies 5 is a non productive due to the inability of these rock types to

contribute to flow and not having storage capability. The porosity of these Petrofacies 5m ranges from 1.6 % to 9.2 % with an average permeability of approximately 0.1mD.

In order to determine whether the core plug data generally conform to Winland or Pittman, a correlation was made with the permeability and the Pittman's equation having a correlation coefficient of 90 % best fit with permeability values (Figure 7.12); therefore it was adopted for rock type classification.

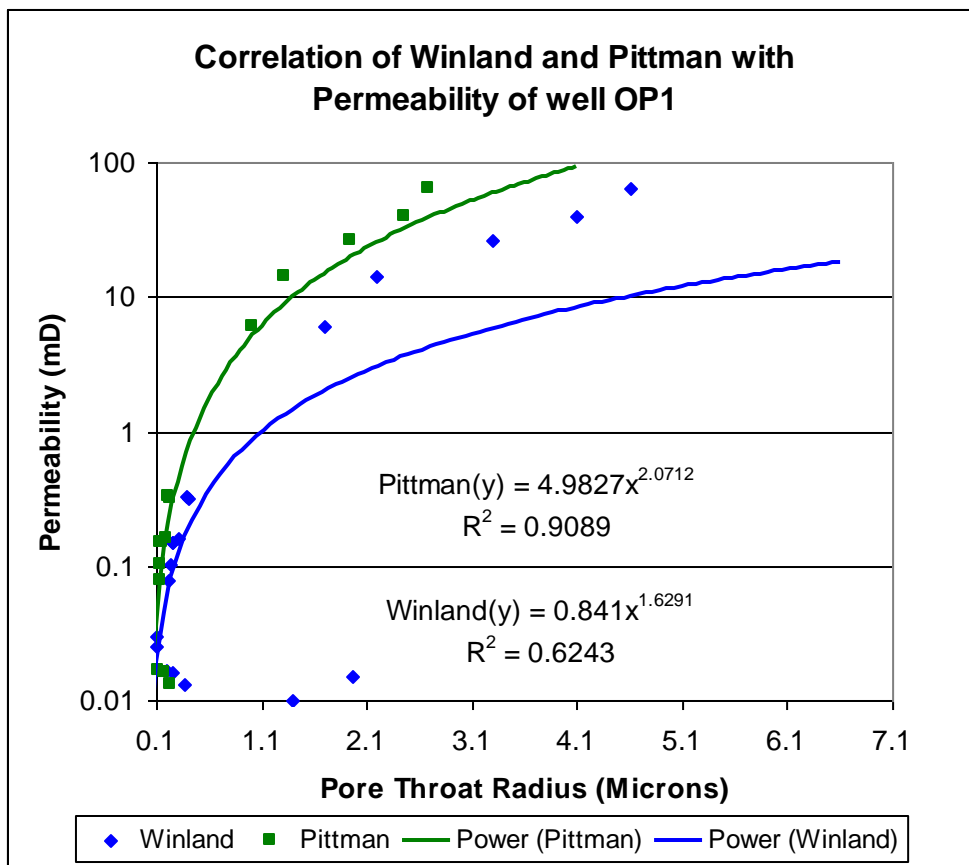


Figure 7.12: Correlation of Winland and Pittman's plots for well OP1

7.5.2 Well OP2 Petrofacies determination

The reservoir rocks in well OP2 were classified based on pore throat radius (r35) of Winland. The characterization was based on the flow capacity and storage carried out

from the routine core porosity and permeability values. Table 7.4 below presents the results from the analysis and rock type classifications.

Table 7.4: Rock types classification based on winland and Pittman calculations for well OP2

Depth (m)	Porosity (%)	Kair (mD)	Winland(r35) (Microns)	Pittman(r45) (Microns)	Petrofacies	Rock Type
3446.20	23.06	392	11.8	7.3	Mega	1
3447.08	24.24	227	8.3	4.9	Macro	2
3447.11	24.17	166	7.1	4.1	Macro	2
3447.83	18.65	14.2	2	1.2	Meso	3
3448.69	22.01	30.3	2.8	1.6	Macro	2
3449.52	20.27	13.3	1.8	1	Meso	3
3450.58	22.32	165	7.4	4.4	Macro	2
3451.70	23.54	366	12.6	6.8	Mega	1
3452.14	23.83	606	14.8	9.2	Mega	1
3452.59	24.01	435	12.6	7.4	Mega	1
3453.68	23.03	296	10	6.1	Mega	1
3454.72	24.25	909	19	11.5	Mega	1
3455.08	22.96	1095	20.1	13.6	Mega	1
3455.55	18.83	28.1	3.1	1.8	Macro	2
3455.86	10.42	2.07	1.1	0.6	Meso	3
3456.15	4.59	.019	0.1	0.1	Nano	5
3456.65	3.37	.021	0.2	0.1	Micro	4
3457.18	3.27	.006	0.1	0.1	Meso	3
3457.74	21.39	225	9.1	5.6	Macro	2
3458.69	21.36	270	10	6.2	Mega	1
3459.59	20.11	213	9.3	5.7	Macro	2
3460.00	21.93	399	12.6	7.7	Mega	1
3460.10	22.05	675	17.4	10.5	Mega	1
3461.48	23.07	473	13.5	8.1	Mega	1
3462.54	18.91	33.1	3.3	1.9	Macro	2
3463.48	19.55	110	6.2	3.9	Macro	2
3464.59	8.19	.100	0.23	0.1	Micro	4
3464.81	4.92	.037	0.2	0.1	Micro	4
3465.40	2.95	.005	0.1	0.1	Nano	5
3466.47	6.23	.015	0.1	0.1	Nano	5
3466.75	4.43	.092	0.4	0.2	Micro	4
3467.50	4.12	.054	0.3	0.2	Micro	4
3467.60	3.89	.018	0.16	0.1	Nano	5
3468.17	5.96	.020	0.1	0.1	Nano	5
3468.89	7.23	.028	0.12	0.1	Nano	5
3470.30	6.80	3.07	2	1.2	Meso	3

A plot of pore throat radius calculated from the Winland and Pittman equations versus the permeability for well OP2 is given in Figure 7.13 below. It was observed from the regression correlation coefficient that the Winland equation best correlate with the permeability values and hence was used to classify the reservoir rocks.

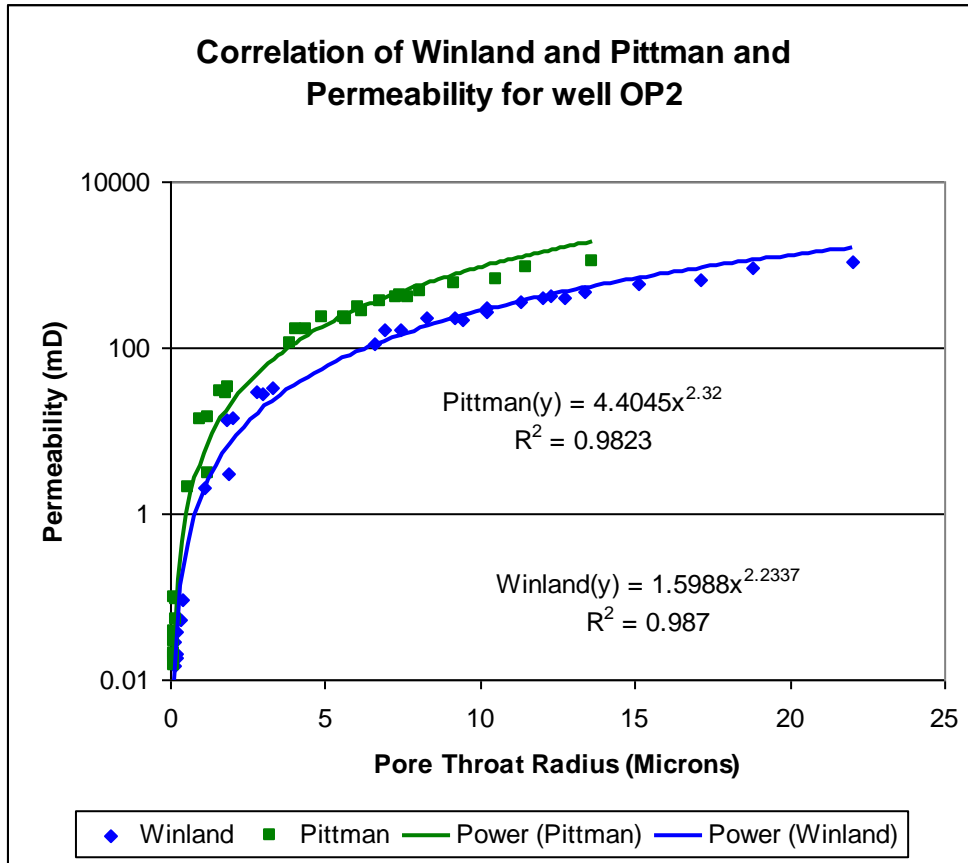


Figure 7.13: Correlation of Winland and Pittman’s plots for well OP2

Five Petrofacies (1, 2, 3, 4, and 5) were identified in this Well as shown in the Table above. The best petrofacies is the mega (Petrofacies 1) which has a pore throat radius of more than 10 microns and classified as petro-facies1. This particular rock type has excellent flow and storage capacity with average porosity value of 22.6 % and permeability of 538 mD. Petrofacies 2 will also contribute to flow and storage capacity because it is dominated with good porosity and permeability. While Petrofacies 5 (nanoporous) could be regarded as non productive rock type and will not contribute to flow due to the poor permeability values of less than 0.1mD exhibited in these rock types.

7.5.3 Well OP3 Petrofacies determination

The Winland and Pittman’s equations were adopted to identify the dominant reservoir rock type based on pore throat radius. Table 7.5 represents the calculated values.

Table 7.5: Reservoir rock classifications of well OP3

Depth (m)	Porosity (%)	Kair (mD)	Winland(r35) (Microns)	Pittman(r45) (Microns)	Rock Type (Petrofacies)	Rock Type
3236.1	24.2	135	6.0	3.6	Macro	2
3236.35	22.6	156	7.0	4.2	Macro	2
3236.51	21.3	86	5.3	3.1	Macro	2
3236.81	21.4	77	4.8	2.9	Macro	2
3237.05	18.1	34	3.6	2.1	Macro	2
3237.26	18.1	43	4.1	2.4	Macro	2
3237.51	15.0	21	3.1	1.9	Macro	2
3237.77	12.9	8.6	2.1	1.2	Meso	3
3237.95	9.1	0.63	0.6	0.4	Meso	3
3238.3	8.9	0.22	0.33	0.2	Micro	4
3238.5	6.3	0.074	0.24	0.1	Micro	4
3238.52	8.8	0.23	0.34	0.2	Micro	4
3239.05	4.3	0.06	0.29	0.2	Micro	4
3243.6	0.6	0.04	1.26	0.9	Meso	3
3283.2	19.2	4.9	1.05	0.6	Meso	3
3283.6	17.8	15	2.2	1.3	Meso	3
3283.85	17.8	30	3.3	1.9	Macro	2
3284.1	20.4	41	3.6	2.1	Macro	2
3284.35	21.3	40	3.3	1.9	Macro	2
3284.45	22	62	4.7	2.5	Macro	2
3285.05	22.2	50	3.6	2.1	Macro	2
3285.3	22.8	47	3.5	2	Macro	2
3285.34	20.6	15	1.9	1.1	Meso	3
3285.83	17.3	4.8	1.2	0.7	Meso	3
3286.08	14.3	45	5.2	3.1	Macro	2
3286.3	20.4	53	3.9	2.4	macro	2
3286.55	22.3	48	3.6	2.1	Macro	2
3286.6	22.2	79	4.7	2.8	macro	2
3287.25	23.3	2.7	0.66	0.3	Meso	3
3287.3	15.8	77	6.2	3.9	macro	2
3287.9	3.7	0.194	0.66	0.4	Meso	3
3290.06	2.3	0.013	0.21	0.1	Micro	4
3291.76	2.7	0.016	0.18	0.1	Nano	5

Four rock types (2, 3, 4 and 5) were identified based on pore throat radius of Winland and Pittman. Petrofacies 2 was identified as the best reservoir rock in this Well and has a flow and storage capacity having porosity range of 23 % to 24 % and permeability values from 57mD to 105mD. Petrofacies 3 (meso porous) is relatively fair to poor rock type which may contribute to flow. Petrofacies 4 and 5 were classified as non productive rock types because of the very low permeability values of less than 0.1mD exhibited.

The plot of the Winland and Pittman equations versus the core permeability is presented in Figure 7.14 below. The Winland correlates better with core permeability values and was used to classify the rock types.

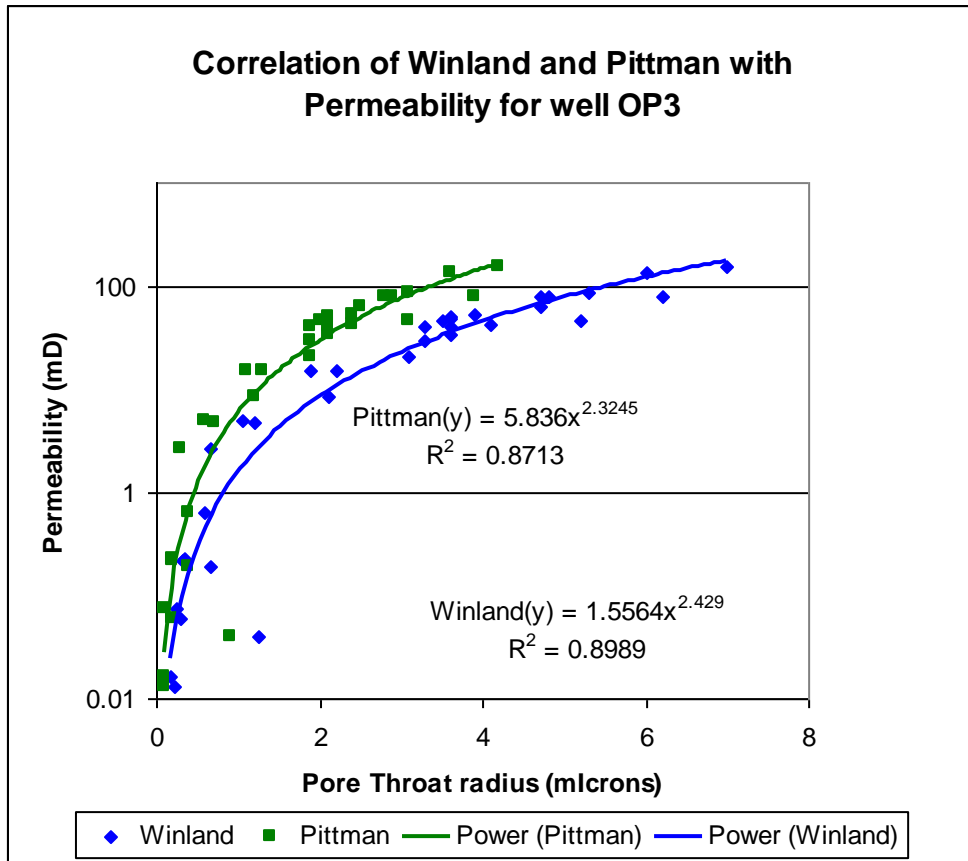


Figure 7.14: Correlation of Winland and Pittman’s plots for well OP3

7.6 COMPARISON OF PETROFACIES AND LITHOFACIES

In terms of pore throat, porosity and permeability, five petrofacies were distinguished. Four rock types (2, 3, 4 and 5) were present in well OP1; five rock types (1, 2, 3, 4 and 5) were present in well OP2; and well OP3 had four rock types (2, 3, 4, and 5) respectively. Six lithofacies were also classified in terms of texture, size, and sorting in the entire well. Lithofacies (A3, A4, A5 and A6) were identified in well OP1; and well OP2 lithofacies identified were (A1,A2, A3, A4, A5 and A6); and well OP3 lithofacies identified were (A3, A4, A5, and A6) respectively.

Presented in Figure 7.15a is the plot of Lithofacies and Petrofacies of well OP1.

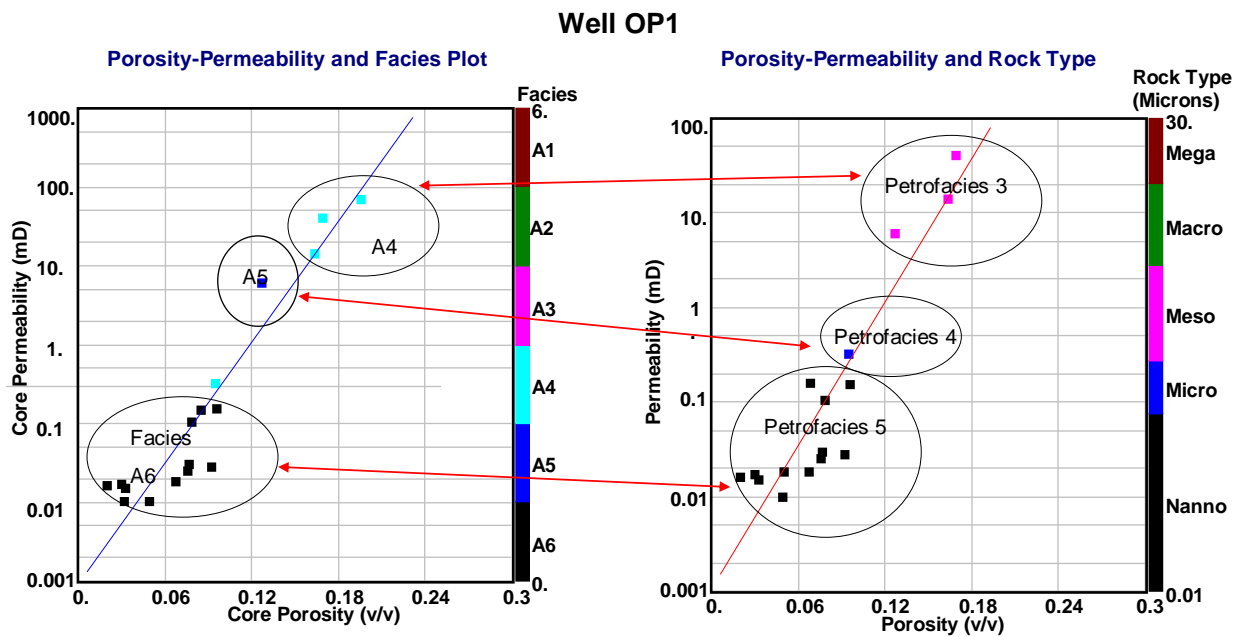


Figure 7.15a: Comparison of lithofacies and petrofacies for well OP1

Three lithofacies and Petrofacies were identified as presented in the Figure 7.12a above. The best reservoir rock quality was identified as petrofacies 3 (meso porous) rocks which correspond to Lithofacies A4. Petrofacies 5 (Nano porous) rock has equivalent lithofacies type A6 which is termed as non reservoir rock.

In well OP2 (Figure 7.13b below), five rock types (Petrofacies) were identified and six lithofacies .

Well OP2

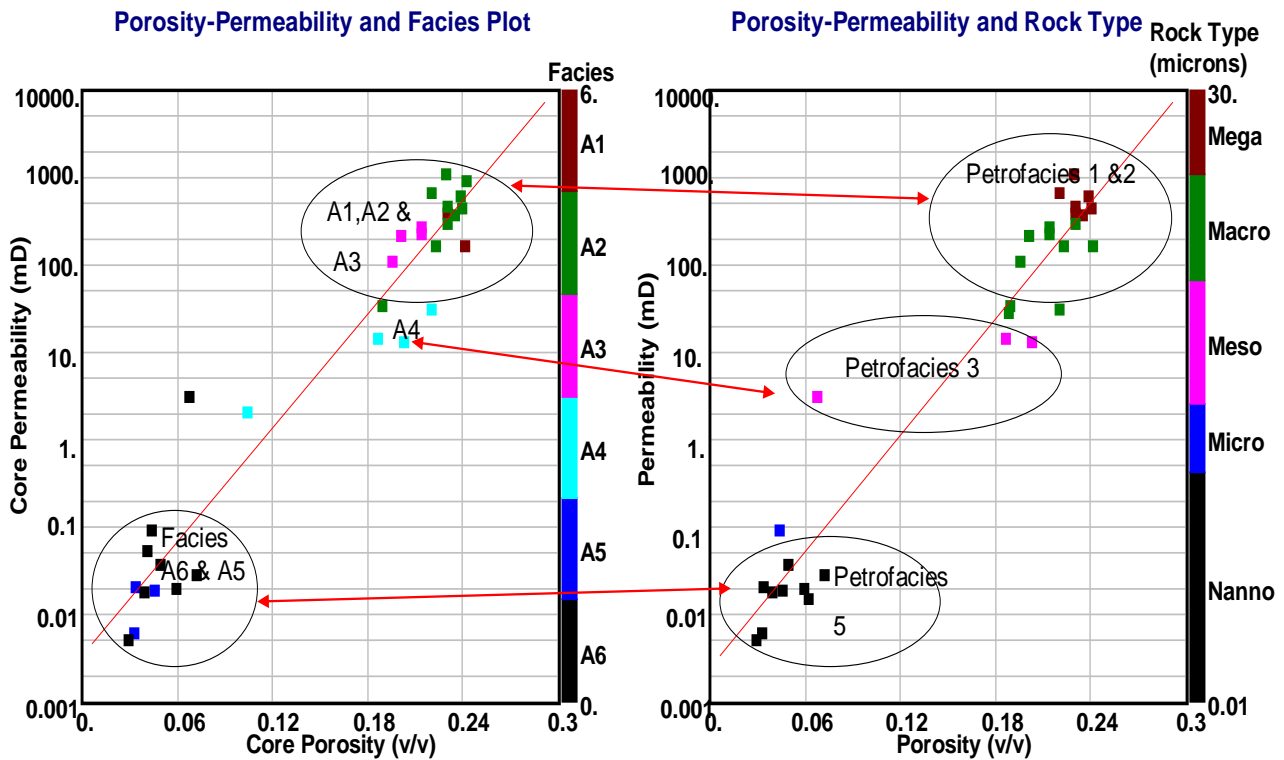


Figure 7.15b: Comparison of lithofacies and petrofacies for well OP2

The best reservoir rock quality were identified as petrofacies 1(mega porous) and 2 (macro porous) rock types which corresponds to lithofacies A1, A2 and A3 respectively. Petrofacies 3 (meso porous) rock type has its equivalent Lithofacies type A4 which is between the best and non reservoir rocks. Petrofacies 5 (Nano porous) rock types corresponds to facies A5 and A6. They possess very low permeability values of less than 0.1mD and porosity less than 8 percent and are classified as the non- reservoir rock types.

The comparison of core lithofacies and petrofacies for well OP3 is presented in Figure 7.15c below.

Well OP3

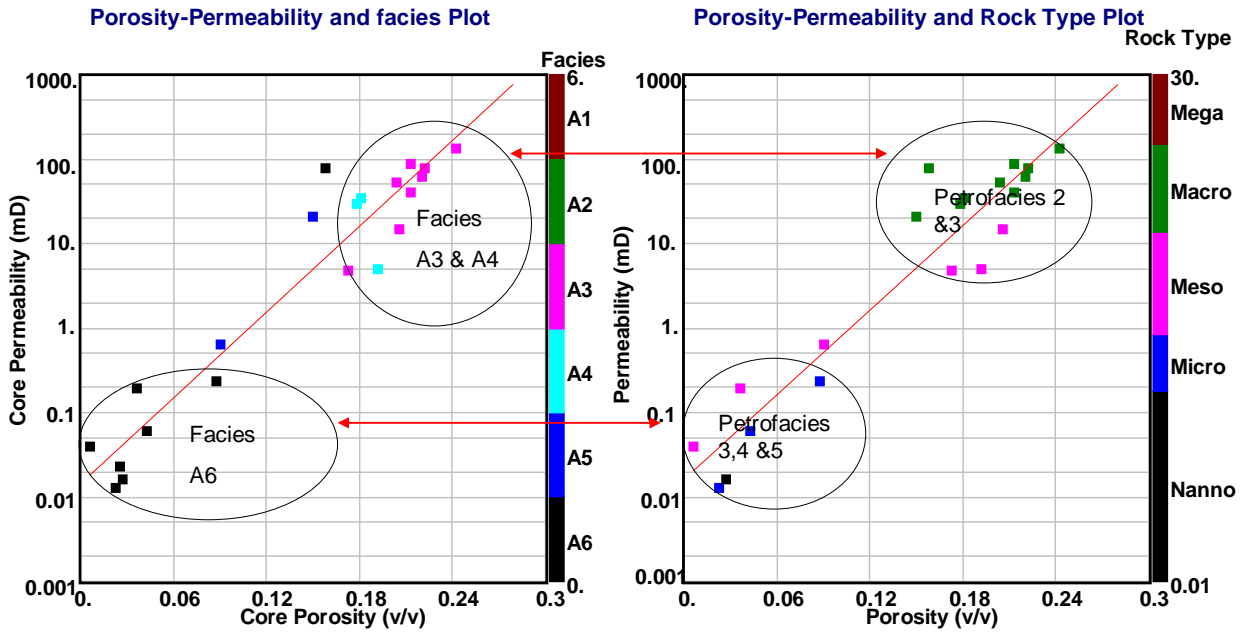


Figure 7.15c: Comparison of lithofacies and petrofacies for well OP3

In well OP3, four petrofacies (macro, meso, micro, and Nanno porous) rock types and four Lithofacies (A3, A4, A5 and A6) were identified as shown above. The best reservoir quality rock in terms of petrofacies is petrofacies 2 (macro porous) rock types which has an equivalent lithofacies as facies A3. This rock type is closely followed by petrofacies 3(meso porous) that corresponds to facies A4. The non reservoir rock (facies A6) has petrofacies 4 and 5 (micro and Nano porous) rock types as its equivalent rock.

Generally, lithofacies with the best characteristics (A1 and A2) correspond to the best quality rock (Petrofacies 1), and non reservoir rock (Petrofacies 5) corresponds to facies A6. It is important to note that lithofacies were classified based on grain size and texture of the cores, Petrofacies were determined based upon the analysis of the pore system of the rock.

The comparison between lithofacies and petrofacies indicates that within a given lithofacies, there may exist different Petrofacies which are indicative of rock quality. Figure 7.15 below presents the comparison of core lithofacies and petrofacies for all wells.

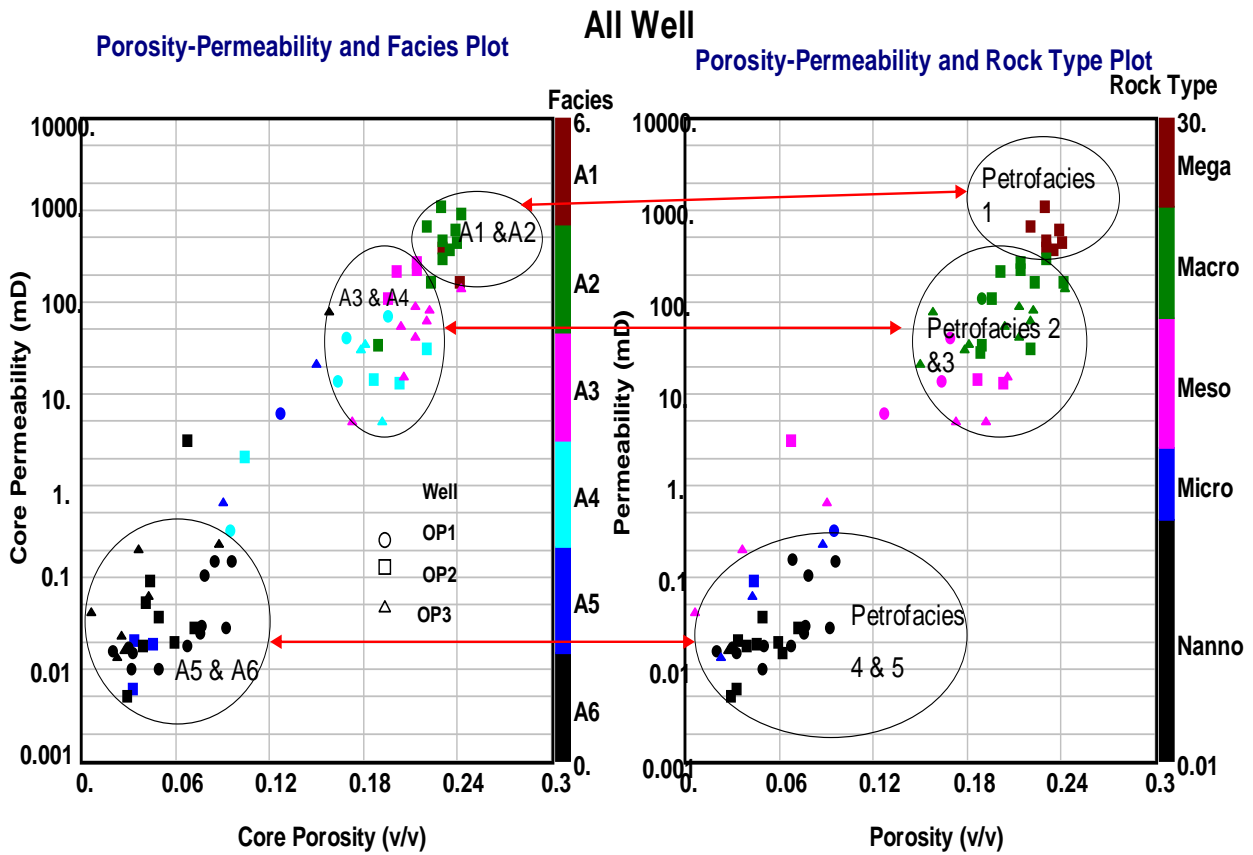


Figure 7.15d: Comparison of lithofacies and petrofacies for all the wells

7.7 K/PHI RELATION

The ratio of the permeability to porosity plot is a useful indicator of flow quality and storage capacity of rocks. It reflects quality of rock expressed in terms of flow efficiency.

When pore systems are dependent on grain size, the plot of porosity versus permeability provides a direct relationship. The plot of porosity versus permeability ratio helps to know the differences in rock types in relation to diagenesis and flow capacity of the rock. The porosity permeability ratios used in this study are as follows

$$K/PHI=0.01$$

$$K/PHI=0.05$$

$$K/PHI=0.5$$

$$K/PHI =5$$

$$K/PHI=50$$

The graphics below (Figure 7.15e) is the result of the application of the above porosity and permeability ratio and Winland pore throat radius for all the wells.

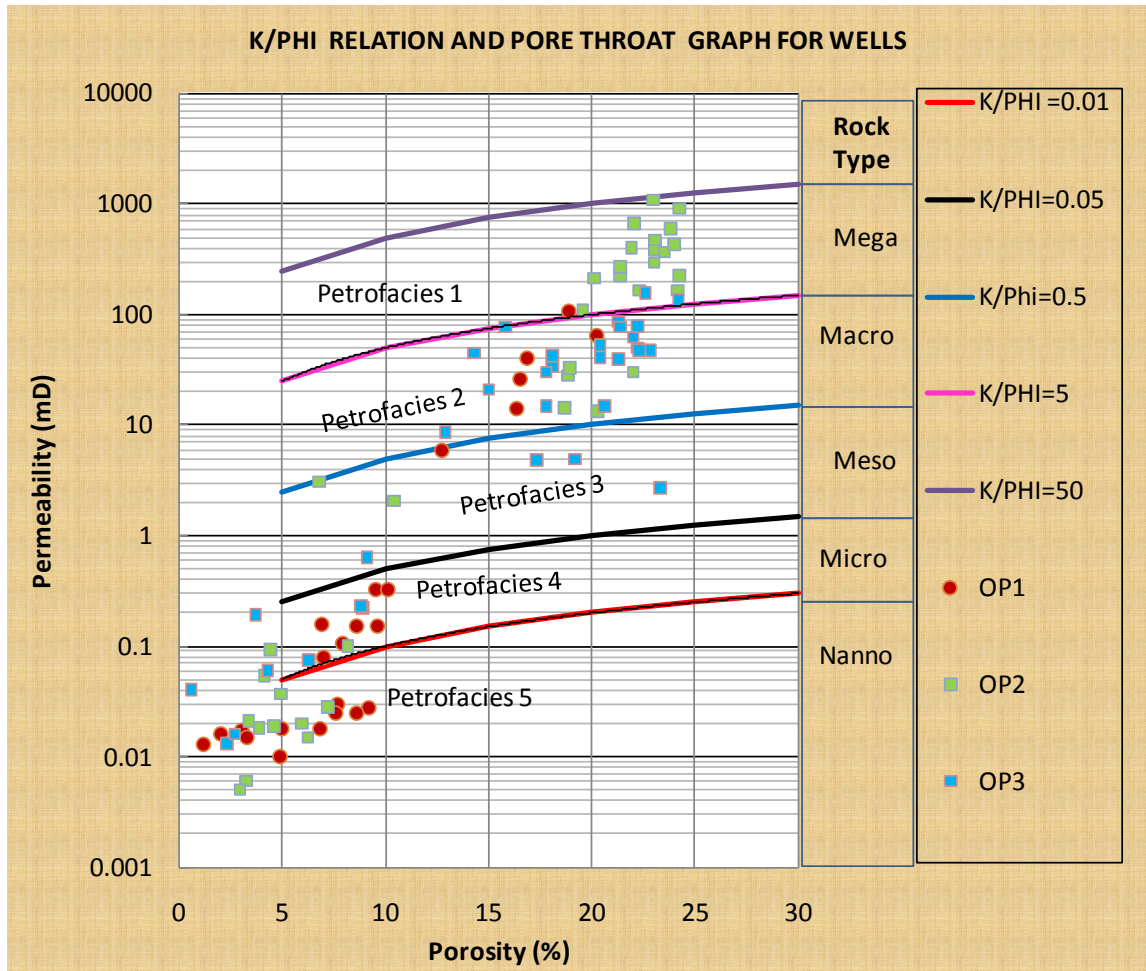


Figure 7.15e: Permeability/Porosity Ratio (K/PHI) for all the wells

Petrofacies 5 with porosity values less than 10 percent and permeability of less than 0.1mD clusters below the K/PHI =0.01 line and corresponds to nano rock type and demonstrate less flow efficiency, smaller pore throat, larger number of smaller pores and will have high surface area and irreducible water saturation. The low flow efficiency observed in this petrofacies is due to the effects of diagenesis on porosity and permeability.

Petrofacies 4 clusters between the 0.01 and 0.05 on the K/PHI line. Porosity and permeability values of less than or equal to 10 percent and 1 mD were indicated. In terms of flow efficiency, this micro porous rock type will have poor flow efficiency.

Petrofacies 3 clusters between the 0.05 and 0.5 K/PHI line and display good storage capacity and fair flow efficiency in gas field. This petrofacies is the meso rock type.

Petrofacies 2 indicates good flow efficiency and larger pore throats and smaller number of larger pores. These facies have lower irreducible water saturations and smaller surface areas. They cluster between the 0.5 and 5 on the K/PHI line.

Petrofacies 1 indicate high flow efficiency and cluster between 5 and 50 on the K/PHI line. The porosity of this facies is between 15 and 25 % which represents a high storage capacity. Flow depends more on permeability than porosity and petrofacies 1 showed permeability values in the range of 85 to 1000 mD. Larger pore throat and low irreducible water saturation play a dominant role in this petrofacies.

7.8 HYDRAULIC FLOW ZONE INDICATOR (FZI)

A Petrophysical flow unit is defined as an interval of sediment with similar petrophysical properties such as porosity, permeability, water saturation, pore throat radius, storage and flow capacity, that are different from the intervals immediately above and below the reservoir intervals (Porras and Campos, 2001). Petrophysical flow units are usually grouped and used in determination of reservoir flow units.

Bear (1972) defined Hydraulic flow units as the representative of elementary volume of the total reservoir rock within which geological and petrophysical properties that affect fluid flow are internally consistent and predictably different from properties of other rock volumes.

Amaefule et al. (1993) showed that it is not possible to get good reservoir description without introducing pore throat parameters and bridging the gap between microscopic attributes from routine core plugs and macroscopic log derived characterization and they introduced the concept of reservoir quality index (RQI) to define the pattern of flow units. The hydraulic flow unit concept (Amaefule et al., 1993) is adopted in this work to identify reservoir rock quality and heterogeneity. The method can be applied to carbonate reservoirs as well as to clastic rocks by subdividing the reservoir into distinct petrophysical types. Each distinct reservoir unit has a unique flow zone indicator (FZI), Reservoir quality index (RQI), and Normalized Porosity Index (NPI) values (Al-Dhafeeri & Nasr-El-Din, 2006).

The combination of porosity and permeability data in terms of flow zone indicator, reservoir quality index, and normalized porosity index is convenient to use with routine core analysis data. The concept of Amaefule et al. (2003) is based on the calculation of two terms, RQI and NPI as defined below:

$$RQI = 0.0314 * \sqrt{K/\Phi} \dots\dots\dots (7.7a)$$

$$NPI = \Phi / (1-\Phi) \dots\dots\dots (7.7b)$$

$$FZI = RQI / NPI \dots\dots\dots (7.7c)$$

Where:

K = Permeability (mD)

Φ = Porosity (Fraction)

RQI and FZI are in microns.

The RQI and NPI values are used to determine FZI which is a unique and useful value to quantify the flow character of a reservoir and also gives a relationship between petrophysical properties at micro scale (core plug) and macro scale (well logs). It is assumed that zones with high values of RQI and FZI should be a high potential for high permeability zone.

The changes in pore geometrical attributes define the existence of hydraulic units with similar fluid flow characteristics. Hydraulic units are related to geological facies distributions but do not necessarily coincide with facies boundaries (Amaefule et al., 1993).

Tables 7.6 to 7.8 below present results of the flow zone indicator calculated for the three wells.

Table 7.6: Well OP1 Calculated values for RQI, NPI and FZI

Depth(m)	Porosity	Kair (mD)	RQI	NPI	FZI
3370.05	0.189	108.00	0.75	0.23	3.22
3370.35	0.196	69.00	0.59	0.24	2.42
3370.6	0.202	64.00	0.56	0.25	2.21
3370.85	0.146	13.00	0.30	0.17	1.73
3371.07	0.169	40.00	0.48	0.20	2.38
3371.4	0.164	14.00	0.29	0.20	1.47
3371.65	0.167	19.00	0.34	0.20	1.68
3371.9	0.165	26.00	0.40	0.20	2.00
3372.03	0.127	6.00	0.22	0.15	1.49
3372.28	0.12	1.30	0.10	0.14	0.76
3372.53	0.095	0.32	0.06	0.10	0.54
3372.82	0.085	0.14	0.04	0.09	0.44
3378.98	0.069	0.16	0.05	0.07	0.64
3373.75	0.05	0.018	0.02	0.05	0.36
3373.88	0.032	0.010	0.02	0.03	0.57
3375.6	0.03	0.017	0.02	0.03	0.71
3375.98	0.02	0.016	0.03	0.02	1.38
3376.62	0.077	0.030	0.02	0.08	0.23
3376.86	0.086	0.151	0.04	0.09	0.43
3377.12	0.101	0.33	0.06	0.11	0.50
3377.36	0.096	0.151	0.04	0.11	0.38
3377.54	0.07	0.079	0.03	0.08	0.42
3377.78	0.079	0.104	0.03	0.09	0.40
3378.23	0.092	0.028	0.02	0.10	0.15
3378.48	0.086	0.025	0.02	0.09	0.17
3378.58	0.076	0.025	0.02	0.08	0.23
3379.24	0.068	0.018	0.02	0.07	0.22
3379.64	0.012	0.013	0.03	0.01	2.59
3379.82	0.049	0.01	0.01	0.05	0.24
3380.15	0.033	0.015	0.02	0.03	0.62

The FZI ranged from 0.15 to 3.22 as indicated in Table 7.6 above. The variation of the FZI appears to be both textural and mineralogically controlled as compared with the lithofacies. The worst hydraulic unit (FZI < 0.7) was observed at interval of 3376m to 3379m which is comprised of laminated claystones with siltstone, poorly sorted tend to exhibit low FZI values (Figure 7.16a) below.

Well OP1

Flow zone Indicator Vs Depth and Rock Type

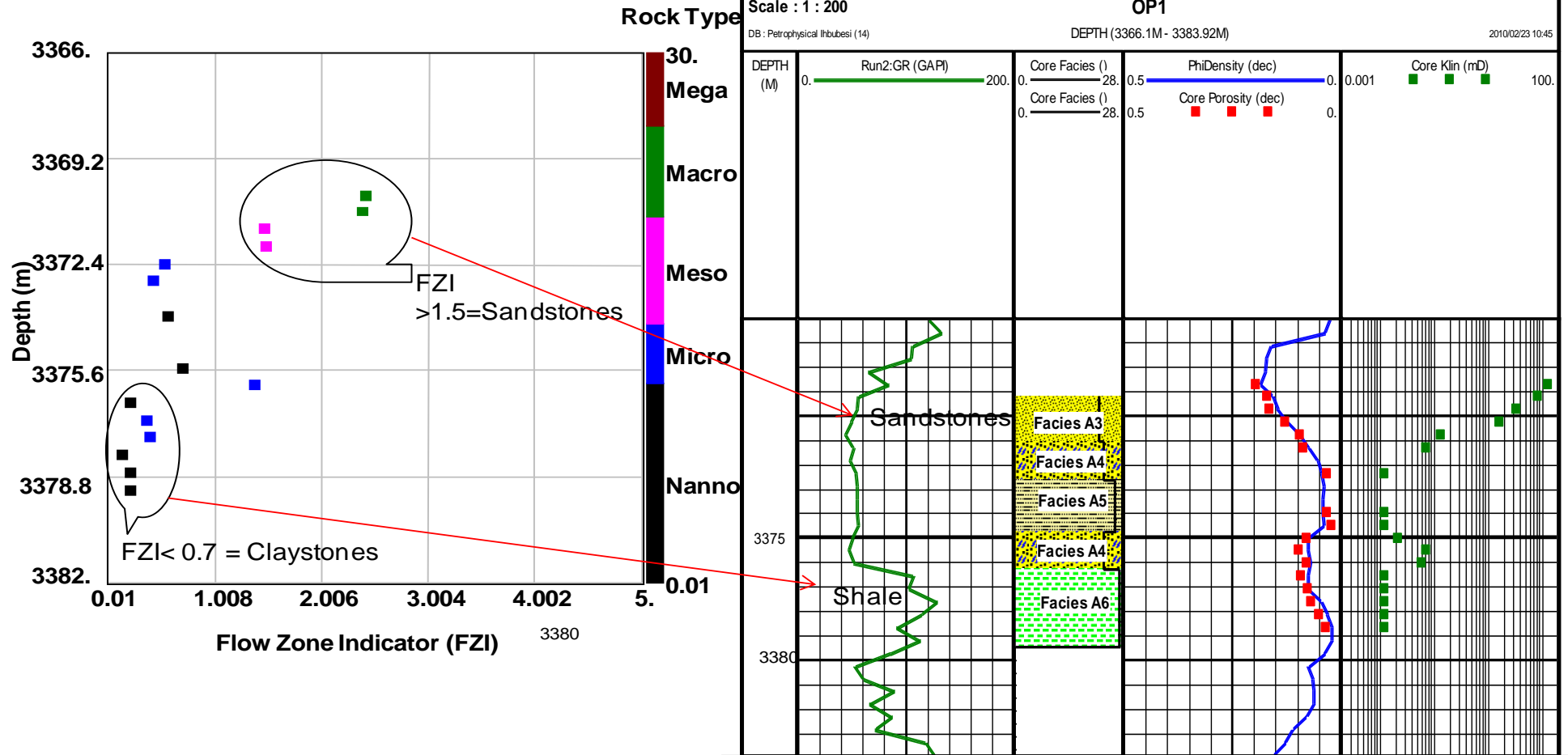


Figure 7.16a: Well OP1 flow zone indicator, rock types and facies plot

In contrast, the massive fine to very fine ,well sorted sandstones at interval of 3370m to 3372m with pore throat radius which are macro to meso porous exhibit high FZI (>1.5) values and hence will contribute to flow. A log-log plot of the normalized porosity versus reservoir quality index is shown in Figure 7.16b. The slope equals FZI.

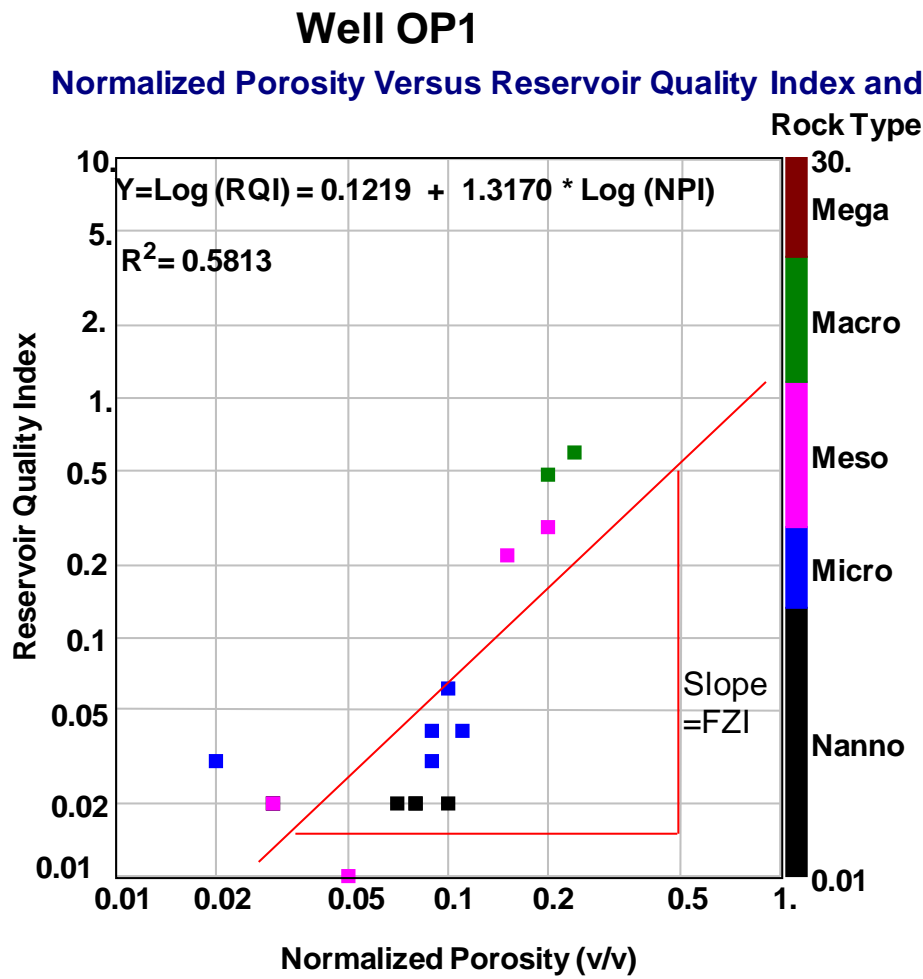


Figure 7.16b: Well OP1 NPI Vs RQI Plot

In well OP2, the FZI ranged from 0.23 to 7.27 as presented in Table 7.7 below.

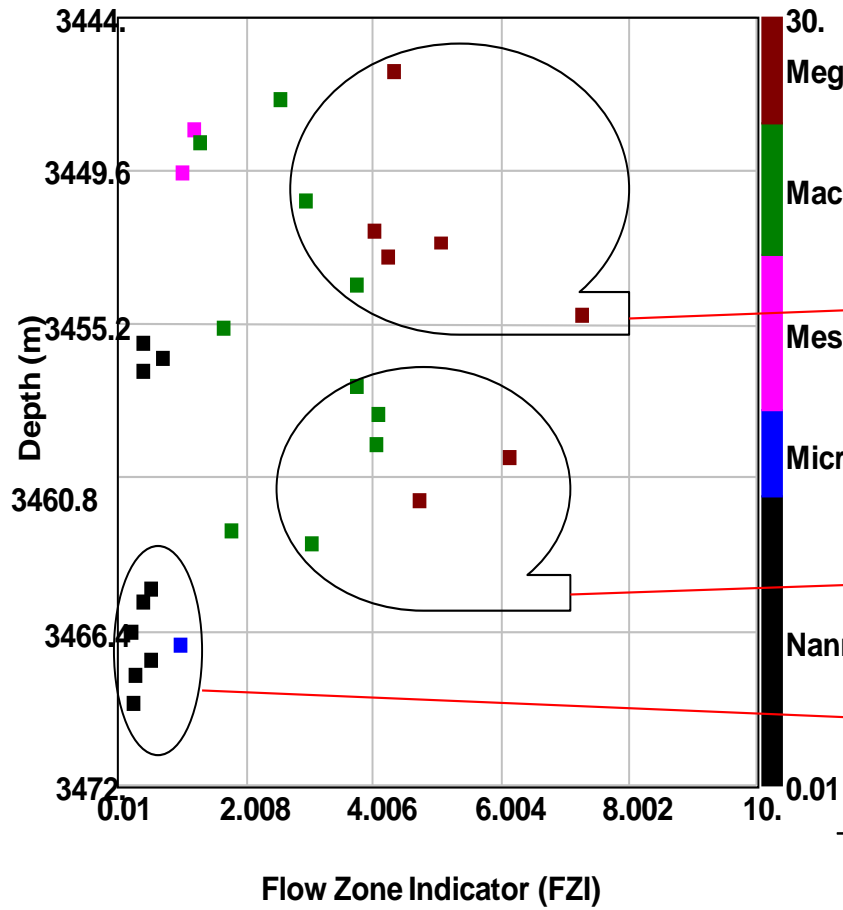
Table 7.7: Well OP2 Calculated values for RQI, NPI and FZI

Depth	Porosity	Kair(mD)	RQI	NPI	FZI
3446.20	23.06	392	1.29	0.30	4.32
3447.08	24.24	227	0.96	0.32	3.00
3447.11	24.17	166	0.82	0.32	2.58
3447.83	18.65	14.2	0.27	0.23	1.19
3448.69	22.01	30.3	0.37	0.28	1.30
3449.52	20.27	13.3	0.25	0.25	1.00
3450.58	22.32	165	0.85	0.29	2.97
3451.70	23.54	366	1.24	0.31	4.02
3452.14	23.83	606	1.58	0.31	5.06
3452.59	24.01	435	1.34	0.32	4.23
3453.68	23.03	296	1.13	0.30	3.76
3454.72	24.25	909	1.92	0.32	6.00
3455.08	22.96	1095	2.17	0.30	7.27
3455.55	18.83	28.1	0.38	0.23	1.65
3455.86	10.42	2.07	0.14	0.12	1.20
3456.15	4.59	.019	0.02	0.05	0.42
3456.65	3.37	.021	0.02	0.03	0.71
3457.18	3.27	.006	0.01	0.03	0.40
3457.74	21.39	225	1.02	0.27	3.75
3458.69	21.36	270	1.11	0.27	4.10
3459.59	20.11	213	1.02	0.25	4.06
3460.00	21.93	399	1.34	0.28	4.76
3460.10	22.05	675	1.74	0.28	6.14
3461.48	23.07	473	1.42	0.30	4.74
3462.54	18.91	33.1	0.42	0.23	1.78
3463.48	19.55	110	0.75	0.24	3.07
3464.59	8.19	.100	0.03	0.09	0.39
3464.81	4.92	.037	0.027	0.05	0.52
3465.40	2.95	.005	0.01	0.03	0.41
3466.47	6.23	.015	0.02	0.07	0.23
3466.75	4.43	.092	0.05	0.05	0.98
3467.50	4.12	.054	0.04	0.04	0.83
3467.60	3.89	.018	0.02	0.04	0.52
3468.17	5.96	.020	0.02	0.06	0.29
3468.89	7.23	.028	0.02	0.08	0.25
3470.30	6.80	3.07	0.21	0.07	2.88

The plot of flow zone indicator with rock types and lithofacies are presented in Figure 7.17a below.

Well OP2

Flow Zone Indicator Vs Depth and Rock Type Plot



Rock Type

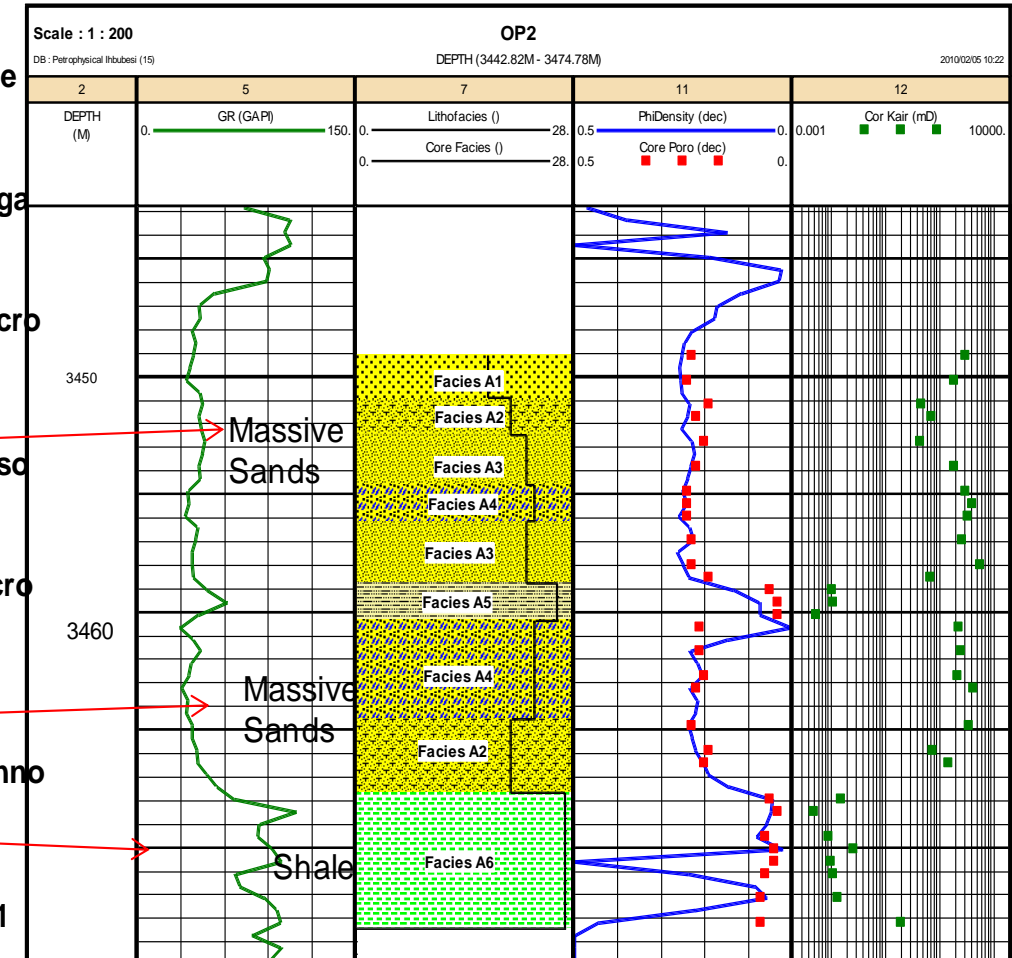


Figure 7.17a: Well OP2 flow zone indicator, rock types and facies plot

The comparison of flow zone indicators with rock types and lithofacies as presented in Figure 7.17a above showed that the mega porous rock types possess the highest hydraulic flow unit with values of more than 4 and corresponds to the massive sandstone intervals (facies A1 and A2). Closely following this interval is hydraulic flow unit of 1.8 to 4 which represents macro porous rock type and corresponds to Lithofacies A3 and A4. The high values of FZI recorded in this interval may due to the medium to fine sands, well sorted grains dominances of this interval.

The intervals of flow zone indicators of less than 1 were represented with nanno porous rock type and correspond to facies A6 (non reservoir rock). The low values of flow zone indicator in this interval can be attributed to the presence of fine grain, poorly sorted sandstones with intercalation of siltstones and laminated shale with minor burrow.

Presented in Figure 7.17b below is the plot of normalized porosity against the reservoir quality index for Well OP2.

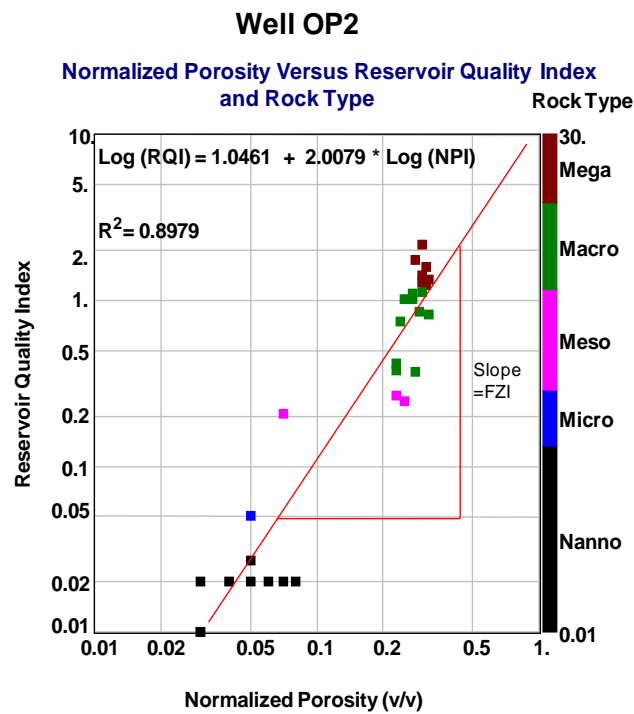


Figure 7.17b: Plot of NPI versus RQI for well OP2

Two distinct zones were clearly shown in the RQI versus NPI plot. The zone with lowest hydraulic flow indicators were dominated with rock types of nanno porous (Petrofacies 5) which reflected a zone of low RQI (less than 0.05) and NPI (less than 0.1) values. Another zone of high hydraulic flow was observed with values of RQI of

0.2 to 2.0) and corresponding NPI values in the range of 0.2 to 0.4. This high flow zone indicator was represented with meso, macro and mega porous rock types. Table 7.8 below present the values of reservoir quality index, normalized porosity and flow zone indicator for well OP3.

Table 7.8: Well OP3 Calculated values for RQI, NPI and FZI

Depth (m)	Kair (mD)	Porosity (v/v)	RQI	NPI	FZI
3236.1	135	0.242	0.74	0.32	2.32
3236.35	156	0.226	0.82	0.29	2.83
3236.51	86	0.213	0.63	0.27	2.33
3236.81	77	0.214	0.60	0.27	2.19
3237.05	34	0.181	0.43	0.22	1.95
3237.26	43	0.181	0.48	0.22	2.19
3237.51	21	0.15	0.37	0.18	2.10
3237.77	8.6	0.129	0.26	0.15	1.73
3237.95	0.63	0.091	0.08	0.10	0.82
3238.3	0.22	0.089	0.05	0.01	0.50
3238.5	0.074	0.063	0.03	0.07	0.51
3238.52	0.23	0.088	0.05	0.10	0.52
3239.05	0.06	0.043	0.04	0.04	0.82
3243.6	0.04	0.006	0.08	0.01	0.01
3283.2	4.9	0.192	0.07	0.24	0.31
3283.6	15	0.178	0.29	0.22	1.33
3283.85	30	0.178	0.41	0.22	1.88
3284.1	41	0.204	0.45	0.26	1.74
3284.35	40	0.213	0.43	0.27	1.59
3284.45	62	0.22	0.53	0.28	1.87
3285.05	50	0.222	0.47	0.29	1.65
3285.3	47	0.228	0.45	0.30	1.53
3285.34	15	0.206	0.27	0.26	1.03
3285.83	4.8	0.173	0.17	0.21	0.80
3286.08	45	0.143	0.56	0.17	3.33
3286.3	53	0.204	0.51	0.26	1.98
3286.55	48	0.223	0.46	0.29	1.60
3286.6	79	0.222	0.59	0.29	2.08
3287.25	2.7	0.233	0.11	0.30	0.35
3287.3	77	0.158	0.69	0.19	3.70
3287.9	0.194	0.037	0.07	0.04	1.88
3290.06	0.013	0.023	0.02	0.02	1.00
3291.76	0.016	0.027	0.02	0.03	0.87
3292.79	0.023	0.026	0.03	0.03	1.11

The RQI ranged from 0.02 to 0.82, NPI ranged from 0.01 to 0.32, and FZI from 0.01 to 3.7. The plot of flow zone indicator, rock type and facies are presented in Figure 7.18a below.

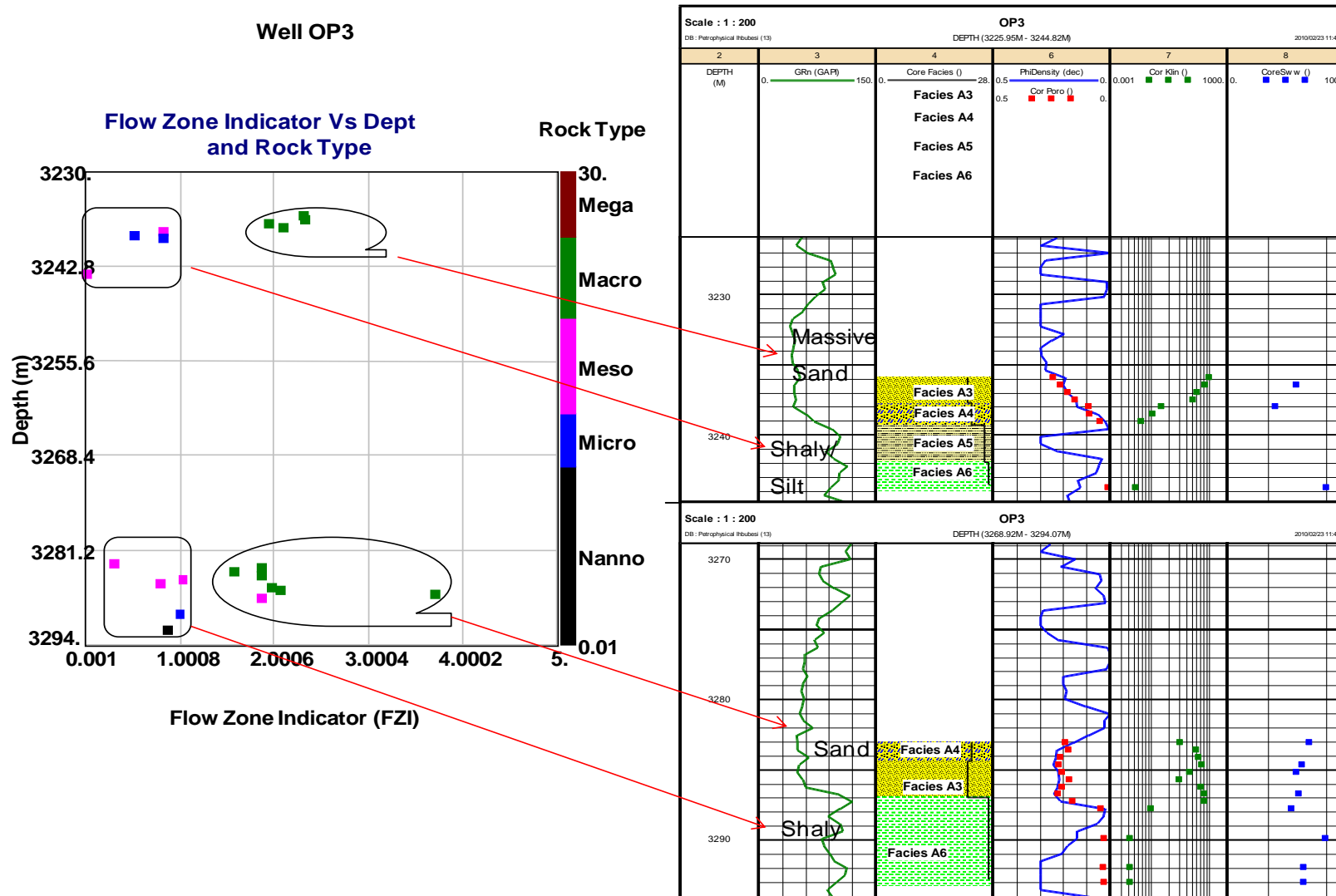


Figure 7.18a: Well OP3 flow zone indicator, rock types and facies plot

The FZI values in the range of 1.6 to 3.7 represent the massive sandstone intervals and correspond to rock types of predominantly macro porous and facies A3 and A4 respectively and have potential for productivity. Intervals of with FZI values of less than 1 represent the shaly/silt and shale intervals and correspond to meso, micro and nano porous rock types. The equivalent facies is facies A5 and A6. This interval of low flow zone indicators were regarded as the un-productive intervals based on flow zone indicators. The low values of FZI recorded may be attributed to the pore lining, pore filling and pore bridging clays as well as fine grained that are poorly sorted as confirmed in the petrography study results.

The log-log cross plot of normalized porosity versus the reservoir quality index is presented in Figure 7.18b below.

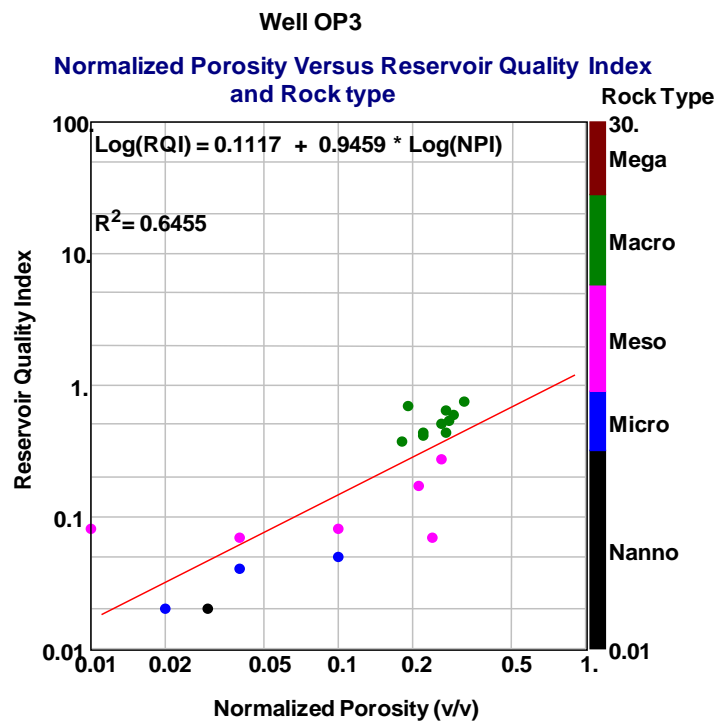


Figure 7.18b: Plot of NPI Versus RQI for well OP3

A regression analysis correlation coefficient of 0.6 was obtained from the cross plot which portray a good agreement between the plotted data. The slope of the plot gives the flow zone indicator.

The plot of normalized porosity and reservoir quality index for all the well is presented in the Figure below.

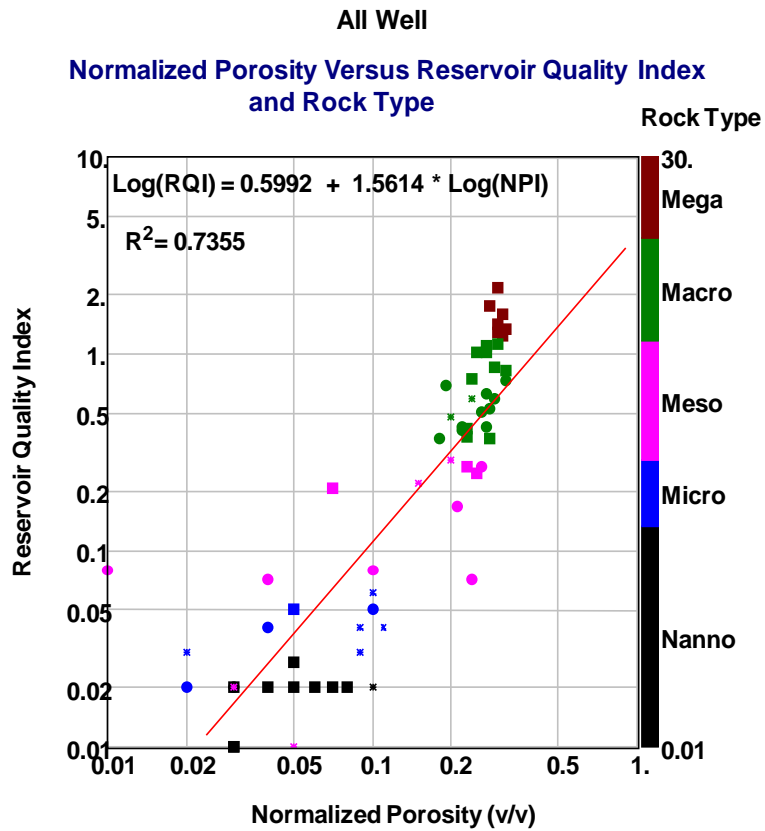


Figure 7.18c: Plot of NPI Versus RQI for Well OP3

The mega porous rocks showed high values of RQI (1 to 2) and NPI (25 % to 32 %) which represent the best reservoir rock quality of the wells studied. The poor reservoir rock quality was observed in the nanno and micro porous rock types which showed values of RQI and NPI of less than 0.1 respectively. A good regression analysis coefficient of correlation of 73 % was realized from the cross plot.

CHAPTER EIGHT

DETERMINATION OF FLUID CONTACT

8.1 INTRODUCTION

The identification of fluid in rocks and possible contacts provides useful information on the petrophysical interpretation. Oil and gas are both fluid and pressure is one of the important elements in characterising the physical behaviours of fluids in the subsurface. The water contact is used to describe the elevation above which fluids (oil/gas) can be found in the pores of the rock. The fluid contacts can be determined by petrophysical interpretation of wire logs and production test results. Oil fingerprinting of residual hydrocarbons from sidewall core extracts can also provide an independent means of identification of reservoir fluid types.

As hydrocarbon and water accumulates in a reservoir, separation occurs as a result of the difference in the specific gravity of various fluids. The less dense fluid like gas rise to the top of the reservoir, and below the gas is a gas to oil transition zone. Below the transition zone in most reservoirs is an oil-water transition zone of varying thickness which is partly filled with oil and water. Beneath the oil-water transition zone is the part of the formation that is completely saturated with water (Link, 1982).

An assessment of the pore fluid types and contacts has been undertaken based on wireline pressure data, log data and saturation estimates from logs as presented in the subsections below.

8.2 WIRELINE PRESSURE DATA ANALYSIS AND INTERPRETATION

Pressure is defined as the measure of force per unit area. Pressure in the subsurface is a function of the densities of the rock and fluids. The normal hydrostatic pressure increases with depth and the rate of pressure change depends only on water density. The pressure-depth relationship is independent of the shape of the fluid container (Dahlberg, 1994). Fluid density is the controlling factor in the normal hydrostatic pressure gradient.

The Table 8.1 below shows typical density ranges and gradients for gas, oil and water that vary with pressure, temperature and composition.

Table 8.1: Ranges of density and pressure gradients for hydrocarbon.

Fluid	Normal density range (g/cm³)	Gradient range (psi/ft)
Gas (gaseous)	0.007-0.30	0.003-1.130
Gas (liquid)	0.200-0.40	0.090-0.174
Oil	0.400-1.12	0.174-0.486
Water	1.000-1.15	0.433-0.500

(Modified after, Gearhart-Owens Industry, 1972)

The wireline pressure data were acquired in some of the wells in the study area in order to establish fluid pressure gradients in several reservoir sands in the study area. The results of the repeat formation tests for wells are given in appendix K. the pressure test may be unsuccessful due to packer seal failure, flow line or probe blockages, poor isolation of the mud column or tight formation. In very low permeability environments, formation layers may become “supercharges” by mud filtrate invasion and pressure points will plot on the high side of the normal pressure gradient line. The supercharged points are neglected in the pressure depth plot because they are not reliable.

The interpretation is performed by constructing pressure versus depth plot to establish pressure distribution and fluid gradients. The intersection of hydrocarbon and water gradients is used to identify the free water level and also define the contact. The fluid densities were deduced from the pressure gradient using the following relationship (Bateman, 1985):

$$\text{Fluid density (g/cc)} = \text{Pressure gradient (psi/ft)} * 2.3072 \dots \dots \dots (8.1)$$

However, equation 8.1 above was modified to express the pore pressure gradients in psi/m using the following equivalent relationship:

$$1 \text{ psi/m} = 0.7034 \text{ g/cc}$$

The RFT was run in eight wells by Schlumberger Company. Gas and water gradients were identified in many of the wells with some variations.

8.2.1 Well OP1

The RFT tool was run in well OP1 to establish formation pressures and fluid gradients in reservoir sands and to obtain a qualitative indication of permeability. However, within the Albian age of the formation, a total of twelve RFT formation pressure tests were measured on well OP1 as presented in appendix K. An interpretation of the result is presented in Figure 8.1 below.

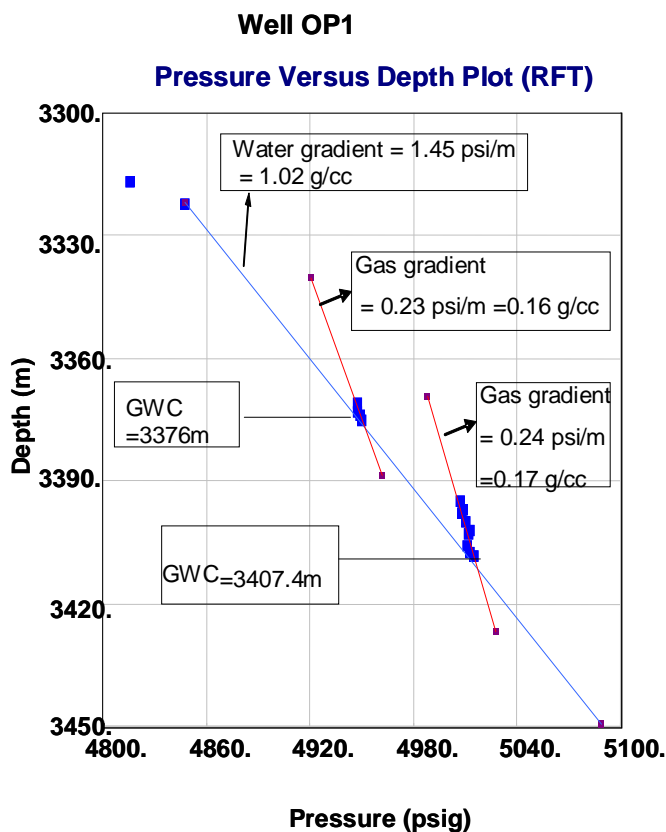


Figure 8.1: Well OP1 pressure versus depth plot for identification of Gas/Water contact (GWC) and fluid densities.

The Figure above present two separate reservoirs of well OP1 using the pressure-depth plot from the repeat formation test measurements (RFT). A communication in aquifer between the two reservoir intervals is represented in the water gradient line (blue) with water density of 1.02 g/cc.

Two gas gradients of 0.16g/cc and 0.17g/cc were calculated from the slope of the plot in the two sandstone intervals. Two Possible gas water contacts (GWC) were

identified at measured depth of 3376m and 3407.4m respectively. This result will be confirmed with the log data.

8.2.2 Well OP2

A total of seventeen RFT pressure test measurements were performed within the measured depth interval of 3300m to 3460m as presented in appendix K. The interpretation is presented in Figure 8.2 below.

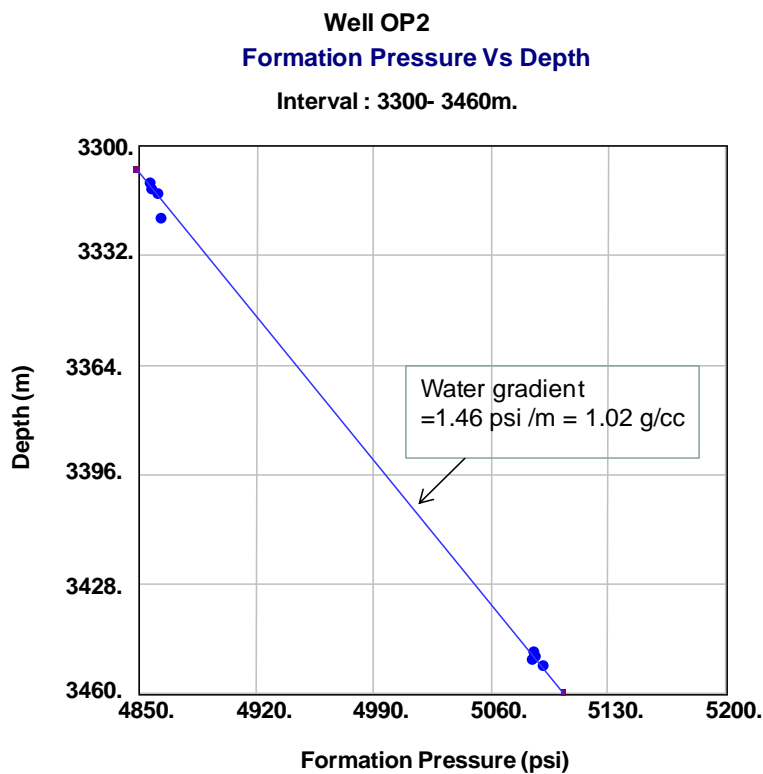


Figure 8.2: Well OP2 pressure versus depth plot

The pressure point that fall on the left of the water gradient line between the interval of 3300m to 3332m may be due to slow pressure build up or to the RFT temperature stabilization. A water gradient of 1.46 psi/m which is equal to water density of 1.02 g/cc represents a water productive reservoir interval. No gas/water contact was identified in this well.

8.2.3 Well OP3

In well OP3, a total of twenty three (23) RFT pressure test measurements were performed. The mud pressure data was corrected to the formation pressure, and a mud weight of approximately 2lb/gal was recorded. The interpreted result is presented in Figure 8.3 below.

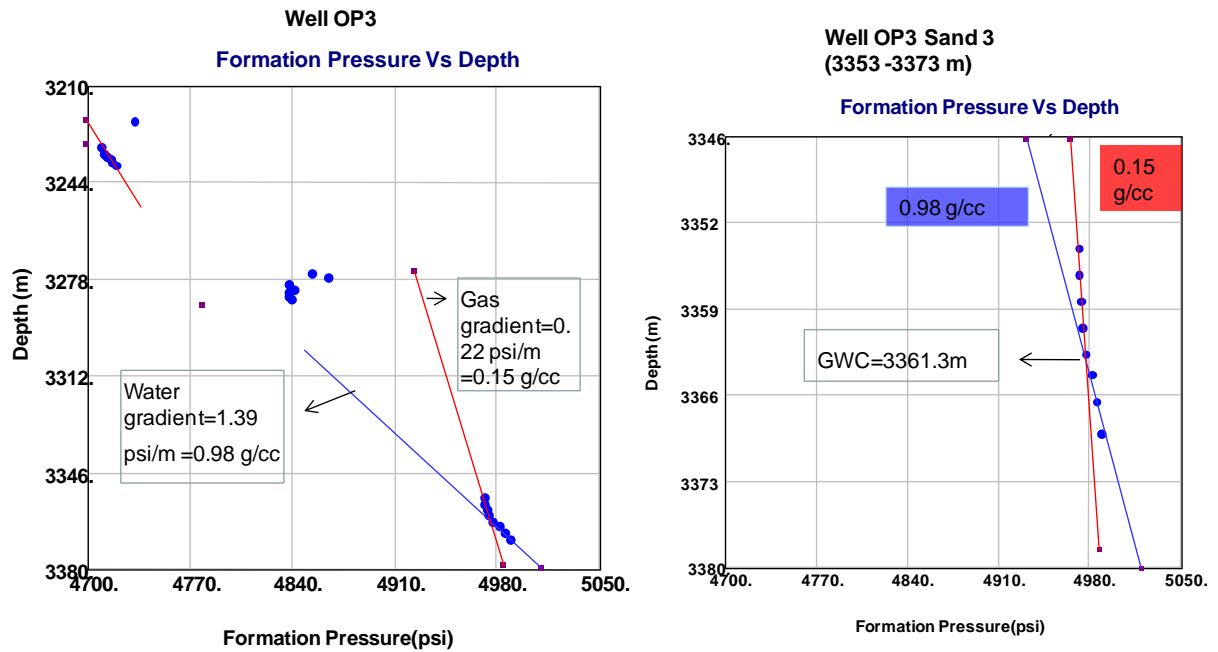


Figure 8.3: Well OP3 pressure versus depth plot showing possible gwc at measured depth 3361.3m

Two separate gas columns at measured between the interval of 3210 -3244m and 3278 -3312m were observed as shown in the Figure above. A possible gas-water contact at measured depth of 3361.3m was observed. A calculated water density of 0.98 g/cc and gas density of 0.15 g/cc were obtained from the slope of the plot.

8.2.4 Well OP4

A total of nineteen RFT pressure test measurements were performed between the interval of 3200m to 3350m as shown in appendix K. A supercharged pressure was also observed. The interpretation of the result is as shown in Figure 8.4 below.

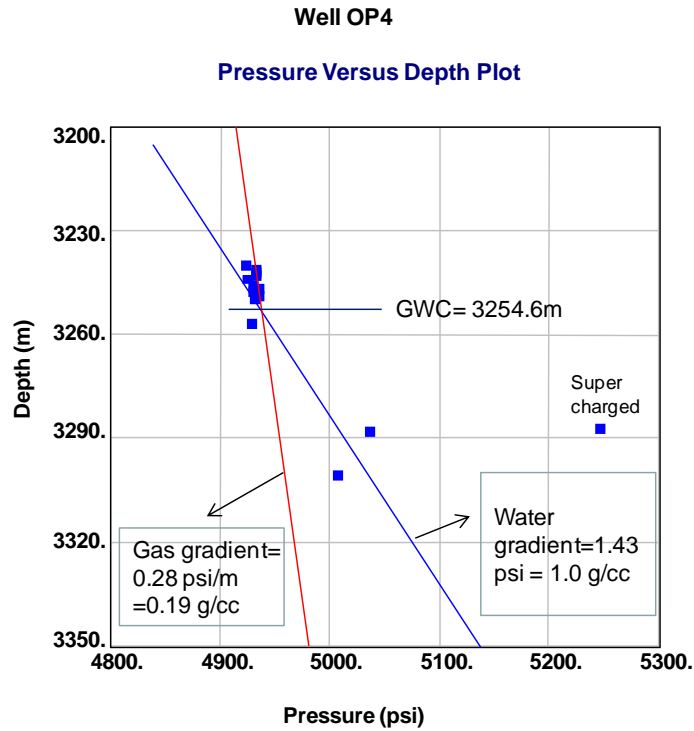


Figure 8.4: Well OP4 pressure versus depth plot

The graphics above showed the water density of 1.0 g/cc and gas density of 0.19 g/cc. A possible gas water contact (GWC) was observed at measured depth 3254.6 m. The water and gas line pressures of less than 5200 psi and 5000 psi respectively were recorded within the interval.

8.2.5 Well OP6

A total of eighteen RFT pressure test measurements were performed within the interval of 3190m to 3230m as presented in appendix I. The plot of the pressure versus depth for the identification of fluid densities and contacts are presented in Figure 8.5 below. A possible gas water contact was noticed at measured depth 3223.5m. The water density of 0.99 g/cc and gas density of 0.25 g/cc were calculated from the slope of the graph.

Well OP 6
Pressure Versus Depth Plot

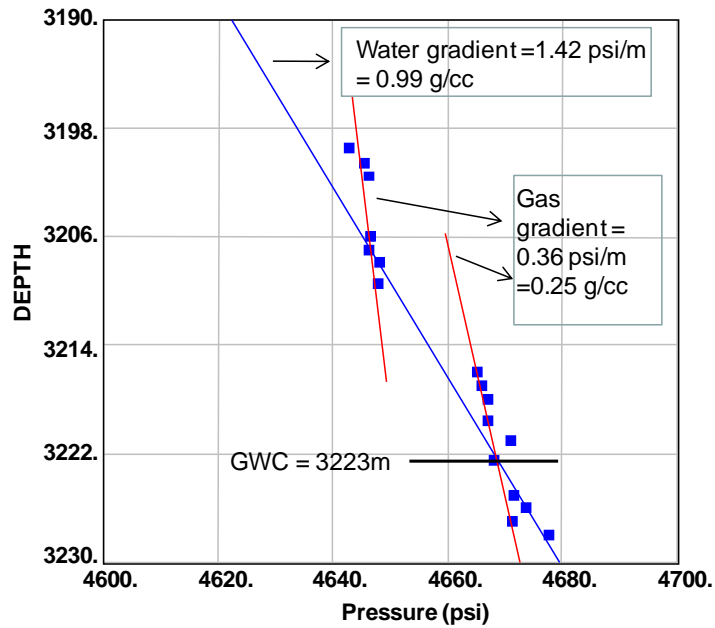


Figure 8.5: Well OP6 pressure versus depth plot

8.2.6 Well MA1

A total of eleven RFT formation pressure test measurements were obtained within the Albian age sandstone reservoir interval of well MA1. The results are presented in appendix K. Shown in Figure 8.6 below is the pressure versus depth plot. The pressure versus depth interval investigated in well MA1 indicated wet sandstone reservoir interval with a gradient of 1.02 g/cc. No gas was intersected in this analysis.

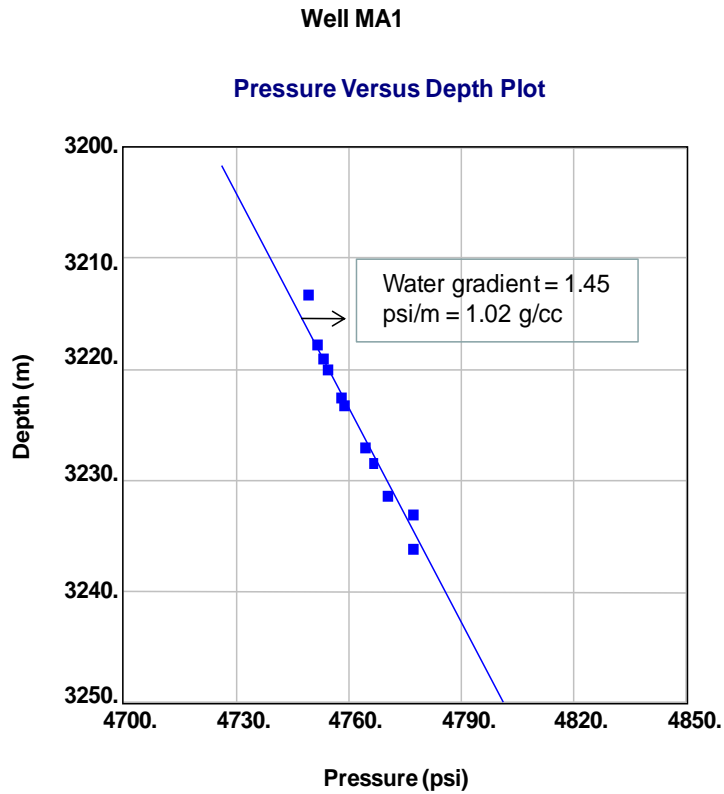


Figure 8.6: Well MA1 pressure versus depth plot

8.2.7 Well MA2

In well MA2, a total of eighteen RFT pressure test measurements were conducted within the Albian age sandstone reservoir formation at a measured depth of 2940 m to 2970 m as shown in appendix K. The pressure versus depth plot for identification of fluids and possible contacts is presented in Figure 8.7 below. Water density of 1.04 g/cc and gas density of 0.24 g/cc were calculated from the slope respectively. A possible gas water contact was observed at measured depth of 2964 m as shown in Figure 8.7.

Well MA2
Formation Pressure Vs Depth

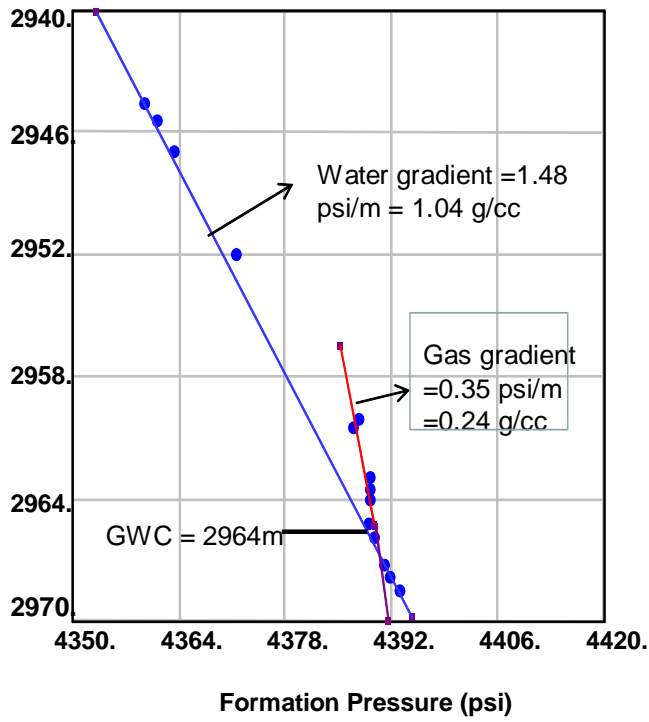


Figure 8.7: Well MA2 pressure versus depth plot

8.2.8 Well MA3

A total of nine successful RFT pressure test measurements were performed within the depth range of 2936m to 3080m of well MA3 as shown in appendix K. The interpretation of the result is presented in Figure 8.8 below.

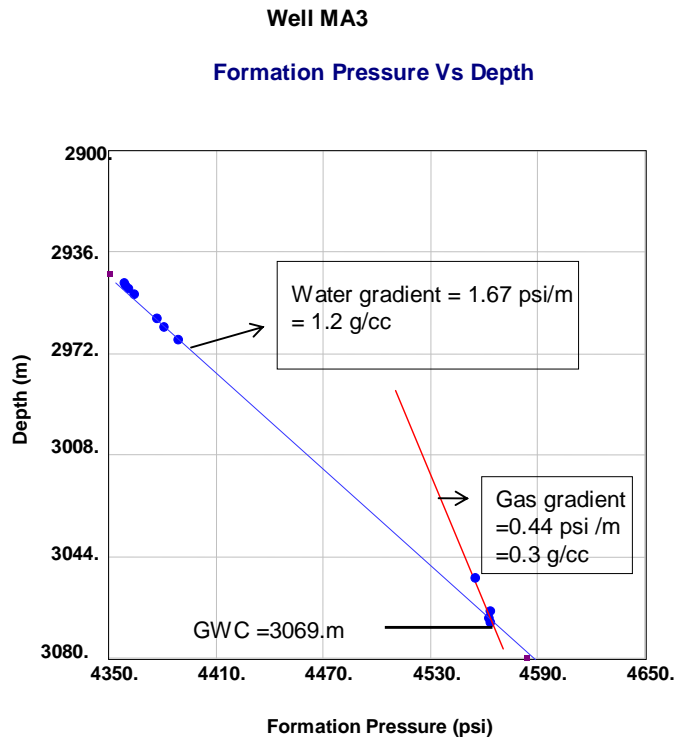


Figure 8.8: Well MA3 pressure versus depth plot

The aquifer density obtained from the calculation was 1.17 g/cc and gas density of 0.3 g/cc respectively. A possible gas water contact was also observed at measured depth of 3069m. The Table 8.2 below summarizes the interpreted water and gas gradients interpreted in each well from the pressure data.

Table 8.2: Summary of pressure gradients and densities for Wells

Well	Water Gradient (psi/m)	Water Gradient (psi/ft)	Density (g/cc)	Gas Gradient (psi/m)	Gas Gradient (psi/ft)	Density (g/cc)
OP1	1.45	0.44	1.02	0.23	0.07	0.16
OP2	1.46	0.44	1.02	-	-	-
OP3	1.39	0.42	0.98	0.22	0.07	0.15
OP4	1.43	0.44	1.00	0.28	0.09	0.19
OP6	1.42	0.43	0.99	0.36	0.11	0.25
MA1	1.45	0.44	1.02	-	-	-
MA2	1.48	0.45	1.04	0.35	0.11	0.24
MA3	1.67	0.51	1.20	0.44	0.13	0.3
Average	1.44	0.44	1.02	0.29	0.09	0.20

In the majority of the wells, the interpreted water gradient ranges from 1.39 -1.48 psi/m (0.98 – 1.04 g/cc equivalent). However, well MA4 indicated a high water gradient of 1.67 psi/m (1.2 g/cc equivalent). Excluding well MA3, the average water gradient of 1.44 psi/m (1.01 g/cc) was obtained which is taken as the field interpreted water gradient from the pressure data.

The interpreted gas gradient in the field range from 0.22 – 0.44 psi/m (0.15 – 0.3 g/cc equivalent). In calculating the field gas gradient, well MA3 was excluded because it gives a significantly high value in comparison with others. An interpreted field gas gradient of 0.29 psi/m (0.20 g/cc equivalent) was interpreted from the pressure data.

The overlay of gas and aquifer gradients in the field is presented in Figure 8.9 below showing the field aquifer gradient line of 0.44 psi/ft (1.01 g/cc).

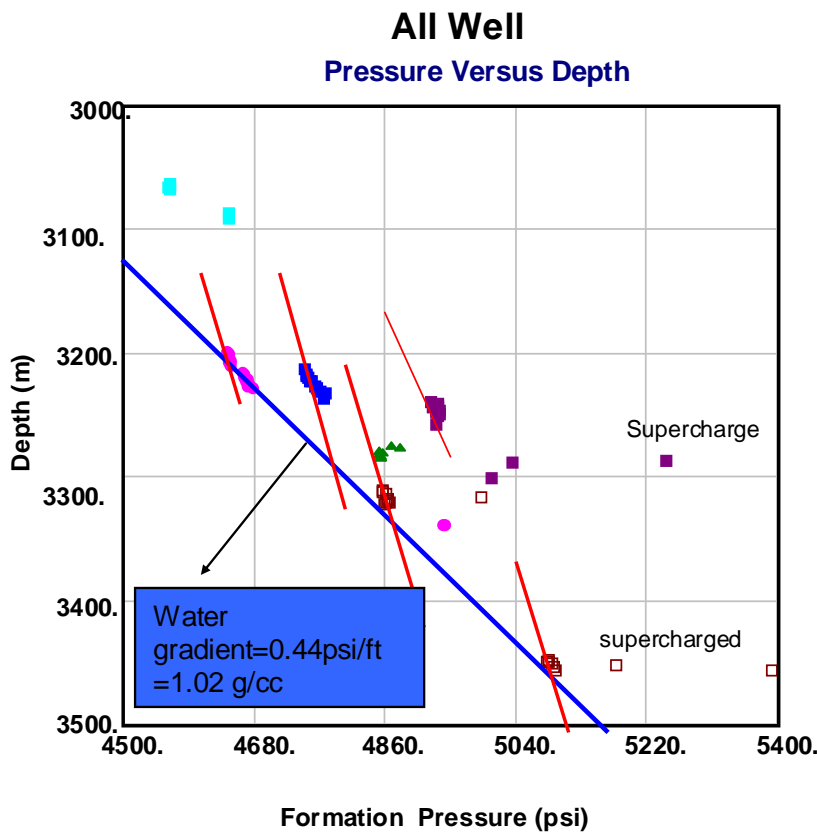


Figure 8.9: Overlaid gas and water gradients in the field

8.3 COMPARISON OF LOG, DST AND RFT DATA FLUID CONTACT

The possible gas producing zone and its contact with water can be identified by the combination of the neutron and density logs. The presence of gas increases the density log porosity and decreases the neutron log porosity (Bassiouni, 1994). The log resistivity and combination of neutron/density data provides an alternate indication of the location of fluid boundaries.

The gas and water contacts can be located from the separation between the neutron and density logs. A reduction in the separation between the neutron and density log within a hydrocarbon column can be indicative of the base of the gas column. The level of this neutron and density log separation is sensitive to reservoir quality and will reduce where reservoir quality becomes poorer due to increased clay volume or cementation. The gas water contacts are picked at the base of apparent saturation zone from the resistivity log data and from the computed water saturation.

The objectives of running the drill stem test (DST) among others are to establish the type of production, collect formation fluids for laboratory analysis and to ascertain if the formation can achieve sustained production. It was used in this study to ascertain the type of fluid present. However, the DST tests were performed in well OP3.

The picked gas and water contacts from logs are comparison with the pressure data measurement contacts are presented in the Figures below.

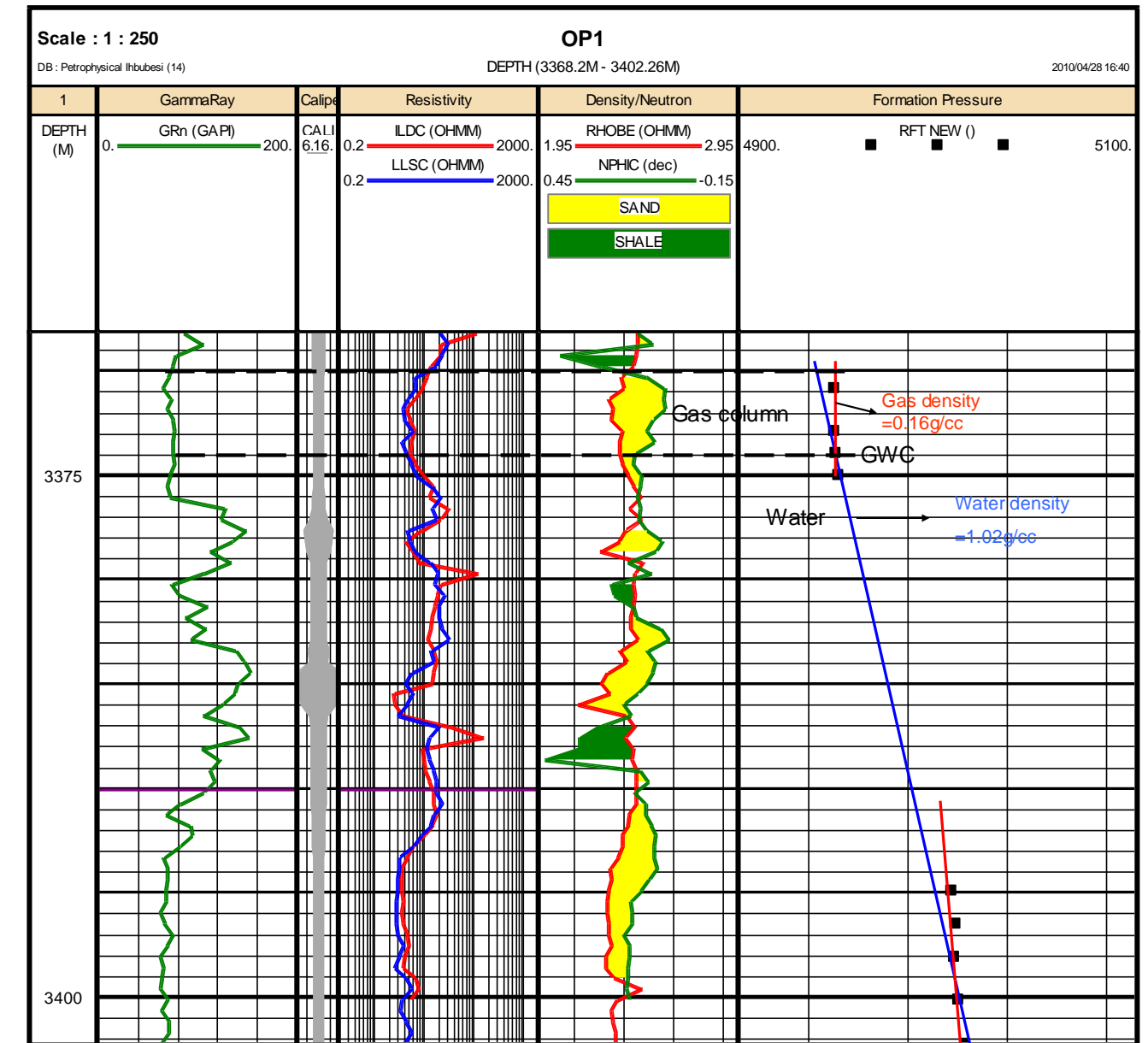


Figure 8.10: Well OP1 comparison of log and pressure data gas water contact

Figure 8.10 present resistivity curves in track 4 and density and neutron curves in track 5. The pressure versus depth is displayed on the right hand side of the Figure showing the gas water contact (GWC) at depth of 3374m.

The gas water contact from the log was picked at a measured depth of 3374m which is a little shallower than the contact obtained from the formation pressure measurement. The gas column of approximately 4m was observed on the log, which is 4m above the gas water contact point. The low resistivity values displayed in this zone may be due to the presence of chlorite mineral as previously presented as the dominant clay.

No drill stem test was conducted in the well.

Shown in Figure 8.11 below is the comparison of log and pressure data gas water contact.

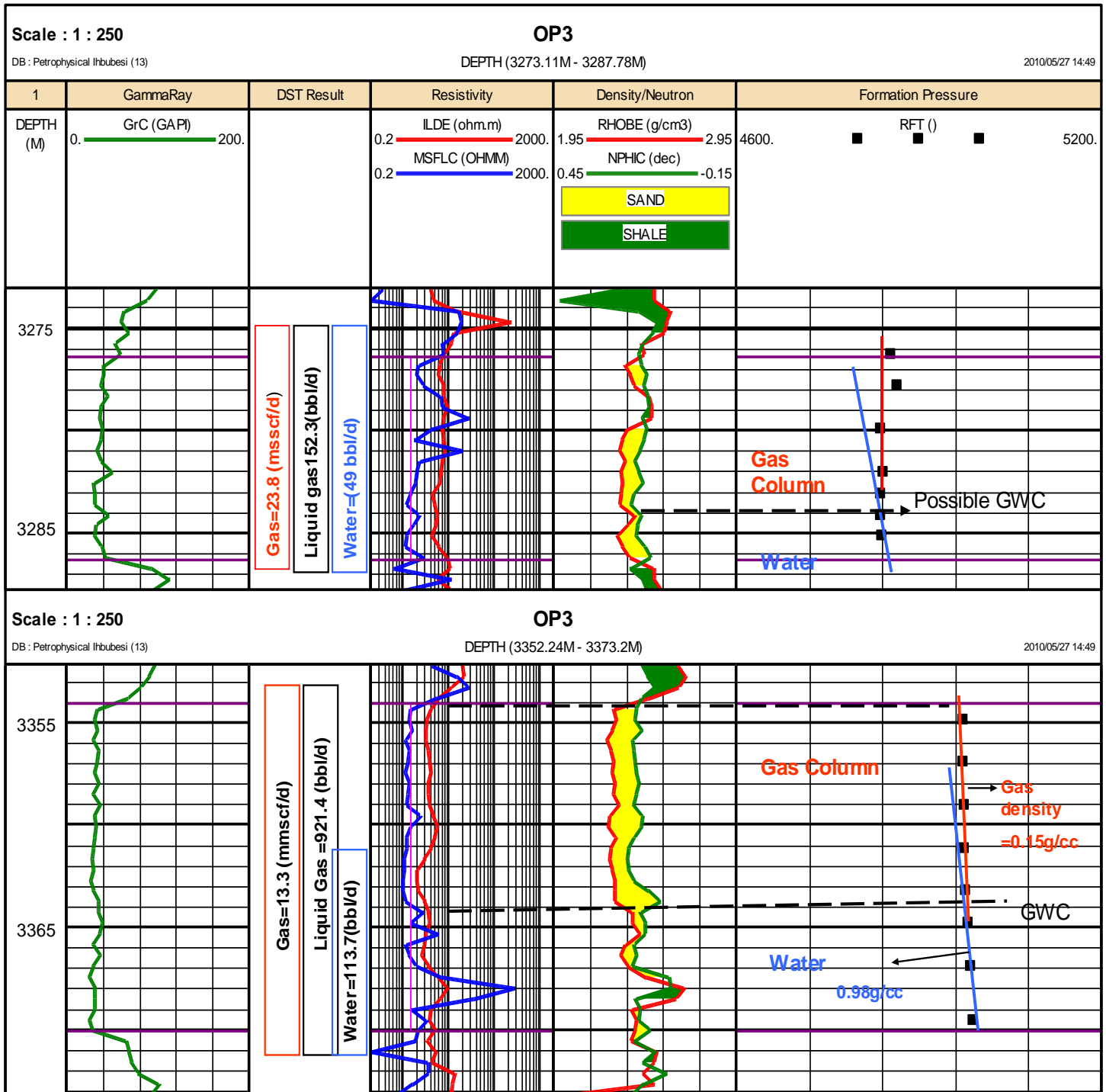


Figure 8.11: Well OP3 Comparison of log and pressure data gas water contact

Figure 8.11 presents the drill stem test results (track3), resistivity curves plotted in track 4 and density with neutron curves in track 5. The formation pressure is plotted in

track 6. The deep resistivity with the density/neutron curves was very useful in identification of the possible gas water contact of the well. The gas water contact was observed at measured depth of approximately 3284m and 3364m respectively .Gas column of 8m and 10m was also identified.

The drill stem test was conducted in open hole in order to test for a possible fracture zone over which high gas values had been recorded while drilling but no flow to surface was recorded. The summary of the results of the DST are presented in track 3 of Figure 8.11 above. The results confirmed the presence of gas and water in the interval analysed. The absence of a significant gas effect in the interval may be attributed to the presence of liquid gas in significant quantities at intervals tested. High production of water was also observed in the interval analysed. Presented in Figure 8.12 below is the comparison for well OP4.

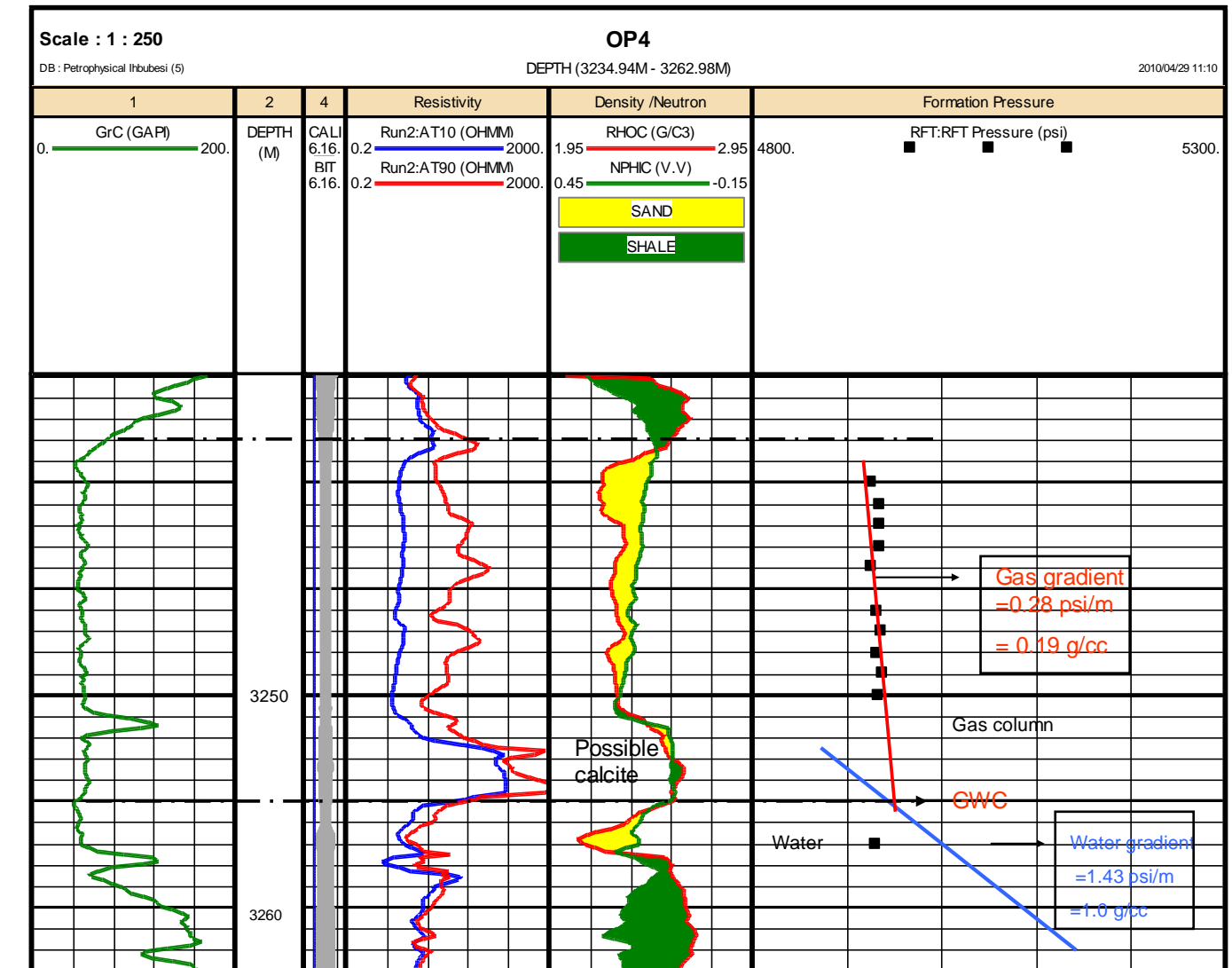


Figure 8.12: Well OP4 Comparison of log and pressure data gas water contact

Figure 8.11 above presents the log curves on the left and pressure data on the right. Track 4 is the resistivity curves and track 5 is the density and neutron curves. There was no visible gas water contact on the log plot but little effect was observed at measured depth 3240m, and below this was interpreted as the possible transition zone where both gas and water could be produce.

However, the pressure data indicated a gas water contact at 3254.6m which coincides with log measured depth of 3255 m. DST tests were carried out but details are not available.

Presented in Figure 8.13 below is log and pressure data comparison for well OP6.

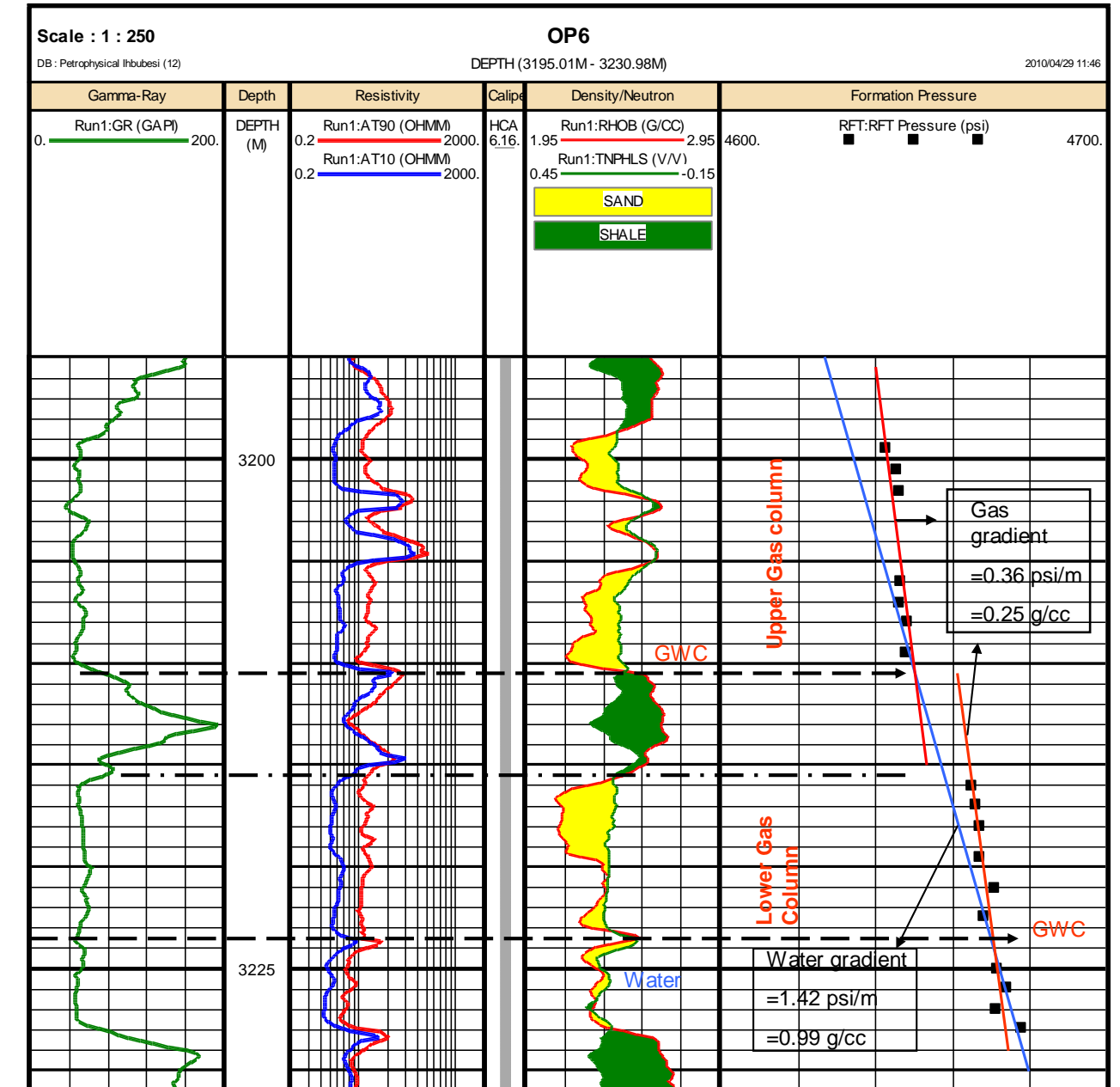


Figure 8.13: Well OP6 Comparison of log and pressure data gas water contact

Track 3 of Figure 8.13 (left) above is the resistivity curves and track 4 is the density and neutron log curves. The separation between the neutron and density curves was not so obvious in the entire gas column. Two separate gas columns of 10m and 7.5m were obtained with possible gas water contacts at measured depth 3210.5m and 3223.5m respectively. The sandstones appear to be hydraulically connected with water gradient of 1.42 psi /m (0.99 g/cc) and gas gradient of 0.36 psi/m (0.25 g/cc). DST was carried out over the intervals but details are not available for comparison.

However, the resistivity curve indicated a gas water contact at 3223.5m which almost coincide with that determined from the pressure data.

Figure 8.14 is the gas water contact comparison for well MA2 presented below.

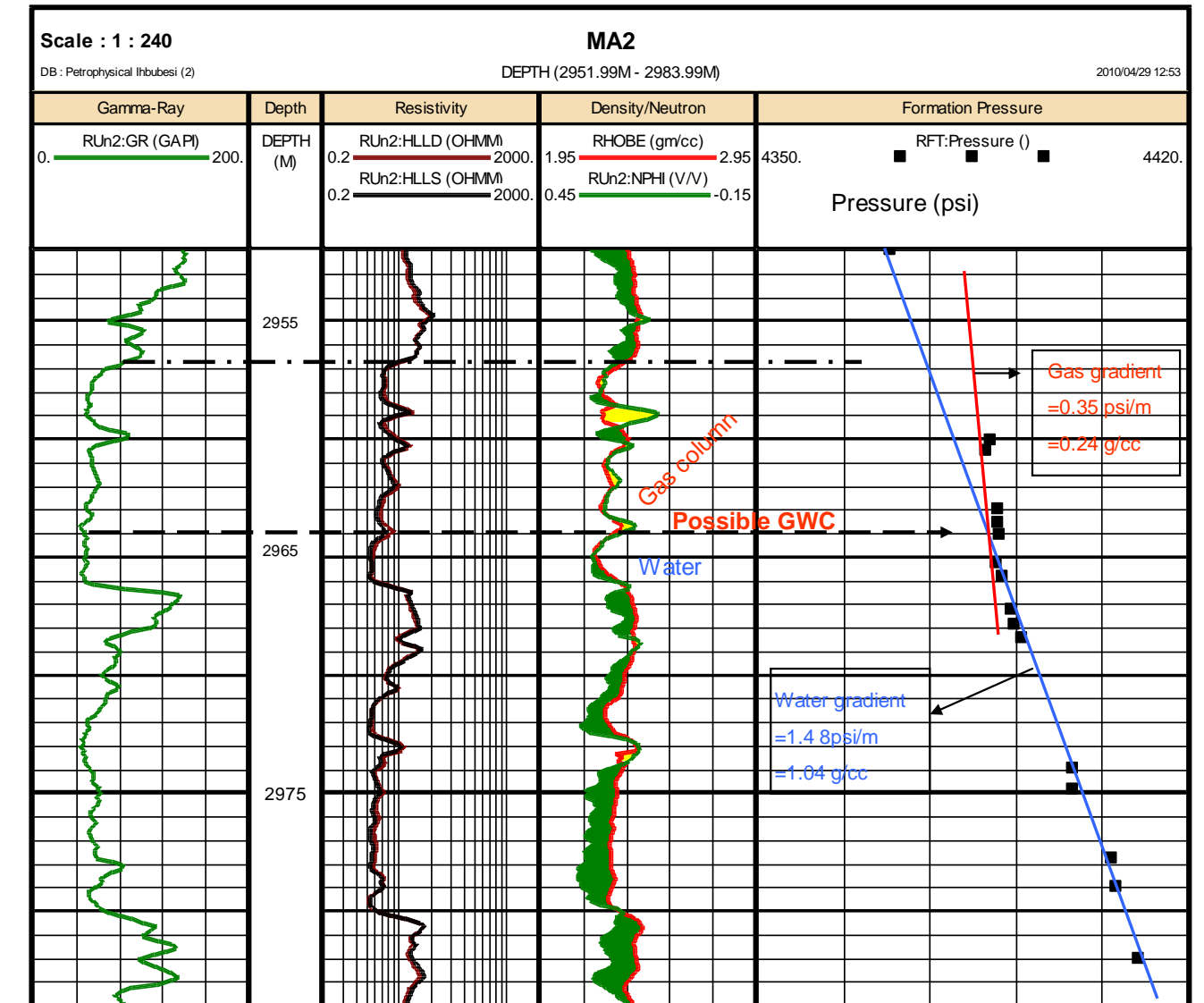


Figure 8.14: Well MA 2 comparison of log and pressure data gas water contact

Presented in Figure 8.15 below is the comparison of well MA3 log and pressure data determined gas water contact.

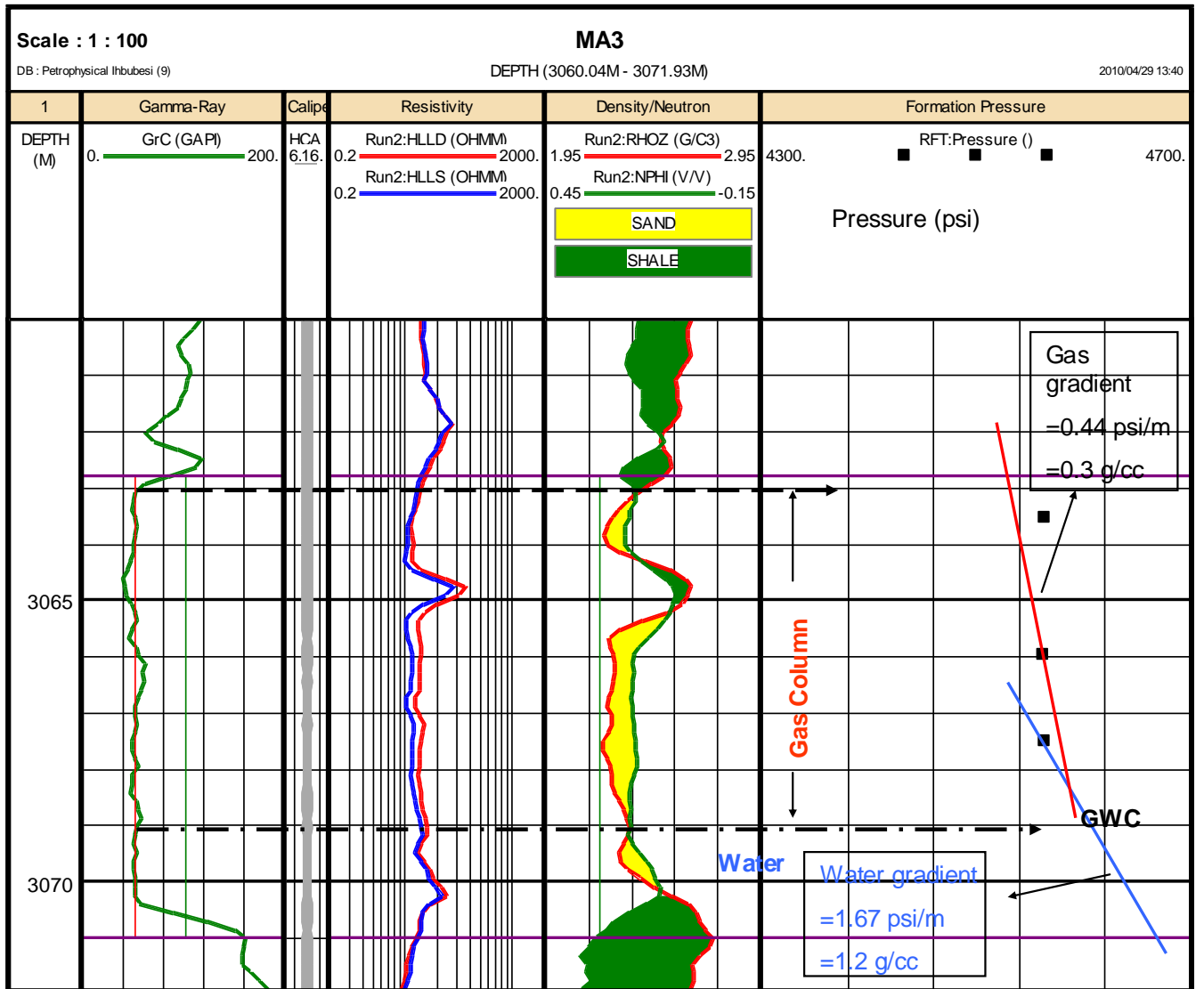


Figure 8.15: Well MA3 comparison of log and pressure data gas water contact

The log and pressure data gas water contact coincides at measured depth of 3069.2m as shown above. Log analysis indicates a gas column of 6 m.

Generally, the gas water contacts determined from log and pressure data are in close agreement. However, in most of the wells, the gas effect was not observed at the gas column which may be due to the dominance of condensate gas (liquid gas) present.

The summary of gas-water contacts identified by wells is presented in Table 8.3 below.

Table 8.3: Summary of gas water contact

Well Name	Interval (m)	Gas Water Contact(GWC) (m)
OP1	3368-3375	3374.0
OP3	3275-3287	3284.0
	3354-3370	3364.0
OP4	3238-3258	3255.0
OP6	3197-3213	3210.5
	3213-3227	3223.5
MA2	2955-2967	2964.0
MA3	3063-3070	3069.0

CHAPTER NINE

APPLICATION OF RESULTS, DETERMINATION OF CUT-OFF AND NET PAY

9.1 INTRODUCTION

One of the major challenges with determination of petrophysical properties from core, wireline logs, and production test is that, data sources measure different physical parameters and represent different sample volumes. Sampling bias also contribute to the challenges. According to Lovell et al (1998), measurements of petrophysical properties in the laboratory or down-hole device would under favourable conditions and experimental experience, produce an accurate measure of the parameter the device was designed to measure. The wireline tools do not record petrophysical properties directly but have to be interpreted (chapter 2), and the degree to which the interpreted values are accurate is difficult to ascertain. To minimize the uncertainty or error associated wireline data, core data was used to calibrate wireline log measurements (chapter 6) in order to obtain accurate measurements.

The methods used to give a better and more reliable estimate of petrophysical properties were based on core data (sedimentological description and petrophysical) which helps in identification of lithofacies, petrofacies and flow zone indicators. Well test effective permeability estimates were available for well OP2 (chapter 7) and a good match with wireline log prediction of permeability using the Morris Biggs gas model was obtained. The absolute permeability (K) was obtained predicted from the porosity estimate using a regression equation established at the core plug scale in chapter 5. Though the expression obtained relating linear porosity to the logarithm of permeability at the core plug scale is not likely the same at the wireline scale. As indicated in chapter 5, diagenesis is present in the studied intervals and as such will influence some of the wireline log measurements. The core plug porosities were corrected for overburden effects and the core permeability for gas effect (Klinkenberg) in order to obtain results close to in situ measurements.

According to Elfenbein et al (2003) and Zhang et al (2004), wells test results when carefully calibrated, actually reproduce in situ measurement results. There exist many

published methods to estimate petrophysical properties from well data. Some of these have been discussed in the previous chapters. This section of the study focused on the estimate of basic petrophysical properties (volume of shale, porosity, permeability and water saturation) in non-cored wells.

9.2 Determination of Petrophysical Properties in Non-Cored Wells.

The petrophysical models of volume of shale, porosity and water saturation derived from the three cored wells (OP1, OP2 and OP3) was applied to non-cored wells as presented in some of the wells below.

The estimation of volume of clay in non-cored wells was based on the Steiber volume of shale correction equation which showed very good agreement with the whole rock mineralogy core data as shown in Figures 6.3 and 6.4 of chapter 6.

The equation 6.13 of chapter 6 was applied to non-cored wells in order to estimate overburden porosities using the sonic porosity log that best correlated with the core porosity data. The sonic porosity log was run in all the wells so it was easier to use it in estimation of the overburden porosity.

The capillary pressure water saturation was used to calibrate log calculated water saturations as discussed in section 6.3 (chapter 6). The Simandoux and Waxman Smith models best matched with capillary pressure estimated water saturations and hence will be used to estimate water saturations in non-cored wells.

Presented in the Figures below are the results obtained from the application of petrophysical obtained models from core to non-cored wells and intervals.

The Gamma-Ray is represented in track 3, porosity (total and effective) in track 4, water saturation (S_w) in track 5, Permeability (Absolute k and effective) in track 6, and volume of clay (track 7) in the graphics presented below.

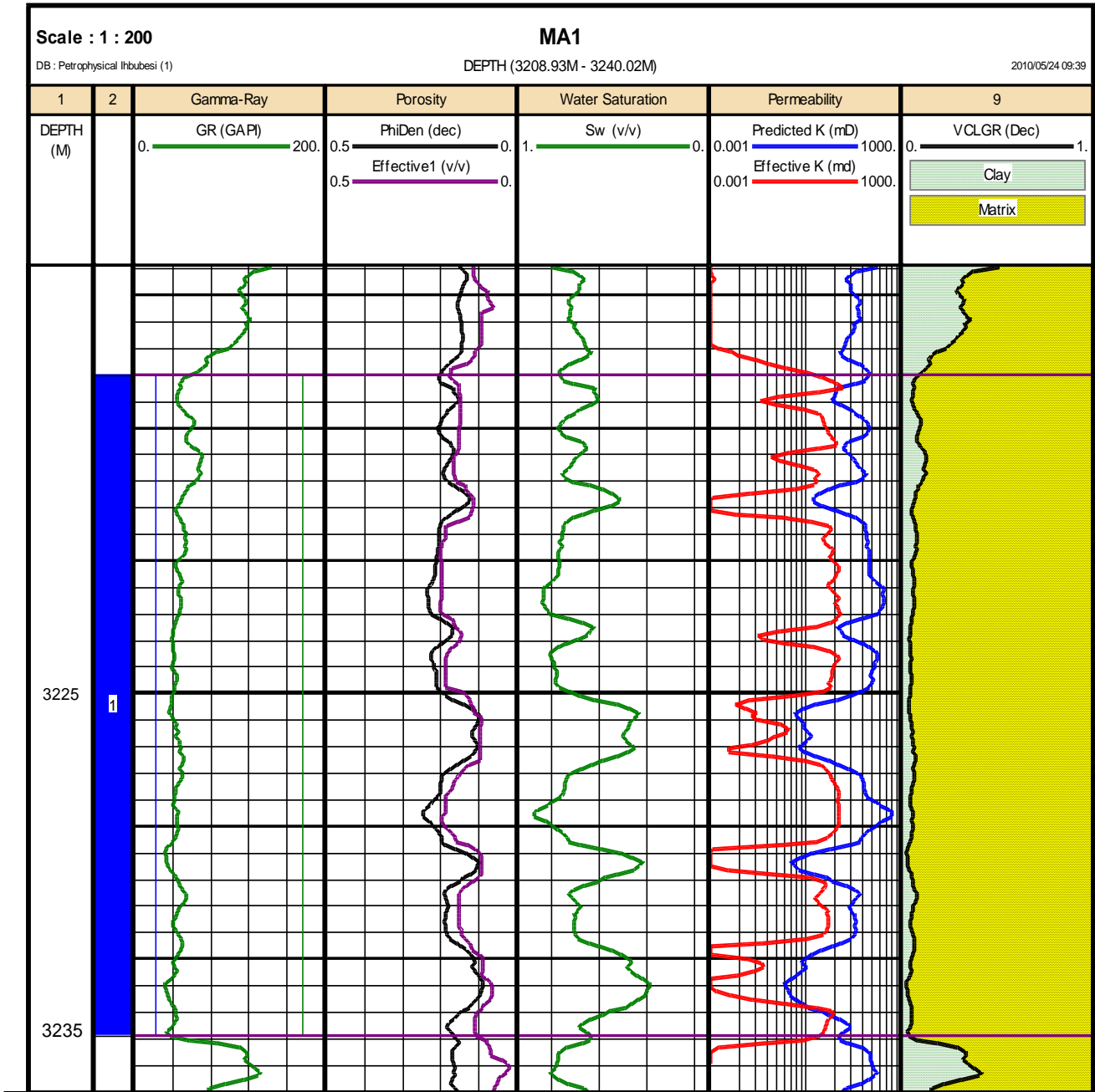


Figure 9.1: Well MA1 results estimated petrophysical properties

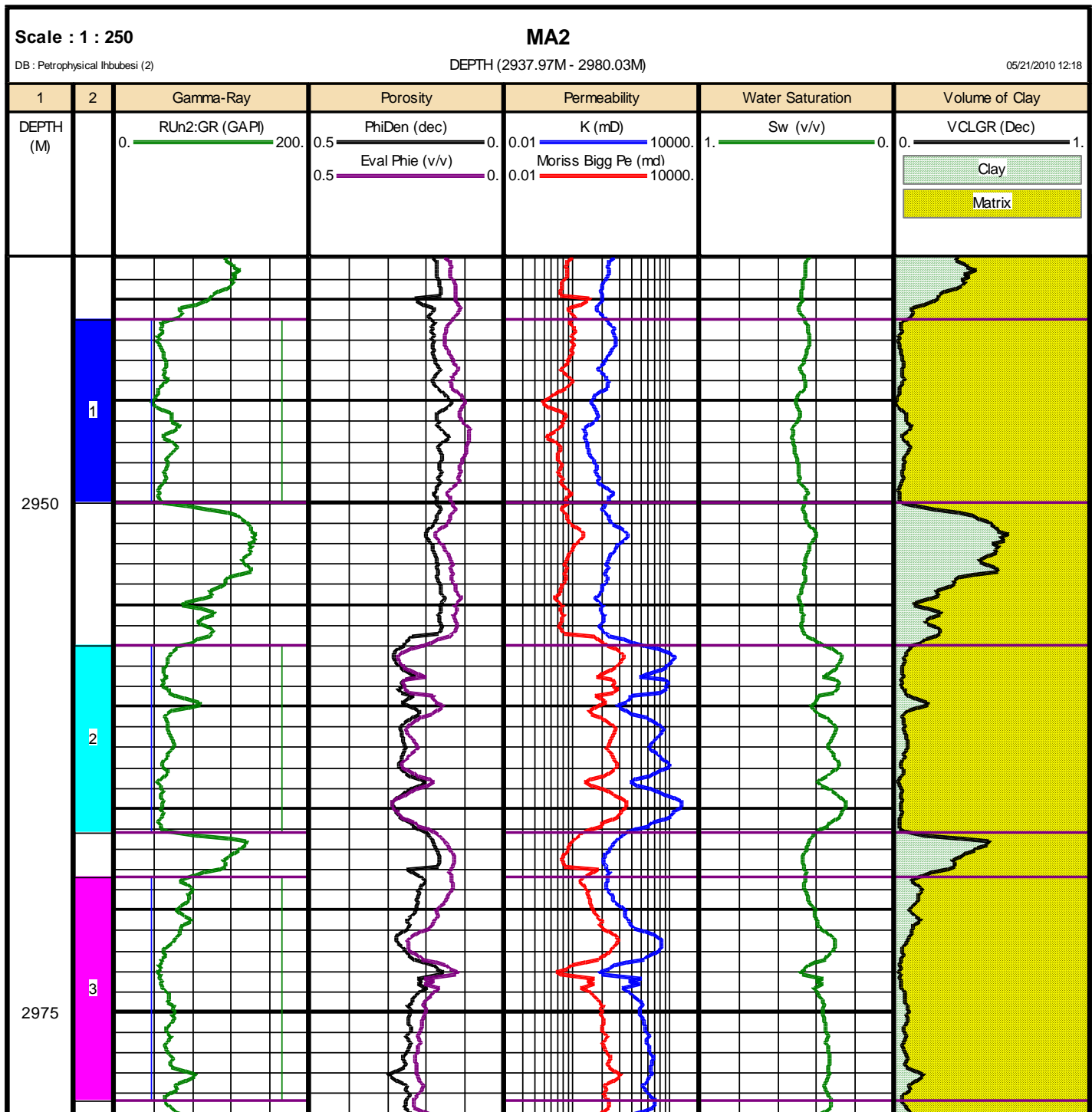


Figure 9.2: Well MA2 results of estimated of petrophysical properties

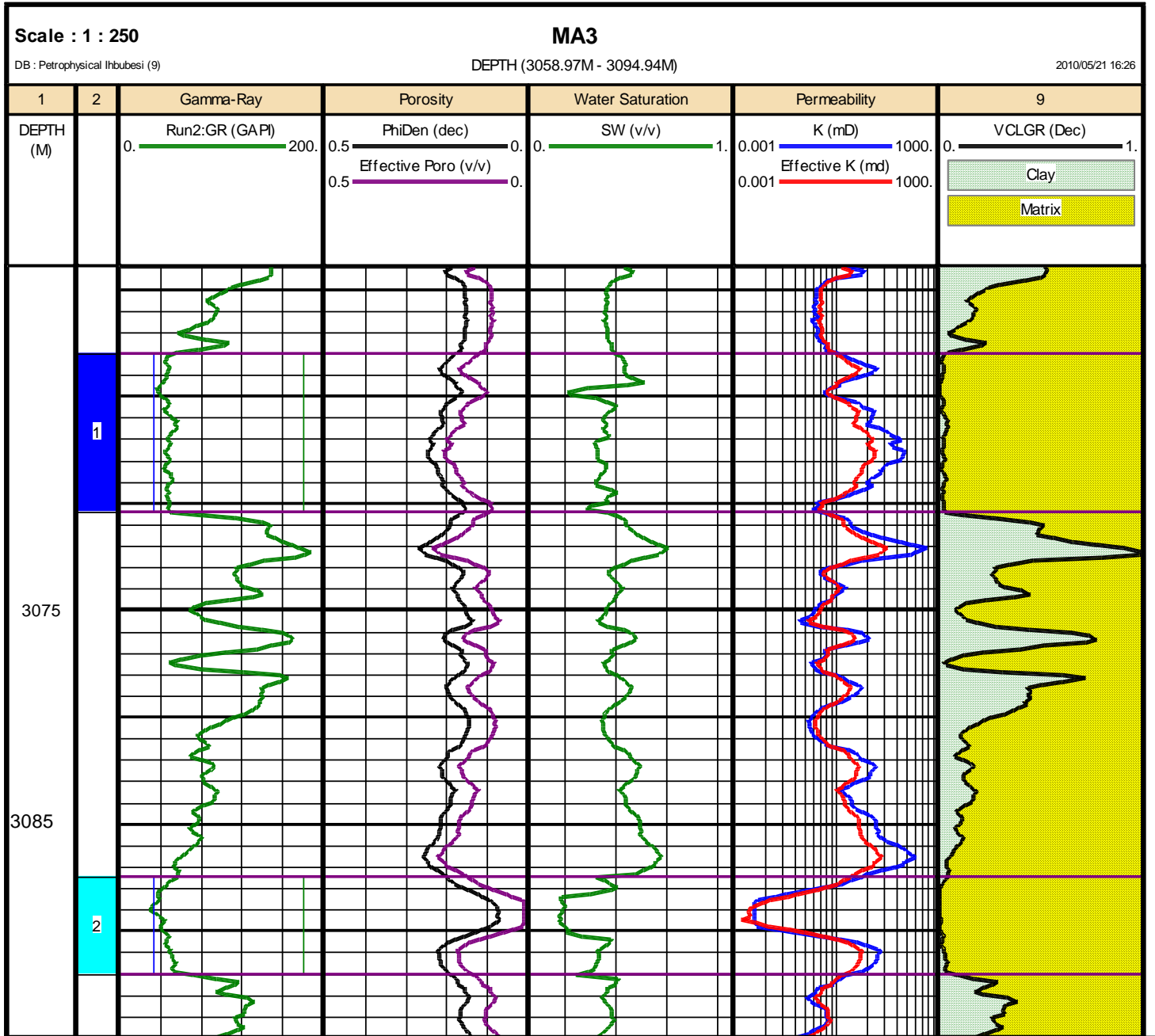


Figure 9.3: Well MA3 results of estimated petrophysical properties

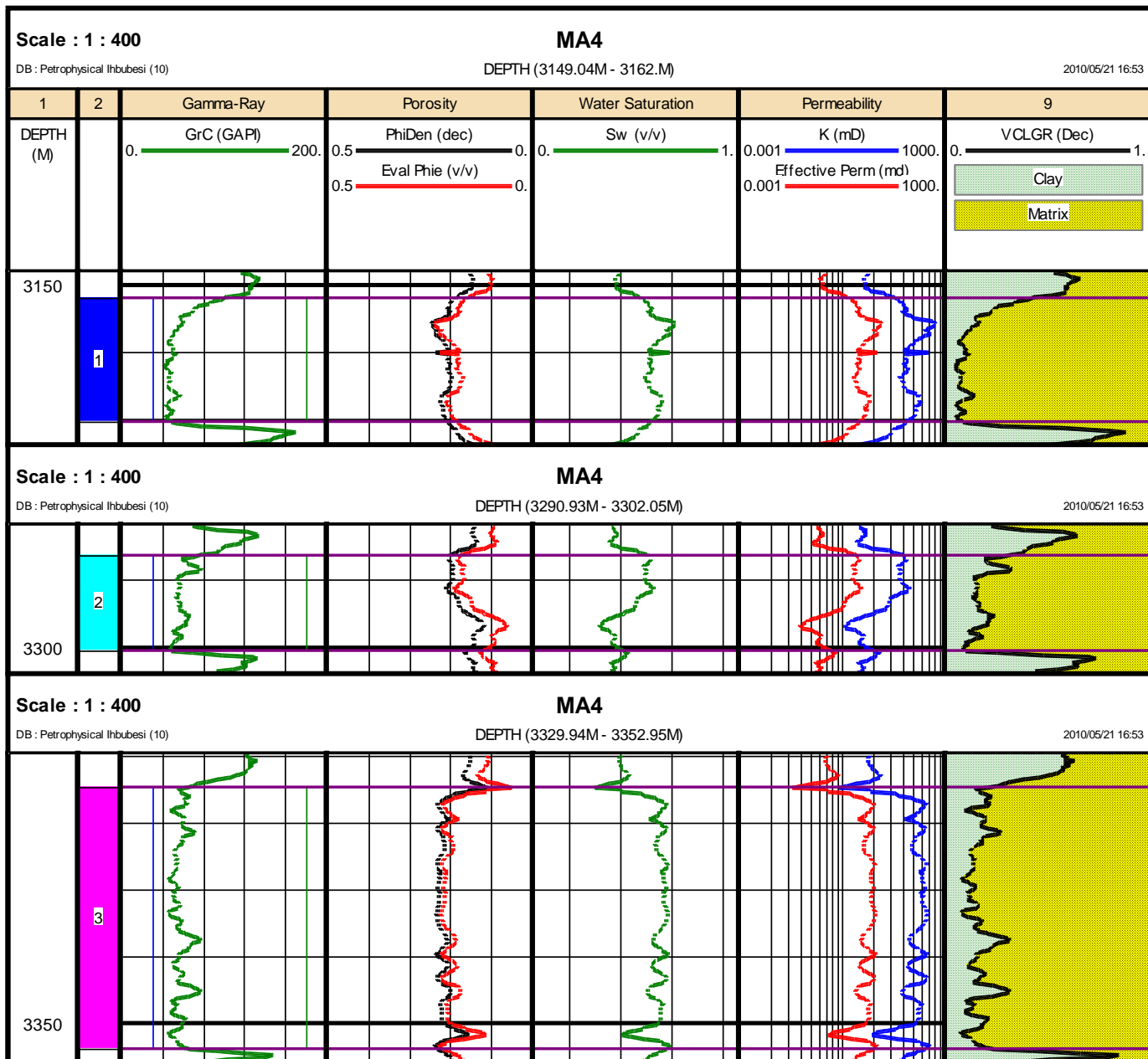


Figure 9.4: Well MA4 results of estimated petrophysical properties

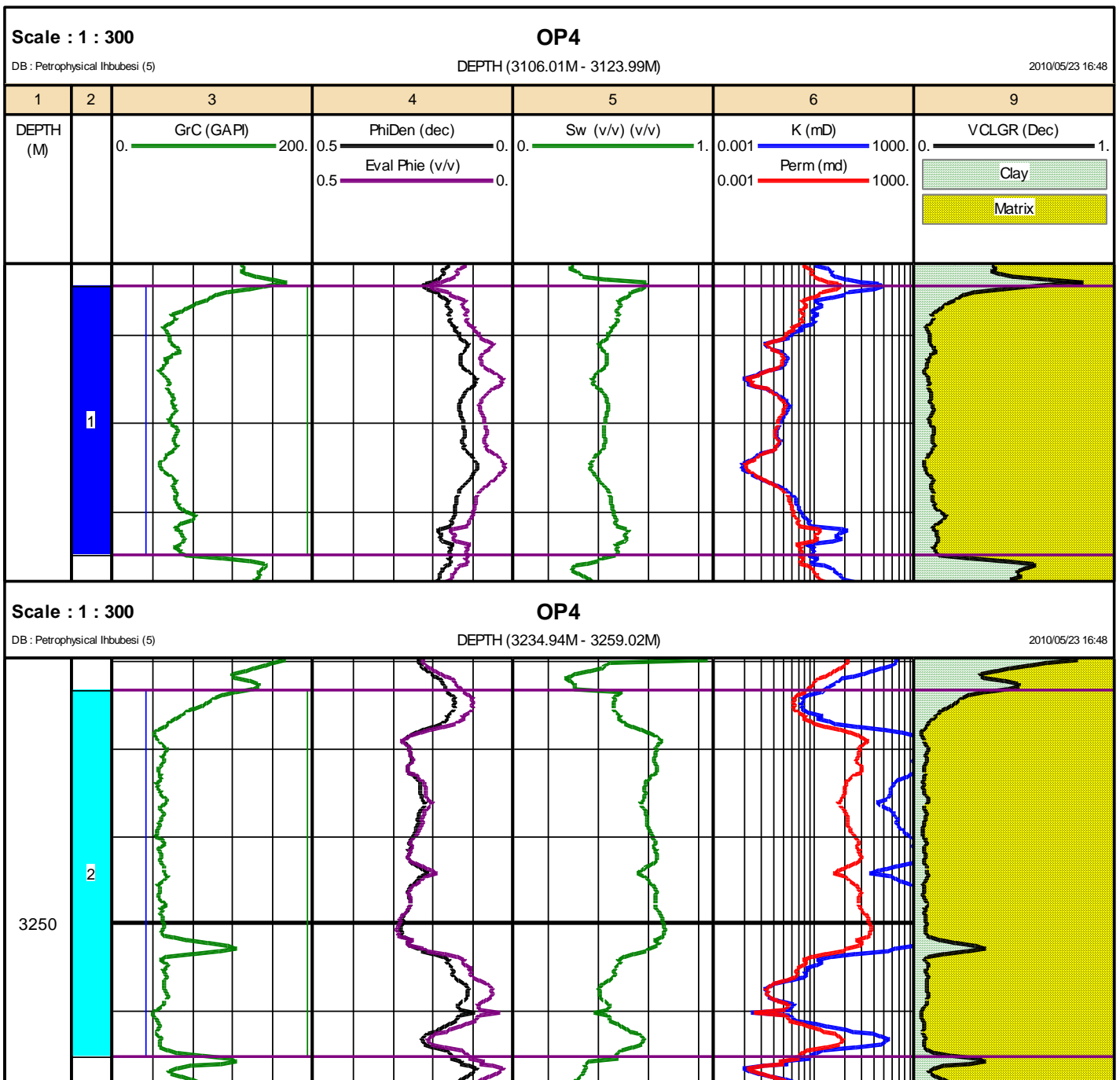


Figure 9.5: Well OP4 results of estimated petrophysical properties

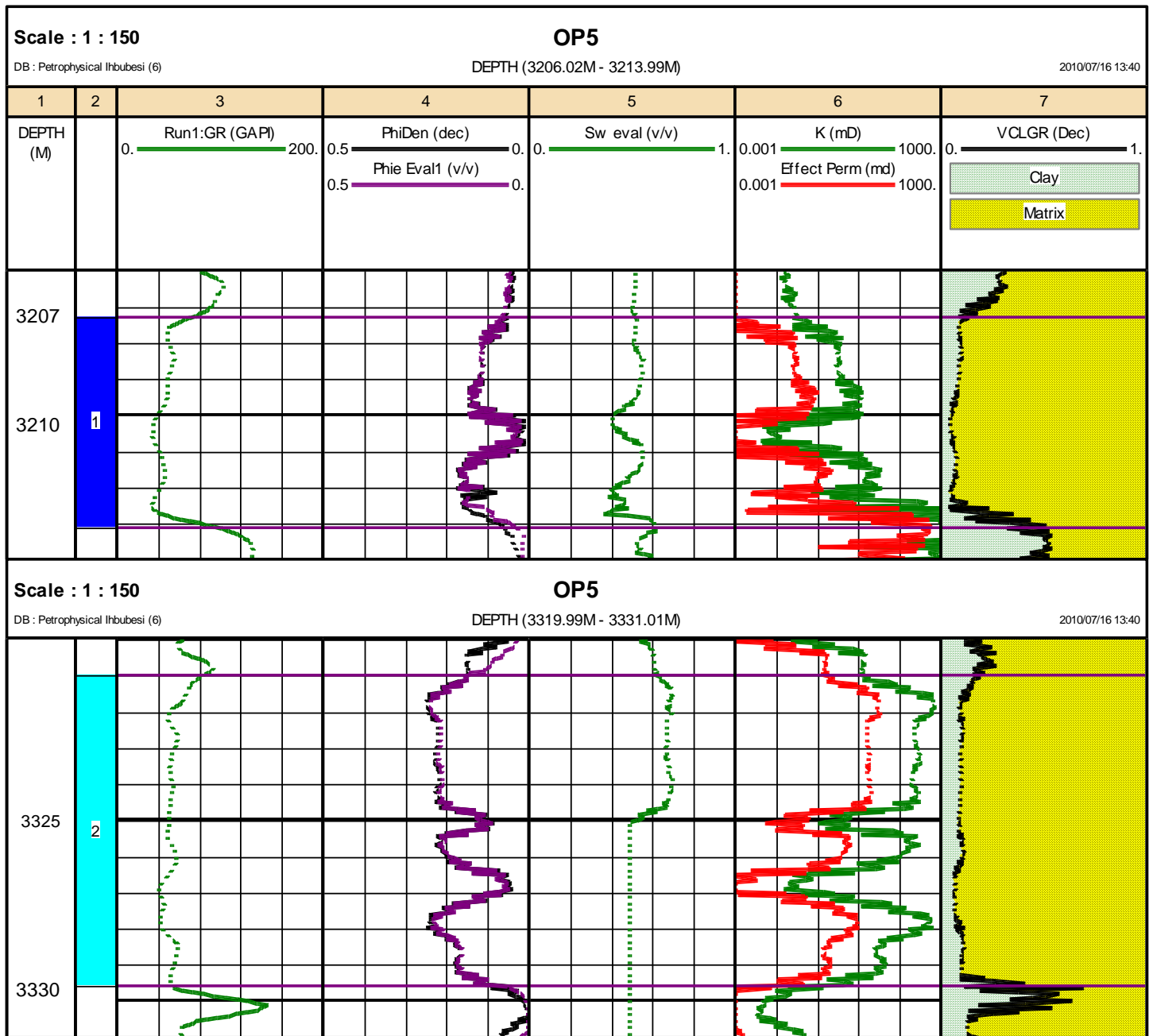


Figure 9.6: Well OP5 results of estimated petrophysical properties

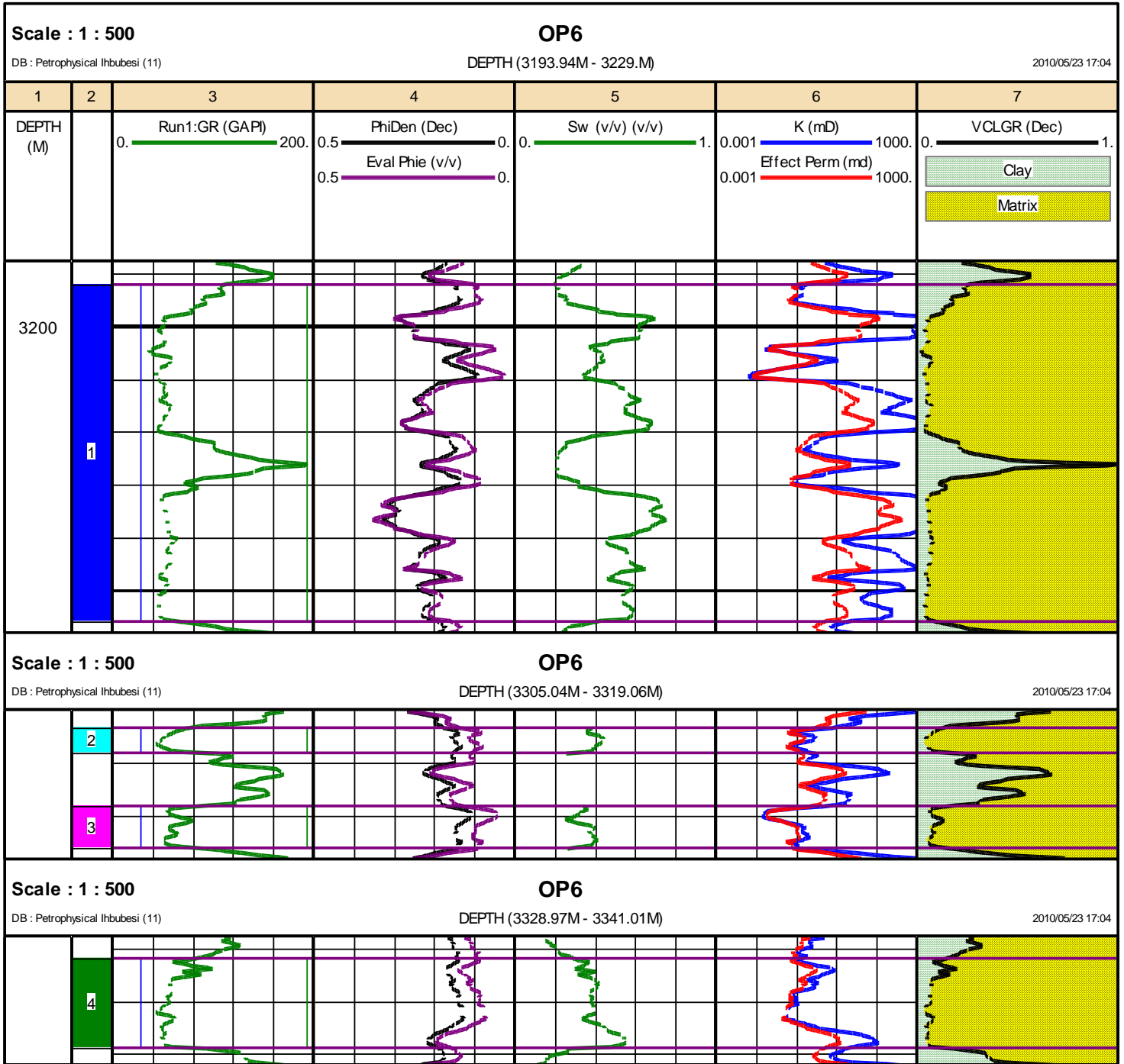


Figure 9.7: Well OP6 results of estimated petrophysical properties

9.3 CUT-OFF DETERMINATION

The cut-off concept is aimed at defining the effective petrophysical properties of a given geological unit in the presence of poor reservoir zones. In order to assess the efficiency of reservoir recovery mechanisms, the initial hydrocarbon volume must relate to reservoir rock. Where it does not, the hydrocarbon will have little chance of being, they may not contribute to reservoir dynamics and they should not be included within the accumulation volume against which recovery is to be assessed (Worthington, 2008).

The starting point in determining cut-off is to identify reference parameter that allows us to distinguish between intervals that have reservoir potential and intervals that do not. There is no single universally applicable approach to the identification of cut-off (Worthington & Cosentino, 2005). One of the most important steps is to establish the linkage between a conventional core measurement and a reference parameter that distinguishes between reservoir and non-reservoir rock. The evaluation of hydrocarbon volumes requires cut-offs so that net reservoir intervals (net pay) that contain sufficient hydrocarbon potentials and allow adequate hydrocarbon flow can be identified.

The net pay is defined on flow rate criteria and the fluids produce. Rocks with sufficient permeability to flow fluids at commercially significant rates are classified as net sandstone or net reservoir. If they produce hydrocarbons at a commercially acceptable hydrocarbon/water ratio, they are classified as net pay (Suzanne & Robert, 2004).

A non reservoir rock may have porosity and permeability that is too low and zero hydrocarbon saturation. The major control is often the lithology. Though shales are classified as non reservoir rocks, they often contain hydrocarbon with high saturations but have porosity and permeability that are too low for the hydrocarbon to be extracted. Sandstones on the contrary could be considered as reservoir rocks provided that they contain sufficiently high hydrocarbon could be extracted without difficulties..

The permeability cut-off is very often considered as the controlling parameter in net pay since it is dependent on a limited number of parameters including the fluid mobility, viscosity; pressure differential and reservoir drive mechanism. A common arbitrary approach of determining permeability cut-off is to set permeability cut-off

for gas reservoir net pay at 0.1mD and oil reservoir net pay at 1.0 mD. This approach is arbitrary since it does not take into consideration the reservoir fluid characteristics (George & Stiles, 1978).

To separate pay from non-pay, this study used the combined plot of porosity-permeability for the cored wells in the field in conjunction with the classified facies and log derived volume of shale and water saturation cut-offs. Also, petrofacies and flow zone indicators identified in the previous chapter was also used to identify rocks in pay and non-pay intervals.

9.3.1 Porosity Cut-Off Determination

To discriminate between reservoir and non-reservoir, each data had to meet a porosity cut-off. The cross plot of conventional core porosity-permeability data corrected to equivalent in situ conditions in wells with facies plot was used to define a porosity equivalent to a minimum permeability considered capable of flowing hydrocarbon.

The Figure 9.8a below presents the porosity-permeability cross plot for the combined wells with core porosity and permeability data used for cut-off determination.

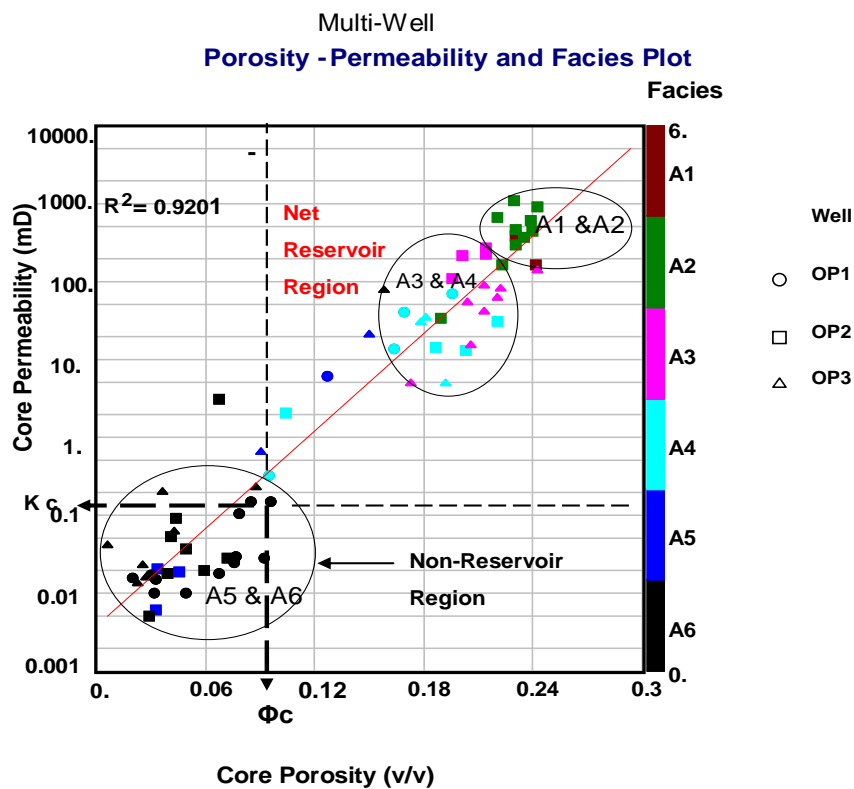


Figure 9.8a: Multi-Well porosity-permeability plot for cut-off determination

The porosity-permeability relationship indicated a conventional core Klinkenberg corrected permeability of approximately 0.1mD corresponding to an approximate overburden corrected porosity of 10 percent as cut-off points for reservoir and non reservoir regions. The points K_c and Φ_c on y and x axis on the plot are the permeability and porosity cut-off points respectively.

Facies A6 dominates the non reservoir region with facies A5 insignificantly distributed in this region. This confirms that facies A6 is a non reservoir rock. The histogram of the frequency distribution of permeability and porosity showing the cut-off points are presented in Figure 9.8b below.

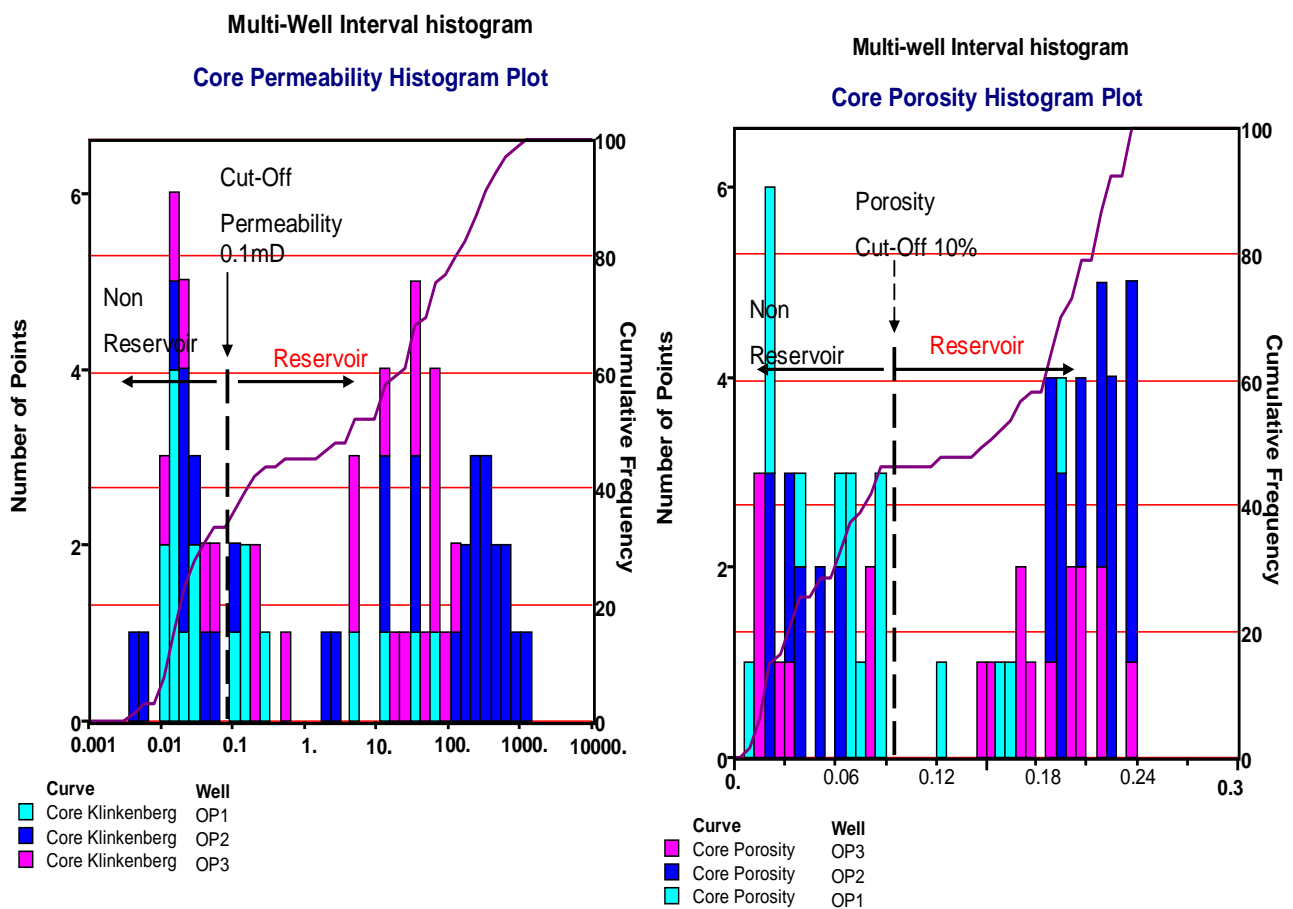


Figure 9.8b: Multi-Well permeability and porosity histogram distributions

The obtained permeability and porosity cut-off criteria were also applied to petrofacies in order to determine petrofacies that meet up the cut-off criteria. The plot indicated a cut-off point on micro-petrofacies. That is, for a rock to be classified as reservoir rock, it must have a pore throat radius of at least 0.2 microns.

The Nano rock type was identified as a non-reservoir rock because it failed to meet the cut-off criteria. The plot is presented in Figure 9.8c below.

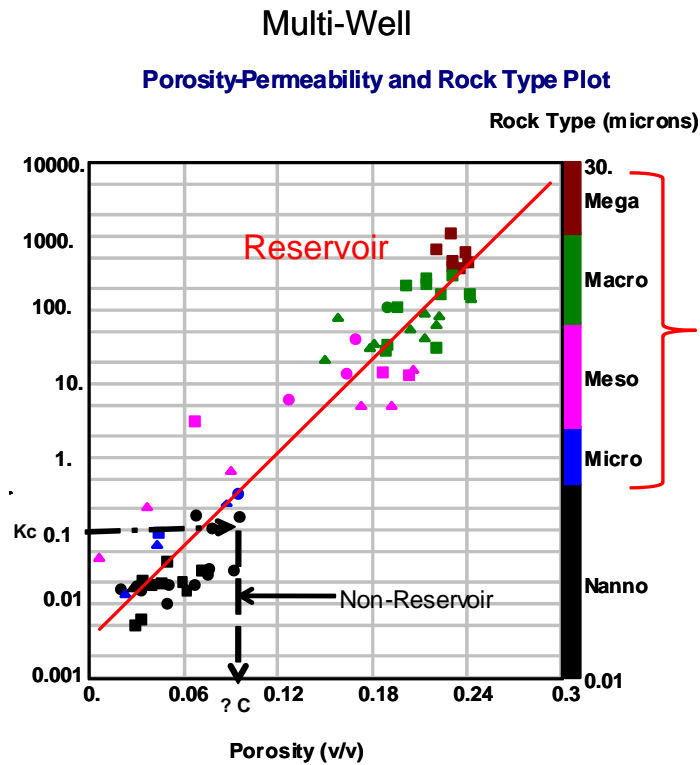


Figure 9.8c: Application of permeability and porosity cut-off to petrofacies

9.3.2 Volume of Shale Cut-Off Determination

The volume shale cut-off is used to discriminate between reservoir and non reservoir rock by allowing all rocks volume of shale equal to or less than certain value of the total reservoir volume.

The multi-well volume of shale versus porosity and gamma-ray log used to determine the volume of shale cut-off is presented in Figure 9.9a below.

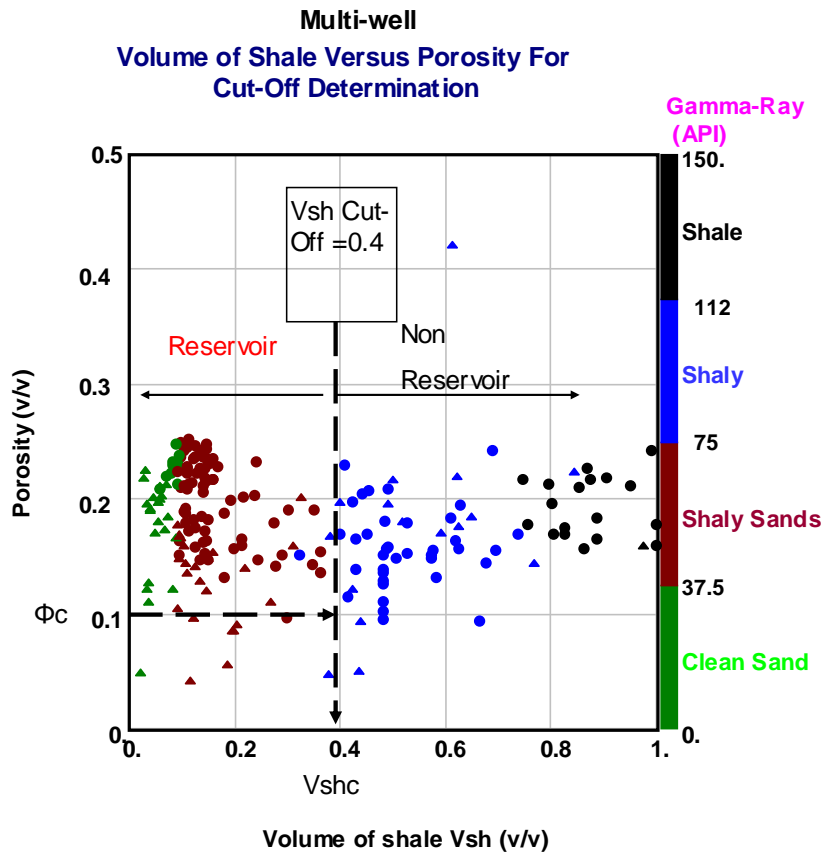


Figure 9.9a: Volume of shale versus porosity and gamma-ray log plot

The plot above showed the volume of shale (V_{shc}) cut-off value for reservoir and non reservoir rock determined at 0.4. That means that rocks with volume of shale value of more than 40 percent was regarded as shale and was not classified as reservoir rock. In contrary, rocks with volume of shale values equal to or less than 40 percent are regarded as reservoir rock.

The frequency distribution histogram of volume of shale and its cut-off point is presented in Figure 9.9b below.

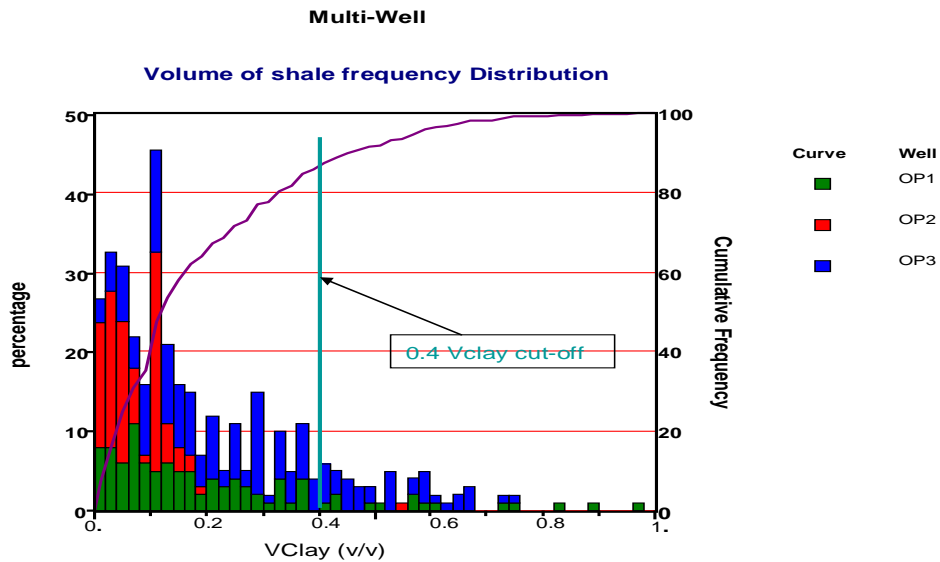


Figure 9.9b: Multi-Well vclay frequency distribution and cut-off point

9.3.3 Water Saturation Cut-Off Determination.

The water saturation cut-off discriminates between hydrocarbon bearing sandstones (pay) and intervals and water (wet) bearing intervals. Intervals that have water saturation greater than 65 percent water saturation were assumed to be wet or non-productive intervals.

Presented in Figure 9.10 below are the water saturation versus porosity cross plot and the water saturation frequency distribution histogram plot.

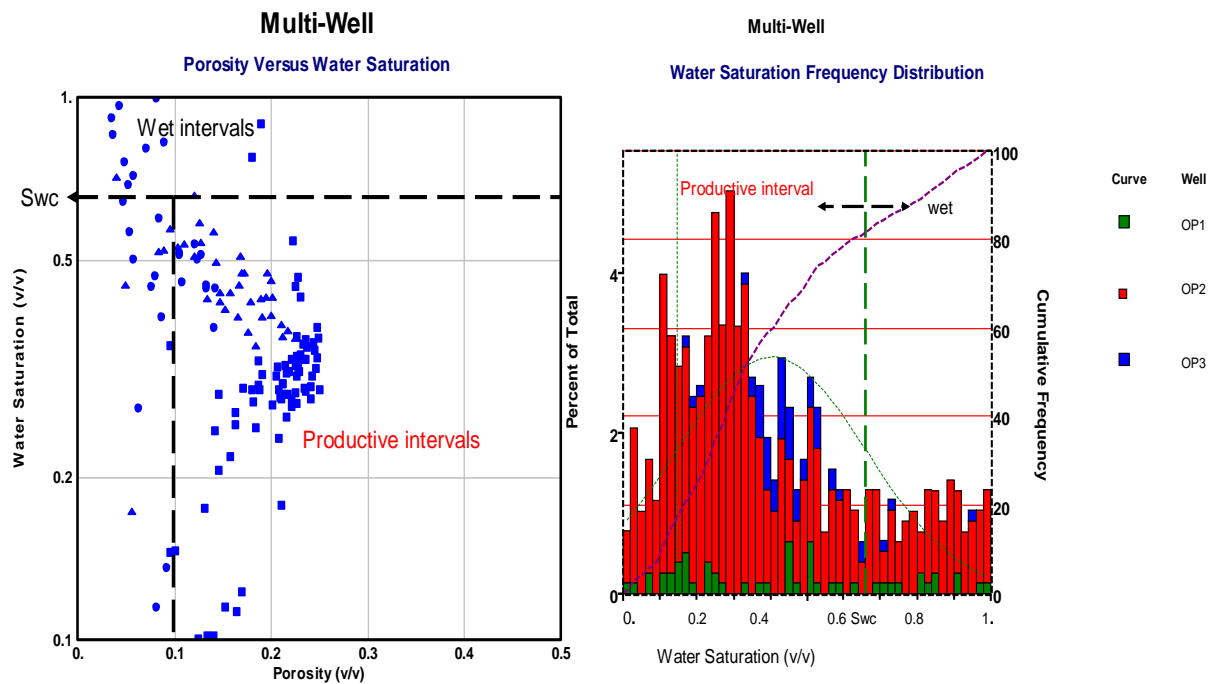


Figure 9.10: Multi-Well porosity vs water saturation and frequency distribution

9.4 Determination of Net Pay

The gross is regarded as the thickness of the reservoir interval that contains zones of which hydrocarbon can be produced and zones which does not favour the production of hydrocarbon. Net pay is any interval within the reservoir that contains producible hydrocarbon at economic rate given a specific production method. It represents the portion of the reservoir that contains high storability and mobility and significant hydrocarbon saturation.

Net pay is used to compute volumetric hydrocarbon in place and to determine the total energy of the reservoir which are both moveable and non-moveable hydrocarbons. Other use of net pay is to evaluate the potential amount of hydrocarbon available for secondary recovery (Cobb & Marek, 1998).

The distinction between gross and net pay is made by applying cut-off values in the petrophysical analysis. In this study, cut-off values of porosity (≥ 0.1), volume of shale (≤ 0.4) and water saturation (≤ 0.65) were used to identify pay intervals. That is,

intervals with porosity equal to and greater than 10 percent and volume of shale less than or equal to 40 percent and water saturation less than or equal to 65 percent were regarded as net pay intervals. Capillary pressure and relative permeability data support this 65 % pay cut-off.

The net to gross ratio is the thickness of net sand divided by the thickness of gross sand. This ratio is often used to represent the quality of a reservoir zone and for volumetric hydrocarbon calculations.

Using the cut-off limits, flag curves were created in the database for net reservoir interval (red colour) and gross reservoir (green). The net to gross ratio determined could be used to calculate the volume of gas originally in place. However, the calculation of volume of hydrocarbon is not part of the scope of this study.

Presented in Table 9.1 to 9.8 below are the calculated net pay summary for wells with the corresponding graphics in Figure 9.11 to 9.20.

Table 9.1: Summary of calculated reservoir pay parameters for Well OP1

Zone Name	Top (m)	Bottom (m)	Gross (m)	Net (m)	N/G	Av Phi (v/v)	Av Sw (v/v)	Av Vcl (v/v)
Reservoir 1	3303	3330.9	27.9	0	0	---	---	---
Reservoir 2	3368	3376.3	8.3	6.29	0.758	0.153	0.521	0.284
Reservoir 3	3390.5	3416	25.5	0	0	---	---	---

Three reservoirs were encountered in well OP1 of which one proved to have net pay (6.29m) having average porosity of 15.3 %, water saturation of 52 % and 28 % volume of shale as presented in Table 9.1 above and Figure 9.11 below.

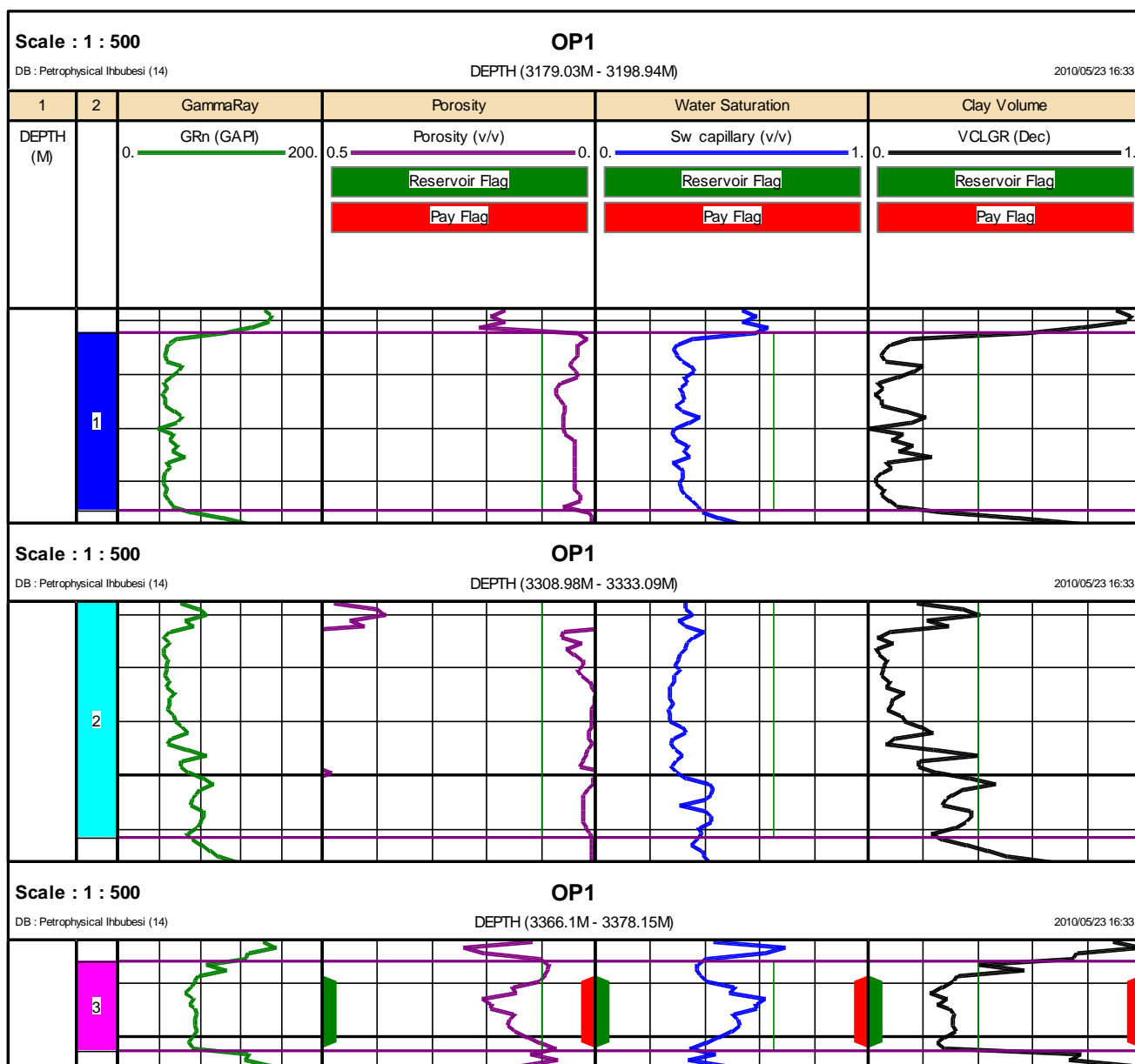


Figure 9.11: Well OP1 showing calculated reservoir parameters and pay flags

In well OP2, three reservoirs were evaluated and all showed net pay potentials as presented in Table 9.2 below. The net thickness range from 1.05m to 4.19m and average porosity from 11 to 12 %, water saturation 60 to 62 % and volume of clay 11 to 17 %.

Table 9.2: Summary of calculated reservoir pay parameters for well OP2

Zone Name	Top (m)	Bottom (m)	Gross (m)	Net (m)	N/G	Av Phi (v/v)	Av Sw (v/v)	Av Vcl (v/v)
14Ct1	3184.4	3203.1	18.7	4.19	0.224	0.113	0.614	0.17
14Dt1	3308.0	3320.7	12.7	1.05	0.083	0.11	0.608	0.11
14Et1	3446.0	3468.2	22.2	1.05	0.047	0.12	0.619	0.13
All Zones	3184.4	3468.2	53.6	6.29	0.117	0.114	0.613	0.153

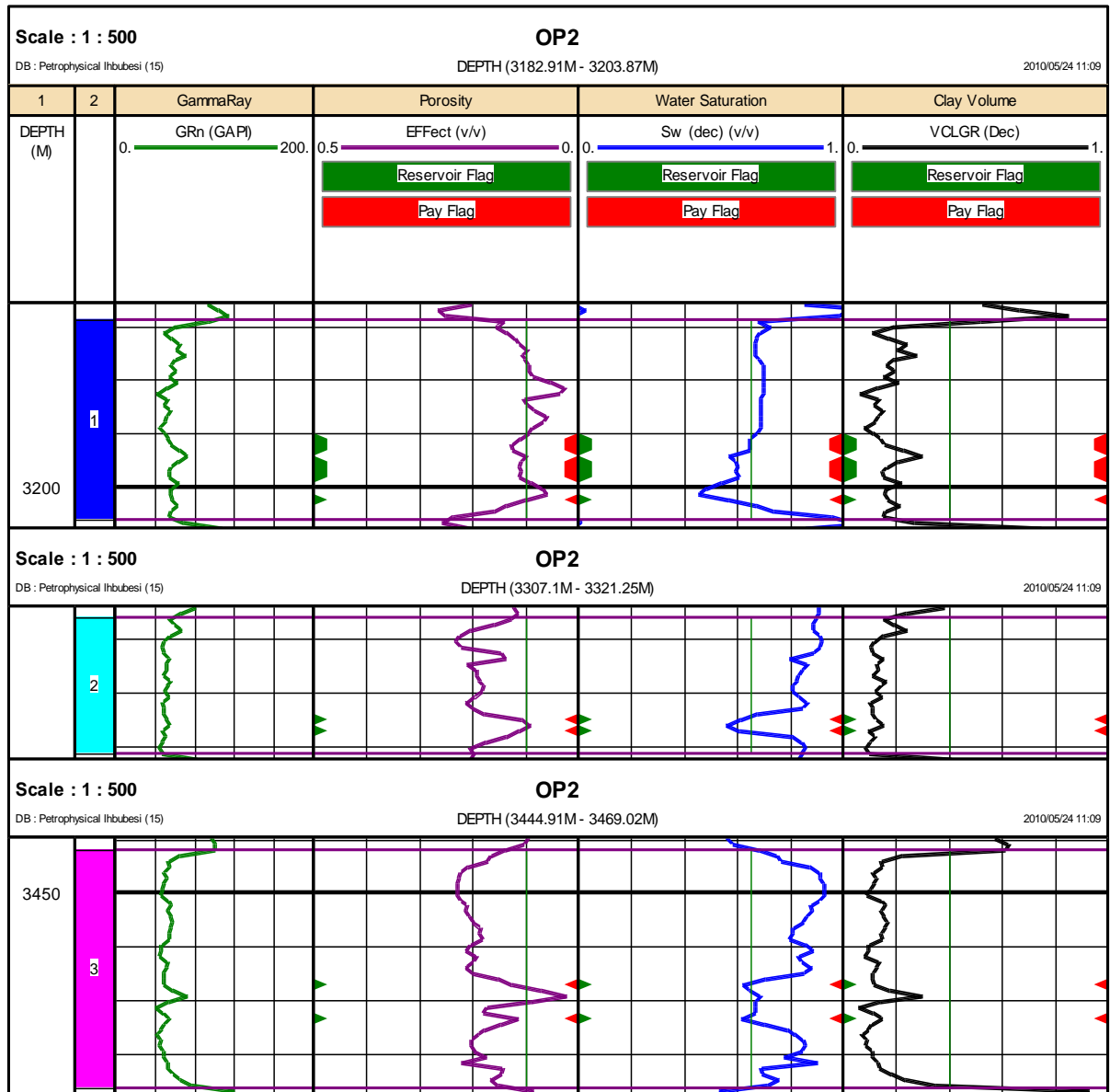


Figure 9.13: Well OP2 showing calculated reservoir parameters and pay flag

In well OP3, the gross thickness range from 9.1 to 16.9 m and net thickness from 2.33 to 13.33 m. An average porosity of 15.7 %, water saturation of 53% and volume of clay of 7 % were calculated as presented in Table 9.3 and Figure 9.14 below.

Table 9.3: Summary of calculated reservoir pay parameters for well OP3

Zone Name	Top (m)	Bottom (m)	Gross (m)	Net (m)	N/G	Av Phi (v/v)	Av Sw (v/v)	Av Vcl (v/v)
14Jt1	3230.1	3239.2	9.1	5.96	0.655	0.143	0.5	0.055
14Et1	3276.4	3286.3	9.9	5.24	0.529	0.161	0.544	0.084
14Et1	3310.1	3317.1	7	2.33	0.333	0.158	0.526	0.055
14Bt1	3354.1	3371	16.9	13.23	0.783	0.161	0.545	0.066
All Zones	3230.1	3371	42.9	26.76	0.624	0.157	0.534	0.066

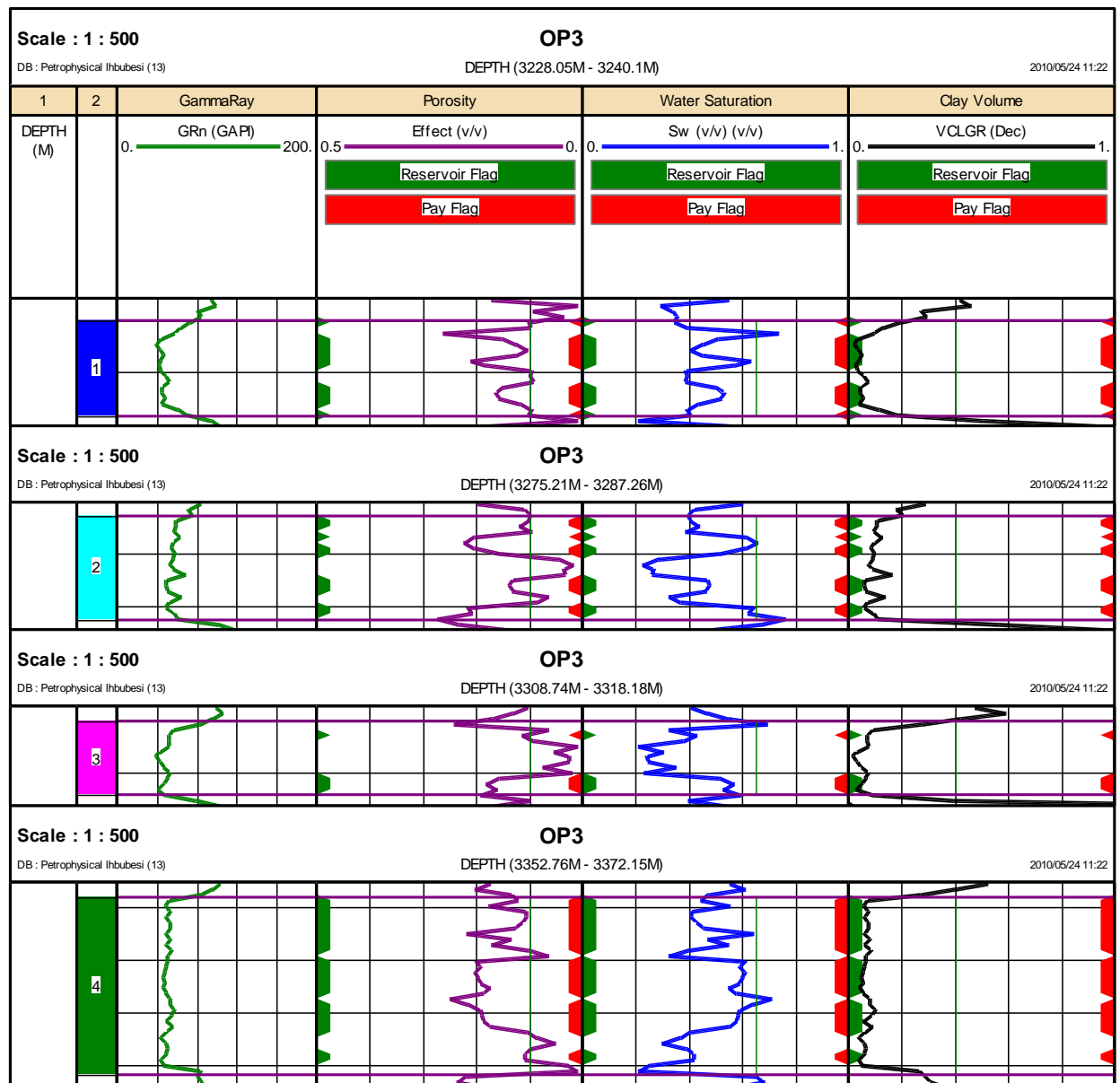


Figure 9.14: Well OP3 graphics of calculated reservoir parameters and flags

Two sandstone reservoirs were evaluated in well OP4 with total gross thickness of 35.8m and net thickness of 22.69m. An average porosity of 19.6 %, water saturation of 65 % and volume of clay of 8.5 % were calculated as shown in Table 9.4 below.

Table 9.4: Summary of calculated reservoir pay parameters for well OP4

Zone Name	Top (m)	Bottom (m)	Gross (m)	Net (m)	N/G	Av Phi (v/v)	Av Sw (v/v)	Av Vcl (v/v)
14Et1	3107.5	3122.5	15	4.48	0.299	0.125	0.534	0.126
14Et1	3236.8	3257.6	20.8	18.21	0.875	0.214	0.671	0.075
All Zones	3107.5	3257.6	35.8	22.69	0.634	0.196	0.654	0.085

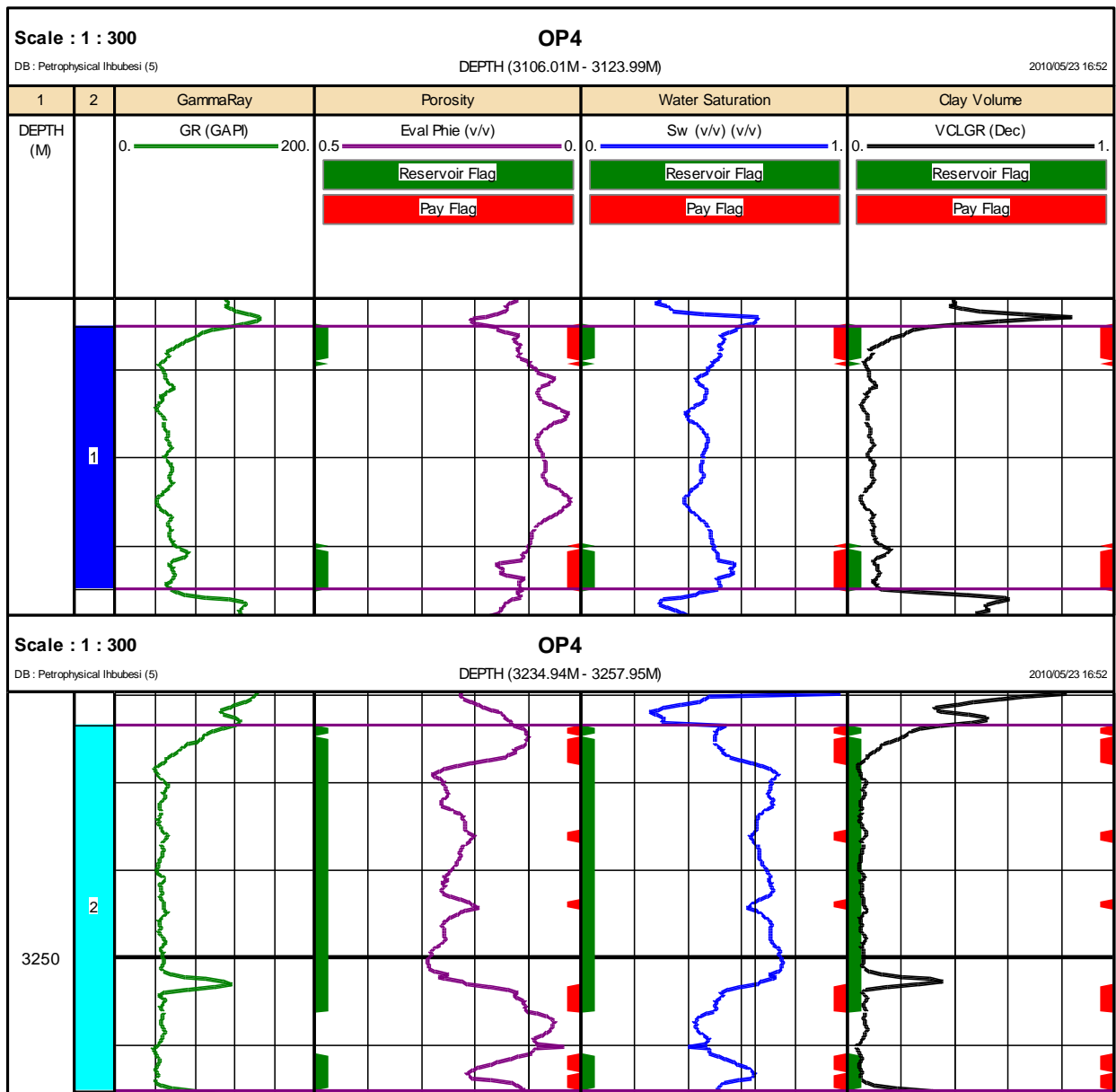


Figure 9.15: Well OP4 showing calculated reservoir parameters and flags

Two sandstone reservoirs were evaluated in well OP5 and total gross thickness of 14.7m and net thickness of 5.47m were calculated. An average reservoir porosity of 16 %, water saturation of 49 % and volume of clay of 9 % were also calculated as presented in Table 9.5 below. The graphics is shown in Figure 9.16 below.

Table 9.5: Summary of calculated reservoir pay parameters for well OP5

Zone Name	Top (m)	Bottom (m)	Gross (m)	Net (m)	N/G	Av Phi (v/v)	Av Sw (v/v)	Av Vcl (v/v)
Reservoir 1	3207.3	3213.1	5.8	2.64	0.455	0.148	0.496	0.085
Reservoir 2	3321.1	3330	8.9	2.83	0.317	0.175	0.493	0.091
All Zones	3207.3	3330	14.7	5.47	0.372	0.162	0.494	0.088

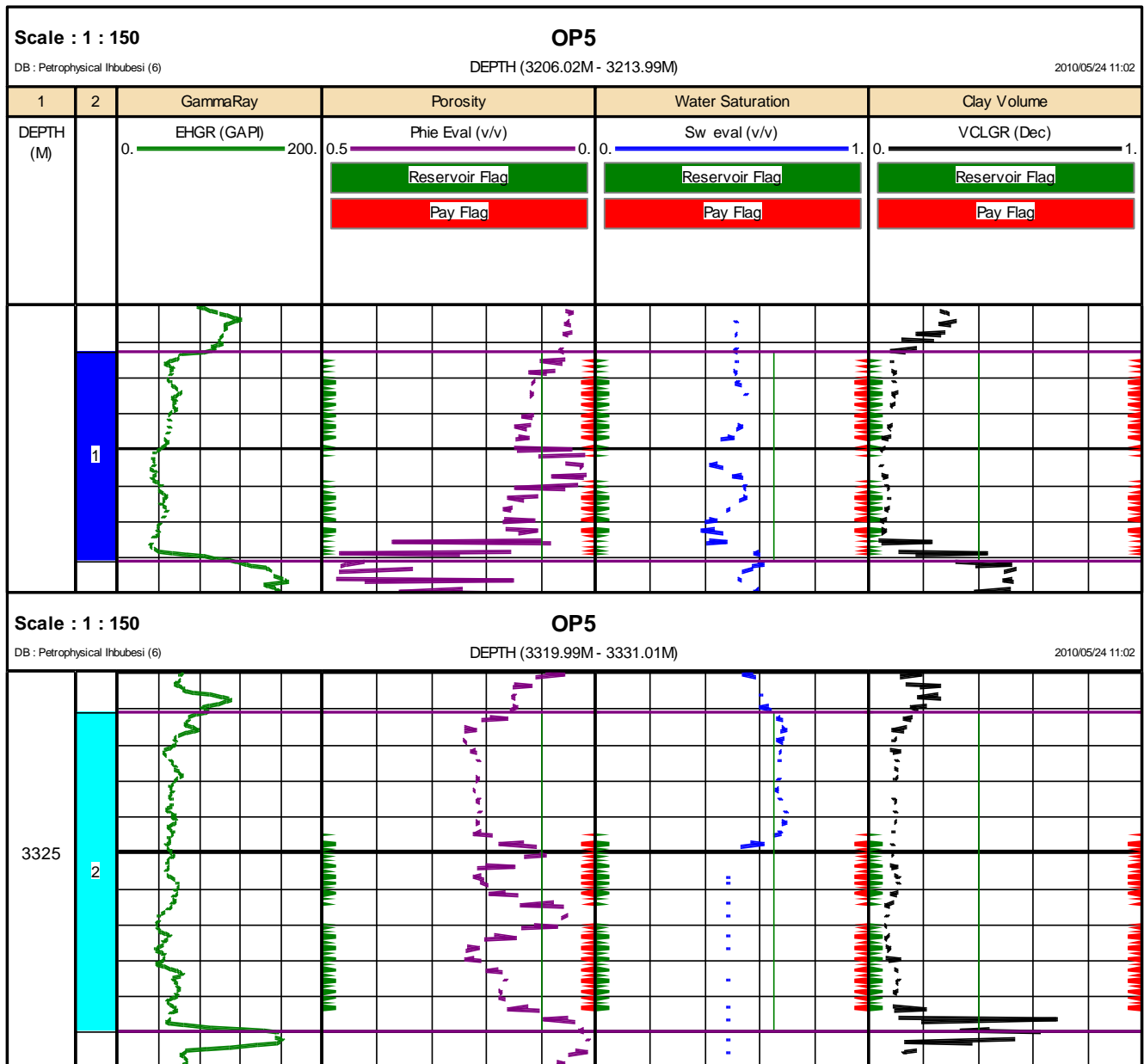


Figure 9.16: Well OP5 showing calculated reservoir parameters and flags

Four reservoir intervals with total gross thickness of 47.7m and net thickness of 28.31m were calculated for well OP6. An average porosity of 17.5 %, water saturation of 51 % and volume of clay of 8 % were also calculated as shown in Table 9.6 below.

Table 9.6: Summary of calculated reservoir pay parameters for well OP6

Zone Name	Top (m)	Bottom (m)	Gross (m)	Net (m)	N/G	Av Phi (v/v)	Av Sw (v/v)	Av Vcl (v/v)
14Et1	3196.0	3227.7	31.7	20.73	0.654	0.191	0.527	0.083
14Et1	3306.6	3309.0	2.4	1.18	0.492	0.111	0.393	0.078
14Et1	3314.0	3318.0	4.0	1.03	0.256	0.105	0.389	0.072
14Dt1	3330.0	3339.6	9.6	5.37	0.56	0.139	0.43	0.088
All Zones	3196.0	3339.6	47.7	28.31	0.593	0.175	0.506	0.083

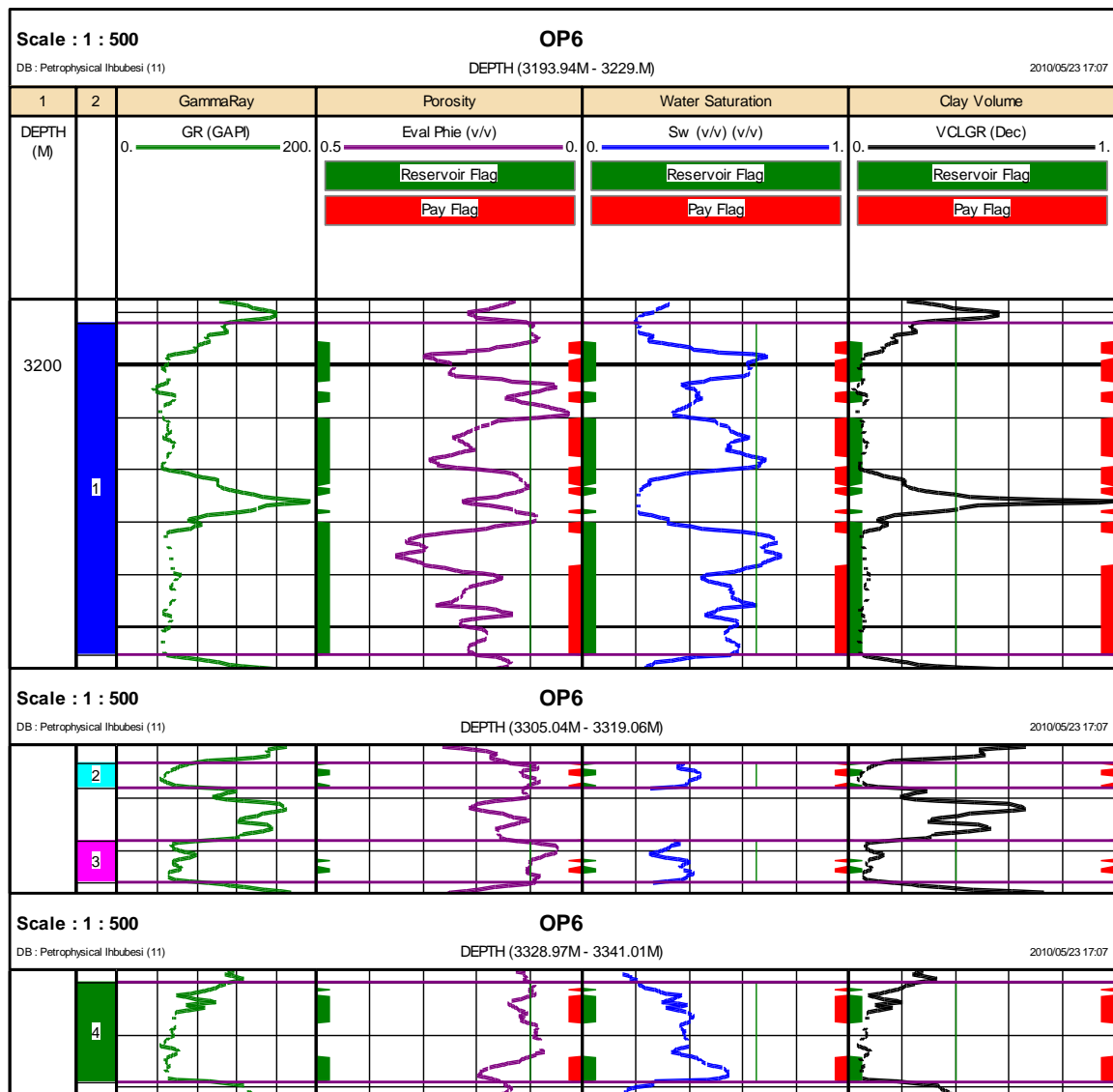


Figure 9.17: Well OP6 showing calculated reservoir parameters and flags

Two reservoirs were evaluated in well MA2 and results shows 32.1m total gross thickness, 30.58m total net thickness and average porosity of 18.7 %, water saturation of 42 % and volume of clay of 6 % were obtained as shown in Table 9.7 and Figure 9.18 below.

Table 9.7: Summary of calculated Reservoir Pay Parameters for well MA2

Zone Name	Top (m)	Bottom (m)	Gross (m)	Net (m)	N/G	Av Phi (v/v)	Av Sw (v/v)	Av Vcl (v/v)
Reservoir One	2939.9	2950.0	10.1	8.58	0.849	0.126	0.229	0.043
Reservoir Two	2956.6	2966.0	9.4	9.4	1.000	0.234	0.587	0.050
Reservoir Three	2968.0	2980.6	12.6	12.6	1.000	0.194	0.364	0.074
All Zones	2939.9	2980.6	32.1	30.58	0.953	0.187	0.424	0.058

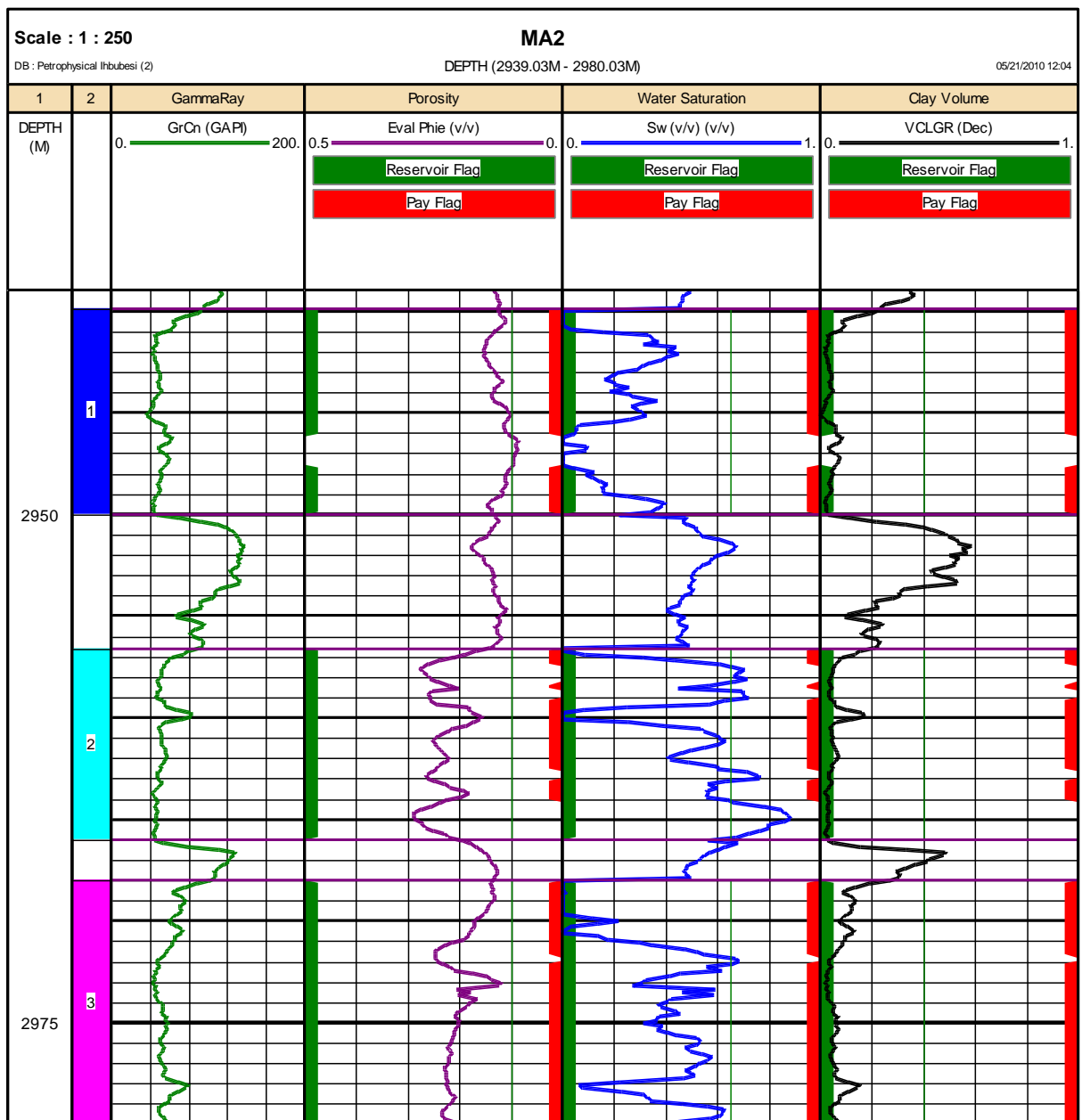


Figure 9.18: Well MA2 showing calculated reservoir parameters and flags

In well MA3, total gross thickness of 13.7m, net thickness of 10.8, average porosity of 16 %; water saturation of 42 % and volume of clay of 3 % were calculated as shown in Table 9.8 and Figure 9.19 below.

Table 9.8: Summary of calculated reservoir pay parameters for well MA3

Zone Name	Top ((m)	Bottom (m)	Gross (m)	Net (m)	N/G	Av Phi (v/v)	Av Sw (v/v)	Av Vcl (v/v)
1	3062.8	3070.4	7.6	6.99	0.92	0.159	0.382	0.019
2	3085.8	3091.9	6.1	3.81	0.625	0.17	0.474	0.038
All Zones	3062.8	3091.9	13.7	10.8	0.789	0.163	0.416	0.026

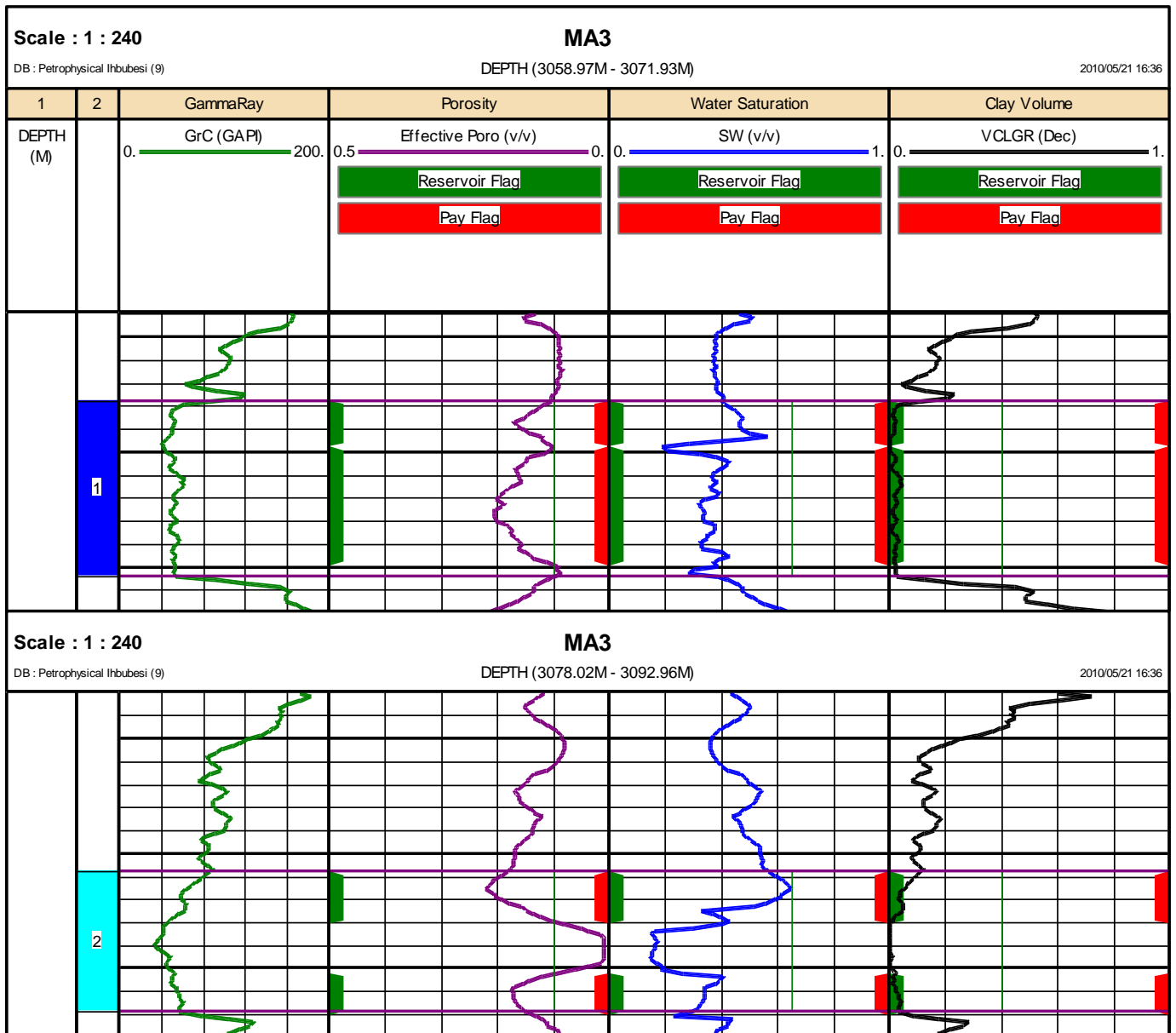


Figure 9.19: Well MA3 showing calculated reservoir parameters and flags

Total gross thickness of 46.1m; net thickness of 36.25m; average porosity of 18.9 %; water saturation of 59 %, and volume of clay of 15% were calculated for well MA4 as shown in Table 9.9 and Figure 9.20 below.

Table 9.9: Summary of calculated reservoir pay parameters for well MA4

Zone Name	Top (m)	Bottom (m)	Gross (m)	Net (m)	N/G	Av Phi (v/v)	Av Sw (v/v)	Av Vcl (v/v)
1	3150.6	3161	10.4	8.53	0.821	0.19	0.584	0.114
2	3293	3301	8	5.16	0.646	0.16	0.528	0.184
3	3332.1	3359.8	27.7	22.56	0.814	0.196	0.602	0.162
All Zones	3150.6	3359.8	46.1	36.25	0.786	0.189	0.589	0.154

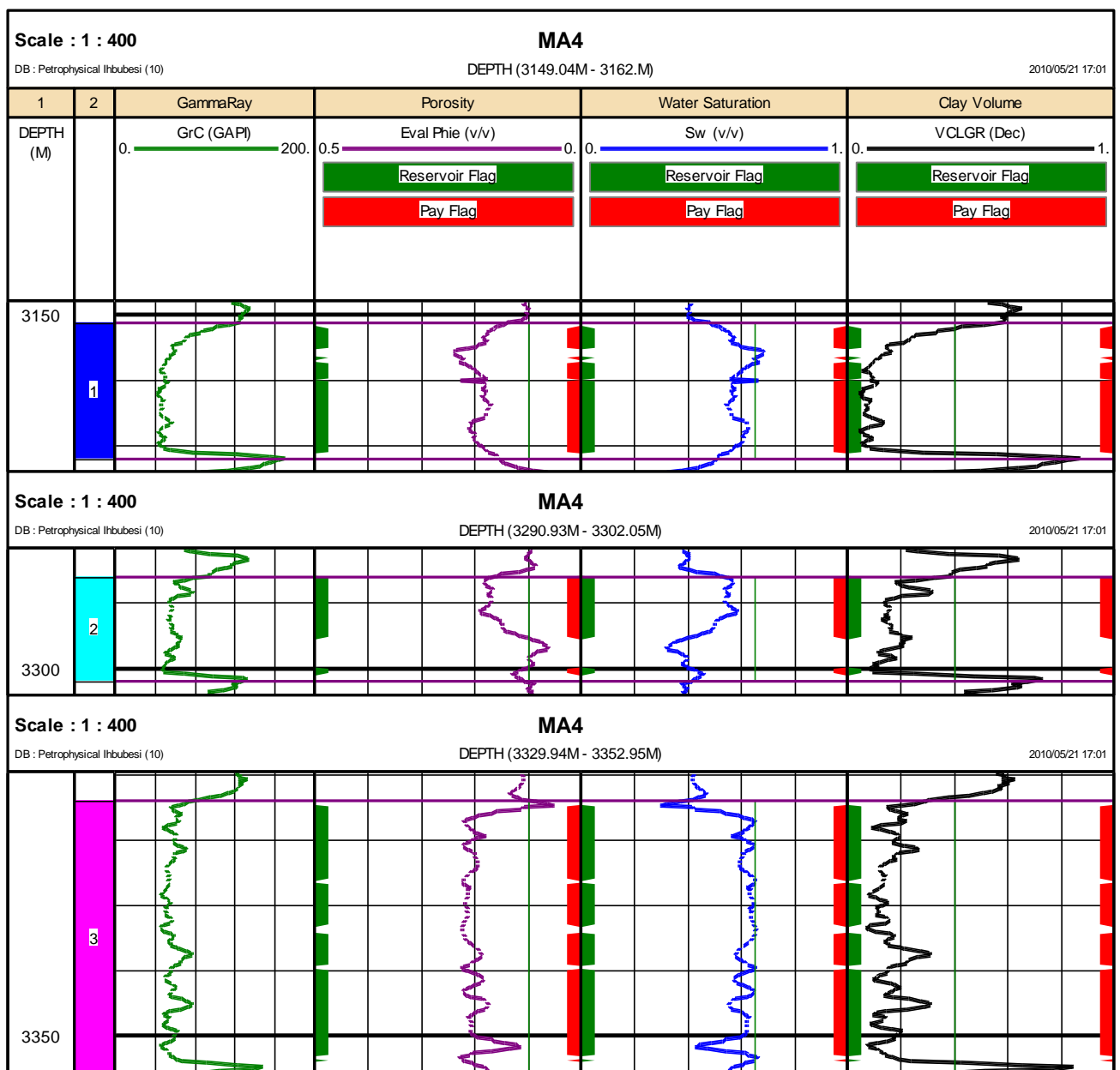


Figure 9.20: Well MA4 graphics of calculated reservoir parameters and flags

CHAPTER TEN

CONCLUSIONS AND RECOMMENDATIONS

The Petrophysical evaluation of Albian age gas bearing sandstone reservoirs of the O-M Field, offshore South Africa has been carried out. It is hoped that this thesis will serve as a guide for future studies on petrophysical evaluations. Due to the complex nature of the O-M field, the petrophysical evaluation approach was chosen to assess the reservoirs within the Albian age formation. In total, ten wells were drilled within the field, and eight of these made gas discoveries with only two being wet. The study was divided into two sections which are the basic concepts (Chapter 1 to 3) and petrophysical evaluations (Chapters 4 to 9). A brief summary of the chapters studied and recommendations for further work are presented below.

Chapter one gives the general introduction and outline to the study. The Albian age gas bearing reservoir sandstones evaluated range between 2800m to 3500m depending on the position of the well. The studied area is zoned into two, the MA zone in the Northern part of the field and the OP zone in the central and Southern part of the field. The reservoirs in the area are in a sequence of fluvial channel sands of Albian to Cenomanian age. The area is predominantly gas prone with gas being sourced from Pre-Hautervarian Lacustrine shales in rift phase half graben sub-basins and terrigenous derived type II kerogen from upper Cretaceous drift sequence. The channels are meandering systems.

Chapter two focused on the principles and uses of wireline logs. The wireline logs were grouped into active and passive tools. The active tools measure the response of formation to some form of excitations. This includes the density, neutron, resistivity and nuclear magnetic resonance tools. The passive tools measure natural occurring phenomena such as gamma radiation that is emitted by elements in the rock or electric potential caused by differences in salinity of the mud in the Well and formation water. Examples are the gamma-ray and spontaneous potential logs.

Chapter three gives the description of fundamental petrophysical properties which includes the porosity, permeability and water saturation. The main petrophysical

properties are porosity, permeability, and saturation. Porosity determines the storage capacity for hydrocarbon and permeability determines the fluid flow capacity of the rock. Saturation is the fraction of the pore spaces that is occupied by hydrocarbon or water. Accurate determination of these petrophysical properties is essential to assess the economic viability of the development of reservoirs.

The petrophysical evaluation section starts with wireline log editing and normalization in chapter four. When raw log data are collected for formation evaluation purposes, it is essential to check the quality of the data and perform editing if necessary before using it for qualitative interpretations. Log editing is a form of log interpretation aimed at removing problems that affect log readings and provide the best possible presentation of the in situ properties measured. Some of the problems encountered in the study and were corrected includes depth matching, environmental corrections, noise removal and curve matching of different RUNs into a continuous curve. After performing the editing processes, curves were normalized. Curve normalization is a mathematical process that adjusts for differences among data from varying sources in order to create a common basis for comparison.

Chapter five is the rate determining step of this research. It discussed the ground truth of conventional and special core analysis results of the key wells (OP1, OP2 and OP3) which was essential for calibration of non-cored wells. The approach adopted by Nieto Rojas (1998) for grouping lithofacies was used and six rock units (facies A1, A2, A3, A4, A5 and A6) were grouped according to textural and structural features and grain sizes. Facies A1, A2, A3, A4 and A5 were classified were classified as reservoir rocks in terms of their porosity and permeability and they showed good reservoir quality while facies A6 was regarded as no reservoir rock. The grain density value for wells showed a range of 2.58 g/cc to 2.72 g/cc with a mean grain density of 2.67 g/cc obtained from the histogram analysis which was used for other evaluations. Core porosity ranged from 1 % to 24.4 % with an average of 13.5 %. The low porosity values were recorded in intervals of clay/siltstones and the high porosity values were associated with clean sandstone intervals. Core permeability ranged from 0.006mD to 1095mD with a mean value of 10mD.

Three types of fluid saturation were obtained from core analysis of well OP1 and OP3. An average water saturation of 57 %, gas saturation of 38 % and oil saturation of 5 % was measured in well OP1. Two cores were taken in well OP3 with core 1 showing 62 % of gas saturation and 38 % of water saturation. Core 2 of the same well showed 65 % of water saturation and 35 % of gas saturation. The conventional core porosity measured at room conditions were converted to net effective overburden stress at in situ reservoir conditions (4830 psi). The cementation exponent (m) of 1.94 and saturation exponent (n) of 1.8 were determined from special core analysis measurements. The petrography study of thin section, x-ray diffraction (XRD) analysis and scanning electron microscopy (SEM) was performed in well OP2 and OP3. The study revealed mineralogy with quartz being the dominant mineral in addition to abundant chlorite as the major clay mineral. The fine textured dispersed pore lining and pore filling chlorite mineral affects the reservoir quality and may be the possible causes of the low resistivity recorded in the area.

Demonstration was made of the cation exchange capacity per pore volume (Q_v) as an effective shaliness indicator. The higher the concentration of Q_v , the higher the amount of saturation of bound water and shaliness. The porous plate method of capillary pressure measurements were performed in well OP1 and OP3, and mercury injection capillary pressure measurements were made in three plugs of well OP2. Results showed that the amount of irreducible water saturation increases, shaliness also increases and permeability decreases. The laboratory measured capillary pressure measurements were converted to reservoir conditions and saturation-height functions and universal J functions were also established.

Chapter six presents the calibration of volume of shale, porosity, and water saturations from the three key wells (OP1, OP2 and OP3). The volume of clay model from the logs was taken from the Gamma-Ray model corrected by Steiber equations. This was based on the observed levels of agreement between log and XRD volume of clay data. Log (density and neutron) and core porosities showed departures from each other at intervals of clay materials and enlarged borehole. The differences observed in both measurements may be due to the effect of authigenic clays and enlarge borehole. An empirical relationship between overburden corrected porosity from core and log

derived porosity from the sonic porosity log was established and used to estimate overburden corrected porosities in non-cored wells and intervals. An average reservoir water resistivity of 0.1 Ohm-m was determined and used in water saturation models. The shaly-sand water saturation models of Simandoux and Dual-Water best match with conventional core and capillary pressure water saturations. However, the Simandoux model was used as the field model because the input parameters could easily be controlled.

Chapter 7 of the study was on permeability, petrofacies and flow zone indicators. An empirical relationship was established from conventional core porosity and permeability plots to predict an absolute permeability in non-cored wells and intervals. Good agreement was obtained between the cored measured Klinkenberg corrected permeability and the reservoir predicted permeability. An effective permeability was determined from the repeat formation test (RFT) measurements and was compared with log estimated permeability of the Timur, Morris Biggs for gas, and the Schlumberger models. The Morris Biggs gas model best matched with the effective permeability determined from the RFT measurements. Hence Morris Biggs gas model was used to estimate effective permeability in non-cored wells.

Pore throat radius was estimated from routine core porosity and permeability measurements. The winland method was used to assess reservoir quality on the bases of pore throat radius. Five petrofacies (Petrofacies 1(mega porous), 2 (macro porous), 3(mesoPorous), 4 (micro porous) and 5(nanoporous) were classified in terms of pore throat radius. Lithofacies A1 and A2 correspond to the best reservoir quality rock (Petrofacies 1) and facies A6 which is a non reservoir rock corresponds to Petrofacies 5. The permeability/porosity (K/PHI) ratio plot was performed to determine flow efficiency. Petrofacies 1 indicated the highest flow efficiency and Petrofacies 5 the lowest flow efficiency. The methodology of Amaefule et al. (1993) was adopted to determine flow zones. Flow zone indicators (FZI) greater than 1.5 were associated with sandstone intervals and values of less than 0.7 were predominant in the clay siltstone intervals. The mega porous rocks showed values of rock quality index (RQI) in the range 1 to 2 while the nanoporous rocks displayed values of less than 0.1.

Fluid contacts from wireline pressure data and wireline logs were determined and compared in chapter 8. The interpreted water gradient ranges from 0.42 -0.45 psi/ft (0.98 -1.02 g/cc equivalent). A field water gradient of 0.44 psi/ft (1.02 g/cc) was obtained. Gas gradient ranged from 0.07 – 0.13 psi/ft (0.15 – 0.3 g/cc equivalent). An interpreted field gas gradient of 0.09 psi/ft was obtained.

The gas water contact (GWC) determined from RFT and Log were generally in close agreement. The log resistivity and combination of neutron/density data were useful in locating fluid boundaries. Gas effects on neutron/density were not observed in most of the wells. Eight gas water contacts were identified in six wells of the area studied.

Results obtained from chapters 4 to 8 were applied to chapter 9 in order to estimate petrophysical properties in non-cored wells and intervals. Cut-off values of 10 % for porosity, 40 % for volume of shale and 65 % for water saturations were used as reference parameters that distinguished between pay and no pay intervals. For an interval to be regarded as having pay, it must have porosity values of at least 10 %, volume of shale of not more than 40 % and water saturation of 65 % or less.

RECOMMENDATIONS

This thesis has only considered the multi-mineral petrophysical evaluation approach by integrating core data, wireline logs and production tests results for better estimate of static reservoir properties. In the future, the following tasks are considered to be important for further developments in the area.

- ❖ The new generation wireline logs (example nuclear magnetic resonance log) be run in the Wells and be integrated with core, seismic and production test data sets to have a better robust models.
- ❖ Artificial neural network method may be used in future studies to predict permeability of the formation and confirm results of this study.
- ❖ The selection of core samples for special core analysis must be done based on different rock types present in order to guarantee greater precision in determining reservoir heterogeneity. If selection is based on rock types, a better correlation between petrofacies and lithofacies is achieved. If the core plugs are not accessible, sidewall rotary core plug could be used for sample selections.

- ❖ Only single phase permeability has been calculated in this thesis. A deterministic petrophysical evaluation approach to evaluate the multiphase flow simulation models should be a topic for further research.
- ❖ Mercury injection capillary pressure measurements to be performed in the key wells in order to obtain a broad range of capillary pressures and reasonably accurate results.
- ❖ The volume of reserve can be estimated based on the determined petrophysical properties of wells studied in order to quantify the gas original in place (GOIP). This was not part of the objective of the present research.

REFERENCES

Adams SJ (2005): Core-to-log Comparison-What's a good match? Society of Petroleum Engineers Annual Technical Conference and Exhibition, Dallas, Texas.

Al-Dhafeeri AM, Nasr-El-Din HA (2006): Characteristics of high-permeability zones using core analysis and production logging data. *Journal of Petroleum Science and Engineering*, doi: 10.1016.

Amaefule JO, Altunbay M, Tiab D, Kersey DG, Keelan DK (1993): Enhanced reservoir description: Using core and log data to identify hydraulic flow units and predict permeability in uncored intervals/wells. Society of Petroleum Engineers, paper 26436, 88th Annual Technical Conference and Exhibition ; 205-220.

Archie GE (1942): The Electrical resistivity log as an aid in determining some reservoir characteristics. *Transaction of AIME* 146; 54.

Asquith GB, Gibson (1983): Basic well Log analysis for geologists' text book. American Association of Petroleum Geologist, Tulsa, Oklahoma, USA; 29.

Bassiouni Z (1994): Theory, Measurement, and interpretation of well logs. Society of Petroleum Engineers, textbook series, vol 4; p.329.

Bastia R (2004): Depositional model and reservoir architecture of tertiary deep-water sedimentation, Krishna-Godavari Offshore Basin, India. *Journal of Geology Society of India* 64; 11-20.

Bateman R (1985): Open-hole log analysis and formation Evaluation: Boston, International Human resources Development Corporation; 647.

Bear J (1972): Dynamics of fluids in porous Media, Elsevier, New York.

Boada E, Barbato R, Porras JC, Quaglia A (2001): Rock Typing: Key Approach for Maximizing use of old well log data in Mature Fields, Santa Rosa field Case study. SPE 69459, Texas, USA.

Boggs Sam Jr (2006): Principles of sedimentation and Stratigraphy, 4th Ed; New Jersey, Pearson Education Incorporated.

Brown LF, Benson JM, Brink GJ (1995): Sequence Stratigraphy in Offshore South Africa divergent basins; An Atlas on Exploration for cretaceous lowstand traps by SOEKOR (pty) ltd. AAPG Studies in Geology 41.

Chi S, Carlos TV, Wu J, Alpak OF (2004): Assessment of mud-filtrate invasion effects on borehole acoustic logs and radial profiling of formation elastic parameters, SPE International, 90; 159.

Clavier C, Coates G, Dumanoir J (1984): Theoretical and Experimental bases for the Dual-water Model for interpretation of shaly-sands. SPE Journal, Vol; 24, no 2; 153-168.

Clavier, Huyle WR, Meunier D (1971): Quantitative Interpretation of T.D.T Logs; Part 1 and 11, Journal of Petroleum Technology, No. 6.

Coates G, Denoo S (1981): The producibility answer product. The technical Review Schlumberger, Houston, No.2; 55-63.

Cobb MW, Marek FJ (1998): Net pay determination and waterflood depletion mechanisms, SPE 48952, in the Annual Technical Conference and Exhibition; 14.

Core Laboratories (1973): A course in the Fundamentals of Core Analysis: Texas core laboratories, Inc; 256.

Core Laboratories (1982): A course in special Core Analysis 5-21, Dallas.

Cosentino L, Sabathier J (2001): Integrated réservoir Studieuse. Institut français du pétrole publications, Édition TECHNIP ; 120.

Crain ER (1986): The log Analysis Handbook; Penn-Well Publishing Company, Tulsa, Oklahoma, USA.

Crain ER (2001): Crain's Petrophysical Handbook, Penn -well.

Cuddy S, Allison G, Steele R (1993): A simple, convincing model for calculating water saturations in Southern North Sea gas fields. SPWLA 34th Annual logging Symposium,

Dalhberg EC (1994): Applied Hydrodynamics in Petroleum Exploration, second Edition, New York, Springer-Verlag ; 295.

Daniel SE (2004): Well log Normalization, Methods and Guides.

De Ros F L, Goldberg K (2007): Reservoir petrofacies tool for quality characterization and Prediction. AAPG, annual convention and exhibition, April 1 -4, long Beach, CA.

Dewan JT (1983b): Essentials of modern open-hole log interpretation, Penn -well Publishing Company, Tulsa, Oklahoma; 239.

Dias MM, Payatakes AC (1986): Network models for two-phase flow in porous media,2,motion of oil ganglia. Journal of Fluid Mechanics,vol 164,pp 337.

Djebbar T, Donaldson EC (1999): Theory and practice of measuring reservoir rock and fluid transport properties.Butterworth-Heimann,USA.

Dresser Atlas (1979): Log Interpretation Charts; Houston, Dresser Industries Inc.

Dullian FAL (1979): Porous Media Fluid Transport and Pore Structure, 1st Edition, Academic Press, New York, USA.

Ebanks Jr WJ (1987): Flow Unit concept-Integrated approach to reservoir description for engineering projects(abstract), AAPG, bul; vol; 71; 55-552.

Elfenbein C, Husby Q, Ringrose PS (2003): Geological-based estimation of kv/kh ratios: An Example from the Garn formation, Tyrihans Field, Mid-Norway. Proceedings of the 6th Petroleum Geology and Global Perspectives. The Geological Society of London.

Ellis DV, Singer JM (1987): Well logging for Earth Scientist.

Emerson DW (2000): The petrophysics of the Hawkesbury sandstones. Geological Society of Australia; Environment and Hydrogeology Specialist group monograph 5; 197.

Engineering Data Book (1977): Gas Processors Suppliers Association, 9th Edition, and Tulsa, Oklahoma.

Fens TW (2000): Petrophysical properties from small rock samples using image analysis techniques. Delft University Press, Stevinweg, Netherlands.

Fertl WH, Stapp WL, Vaello DB, Vercellino WC (1980): Spectral Gamma Ray logging in the Texas Austin Chalk Trend. Journal of Petroleum Technology.

Forest Oil Exploration International (Forest, Report) (2001): Petrography study for Forest Oil International, Republic of South Africa for Wells in Ibhubesi field, Orange Basin, South Africa (unpublished).

Fraser HJ, Gratton LC (1935): Systematic packing of sphere with particular relations to porosity and permeability. Journal of Geology; 785.

Garven G (1986): The role of regional fluid flow in the genesis of the Pine Point deposits, western Canada sedimentary basin. Economical geology, vol 81, no 4, pp1015.

Gauchet R (1993): Capillary Pressure Measurements by centrifuge and mercury Injection. Elf Aquitaine Production-Internal Report No 93.602.

Gearhart-Owens Industries (1972): GO Log Interpretation Reference Data Handbook. Fort Worth, Gearhart-Owens, Industries Inc; 226.

Genliang G, Marlon AD, Francisco, Smalley J, Eric AW (2007): Rock typing as an effective tool for permeability and water saturation modelling: A case study in a clastic reservoir in the Oriente Basin. SPE Reservoir Evaluation and Engineering, vol; 10; No 6; 730.

George CJ, Stile LH (1978): Improve techniques for evaluating carbonate waterfloods in West Texas, Journal of Petroleum Technology, vol 30, no 6; 1547 -1554.

Guest (1990): The use of core derived quantitative mineralogical data to improve formation Evaluation; European core analysis Symposium; 187.

Gunter GW, Finneran JM, Hartman DJ, Miller JD (1997): Early determination of reservoir flow units using an integrated Petrophysical method. SPE 38679, San Antonio Texas.

Hagelberg T, Shackleton N, Pisia N, Shipboard Scientific Party (1992): Development Of composite depth sections for sites 844 through 854 in Mayer, LPisia N et al; Proc.ODP, Init Repts, 138(pt1): College Station Texas.

Halliburton (2001): Basic Petroleum Geology and Log Analysis; 35, 72.

Harrison, Jing XD (2001): Saturation height methods and their impact on volumetric hydrocarbon in place estimates. SPE, ATCE, New Orleans, Louisiana.

Hartman DJ, Coalson EB (1990): Evaluation of the Morrow sandstones in the Sorrento field, Cheyenne County, Colorado. RMAG Symposium; 91.

Hartmann DJ, Beaumont EA, Coalson E (2000): Prediction sandstone reservoir system quality and example of petrophysical evaluation. Search and discovery 40005.

Hearn CL, Ebank WJ, Tye RS, Ranganathan (1984): Geological factors influencing reservoir performance of the Hartzog draw field, Wyoming. *Journal of Petroleum technology* 46; 1335.

Helander DP (1984): *Fundamental of Formation Evaluation*. Publisher; Oil and gas Consultants, 2nd Edition.

Heslop A (1972): Gamma-Ray Log response of shaly sandstones: Canadian Well Logging Society, vol 5; 29.

Heslop K, Heslop A (2003): *Interpretation of Shaly-Sands*: Logx Inco; Anadarko Canada Corp, archive//heslop_shaly-sands.htm.

Hilchie DW (1978): *Applied Open Hole log Interpretation*, Golden Company.

Hill HJ, Shirley OJ, Klein GE (1979): Bound water in shaly sands-its relation to Qv and other formation properties. *The log Analyst*.

Holmes M (2002): *Capillary Pressure and Relative Permreability Petrophysical Reservoir models*. Digital formation Incorporated, Denver, Colorado, USA. pp3. www.digitalformation.com

Hughes B (2002): *Introduction to Wireline Log Analysis*; Baker Hughes Inc.

Hunt JH (1990): generation and migration of petroleum from abnormal pressured fluid compartments. *American Association of Petroleum Geologist Bulletin*, 74; 1-2.

Hurst A (1987): Problem of reservoir characterisation in some North Sea sandstone reservoirs solved by the application of Micro scale geological data. *North Sea Oil and Gas reservoirs*, Graham and trot man; 153.

Hurst A, Archer JS (1986): Some application of clay mineralogy to reservoir description. *Clay Minerals*, vol 21; 811-826.

Hurst J, Archer JS (1986): Sandstone reservoir description: An overview of the role of Geology and Mineralogy. Clay minerals 21; 791-809.

John D, Marin P (2006): Practical Advances in core based water saturation analysis of shaly tight gas sands. Core laboratories, Houston, Texas; 3-14.

Johnson A (1987): Permeability averaged capillary data; A supplement to log analysis in field studies. SPWLA, 28th Annual logging Symposium.

Juhasz I (1981): Normalized Q_v - the key to shaly sand evaluation using the Waxman-smith's equation in the absence of core data. Transaction of SPWLA 22nd Annual logging Symposium,p. 1-36.

Juhasz I (1990): Core Analysis: Opportunities and challenges in the 1990s: European core analysis Symposium; 1-15.

Jungslager EHA (1999): Petroleum habitats of the Atlantic margin of South Africa. Geological Society London, Special Publications; 153.

Kamel MH, Mabrouk WM (2002): An equation for estimating water saturation in clean formations utilizing resistivity and sonic logs: Theory and application. Journal of Petroleum Science and Engineering, vol. 36; 2.

Keith K (2008): What is Shale to a petrophysicist? The leading Edge,vol 27; no.6; p.738.

Kolodzie S (1980): Analysis of Pore throat size and use of the Waxman-Smits equation to determine OOIP in Spindle field, Colorada; SPE 55th Annual fall Technology Conference; 10.

Krygowski DA (2003): Guide to petrophysical Interpretation. Austin Texas USA.

Leverett MC (1941): Capillary behaviour in porous solids. Petroleum transactions of AIME, 142; 152.

Levorsen AI (1967): Geology of Petroleum, 2nd Edition; W.H Freeman and Co; San Francisco.

Link PK (1982): Basic petroleum Geology, 2nd Edition. OGCI Publications, Tulsa, OK; 425.

Lovell MA, Harvey PK, Jackson PD, Brewer TS, Williamson G, Williams C (1998) : Interpretation of log and core data-Integration or Calibration? Geological Society of London, Special Publication, vol.136, p.39-51.

Luca C, Jean-Claude S (2001): Integrated réservoir Studies. Institut français du pétrole publications, édition TECHNIP, pp120.

Mabrouk WM (2005): BVW as an indicator for hydrocarbon and reservoir homogeneity. Journal of Petroleum Science and Engineering, Elsevier, vol; 49; 57-62.

Michael H (2002): Capillary Pressure and Relative Permeability Petrophysical Reservoir Model. Digital Information Inc.; Denver, Colorado, USA ; 3.

Mishra BK, Sharma MM (1988): Measurement of Pore size distributions from capillary pressure curves. ALCHE Journal, April 1988; vol34, No 4.

Moran K (1995): Sediments elastic properties applied to the Ocean drilling Program composite depth scale: examples from Leg 154, Ceara rise. 5th International Conference of Paleocoenogram. Halifax (Abstract).

Morris RL, Biggs WP (1967): Using log derived values of water saturation and Porosity. Trans; SPWLA, Annual logging Symposium.

Mostafa HK, Walid MM (2002): An equation for estimating water saturation in clean formations utilizing resistivity and sonic logs: theory and applications. Journal of Petroleum Science and Engineering, vol. 36, p.159-168.

Muntingh A (1993): Geology, prospects in Orange Basin offshore western South Africa. Oil and Journal 25; 106-108

Newman ACD (1987): The interaction of water with clay mineral surfaces. In chemistry of clay and clay minerals, Harlow, England. Longman scientific and Technical; 237-274.

Nieto, Rojas N (1998): Caracterización geológica y petrofísica del yacimiento K2 en los campos Apiay, Suria y Libertad. ECOPETROL, Internal reporte.

Nyberg O, Lien K, Lingberg PA, Smistad JK (1978): Mineral composition, an aid classical log analysis used Jurassic sandstones of the Northern Sea: SPWLA 19th Annual Logging Symposium; 1- 35.

Omaregie ZS (1986): Factors affecting the Equivalency of different capillary pressure measurement techniques. SPE 15386.

Patchett JG, Coalman EB (1982): The determination of porosity in sandstone and shaly sandstone, part2, SPWLA 23rd Annual Logging Symposium; 36.

Pelliaier-Combescure J, Pollock D, Wittmann M (1979): Application of Repeat Formation Tester pressure measurements in the Middle East. SPE, 7775.

Person GG, Raffensperger M (1996): Basin scale hydrological Modeling, Rev Geophysics' 34 (1); 67-87.

Petroleum Agency of South Africa (PASA report) (1989): Petroleum agency brochure (unpublished).

Petroleum Agency of South Africa (2000): Petroleum Agency of South Africa Bulletin; South Africa Petroleum Exploration opportunities.

Petroleum Agency of South Africa (PASA Report) (2001): Petroleum Agency Brochure (unpublished).

Petroleum Agency of South Africa (PASA report) (2005): Petroleum agency brochure.

Petrolog (2006): Software module overview. Petrolog Vol 10.2 help manual

Pirson SJ (1958): Oil Reservoir Engineering, 2nd edition, New York; McGraw-Hill; 735.

Pittman ED (1992): Relationship of Porosity and Permeability to various parameters derived from mercury injection capillary pressure curves for sandstones; AAPG Bulletin, vol 76, No.2; 191-198.

Porras JC, Barbato R, Khazen L (1999): Reservoir flow units: A comparison between three different models in the Santa Barbara and Pirital fields, North Monagas area, Eastern Venezuela Basin: SPE Latin American and Caribbean Petroleum Engineering Conference, SPE paper 53671; 7.

Porras JC, Campos N (2001): Rock typing: A key Approach for Petrophysical characterization and definition of flow Units, Santa Barbara field, Eastern Venezuela Basin. SPE 69458.

Poupon A, Leveaux J (1971): Evaluation of water saturation in shaly formations; Trans. SPWLA 12th Annual Logging Symposium; 2.

Raymer LL, Hunt ER (1980): An improved sonic transit time to porosity transform. SPWLA 21st Annual logging symposium, Lafayette, LA.

Rider MH (1996): The geological Interpretation of well logs; John Wiley and sons, New York.

Roger GW, Noel PJ (1992): Facies Models response to sea level change. Geological association of Canada. Love Printing service Ltd, Stilts Ville, Ontario, pp2.

Russel WL (1944): The Total Gamma- Ray Activity of Sedimentary Rocks as indicated by Geiger-Counter Determinations. Geophysics, April 1944.

Saibal B, Alan PB, Watney WL, John HD (2008): Flow unit modelling and fine-scale predicted permeability validation in Atokan sandstones: Norcan east field, Kansas. AAPG Bulletin, vol 92, no 6; 709-732.

Schlumberger Ltd (1972): Log Interpretations Principles. Volume 1.

Schlumberger (1987): Log Interprétation Principles/Applications. New York.

Schlumberger Ltd (1989): Log Interpretation Principles/Applications. New York.

Schlumberger ltd (1995): Log Interpretation charts, Houston, Texas.

Schutjens PM (1991): Intergranular pressure solution in halite aggregates and quartz sands; an experimental investigation, PhD thesis, University of Utrecht, Netherlands.

Scott G, Manuel J, Robert RC, Charles EG, Ken M (2004): Well log Normalization and Comparative volumetric analyses of gas hydrate and free-gas resources, Central North Slope, Alaska.

Serra O (1984): Fundamental of well logging Interpretation. Elsevier Science Publisher, BV; 142.

Serra O (1986): Developments in petroleum science: Fundamentals of well log interpretation 2. The interpretation of logging data, v15b; New York, Elsevier science publishing Company incorporated; 684

Shier ED (2004): Well log Normalization, Methods and Guides.

Simandoux P (1963): Dielectric Measurements on Porous Media: Application to measurement of water saturation. Study of the behaviour of argillaceous formation. SPWLA, Houston, vol; 97-124.

Skelt C, Harrison (1995): An integrated approach to saturation height analysis. SPWLA 36th Annual logging Symposium.

SPWLA (1984): Society of Petrophysicists and Well Log Analysts. www.spwla.com

Steiber RG (1973): Optimization of Shale Volumes in Open Hole Logs. Journal of Petroleum Technology.

Stolz, A, Graves RM (2003): Sensitivity study of flow unit definition by use of reservoir simulation: SPE paper 84277; 14.

Sua J, Spurlin J (1982): Interpretation of micaceous sandstones in the North Sea. SPWLA 16th Annual logging symposium; 32.

Suzanne GC, Robert MC (2004): Petrophysics of the Lance Sandstone Reservoirs in Jonah Field, Sublette County, Wyoming. AAPG Studies in Geology 52 and Rocky Mountain Association of Geologists 2004 Guidebook; 226-227.

Tiab D, Donaldson EC (1999): Theory and Practice of measuring reservoir rock and fluid transport properties. Butterworth-Heimann, USA.

Timmerman EH (1982): Practical Reservoir Engineering, Part 1. Methods for improving accuracy or input into equations and computer programs. Pennwell Publishing Company, Tulsa, Oklahoma; 102.

Timur A (1968): An investigation of Permeability, Porosity, and Residual water Saturation Relationships for Sandstone Reservoirs. Log Analyst, 9, 4; 8-17.

Van der Spuy D (2002): What of the synrift? Graben plays in the Orange Basin, South Africa. First annual International symposium .Poster 7.PESGB, London.

Walid MM (2005) : BVW as an indicator for hydrocarbon and reservoir homogeneity. Journal of Petroleum Science and Engineering,vol; 49,p.57-62.

Walker RG, James NP (1992): Facies Models response to sea level change. Geological Association of Canada. Love Printing service Ltd, Stiltsville, Ontario; 2.

Waxman MH, Smith LJ (1968): Electrical conductivities in oil bearing shaly-sands. Journal of Petroleum Technology; 107.

Winland HD (1972): Oil accumulation in response to pore size changes, Weyburn field, Saskatchewan. Amaco Production Research Report, No. F72-G-25.

Winsauer WO, McCardell WM (1953) : Ionic double layer conductivity in reservoir rocks. Transactions of AIME,vol 198,p.129.

Worthington PE (1985): The evaluation of shaly sand concepts in reservoir evaluation. The log Analyst.

Worthington PF (2008): The Application of Cut-Offs in Integrated Reservoir Studies. SPE Reservoir Evaluation and Engineering (SPE 95428).

Worthington PF, Cosentino (2005): The role of Cut-Offs in Integrated Reservoir Studies. SPE Reservoir Evaluation and Engineering (4). SPE 84387.

Wyllie MRJ (1963): The fundamentals of Well Log Interpretation. New York Academic Press.

Wyllie MRJ, Gregory AR, Gardner GHF (1958): An experimental Investigation of factors affecting elastic wave velocities in porous media.Geophysics, vol.23.

Wyllie MRJ, Rose WD (1950): Some theoretical considerations related to the Quantitative Evaluation of Physical Characteristics of reservoir Rock from Electrical log Data. Trans; AIME, 189.

Yan J, Lubbe R, Waters K, Pillar N, Anderson E (2008): Log quality assessment and data correction for AVO.& 10th EAGE Conference and Exhibition, Rome Italy.

Zhang P, Ringrose P, Langeland H, Nordahl K, Elfenbein C, Naess A (2004): Permeability Re-Scaling and near well bore Modeling of heterogeneities in the lower Jurassic tidal influenced tilje Formation, Heidrun Field.

APPENDICES

APPENDIX A: LOGGING TOOL CODE AND TOOL DESCRIPTION

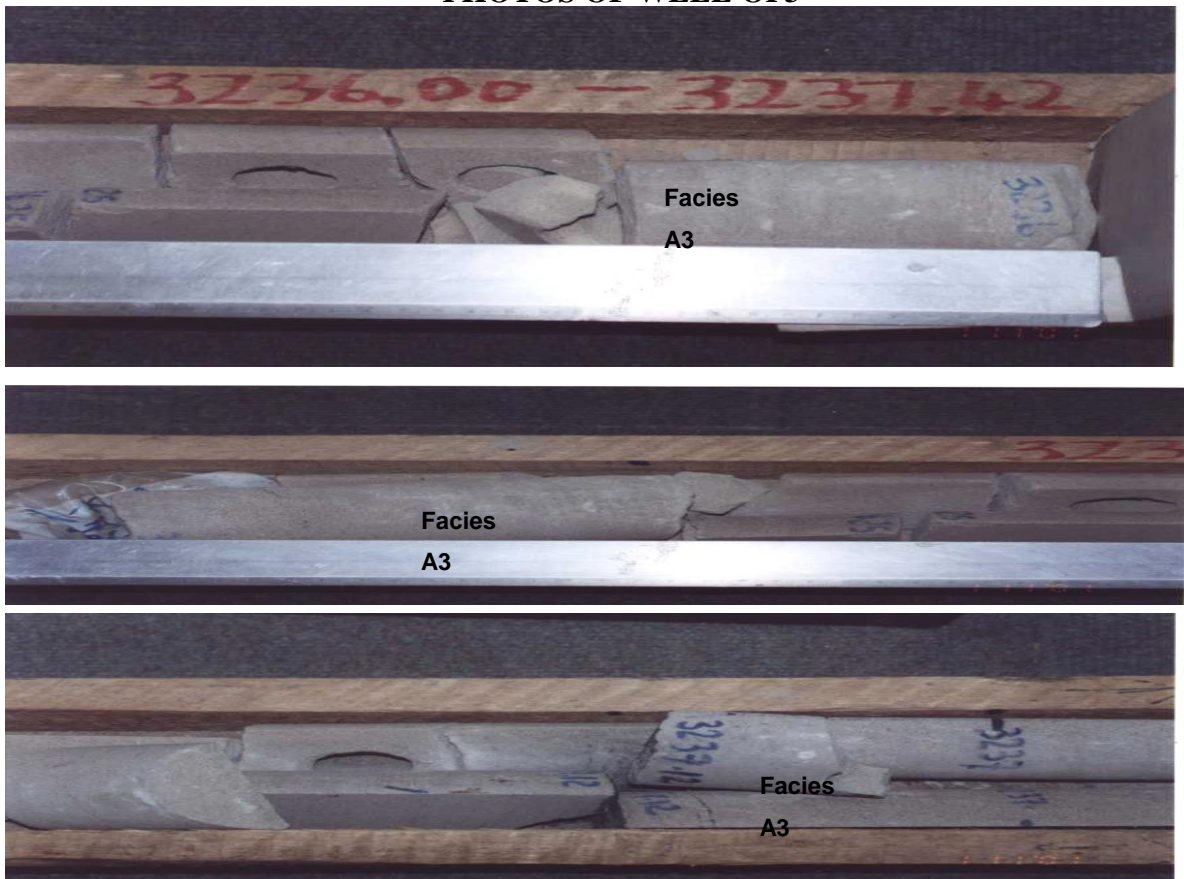
Tool Code	Tool description
AIT	Array Induction Imager
CNL	Compensated Neutron log
DSI	Dipole Shear Sonic Imager
GR	Gamma Ray
HALS	High Resolution Azimuth Laterlog sonde
LDT	Litho Density
MCFL	Micro-Cylindrically Focused Log
SHDT	Stratigraphic High Resolution Dipmeter Tool
SP	Spontaneous Potential
TLD	Three Detector Lithology Density
NGT	Natural Gamma Ray Spectrometry
VSP	Vertical seismic Profile
PEX	Bulk Density Photo-electric Effect log
BHC	Borehole Compensated Sonic tool
ISF	Induction spherical Focused Log

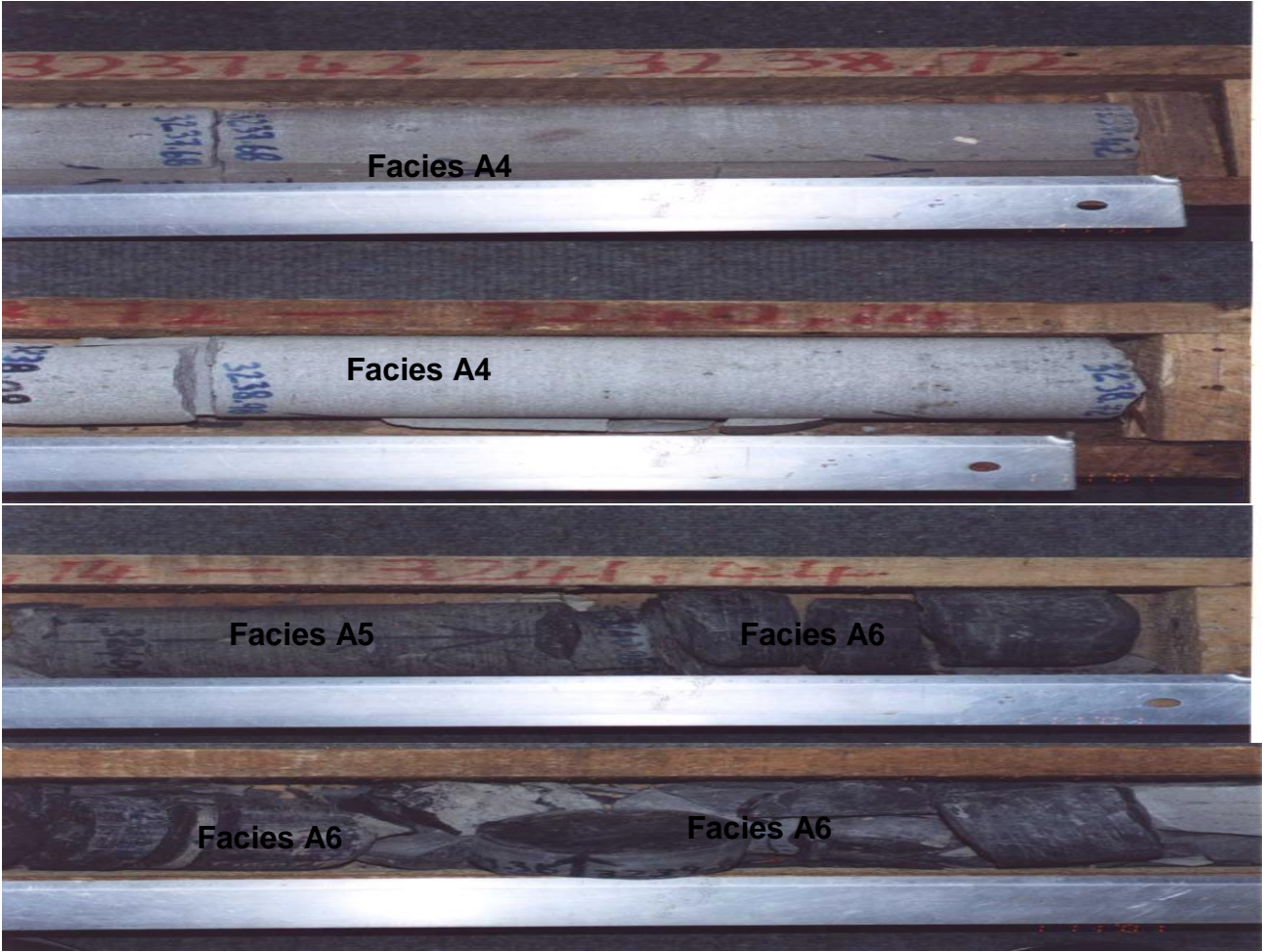
APPENDIX B: CORE PHOTOS

WELL OPI CORE PHOTOS



PHOTOS OF WELL OP3

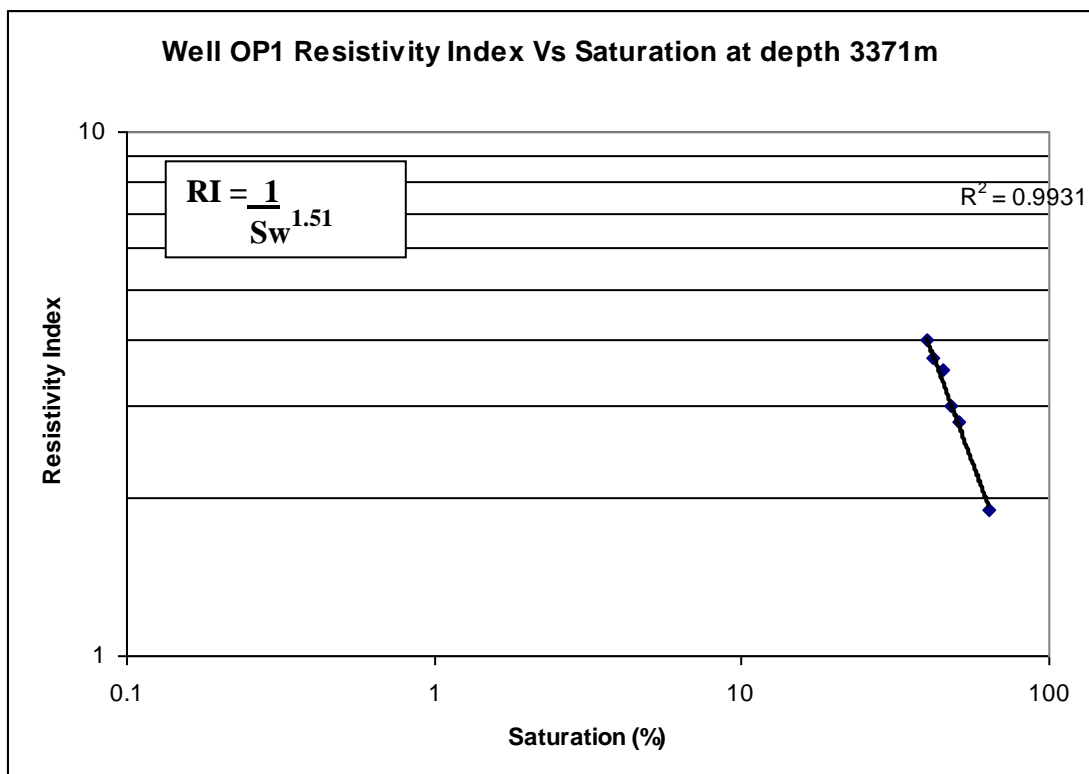
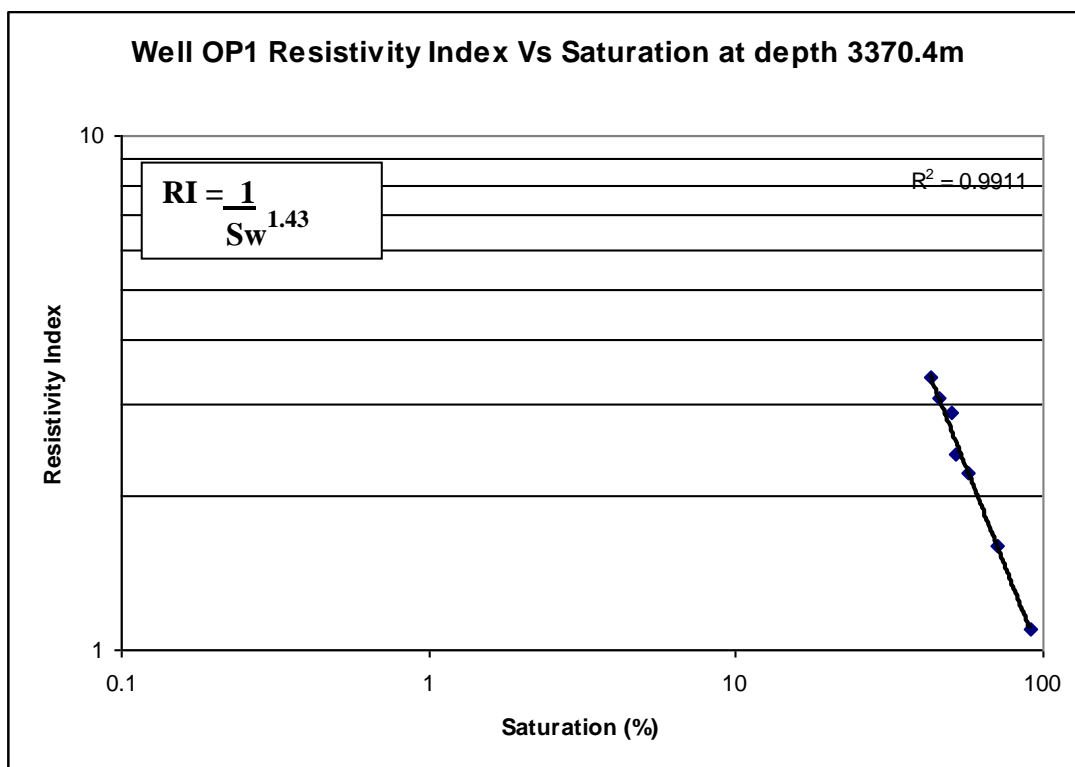


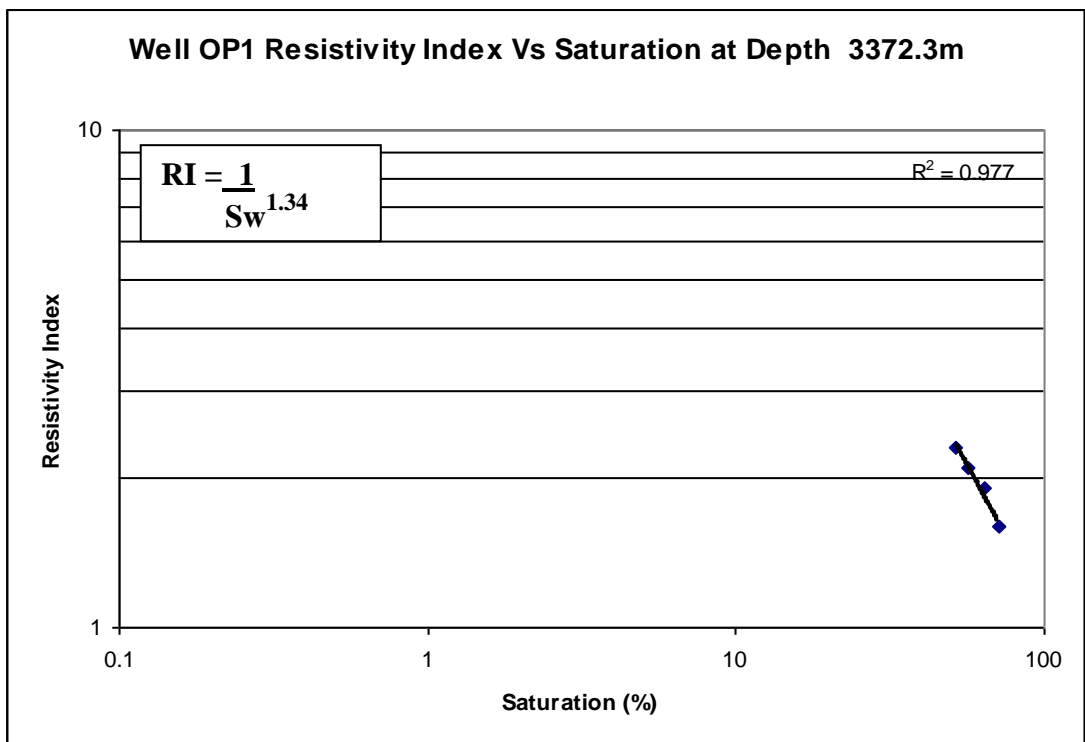
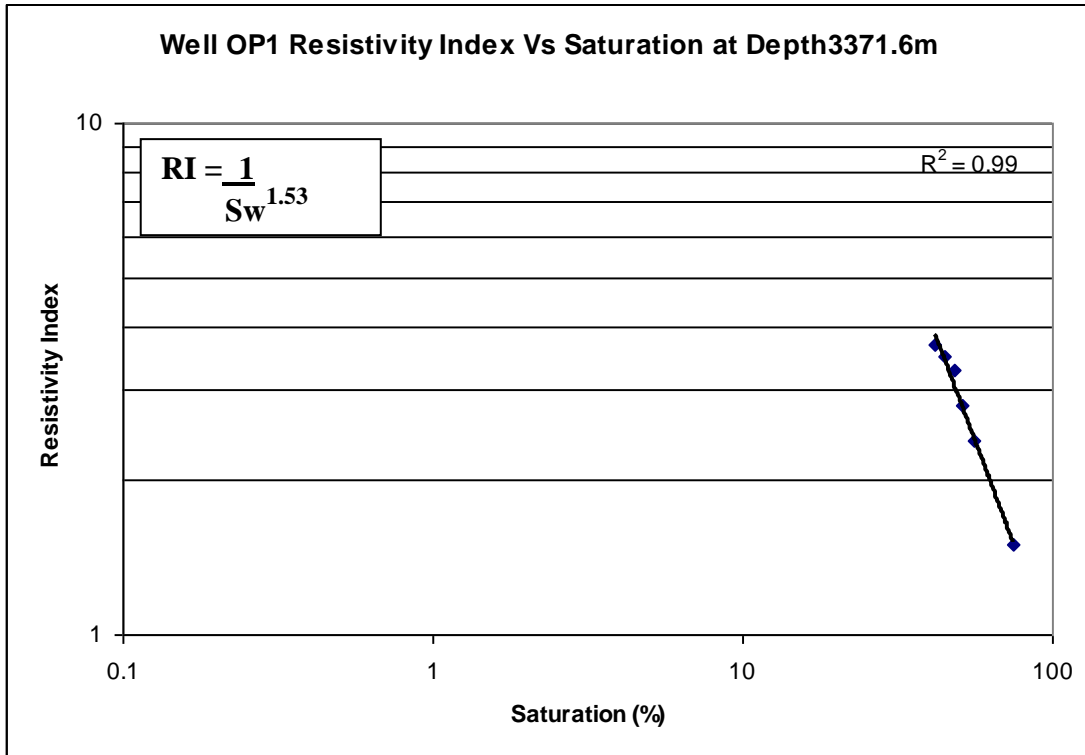


WELL OP2 CORE PHOTO

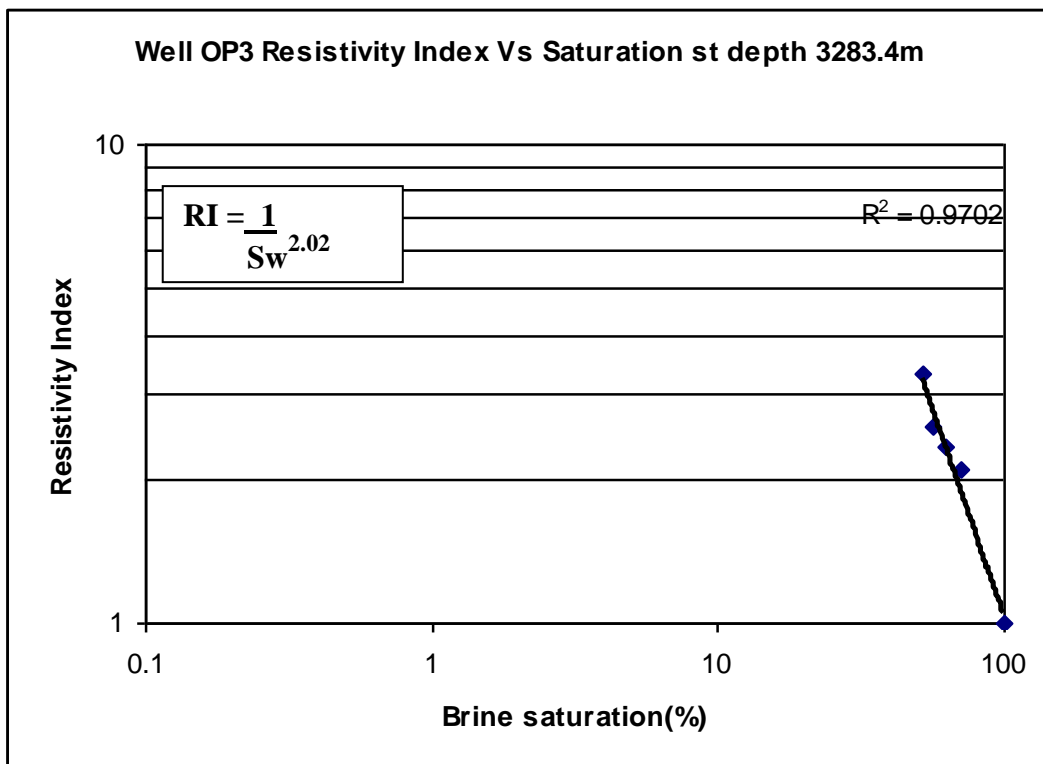
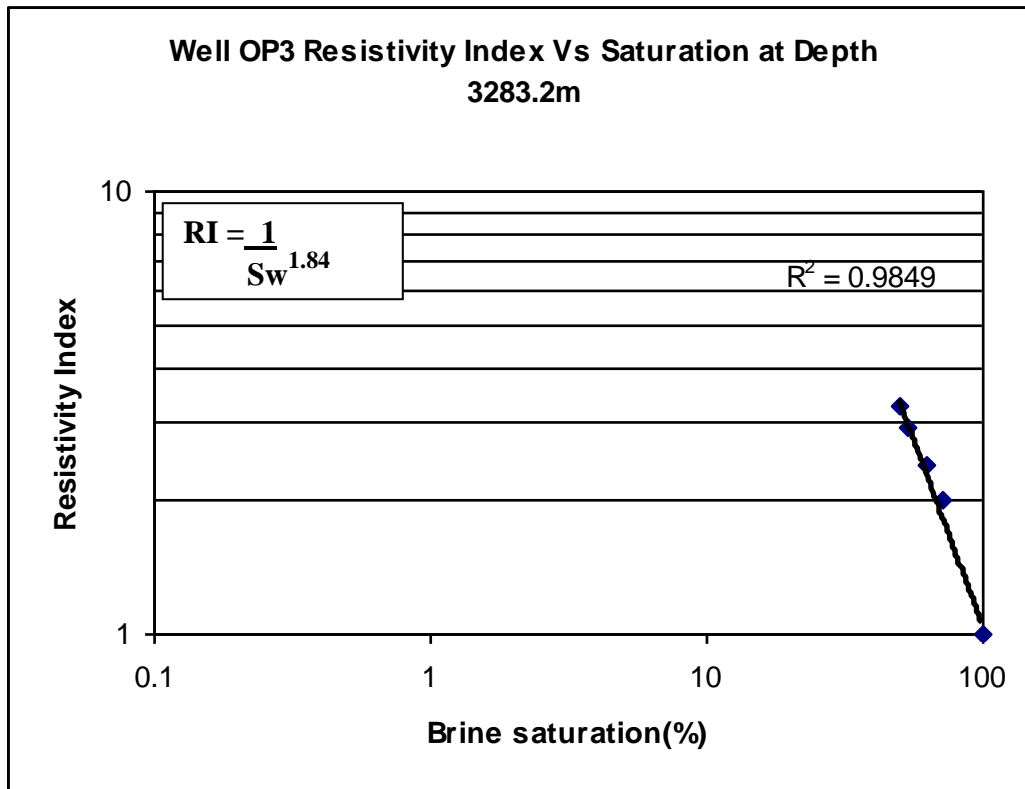


APPENDIX C: WELL RESISTIVITY INDEX VS SATURATION PLOTS

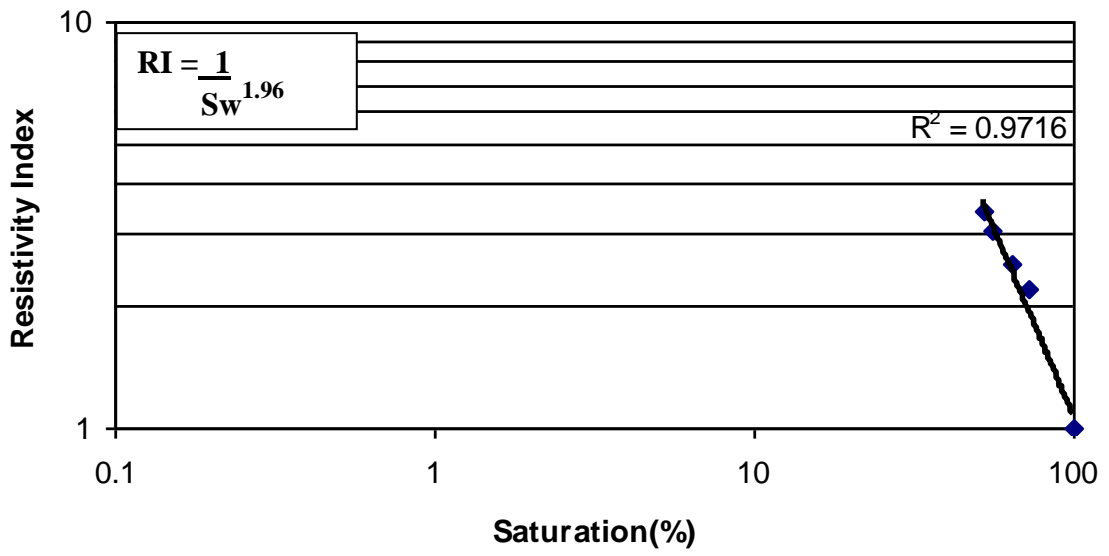




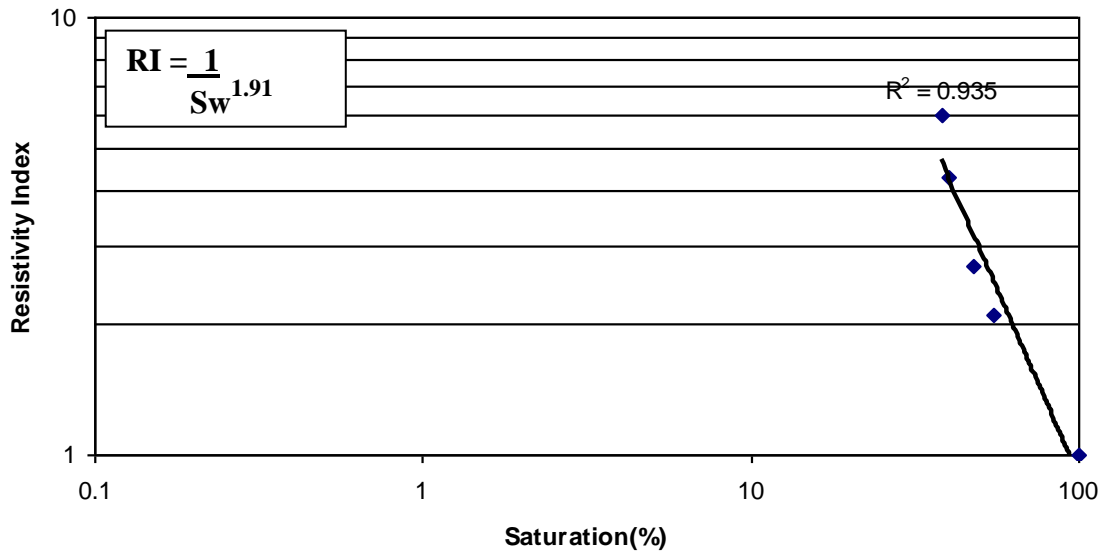
WELL OP3 RESISTIVITY INDEX VS SATURATION PLOTS

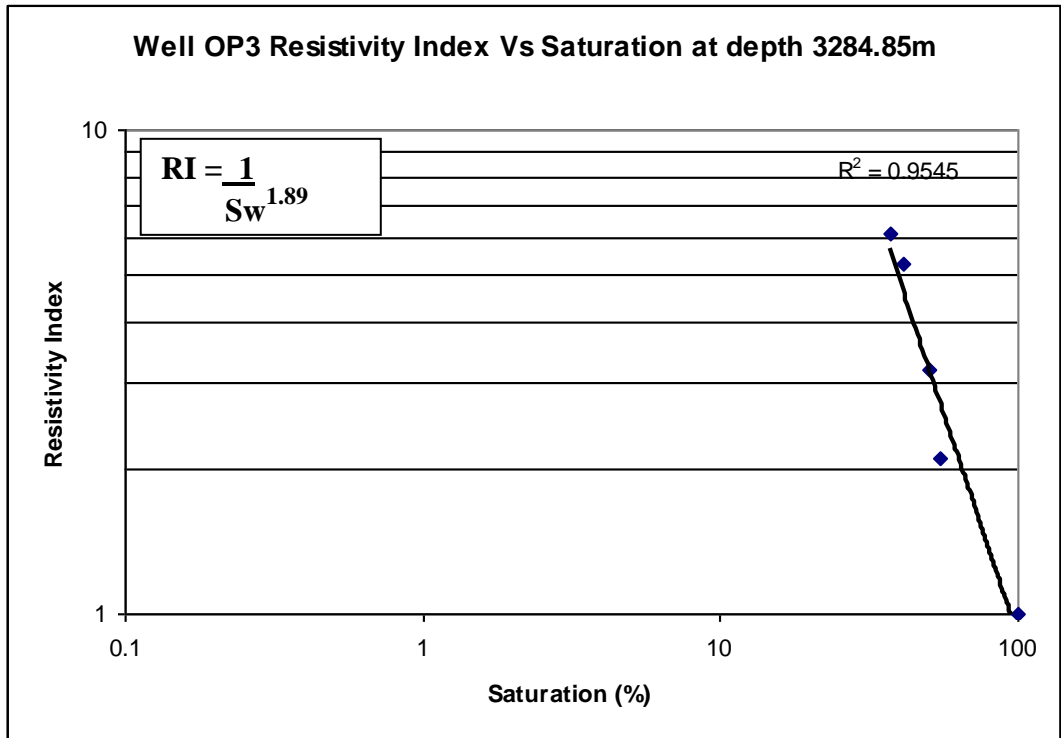
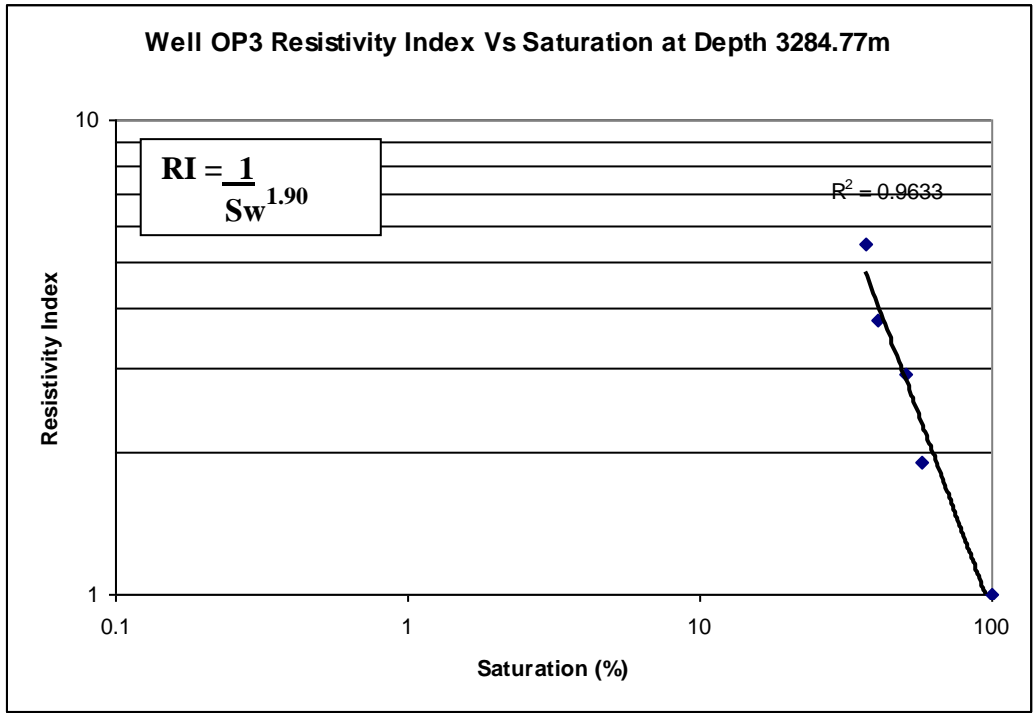


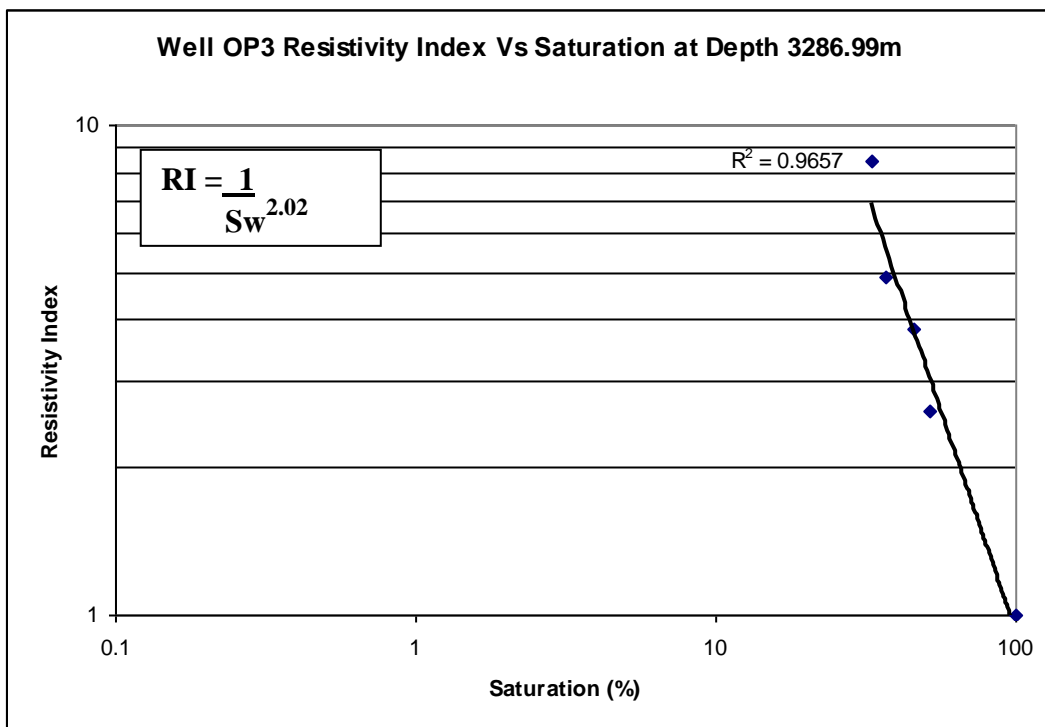
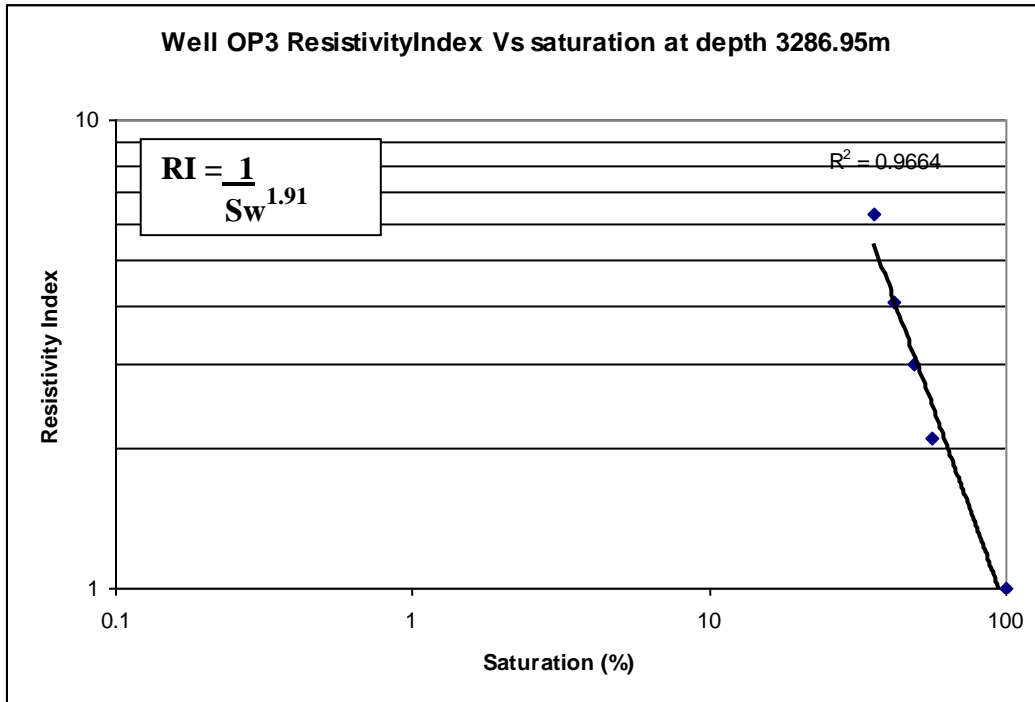
Well OP3 Resistivity Index Vs Saturation at Depth 3283.5m

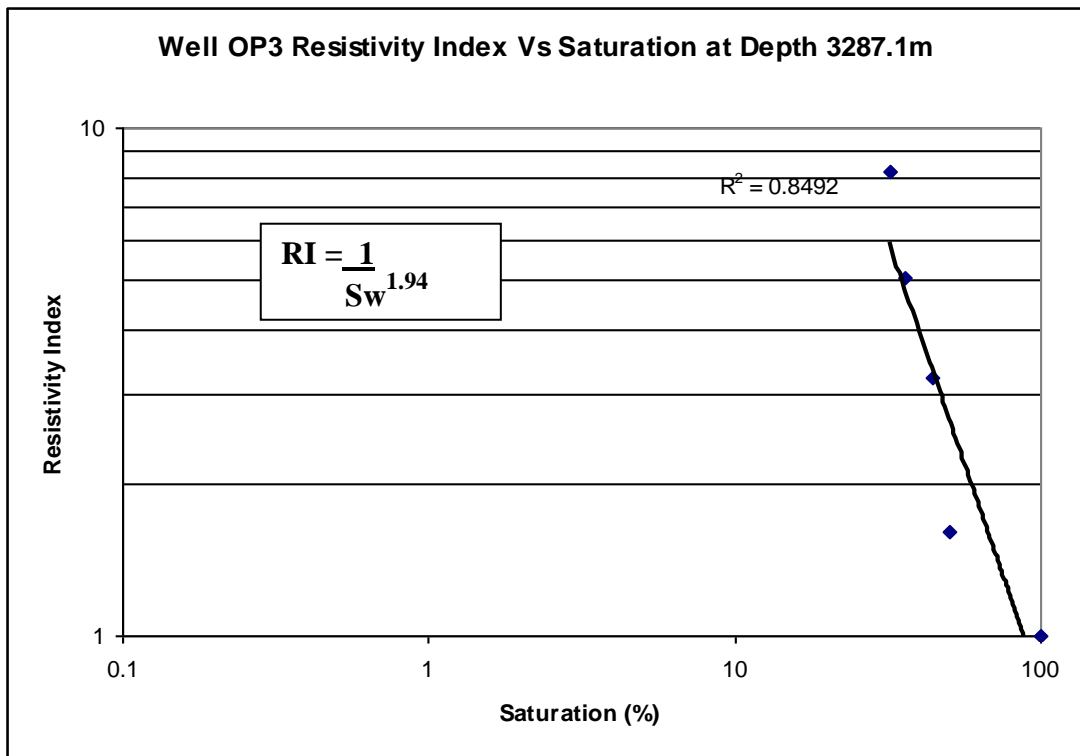
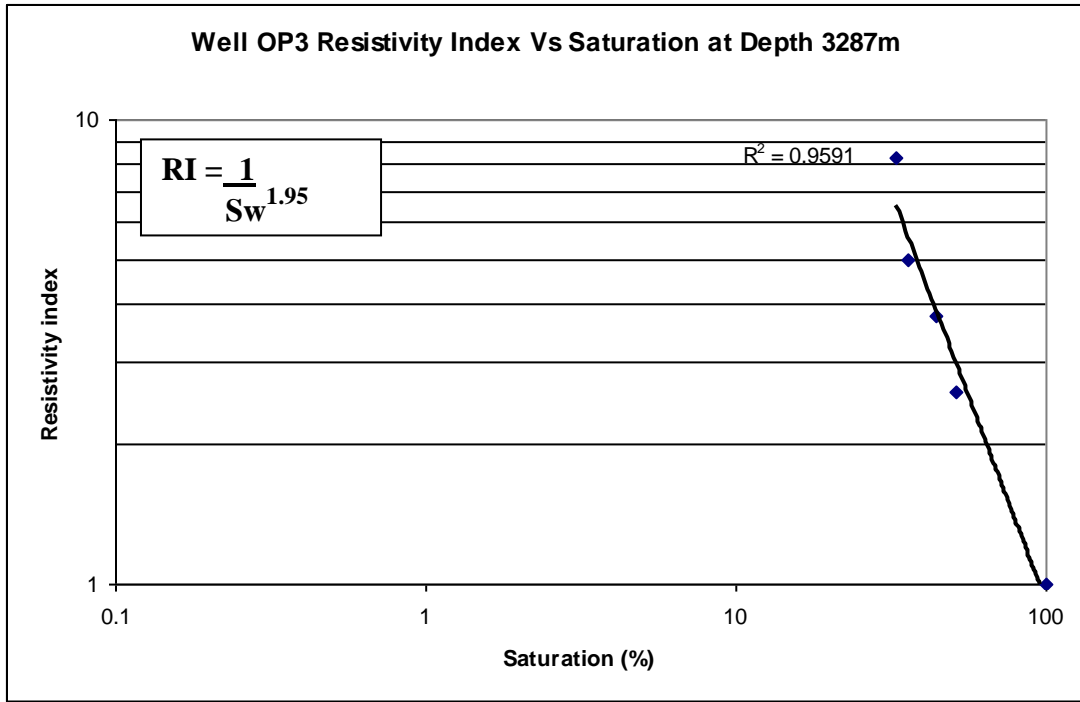


Well OP3 Resistivity Index Vs saturation at depth 3284.74m









APPENDIX D: WELL OP2 CAPILLARY PRESSURE DATA

Well OP2 Mercury Injection Capillary Pressure Data					
Depth=3447.08m Permeability=224mD Porosity=24.6 %		Depth=3560m Permeability=673mD Porosity=22.6%		Depth=3467.5m permeability=0.036mD Porosity=4.6%	
Injection Pressure, psia	1.0-Mercury Saturation, fraction	Injection Pressure, psia	1.0-Mercury Saturation, fraction	Injection Pressure, psia	1.0-Mercury Saturation, fraction
1.01	1.000	1.01	1.000	1.08	1.000
2.01	1.000	2.01	1.000	2.07	1.000
3.00	1.000	3.00	1.000	3.07	1.000
4.01	1.000	4.01	0.984	4.06	1.000
4.99	1.000	4.99	0.939	5.06	1.000
6.0	1.000	6.0	0.824	6.1	1.000
7.5	1.000	7.5	0.700	7.5	1.000
9.0	0.988	9.0	0.636	9.0	1.000
11.0	0.910	11.0	0.593	11.0	1.000
14.0	0.757	14.0	0.558	14.0	1.000
16.9	0.695	16.9	0.554	17.0	1.000
19.9	0.662	19.9	0.547	20.0	1.000
23.0	0.640	23.0	0.535	23.0	1.000
25.9	0.627	25.9	0.527	26.0	1.000
29.9	0.614	29.8	0.516	30.2	1.000
35	0.603	35	0.508	36	1.000
40	0.592	40	0.503	40	1.000
50	0.579	50	0.494	50	1.000
60	0.568	60	0.488	61	1.000
75	0.554	75	0.478	75	0.994
90	0.541	90	0.467	90	0.989
120	0.520	120	0.451	120	0.983
150	0.505	150	0.437	150	0.977
190	0.481	190	0.420	190	0.972
250	0.452	250	0.400	250	0.966
350	0.410	350	0.374	350	0.949
450	0.380	450	0.355	450	0.938
610	0.339	610	0.335	600	0.915
800	0.295	800	0.314	820	0.893
1000	0.259	1000	0.294	1020	0.876
1300	0.222	1300	0.275	1300	0.864
1600	0.188	1600	0.246	1600	0.853
2000	0.164	2000	0.219	2000	0.842
2500	0.148	2500	0.196	2500	0.842
3100	0.136	3100	0.185	3100	0.842
4000	0.123	4000	0.174	4000	0.842
5000	0.112	5000	0.165	5000	0.842
6500	0.106	6500	0.155	6500	0.842
8000	0.099	8000	0.152	8000	0.836
10000	0.093	10000	0.144	10000	0.814
12000	0.089	12000	0.140	12000	0.780
14000	0.086	14000	0.133	14000	0.751
16900	0.079	16900	0.130	17000	0.700
20000	0.077	20000	0.121	19900	0.655
23400	0.072	23400	0.107	23400	0.599
27400	0.068	27400	0.099	27400	0.537
31400	0.061	31400	0.090	31500	0.469
35000	0.055	35000	0.081	34800	0.429
39900	0.051	39900	0.068	39800	0.361
44900	0.047	44900	0.052	45000	0.288
49800	0.041	49800	0.041	49800	0.243
54900	0.033	54900	0.030	54800	0.209

APPENDIX E: WELL J-FUNCTION AND HEIGHT PARAMETERS

Interfacial Tension and Contact Angle Values (Core Laboratories, 1982) used for Well OP1 and OP3.

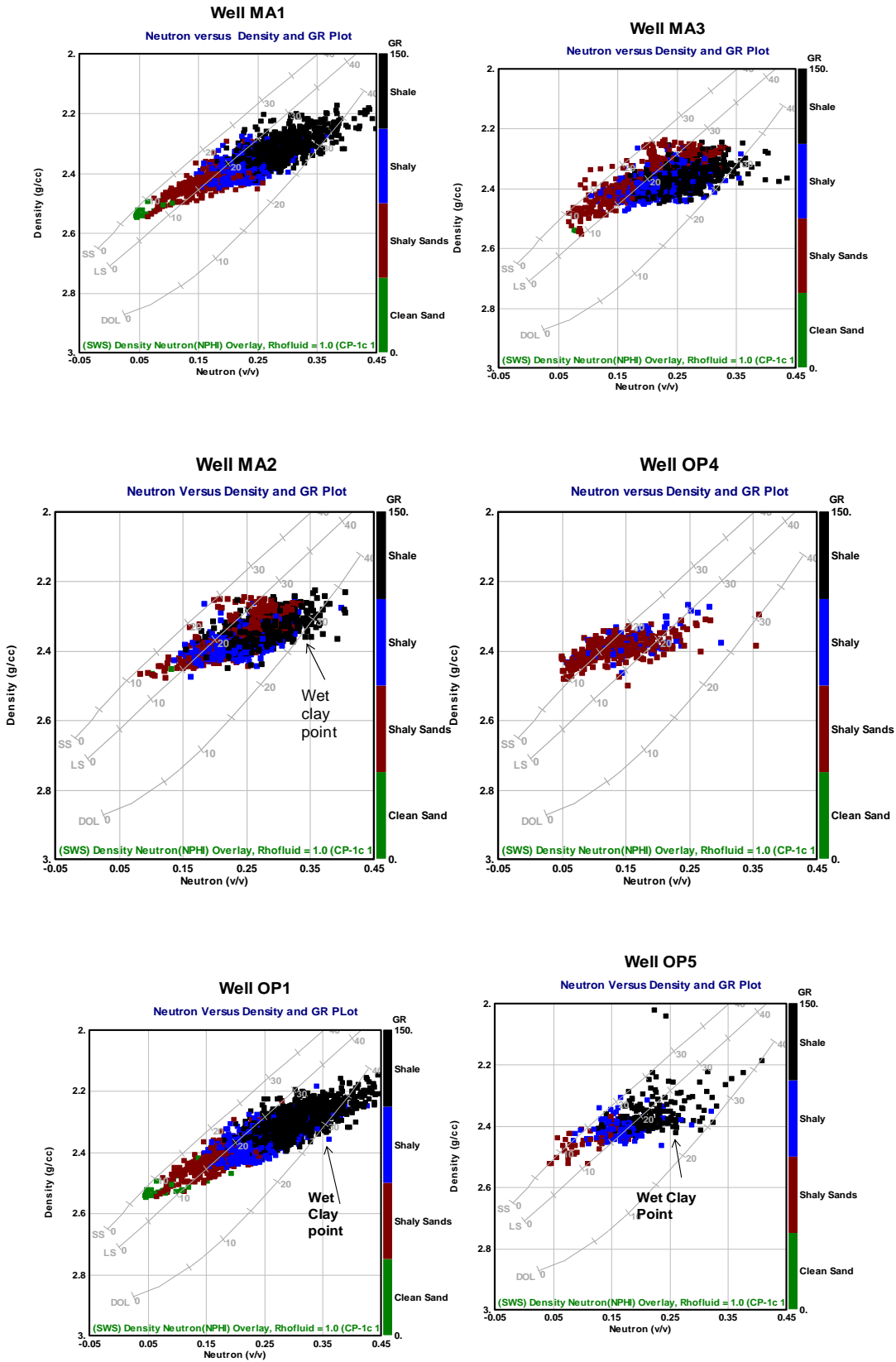
<i>Wetting Phase</i>	<i>Non-Wetting Phase</i>	<i>Conditions: Temperature(T) Pressure(P)</i>	<i>Contact Angle(σ)</i>	<i>Interfacial Tension (dynes/cm)</i>	<i>Comment</i>
Brine	Oil	Reservoir,T,P	30	30	Not Used
Brine	Oil	Laboratory,T,P	30	48	Not Used
Brine	Gas	Laboratory,T,P	0	72	Used
Brine	Gas	Reservoir,T,P	0	50	Used
Oil	Gas	Reservoir,T,P	0	4	Not Used
Gas	Mercury	Laboratory,T,P	140	480	Not used

WELL OP1 J-FUNCTION PARAMETERS							
Depth=3370.4m;K=38mD;Poro=0.177							
Brine Sw	Pc	Pc*coso	cos lab	Pc res	0.3048*Pc	Ht	Nor(J(Sw))
90.5	2	100	72	1.388889	0.423333	1.286727	0.09
71	4	200	72	2.777778	0.846667	2.573455	0.18
57.1	8	400	72	5.555556	1.693333	5.14691	0.35
52.4	15	750	72	10.41667	3.175	9.650456	0.66
49.8	35	1750	72	24.30556	7.408333	22.51773	1.54
46.2	80	4000	72	55.55556	16.93333	51.4691	3.53
43.2	180	9000	72	125	38.1	115.8055	7.93
Depth=3371.0m;K=38mD;Poro=.186							
Brine Sw	Pc						
64	4	200	72	2.777778	0.846667	2.573455	0.17
51.1	8	400	72	5.555556	1.693333	5.14691	0.34
47.5	15	750	72	10.41667	3.175	9.650456	0.64
45.2	35	1750	72	24.30556	7.408333	22.51773	1.5
42.3	80	4000	72	55.55556	16.93333	51.4691	3.44
39.7	180	9000	72	125	38.1	115.8055	7.74
Depth=3371.6m;K=17mD;Poro=0.167							
Brine Sw	Pc						
74.9	4	200	72	2.777778	0.846667	2.573455	0.12
55.9	8	400	72	5.555556	1.693333	5.14691	0.24
50.8	15	750	72	10.41667	3.175	9.650456	0.46
48.2	35	1750	72	24.30556	7.408333	22.51773	1.06
44.5	80	4000	72	55.55556	16.93333	51.4691	2.43
42.4	180	9000	72	125	38.1	115.8055	5.47
Depth=3372.3m;K=1.1mD;Poro=0.117							
Brine Sw	Pc						
71.3	15	750	72	10.41667	3.175	9.650456	0.14
63.7	35	1750	72	24.30556	7.408333	22.51773	0.33
56.7	80	4000	72	55.55556	16.93333	51.4691	0.75
52.2	180	9000	72	125	38.1	115.8055	1.68

WELL OP3 J-FUNCTION AND HEIGHT PARAMETERS

WELL OP3 J-FUNCTION PARAMETERS									
Depth(m)	Sw(%)	Pc(psi)	Pc Cosθ	Cosθ lab	Pc res	0.3048*Pc	Ht	Nor(J Sw)	
3283.2 K=6mD Porosity=20.2	100	1	50	72	0.694444	0.211667	0.643364	0.02	
	100	2	100	72	1.388889	0.423333	1.286727	0.03	
	98.4	4	200	72	2.777778	0.846667	2.573455	0.07	
	82.7	8	400	72	5.555556	1.693333	5.14691	0.13	
	71.4	15	750	72	10.41667	3.175	9.650456	0.25	
	63.2	35	1750	72	24.30556	7.408333	22.51773	0.57	
	53.3	100	5000	72	69.44444	21.16667	64.33637	1.64	
	50	180	9000	72	125	38.1	115.8055	2.95	
3283.4 K=4.4mD Porosity=18.7	100	1	50	72	0.694444	0.211667	0.643364	0.01	
	100	2	100	72	1.388889	0.423333	1.286727	0.03	
	97.9	4	200	72	2.777778	0.846667	2.573455	0.06	
	83.9	8	400	72	5.555556	1.693333	5.14691	0.12	
	71.2	15	750	72	10.41667	3.175	9.650456	0.22	
	62.7	35	1750	72	24.30556	7.408333	22.51773	0.51	
	55.7	100	5000	72	69.44444	21.16667	64.33637	1.46	
	52.1	180	9000	72	125	38.1	115.8055	2.63	
3283.5 K=3.5 Porosity=17.7	100	1	50	72	0.694444	0.211667	0.643364	0.01	
	100	2	100	72	1.388889	0.423333	1.286727	0.03	
	97.8	4	200	72	2.777778	0.846667	2.573455	0.05	
	87.6	8	400	72	5.555556	1.693333	5.14691	0.11	
	72.8	15	750	72	10.41667	3.175	9.650456	0.2	
	63.5	35	1750	72	24.30556	7.408333	22.51773	0.47	
	55.9	100	5000	72	69.44444	21.16667	64.33637	1.34	
	51.6	180	9000	72	125	38.1	115.8055	2.41	
3284.74 K=80mD Porosity=23.5	100	1	50	72	0.694444	0.211667	0.643364	0.06	
	94.8	2	100	72	1.388889	0.423333	1.286727	0.11	
	67.6	4	200	72	2.777778	0.846667	2.573455	0.22	
	59.8	8	400	72	5.555556	1.693333	5.14691	0.44	
	54.9	15	750	72	10.41667	3.175	9.650456	0.83	
	48.1	35	1750	72	24.30556	7.408333	22.51773	1.94	
	40.3	100	5000	72	69.44444	21.16667	64.33637	5.55	
	37.9	180	9000	72	125	38.1	115.8055	9.99	
3284.77 K=57mD Porosity=23.4	100	1	50	72	0.694444	0.211667	0.643364	0.05	
	95.7	2	100	72	1.388889	0.423333	1.286727	0.09	
	72.6	4	200	72	2.777778	0.846667	2.573455	0.19	
	62.9	8	400	72	5.555556	1.693333	5.14691	0.38	
	57.6	15	750	72	10.41667	3.175	9.650456	0.7	
	50.5	35	1750	72	24.30556	7.408333	22.51773	1.64	
	41.2	100	5000	72	69.44444	21.16667	64.33637	4.69	
	38	180	9000	72	125	38.1	115.8055	8.45	
3284.85 K=69mD Porosity=23.6	100	1	50	72	0.694444	0.211667	0.643364	0.05	
	96.1	2	100	72	1.388889	0.423333	1.286727	0.1	
	68.4	4	200	72	2.777778	0.846667	2.573455	0.21	
	60.4	8	400	72	5.555556	1.693333	5.14691	0.41	
	55.2	15	750	72	10.41667	3.175	9.650456	0.77	
	49.7	35	1750	72	24.30556	7.408333	22.51773	1.8	
	40.9	100	5000	72	69.44444	21.16667	64.33637	5.14	
	37.4	180	9000	72	125	38.1	115.8055	9.26	
3286.95 K=59mD Porosity=24.2	97.9	1	50	72	0.694444	0.211667	0.643364	0.05	
	85.8	2	100	72	1.388889	0.423333	1.286727	0.09	
	68	4	200	72	2.777778	0.846667	2.573455	0.19	
	61.2	8	400	72	5.555556	1.693333	5.14691	0.38	
	56	15	750	72	10.41667	3.175	9.650456	0.7	
	49	35	1750	72	24.30556	7.408333	22.51773	1.64	
	41.8	100	5000	72	69.44444	21.16667	64.33637	4.69	
	36.3	180	9000	72	125	38.1	115.8055	8.45	
3286.99 K=105mD Porosity=24.3	98.2	1	50	72	0.694444	0.211667	0.643364	0.06	
	80.7	2	100	72	1.388889	0.423333	1.286727	0.13	
	62.9	4	200	72	2.777778	0.846667	2.573455	0.25	
	57.2	8	400	72	5.555556	1.693333	5.14691	0.5	
	52.4	15	750	72	10.41667	3.175	9.650456	0.94	
	45.5	35	1750	72	24.30556	7.408333	22.51773	2.19	
	37.3	100	5000	72	69.44444	21.16667	64.33637	6.26	
	33	180	9000	72	125	38.1	115.8055	11.26	
3287 K=79mD Porosity=24.3	97.6	1	50	72	0.694444	0.211667	0.643364	0.05	
	78.7	2	100	72	1.388889	0.423333	1.286727	0.11	
	60.9	4	200	72	2.777778	0.846667	2.573455	0.22	
	55.4	8	400	72	5.555556	1.693333	5.14691	0.43	
	50.7	15	750	72	10.41667	3.175	9.650456	0.81	
	44.4	35	1750	72	24.30556	7.408333	22.51773	1.89	
	35.9	100	5000	72	69.44444	21.16667	64.33637	5.42	
	32.5	180	9000	72	125	38.1	115.8055	9.75	
3287.1 K=90mD Porosity=24.4	97.1	1	50	72	0.694444	0.211667	0.643364	0.06	
	78.8	2	100	72	1.388889	0.423333	1.286727	0.12	
	60.7	4	200	72	2.777778	0.846667	2.573455	0.23	
	55	8	400	72	5.555556	1.693333	5.14691	0.46	
	50.4	15	750	72	10.41667	3.175	9.650456	0.87	
	44.2	35	1750	72	24.30556	7.408333	22.51773	2.02	
	35.7	100	5000	72	69.44444	21.16667	64.33637	5.78	
	32.4	180	9000	72	125	38.1	115.8055	10.39	

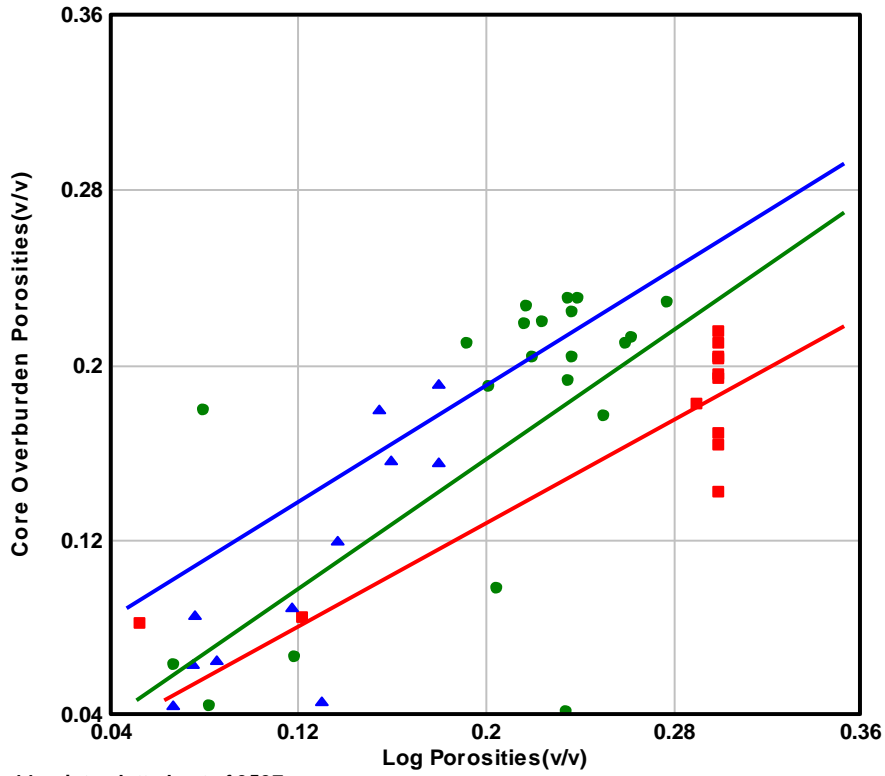
APPENDIX F: NEUTRON VERSUS DENSITY AND GR LOG PLOTS



APPENDIX G: LOG VERSUS CORE POROSITY PLOT

All Well

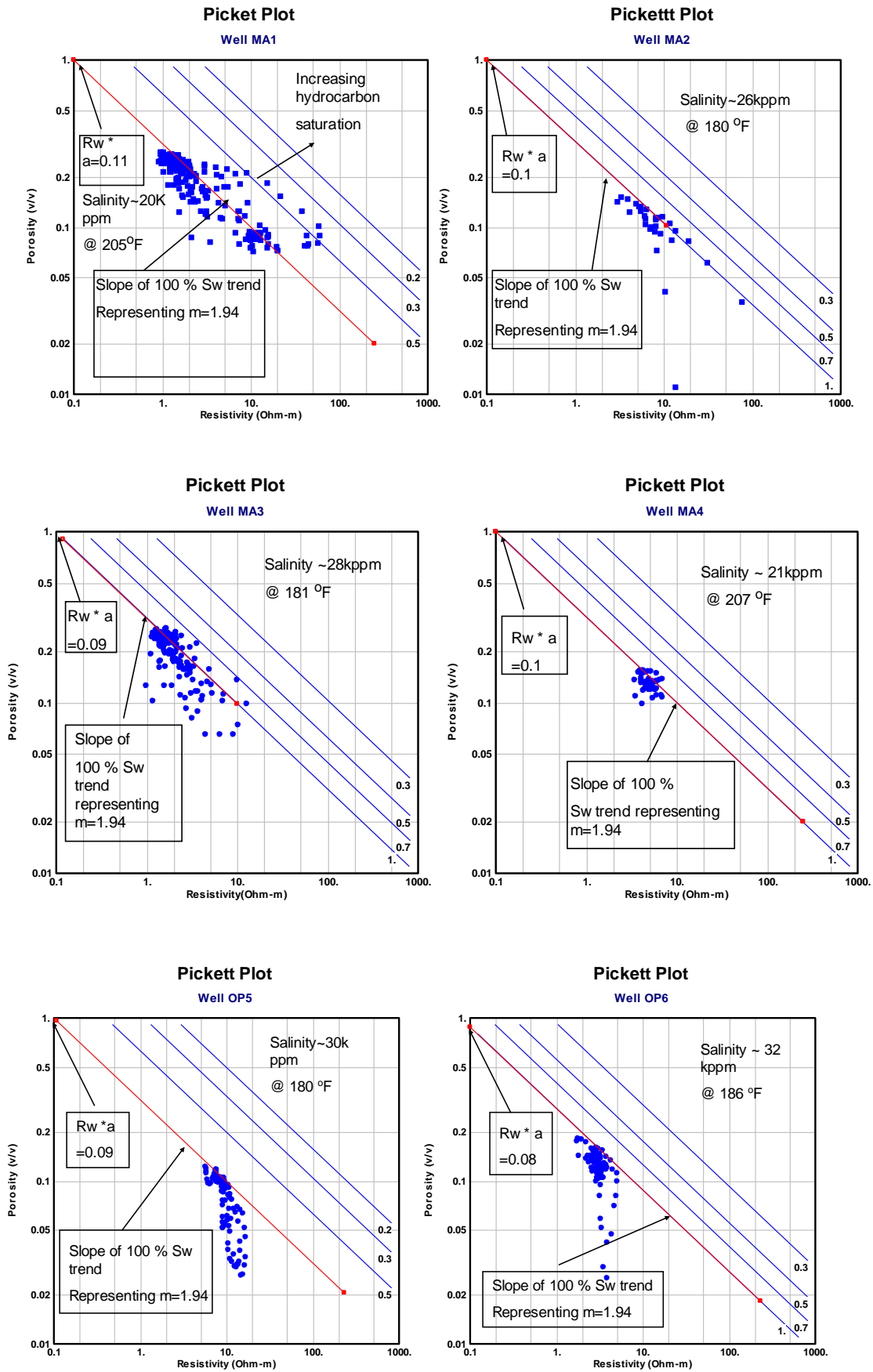
Log Versus Core Overburden Porosity
Multi well Interval plot



44 points plotted out of 3537

Well	Depths
OP3	3000.M - 3500.M
OP1	3000.M - 3751.76M
OP2	3000.M - 3600.02M

APPENDIX H: PICKETT PLOT FOR WELLS



APPENDIX I: RESULTS OF RFT MEASUREMENTS FOR WELLS

WELL OP2

DEPTH (primary gauge)		IHP (primary gauge)	FHP (primary gauge)	Vol (cc)	Time Set	PRE-TEST DATA		SIP EMW to RT (ppg)	SIP EMW to SS (ppg)	Temp (deg F)	Mobility (md/cp)
meters (RTMD)	feet (TVDmd)	(psia)	(psia)			Flow time (mins)	SIP (psia)				
3448.0	11312.3	6113.3	6102.1	20.0	3:15	10.0	5085.24	8.644817	8.7084812	197.3	91.9
3449.0	11315.6	6099.8	6097.4	20.0	3:36	3.0	5086.46	8.6443839	8.7080263	205.0	165.0
3450.0	11318.9	6067.0	6067.0	20.0	4:44	4.0	5083.90	8.6375288	8.7011022	209.3	507.0
3451.5	11323.8	6102.4	6099.5	20.0	3:32	3.5	5090.93	8.6457138	8.7093196	201.8	70.4
3453.0	11328.7	6099.0	6090.0	20.0	3:43	15.0	5179.38	8.7921037	8.8567582	203.3	3.4
3454.5	11333.7	6078.4	6078.7	20.0	4:32	5.0	5092.01	8.6400381	8.7035465	208.8	58.9
3456.0	11338.6	6095.8	6093.4	20.0	4:02	6.0	5095.20	8.6416984	8.7051913	206.2	223.6
3456.5	11340.2	6089.5	6083.7	20.0	4:12	15.0	5392.13	9.1439827	9.2111563	207.4	12.7

Well OP3

Depth	P mud Before	P res psia	P mud After psia	Time		QC	Remarks
				From	To		
3276.04	5735	4854	5735	13:31	13:38	1	Drawdown to 550psi, Erratic BU Plugging (?) building slowly at end
3278.05	5741	4865	5740	13:39	13:49	1	Deep drawdown to 250psi slow but smooth BU. Still Building
3280.05	5745	4838	5744	13:50	13:56	2	Deep drawdown to 500psi Reasonable BU. Stabilizing at end
3282.04	5749	4842	5749	13:58	14:05	2	Deep drawdown to 500psi, rapid BU, Fairly stable
3283.05	5751	4838	5751	14:06	14:11	4	shallow drawdown, stable
3284.05	5754	4838	5754	14:12	14:16	4	Very shallow drawdown, stable at end.
3285.04	5756	4840	5756	14:18	14:23	4	Very shallow drawdown, stable at end.
3312.05	5804	4885	5803	14:27	14:33	4	shallow drawdown, stable at end.
3314.05	5808		5806	14:33	14:39	0	Drawdown to 160psi, no BU
3316.04	5812	4891	5811	14:41	14:46	4	Very shallow drawdown, stable
3322.05	5826	leakage	5825	14:48	14:57	0	Deep drawdown to 170psi, BU to 5323, then down to 5034 (not stable)
3355.04	5883	4972	5881	15:01	15:06	4	Very shallow drawdown, stable
3357.05	5885	4972	5885	15:07	15:12	4	Very shallow drawdown, stable
3359.03	5889	4974	5888	15:13	15:19	4	Very shallow drawdown, stable
3361.05	5893	4975	5893	15:20	15:24	4	Very shallow drawdown, stable
3363.04	5898	4978	5898	15:26	15:30	4	Very shallow drawdown, stable
3365.04	5902	4982	5902	15:32	15:37	4	Low drawdown, stable
3367.05	5907	4986	5907	15:39	15:43	4	Very low drawdown, stable
3369.55	5913	4990	5912	15:46	15:50	3	medium drawdown, stable

WELL OP4

DEPTH		IHP	FHP	PRE-TEST DATA							
(primary gauge)		(primary gauge)		Vol	Time	Flow	SIP	SIP	SIP	Temp	Mobility
meters	feet				Set	time		EMW to RT	EMW to SS		
(RTMD)	(TVDmd)	(psia)	(psia)	(cc)		(mins)	(psia)	(ppg)	(ppg)	(deg F)	(md/cp)
3240.0	10629.9	5679.0	5675.6	20.0	16:04	4.6	4929.75	8.9184933	8.9884226	227.0	91.5
3240.0	10629.9	5674.4	5668.8	20.0	13:32	8.0	4924.64	8.9092487	8.9791055	221.0	
3241.0	10633.2	5684.8	5684.4	20.0	20:13	5.0	4933.60	8.9227045	8.992645	229.0	245.2
3242.0	10636.5	5686.3	5686.1	20.0	20:04	4.2	4933.39	8.9195726	8.9894668	229.0	92.1
3243.0	10639.8	5688.6	5687.9	20.0	19:55	4.0	4933.82	8.9175994	8.9874564	229.0	68.6
3244.0	10643.0	5680.4	5675.6	20.0	13:46	9.0	4925.71	8.9001966	8.9698956	224.0	76.0
3246.0	10649.6	5688.3	5685.5	20.0	15:08	2.5	4931.52	8.9052043	8.9748993	227.0	561.9
3247.0	10652.9	5694.6	5694.3	20.0	19:44	5.0	4935.82	8.9102242	8.9799368	229.0	1.1
3248.0	10656.2	5690.2	5686.8	20.0	15:15	4.0	4931.25	8.8992336	8.9688386	226.0	246.5
3249.0	10659.4	5703.0	5698.2	20.0	19:20	18.0	4936.70	8.9063269	8.9759658	229.0	331.9
3250.0	10662.7	5693.3	5891.2	20.0	15:26	8.5	4932.55	8.8961017	8.9656391	226.0	186.7
3253.0	10672.6	5700.2	5704.4	20.0	15:41	4.0		0	0	226.0	
3255.0	10679.1	5702.4	5700.3	20.0	15:50			0	0	227.0	
3255.2	10679.8	5702.6	5707.1	20.0	15:57			0	0	227.0	
3257.0	10685.7	5713.7	5701.1	20.0	14:01	19.0	4930.17	8.8726988	8.9419031	225.0	86.3
3287.5	10785.8	5782.9	5769.7	20.0	18:33	29.5	5247.40	9.3559957	9.4282873	233.0	0.1
3288.5	10789.0	5780.4	5760.2	20.0	14:30	28.0	5036.42	8.9770925	9.0464351	227.0	0.5
3301.0	10830.1	5821.3	5791.5	20.0	16:20	24.1	5007.70	8.8921009	8.9605249	230.0	20.4

WELL OP6

DEPTH		IHP	FHP		PRE-TEST DATA						
(primary gauge)		(primary gauge)		Vol	Time	Flow	SIP	SIP	SIP	Temp	
meters	feet				Set	time		EMW to RT	EMW to SS		
(RTMD)	(TVDmd)	(psia)	(psia)	(cc)		(mins)	(psia)	(ppg)	(ppg)	(deg F)	
3199.5	10414.4	5799.6	5787.6	20.0	23:36	5.0	4642.88	8.573361	8.6419866	206.0	
3200.5	10417.7	5783.5	5776.1	20.0	23:50	10.0	4645.47	8.5754428	8.6440633	208.0	
3201.5	10420.9	5775.6	5776.3	20.0	0:06	10.0	4646.27	8.5742192	8.6428081	209.0	
3206.0	10435.7	5789.6	5783.1	20.0	0:23	11.0	4646.69	8.5628627	8.631263	210.0	
3216.0	10468.5	5808.9	5798.9	20.0	1:30	11.0	4665.00	8.5696626	8.637901	212.0	
3217.0	10471.8	5800.0	5800.6	20.0	1:47	4.0	4665.85	8.5685385	8.6367465	212.0	
3218.0	10475.1	5800.7	5802.0	20.0	1:56	7.0	4666.85	8.5676905	8.6358702	212.0	
3219.5	10480.0	5802.3	5803.8	20.0	2:08	9.5	4666.95	8.563851	8.6319678	212.0	
3221.0	10484.9	5805.5	5806.1	20.0	2:23	10.0	4670.93	8.5671307	8.6352414	213.0	
3222.5	10489.8	5809.7	5797.2	20.0	2:38	6.0	4668.12	8.5579601	8.6259658	214.0	
3225.0	10498.0	5815.4	5814.9	20.0	2:48	6.0	4671.42	8.557319	8.625266	214.0	
3226.0	10501.3	5812.1	5817.3	20.0	3:00	7.5	4673.90	8.5591869	8.6271273	215.0	
3227.0	10504.6	5814.1	5814.6	20.0	3:12	10.0	4671.10	8.5513876	8.6192447	215.0	
3228.0	10507.9	5813.9	5817.6	20.0	3:27	10.0	4677.73	8.5608512	8.6287621	216.0	

WELL MA1

DEPTH			STRAIN GAUGE						HP GAUGE					
			HYD PRESSURE	EMW	FORMATION PRESSURE	EMW	HYD PRESSURE	EMW	HYD PRESSURE	EMW	FORMATION PRESSURE	EMW	HYD PRESSURE	EMW
(m MD)	(mTVD)	(mTVDS) (MSL)	BEFORE	PPG EMW		PPG EMW	AFTER	PPG EMW	BEFORE	PPG EMW		PPG EMW	AFTER	PPG EMW
3213.4	3213.4	3191.9	5557.06	10.14	4733.27	8.69	5557.01	10.14	5572.6	10.16	4749.3	8.72	5572.8	10.17
3217.7	3217.7	3196.2	5564.20	10.14	4736.99	8.69	5564.56	10.14	5580.3	10.17	4751.6	8.71	5580.4	10.17
3219.0	3219.0	3197.5	5566.71	10.14	4738.56	8.69	5566.72	10.14	5582.6	10.17	4753.1	8.71	5582.5	10.17
3220.0	3220.0	3198.5	5568.21	10.14	4739.80	8.69	5568.44	10.14	5584.2	10.17	4754.4	8.71	5584.2	10.35
3222.5	3222.5	3201.0	5572.53	10.14	4743.22	8.69	5572.61	10.14	5588.6	10.17	4757.9	8.71	5588.4	10.17
3223.2	3223.2	3201.7	5573.65	10.14	4744.09	8.69	5573.54	10.14	5589.4	10.16	4758.8	8.71	5588.3	10.16
3227.0	3227.0	3205.5	5580.11	10.14	4749.77	8.69	5580.11	10.14	5595.9	10.16	4764.3	8.71	5595.7	10.16
3228.5	3228.5	3207.0	5582.51	10.14	4751.81	8.69	5582.41	10.14	5598.4	10.16	4766.5	8.71	5598.1	10.16
3231.3	3231.3	3209.8	5587.18	10.14	4755.93	8.69	5587.14	10.14	5603.0	10.16	4770.5	8.71	5602.8	10.16
3233.0	3233.0	3211.5	5589.78	10.13	4761.40	8.69	5589.27	10.13	5605.7	10.16	4777.4	8.72	5606.4	10.16
3236.2	3236.2	3214.7	5594.77	10.13	4762.64	8.68	5594.86	10.13	5611.0	10.16	4777.3	8.71	5610.6	10.16

WELL MA2:

			HP GAUGE					
DEPTH			HYD PRESSURE	EMW	FORMATION PRESSURE	EMW	HYD PRESSURE	EMW
(m MD)	(mTVD)	(mTVDSS) (MSL)	BEFORE	ppg		ppg	AFTER	ppg
2944.5	2941.5	2920.0	5143.8	10.25	4359.5	8.75	5143.7	10.25
2945.5	2942.5	2921.0	5145.6	10.25	4361.2	8.75	5145.3	10.25
2947.0	2944.0	2922.5	5148.3	10.25	4363.3	8.75	5147.9	10.25
2952.0	2949.0	2927.5	5156.6	10.25	4371.6	8.75	5156.3	10.25
2960.5	2957.5	2936.0	5170.3	10.25	4387.1	8.76	5169.9	10.25
2963.5	2960.5	2939.0	5175.5	10.25	4389.2	8.75	5175.1	10.25
2965.3	2962.3	2940.8	5178.8	10.25	4389.0	8.75	5178.2	10.25
2967.2	2964.2	2942.7	5181.3	10.25	4391.2	8.75	5180.8	10.24
2967.8	2964.8	2943.3	5182.0	10.25	4391.9	8.75	5181.7	10.24
2968.5	2965.5	2944.0	5183.2	10.25	4393.1	8.75	5182.9	10.24
2974.0	2971.0	2949.5	5192.2	10.24	4401.4	8.75	5191.6	10.24
2974.8	2971.8	2950.3	5191.9	10.24	4401.2	8.74	5191.6	10.24
2977.7	2974.7	2953.2	5197.8	10.24	4407.5	8.75	5197.1	10.24
2979.0	2976.0	2954.5	5199.5	10.24	4408.3	8.75	5198.9	10.24
2982.0	2979.0	2957.5	5203.7	10.24	4412.1	8.74	5203.2	10.24
2960.0	2957.0	2935.5	5165.2	10.24	4387.8	8.76	5165.1	10.24
2963.0	2960.0	2938.5	5170.3	10.24	4389.2	8.76	5169.9	10.24
2964.0	2961.0	2939.5	5172.0	10.24	4389.3	8.75	5171.7	10.24
2965.8	2962.8	2941.3	5175.2	10.24	4389.8	8.75	5174.7	10.24

WELL MA3

			HP GAUGE					
DEPTH			HYD PRESSURE	EMW	FORMATION PRESSURE	EMW	HYD PRESSURE	EMW
(m MD)	(mTVD)	(mTVDSS) (MSL)	BEFORE	ppg		ppg	AFTER	ppg
2944.5	2941.5	2920.0	5143.8	10.25	4359.5	8.75	5143.7	10.25
2945.5	2942.5	2921.0	5145.6	10.25	4361.2	8.75	5145.3	10.25
2947.0	2944.0	2922.5	5148.3	10.25	4363.3	8.75	5147.9	10.25
2952.0	2949.0	2927.5	5156.6	10.25	4371.6	8.75	5156.3	10.25
2960.5	2957.5	2936.0	5170.3	10.25	4387.1	8.76	5169.9	10.25
2963.5	2960.5	2939.0	5175.5	10.25	4389.2	8.75	5175.1	10.25
2965.3	2962.3	2940.8	5178.8	10.25	4389.0	8.75	5178.2	10.25
2967.2	2964.2	2942.7	5181.3	10.25	4391.2	8.75	5180.8	10.24
2967.8	2964.8	2943.3	5182.0	10.25	4391.9	8.75	5181.7	10.24
2968.5	2965.5	2944.0	5183.2	10.25	4393.1	8.75	5182.9	10.24
2974.0	2971.0	2949.5	5192.2	10.24	4401.4	8.75	5191.6	10.24
2974.8	2971.8	2950.3	5191.9	10.24	4401.2	8.74	5191.6	10.24
2977.7	2974.7	2953.2	5197.8	10.24	4407.5	8.75	5197.1	10.24
2979.0	2976.0	2954.5	5199.5	10.24	4408.3	8.75	5198.9	10.24
2982.0	2979.0	2957.5	5203.7	10.24	4412.1	8.74	5203.2	10.24
2960.0	2957.0	2935.5	5165.2	10.24	4387.8	8.76	5165.1	10.24
2963.0	2960.0	2938.5	5170.3	10.24	4389.2	8.76	5169.9	10.24
2964.0	2961.0	2939.5	5172.0	10.24	4389.3	8.75	5171.7	10.24
2965.8	2962.8	2941.3	5175.2	10.24	4389.8	8.75	5174.7	10.24